

**TOPICS IN  
STEREOCHEMISTRY**

**VOLUME 25**

## **ADVISORY BOARD**

**GUY BERTRAND**, *Paul Sabatier University, Toulouse, France*

**HENRI BRUNNER**, *University of Regensburg, Regensburg, Germany*

**DAVID E. CANE**, *Brown University, Providence, Rhode Island, USA*

**GAUTAM R. DESIRAJU**, *University of Hyderabad, Hyderabad, India*

**FRANÇOIS DIEDERICH**, *Eidgenössische Technische Hochschule, Zurich, Switzerland*

**ERNEST L. ELIEL**, *University of North Carolina/Chapel Hill, Chapel Hill, North Carolina, USA*

**MARK M. GREEN**, *Polytechnic University, Brooklyn, New York, USA*

**CLAYTON H. HEATHCOCK**, *University of California/Berkeley, Berkeley, California, USA*

**KENDALL N. HOUK**, *University of California/Los Angeles, Los Angeles, CA, USA*

**DANIEL S. KEMP**, *Massachusetts Institute of Technology, Cambridge, Massachusetts, USA*

**JEAN-MARIE LEHN**, *Université Louis Pasteur, Strasbourg, France*

**STEVEN V. LEY**, *Cambridge University, Cambridge, England*

**EIICHI NAKAMURA**, *University of Tokyo, Tokyo, Japan*

**RYOJI NOYORI**, *Nagoya University, Nagoya, Japan*

**NED A. PORTER**, *Vanderbilt University, Nashville, Tennessee, USA*

**STUART L. SCHREIBER**, *Harvard University, Cambridge, Massachusetts, USA*

**K. BARRY SHARPLESS**, *Scripps Institute, La Jolla, California, USA*

**DAVID M. WALBA**, *University of Colorado/Boulder, Boulder, Colorado, USA*

TOPICS IN

# STEREOCHEMISTRY

EDITORS

**SCOTT E. DENMARK**

*Department of Chemistry*

*University of Illinois, Urbana-Champaign  
Urbana, Illinois*

**JAY S. SIEGEL**

*Organic Chemistry Institute  
University of Zurich*

VOLUME 25



A JOHN WILEY & SONS, INC., PUBLICATION

Copyright © 2006 by John Wiley & Sons, Inc. All rights reserved

Published by John Wiley & Sons, Inc., Hoboken, New Jersey

Published simultaneously in Canada

No part of this publication may be reproduced, stored in a retrieval system, or transmitted in any form or by any means, electronic, mechanical, photocopying, recording, scanning, or otherwise, except as permitted under Section 107 or 108 of the 1976 United States Copyright Act, without either the prior written permission of the Publisher, or authorization through payment of the appropriate per-copy fee to the Copyright Clearance Center, Inc., 222 Rosewood Drive, Danvers, MA 01923, (978) 750-8400, fax (978) 750-4470, or on the web at [www.copyright.com](http://www.copyright.com). Requests to the Publisher for permission should be addressed to the Permissions Department, John Wiley & Sons, Inc., 111 River Street, Hoboken, NJ 07030, (201) 748-6011, fax (201) 748-6008, or online at <http://www.wiley.com/go/permission>.

**Limit of Liability/Disclaimer of Warranty:** While the publisher and author have used their best efforts in preparing this book, they make no representations or warranties with respect to the accuracy or completeness of the contents of this book and specifically disclaim any implied warranties of merchantability or fitness for a particular purpose. No warranty may be created or extended by sales representatives or written sales materials. The advice and strategies contained herein may not be suitable for your situation. You should consult with a professional where appropriate. Neither the publisher nor author shall be liable for any loss of profit or any other commercial damages, including but not limited to special, incidental, consequential, or other damages.

For general information on our other products and services or for technical support, please contact our Customer Care Department within the United States at (800) 762-2974, outside the United States at (317) 572-3993 or fax (317) 572-4002.

Wiley also publishes its books in a variety of electronic formats. Some content that appears in print may not be available in electronic formats. For more information about Wiley products, visit our web site at [www.wiley.com](http://www.wiley.com).

Library of Congress Catalog Card Number: 67-13943

ISBN-13 978-0-471-68244-8

ISBN-10 0-471-68244-6

Printed in the United States of America

10 9 8 7 6 5 4 3 2 1

## INTRODUCTION TO THE SERIES

From 1967 until 1993 the Topics in Stereochemistry series appeared in 21 volumes edited by Ernest Eliel with assistance in part from Lou Allinger (1967–1986) and Sam Wilen (1982–1993). This highly visible and quoted series provided an avenue for the publication of new treatises in stereochemistry as well as a repository for gold standard reference works. Students and veteran practitioners referred regularly to the pages of Topics in Stereochemistry to stay on top of one of chemistry's unifying disciplines.

For five years there was a short dormancy in the series but not in the field, and it became clear that the empowering tools of stereochemistry (spectroscopy and selective synthesis) soon would parallel the importance of stereochemistry's conceptual basis. Such a development required a renewed platform from which Stereochemistry, broadly defined, could be presented. The series was revitalized in 1998 by Scott Denmark. He single-handedly edited two excellent volumes and commissioned a third in the form of a special volume on Materials Chemistry, edited by Mark Green, Roeland Nolte, and Bert Meier. It was at that point we joined forces and developed an extended vision of the series, balanced between special-theme and general-advances issues.

Stereochemistry embraces diverse aspects of chemistry as well as the fields that depend on chemistry. The fundamentals are rooted in the idea that molecular shape and structure determine material and biological properties. The simple fact that real matter is not limited by the intellectual boundaries of chemistry with physics or biology, means that the principles of stereochemistry are consequential for all natural sciences. Topics in Stereochemistry was therefore envisioned to serve as a multidisciplinary series that enriches all of chemistry.

We have been fortunate to enlist the help of an able-bodied board of Editorial Advisors. Their guidance on chapter selection and choices for thematic issues is gratefully appreciated. For all things that remain to be improved on Topics in Stereochemistry, we hold ourselves and the authors responsible.

SCOTT E. DENMARK  
JAY S. SIEGEL

## FOREWORD

Volume 25 is the fourth volume of Topics in Stereochemistry to appear since the reestablishment of this series by Scott Denmark. As in Volume 24, stereochemistry in the crystalline phase is the thematic issue. This time the guest editing is provided by Professor Fumio Toda of Okayama Science and Technology University. Professor Toda is an expert in the area of solid state reaction phenomena, and Scott and I are very happy to have him on board for this adventure.

Stereochemistry continues to be a unifying theme in chemistry, and the stereochemistry in crystalline phases brings together aspects of molecular recognition, supramolecular chemistry, conformational analysis, crystal engineering, stereoselective synthesis, and chiroptical phenomena. The roots of this chemistry can be found in the photochemical dimerization of cinnamic acid, which dates back to the 1899 work by Marckwald; however, from a modern perspective the 1960s work of Gerhard Schmidt at the Weizmann Institute in Rehovot really expanded this important field. Schmidt pioneered the idea of topochemical reaction control in crystals in which reactions occur selectively, owing to the restricted orientation of the components in the solid state. An earlier perspective on the related stereochemistry in organic solid state reactions came from Green, Arad-Yellin, and Cohen in Volume 16, Chapter 3, of this series. The principle of least motion in crystal reactions was exploited in stereoselective reactions. In addition form and structure in crystals were used analytically to detect the chirality of tailored additives, and were so elegantly explained by Lehav, Leiserovitz, and Addadi in Chapter 1 of Volume 16.

It was by the Editor's own admission "by chance rather than by design" that two chapters of Volume 16 happened to deal with stereochemistry in solid state. In contrast, Volume 25 contains 10 handpicked chapters collected with the intent of demonstrating how far this field has come and how broadly it applies. The eclectic compilation of chapters accomplishes this task well.

I would like to thank Darla Henderson, Shirley Thomas, and Kellsee Chu for enormous editorial assistance in putting together this larger than average volume. In the past this would have been the material of about two or three volumes of Topics in Stereochemistry, and it would not have come together without them. In this my first Foreword introducing the series, let me express how happy I am to be working with Scott Denmark, and I look forward to continued success for Topics in Stereochemistry.

JAY S. SIEGEL

## PREFACE

Shape and symmetry strongly influence the reactivity of a molecule. The state-of-the-art methods for determining molecular structure make it easy to elucidate the stereochemistry of molecules. Various physical methods such as vibrational and microwave spectroscopy, and X-ray or electron diffraction analysis, are mature analytical methods. Among these methods, automated structural studies of molecules in crystals by X-ray analysis is the most powerful method for analyzing stereochemistry. The stereochemistry elucidated in the crystal provides a basis for interpreting chemical reactions and properties of compounds, in the solid state and in solution. Although differences may arise between solid and solution, the quantitative geometric data obtained for molecules in crystals can often help us explain those differences as well.

It is well established that solid state reactions can be exploited as useful synthetic methods. The stereochemistry of molecules in crystals provides the basis to rationalize the steric course and mechanism of solid state reactions. In some cases, the stereochemistry of molecules can be controlled by formation of an inclusion crystal with a host compound. In the inclusion crystal, molecules are ordered enabling the reaction to proceed through a stereospecific course. In other cases, one tautomer can be isolated in a pure state from an equilibrium mixture by formation of an inclusion crystal with a host, and the stereochemistry of the tautomer can be studied by X-ray crystallographic analysis. Study of the stereochemistry of molecules in crystals is also advantageous in clarifying the intermolecular and intramolecular interactions, which are important factors controlling molecular shape and molecular arrangement in the crystal. Furthermore, from data obtained during the stereochemical study of molecules in crystals, new crystals and inclusion crystals that are useful as new materials and are applicable to stereoselective reactions can be designed.

The study of the stereochemistry of molecules in crystals is important for the lofty goal of crystal engineering. If chemists are ever going to achieve this, it will first be necessary to have a far greater and more refined understanding of the structure-property principles encoded in the stereochemistry of crystals.

The chapters of this volume are written by academic scientists who are actively engaged in research in this field. The topics cover a multitude of themes. In the first chapter, I review the progress made in inclusion crystals on the stereochemistry of molecules. Professor Ogawa reveals the extent to which one must go to truly understand the conformational effects in crystal structure determination.

Professors Goldberg and Nangia regale us on the fascinating network structures that arise from cooperative supramolecular interactions in crystals. The importance of supramolecular effects is further expanded by Professor Nishio on CH-pi interactions and Professor Kato on structure-property effects induced by intermolecular interactions in crystalline platinum complexes. Beautiful examples of controlled molecular reactivity in crystals, a type of crystal engineering, are found in chapters by Professors Kaupp and Garcia-Garibay. Professor Harada discusses the design of powerful chiral auxiliaries for enantiomeric resolution and the determination of absolute configuration. Hetero and Homochirality in crystals is critically reviewed by Professors Levkin, Torbeeve, Lenev, and Kostaynovsky.

It has been a pleasure working with these authors to create this volume of Topics in Stereochemistry. As guest editor, I hope this book will be useful for chemists who are interested in the stereochemistry of molecules, solid state chemistry and crystal engineering.

FUMIO TODA

## CONTRIBUTORS

**Miguel A. Garcia-Garibay**

University of California, Los Angeles  
Department of Chemistry and  
Biochemistry  
607 Charles E. Young Drive East  
Los Angeles, CA 90095-1569  
[mgg@chem.ucla.edu](mailto:mgg@chem.ucla.edu)

**Israel Goldberg**

School of Chemistry  
Sackler Faculty of Exact  
Sciences  
Tel-Aviv University  
69978 Ramat-Aviv, Tel-Aviv, Israel  
[goldberg@post.tau.ac.il](mailto:goldberg@post.tau.ac.il)

**Jun Harada**

Department of Basic Science  
Graduate School of Arts and  
Sciences  
The University of Tokyo  
3-8-1 Komaba, Meguro-ku,  
Tokyo 153-8902, Japan  
[harada@ramie.c.u-tokyo.ac.jp](mailto:harada@ramie.c.u-tokyo.ac.jp)

**Nobuyuki Harada**

Institute of Multidisciplinary Research  
for Advanced Materials  
Tohoku University  
2-1-1 Katahira, Aoba, Sendai  
980-8577 Japan

**Masako Kato**

Graduate School of Humanities and  
Sciences  
Nara Women's University

**Kitauoyahigashi-machi,**

Nara 630-8506  
[kato@cc.nara-wu.ac.jp](mailto:kato@cc.nara-wu.ac.jp)

**Gerd Kaupp**

University of Oldenburg  
P.O. Box 2503  
D-26111 Oldenburg, Germany  
[kaupp@kaupp.chemie.  
uni-oldenburg.de](mailto:kaupp@kaupp.chemie.uni-oldenburg.de)

**Remir G. Kostyanovsky**

N.N. Semenov Institute of Chemical  
Physics  
Russian Academy of Sciences  
119991 Moscow, Russian Federation  
[kost@chph.ras.ru](mailto:kost@chph.ras.ru)

**Denis A. Lenev**

N.N. Semenov Institute of Chemical  
Physics  
Russian Academy of Sciences  
119991 Moscow, Russian Federation

**Pavel A. Levkin**

N.N. Semenov Institute of Chemical  
Physics  
Russian Academy of Sciences  
119991 Moscow, Russian Federation

**Christopher J. Mortko**

University of California, Los Angeles  
Department of Chemistry and  
Biochemistry  
607 Charles E. Young Drive East  
Los Angeles, CA 90095-1569

**Ashwini Nangia**  
School of Chemistry  
University of Hyderabad  
Hyderabad 500 046, India  
[ansc@uohyd.ernet.in](mailto:ansc@uohyd.ernet.in)

**Motohiro Nishio**  
The CHP Institute  
3-10-7 Narusedai  
Machida, Tokyo 194-0043, Japan  
[dionisio@tim.hi-ho.ne.jp](mailto:dionisio@tim.hi-ho.ne.jp)

**Keiichiro Ogawa**  
Department of Basic Science  
Graduate School of Arts and Sciences  
The University of Tokyo

3-8-1 Komaba, Meguro-ku,  
Tokyo 153-8902, Japan  
[ogawa@ramie.c.u-tokyo.ac.jp](mailto:ogawa@ramie.c.u-tokyo.ac.jp)

**Fumio Toda**  
Department of Chemistry  
Okayama University of Science  
Ridia-chol-1  
Okayama, 700-0005 Japan  
[toda@chem.ous.ac.jp](mailto:toda@chem.ous.ac.jp)

**Vladimir Yu. Torbeev**  
N.N. Semenov Institute of Chemical  
Physics  
Russian Academy of Sciences  
119991 Moscow, Russian Federation

# CONTENTS

<b>1 STEREOCHEMISTRY OF MOLECULES IN INCLUSION CRYSTALS</b>	<b>1</b>
<i>By Fumio Toda</i>	
<b>2 TORSIONAL MOTION OF STILBENE-TYPE MOLECULES IN CRYSTALS</b>	<b>31</b>
<i>By Jun Harada and Keiichiro Ogawa</i>	
<b>3 SUPRAMOLECULAR NETWORKS OF PORPHYRINS</b>	<b>49</b>
<i>By Israel Goldberg</i>	
<b>4 HOMO- AND HETEROCHIRALITY IN CRYSTALS</b>	<b>81</b>
<i>By Pavel A. Levkin, Vladimir Yu. Torbeev, Denis A. Lenev and Remir G. Kostyanovsky</i>	
<b>5 SUPRAMOLECULAR SYNTHESIS OF 1D CHAINS AND 2D LAYERS IN HYDROGEN BOND NETWORKS OF UREAS AND 2-PYRIMIDINONES</b>	<b>135</b>
<i>By Ashwini Nangia</i>	
<b>6 CHIRAL AUXILIARIES POWERFUL FOR BOTH ENANTIOMER RESOLUTION AND DETERMINATION OF ABSOLUTE CONFIGURATION BY X-RAY CRYSTALLOGRAPHY</b>	<b>177</b>
<i>By Nobuyuki Harada</i>	
<b>7 ENGINEERING STEREOSPECIFIC REACTIONS IN CRYSTALS: SYNTHESIS OF COMPOUNDS WITH ADJACENT STEREOGENIC QUATERNARY CENTERS BY PHOTODECARBOXYLATION OF CRYSTALLINE KETONES</b>	<b>205</b>
<i>By Christopher J. Morthko and Miguel A. Garcia-Garibay</i>	

<b>8 THE CH/HYDROGEN BOND: AN IMPORTANT MOLECULAR FORCE IN CONTROLLING THE CRYSTAL CONFORMATION OF ORGANIC COMPOUNDS AND THREE-DIMENSIONAL STRUCTURE OF BIOPOLYMERS</b>	<b>255</b>
<i>By Motohiro Nishio</i>	
<b>9 STEREOSELECTIVE THERMAL SOLID-STATE REACTIONS</b>	<b>303</b>
<i>By Gerd Kaupp</i>	
<b>10 CRYSTAL STRUCTURES AND FUNCTIONALITIES OF PLATINUM(II) COMPLEXES CONTROLLED BY VARIOUS INTERMOLECULAR INTERACTIONS</b>	<b>351</b>
<i>By Masaka Kato</i>	
<b>SUBJECT INDEX</b>	<b>375</b>
<b>CUMULATIVE AUTHOR INDEX, VOLUMES 1-25</b>	<b>391</b>
<b>CUMULATIVE TITLE INDEX, VOLUMES 1-25</b>	<b>397</b>

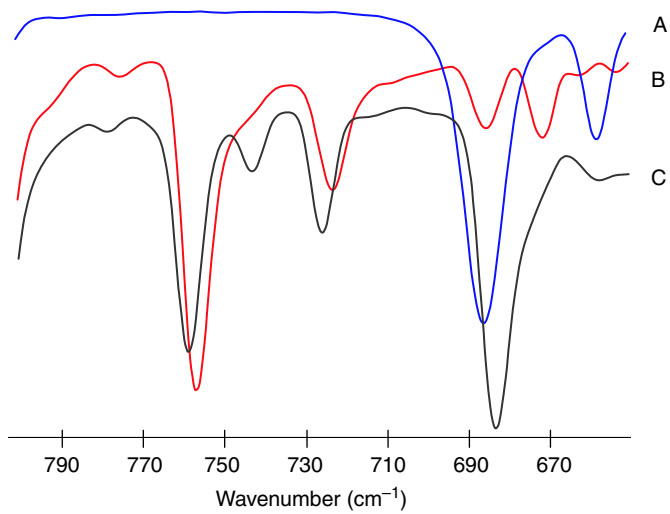


Figure 1.4. IR spectra of **31** (neat), **32** and **34** using ATR (attenuated total reflection) method. (A) **31**; (B) **32**; (C) **34**.

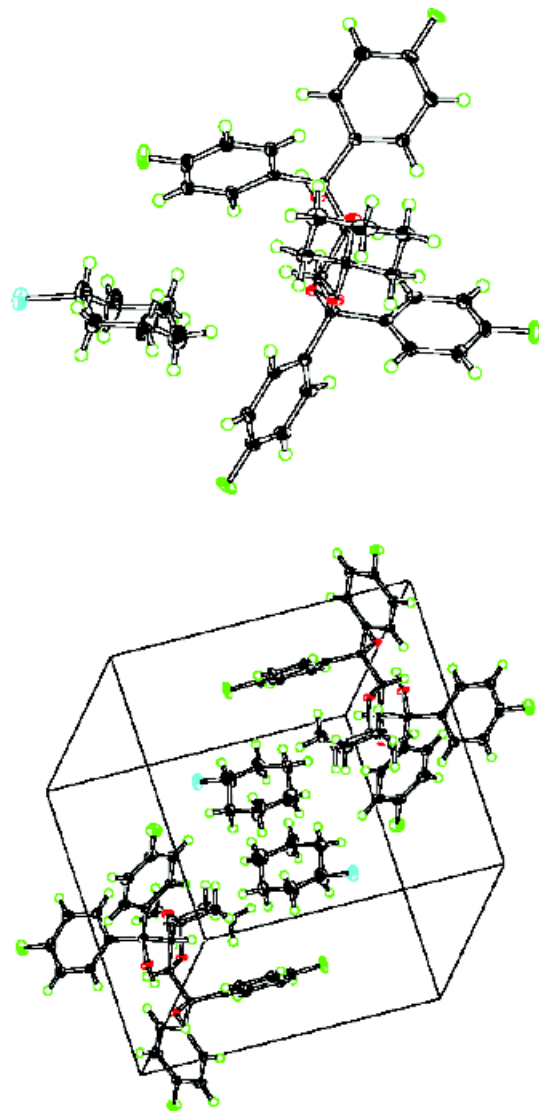


Figure 1.5. X-ray structure of a 1:1 complex of **30a** and **32**.

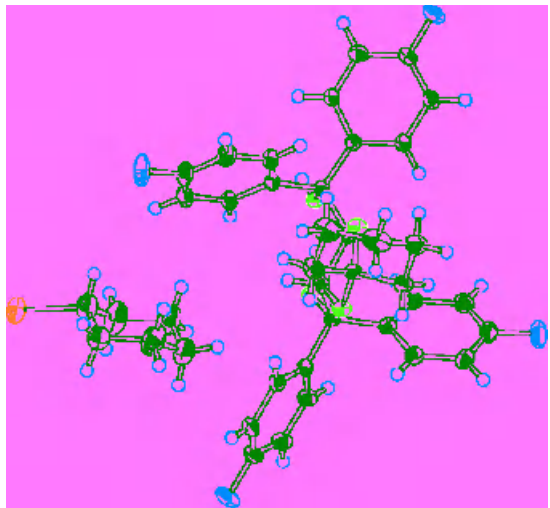


Figure 1.6. X-ray structure of a 1:1 complex of **31a** and **32**.

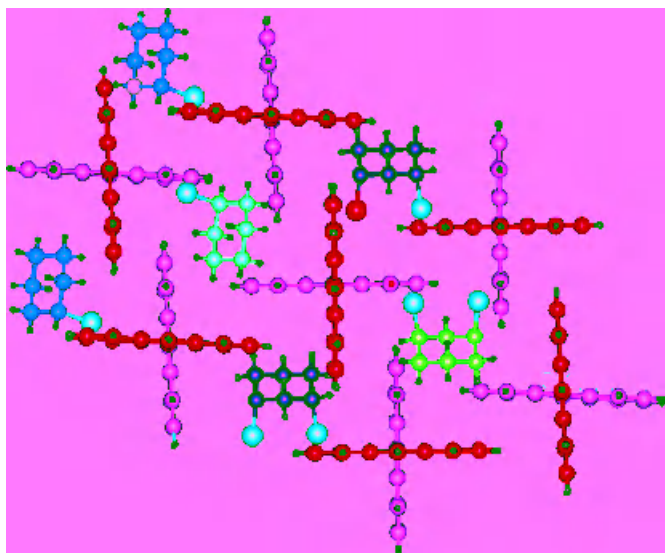


Figure 1.7. X-ray structure of a 1:1 complex of **30b** and **18**. Half of the **30b** molecules are disordered.

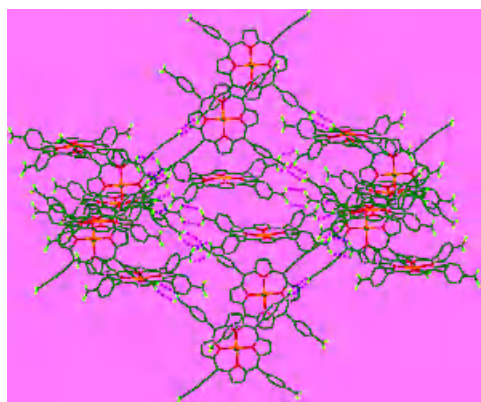
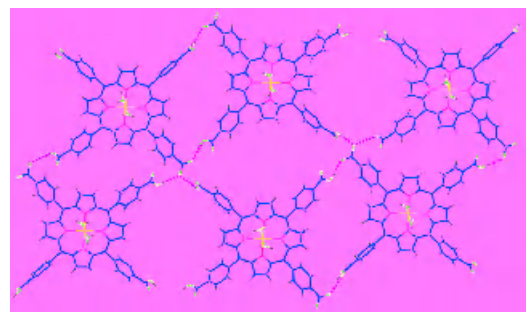
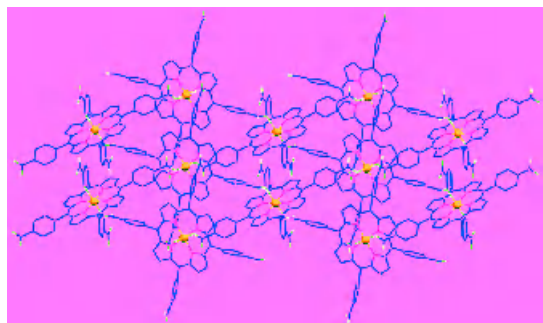


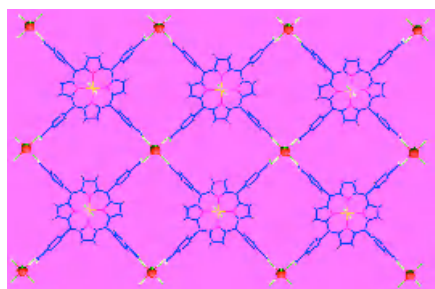
Figure 3.5. Illustration of crystal structure in which such networks doubly interpenetrate into one another.



(a)

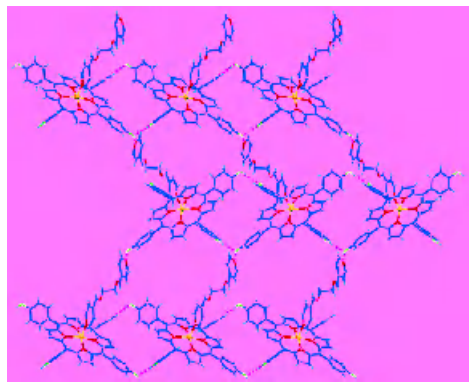


(b)

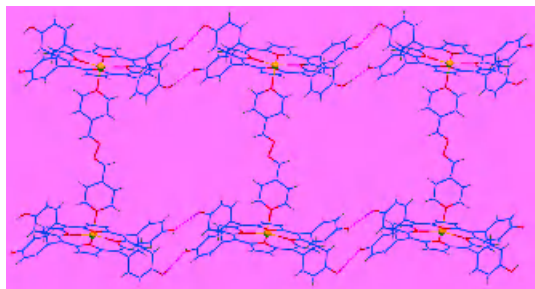


(c)

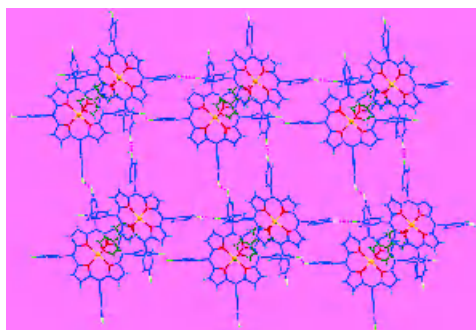
*Figure 3.10.* Illustration of the versatile self-assembly modes utilized by the Mn-9 building blocks.<sup>27</sup> (a) An array of multiply hydrogen bonded Mn(H<sub>2</sub>O)<sub>2</sub>-9. (b) Two-dimensional coordination polymer of Mn-9. (c) Intercoordination of Mn(H<sub>2</sub>O)<sub>2</sub>-9 units through exocyclic K<sup>+</sup> auxiliaries (unpublished results).



(a)



(b)



(c)

*Figure 3.13.* Various network arrays formed by porphyrin 7 with the aid of bipyridyl-type bridging ligands, exhibiting a concerted metal-ligand coordination and cooperative hydrogen-bonding mechanism.<sup>48</sup> (a) Axial coordination and lateral hydrogen bonding of the porphyrin units through the ligand auxiliary. (b) Hydrogen-bonded chains of porphyrin dimeric entities intercoordinated axially by the ligand. (c) Two-dimensional arrays of (7)<sub>2</sub>-bipyridyl units stabilized by porphyrin-porphyrin hydrogen bonds.



Maybe the first true image  
of homochirality in art.  
Nefertari (the queen-wife  
of Ramses II) and goddess  
Izida. From Valley of the  
Queens in Thebes -  
tomb of Nefertari - XIXth  
Dynasty, Egypt (1255 BC).

Heterochirality in art. Natalia  
Goncharova (1881-1962),  
“Two spanish women in a  
garden” (1920s-early 1930s).  
From the State Treliakov  
gallery (Moscow, Russia).



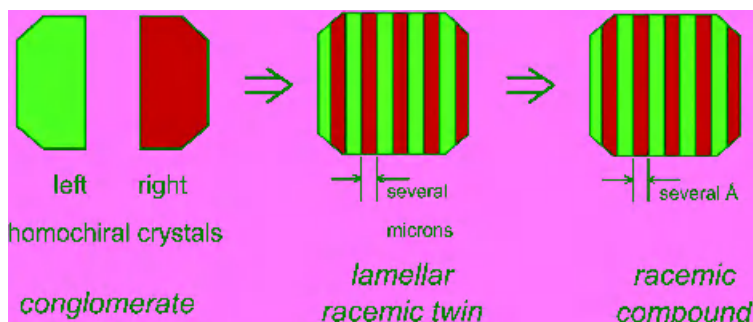


*Figure 4.2.* Crystallization behavior of racemate. (a) As separate left- and right-handed homochiral crystals (conglomerate); (b) as racemic twin consisting of domains of opposite chirality with micron dimensions; (c) as a racemic compound whose “domains” have molecular dimensions.

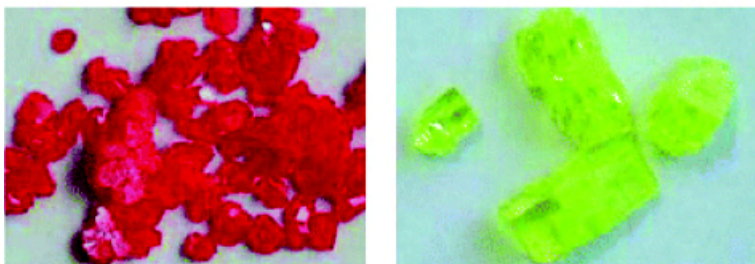
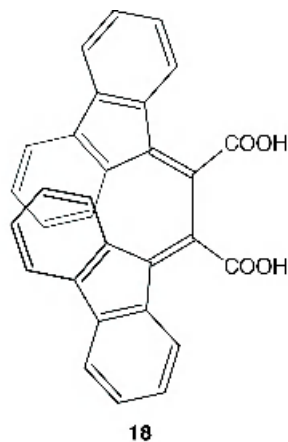


Figure 4.7. Photographs of racemic compound crystals of free host **18** (left) and conglomerate crystals of the 1:1 inclusion complex of **18** with acetone (right). An example of chirodichro(m)ism (for the first case, see Schurig<sup>57b</sup>). Reproduced with the permission of the authors.<sup>68</sup>

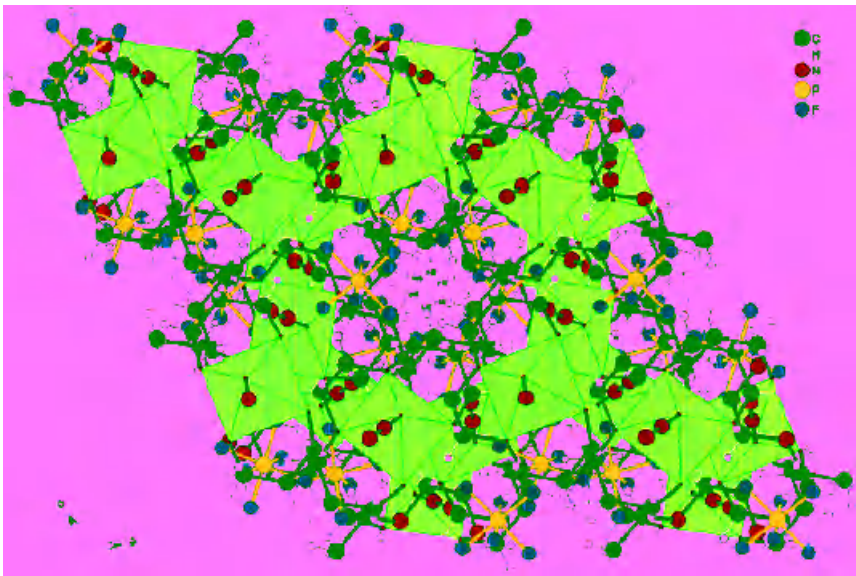


Figure 4.9. View of the cavities along *c*-axis for compound  $[(3,2,3\text{-tet})\text{Co}(\text{N}_3)_2]\text{PF}_6$ . For clarity, P–F bonds are indicated by a purple color, and other bonds are in black. Clusters of cations are packed in a spiral array generated by the  $6_1$  screw as regular, hexagonal cavities parallel to the *c*-axis. Adjacent helices are held together by the  $\text{PF}_6^-$ -anions.<sup>77</sup> Reproduced with the permission of the American Chemical Society ©.

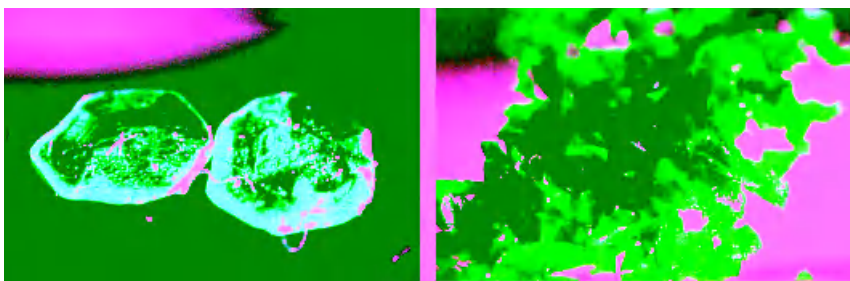


Figure 4.17. Chirodichro(m)ism in the solid state of dicarbonyl-rhodium(I) 3-(trifluoroacetyl)-(1*R*)-camphorate. Left: Crystals of the pure enantiomer (1*R*)-**50**. Right: Crystals of the racemate (1*R*/1*S*)-**50**.<sup>57b</sup> Reproduced with the permission of the author.

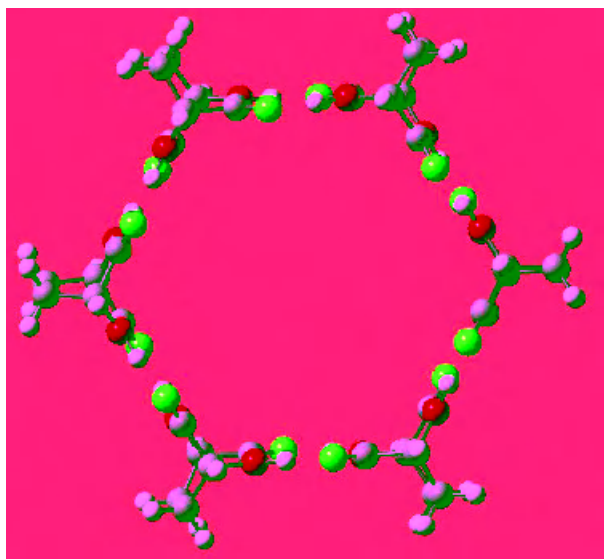


Figure 4.18. *Ab initio* RHF/STO-3G optimized structure of  $D_6$ -symmetric Lehn's bracelet.<sup>104a</sup>

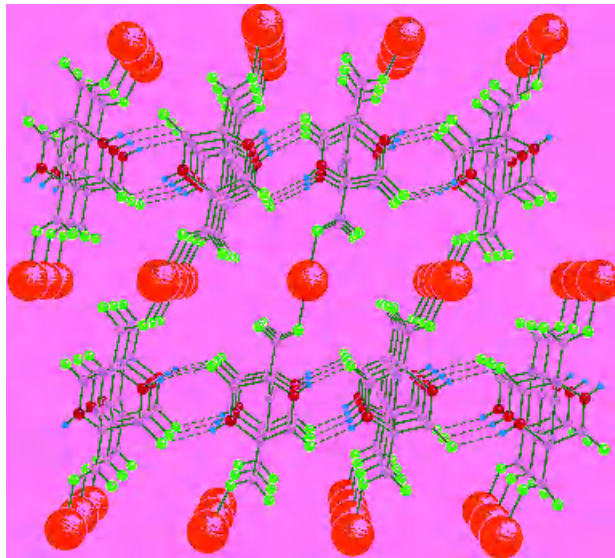


Figure 4.19. Molecular brick walls with inorganic coating in the crystal structures of metal **54**-dicarboxylates.<sup>104m</sup>

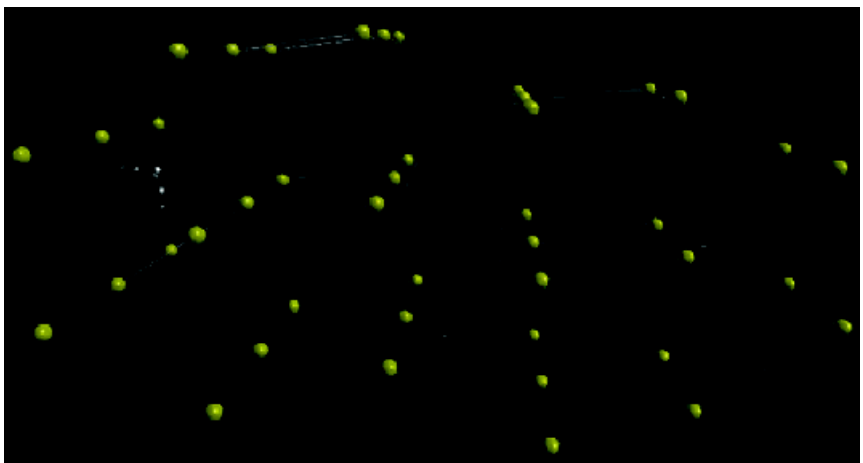


Figure 4.20. Diamondoid H-bonding network in the crystal structure of **64** ( $X = \text{H}$ ,  $Y = \text{Me}$ ).<sup>104p</sup> The balls denote centers of the molecules, and the lines unite molecules by  $\text{NH}\cdots\text{O}$ -bonding pathways.

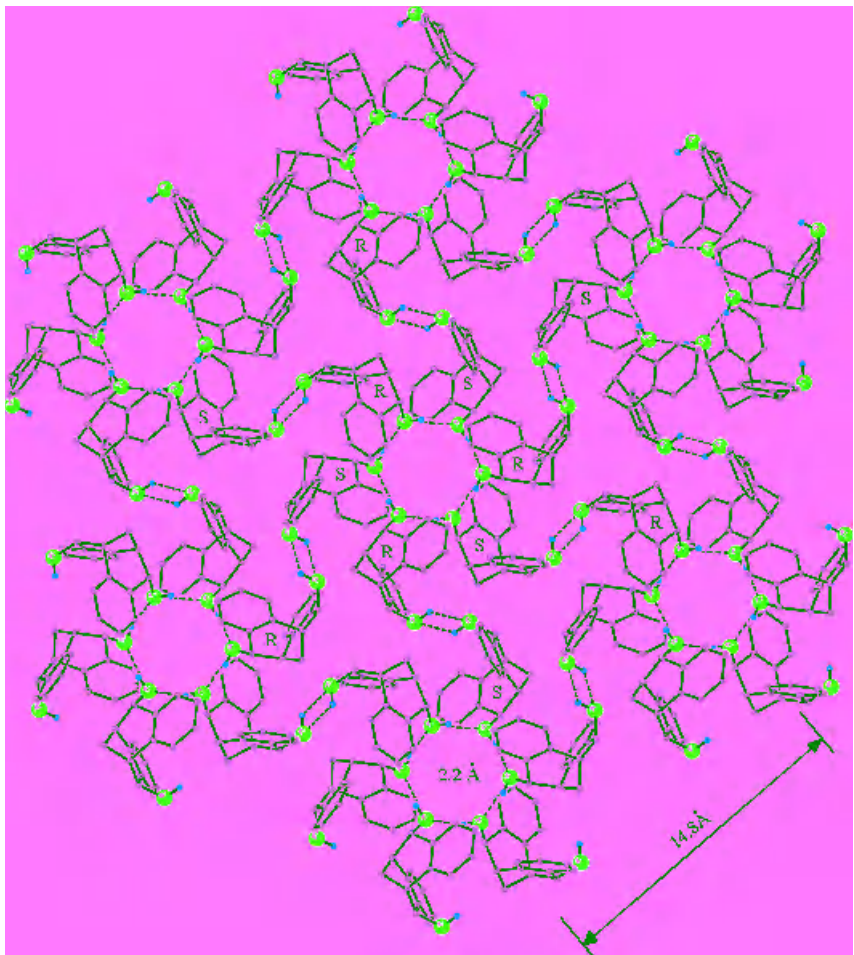


Figure 4.21. View of porous crystal structure of **71** along the crystallographic *c*-axis. The diameter of the canals, 2.2 Å, given here takes into account atomic van der Waals radii.

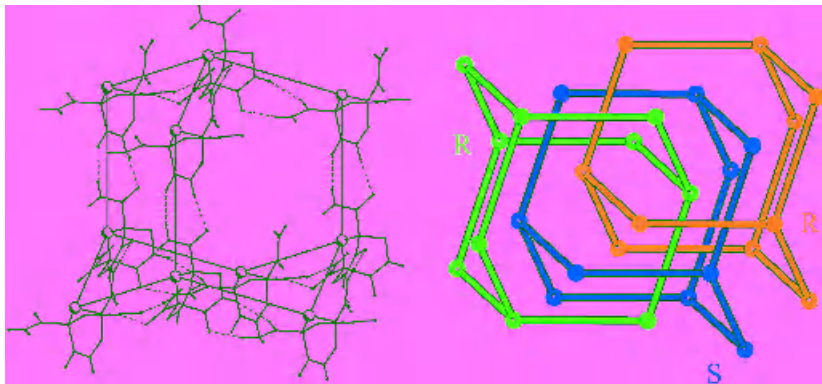


Figure 4.22. Homochiral threefold interpenetrated H-bonded diamondoid networks in the crystal structure of **61** ( $X = \text{CONH}_2$ ).<sup>6</sup>

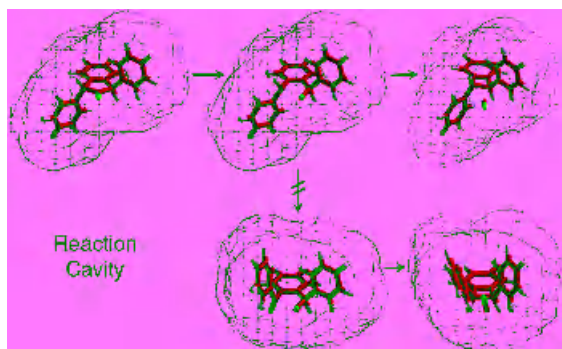


Figure 7.2. Idealized representation of the reaction cavity for the photodecarbonylation of *trans*-diphenyl-2-indanone **5** illustrating the reactant, the acyl-alkyl biradicals, and the final product with the molecules of CO trapped near its original lattice site. The excited states, biradical intermediates, and final products must fit within the space originally reserved for the ground state reactant.

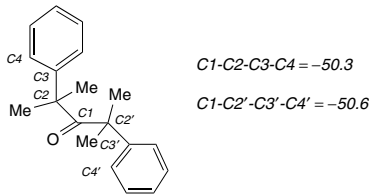


Figure 7.10. Reaction cavity of ketone **36** derived from its X-ray crystal structure with the equivalent line formula illustrating the dihedral angles that determine the extent of benzylic stabilization.

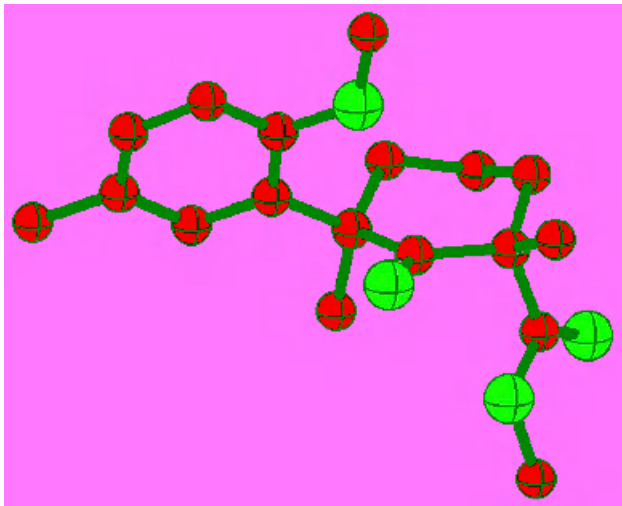


Figure 7.17. Molecular structure of ketone **57**. A crystalline precursor for the synthesis of Herberatenolide.

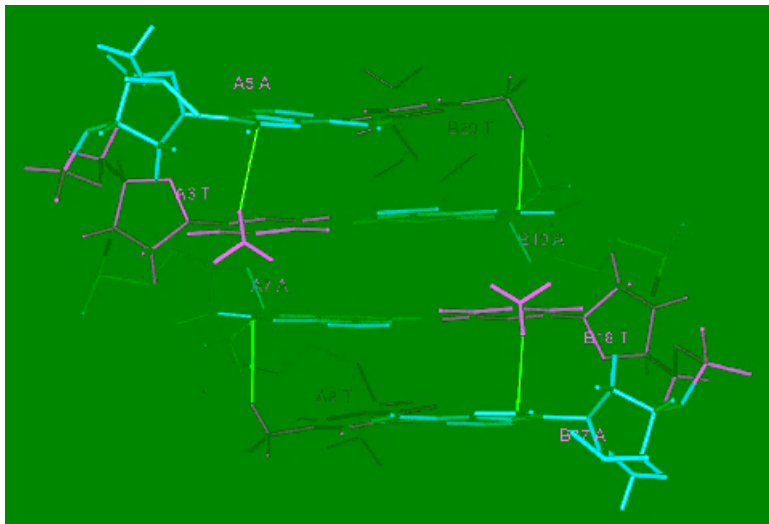


Figure 8.36. Crystal structure of the ATAT portion of a DNA CGCGATATCGCG (NDB code BDL078). T in white and A in yellow. Red sticks indicate CH/π contacts.

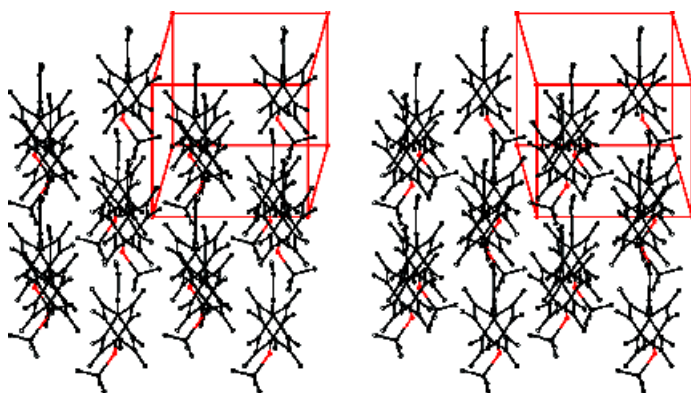


Figure 9.1. Stereoscopic view of the (100) face of 1-(4-anisyl)-1-phenylethene (Cc).

# Chapter 1

## Stereochemistry of Molecules in Inclusion Crystals

FUMIO TODA

*Department of Chemistry, Okayama University of Science,  
Ridia-cho1-1, Okayama 700-0005, Japan*

- I. Introduction
- II. Separation of Stereoisomers
  - A. Separation of a Component of an Equilibrium Mixture
  - B. Separation of Conformational Isomers of  $\alpha$ - and  $\beta$ -Ionones, Acrylic Acid, and 1,2-Dichloroethane
  - C. Separation of Conformational Isomers of Cyclohexane Derivatives
- III. Chiral Conformers of Achiral Molecules in Their Own Crystals
- IV. Control of Stereochemistry of Molecules in Crystals for Selective Reactions
  - Acknowledgments
  - References

### I. INTRODUCTION

A stereoisomer can be studied precisely if it is isolated in a pure state from a mixture of stereoisomers. When the stereoisomer is a component of an equilibrium mixture, its isolation in a pure state is more difficult. The usual method is X-ray crystallographic analysis for the structural study of molecules whereby the stereoisomers are isolated as inclusion crystals with a host compound. By the inclusion method the isomeric molecule of gas, liquid, or solid can be isolated as an inclusion complex in a pure state. The separation of one enantiomer of a racemic compound can be accomplished by using a chiral host compound. In some cases the racemic compound easily forms a conglomerate by complexation with an achiral host compound and thus is separated into enantiomers very efficiently. Once the stereoisomer is trapped in an inclusion crystal, a stereoselective reaction

of a symmetrical molecule can be accomplished by carrying out the reaction within a host compound that controls the steric course of the reaction in the solid state. In some cases achiral molecules can be arranged in chiral form in their own crystal, and their reaction in the solid state proceeds stereoselectively to give an optically active product. Stereochemical study of the absolute asymmetric reaction in a crystal is an interesting subject as well.

In this chapter separation of stereoisomers in a pure state by inclusion complexation with a host compound, and stereochemical study of these stereoisomers in inclusion complexes by X-ray analysis are described. The solid state reactions in the inclusion complex that give stereoselective reaction products is also described.

## II. SEPARATION OF STEREOISOMERS

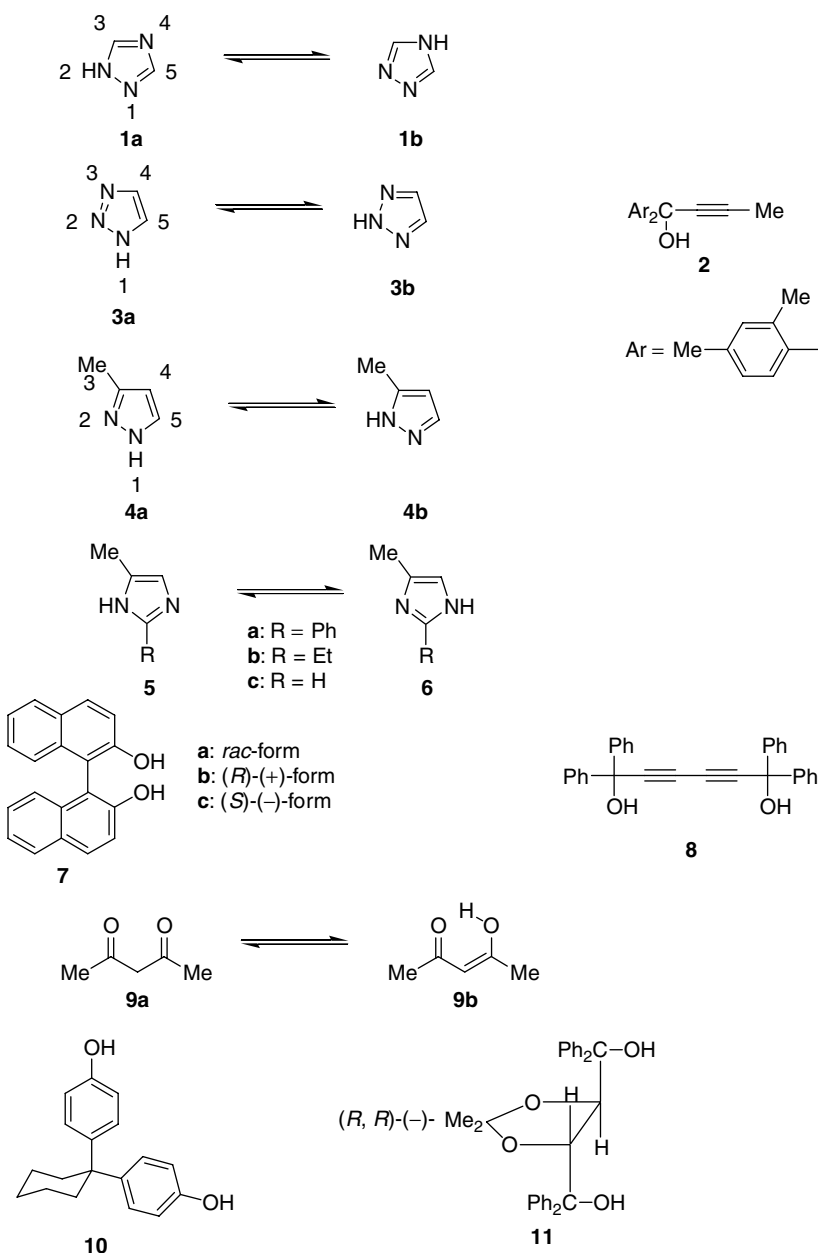
### A. Separation of a Component of an Equilibrium Mixture

We developed a method to separate one stereoisomer from a mixture based on inclusion complexation with a host compound. We began by testing whether the method is useful for separation of one component of an equilibrium mixture.

Since 1,2,4-triazole (**1**) exists as an equilibrium mixture of the two tautomers, 1,2,4-triazacyclopenta-3,5-diene (**1a**) and 1,2,4-traza-2,5-diene (**1b**), we had trouble isolating a single tautomer in a pure state in order to study its structure. We succeeded in freezing out the equilibrium by inclusion complexation with 1,1-di(2,4-dimethylphenyl)but-2-yn-1-ol host (**2**). We could thus isolate the more stable **1a** in a pure state as a 1:1 complex with **2**.<sup>1</sup> X-ray crystallographic analysis of the 1:1 complex showed that **1a** is included by formation of a hydrogen bond between its N(84) and the hydroxyl group of **2**.

1,2,3-Triazole (**3**) and 3(5)-methylpyrazole (**4**) also exist as an equilibrium mixture of two tautomers whose stability is not very different, 1*H*- (**3a**) and 2*H*-1,2,3-triazole (**3b**) and 3- (**4a**) and 5-methylpyrazole (**4b**), respectively. Likewise the structures of these tautomers have not been studied because of difficulty in obtaining them in a pure state. By inclusion complexation of **3** with **2**, we isolated the relatively unstable **3a** in a pure state as a 1:1 complex with **2**. In the case of **4**, both **4a** and **4b** were isolated as a 1:1:1 complex of **4a**, **4b**, and **2**. These are the first isolations of tautomers having almost the same stability. X-ray crystallographic analysis showed that hydrogen bond networks and cyclic hydrogen bonding play an important role in constructing the former and the latter inclusion crystalline lattices, respectively (Figure 1.1).<sup>2</sup>

Of the two possible tautomers, 2-phenyl-5-methylimidazole (**5a**) and 2-phenyl-4-methylimidazole (**6a**), the isomer **5a** was isolated in a pure state as a 1:1 inclusion



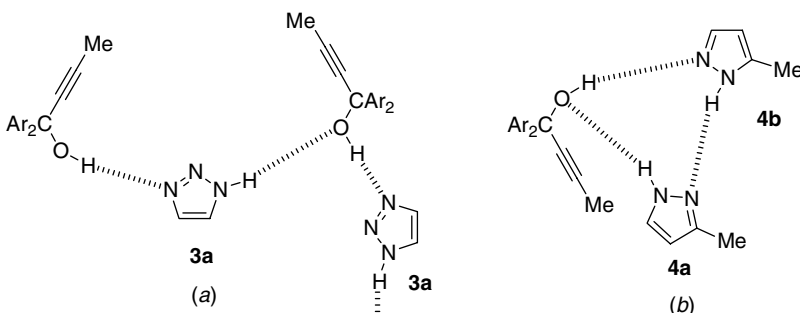
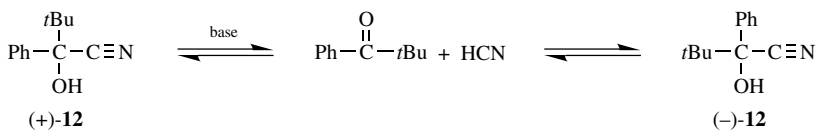


Figure 1.1. Schematic view of the molecular structures and hydrogen bonding patterns in a 1:1 complex of **3a** with **2** (*a*) and a 1:1:1 complex of **4a** and **4b** with **2** (*b*).

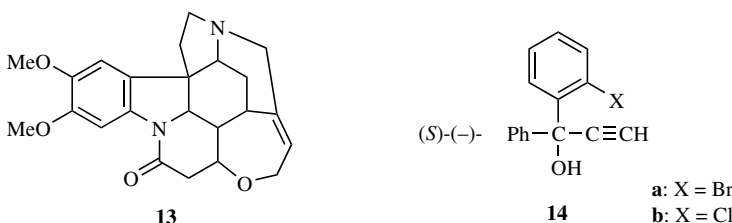
complex with the *rac*-2,2'dihydroxy-1,1'-binaphthyl (**7a**).<sup>3</sup> X-ray analysis of the crystalline complex showed that **5a** is accommodated in the inclusion cavity by formation of a hydrogen bond between the hydroxyl group of **7a** and the  $\text{sp}^2$ -nitrogen atom of **5a**. This hydrogen bond formation is more favorable than that between **7a** and the  $\text{sp}^2$ -nitrogen atom of **6a** because the latter atom is more sterically hindered due to the methyl substituent.<sup>3</sup>

In the case of the equilibrium mixture of 2-ethyl-5-methylimidazole (**5b**) and 2-ethyl-4-methylimidazole (**6b**), the tautomer **5b** was included by the host 1,1,6,6-tetraphenylhexa-2,4-diyne-1,6-diol (**8**) on recrystallization from ether as a 2:1:1 complex of **5b**, **8**, and ether. X-ray analysis showed that hydrogen bond formation between the hydroxyl group of **6** and the  $\text{sp}^2$ -nitrogen atom of **5b** is also favored due to steric factors.<sup>3</sup> In the case of 3-methylimidazole, however, **7a** trapped **6c** to form a 1:1 inclusion complex.<sup>3</sup>

We were able to isolate an enol form of acetylacetone (**9b**) in a pure state. By recrystallization of 1,1-di(*p*-hydroxyphenyl)cyclohexane (**10**) from acetylacetone, a 1:1:1 inclusion complex of **9b**,  $\text{H}_2\text{O}$  and **10** was formed as colorless plates. X-ray crystallographic analysis of the complex showed that the  $\text{C}=\text{O}$ ,  $\text{C}-\text{O}$ ,  $\text{C}=\text{C}$  and  $\text{C}-\text{C}$  bond lengths are 1.258(5), 1.284(5), 1.361(5), and 1.398(6) Å, respectively. From these data it is clear that the enol form (**9b**) isolated as an inclusion complex with **10** is in a pure state. A 2:2 inclusion complex of **9** and (*R,R*)-*(−)*-*trans*-4,5-bis(hydroxydiphenyl)-2,2-dimethyl-1,3-dioxacyclopentane (**11**) was obtained by recrystallization of **11** from **9** as colorless crystals. X-ray crystallographic analysis showed that two independent acetylacetone molecules are accommodated in the complex. The two independent enolic molecules (**9b**) have the same geometry, first molecule:  $\text{C}=\text{O}$  1.263(3),  $\text{C}-\text{O}$  1.323(3),  $\text{C}=\text{C}$  1.365(3), and  $\text{C}-\text{C}$  1.419(3) Å; second molecule:  $\text{C}=\text{O}$  1.258(3),  $\text{C}-\text{O}$  1.321(3),  $\text{C}=\text{C}$  1.357(3), and  $\text{C}-\text{C}$  1.415(3) Å.<sup>4</sup>



*Scheme 1.1.* Base-catalyzed racemization of **12**.



Cyanohydrins exist as an equilibrium mixture of enantiomers in the presence of base as indicated, for 1-cyano-2,2-dimethyl-1-phenylpropanol (**12**) in Scheme 1.1.<sup>5</sup> When (+)-**12** is trapped out of the equilibrating mixture, excess (-)-**12** is transformed into *rac*-**12** through the equilibrium, and thus more (+)-**12** of the *rac*-**12** is trapped. As the processes continue, *rac*-**12** is completely transformed into (+)-**12** by a 1st order asymmetric transformation.

The transformation of *rac*-**12** into (+)-**12** was accomplished by use of brucine (**13**) as the host and base. When a solution of *rac*-**12** (1.0 g, 5.3 mmol) and **13** (2.1 g, 5.3 mmol) in MeOH (2 ml) was kept in a capped flask for 12 h, a 1:1 brucine complex of (+)-**12** (2.08 g, 67% yield, m.p. 112–114°C) separated out as colorless prisms. Decomposition of the complex with dil HCl gave (+)-**12** of 97% ee (0.67 g, 67% yield).<sup>5</sup> A yield of (+)-**12** of more than 50% shows a conversion of (−)-**12** into (+)-**12** through racemization during the complexation. The yield of (+)-**12** increased to 100% by leaving the MeOH solution to evaporate gradually during the complexation. For example, when a solution of *rac*-**12** (1.0 g) and **13** (2.1 g) in MeOH (2 ml) was kept in an uncapped flask at room temperature for 24 h, the amount of solvent decreased to 0.6 ml. From the MeOH solution the inclusion complex of (+)-**12** and **13** was isolated quantitatively, which upon treatment with dil HCl gave (+)-**12** of 100% ee in 100% yield.

Stereochemical study of the inclusion complex with **13** was carried out for the 1:1 complex of tertiary acetylenic alcohol, (*S*)-(-)-1-(*o*-bromophenyl)-1-phenylprop-2-yn-1-ol (**14a**) instead of (+)-**12**, since the brucine complex of **12** does not form suitable crystals for X-ray crystallographic analysis.<sup>6</sup> The brucine complex of **14a** is constructed by formation of a hydrogen bond between the

hydroxyl group of **14a** and the tertiary amine nitrogen atom of **13**. In the complex, mutual chiral recognition between **13** and **14a** occurs precisely. We used this inclusion complexation with chiral amines such as **13**<sup>6</sup> and sparteine<sup>7</sup> and obtained **14a** and **14b** of 100% ee.

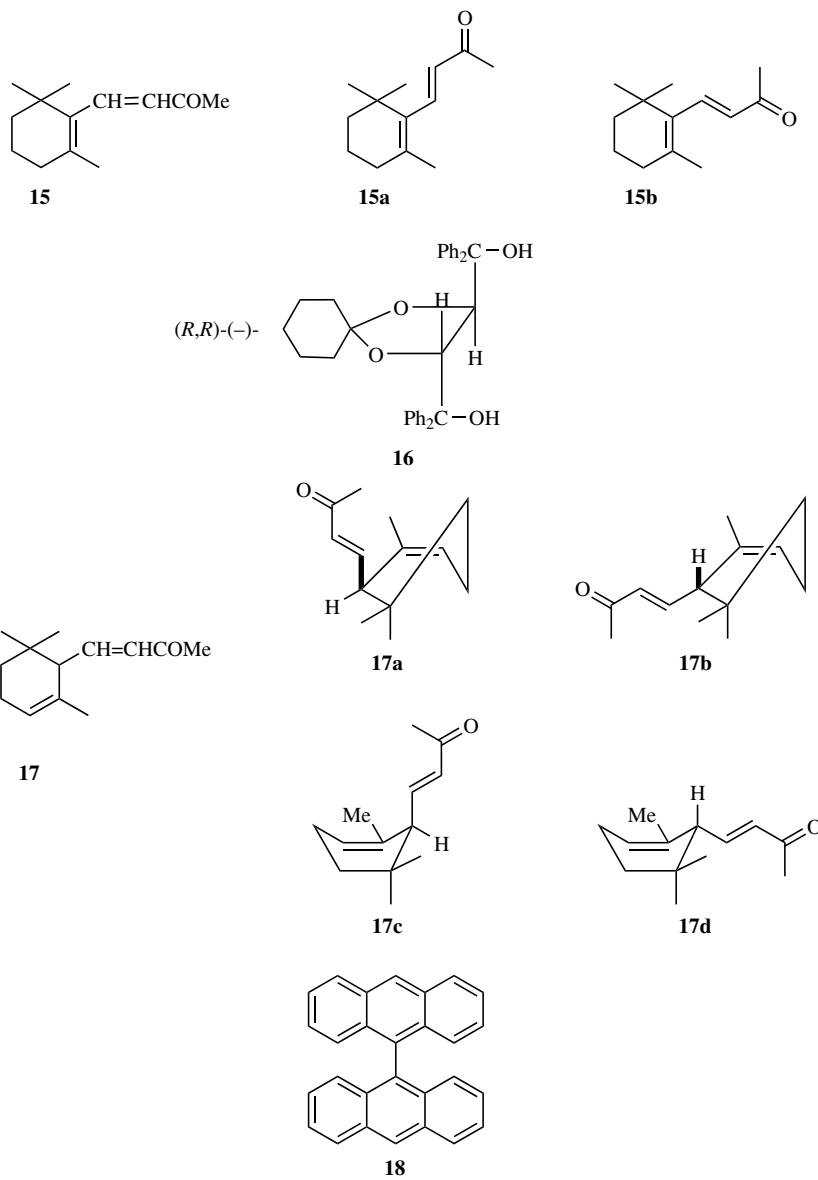
## B. Separation of Conformational Isomers of $\alpha$ - and $\beta$ -Ionones, Acrylic Acid, and 1,2-Dichloroethane

As we noted in Section A, it is not difficult to isolate one component of an equilibrium mixture by inclusion complexation with a host compound to study its stereochemistry by X-ray analysis. By this method, conformational isomers of  $\alpha$ - and  $\beta$ -ionones, acrylic acid, and 1,2-dichloroethane have been isolated in a pure state, and their stereochemical structures have been studied.

Conformational study of  $\beta$ -ionone (**15**) has long been interesting because **15** is closely related to the retinal chromophore, whose binding within rhodopsin is known to be conformationally dependent. However, no conformational isomer of **15** has yet been isolated in a pure state until 1990, although NMR studies of the solution conformation of **15** have shown it to exist mainly in the *s-cis* form (**15b**).<sup>8</sup> The *s-trans* conformer (**15a**) and the *s-cis* conformer (**15b**) were isolated in pure state as inclusion complexes with the host compounds **10** and (*R,R*)-(*–*)-*trans*-2,3-bis(diphenylhydroxymethyl)-1,4-dioxaspiro[4.5]decane (**16**), respectively.<sup>9</sup> The quasi-chair form (**17a**) of  $\alpha$ -ionone (**17**) was also isolated in a pure state as an inclusion complex with 9,9'-bianthryl (**18**).<sup>9</sup>

X-ray crystallographic analysis of a 2:1 inclusion complex of **10** and **15a** showed that molecule **15a** is accommodated in an almost planar *s-trans*-form between two molecules of the host **10**. Energywise is easier for **10** to form a cavity that accommodates **15a** through van der Waals and hydrogen-bonding interactions.<sup>9</sup> Conversely, **16** formed a 1:1 inclusion complex with **15b**. Although an X-ray crystal structure analysis of the complex with **15b** could not be carried out because of difficulty in obtaining a good crystal, the *s-cis* conformation was determined spectroscopically. In the IR spectrum,  $\nu\text{C=O}$  at  $1675\text{ cm}^{-1}$  of **15b** in the complex with **16** was at higher frequencies than the  $\nu\text{C=O}$  at  $1590\text{ cm}^{-1}$  of **15a** in the complex with **10**. It has been well established that *s-cis* enones show  $\nu\text{C=O}$  at higher frequencies than do the *s-trans* isomers. In the UV spectrum in the solid state, **15b** in the complex with **16** showed  $\lambda_{\max}$  at shorter wavelengths than did **15a** in the complex with **10**. It has also been established that *s-cis* enones absorb in the UV at shorter wavelengths than do *s-trans* enones.

Interestingly  $\alpha$ -ionone (**17**) and **18** formed a 1:1 inclusion complex, in which the quasi-chair form with an axial enone group (**17a**) is present. The X-ray crystal structure analysis of the complex showed that the molecules of **18** are arranged so as to form a channel-type complex with **17a**. In a channel, two molecules



of **17a** of the same chirality face each other and display contacts through their acyl groups.<sup>9</sup> The cavity formed by **18** is suitable to accommodate **17a** but not the equatorial quasi-chair form (**17b**), the axial quasi-boat form (**17c**), or the equatorial quasi-boat form (**17d**).

Carboxylic acids exist as cyclic dimers in the gas, liquid, and solid states. For example, acrylic acid (**19**) has been shown to exist as two different cyclic dimers, *s-trans*-**19**···*s-trans*-**19** and *s-cis*-**19**···*s-cis*-**19**. However, no monomeric rotational isomer of **19**, neither *s-trans*-**19** nor *s-cis*-**19**, has ever been isolated in a pure state. In 1998 monomeric *s-trans*-**19** was isolated in a pure state as an inclusion complex with 2,2'-bis(hydroxydiphenylmethyl)-1,1'-biphenyl (**20**).<sup>10</sup> X-ray crystal structure analysis of the complex showed that the *s-trans*-**19** has bond lengths and a dihedral angle between vinyl and carboxylic acid groups as shown in Figure 1.2.<sup>10</sup>

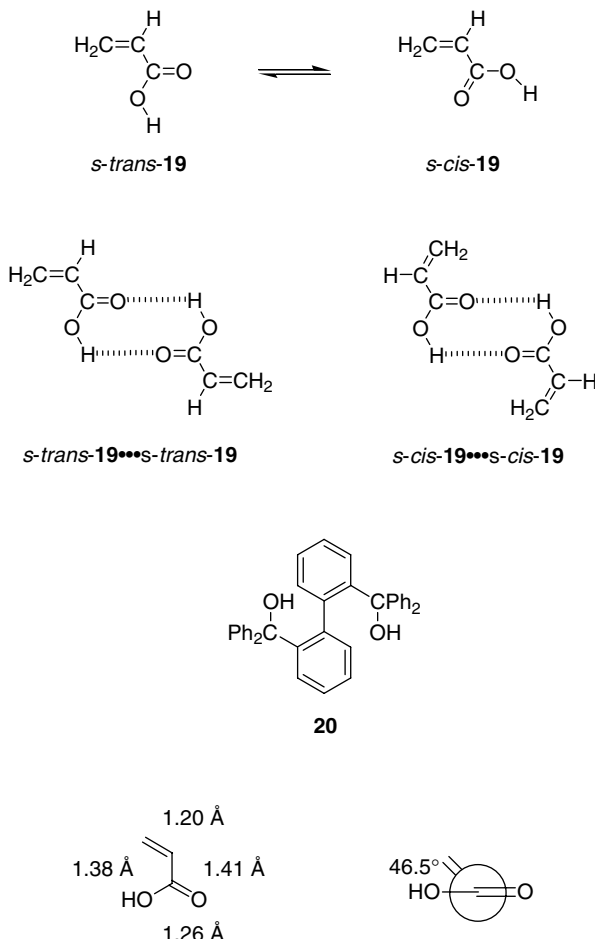
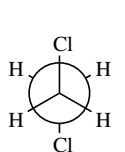
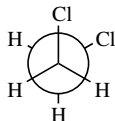
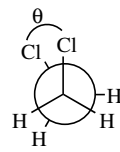
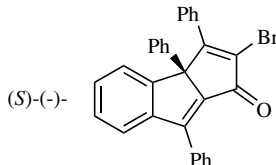
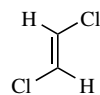


Figure 1.2. X-ray analytical data for *s-trans*-**19** in its inclusion complex with **20**.

By an inclusion complexation similar to **20**, monomeric formic, acetic, propionic, and butanoic acids were isolated in their pure states, and their X-ray crystal structures were studied.<sup>11</sup>

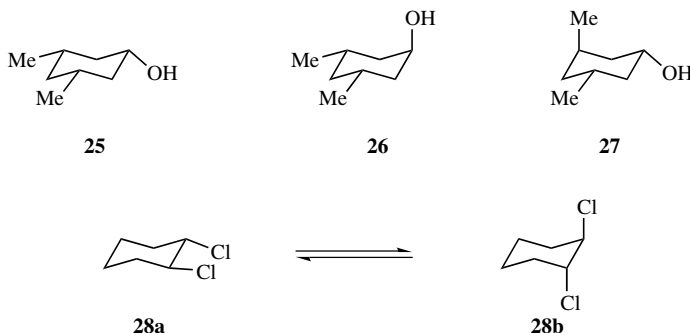
**21a****21b****21c***trans-form**gauche-form**eclipsed-form***22****23****24**

It has been established that the energetically most stable rotational isomer around the C–C bond of 1,2-disubstituted ethane is the *trans*-form. For example, 1,2-dichloroethane (**21**) exists in the *trans*-form (**21a**), although the energy difference between the *trans* (**21a**) and gauche form (**21b**) is estimated to be small. The existence of **21** in the eclipsed form of the two chlorine atoms (**21c**,  $\theta = 0^\circ$ ) is excluded because of its instability, which is due to a strong repulsion between not only the chlorine atoms but also the carbon-hydrogen bonds. Isolation of the eclipsed form has never been reported. In 1997, however, a nearly eclipsed form (**21c**,  $\theta = 32(2)^\circ$ ) was isolated as a 1:1 inclusion complex with the optically active host compound (S)-(-)-2-bromo-3,3a,8-triphenyl-1,2a-dihydrocyclopenta[a]inden-1-one (**22**).<sup>12</sup> X-ray analysis of the complex showed that only one enantiomer of **21c**, the left-handed helical form (*M*)-**21c**, is accommodated, since **22** is an optically active (S)-(-)-host compound.<sup>12</sup>

There is no relatively strong interaction between the host and guest molecules. Isomer **21c** is just accommodated through a van der Waals interaction in a small cavity constructed with its host **22**, since the cavity is too small to include sterically bulky **21a** and **21b**. For the same reason **22** includes sterically less bulky *cis*-1,2-dichloroethane (**23**) but not its *trans* isomer (**24**).<sup>12</sup>

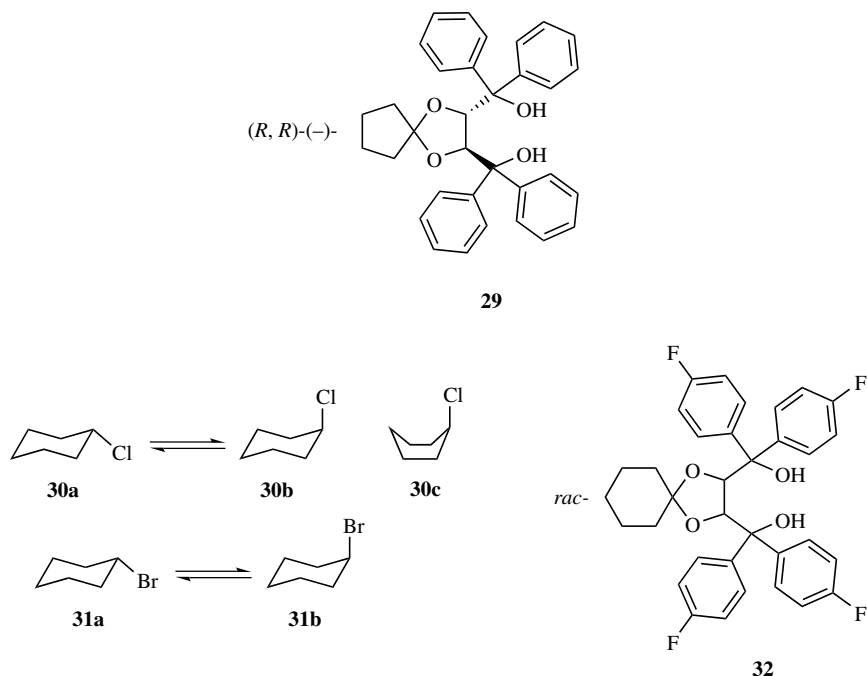
### C. Separation of Conformational Isomers of Cyclohexane Derivatives

Stereoisomerism of cyclohexane derivatives can easily be recognized in an inclusion complex with a host compound. By way of this phenomenon, stereoisomers of cyclohexane derivatives can be separated efficiently. For example, the inclusion complexation of a commercially available mixture of three 3,5-dimethylcyclohexanols **25** (63%), **26** (22%), and **27** (15%) in the composition indicated with 1,1,6,6-tetraphenylhexa-2,4-diene-1,6-diol (**8**) gives a 1:2 complex of **8** and **25** as colorless crystals (69% yield, m.p. 90–91°C). Heating of the complex in vacuo gives **25** of 99.7% purity in 65% yield.<sup>13</sup> X-ray analysis of the 1:2 complex of **8** and **25** shows that two **25** molecules are binding to the two OH groups of **8** through hydrogen bond formation.<sup>13</sup> Only the all equatorial isomer **25** is accommodated in the crystalline cavity, and this is probably because of its less bulky structure.



The only example of isolation of the optically active *trans*-1,2-dihalocyclohexane is (*R,R*)-(*–*)-diequatorial isomer (**28a**) of *trans*-1,2-dichlorocyclohexane (**28**). The isomer was isolated in an enantiomerically pure form as an inclusion complex with the chiral host (*R,R*)-(*–*)-*trans*-2,3-bis(hydroxydiphenylmethyl)-1,4-dioxaspiro[4.4]nonane (**29**), and the diequatorial structure and (*R,R*)-configuration were elucidated by X-ray study.<sup>14</sup> This is the first X-ray structural report to confirm the direct conformation of a halocyclohexane derivative. In this case, however, it was easier to isolate **28a**, since the diaxial conformer (**28b**) is energetically very unfavorable.

Conformational studies of cyclohexanes substituted with one sterically less bulky group, such as chloro- (**30**) and bromocyclohexane (**31**), are of considerable interest. Nevertheless, it is not easy to isolate conformational isomers of halocyclohexanes in a pure state at room temperature because of the dynamic equilibrium between the equatorial and axial conformers even though in the solid state at sufficiently low temperature or high pressure **30** and **31** exist only in the equatorial form (**30a**, **31a**).<sup>15</sup>



Attempts to isolate conformational isomers of **30** and **31** in a pure form at room temperature have been reported. Chlorocyclohexane (**30**), which is included with a thiourea host, has been shown by IR and Raman spectroscopy to adopt the axial conformation (**30b**).<sup>16</sup> However, X-ray crystal structural study of the inclusion complex of **30** with thiourea shows that the substructure of **30** to be substantially disordered, and its structure has not yet been analyzed clearly.<sup>17</sup> Conformational studies by IR spectroscopy and X-ray crystallographic analysis of **30**, which is included in the tri-*o*-thymotide host compound, have been reported.<sup>18</sup> The data showed that a 2:1 inclusion complex of the host and **30** contains both axial chair (**30b**) and axial boat conformers (**30c**) in a 2:1 ratio and that these two overlap in

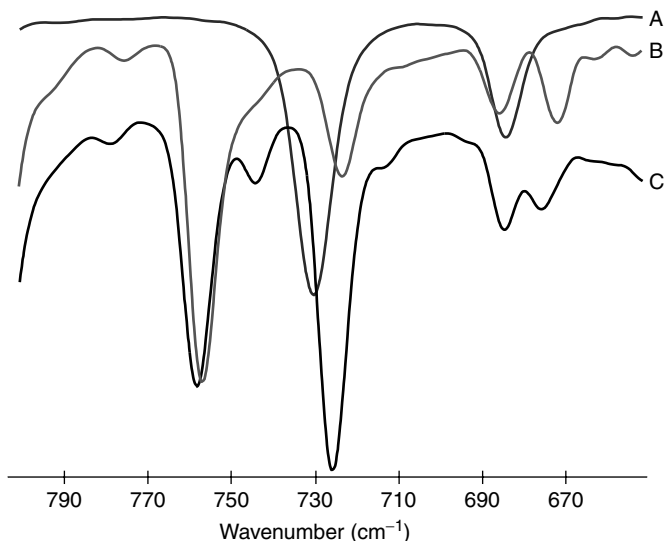
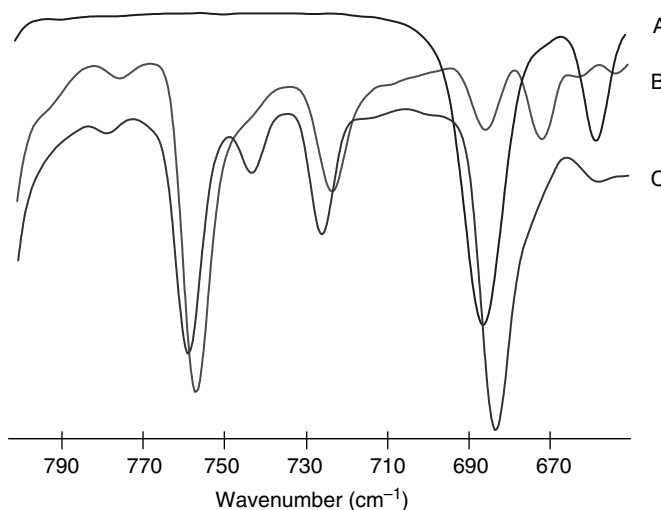


Figure 1.3. IR spectra of **30** (neat), **32** and **33** using the ATR (attenuated total reflection) method (A **30**; (B) **32**; (C) **33**.

the same crystalline lattice. Finally, the equatorial (**30a**, **31a**) and axial conformers (**30b**, **31b**) could not be isolated in pure form at room temperature.

However, in 2004 the equatorial conformers of chloro- (**30a**) and bromo-cyclohexanes (**31a**) were isolated in a pure state as inclusion complexes with the racemic *p*-fluoro-substituted derivative of **16** (**32**), and structural study of these conformers was accomplished by IR spectroscopic and X-ray crystallographic analysis. Inclusion complexes of **30** and **31** with host **32** were prepared by recrystallization of the host from neat **30** and **31** to give 1:1 inclusion complexes of **30a** with **32** (**33**) (m.p. 227.5–228.0°C) and of **31a** with **32** (**34**) (m.p. 226.5–227.0°C), respectively, as colorless crystals. These complexes showed sharp melting points as indicated. The host:guest molar ratios were determined from <sup>1</sup>H NMR spectra.

The equatorial conformers of **30a** and **31a** in their inclusion complexes were first elucidated from their IR spectra using the ATR (attenuated total reflection) method. As shown in Figure 1.3, the neat IR spectrum of **30** shows equatorial and axial C–Cl stretches at 732 and 685 cm<sup>-1</sup>, respectively. In the spectrum of **33**, a very strong equatorial C–Cl stretch appears at 726 cm<sup>-1</sup> but without significant axial C–Cl absorption. The absorption at around 690 cm<sup>-1</sup> is probably due to the host compound. In Figure 1.4, isomer **34** also shows very strong equatorial C–Br absorption at 684 cm<sup>-1</sup>, which corresponds to that of **31a** at 687 cm<sup>-1</sup>, but no axial absorption at around 660 cm<sup>-1</sup>.



*Figure 1.4.* IR spectra of **31** (neat), **32** and **34** using ATR (attenuated total reflection) method. (A) **31**; (B) **32**; (C) **34**. See color insert.

The equatorial structures were finally determined by X-ray crystallographic analysis of **33** and **34**. In the inclusion complexes, **30** and **31** are accommodated as equatorial conformers, **30a** (Figure 1.5) and **31a** (Figure 1.6), respectively. In both cases no significant host–guest interaction is present. Guest molecules are just accommodated in the cavity constructed by the host molecules. The cavity must be large enough to accommodate the somewhat longer equatorial conformer than the axial one. A cavity not long enough to accommodate the equatorial conformer will accommodate an axial conformer of a more cubic shape. With this idea in mind, it is possible to design an inclusion complex to accommodate the axial conformer. Isolation of the axial conformer **30b** was obtained by complexation with the hydrocarbon host **18** (Figure 1.7).

### III. CHIRAL CONFORMERS OF ACHIRAL MOLECULES IN THEIR OWN CRYSTALS

Some achiral molecules are arranged in chiral form in their own crystal. The chiral crystal can be obtained in large quantity and converted into an optically active product by a chemical reaction. So here we discuss an asymmetric synthetic method without using a chiral source called an absolute asymmetric synthetic procedure. Some examples of chiral arrangements of achiral molecules in crystals

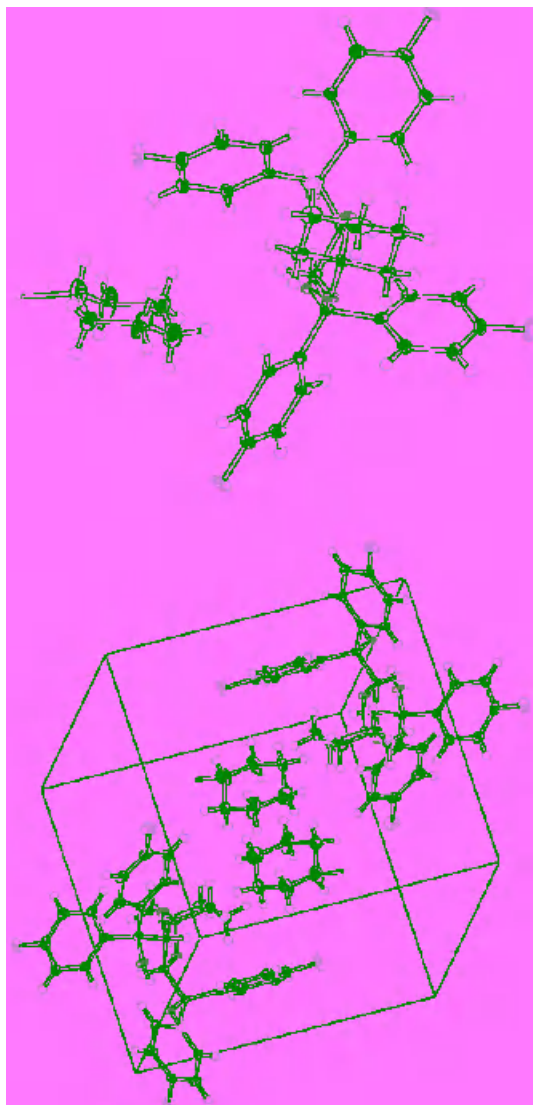


Figure 1.5. X-ray structure of a 1:1 complex of **30a** and **32**. See color insert.

and their absolute asymmetric synthetic reaction in the solid state are described in this section.

Recrystallization of the oxoamide (**35**) from benzene gives colorless prisms. Each crystal is confirmed to be chiral by a photochemical conversion into the

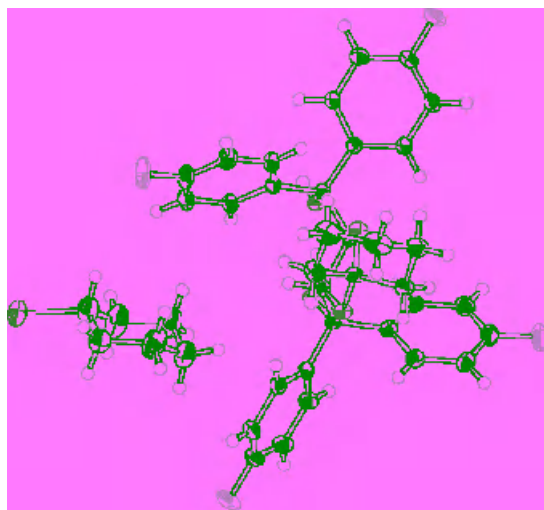


Figure 1.6. X-ray structure of a 1:1 complex of **31a** and **32**. See color insert.

enantiomerically enriched  $\beta$ -lactam (**36**).<sup>19</sup> Crystals that give (+)- and (-)-**36** on photocyclization are provisionally labeled (+)- and (-)-**35** crystals, respectively. Crystals of (+)- and (-)-**35** can easily be prepared in large quantities by seeding with finely powdered crystals of (+)- and (-)-**35** during recrystallization of **35**.

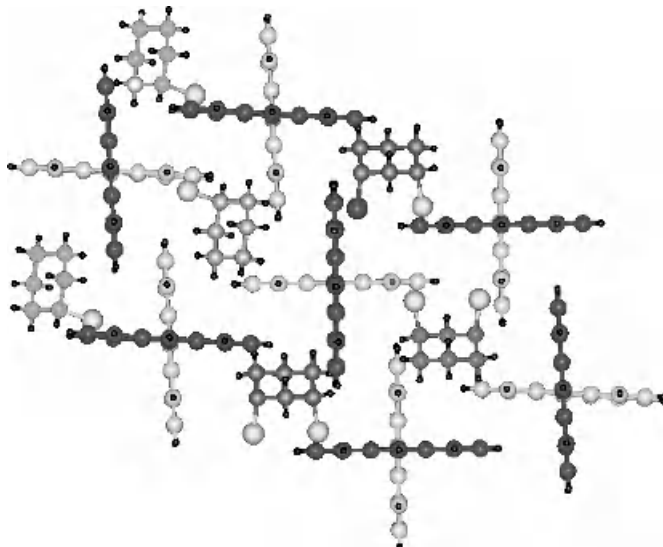
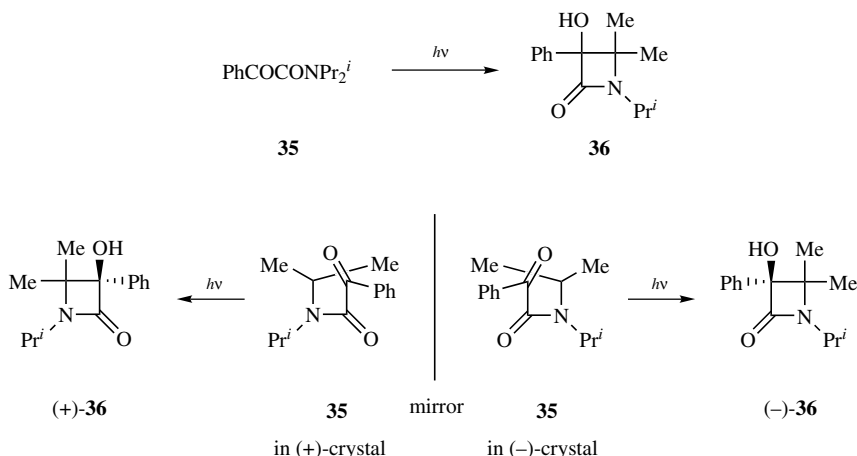


Figure 1.7. X-ray structure of a 1:1 complex of **30b** and **18**. Half of the **30b** molecules are disordered. See color insert.



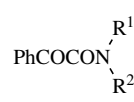
*Scheme 1.2.* A possible mode of formation of optically active **36** from achiral **35** in its chiral crystal.

from benzene. Irradiation of powdered (+)-**35** crystals (200 mg) in the solid state gives (+)-**36** of 93% ee (148 mg, 74% yield).<sup>19</sup>

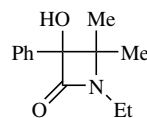
X-ray crystallographic analysis of the (+)-**35** single crystal shows that the molecules of **35** are arranged in a chiral form as indicated in Scheme 1.2.<sup>20</sup> Note that in the (-)-**35** crystal, molecules of **35** are arranged in a mirror-imaged chiral form (Scheme 1.2). Finally, photocyclizations of the (+)- and (-)-**35** in their chiral crystal give (+)- and (-)-**36**, respectively. The chiral conformational structure of **35** in a crystal has been studied in detail by using the HAUP (high-accuracy universal polarimeter) method.<sup>21</sup>

The relationship between the chiral arrangement and the different substituents on the oxoamide molecule has been studied. Of the four oxoamide derivatives tested (**37a–d**), only the *N*-ethyl-*N*-isopropyl (**37c**) formed a chiral crystal, and irradiation of the chiral crystal gave optically active  $\beta$ -lactam (**38**) of 80% ee in 55% yield.<sup>22</sup> The other oxoamides (**37a–b** and **37d**) formed achiral crystals. Cyclohexyl and benzyl substituents on the nitrogen of the oxoamide were also not effective in forming a chiral crystal.<sup>23</sup> These data show that the isopropyl group is effective in this regard.

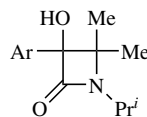
X-ray analysis of the chiral crystal of **37c** showed that the isopropyl but not the ethyl group is situated close to the benzoyl carbonyl carbon. The isopropyl group then reacts with the benzoyl carbonyl carbon to give finally the *N*-ethyl-substituted  $\beta$ -lactam (**38**). X-ray analysis also clarified that the chiral crystal of **37c**, which shows a (+)-Cotton effect in a CD spectrum in the solid state has the (*R*)-configuration, and that the (+)- $\beta$ -lactam derived from the (*R*)-(+)-**37c**, has also the (*R*)-configuration.<sup>22</sup>



- a:** R<sup>1</sup> = R<sup>2</sup> = Me
- b:** R<sup>1</sup> = Me; R<sup>2</sup> = Pr<sup>i</sup>
- c:** R<sup>1</sup> = Et; R<sup>2</sup> = Pr<sup>i</sup>
- d:** R<sup>1</sup> = Pr<sup>n</sup>; R<sup>2</sup> = Pr<sup>i</sup>

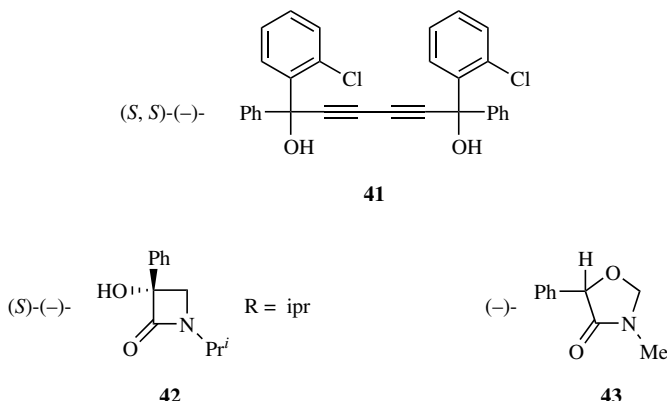


- |  |  |
|--|--|
| <b>a:</b> Ar = <i>m</i> -ClC <sub>6</sub> H <sub>4</sub><br><b>b:</b> Ar = <i>m</i> -BrC <sub>6</sub> H <sub>4</sub><br><b>c:</b> Ar = <i>m</i> -MeC <sub>6</sub> H <sub>4</sub><br><b>d:</b> Ar = <i>p</i> -ClC <sub>6</sub> H <sub>4</sub><br><b>e:</b> Ar = <i>p</i> -BrC <sub>6</sub> H <sub>4</sub><br><b>f:</b> Ar = <i>p</i> -MeC <sub>6</sub> H <sub>4</sub> | <b>g:</b> Ar = <i>o</i> -ClC <sub>6</sub> H <sub>4</sub><br><b>h:</b> Ar = <i>o</i> -BrC <sub>6</sub> H <sub>4</sub><br><b>i:</b> Ar = <i>o</i> -MeC <sub>6</sub> H <sub>4</sub><br><b>j:</b> Ar = <i>m, p</i> -Me <sub>2</sub> C <sub>6</sub> H <sub>3</sub><br><b>k:</b> Ar = <i>m, m</i> -Me <sub>2</sub> C <sub>6</sub> H <sub>3</sub> |
|--|--|



A substituent on the benzene ring of **35** is also important for the formation of a chiral crystal. Of the eleven derivatives (**39a–k**), three *m*-substituted derivatives (**39a–c**), one *o*-substituted derivative (**39i**), and one *m,p*-disubstituted derivative (**39j**) formed chiral crystals, and their irradiation in the solid state gave the corresponding optically active β-lactam **40a** (75% yield, 100% ee), **40b** (97% yield, 96% ee), **40c** (63% yield, 91% ee), **40i** (54% yield, 92% ee), and **40j** (62% yield, 54% ee), respectively, in the chemical and optical yields indicated.<sup>23</sup> The reason why an *m*-substituent on the benzene ring is effective for the formation of the chiral crystal was studied by X-ray analysis of **39c**.<sup>24</sup> Crystal structures of **39f**, **49i**, and **49j** have also been analyzed.<sup>25</sup>

Even when a chiral arrangement of oxoamide molecules in their own crystal is difficult or impossible to achieve, an chiral arrangement can easily be obtained by formation of an inclusion complex with a chiral host compound. Photoirradiation of the inclusion complex in the solid state gives the optically active β-lactam very efficiently. For example, irradiation of a 1:1 complex of the chiral host, (*S,S*)-(*–*)-1,6-di(*o*-chlorophenyl)-1,6-diphenylhexa-2,4-diyne-1,6-diol (**41**, a dimer of **14b**) with **37a** in the solid state for 27 h gives (*S*)-(*–*)-β-lactam (**42**) of 100% ee

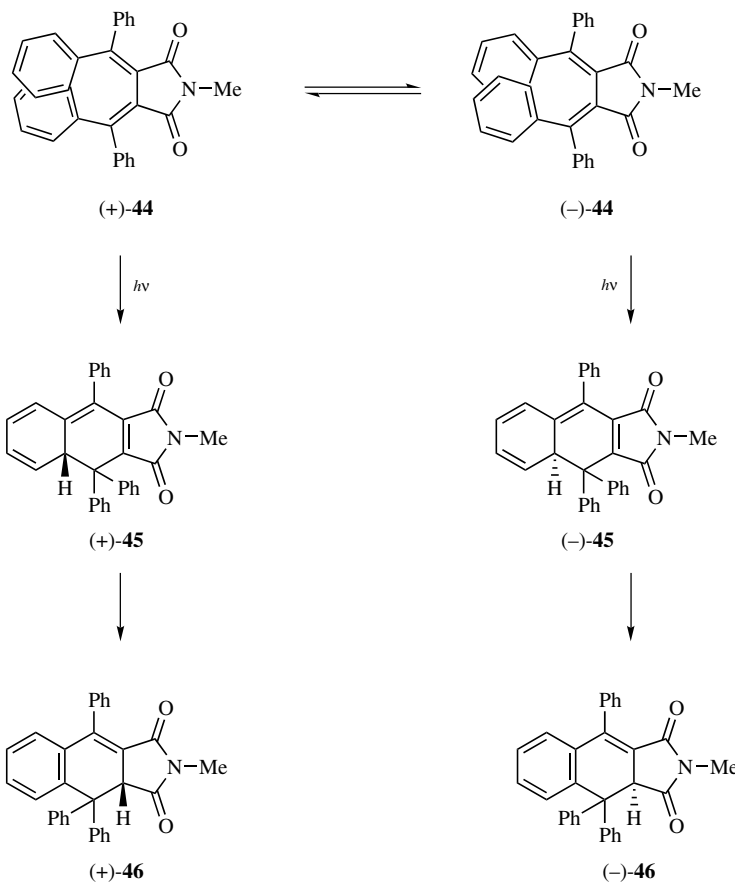


in 100% yield. X-ray crystallographic analysis of the complex shows achiral **37a** molecules arranged in chiral form so as to give **42** by photocyclization in the chiral crystalline lattice induced by the chirality of the host **41**.<sup>26</sup> Irradiation of a 2:1 inclusion complex of **16** with **37a** also gives **42** of 100% ee in 40% yield. However, irradiation of a 2:1 complex of **29** with **37a** gives **42** of 67% ee (40% yield) and (-)-oxazolidinone (**43**) of 100% ee (55% yield) in the yields indicated.<sup>27</sup>

The chiral arrangement of molecules of **37a** in an inclusion crystalline cavity changes depending on the slight difference of the host molecule. The difference in the chiral arrangement of **37a** molecules in their inclusion complex has been studied by X-ray analysis.<sup>28</sup>

The chiral arrangement of the 3,4-bis(diphenylmethylene)-*N*-methylsuccinamide molecule (**44**) in its crystal has been reported.<sup>29</sup> Recrystallization of **44** from acetone formed a chiral crystal as an orange plate (**A**, converts to **C** by heating at 260°C) and two racemic crystals as orange plates (**B**, mp 302°C) and yellow rectangular plates (**C**, mp 297°C). These can be easily separated by manual selection. In one section of the **A** crystal, for example, (+)-**44** molecules are packed together, while (-)-**44** molecules are packed together in another section of the **A** crystal. These chiral crystals are provisionally labeled (+)-**A** and (-)-**A** crystals, respectively. The chirality of the achiral compound **44** generated in the crystal is due to the helical structure produced by the overlapping of the inner two phenyl rings, as shown in Scheme 1.3. X-ray crystal structural analysis has proved the helical stereochemistry of molecules of **44** in the **A** crystal.<sup>30</sup>

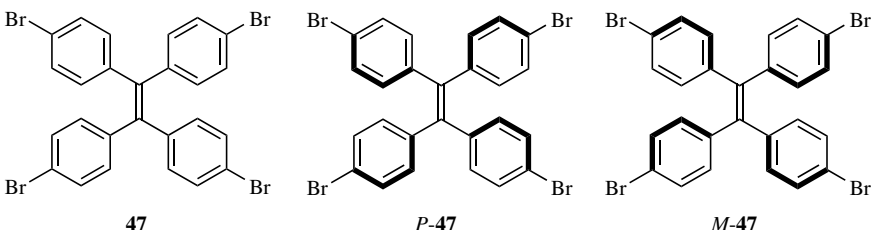
The chirality of **44** in its chiral crystal **A** was frozen by a photocyclization reaction in the solid state. Photoirradiation of the (+)-**A** and (-)-**A** crystals gives (+)-**46** of 65% ee and (-)-**46** of 64% ee, respectively, in quantitative yields.<sup>29</sup> The relatively low optical yield of **46** is probably due to the stereoselective two-step reactions that proceed via **45** (Scheme 1.3).



Scheme 1.3. Photoreaction of chiral helicene **44** in crystal.

The thermal conversion of the chiral **A** crystal into racemic **C** crystal in the solid state is interesting. The conversion suggests that one-half of the chiral molecules is easily inverted into enantiomers in the crystal. X-ray crystallographic analysis of the **C** crystal showed that the inversion occurs in a very orderly fashion.<sup>30</sup>

Achiral tetra(*p*-bromophenyl)ethylene molecules (**47**) arrange in a chiral form in their inclusion complexes with acetone (1:2), 1,4-dione (1:1), benzene (1:1), and *p*-xylene (1:1) obtained in the **47**:guest ratios indicated by recrystallization of **47** from these liquid guests.<sup>31</sup> The chirality of **47** is generated by twisting of the *p*-bromophenyl groups, as shown in *P*-**47** and *M*-**47**. In the complexes with cyclohexanone (1:1), THF (1:2), toluene (1:1), and  $\beta$ -picoline (1:1) obtained in the ratios indicated by recrystallization of **47** from these liquid guests, no chirality

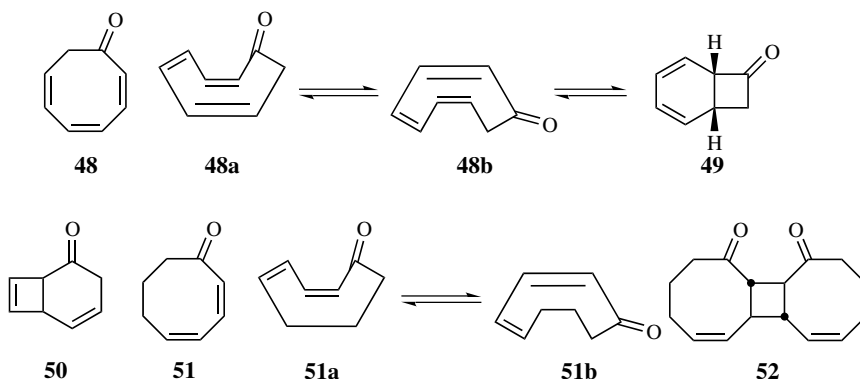


is generated. Interestingly, however, when **47** was exposed to the following guest vapor at room temperature for 24 h, a single crystal of pure **47** was gradually changed into the chiral polycrystalline inclusion complexes with THF (1:2), 1,4-dioxane (1:1), benzene (1:1), *p*-xylene (1:1), and  $\beta$ -picoline (1:1) in the host:guest ratios indicated. The generation of chirality in a crystal through gas–solid reaction is an interesting phenomenon. X-ray structural study of these inclusion complexes of *P*-**47** and *M*-**47** has been performed.<sup>31</sup>

#### IV. CONTROL OF STEREOCHEMISTRY OF MOLECULES IN CRYSTALS FOR SELECTIVE REACTIONS

Molecules are arranged regularly in a crystal. The host–guest inclusion crystallization technique is particularly useful in arranging molecules regularly for selective reactions. When a chiral host compound is used, the achiral molecule can be arranged in a chiral form, and its reaction in the solid state proceeds enantioselectively to give optically active product. These methods are useful especially for liquid guest material. Since various successful examples of such selective organic solid state reactions have been summarized so far,<sup>32</sup> only some typical cases are described in this section.

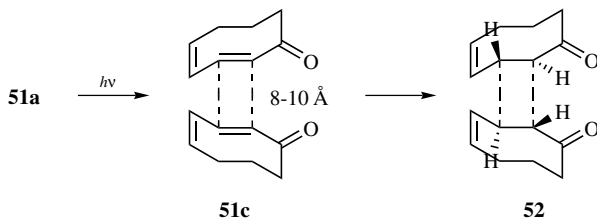
Cycloocta-2,4,6-trien-1-one (**48**) exists as an equilibrium mixture of a stable boat form (**48a** and **48b**) and an unstable bicyclic form (**49**) in a 95:5 ratio at 20°C. Conversion between the two optical conformers **48a** and **48b** is rapid at around room temperature with an activation energy of about 12 kcal/mole. By inclusion complexation with **41**, the flipping equilibrium of **48** was frozen in one conformer as a 1:2 host:guest complex. The IR spectrum of the complex did not show any carbonyl absorption assignable to **49**. When the 1:2 complex of **41** and **48** was irradiated in the solid state for 168 h, 50% conversion occurred and (−)**50** was obtained in 28% yield ( $[\alpha]_D -69.0^\circ$  (c.0.12,  $\text{CHCl}_3$ )).<sup>33</sup> However, the optical purity of the (−)**50** obtained was not determined. Photoreaction of **48** in pentane has been reported to give racemic **50** in 30% yield after irradiation for 21



days.<sup>34</sup> Therefore it is obvious that the photoreaction of **48** in the complex with **41** proceeds not only enantioselectively but also much more efficiently.<sup>33</sup>

X-ray crystallographic analysis of the 1:2 complex of **41** with **48** clarified, that the enantiomers **48a** and **48b** are included in the complex by the formation of a hydrogen bond between the hydroxyl groups of **41** and the carbonyl oxygen of **48**. In the complex, **48a** is enclosed loosely but **48b** is enclosed tightly. Therefore reaction of **48b**, proceeds more efficiently and/or enantioselectively to give (*-*)-**50**, predominantly.<sup>35</sup>

Irradiation of cycloocta-2,4-dien-1-one (**51**) in pentane for 1 h gives racemic **52** in 10% yield along with polymeric materials.<sup>36</sup> However, irradiation of a 3:2 complex (**53**) of **41** and **51** in the solid state for 48 h gave (*-*)-**52** of 78% ee in 55% yield.<sup>33</sup> By X-ray analysis of the complex (**53**), the mechanism of the enantioselective reaction of **51** in the complex has been studied.<sup>35</sup> In **53**, **51a** is included selectively. First of all, the boat form (**51a**) has to be isomerized to the chair form (**51c**), since the reaction product has an all trans structure (**52**). The intermolecular reaction-site distances between the olefinic carbons of two **51a** molecules in **53** were 8 to 10 Å (Scheme 1.4). Schmidt's rule for photodimerization



Scheme 1.4. Enantioselective photodimerization of **51a** in the complex **53**.

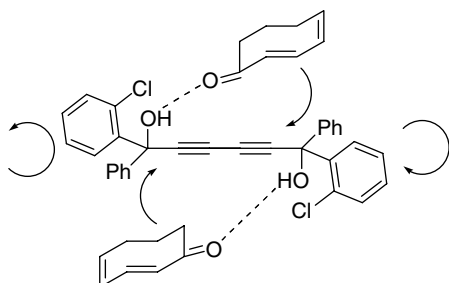
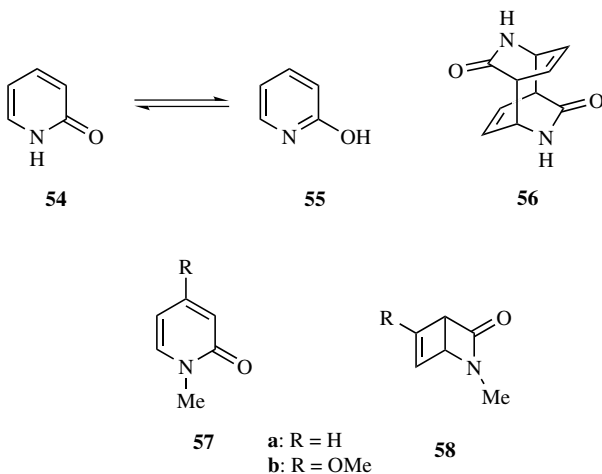


Figure 1.8. Schematic drawing of stereoscopic view of the molecular structure of **51c** and **41** in **51c** and molecular rotation along the arrows during the photodimerization reaction of **51c**.

of an olefin in the solid state states that the distance between the reaction centers should not be longer than 4.2 Å.<sup>37</sup> Therefore, in order to dimerize, two molecules of **51c** have to move close to one another in the crystal. One possible movement is by a rotation around the hexa-2,4-diyne linkage of **41**, as schematically depicted in Figure 1.8. This interesting example appears not fit Schmidt's rule.

Since 2-pyridone (**54**) exists as an equilibrium mixture with 2-hydroxypyridine (**55**), it is difficult to isolate **54** in a pure state. However, the inclusion complexation method with a host is applicable for an isolation of the *keto*-form (**54**) in a pure state. For example, **54** was isolated by complexation with **8** as a 1:2 complex. Photoirradiation of the 1:2 complex in the solid state for 6 h gave the *trans-anti*-dimer **56** in 76% yield.<sup>38</sup> This efficient reaction contrasts with that of an equilibrium mixture of **54** and **55** in solution, which gave **56** in 40% yield after irradiation for 72 h.<sup>39</sup> X-ray crystallographic analysis of the 1:2 complex of **8** and



**54** showed that two molecules of **55** are arranged in the positions, which gives the *trans-anti*-dimer **56** by dimerization, and that the distance between the reaction centers is very short (3.837 Å).<sup>40</sup>

Formation of β-lactam derivatives **58** by an intramolecular photoreaction of pyridones (**57**) is even more interesting. When the cyclization reaction proceeds enantioselectively, it is a useful synthetic method to obtain the optically active β-lactam. Photoirradiation of a 1:1 inclusion complex of **41** and **57b** in the solid state for 47 h gives (−)-**58b** of 100% ee in 97% yield, after 50% conversion.<sup>41</sup> Similar irradiation of 1:1 inclusion complexes of **11** with **57a** and **57b** gives (+)-**58a** of 100% ee and (+)-**58b** of 72% ee in 93% and 99% yields, respectively, after 15% conversion.<sup>41</sup>

Irradiation of a 1:2 inclusion complex **59** of biphenyl-2,2'-dicarboxylic acid (**60**) and **54** for 20 h in the solid state gives **56** in 92% yield (Figure 1.9).<sup>42</sup> X-ray crystallographic analysis of the complex (**59**) shows that two **54** molecules form a cyclic dimer and that the dimer binds to **60** through a hydrogen bond formation. Since two dimer units are arranged at close positions, photodimerization of **54** occurs easily, as depicted in Figure 1.9.<sup>42</sup> In this case **59** can be easily prepared by a simple mixing of the components in the solid state. By combining the mixing and photoirradiation procedures in the solid state, an interesting photochemical process can be established. For example, photoirradiation of a 1:2 mixture of powdered **54** and **60** for 20 h under grinding occasionally by pestle and mortar gave **56** in 90% yield. Since the photodimerization of **54** does not occur in its own crystal, it is very clear that **59** is formed before the photodimerization reaction. A much more interesting catalytic reaction process in the solid state was accomplished. Photoirradiation of a 1:4 mixture of **60** and **54** for 20 h in the solid state gave **56** in 81% yield. These data clearly show that molecules of **60** functioned twice as a host. That is, the mixing of **60** and **54** produces the complex **59** and its photoirradiation gives **56** and **60**. By further mixing, excess **54** becomes included with the released host **60**, which upon continuous irradiation forms the dimer **56**.

Isolation of 4-pyridone (**61**) from an equilibrium mixture with 4-hydroxypyridine (**62**) was accomplished by inclusion complexation with **7a** to give a 1:1 complex **63** of **7a** and **61**. Since so far photodimerization of **61** has never succeeded, complex **63** is an interesting target compound for photoirradiation experiments. Nevertheless, complex **63** was photochemically inert. X-ray crystallographic analysis of **63** showed that the crystal packing is composed of alternating host and guest layers.<sup>42</sup> Within a guest layer, pairs of molecules **61** are formed surrounded by four **7a** molecules as though contained in a kind of nanovessel (Figure 1.10). Each molecule of **61** forms very strong hydrogen bonds with three different **7a** molecules. On the one side, the pyridone oxygen atom forms two strong hydrogen bonds with the hydroxyl groups of two different **7a** molecules. On the other side, the N–H group of **61** is hydrogen-bonded to the OH group of a third molecule

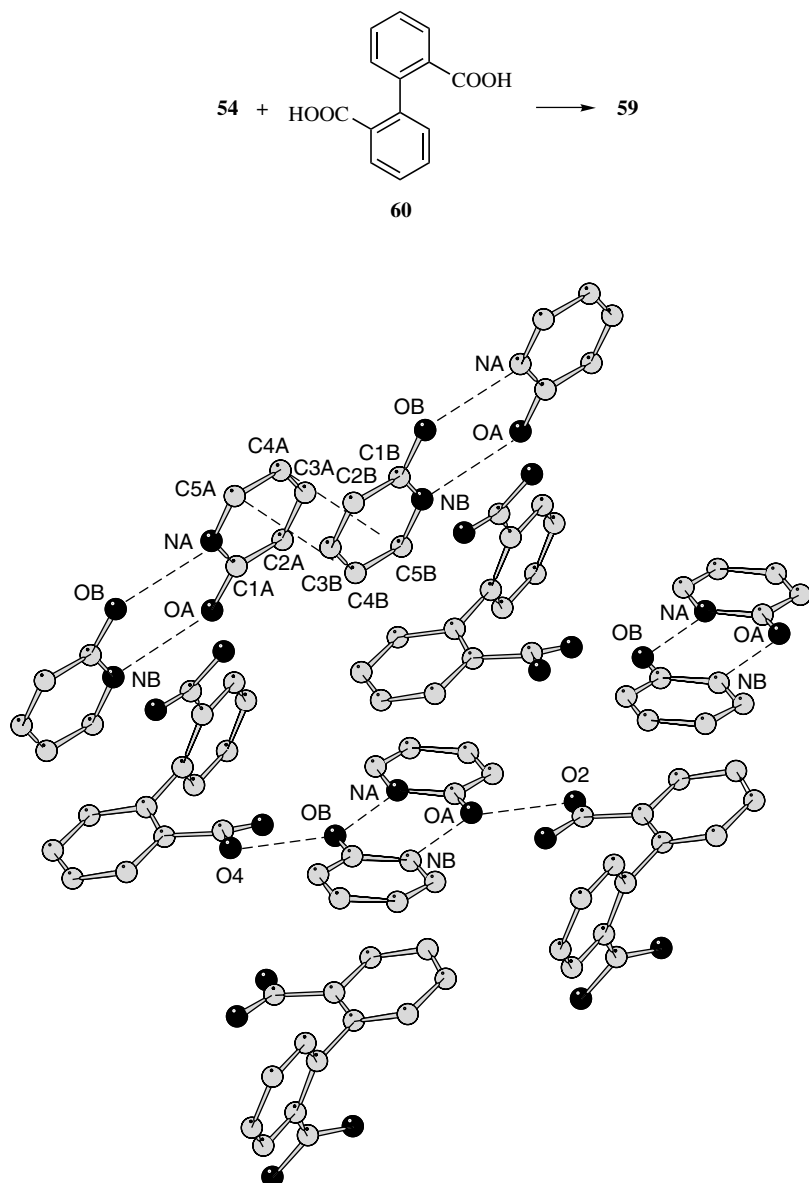
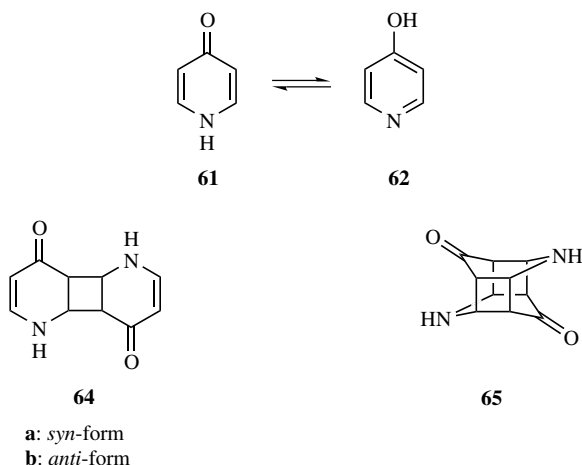


Figure 1.9. X-ray structure of **59**, a 1:2 complex of **60** and **54**.



of **7a**. Moreover there are many C–H···π interactions (at distance around 3 Å) between the molecule of **61** and the aryl groups of **7a**. The pyridone molecules in each pair are antiparallel with a mean interplane distance of 3.69 Å, and thus in an appropriate geometry to give cyclic dimer (**64** or **65**) by photodimerization. However, irradiation of **63** in the solid state did not give any photoproduct, and the crystal structure cannot provide any explanation for that.

Photoirradiation of a 1:1 inclusion complex of **29** with **66** in the solid state gave (−)-**67** of 98% ee in 46% yield.<sup>43</sup> By X-ray analytical study, this reaction was proved to proceed via a partial single-crystal to single-crystal photocyclization

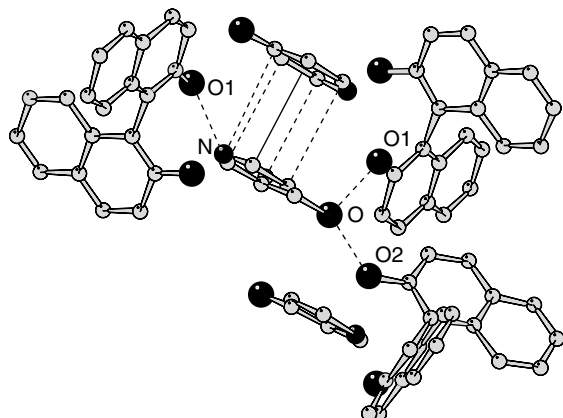
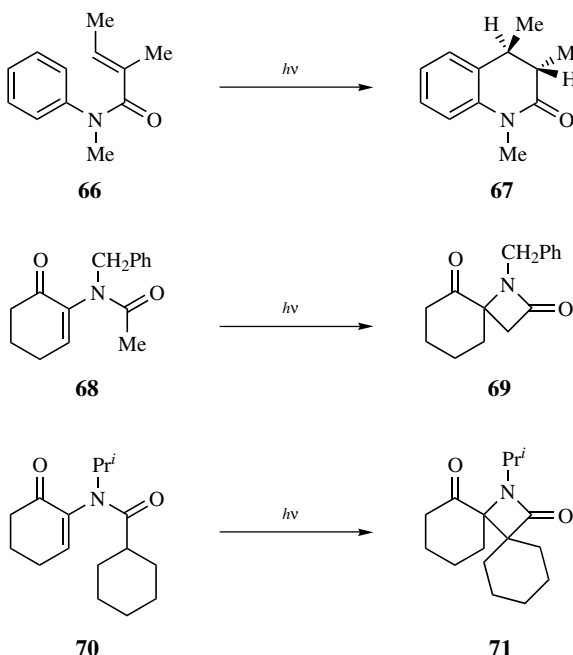


Figure 1.10. X-ray structure of **63**, a 1:1 complex of **61** and **7a**.



transformation.<sup>43</sup> Photoirradiation of a 1:2 inclusion complex of **16** with **68** gave (*-*)-**69** of 97% ee in 42% yield.<sup>44</sup> Similar irradiation of a 1:1 complex of **29** with **70** gave (*-*)-**71** of >99.9% ee in 61% yield.<sup>44</sup> All these highly enantioselective photocyclization reactions can be accomplished because achiral guest molecules are arranged in a chiral form in these inclusion crystalline lattices together with the chiral host molecule.

Photoirradiation of a 1:1 inclusion complex of **41** with coumarin (**72a**) and of a 1:2 inclusion complex of *meso*-1,6-bis(2,4-dimethylphenyl)-1,6-diphenylhexa-2,4-diyne-1,6-diol (**73**) with **72a** gave the dimers **74a** and **75a**, respectively. Interestingly, however, irradiation of a 1:1 inclusion complex of **11** with **72a** prepared by recrystallization of the two components from ethyl acetate gave (*-*)-*anti*-head-to-head dimer **76a** of 96% ee in quantitative yield, although the same irradiation of a 1:1 inclusion complex of **11** with **72a** prepared by recrystallization from toluene-hexane gave *syn*-head-to-head dimer **74a**.<sup>45</sup> The enantioselective reaction of **72a** in the complex with **11** was found to proceed by a single-crystal to single-crystal transformation by X-ray study.<sup>46,47</sup> Since the crystalline lattice of the 1:1 inclusion complex of **11** with **72a** is very similar to that of the 2:1 inclusion complex of **11** with (*-*)-**76a**, the photoreaction would proceed without destroying the crystalline lattice. Similar enantioselective photoreaction of thiocoumarin (**72b**) in an inclusion complex with **29**, which also proceeds by single-crystal to

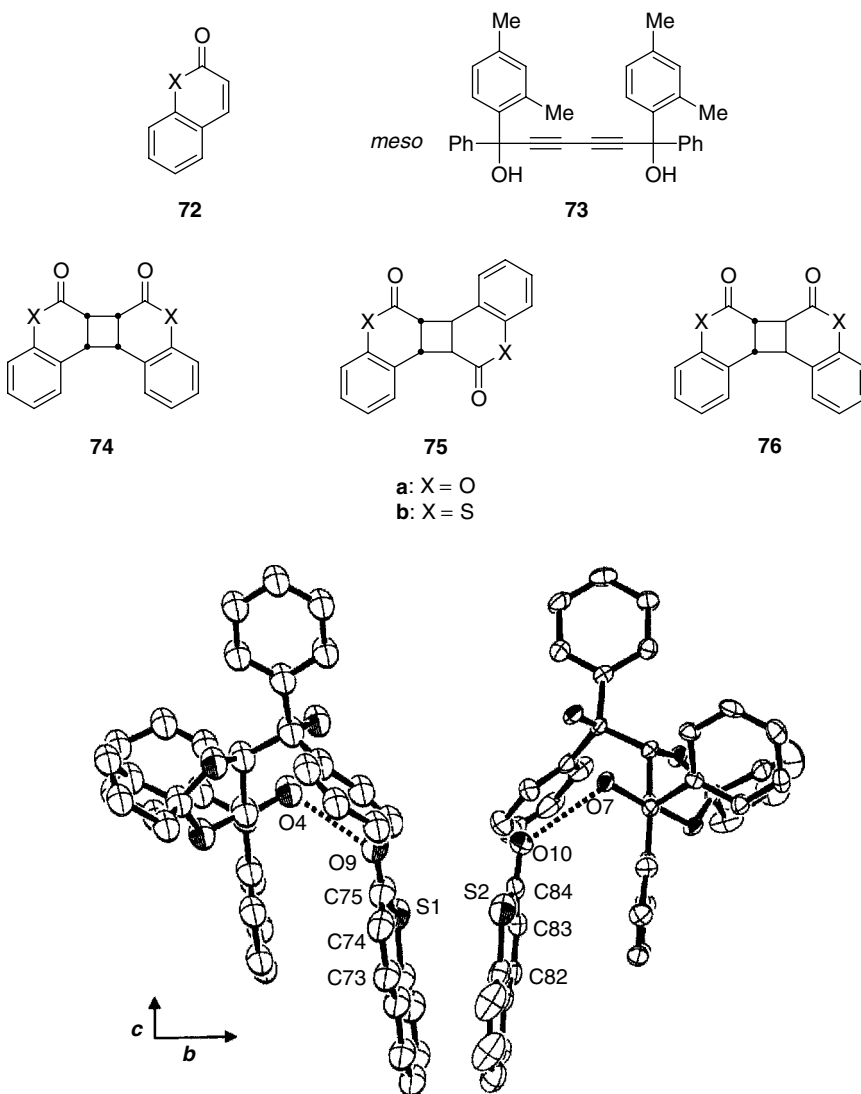


Figure 1.11. X-ray structure of 1:1 complexes of **29** and **72b**.

single-crystal transformation and finally gives (+)-*anti*-head-to-head dimer (**76b**) of 100% ee, has been reported.<sup>46,47</sup> To clarify the mechanism of the single crystal-to-single crystal reaction, X-ray crystallographic analysis was carried out twice for the complex crystal **29–72b** before the irradiation and after the irradiation. Before the irradiation, two molecules of **72b** are arranged in the complex at very

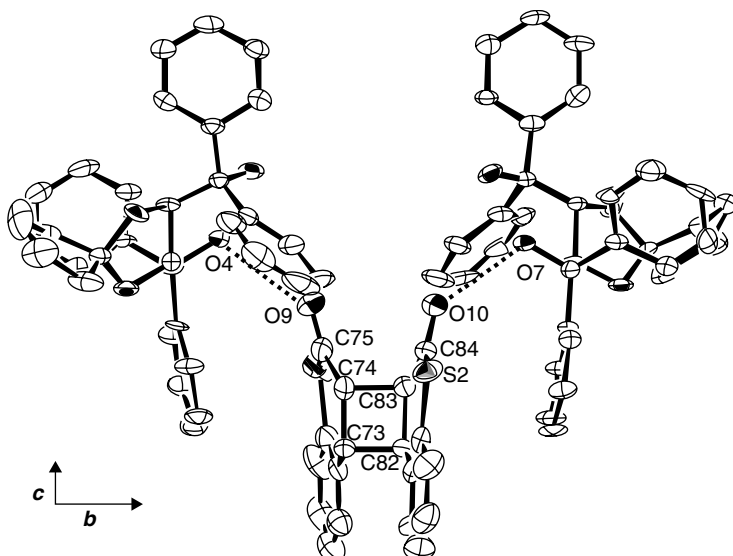


Figure 1.12. X-ray crystal structure of a 2:1 complex of **29** and **76b**.

close positions as shown in Figure 1.11. After the irradiation, the molecule of the photodimer (+)-**76b** produced is arranged at almost the same position as the two molecules of **72b** had been before the irradiation (Figure 1.12). By the photodimerization from **72b** to (+)-**76b**, no big change of the crystalline cavity happened in the complex.<sup>46,47</sup> This is the rationale for the single-crystal to single-crystal reaction.

## ACKNOWLEDGMENTS

The author is grateful to his coworkers whose names appear in the references. The author also would like to thank Ph.D. students Kazuhiro Yoshizawa and Shinya Hirano for their technical assistance in the preparation of this chapter.

## REFERENCES

1. Toda, F.; Tanaka, K.; Elguero, J.; Nassimbeni, L. R.; Niven, M. *Chem. Lett.* **1987**, 2317.
2. Toda, F.; Tanaka, K.; Elguero, J.; Stein, Z.; Goldberg, I. *Chem. Lett.* **1988**, 1061.
3. Yagi, M.; Hirano, S.; Toyota, S.; Kato, M.; Toda, F. *CrystEngComm.* **2002**, 4, 143.
4. Urbanczyk-Lipkowska, Z.; Yoshizawa, K.; Toyota, S.; Toda, F. *CrystEngComm.* **2003**, 5, 114.

5. Toda, F.; Tanaka, K. *Chem. Lett.* **1983**, 661.
6. Toda, F.; Tanaka, K.; Ueda, H. *Tetrahedron Lett.* **1981**, 4669.
7. Toda, F.; Tanaka, K.; Ueda, H.; Oshima, T. *J. Chem. Soc., Chem. Commun.* **1983**, 743.
8. Mullen, K.; Schmickler, H.; Frei, B.; Wolf, H. R. *Tetrahedron Lett.* **1986**, 27, 477.
9. Toda, F.; Tanaka, K.; Fujiwara, T. *Angew. Chem. Int. Ed. Engl.* **1990**, 29, 662.
10. Toda, F.; Tanaka, K.; Koshima, H.; Khan, S. I. *Chem. Comm.* **1998**, 2503.
11. Csoeregh, I.; Hirano, S.; Toyota, S.; Bombicz, P.; Toda, F. *CrystEngComm.* **2004**, 6, 60.
12. Toda, F.; Tanaka, K.; Kuroda, R. *Chem. Comm.* **1997**, 1227.
13. Toda, F.; Tanaka, K.; Kai, A.; Tanaka, N.; Tsugiyama, Y.; Hamada, K.; Fujiwara, T. *Chem. Lett.* **1988**, 537.
14. Kato, M.; Tanaka, K.; Toda, F. *Supramol. Chem.* **2001**, 13, 175.
15. Klaebe, P. *Acta Chem. Scand.* **1969**, 23, 2641.
16. (a) Nishikawa, M. *Chem. Pharm. Bull.* **1963**, 11, 977. (b) Fukushima, K. *J. Mol. Struct.* **1976**, 34, 67. (c) Allen, A.; Fawcett V.; Long, D. A. *J. Raman Spectrosc.* **1976**, 4, 285.
17. Harris, K. D. M.; Thomas, J. M. *J. Chem. Soc. Faraday Trans.* **1990**, 86, 1095.
18. Gerdil, R.; Frew, A. J. *Inclu. Phenom.* **1985**, 3, 335.
19. Toda, F.; Yagi, M.; Soda, S. *J. Chem. Soc., Chem. Commun.* **1987**, 1413.
20. Sekine, A.; Hori, K.; Ohashi, Y.; Yagi, M.; Toda, F. *J. Am. Chem. Soc.* **1989**, 111, 697.
21. Asahi, T.; Nakamura, M.; Kobayashi, J.; Toda, F.; Miyamoto, H. *J. Am. Chem. Soc.* **1997**, 119, 3665.
22. Toda, F.; Miyamoto, H.; Koshima, H.; Urbanczyk-Lipkowska, Z. *J. Org. Chem.* **1997**, 62, 9261.
23. Toda, F.; Miyamoto, H. *J. Chem. Soc., Perkin Trans. 1* **1993**, 1129.
24. Hashizume, D.; Kogo, H.; Ohashi, Y.; Miyamoto H.; Toda, F. *Anal. Sci.* **1998**, 14, 1187.
25. Hashizume, D.; Kogo, H.; Sekine, A.; Ohashi, Y.; Miyamoto, H.; Toda, F. *Acta Cryst.* **1995**, C51, 929.
26. Kaftory, M.; Yagi, M.; Tanaka, K.; Toda, F. *J. Org. Chem.* **1988**, 53, 4391.
27. Toda, F.; Miyamoto, H.; Matsukawa, R. *J. Chem. Soc., Perkin Trans.* **1992**, 1, 916.
28. Hashizume, D.; Uekusa, H.; Ohashi, Y.; Matsukawa, R.; Miyamoto, H.; Toda, F. *Bull. Chem. Soc. Jpn.* **1994**, 67, 985.
29. Toda, F.; Tanaka, K. *Supramol. Chem.* **1994**, 3, 87.
30. Toda, F.; Tanaka, K.; Stein, Z.; Goldberg, I. *Acta Cryst.* **1995**, B51, 856.
31. Tanaka, K.; Fujimoto, D.; Oeser, T.; Irlgartinger, H.; Toda, F. *Chem. Comm.* **2000**, 413.
32. Toda, F. *Acc. Chem. Res.* **1995**, 28, 480; Tanaka, K.; Toda, F. *Chem. Rev.* **2000**, 100, 1025; Toda, F., ed. 'Organic Solid State Reactions,' Kluwer Acad. Pub. 2002.
33. Toda, F.; Tanaka, K.; Oda, M. *Tetrahedron Lett.* **1988**, 29, 653; Toda, F. *Pure Appl. Chem.* **1990**, 62, 417.
34. Buchi, G.; Burgess, E. M. *J. Am. Chem. Soc.* **1962**, 84, 3104.
35. Fujiwara, T.; Nanba, N.; Hamada, K.; Toda, F.; Tanaka, K. *J. Org. Chem.* **1990**, 55, 4532.
36. Cantrell, T. S.; Solomon, J. S. *J. Am. Chem. Soc.* **1970**, 92, 4656.
37. Schmidt, G. M. *Pure Appl. Chem.* **1971**, 27, 647.
38. Tanaka, K.; Toda, F. *Nippon Kagaku Kaishi* **1984**, 141.
39. Taylor, E. C.; Kan, R. O. *J. Am. Chem. Soc.* **1963**, 85, 776.
40. Kaftory, M. *Tetrahedron* **1987**, 43, 1503.
41. Toda, F.; Tanaka, K. *Tetrahedron Lett.* **1988**, 29, 4299.
42. Yagi, M.; Hirano, S.; Toyota, S.; Toda, F.; Giastas, P.; Mavridis, I. *Heterocycles* **2003**, 59, 735.
43. Hosomi, H.; Ohba, S.; Tanaka, K.; Toda, F. *J. Am. Chem. Soc.* **2000**, 122, 1818.
44. Toda, F.; Miyamoto, H.; Inoue, M.; Yasaka, S.; Matijasic, I. *J. Org. Chem.* **2000**, 65, 2778.
45. Tanaka, K.; Toda, F. *J. Chem. Soc., Perkin Trans.* **1992**, 1, 914.
46. Tanaka, K.; Toda, F.; Mochizuki, E.; Yasui, N.; Kai, Y.; Miyahara, I.; Hirotsu, K. *Angew. Chem. Int. Ed. Engl.* **1999**, 38, 3523.
47. Tanaka, K.; Mochizuki, E.; Yasui, N.; Kai, Y.; Miyahara, I.; Hirotsu, K.; Toda, F. *Tetrahedron* **2000**, 56, 6853.

# Chapter 2

## Torsional Motion of Stilbene-type Molecules in Crystals

JUN HARADA and KEIICHIRO OGAWA

*Department of Basic Science, Graduate School of Arts and Sciences,  
The University of Tokyo, 3-8-1 Komaba, Meguro-ku, Tokyo 153-8902, Japan*

- I. Introduction
- II. Apparent Shortening of the Central Bond of (*E*)-Stilbene-type Molecules
- III. Conformational Change of Stilbene-type Compounds in Crystal
- IV. Pedal Motion and Solid State Reactivity
  - A. Photochronism of Salicylideneanilines
  - B. Photodimerization of *trans*-Cinnamamide
- V. Torsional Vibration, Pedal Motion, and Disorder
- VI. Conclusion
- References

### I. INTRODUCTION

Molecular motions in crystals have been extensively studied for more than three decades because they are closely related to the physical properties and chemical reactivities of the crystals.<sup>1</sup> The variety of molecular motions known to chemists and crystallographers are, however, extremely limited (Figure 2.1). Only a few types of molecular motions have systematically been studied: for example, the reorientation of the groups with approximate conical symmetry, such as methyl groups and *tert*-butyl groups;<sup>2</sup> the twofold reorientation of phenyl groups;<sup>3</sup> the in-plane reorientation of flat disklike molecules, such as benzene;<sup>4</sup> and the overall rotation of globular molecules, such as adamantane<sup>5</sup> and fullerene.<sup>6</sup>

---

*Topics in Stereochemistry, Volume 25*, edited by Scott E. Denmark and Jay S. Siegel  
Copyright © 2006 John Wiley & Sons, Inc.

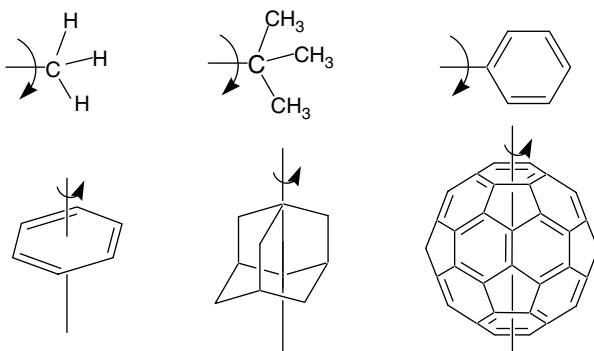


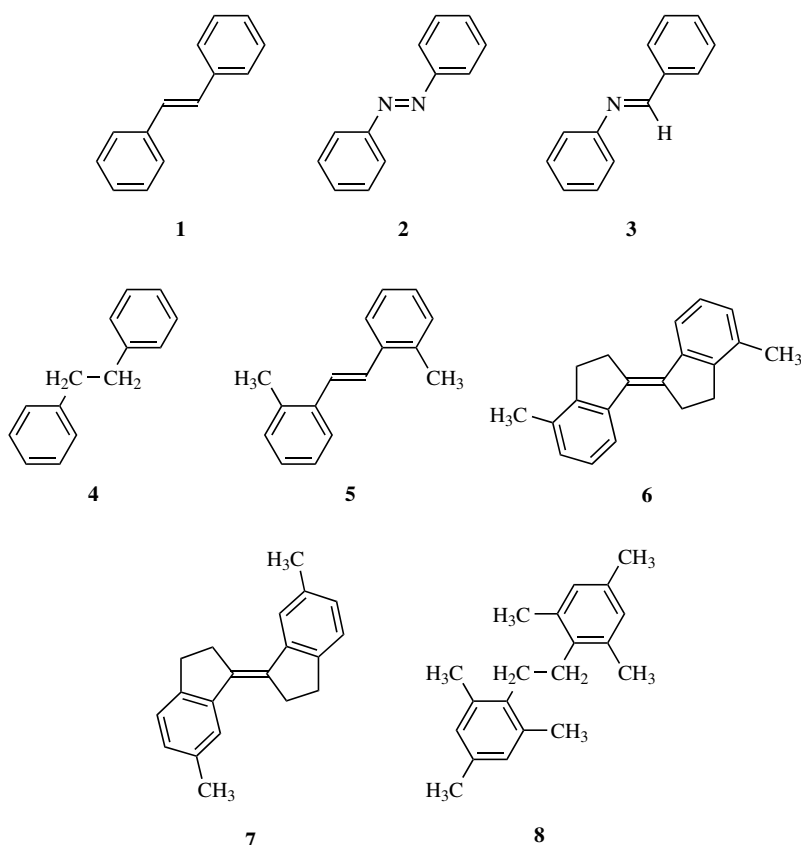
Figure 2.1. Molecular motion in organic crystals.

Recently it has been found that (*E*)-stilbene (**1**) and its congeners undergo a characteristic torsional motion of the C–Ph bonds in crystals and that the torsional motion is a common type of motion that allows one to understand both static and dynamic aspects of the crystals of stilbene-type compounds.

There are two remarkable phenomena for which the torsional motion is responsible. One is an apparent shortening of the central bond in the crystal structure, which is determined by X-ray diffraction analysis.<sup>7,8</sup> Apparent shortening of the central bond by a maximum of 0.05 Å is commonly observed in the crystal structures of (*E*)-stilbene (**1**),<sup>8</sup> azobenzene (**2**),<sup>9</sup> *N*-benzylideneaniline (**3**),<sup>10</sup> 1,2-diphenylethane (**4**),<sup>11,12</sup> and their derivatives. The other is conformational change through a pedal motion in crystals.<sup>9,12,13,14,15</sup> The pedal motion also takes place commonly in the stilbene-type compounds and often plays an essential role in solid state photochemical reactions. This account describes these two phenomena as they are revealed by our X-ray crystallographic studies.

## II. APPARENT SHORTENING OF THE CENTRAL BOND OF (*E*)-STILBENE-TYPE MOLECULES

The length of a covalent bond has almost a constant value for a bond type with the same constituent atoms.<sup>16</sup> For example, the length of carbon–carbon single bond is typically 1.54 Å.<sup>17</sup> The standard lengths of carbon–carbon double and triple bonds are 1.34 and 1.20 Å, respectively.<sup>17</sup> These values have been determined mainly by X-ray diffraction analysis, which is the most reliable experimental method for determination of bond lengths. Use of modern X-ray crystallographic technique can easily give reliable bond lengths with a precision of a few thousandths of an angstrom.



However, the bond length determined by X-ray diffraction analysis often deviates from the typical one for the same kind of bond. If the deviation is very large, such as 0.05 Å for carbon–carbon bonds, considerable attention must be given to the origin of the deviation.

Such an example is an unusual shortening of the central ethylene bond in (*E*)-2,2'-dimethylstilbene (**5**).<sup>7,8</sup> The ethylene bond length determined by X-ray diffraction analysis was 1.283(3) Å at 298 K (Table 2.1). This is surprisingly shorter than the standard experimental value of carbon–carbon double bonds, 1.34 Å. There was, however, no serious error in the X-ray crystallographic data. The lengths of all the other carbon–carbon bonds were normal. Only the length of the central ethylene bond was anomalous.

To elucidate the origin of the anomaly in the length of the ethylene bond, the X-ray diffraction measurements were carried out at 118 K. The observed length of the ethylene bond was 1.321(2) Å, which increased by 0.04 Å compared with

Table 2.1  
Central Bond Length of Stilbene-type Compounds

Compound	Bond Type	Origin	T (K)	Distance (Å)	Reference
<b>1</b>	C=C	X-ray	300	1.324(3)	13
			90	1.337(2)	14
		calc	MMP2	1.356	8
<b>2</b>	N=N	X-ray	300	1.242(2)	14
			90	1.256(2)	
		calc	B3LYP/6-31G*	1.261	9
<b>3</b>	C=N	X-ray	300	1.254(2)	10
			90	1.276(1)	
		calc	B3LYP/6-31G*	1.281	
<b>4</b>	C–C	X-ray	300	1.504(3)	12
			90	1.530(2)	
		calc	MP2/6-31G*	1.540	
<b>5</b>	C=C	X-ray	298	1.283(3)	8
			118	1.321(2)	
			MMP2	1.353	
<b>6</b>	C=C	X-ray	296	1.353(2)	20
			120	1.355(2)	
		calc	MM3	1.362	
<b>7</b>	C=C	X-ray	296	1.362(2)	20
			120	1.358(3)	
		calc	MM3	1.362	
<b>8</b>	C–C	X-ray	300	1.536(3)	12
			90	1.541(2)	
		calc	MP2/6-31G*	1.546	

the length at 298 K (Table 2.1). Despite the marked temperature dependence of the ethylene bond, the other bond lengths changed little with variation in the temperature and showed no anomaly.

It is well known that the interatomic distance determined by X-ray diffraction is often apparently shorter than the true one. The apparent shortening of interatomic distances in crystal structures has usually been interpreted in terms of a rotational oscillation of the molecule regarded as a rigid body (the rigid-body model).<sup>18</sup> The shortening of the ethylene bond in **5**, however, cannot be explained by this model because the temperature dependence of the observed geometry appears only in the central part of the molecules.

The unusual shortening of the ethylene bond can be regarded as an artifact caused by the torsional vibration of the C–Ph bonds. The vibration is supposed to take place with minimum movement of the benzene rings. During torsional vibration, the orientation of the two benzene rings relative to the crystal lattice

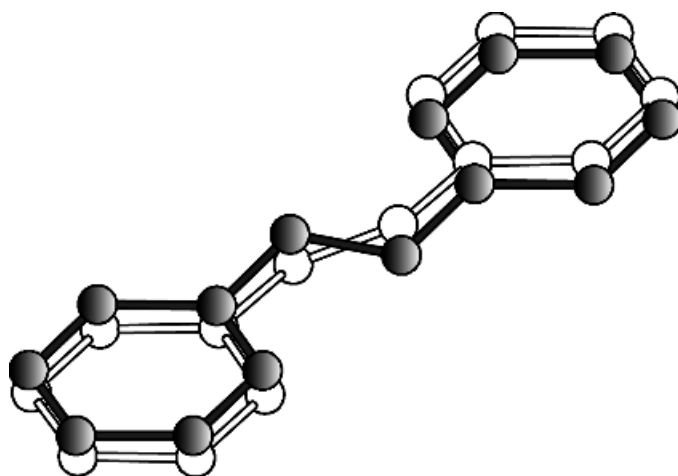


Figure 2.2. Example of torsional vibration of the C–Ph bonds of (*E*)-stilbenes in crystals.

does not change but that of the ethylene moiety does. Such a torsional vibration can be illustrated as an interconversion between two conformations (Figure 2.2). The two conformations are not the stable ones at energy minima on the torsional potential energy surface, though they exist on the surface. During the vibration the ethylene carbon atoms move along the arcs (Figure 2.3). However, the ethylene carbon atoms are treated as vibrating at the points inside the arcs, P and P', with a direction perpendicular to the molecular plane, because the magnitude and direction of thermal vibration of atoms are modeled as thermal ellipsoids in the X-ray diffraction analyses. The longest axes of the thermal ellipsoids of the ethylene carbon atoms are actually nearly perpendicular to the molecular plane (Figure 2.4). As a result the observed length of the ethylene bond becomes the distance between *P* and *P'*, which is shorter than the true length *A*–*A'* or *B*–*B'*. As the temperature is lowered, the amplitude of the vibration decreases; the length

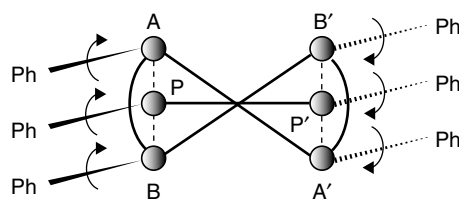


Figure 2.3. Movement of the central atoms in the torsional vibration of the C–Ph bonds.

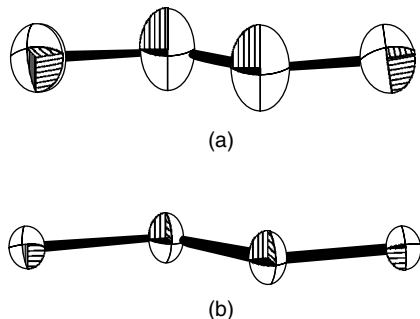


Figure 2.4. Thermal ellipsoids of the central atoms of (*E*)-2,2'-dimethylstilbene (**5**). (a) at 300 K; (b) at 90 K<sup>19</sup>.

of the ethylene bond approaches the true value and becomes longer. This model also reveals that the rotational oscillation does not occur in other bonds because all the corresponding C–C bonds except the ethylene bond are parallel to each other between the two interchanging conformations. Thus the unusual shortening of bond occurs only in the central ethylene bond.

Strong support for this model was obtained from the X-ray crystallographic study of stiff stilbenes **6** and **7**.<sup>20</sup> Because in these compounds the torsional vibration of the C–Ph bonds is severely restricted by the alkylene chains, the ethylene bond of these compounds is not expected to show shrinkage but to maintain normal length even at room temperature. Accordingly the ethylene bond lengths of these compounds proved to be independent of temperature and measured 1.35 to 1.36 Å, which are values that agree with the value of 1.36 Å that was estimated from the molecular mechanics calculations.

Similarly anomalous shortening and temperature dependence of the length of the central ethylene bond have been widely observed in other stilbenes, including their parent compound (**1**). Azobenzenes, *N*-benzylideneanilines, and 1,2-diphenylethylenes show the same tendency in the central bond length as well (Table 2.1). Although the magnitude of shrinkage depends on the compound and is usually less remarkable than that in **5**, it is certain that the central bonds shortening is a general phenomenon in stilbene-type compounds. From the temperature dependences of the observed bond lengths compared with the theoretically estimated bond lengths, the true lengths of C=C bond in (*E*)-stilbenes, N=N bond of azobenzenes, and C=N bond of benzylideneanilines can be safely estimated to be 1.35 to 1.36, 1.26 to 1.27, and 1.28 to 1.29 Å, respectively.

Bond lengths obtained by X-ray diffraction analysis are usually accepted because this is the most reliable experimental method for the determination of

accurate molecular structures. When an unusual bond length is obtained by X-ray diffraction analysis, chemists are inclined to explain the anomaly by invoking some electronic effects. However, intramolecular motions in crystals often give some apparent shortening of the bond length without any other anomalous features in the observed structures. To understand correctly the anomaly in bond length, it is therefore essential to study the temperature dependence of the crystal structures before multiplying hypothesis. An instructive example is given below.

The length of the central ethane bond in 1,2-diphenylethane (**4**) had been a subject of considerable interest for more than half a century.<sup>21,22</sup> It was pointed out that the ethane bond could be anomalously long due to the through-bond interaction of the  $\sigma$  orbitals of the ethane bond with the  $\pi$  orbitals of the benzene rings in the antiperiplanar conformation.<sup>23</sup> The length determined by X-ray diffraction (1.50 Å), however, was significantly shorter than the standard value of the carbon–carbon single bond (1.541(3) Å). The phenomenon seemed to be closely related to the ethane bond length problem of hexaphenylethyanes, which had been a subject of much controversy.<sup>24</sup> Variable temperature X-ray crystallographic analyses of **4** showed that the ethane bond increases in length as the temperature is lowered (1.530(2) Å at 90 K) and consequently revealed that the unusual shortening of the ethane bond length of **4** is an artifact caused by the torsional vibration of the C–Ph bonds in crystals (Figure 2.5).<sup>11,12</sup> The true length of the ethane bond was safely estimated to be 1.54 Å. Thus it was not necessary to resort to an electronic effect to explain the anomaly in the ethane bond length of 1,2-diphenylethane (**4**).<sup>11,12,25</sup>

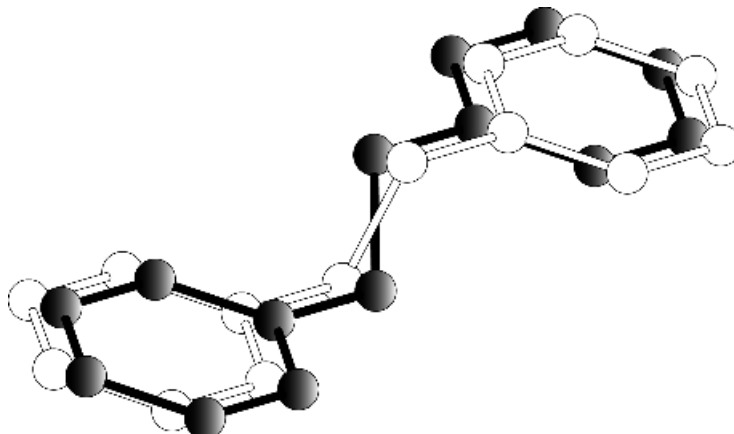


Figure 2.5. Example of torsional vibration of the C–Ph bonds of 1,2-diphenylethane (**4**) in crystals.

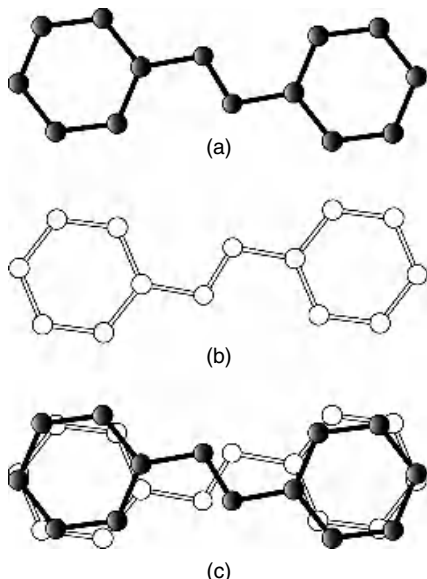


Figure 2.6. Orientational disorder in azobenzene (**2**): (a) Major conformer; (b) minor conformer; (c) observed structure (orientational disorder).

### III. CONFORMATIONAL CHANGE OF STILBENE-TYPE COMPOUNDS IN CRYSTALS

In addition to the torsional vibration of the C–Ph bonds, a conformational change was observed in the crystals of stilbene-type compounds. The conformational change was revealed by X-ray diffraction analyses of azobenzene (**2**).<sup>9,14</sup> There was an orientational disorder (a misorientation of the molecules in the crystal lattice) in the crystal structure at room temperature;<sup>26</sup> the molecules adopt two conformations related by an approximate twofold rotation about the longest axes of the molecules (Figure 2.6). If two conformations mutually interconvert and a dynamic equilibrium is established through the conformational interconversion, the populations of the conformers would vary with temperature according to the Boltzmann distribution law. Variable temperature X-ray diffraction measurements have revealed that the populations of two conformers changed with variation of the temperature:<sup>9</sup> 81.5(9): 18.5(9) at 296 K and 1: 0 at 82 K; thus the disorder was dynamic and disappeared at 82 K. This means that the population of the minor conformer is less than the detection limit of a few percent. This indicates that a conformational change takes place in the crystals of **2** and that the populations of the interchanging conformers vary with the temperature.

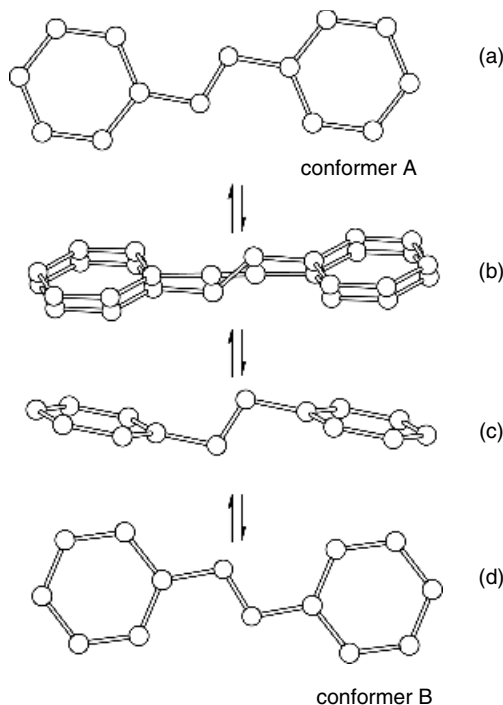


Figure 2.7. Pedal motion of azobenzene (2).

The conformational change is most likely to occur as shown in Figure 2.7. A molecule that adopts conformer A (Figure 2.7a), one of two orientations in the crystals, undergoes the torsional vibration of the C–Ph bonds during which the two benzene rings remain parallel to each other. This torsional vibration is just the same as that described in the previous section and causes an apparent shortening of the N=N bond (Figure 2.7b). When vibration with much larger amplitude takes place, conformer A could change to the other orientation, conformer B (Figure 2.7d), through the conformation in which the C(Ph)–N=N–C(Ph) moiety is perpendicular to the benzene rings (Figure 2.7c). This conformational change can be regarded as taking place through a pedal motion: a pair of benzene rings moving like the pedals of a bicycle. The populations of the two conformers will show the temperature dependence if the two conformers have different stabilities in the crystals. The conformational change through a pedal motion is therefore detected as dynamic disorder by variable temperature X-ray diffraction measurements.

A similar conformational change was observed in the crystals of (*E*)-stilbene (**1**),<sup>13,14</sup> whose crystal structure is isomorphous to that of azobenzene (**2**), and also in other

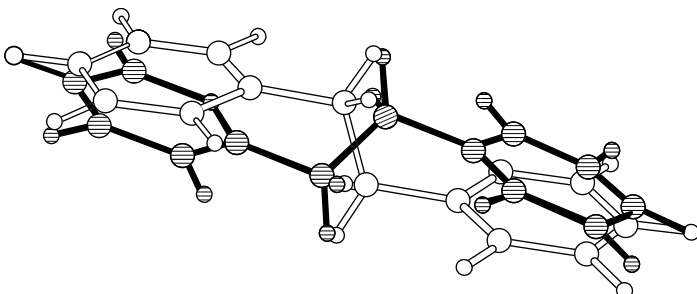


Figure 2.8. Orientational disorder in 1,2-diphenylethane (**4**)<sup>12</sup>.

(*E*)-stilbenes, azobenzenes,<sup>9,13,14</sup> *N*-benzylideneanilines,<sup>27</sup> and 1,2-diphenylethylenes (Figure 2.8).<sup>12</sup> Thus the conformational interconversion through the pedal motion takes place in the crystals of a wide range of stilbene-type compounds.

Although the pedal motion is detected by the facts that the crystal structure has the orientational disorder at room temperature and that the populations of the two conformers varies with the temperature, it was discovered that the pedal motion occurs even if the orientational disorder is not detected at room temperature. Such is the case of the crystal structure of (*E*)-3,3',4,4'-tetramethylazobenzene (**9**).<sup>13</sup>

Figure 2.9 shows difference Fourier maps of **9** at various temperatures. At room temperature, only one conformer is observed and there are no residual peaks corresponding to a misoriented minor conformer (Figure 2.9a). However, at 373 K, two residual peaks (peaks A and A') appear around the N=N bond (Figure 2.9b). The two peaks are due to the nitrogen atoms of the misoriented minor conformer. These results indicate that conformational interconversion through the pedal motion takes place in the crystal of **9**. The minor conformer is too small in population to detect at room temperature, but it becomes detectable at higher temperature because of the increase in population. Pedal motion should therefore be always considered to occur in the crystals of stilbene-type compounds, even if the orientational disorder is not detected.

#### IV. PEDAL MOTION AND SOLID STATE REACTIVITY

The pedal motion was recently found to be a key process of photochemical reactions in the solid state. Two examples are given below.

##### A. Photochromism of Salicylideneanilines

Salicylideneaniline (**10**) and its derivatives, which have a molecular skeleton similar to (*E*)-stilbene, are well known to exhibit a photochromism, a reversible

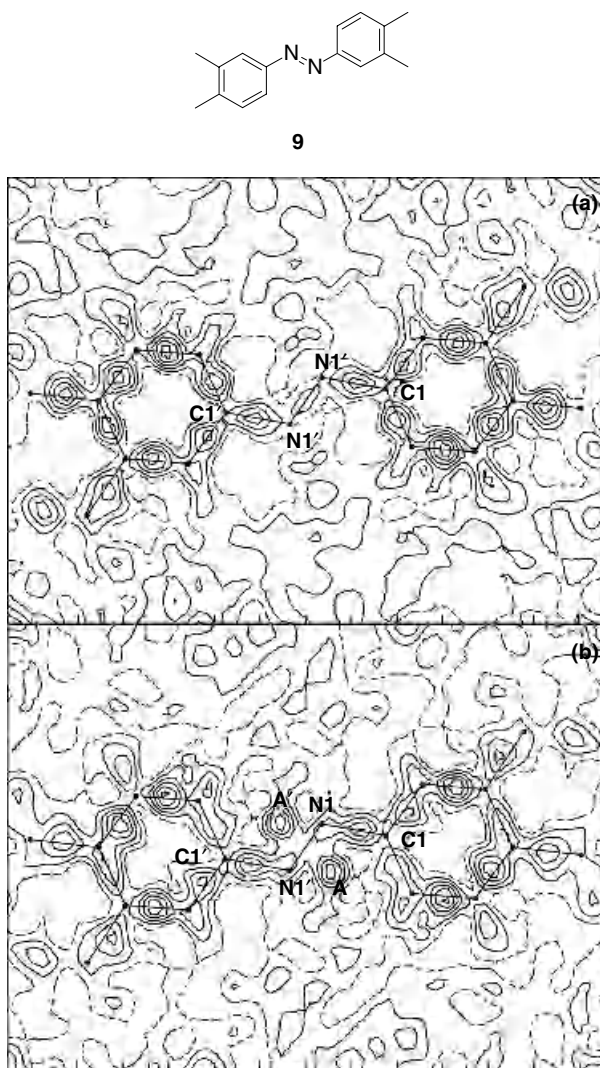
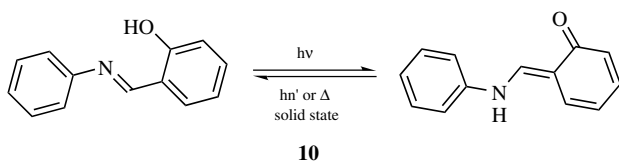
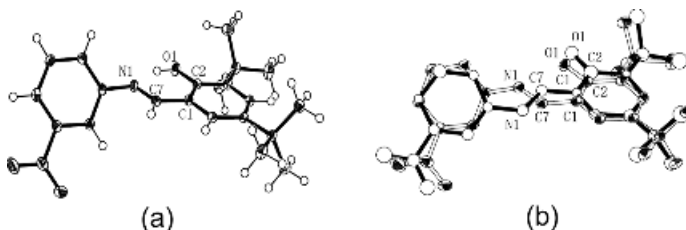
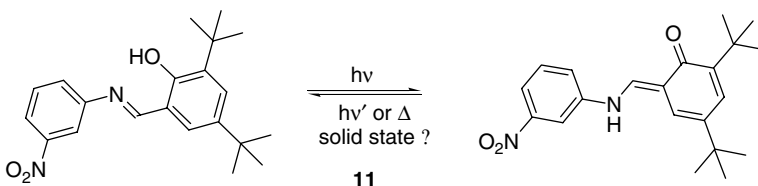


Figure 2.9. Difference Fourier map of (*E*)-3,3',4,4'-tetramethylazobenzene (**9**). The section of each map contains C1, N1, N1', and C1'. The contour lines are at  $0.05 \text{ e}\text{\AA}^{-3}$  intervals. Negative contours lines are indicated by broken lines (a) at 300 and (b) at 373 K.<sup>13</sup>

color change caused by irradiation of light, in the solid state.<sup>28,29,30</sup> Photochromic salicylideneanilines are usually yellow and exist in the enol form in crystals. On irradiation with ultraviolet light, the *trans*-keto form is produced as a red photoproduct via the translocation of the proton bonded to the oxygen atom of the enol form to



the imine nitrogen atom and a subsequent geometrical rearrangement in the excited state. When the red photoproduct is irradiated with visible light or left in the dark, the enol form is regenerated as a yellow crystal. The structural change associated with



**Figure 2.10.** Molecular structure of *N*-3,5-di-*tert*-butylsalicylidene-3-nitroaniline (**11**): (a) Before light irradiation; (b) after light irradiation.<sup>31</sup>

the reversible photochromic reaction was observed by X-ray diffraction analysis of **11**. The crystal structure of the red photoproduct exhibits a similar disorder as observed in the crystals of stilbene-type compounds (Figure 2.10):<sup>31</sup> the enol and *trans*-keto forms coexist in the crystal, which indicates that a pedal motion occurs in the excited state of the photochromic reaction. The pedal motion plays therefore a key role in the photochromism of salicylideneanilines in crystals.

## B. Photodimerization of *trans*-Cinnamamide

The molecular skeleton of *trans*-cinnamamide (**12**) is similar to that of (*E*)-stilbene, except that **12** has only one phenyl group. The photochemical dimerization of

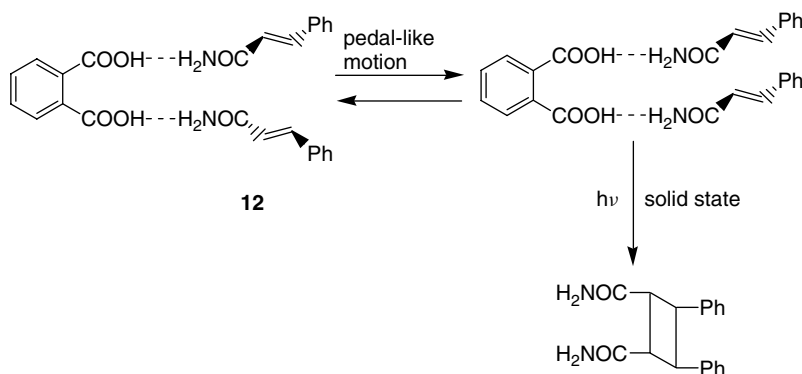


Figure 2.11. Photodimerization of *trans*-cinnamamide (**12**) in cocrystals with phthalic acid.

olefins such as cinnamic acids and their derivatives in the solid state generally occurs with a minimum amount of atomic or molecular movement to give cyclobutane derivatives. The photochemical reactivity of the reactants and the molecular structure of the product depend on the geometric relation of the two reactant molecules in the crystal lattice.<sup>32,33</sup>

In the cocrystals of *trans*-cinnamamide (**12**) with phthalic acid, two cinnamamide molecules are nearest neighbors, but their C=C bonds are in a crisscrossed arrangement (Figure 2.11). These crystals are expected to be inert for the photodimerization because the crisscrossed arrangement of the C=C bonds is geometrically unfavorable for the photodimerization. Nevertheless, the photodimerization proceeds in crystals topochemically.<sup>34</sup> The apparent discrepancy between the molecular rearrangement and the photochemical reactivity can be explained by the assumption that the pedal motion prior to the photodimerization produces the parallel arrangement of the nearest neighboring C=C bonds, which is conducive to photodimerization.

## V. TORSIONAL VIBRATION, PEDAL MOTION, AND DISORDER

To explain better how torsional vibration, pedal motion, and orientational disorder relate to one another, we illustrate this schematically in Figure 2.12 using the potential energy profile associated with the torsional vibration of the C–Ph bonds and the pedal motion of the crystals.

In this figure, in the crystal structures that do not show disorder, only the most stable conformer A is observed. In conformer A the torsional vibration takes place within a small range of the torsion angle change ( $\Delta\omega$ ). This torsional vibration causes an apparent shortening of the central bond. The magnitude of the bond

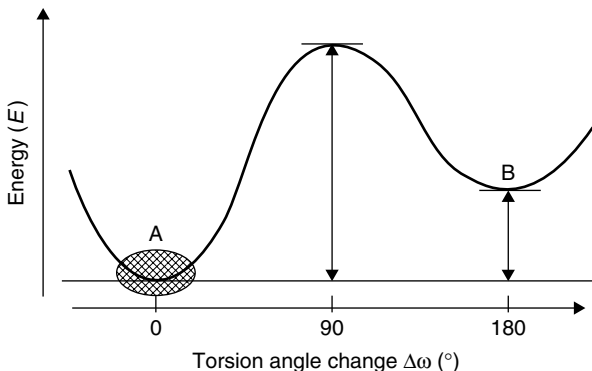


Figure 2.12. Potential energy profile associated with the torsional vibration of the C–Ph bonds and pedal motion.

shortening depends on the amplitude of the torsional vibration, which depends on the curvature of the potential energy profile. When the curvature is small, meaning the profile is depressed, the amplitude is large and the bond shortening is extreme. When the curvature is strong, meaning the profile is steep, the amplitude is small and the bond shortening is minimal. Thus the apparent shortening of the central bond depends on the curvature of the potential energy profile of the torsional vibration.

In the most of the compounds that we have investigated, a significant bond shortening was observed at room temperature, although the magnitude of the shortening varied with the compounds. The shortening of the central bond is therefore generally apparent in stilbene-type compounds. The potential energy profile depends on the intramolecular torsional potential and intermolecular interactions in the crystals. If the torsional vibration is suppressed by alkylene chains or bulky substituents, the curvature becomes large and the bond shortening is not observed even at room temperature. It is the case that no shortening or anomaly in the central bond length was observed in stiff stilbenes (**6** and **7**)<sup>20</sup> and in 1,2-diphenylethyanes with substituents at ortho positions (**8**).<sup>12</sup>

As the torsion angle change ( $\Delta\omega$ ) increases, meaning the C–Ph bonds become greatly twisted, the molecule passes over the energy barrier to reach another conformer B. Then the pedal motion takes place. The pedal motion is detected by X-ray diffraction analysis as an orientational disorder. Whether or not the disorder is observable depends on the energy difference between the two conformers A and B. They have a similar energy in the gas phase, but the energy difference arises from intermolecular interactions in the crystals. For the disorder is to be observed, the energy difference must be small. If the energy difference is too large, the disorder cannot be observed, even if the pedal motion is taking place. The

pedal motion in **9** corresponds to this case. In the crystals of **9**, the orientational disorder was not detected at room temperature but rather at 373 K. This is thought to indicate that the pedal motion occurs even at room temperature, although the disorder cannot be detected.

## VI. CONCLUSION

Unusual shortening in the length of the central bond is commonly observed in the crystals of stilbene-type compounds: (*E*)-stilbenes, azobenezenes, *N*-benzylideneanilines, and 1,2-diphenylethylenes. The shortening is an artifact that is caused by the torsional vibration of the C–Ph or N–Ph bonds. In these crystals a conformational change through the pedal motion also takes place. The pedal motion appears to be a general phenomenon in crystals of stilbene-type compounds and often plays an essential role in solid state photochemical reactions. These two phenomena must therefore be always taken into account when interpreting the static and dynamic aspects of the crystals of stilbene-type compounds.

## REFERENCES

- (a) Paul, I. C.; Curtin, D. Y. *Acc. Chem. Res.* **1973**, *6*, 217–225. (b) Gavezzotti, A.; Simonetta, M. *Chem. Rev.* **1982**, *82*, 1–13. (c) Trueblood, K. N.; Dunitz, J. D. *Acta Crystallogr.* **1983**, *B39*, 120–133. (d) Lascombe, J., ed. *Dynamics of Molecular Crystals. Studies in Physical and Theoretical Chemistry 46*. Elsevier, Amsterdam, **1987**. (e) Gavezzotti, A.; Simonetta, M. In *Organic Solid State Chemistry: Studies in Organic Chemistry 32*, Desiraju, G. R., ed. Elsevier, Amsterdam, **1987**, ch 11. (f) Dunitz, J. D.; Maverick, E. F.; Trueblood, K. N. *Angew. Chem. Int. Ed. Engl.* **1988**, *27*, 880–895. (g) Dunitz, J. D.; Schomaker, V.; Trueblood, K. N. *J. Phys. Chem.* **1988**, *92*, 856–867. (h) Harris, K. D. M.; Aliev, A. E. *Chem. Br.* **1995**, *132–136*. (i) Bürgi, H. B. *Annu. Rev. Phys. Chem.* **2000**, *51*, 275–296.
- (a) Riddell, F. G.; Arumugam, S.; Anderson, J. E. *J. Chem. Soc., Chem. Commun.* **1991**, 1525–1527. (b) Barrie, P. J.; Anderson, J. E. *J. Chem. Soc., Perkin Trans. 2* **1992**, 2031–2034. (c) Riddell, F. G.; Arumugam, S.; Harris, K. D. M.; Rogerson, M.; Strange, J. H. *J. Am. Chem. Soc.* **1993**, *115*, 1881–1885. (d) Riddell, F. G.; Bernáth, G.; Fülöp, F. J. *Am. Chem. Soc.* **1995**, *117*, 2327–2335. (e) Riddell, F. G.; Rogerson, M. *J. Chem. Soc. Perkin Trans. 2* **1996**, 493–504.
- (a) Hiyama, Y.; Silverton, J. V.; Torchia, D. A.; Gerig, J. T.; Hammond, S. J. *J. Am. Chem. Soc.* **1986**, *108*, 2715–2723. (b) Twyman, J. M.; Dobson, C. M. *J. Chem. Soc., Chem. Commun.* **1988**, 786–788. (c) Fattah, J.; Twyman, J. M.; Heyes, S. J.; Watkin, D. J.; Edwards, A. J.; Prout, K.; Dobson, C. M. *J. Am. Chem. Soc.* **1993**, *115*, 5636–5650. (d) Riddell, F. G.; Bremner, M.; Strange, J. H. *Magnet. Reson. Chem.* **1994**, *32*, 118–121. (e) Riddell, F. G.; Bruce, P. G.; Lightfoot, P.; Rogerson, M. *J. Chem. Soc., Chem. Commun.* **1994**, 209–211. (f) Wendeler, M.; Fattah, J.; Twyman, J. M.; Edwards, A. J.; Dobson, C. M.; Heyes, S. J.; Prout, K. *J. Am. Chem. Soc.* **1997**, *119*, 9793–9803.
- (a) Andrew, E. R. *J. Chem. Phys.* **1950**, *18*, 607–618. (b) Andrew, E. R.; Eades, R. G. *Proc. Roy. Soc.* **1953**, *218A*, 537–552. (b) Anderson, J. E. *J. Chem. Phys.* **1965**, *43*, 3575–3579. (c) Boden,

- N.; Clark, L. D.; Hanlon, S. M.; Mortimer, M. *Faraday Symp. Chem. Soc.* **1978**, *13*, 109–123.  
 (d) Fujara, F.; Petry, W.; Schnauss, W.; Sillescu, H. *J. Chem. Phys.* **1988**, *89*, 1801–1806. (e) Ok, J. H.; Vold, R. R.; Vold, R. L.; Etter, M. C. *J. Phys. Chem.* **1989**, *93*, 7618–7624. (f) Goc, R. Z. *Naturforsch. Teil A* **1997**, *52*, 477–484.
5. (a) McCall, D. W.; Douglass, D. C. *J. Chem. Phys.* **1960**, *33*, 777–778. (b) Smith, G. W. *J. Chem. Phys.* **1961**, *35*, 1134–1135. (c) Resing, H. A. *J. Chem. Phys.* **1965**, *43*, 1828–1829. (d) H. A. Resing, *Mol. Cryst. Liq. Cryst.* **1969**, *9*, 101–132. (e) Liu, N.-I.; Jonas, J. *Chem. Phys. Lett.* **1972**, *14*, 555–558. (f) Wasylischen, R. E.; Pettitt, B. A. *Can. J. Chem.* **1980**, *58*, 655–657.
  6. (a) Yannoni, C. S.; Johnson, R. D.; Meijer, G.; Bethune, D. S.; Salem, J. R. *J. Phys. Chem.* **1991**, *95*, 9–10. (b) Tycko, R.; Haddon, R. C.; Dabbagh, G.; Glarum, S. H.; Douglass, D. C.; Mujce, A. M. *J. Phys. Chem.* **1991**, *95*, 518–520. (c) Tycko, R.; Dabbagh, G.; Fleming, R. M.; Haddon, R. C.; Makhija, A. V.; Zahurak, S. M. *Phys. Rev. Lett.* **1991**, *67*, 1886–1889. (d) Johnson, R. D.; Yannoni, C. S.; Dorn, H. C.; Salem, J. R.; Bethune, D. S. *Scienc.* **1992**, *255*, 1235–1238. (e) David, W. I. F.; Ibberson, R. M.; Dennis, T. J. S.; Hare, J. P.; Prassides, K. *Europhys. Lett.* **1992**, *18*, 219–225.
  7. Ogawa, K.; Suzuki, H.; Sakurai, T.; Kobayashi, K.; Kira, A.; Toriumi, K. *Acta Cryst.* **1988**, *C44*, 505–508.
  8. Ogawa, K.; Sano, T.; Yoshimura, S.; Takeuchi, Y.; Toriumi, K. *J. Am. Chem. Soc.* **1992**, *114*, 1041–1051.
  9. Harada, J.; Ogawa, K.; Tomoda, S. *Acta Cryst.* **1997**, *B53*, 662–672.
  10. Harada, J.; Harakawa, M.; Ogawa, K. *Acta Cryst.* **2004**, *B60*, 578–588.
  11. Harada, J.; Ogawa, K.; Tomoda, S. *J. Am. Chem. Soc.* **1995**, *117*, 4476–4478.
  12. Harada, J.; Ogawa, K. *Struct. Chem.* **2001**, *12*, 243–250.
  13. Harada, J.; Ogawa, K. *J. Am. Chem. Soc.* **2001**, *123*, 10884–10888.
  14. Harada, J.; Ogawa, K. *J. Am. Chem. Soc.* **2004**, *126*, 3539–3544.
  15. Harada, J.; Harakawa, M.; Ogawa, K. *Acta Cryst.* **2004**, *B60*, 589–597.
  16. Eliel, E. L.; Wilen, S. H. *Stereochemistry of Organic Compounds*. Wiley, New York, **1994**, ch. 2.
  17. *International Tables for X-ray Crystallography*, Vol. 3. Kynoch Press, Birmingham, England, **1968**.
  18. (a) Cruickshank, D. W. J. *Acta Cryst.* **1956**, *9*, 757–758. (b) Busing, W. R.; Levy, H. A. *J. Chem. Phys.* **1957**, *26*, 563–568. (c) Dunitz, J. D.; Schomaker, V.; Trueblood, K. N. *J. Phys. Chem.* **1988**, *92*, 856–867. (d) Dunitz, J. D.; Maverick, E. F.; Trueblood, K. N. *Angew. Chem. Int. Ed. Engl.* **1988**, *27*, 880–895.
  19. Harada, J.; Ogawa, K. Unpublished results.
  20. Ogawa, K.; Harada, J.; Tomoda, S. *Acta Cryst.* **1995**, *B51*, 240–248.
  21. (a) Jeffrey, G. A. *Natur.* **1945**, *156*, 82–83. (b) Jeffrey, G. A. *Proc. R. Soc. London*, **1947**, *(A) 188*, 222–236. (c) Cruickshank, D. W. J. *Acta Cryst.* **1949**, *2*, 65–82. (d) Winter, W.; Butters, T.; Riekern, A.; Butsugan, Y. Z. *Naturforsch.* **1982**, *37b*, 855–862.
  22. Kahr, B. Dissertation, Princeton University, 1988.
  23. (a) Gleiter, R. *Angew. Chem., Int. Ed. Engl.* **1974**, *13*, 696–701. (c) Osawa, E.; Kanematsu, K. *Molecular Structure and Energetics*, Vol. 3, Greenberg, A.; Lieberman, J. F., eds.; Verlag Chemie International, Deerfield Beach, FL, 1986, ch 7.
  24. (a) Stein, M.; Winter, W.; Rieker, A. *Angew. Chem., Int. Ed. Engl.* **1978**, *17*, 692–694. (b) Osawa, E.; Onuki, Y.; Mislow, K. *J. Am. Chem. Soc.* **1981**, *103*, 7475–7479. (c) Kahr, B.; Engen, D. V.; Mislow, K. *J. Am. Chem. Soc.* **1986**, *108*, 8305–8307. (d) Yannoni, N.; Kahr, B.; Mislow, K. *J. Am. Chem. Soc.* **1988**, *110*, 6670–6672.

25. Kahr, B.; Mitchell, C. A.; Chances, J. M.; VernonClark, R.; Gantzel, P.; Baldridge, K. K.; Siegel, J. S. *J. Am. Chem. Soc.* **1995**, *117*, 4479–4482.
26. (a) Robertson, J. M.; Woodward, I. *Proc. R. Soc. London Ser. A* **1937**, *162*, 568–583. (b) Lange, J. J. de; Robertson, J. M.; Woodward, I. *Proc. R. Soc. London* **1939**, *A171*, 398–410. (c) Brown, C. J. *Acta Crystallogr.* **1966**, *21*, 146–152. (d) Bouwstra, J. A.; Schouten, A.; Kroon, J. *Acta Crystallogr. Sect. C* **1983**, *39*, 1121–1123.
27. Harada, J.; Harakawa, M.; Ogawa, K. *Acta Cryst.* **2004**, *B60*, 589–597.
28. (a) Crano, J. C.; Guglielmetti, R. J., eds. *Organic Photochromic and Thermochromic Compounds*, Vols. 1 and 2. Kluwer Academic, New York, **1999**. (b) Irie, M. *Chem. Rev.* **2000**, *100*, 1683–1683. (c) Bamfield, P. *Chromic Phenomena. Technological Applications of Colour Chemistry*, Royal Society of Chemistry: Cambridge, 2001. (d) Dürr H.; Bouas-Laurent H., eds. *Photochromism. Molecules and Systems*, rev. ed., Elsevier, Amsterdam, **2003**.
29. Cohen, M. D.; Schmidt, G. M. *J. Phys. Chem.* **1962**, *66*, 2442–2445.
30. Fujiwara, T.; Harada, J.; Ogawa, K. *J. Phys. Chem. B* **2004**, *108*, 4035–4038.
31. Harada, J.; Uekusa, H.; Ohashi, Y. *J. Am. Chem. Soc.* **1999**, *121*, 5809–5810.
32. Schmidt, G. M. *J. Chem. Soc.* **1964**, 2014–2021.
33. Schmidt, G. M. *J. Pure Appl. Chem.* **1971**, *27*, 647–678.
34. (a) Ito, Y.; Hosomi, H.; Ohba, S. *Tetrahedron* **2000**, *56*, 6833–6844. (b) Ohba, S.; Hosomi, H.; Ito, Y. *J. Am. Chem. Soc.* **2001**, *123*, 6349–6352.

# Chapter 3

## Supramolecular Networks of Porphyrins

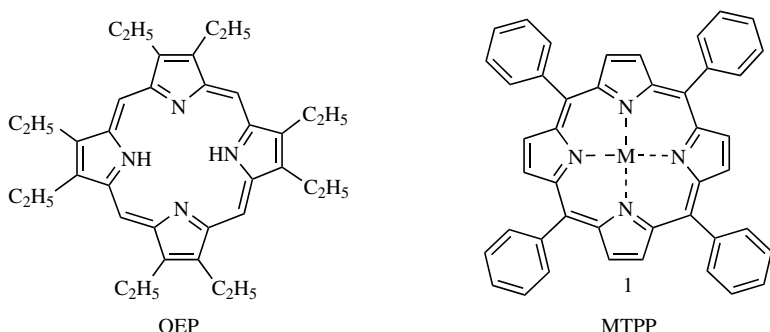
ISRAEL GOLDBERG

*School of Chemistry, Sackler Faculty of Exact Sciences,  
Tel-Aviv University, 69978 Ramat-Aviv, Tel-Aviv, Israel*

- I. Introduction
- II. Molecular Layers Sustained by Weak Interactions
  - A. Open Assemblies Enforced by Dipolar Attractions
  - B. Extended Networks Tessellated by Hydrogen Bonds
- III. Networks Directed by Metal-Ligand Coordination
  - A. Porphyrin Coordination Polymerization without External Auxiliaries
  - B. Polymeric Arrays Tailored by Metal Ion Linkers
    - 1. Pyridylporphyrins as Building Blocks
    - 2. Carboxyporphyrins as Building Blocks
  - C. Interporphyrin Coordination through Organic Ligands
- IV. Concerted Mechanisms of Supramolecular Assembly
- V. Final Remarks
- VI. Acknowledgments
- References

### I. INTRODUCTION

Porphyrins and metalloporphyrins are among the most widely studied chemical systems in solution and in the solid state due to their remarkable structural, thermal and oxidative robustness, interesting photophysical properties, high relevance to catalysis and to electron- and energy-transfer processes. The coordination properties of the metal entity in the center of the porphyrin ring along with tailored functionality of the molecular periphery by suitable substituents provide diverse “programming” elements for the design of



Scheme 3.1.

extended network (supramolecular) materials.<sup>1–2</sup> In addition the flat porphyrin core is characterized by extensive conjugation, and reveals high propensity for characteristic  $\pi$ - $\pi$  stacking interactions (whether between porphyrin molecules or with other aromatic species).<sup>3</sup> Straightforward chemical synthesis affords most readily porphyrin derivatives with either alkyl substituents at the *beta* positions of the macrocycle (e.g., the 2,3,7,8,12,13,17,18-octaethylporphyrin, OEP) or aryl substituents at the *meso* positions of the porphyrin ring (e.g., the 5,10,15,20-tetraphenylporphyrin, TPP; Scheme 3.1). Facile preparative processes of mixed alkyl-aryl porphyrin derivatives and of their metallated products (with metal ions inserted into the porphyrin core) are also available. The square-planar (M)TPP system (**1**; Scheme 3.1) is remarkably stable and thus provides a perfect model compound for application in catalysis, in studies of natural photophysical processes (e.g., as light harvesting antenna devices), and in the design of new materials consisting of multiporphyrin supramolecular assemblies. On the other hand, **1** has a corrugated surface, cannot pack effectively in three dimensions in the condensed crystalline phase, and thus reveals high tendency to form multicomponent systems (clathrates). The latter feature lays the ground work for a tailored construction of composite solids with interesting properties. This review describes the progress made to this end, focusing on the solid state synthesis and structural features of TPP-based solids, from simple clathrate materials, through supramolecular networks, to single-framework porous structures that bear structural as well as functional resemblance to the inorganic zeolites.

The stereochemistry studies of molecular porphyrins in crystals matured more than ten years ago with the systematic evaluation of the molecular structure variants and of the intermolecular organization features of the TPP's. Characteristic core conformations of *meso*-tetraaryl-substituted species, and how they are affected by the presence of axial ligands attached to the metal ion centers or by crystal packing features have been examined in detail by Scheidt et al.<sup>4</sup> Strouse and coworkers explored the structural systematics of the

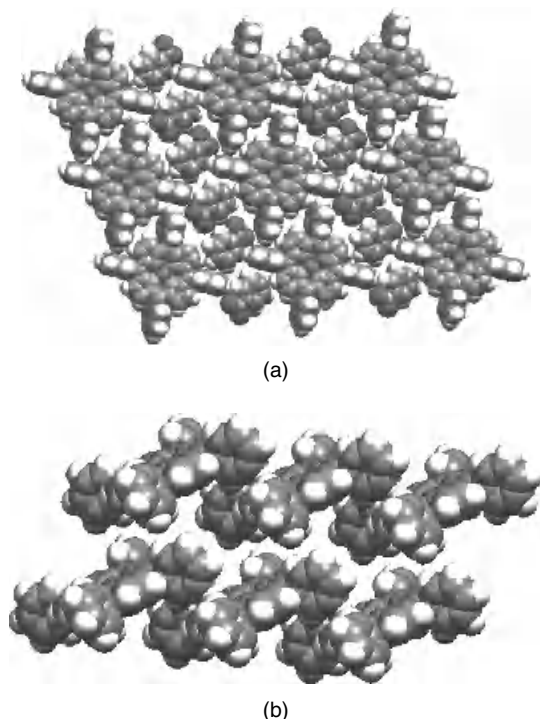


Figure 3.1. (a) Typical layered arrangement observed in clathrates of tetraphenyl metalloporphyrins, with rows of the porphyrin moieties interspaced by rows of nitrobenzene guest molecules. (b) Characteristic offset stacking of the TPP layers in crystals.<sup>5–6</sup>

TPP-based clathrates (examining more than 500 known crystalline compounds), along with the thermodynamic and kinetic properties of guest binding and exchange in these materials.<sup>5–6</sup> They discovered a remarkable conservation of the porphyrin host structure in two-dimensions, observing that the majority of these clathrates contain two-dimensional sheets of porphyrin moieties with guest molecules intercalated within and between the sheets (Figure 3.1). In the absence of any specific interaction between the TPP domains in the crystal other than dispersion forces (within the domains the porphyrins are arranged by stacking interactions in a typical offset-stacked manner), the spacing between them expands or contracts according to the size and shape of the intercalated guest. This imparts a sponge character to these materials, which were hence termed as “expansible porphyrin clathrates” or simply “porphyrin sponges”.<sup>5–6</sup>

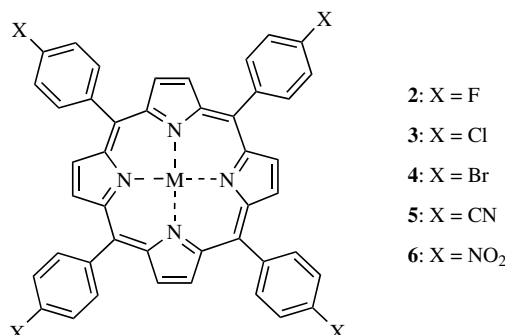
In the last decade considerable effort was devoted to the design and fabrication, by the crystal-engineering approach, of more rigidly assembled supramolecular arrays and of porphyrin-based lattice architectures with better

defined dimensionality, porosity, and guest selectivity. Such modification of the spontaneous buildup of the porphyrin lattice requires suitable functionalization of the metallocporphyrin framework at the core as well as on its periphery, in order to direct the self-assembly process by introducing molecular recognition algorithms. This includes substitution of sensor groups capable of forming specific interactions with the neighboring building blocks (directly or through a bridging metal ion, or through an organic ligand auxiliary) *via* coordination, hydrogen bonding, and/or strong dipolar attractions. Most effective results were obtained when the structural modifications tailored into the TPP system preserved its approximate square-planar geometry. The design strategies for the targeted solid state synthesis of porphyrin-based networks,<sup>7</sup> and the recent developments achieved in this area since 1994, are summarized below.

## II. MOLECULAR LAYERS SUSTAINED BY WEAK INTERACTIONS

### A. Open Assemblies Enforced by Dipolar Attractions

The initial systematic deviation from the basic (M)TPP framework involved the introduction a polar, yet nonprotic, functions at the 4-position of all four phenyl groups. This includes halogen atoms as F, Cl, and Br as well as the nitro and cyano substituents (Scheme 3.2).<sup>8–10</sup> These functions are perfectly suited for invoking the formation of multiporphyrin layers by effective H-bond-assisted dipolar attractions. For example, the linear –CN function is strongly polar and its nitrogen site is a good proton acceptor in hydrogen bonds. Survey of the Cambridge Crystallographic Database shows in fact that the dimeric aggregate of the CN-aryl fragments aligned in an anti-parallel fashion is a very robust supramolecular interaction synthon in organic crystals. Its contribution to the stabilization energy of the intermolecular aggregate was estimated within the



approximate range of 5 to 8 kcal/mol. Similar considerations apply to the polar  $-NO_2$  and halogeno substituents that can also act as acceptors in hydrogen bonds. This functionality, along with the fourfold molecular shape features of the symmetrically substituted porphyrin frameworks (with diminished capacity for competing axial coordination to the porphyrin core), dictates in most cases the formation of layered supramolecular aggregates consisting of flat and *hollow* multiporphyrin assemblies (Figure 3.2a). The porphyrin units within these arrays are interlinked in one or two dimensions by dipolar forces (the perpendicular distance between the anti-parallel aryl-X axes being within 3.4–4.0 Å) assisted

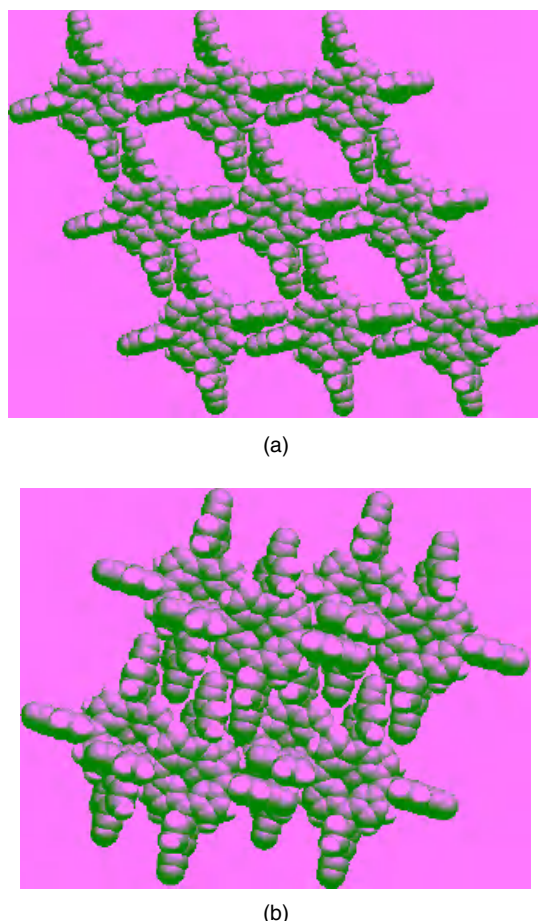


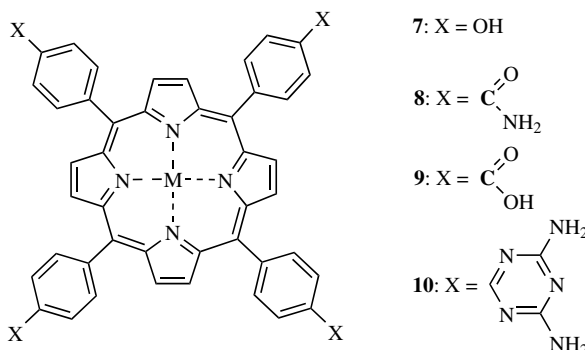
Figure 3.2. (a) Open network formed tetra(4-cyanophenyl)metalloporphyrin, sustained by dipolar attractions assisted by hydrogen bonding. (b) Top view of two overlapping layers, revealing a typical offset arrangement.<sup>10</sup>

by weak C–H···X hydrogen bonding. The layered aggregates, with cavity dimensions affected by the type of the interacting functional groups, give rise to the incorporation of suitably shaped guest components in the crystal. In fact the cavity size characteristics were found to be significantly different in structures based on the tetra(4-fluorophenyl) (**2**), tetra(4-chlorophenyl) (**3**), tetra(4-bromophenyl) (**4**), tetra(4-cyanophenyl) (**5**), and tetra(4-nitrophenyl) (**6**) porphyrin derivatives (Scheme 3.2). The corresponding van der Waals widths of the open space within the interacting chains and networks are 5.0 to 5.5 Å in the halogenophenyl compounds (allowing them to accommodate a flattened aryl moiety or two molecules of smaller guests such as DMSO), and 6.4 to 10.0 Å (suitable to accommodate two chloroform units or two larger aryl entities, respectively).<sup>8–10</sup>

In the crystal, the mixed porphyrin-guest layers stack one on top of the other along a direction normal to the porphyrin plane at regular intervals (typical within a narrow distance range of 4–5 Å) in a typical offset manner (Figure 3.2b).<sup>10</sup> The offset stacking geometry conserved in these structures represents a fundamental property of the porphyrin–porphyrin interaction required to optimize van der Waals stabilization in these solids, in the absence of specific linkages in the axial direction. Evidently many of these materials exhibit limited stability outside their natural crystallization environment. The intercalated guest components act in fact as templates around which the multiporphyrin layered-motifs assemble. Loss of the volatile guest components from the crystal in open air degrades the original three-dimensional lattice (this process may extend over minutes, hours, or days depending on the nature of the component species), often resulting in the formation of other phases as previously observed with the porphyrin sponges.<sup>5–6</sup> However, since upon re-exposure of the deteriorated solid to the vapor or liquid of the same or similar guest species the porphyrin-guest structure is restored, these materials are particularly suitable for guest-release applications.

## B. Extended Networks Tessellated by Hydrogen Bonds

The next stage of these investigations was based on multiple hydrogen bonding interactions as the main molecular recognition algorithm. To this end we introduced several building blocks with different functionalities, which included the 4-hydroxyphenyl (**7**),<sup>8</sup> 4-amidophenyl (**8**),<sup>10b,11</sup> 4-carboxyphenyl (**9**),<sup>12</sup> and 4-(3,5-diaminotriazino)phenyl (**10**)<sup>13</sup> groups (Scheme 3.3). All these building blocks have complementary (i.e., may act simultaneously as proton donors and proton acceptors) and multiple hydrogen-bonding capacity. The cooperative effect of multiple hydrogen bonding is of utmost importance in stabilizing hollow network aggregates in the solid, as the enthalpies of such interactions when considered alone are relatively small (e.g., 5–8 kcal/mol for hydrogen bonds



in a carboxylic acid dimer).<sup>14</sup> Only a cooperative interaction mechanism can provide enough mechanical strength to sustain a large amount of empty space in organic crystals. The actual pattern of the supramolecular assemblies that form in these cases depends also on the nature of the crystallization environment (e.g., pH, presence of solvent with competing H-bonding functions, size of the guest component, which often templates the intermolecular organization, etc.).

The most common mode of H-bonding-assisted assembly of **7** involves self-association through the *cis*-related hydroxyphenyl residues of neighboring moieties. The basic motif is a continuous one-dimensional polymer of linked porphyrin species (Figure 3.3*a*). In some cases these linear porphyrin arrays are sufficiently close to afford direct interporphyrin H-bridges between the chains as well, leading to the formation of two-dimensional arrays. The interporphyrin voids created along the chains are characterized by a van der Waals width of 3.5 Å, suitable to accommodate an aromatic moiety edge-on.<sup>8</sup> As in the previous examples, the crystal structures that form here consist of layered interlinked porphyrin domains which stack one on top of the other in an offset manner. Often the guest components that fill the voids in one layer act also as axial ligands to the metalloporphyrin cores of neighboring layers, thus optimizing the dispersive interactions and imparting stability to the stack-layered architecture. Occurrence of the interlinked porphyrin motif appears to be little dependent on space symmetry and the nature of the occluded guest. Instead of the layered motifs, it is also feasible to induce the formation of supramolecular columnar motifs by replacing the 4-hydroxyphenyl by 3,5- or 2,6-dihydroxyphenyl sensor groups (**11**, **12**; Scheme 3.4).<sup>15</sup> In crystal structures based on the two latter units, large solvent-filled 6 to 7 Å-wide channels are present between the porphyrin molecules (Figures 3.3*b*, *c*). The advantage of the porphyrin columns held together by links between the side arms is that they allow free access to the metalloporphyrin core,

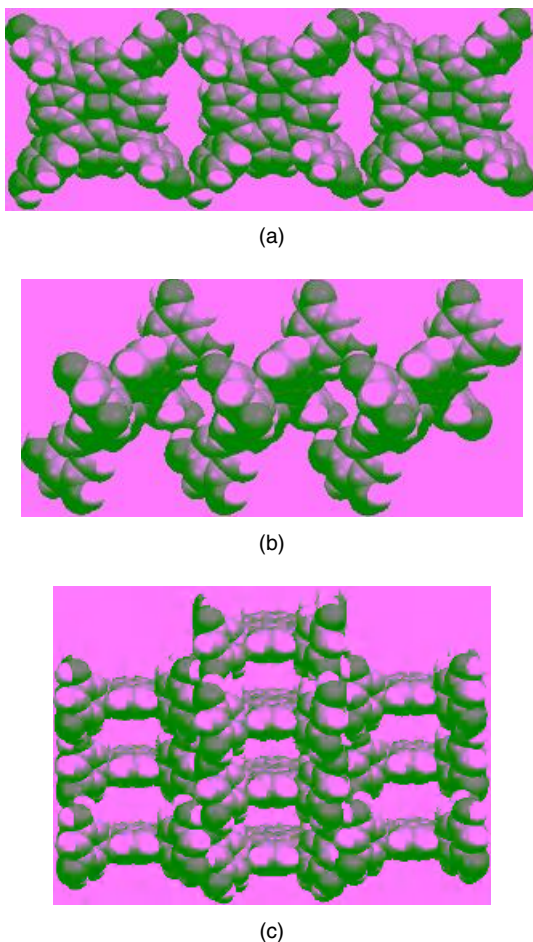
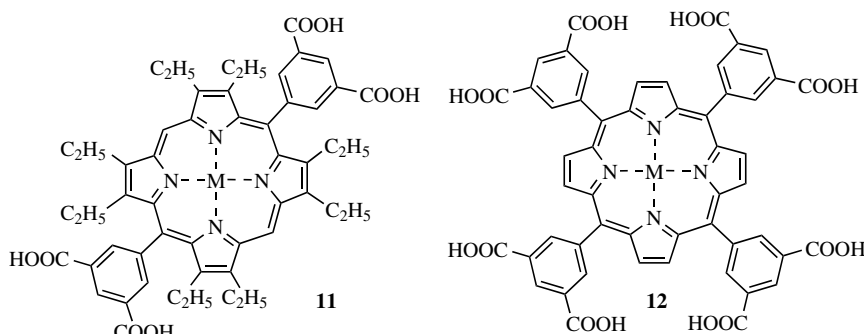


Figure 3.3. (a) Chain formation (which can be extended to layers) by interporphyrin hydrogen bonding of the tetra(4-hydroxyphenyl)porphyrin moieties.<sup>8</sup> Flexible columnar arrangements obtained with porphyrin building blocks bearing the 3,5-dihydroxyphenyl functions are shown in (b) and (c).<sup>15</sup>

which makes these materials potentially suitable as heterogeneous catalysts. This may be severely hampered, however, by the fact that the multiporphyrin columns assemble in a flexible manner rather than in the form of rigid three-dimensional networks.

The hydrogen-bonding interaction pattern of hosts **8** and **9** can be of either the cyclic dimeric or the chain polymeric type, depending to a large extent on the shape of the template applied and the polarity of the crystallization



Scheme 3.4.

environment. A compact layered arrangement of regularly spaced porphyrin units is readily obtained in the presence of small crystallization template moieties. The corresponding motifs form by direct hydrogen bonding between the *cis*-related arms of adjacent species in nearly perpendicular directions parallel to the porphyrin plane, and contain open spaces between the porphyrin connecting units that are accessible to guest molecular components. Suitable examples are provided by networks of Zn-**8** organized by the DMSO template (Figure 3.4a),<sup>10b,11</sup> and networks of Zn-**9** (involving chain-polymeric type interaction between the carboxylic groups of adjacent porphyrins) templated by potassium 18-crown-6 (Figure 3.4b).<sup>16</sup> Correspondingly, the size of the intralayer interporphyrin cavities is  $6.8 \times 10 \text{ \AA}^2$  in the former, and  $8.5 \times 11 \text{ \AA}^2$  in the latter. It is considerably smaller than the size of the individual porphyrin building block, which makes interpenetration of the network patterns improbable. An effective crystal packing of the molecular layers involves offset interlayer stacking (Figure 3.4c). In structures based on **9**, which contain a cationic template, ion-pairing forces stabilize the intermolecular organization as well. It is further facilitated by the absence of separate anionic entities in the lattice, as suitable deprotonation of the porphyrin entity itself accounts for the charge balance, a capacity of utmost importance in the design of porous solids (see below).

Variation of the binding pattern of **9**, from chain-polymeric to cyclic-dimeric, results in the formation of two-dimensional networks with much wider interporphyrin voids (c.  $16 \times 16 \text{ \AA}^2$ ). In these networks every unit interacts with four other porphyrin molecules along the equatorial molecular axes, being involved in eight O–H…O hydrogen bonds (Figure 3.5a). Here the interporphyrin cavities are already larger than a single square-shaped monomeric unit of the hydrogen-bonded polymer (the approximate van der Waals dimensions of **9** are  $12 \times 12 \text{ \AA}^2$ ). Thus, in the absence of a suitable

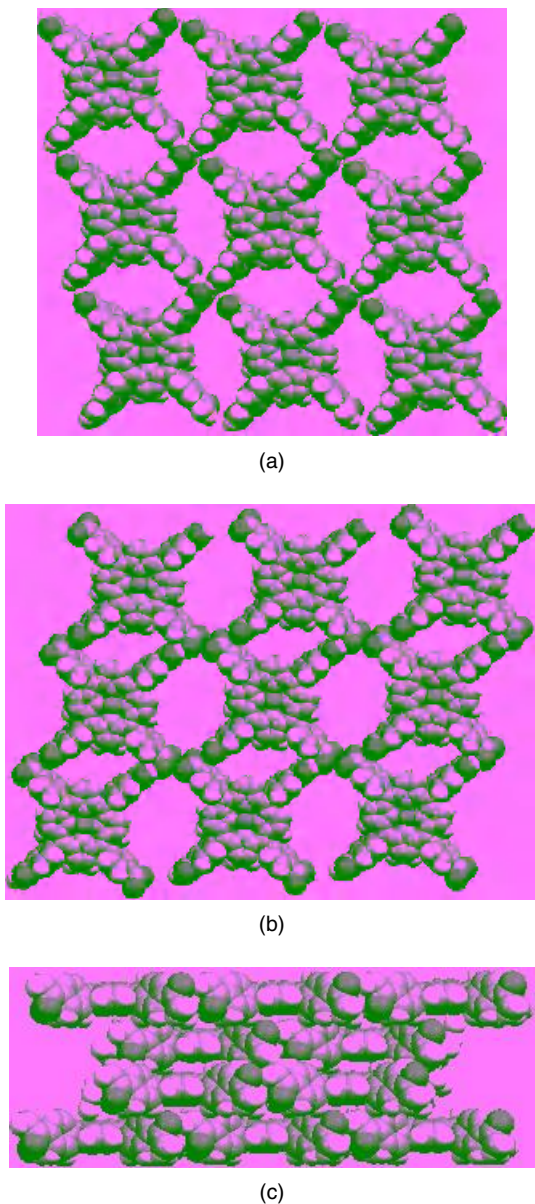
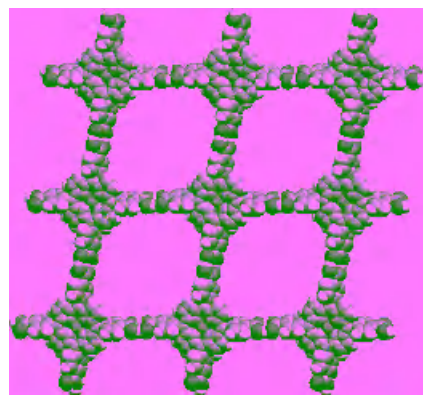
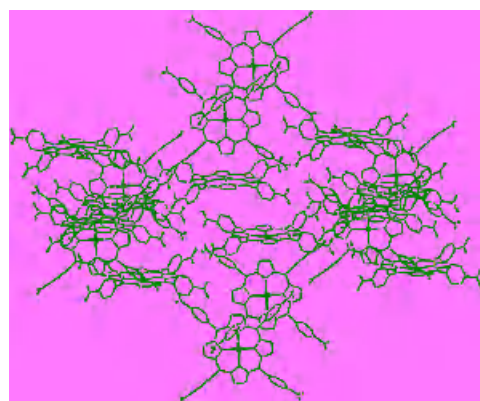


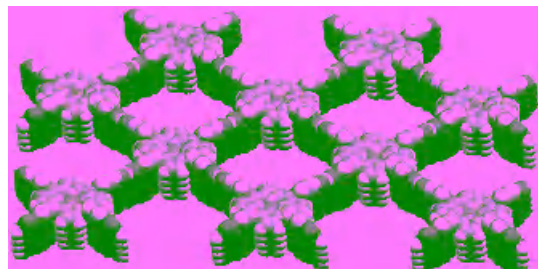
Figure 3.4. Open networks with relatively small interporphyrin cavities formed by the (a) tetra(4-amidophenyl)porphyrin,<sup>11</sup> and (b) tetra(4-carboxyphenyl)porphyrin building blocks.<sup>16</sup> Stacking of such flat networks along the axial direction normal to the porphyrin layers is depicted in (c).



(a)



(b)



(c)

Figure 3.5. (a) Multiply hydrogen-bonded network of the tetra(4-carboxyphenyl) metalloporphyrin with 16 Å wide voids.<sup>17</sup> (b) Illustration of crystal structure in which such networks doubly interpenetrate into one another. (c) View of a molecular sieve-type structure in which the hydrogen bonded layers are tightly stacked in a parallel manner, creating open channels propagating through the crystal. See color insert.

template, these networks mutually interpenetrate (doubly) each another in order to fill the void space (Figure 3.5*b*).<sup>12</sup> The use of sizable templating agent with low tendency to interact with Zn-**9**, in the form of tetra(aminophenyl)porphyrin, finally led to a unique layered structure in which the wide open networks do not concatenate (Figure 3.5*c*).<sup>17a</sup> In the resulting solid the H-bonded layers stack in a largely overlapping manner along the normal direction, at an average distance of 4.7 Å. As a result it contains 15 Å wide channels that propagate through the crystal, and can accommodate a noninteracting lipophilic solvent within them. The stacked organization of the layers occupies less than 40% of the crystal volume. With a nitrobenzene guest molecule occluded within the channels the structure is, however, remarkably stable, preserving its crystallinity up to 80°C. The observed crystalline architecture resembles features of common molecular-sieve materials. Nearly identical assembly formed in the solvothermal reaction of **9** with FeCl<sub>2</sub>—to yield Fe(Cl)-**9**—in glacial acetic acid and in the presence of KOH as a base and ytterbium acetate as a template.<sup>17b</sup>

Formulation of extended network motifs with even larger void volumes has been achieved by incorporation of the diaminotriazine functions to the TPP building blocks in **10**. These sensor groups have much higher H-bonding capacity and spatial flexibility than the carboxylic group. Molecules of **10** assemble into flat multiporphyrin networks with unprecedently large voids of 22 × 22 Å<sup>2</sup>, where every porphyrin unit is involved in eight intralayer hydrogen bonds (Figure 3.6*a*).<sup>13</sup> Evidently the size of the monomeric **10** is considerably smaller. As no suitable template could be found in this case, the interweaving of such open networks could not be avoided. However, the resulting structure still represents a molecular sieve type material with straight 6 Å wide channels, which propagate through the crystal between the interwoven networks (Figure 3.6*b*). These channels are readily accessible to guest solvent components as THF or DMF.

### III. NETWORKS DIRECTED BY METAL-LIGAND COORDINATION

#### A. Porphyrin Coordination Polymerization without External Auxiliaries

Formation of polymers of tetraarylporphyrins by direct coordination requires their functionalization on the periphery by effective sites for metal ligation, along with the presence of metal ions with five or six coordination preference in the porphyrin core. In this manner bonding association of the peripheral substituents of one porphyrin to the metal ion cores of neighboring units may occur. Pyridyl-type functions (along with other groups containing N: sites) are

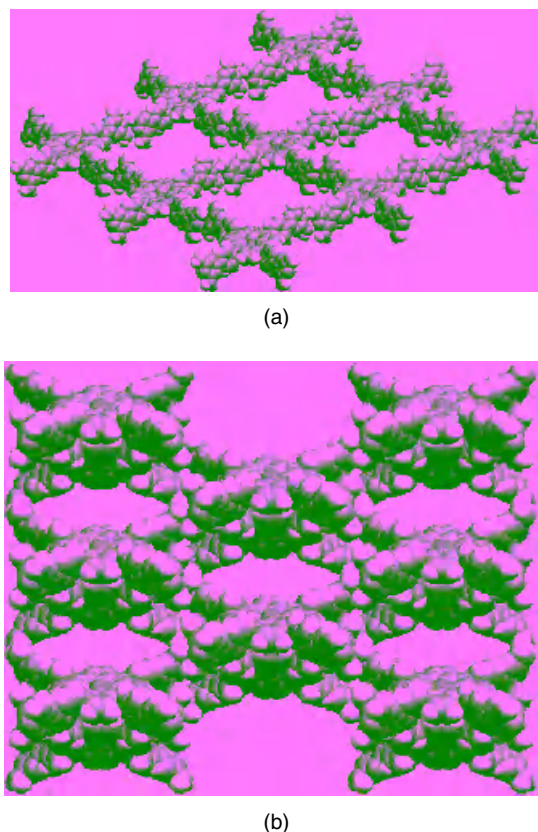
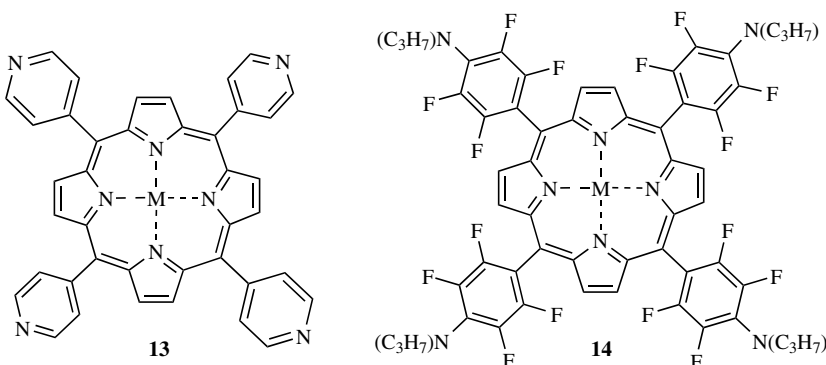


Figure 3.6. (a) Multiply hydrogen-bonded networks of porphyrin **10**, characterized by 22 Å wide voids.<sup>13</sup> (b) Illustration of the crystal structure of **10** perforated by 6 Å wide voids, showing interpenetration of the layered multiporphyrin networks.

particularly suitable to his end (**13–14**; Scheme 3.5), as they tend to coordinate readily to divalent zinc and other metal ions. Ligation of pyridyl moieties to the metal center of metalloporphyrins, and their utilization in templated synthesis have previously been reported.<sup>18</sup> A pioneering work in this area was carried out by Fleischer and coworkers who introduced the mono-, di-, and tetra-pyridylporphyrin moieties and studied extensively their self-assembly features in solution as well as in the solid state.<sup>19</sup> The crystal formation of chain coordination polymers by the monopyridyl and tetrapyridyl zinc-porphyrins<sup>19–20</sup> and their tetra-(*o*-nicotinamidophenyl)-Fe-porphyrin analogue<sup>21</sup> have been confirmed.



Scheme 3.5.

The tetrapyridyl-metallocporphyrin unit (**13**), and to a lesser extend the tetra(4-cyanophenyl)porphyrin (**5**) have become since then very attractive building blocks for the construction of polymeric materials (see below). Several milestone publications on crystalline coordination polymers of TPP's, which highlighted the potential of these materials in the formulation of new porous solids, appeared about ten years ago and stimulated extensive research on extended porphyrin networks. They include the synthesis of crystalline *homogeneous* polymers of **13** that consist of a single-framework porous architecture.<sup>20</sup> Important pioneering discoveries were made by Robson et al., who characterized *heterogeneous* coordination polymers of **5** and **13** that are sustained by metal ion bridging auxiliaries;<sup>22</sup> these will be discussed in Section III.B below.

In the former case we showed that Zn-**13** readily self-assembles in polar solvents into a uniquely structured three-dimensional single-framework coordination polymer, through direct interporphyrin interaction, where the pyridyl function of one unit binds to the metal center of a neighboring unit.<sup>20</sup> In this self-complementary coordination scheme, each molecule coordinates to four other species by attracting the pyridyl ligands of two neighboring units to its zinc metal center, while donating two of its own pyridyl functions to two other metallocporphyrin cores. The resulting polymer reveals high thermal stability (up to about 400 °C), and is characterized by honeycomb architecture. It represents the first published example of a stable porphyrin-based molecular sieve material with nearly 6 Å wide channels, capable of adsorbing and desorbing in a reversible manner small polar molecules (Figure 3.7a). Identically structured polymers with similar properties based on Co-**13** and Mn-**13** building blocks could be constructed as well.<sup>23</sup> The metal ions that reside within the porphyrin core of these compounds are six-coordinate. Recently we reported also another ladder-type homogeneous coordination polymer of Zn-**13**, which is composed of two

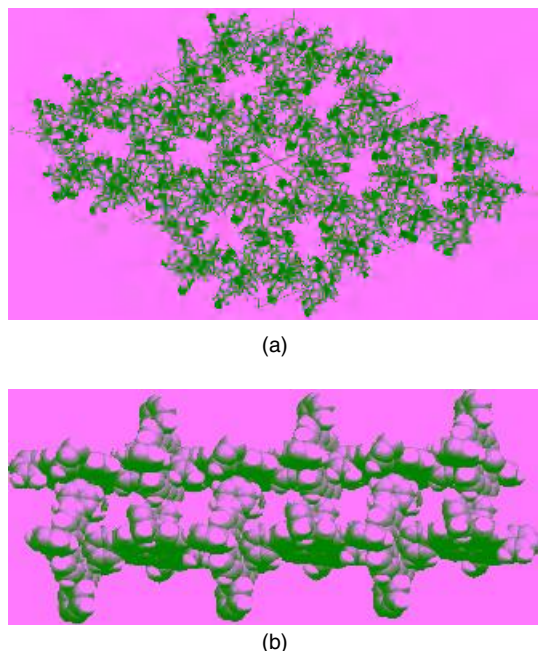


Figure 3.7. (a) Illustration of the honeycomb molecular sieve structure of Zn-13, with open channels propagating through the structure, viewed down the channel axis.<sup>20,23</sup> (b) Ladder-type assembly of Zn-13, consisting of five-coordinate and six-coordinated metalloporphyrin units.<sup>24</sup>

crystallographically independent porphyrin units oriented perpendicularly to one another, one with a five-coordinate and the other with a six-coordinate zinc ion.<sup>24</sup> These two species are arranged in an alternating manner along the polymer, each of the building blocks having three connections to the neighboring molecules (Figure 3.7b). The polymeric ladders are arranged in the crystal structure parallel to one another. They incorporate open interporphyrin voids, with cross section van der Waals dimensions of approximately  $4\text{ \AA} \times 5\text{ \AA}$ , which are accommodated by noncoordinated guest species. More recently reaction of **13** with ferrocene under solvothermal conditions resulted in iron insertion into the porphyrin core and self-coordination of the metalloporphyrin species into a homogeneous coordination polymer of Fe<sup>II</sup>-**13**.<sup>25</sup> It forms a layered structure with two-dimensional paddle-wheel-like pattern. The coordination geometry around each iron center is octahedral, with the pyrrole groups of the porphyrin ligand occupying the equatorial positions, and two pyridine nitrogen atoms from adjacent porphyrin entities occupying the axial sites. In the resulting network all neighboring porphyrins are mutually perpendicular to each other. These solid polymers reveal a remarkable thermal stability, and their structures remain intact up to 550°C under

a nitrogen atmosphere.<sup>25</sup> A very similar two-dimensional coordination pattern was obtained when the Fe-**13** building block was replaced by tetra(4-*n*-propylamino-tetrafluorophenyl)porphyrinato-zinc(II) (**Zn-14**), wherein the pyridyl functions were replaced by the secondary amine groups.<sup>26</sup> It also represents a two-dimensional network composed of hexacoordinated chromophores orthogonally oriented with respect to one another.

Suitably metallated porphyrin-**5** can also self-coordinate, to afford polymeric structures. However, the lower basicity and ligating capacity of the cyano functional groups allows for the formation of open structure with diminished stability.<sup>10a</sup> A homogeneous two-dimensional coordination polymer composed of the Mn-**9** unit has been constructed more recently as well, by controlled crystallization from polar but aprotic reaction mixture (see below).<sup>27</sup>

## B. Polymeric Arrays Tailored by Metal Ion Linkers

### 1. Pyridylporphyrins as Building Blocks

The formulations of porphyrin-based polymeric assemblies by coordination could be immensely diversified by the use of external metal ion auxiliaries of bridging capacity between suitably functionalized building blocks. External linkers with different coordination preferences can be used, and they are less affected by steric constraints of interporphyrin packing in the crystal, which enhances the propensity of forming stable polymeric aggregates. Porphyrin **13** served as a perfect platform to this end, being capable of forming relatively strong multiple bonds to a large variety of metal ions. Not surprisingly, such coordination chemistry of porphyrins has therefore been widely studied not only in the solid state but also in solution. In this context the work published by Robson et al. in 1991 and 1994 represents outstanding examples of Pd<sup>II</sup>-**13** and Cu<sup>II</sup>-**13** porphyrin three-dimensional frameworks sustained by linear Cd<sup>II</sup> and tetrahedral Cu<sup>I</sup> linkers, respectively.<sup>22a,b</sup> While the Pd<sup>II</sup>-**13** structure is relatively dense, the crystalline lattice of the Cu<sup>II</sup>-**13** material contains >1 nm wide channels propagating through the crystal that are occupied by disordered anions and nitrobenzene solvent species (Figure 3.8). It was reported, however, that upon removal of the solvent, the lattice collapses, which makes it unsuitable for molecular sieve-type applications.

Robson's report was soon followed by extended studies from other investigators, using the same porphyrin building block but other metal ion linkers. The preparative procedures have been diversified as well from conventional crystallizations to hydrothermal/solvothermal reactions. The latter lead often to the formation of metal ion clusters, which may represent even stronger linkers than individual metal ions. A noteworthy example is the self-assembly of rigid microporous organic-inorganic hybrid frameworks constructed from Cu<sup>II</sup>-**13** and Fe<sup>II</sup>-**13** and bimetallic oxide chains and oxide clusters such as Cu<sub>2</sub>Mo<sub>3</sub>O<sub>11</sub> and Fe(Mo<sub>6</sub>O<sub>19</sub>)<sub>2</sub>.<sup>28</sup> In the former case, the two Cu bridges exhibit square-pyramidal CuN<sub>2</sub>O<sub>3</sub> and octahedral CuN<sub>2</sub>O<sub>4</sub>

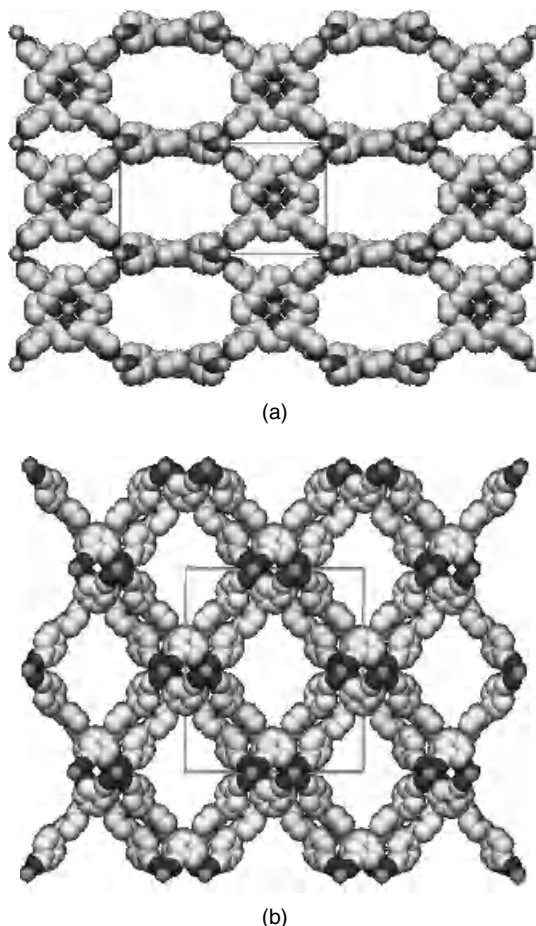
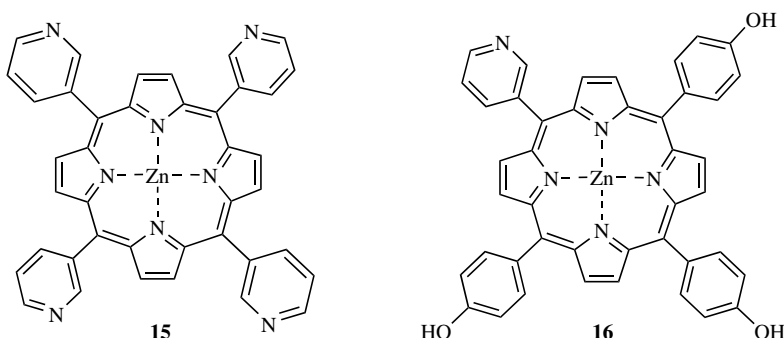


*Figure 3.8.* Open coordination networks with large channel voids sustained by external Cu-ion auxiliaries based on (a) porphyrin **13**, and (b) porphyrin **5**.<sup>22b</sup>

ligation through coordination to the pyridyl nitrogens of adjacent porphyrins and the molybdenum-oxo groups. The iron compound represents a more diversified case, as the metal center within the porphyrin core exhibits additional axial coordination from above and below to a pyridyl nitrogen atom from two adjacent porphyrin units. As a result, the external iron auxiliary links between the pyridyl groups of six converging porphyrins adapting an octahedral coordination environment. The large voids generated within such interconnected lattice are accommodated by the  $\text{Mo}_6\text{O}_{19}$  anionic clusters and water solvent.<sup>28</sup> Solid-state supramolecular arrays of free-base **13** tessellated by heavy metal (Cd, Hg, and Pb) halides were reported as well.<sup>29,30</sup> These form either one-dimensional chains or two-dimensional, highly-organized

polymeric arrays. It was shown that the porphyrin cores within these networks can be additionally populated by various metal cations without distorting the supramolecular arrangement. The tunable mix-metallated content of the multiporphyrin arrays can be particularly relevant to the design of light-harvesting model systems and sensor materials.<sup>29</sup> The noncomplementary crystal packing of the multichromophoric arrays allows commonly for the inclusion of variable amounts of guest solvent components in the interporphyrin voids of the lattice. Similar reactions of different silver salts with free-base **13** and Zn<sup>II</sup>-**13** have led to multiporphyrin architectures interlinked by silver ion bridges.<sup>31,32</sup> Depending on reaction component stoichiometries and the crystallization conditions, it is possible to obtain one-dimensional linear chains,<sup>32</sup> noninterpenetrating two-dimensional square grids, as well as interpenetrating three-dimensional nets.<sup>31</sup> The latter structures turn out to be quite robust, although they exhibit interporphyrin voids that consist more than 50% of the crystal volume partly occupied by reversibly removable guest solvent molecules. Evaporation of the latter by slow heating results in a progressive loss of crystallinity, but which can be readily restored by immersion of the depleted crystals in solution of the guest component. The versatility of the silver cation affords a variety of coordination geometries in these compounds: linear two-coordinate, T-shape three-coordinate, and square-planar four-coordinate, giving rise to somewhat unusually modulated supramolecular patterns of the porphyrin assemblies.<sup>31</sup>

Porphyrin **13** and its functional variants were found to be useful for the synthesis of high-order, yet discrete, supramolecular assemblies (“porphyrin supermolecules”) mediated by one or two different transition metals. For example, various pyridine-containing porphyrin derivatives were applied to the syntheses of molecular squares, sandwiches, and hollow capsules utilizing Pd, Re, and Ru metal ions as external linkers.<sup>33–37</sup> The capsules (based in one case on the tetra(3-pyridyl)porphyrin building blocks—**15**; Scheme 3.6) have a prismlike cage structure with hydrophobic interior lined by the porphyrin macrocycles, capable of accommodating neutral organic molecules.<sup>33</sup> A most recent example in this area



*Scheme 3.6.*

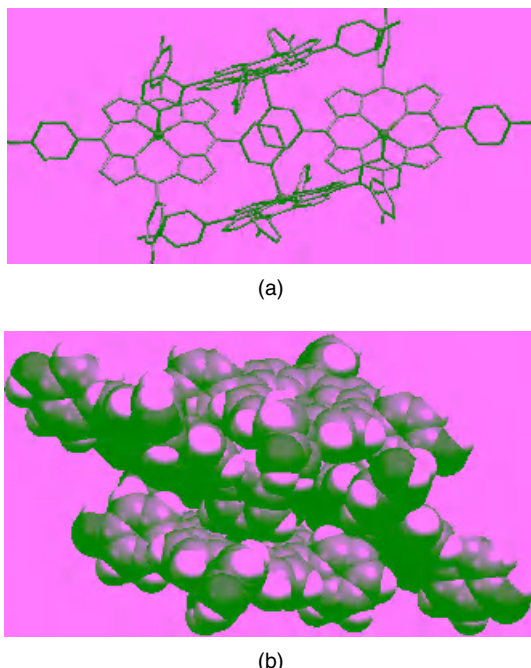


*Figure 3.9.* A cyclic discrete tetramer of zinc-(3-pyridyl)-tri(4-hydroxyphenyl)porphyrin **16** illustrated in (a) wire-frame, and (b) space-filling representations.<sup>38</sup> The van der Waals dimensions of this oval-shaped species are  $3.5 \times 2.1 \times 1.6$  nm.

relates to the successful synthesis of a nanosized cyclic tetramer of zinc-(3-pyridyl)-tri(4-hydroxyphenyl)-porphyrin (**16**; Scheme 3.6, Figure 3.9).<sup>38</sup> In this case the 3-pyridyl function was used for convergent interporphyrin coordination, while the hydroxyphenyl functions served to stabilize the interparticle organization and facilitate the formation of ordered solids. Indeed, in many potential applications the carefully programmed self-assembly of macroscopic arrays and tapes of the discrete pyridyl-porphyrin supermolecules is of particular interest.<sup>37a</sup> Further discussion of the discrete systems is, however, beyond the scope of this review article.

## 2. Carboxyporphyrins as Building Blocks

Although the mononuclear and polynuclear metallocarboxylate complexes are abundant among organometallic compounds, they were introduced to porphyrin supramolecular chemistry only about five years ago.<sup>39</sup> In the present context we have shown that the tetra(carboxyphenyl)-metalloporphyrin (**M-9**) moiety is an extremely versatile building block for effective supramolecular assembly of new

polymeric materials. It can self-assemble into a supramolecular aggregates via diverse intermolecular interaction mechanisms, including cooperative hydrogen bonding (see above), direct porphyrin-to-porphyrin coordination, as well as with the aid of external metal-ion linkers.<sup>27</sup> This is illustrated for Mn-9 in Figure 3.10.

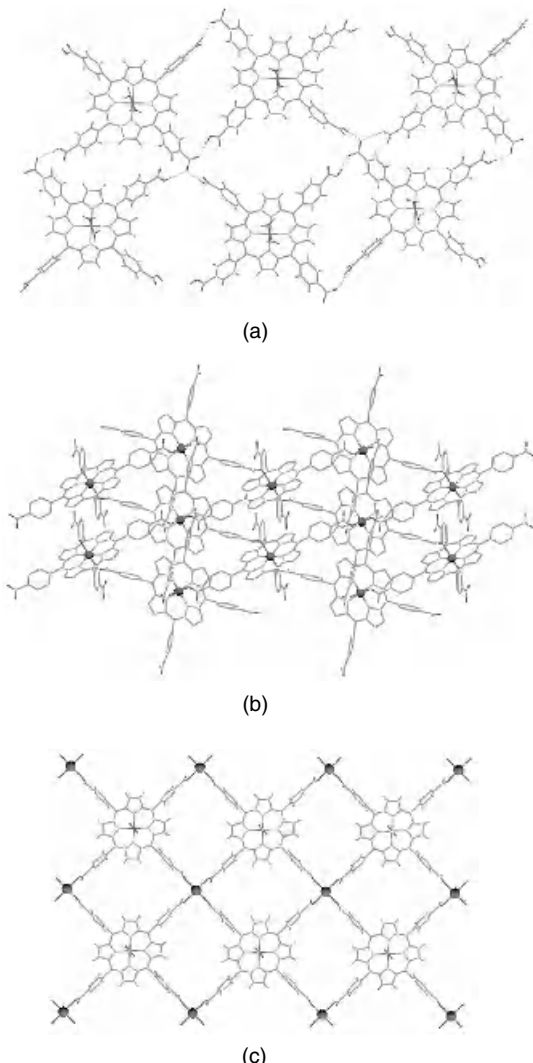
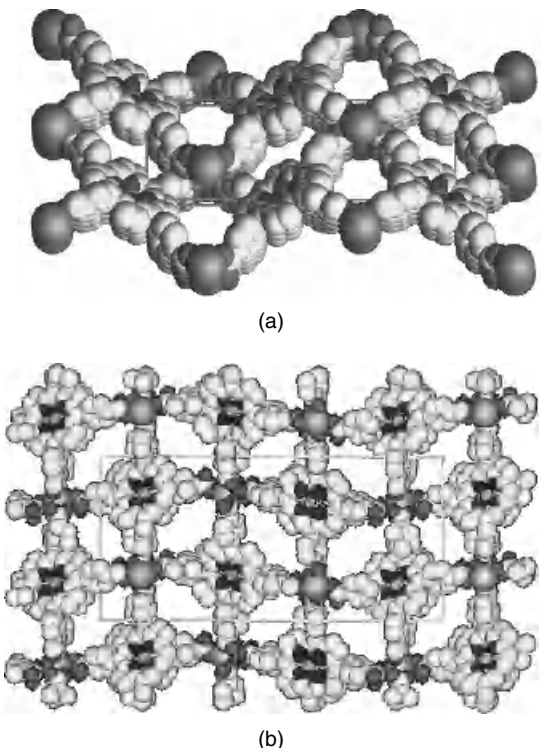


Figure 3.10. Illustration of the versatile self-assembly modes utilized by the Mn-9 building blocks.<sup>27</sup> (a) An array of multiply hydrogen bonded Mn(H<sub>2</sub>O)<sub>2</sub>-9. (b) Two-dimensional coordination polymer of Mn-9. (c) Intercoordination of Mn(H<sub>2</sub>O)<sub>2</sub>-9 units through exocyclic K<sup>+</sup> auxiliaries (unpublished results). See color insert.

In some respects the use of **9** in the formulations of the hybrid organic-inorganic coordination polymers is advantageous compared to that of **11**. Thus the carboxylic groups of **9** can be readily deprotonated in neutral and basic environments to yield anionic porphyrin units, and balance the charge of the cationic metal bridges. This attraction leads to an enforced coordination of synthons assisted by ion pairing interactions, and eliminates the need to incorporate into the crystalline lattice external anionic moieties, thus enhancing the propensity of forming open architectures. The metal cations can readily interact with, and bridge firmly between, the deprotonated carboxylic functions of several adjacent building blocks. The geometry of this interaction of synthons is affected by the preferred coordination environment of the metal centers, and whether the bridging elements consist of single ions, clusters of ions, or metal-ion complexes. Different auxiliaries have been successfully applied thus far in formulations of coordination polymers based on the carboxyphenyl porphyrins. These include the  $\text{Na}^+$ ,<sup>39-41</sup>  $\text{K}^+$ ,<sup>40,42</sup>  $\text{Ca}^{2+}$ ,<sup>43</sup>  $\text{Co}^{2+}$ ,<sup>44</sup>  $\text{Cu}^{2+}$ ,<sup>42</sup>  $\text{Zn}^{2+}$ ,<sup>39,45</sup>  $\text{Pd}^{2+}$ ,<sup>42</sup> and  $\text{Pt}^{2+}$ ,<sup>42</sup> ions or ion clusters, as well as complexes such as  $[\text{Cu}(\text{NH}_3)_6]^{2+}$ .<sup>42</sup> The dimensionality and topology of the polymeric networks that form is affected to a large extent by the composition and preferred coordination geometries of the bridging elements and clusters.

The free-base **9** and its Cu-, Pd-, and Pt-complexes, which lack axial coordination capacity, in combination with other metal ions as external tessellating auxiliaries (e.g.,  $\text{Cu}^{2+}$ ,  $\text{Na}^+$ ,  $\text{K}^+$ ) self-assemble into flat (either planar or somewhat wavy) open polymeric networks with about 5 Å wide interporphyrin cavities.<sup>39,41,42</sup> Sometimes, the Zn-**9** porphyrin also yields flat-layered assemblies, the either four-coordinate or five-coordinate (with an axially attached water or methanol) zinc ion in the center of the porphyrin core playing no role in the intermolecular organization mechanism. The immediate environment around each porphyrin building block in these assemblies is characterized approximately by a square planar symmetry. Tight overlapped stacking of such layers (typically with interlayer separation of about 4.5 Å) yields extended channel voids that propagate through the crystal, and are selectively accessible to exchangeable guest species of suitable size (Figure 3.11). We found that the alkali metal-ion bridges, while maintaining the layered porphyrin organization, can also be uniformly displaced between, rather than contained within, the layers.<sup>41</sup> Moreover they can appear as dinuclear or polynuclear, rather than mononuclear, clusters. This allows for a more complex connectivity, as the metal bridges may now link between porphyrin units located within a given layer as well as in different layers. This gives rise to a bilayered or multilayered connectivity in the structure and adds robustness to it.<sup>41</sup> Interestingly, most of these porphyrin-layered polymeric architectures reveal porosity features and resemble molecular-sieve materials. They contain 4 to 5 Å-wide channel voids that propagate through the corresponding crystals perpendicular to the porphyrin layers, and are accommodated by noncoordinated guest solvent components.



*Figure 3.11.* Typical aggregation patterns based on either free-base or metallated porphyrin **9**, sustained by  $\text{Na}^+$ -ion linkers, which yield molecular sieve-type structures perforated by 5 Å wide channel voids.<sup>41</sup>

The metal-assisted formation of the multiporphyrin coordination polymers can be diversified by changing the nature the bridging auxiliaries. The use of metal-ion complexes, for example, instead of metal ions, provides larger connectors, thus increasing the spacing between the porphyrin building blocks and widening the interporphyrin channel voids. This phenomenon is illustrated by the structure assembled from Pt-**9** units and  $\text{Cu}(\text{NH}_3)_6$  bridging cations in Figure 3.12a.<sup>42</sup> This porphyrin sieve is characterized now by 6.5 Å wide open channels accessible to other components that propagate through the structure. The nature of the interporphyrin organization can be further modified by applying bridges of different coordination directionality. A suitable example is provided by the  $\text{Zn}^{2+}$ -ion linker, which exhibits a tetrahedral coordination environment. Indeed, the self-assembly reactions of Zn-**9**, Pd-**9**, and Pt-**9** templated by the zinc external auxiliary lead to open three-dimensional diamondoid-type architectures.<sup>39,45</sup> To fill space, the formation of a thermodynamically stable, condensed crystalline phase is most often associated with interweaving of the diamondoid networks into one another.

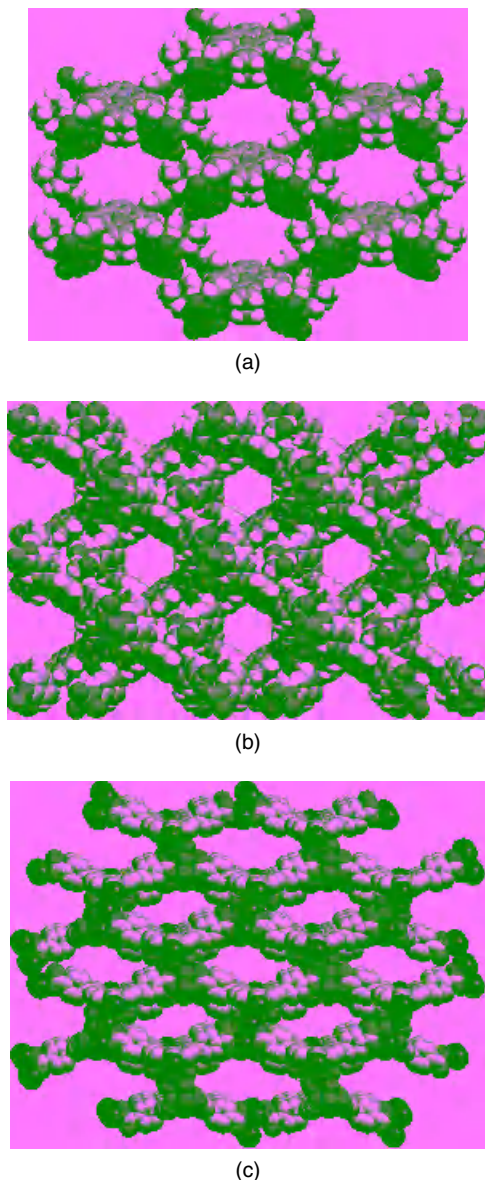


Figure 3.12. Open crystalline architectures consisting of hybrid organic-inorganic coordination polymers of the M-9 unit interlinked by metal ions, metal complexes, or metal ion clusters. (a) Networks of Pt/Pd-9 sustained by Cu(NH<sub>3</sub>)<sub>6</sub> complexes with 6.5 Å wide channels.<sup>42</sup> (b) Diamondoid lattice of Zn-9 tessellated by Zn<sup>2+</sup> ions.<sup>39</sup> The van der Waals cross section of the channel voids is around 7.5 Å. (c) Zeolite-type structure of Co-9 tailored by clusters of cobalt ions.<sup>44</sup> The width of the open channels that propagate through the structure is ≥10 Å.

The geometrically rigid diamondoid organization of Zn-**9** tailored by external zinc ions is depicted in Figure 3.12b.<sup>39</sup> The host framework occupies only about 40% of the crystal volume, and contains continuous channels of approximately 7.5 Å van der Waals diameter that penetrate the crystal between the interlocked polymeric arrays with tetrahedral zinc-ion nodes. Furthermore higher enthalpic stabilization (mostly due to larger electrostatic contribution) can be achieved by interporphyrin bridging entities that consist of metal clusters rather than single ions. This was recently demonstrated by mixing **9** with cobalt-ion auxiliaries under solvothermal conditions in a basic environment.<sup>44</sup> During this reaction metallation of the porphyrin core by Co<sup>2+</sup>, as well as intercoordination of porphyrin species by clusters of the cobalt ions, occurred simultaneously. The Co<sup>2+</sup> ions are too small to fill effectively the cavity within the porphyrin macrocycle, thus allowing for its considerable distortion from planarity. These features lead to the formation of a single-framework three-dimensional intercoordinated architecture, which consists of bent metalloporphyrin entities tessellated to each other by trimeric clusters of the cobalt ions. The resulting solid represents a zeolite-type material. It is thermally robust, containing large tridirectional channels with cross sections of nearly nanometric dimensions (Figure 3.12c). It reveals a remarkably high affinity for water and amines, and is capable of removing effectively (by sorption of the porphyrin lattice) water from common organic solvents.<sup>44</sup> The potential applications of the other polymeric network materials in molecular sieving or slow-release processes have not been fully explored as yet.

### C. Interporphyrin Coordination through Organic Ligands

Organic ligands can also provide a very attractive tool for the tessellation of multiporphyrin assemblies by axial bridging between the centers of adjacent metalloporphyrin units by metal-ligand coordination, and/or by equatorial hydrogen bonding between the peripheral sensor groups of neighboring units. Bidentate amines, particularly those of the bipyridyl type, reveal high affinity for transition metals as well as for hydrogen bonding. “Shish-kebab” type chain polymers with alternating Mn-porphyrin (with six-coordinate metal centers) and bipyridyl ligand units along it, as well as oligomeric species of ligand-bridged dimers of, for example, Zn-porphyrin (with five-coordinate metal centers), are particularly well known to this end.<sup>11,46</sup> Such linear coordination polymers when composed of cationic Mn<sup>3+</sup>-porphyrin and bridging radical anions were shown to be relevant, for example, as organic magnets.<sup>47</sup>

In a different study, the reactions of Zn-**7** with a variety of bipyridyl ligands, have led to a series of products of different porphyrin-ligand stoichiometries. This resulted mainly from the possibility to bridge the protic porphyrin entities to each other by the organic linkers not only in the axial direction, but also sideways via cooperative O—H···N bonds.<sup>48</sup> Figure 3.13a gives a representative example

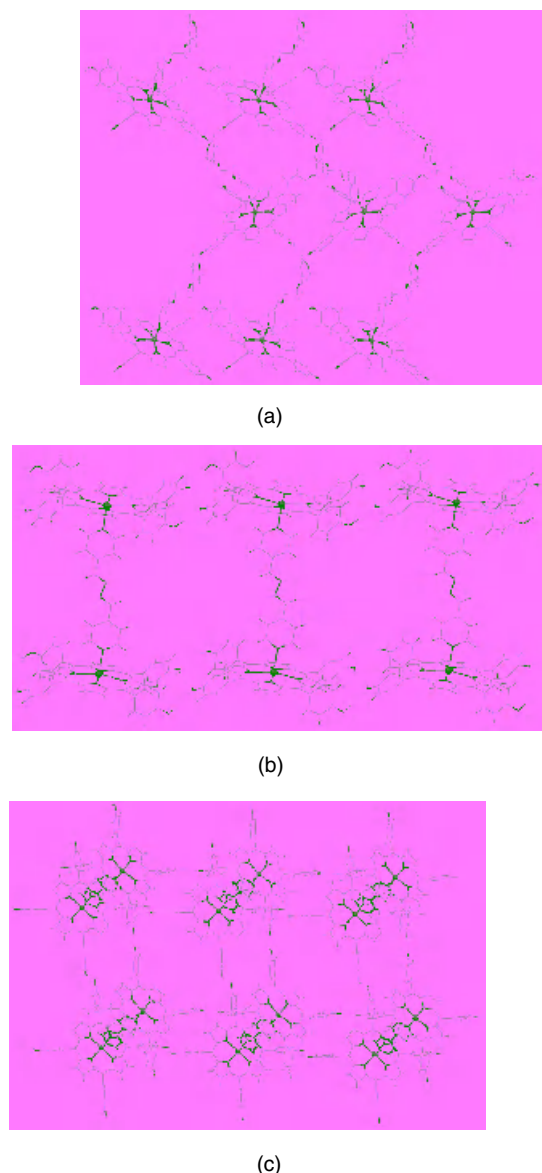


*Figure 3.13.* Various network arrays formed by porphyrin 7 with the aid of bipyridyl-type bridging ligands, exhibiting a concerted metal-ligand coordination and cooperative hydrogen-bonding mechanism.<sup>48</sup> (a) Axial coordination and lateral hydrogen bonding of the porphyrin units through the ligand auxiliary. (b) Hydrogen-bonded chains of porphyrin dimeric entities intercoordinated axially by the ligand. (c) Two-dimensional arrays of  $(7)_2$ -bipyridyl units stabilized by porphyrin-porphyrin hydrogen bonds. See color insert.

of an open multiporphyrin assembly mediated axially as well as equatorially by bridging ligands *via* cooperative hydrogen bonding, in which the hydrogen bonding features of the interacting components are used to capacity. It represents also a realization of a supramolecular assembly of porphyrin-based materials by a concerted molecular recognition algorithm to afford an extended noncovalent connectivity in three dimensions. The latter issue is referred to in more detail in the next section.

#### IV. CONCERTED MECHANISMS OF SUPRAMOLECULAR ASSEMBLY

The fabrication of multiporphyrin networks exploits the square-planar symmetry of the flat porphyrin unit, the diverse cooperative and convergent molecular recognition algorithms (other than dispersion forces) tailored into the porphyrin building blocks, and the use of external metal-ion and organic-ligand auxiliaries for induced coordination and organization. In addition to materials the formation of which is directed primarily by either hydrogen-bonding (Section II) or metal-ligand coordination (Section III), further crystal-engineering efforts involved a concerted expression of two or more different interaction synthons in a single material. From the crystal-engineering point of view, several different concerted mechanisms of porphyrin-based network formation are feasible to this end. They include mainly (1) direct interporphyrin hydrogen bonding in the equatorial directions, along with axial intercoordination between the porphyrin moieties through a bridging organic ligand, (2) peripheral coordination of the porphyrins through metal ion linkers, combined with axial intercoordination through a bridging ligand, and (3) equatorial as well as axial interporphyrin association through organic ligand auxiliaries. These syntheses require functionalized metalloporphyrin building blocks with metal ions having axial coordination capacity (e.g., as  $Zn^{2+}$ ,  $Mn^{2+}$ , or  $Mn^{3+}$ ), and with peripheral functions attached to the macrocycle with favorable hydrogen bonding (e.g., as PhOH in **7** or PhCOOH in **9**) or coordination (e.g., as pyridyl in **13**, and PhCOOH or PhCOO<sup>-</sup> in **9**) capacities.

The above-mentioned possible combinations of intermolecular interaction synthons for the assembly of multiporphyrin networks are illustrated by the following representatives examples. In the structures obtained by reacting Zn-**7** with bipyridyl ligands a combined mechanism of axial coordination to the zinc ions of neighboring porphyrins and lateral multiple hydrogen bonding provides the organizing force for the network assembly of the component species. The hydrogen-bonding linkage may take place either directly between the porphyrin entities (Figures 3.13b, c), or through the bipyridyl bridges with their N-sites acting as proton acceptors, or both (Figure 3.13a). The thermodynamic lability of these interactions allows for spontaneous interpenetration of the open polymeric

arrays into one another, and full utilization of the self-complementary molecular recognition elements during crystallization. These architectures still contain wide intra-lattice voids accessible to solvent nitrobenzene components.

Another variant of effective simultaneous coordination polymerization and hydrogen bonding was achieved in the reaction of Zn-9 with a [2]pseudorotaxane ligand 1,2-bis(4,4'-bipyridinium)ethane-dibenzo-24-crown-8.<sup>41b</sup> The latter represents a linear doubly charged species containing pyridyl fragments at both ends. The crown ether ring is threaded on the molecular axle of the bidentate bipyridinium ligand, imparting bulkiness and geometric rigidity to the system. The charge balance comes from deprotonation of two of the carboxylic groups in 9. Indeed, the [2]pseudorotaxane dication turned out to be an excellent axial bridging between the metalloporphyrin cores, by coordinating from both sides to their zinc-ion centers and leading to the formation of linear multiporphyrin polymers that extend through the crystal. Simultaneously the porphyrin units associate in the equatorial plane into continuous open networks through cooperative charge-assisted strong hydrogen bonding between the carboxylic and carboxylate groups (at O—H $\cdots$ O— distance of 2.45 Å). These H-bonding networks are characterized by an approximate square-planar symmetry where every Zn-9 unit in the net is linked to four neighboring molecules at the corners of the square framework, and a wide-open architecture. The linear coordination polymers that propagate in a direction roughly perpendicular to the porphyrin plane interpenetrate through the hydrogen-bonded porphyrin network. The [2]pseudorotaxane ligands that are embedded within a given layer link to porphyrin units of neighboring layers located above and below. In other words, the linear coordination polymers sustained by the pseudorotaxane bridging ligands interlock in the crystal into the multiporphyrin molecular networks held together by cooperative hydrogen bonding, thus yielding a molecular solid with a fascinating three-dimensional architecture (Figure 3.14).<sup>41b</sup>

The final example represents another fascinating single-framework polymeric structure tailored by cooperative metal-ligand coordination in all three dimensions.<sup>40</sup> It was obtained by reacting Zn-9 with 4,4'-bipyridyl (as axial bridging auxiliaries), and in the presence of sodium ions (as equatorial linkers to the carboxylic/carboxylate functions). The assembled open multiporphyrin architecture represents an “organic zeolite” (Figure 3.15). It consists of porphyrin bilayers held together by ion-pairing forces through the sodium ions. The latter coordinate to the carboxylate groups of several porphyrin units, creating an effective interaction assisted by interporphyrin hydrogen bonding in the equatorial plane. The successively displaced bilayers are then cross-linked in the axial directions from both sides by the bipyridyl ligands, which coordinate to the metallated porphyrin cores. The lattice thus formed is perforated by nearly 1 nm wide-open galleries that extend between the bipyridyl pillars in different directions parallel to the plane of the porphyrin bilayers. The lattice framework occupies less than 40%

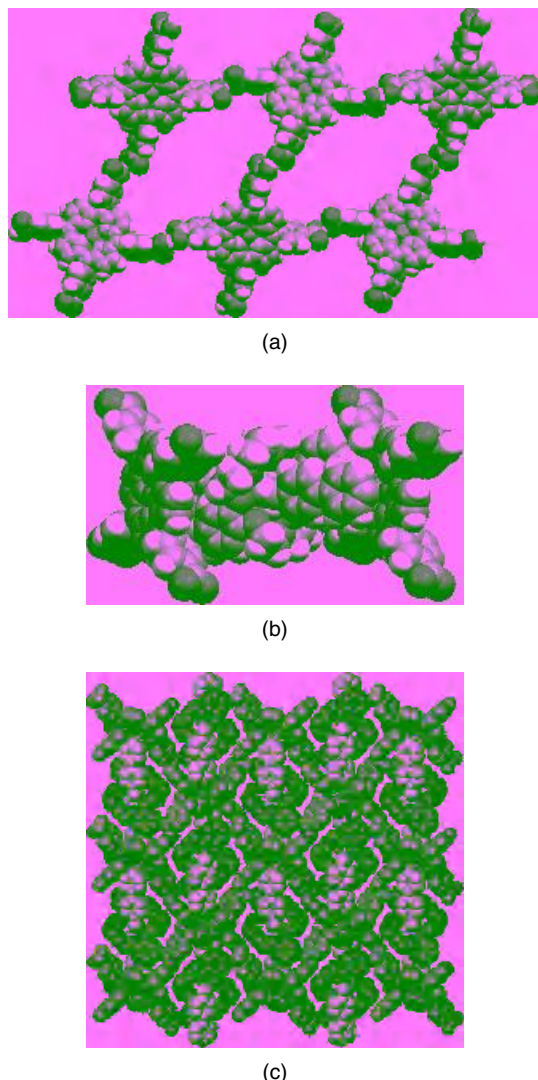


Figure 3.14. A unique three-dimensional lattice (with Zn-9) directed by simultaneous interporphyrin hydrogen bonding and coordination through a bifunctional [2]-pseudorotaxane ligand.<sup>41b</sup> (a) Illustration of the interporphyrin hydrogen-bonding pattern in the form of wide-open networks. (b) Two-porphyrin units linked to each other by the bridging ligand. (c) View of the concatenated architecture.

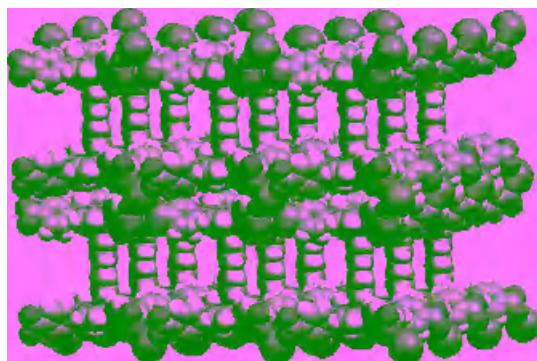


Figure 3.15. Three-dimensional zeolite-like architecture in which porphyrin Zn-9 bilayers, sustained by  $\text{Na}^+$  ions, are intercoordinated axially by bipyridyl pillars. The structure is perforated by  $\geq 1\text{nm}$  wide channel voids that propagate through the crystal in perpendicular directions parallel to the porphyrin bilayers.<sup>40</sup>

of the crystal volume, and the channel voids that propagate through the crystal can accommodate a wide range of other species. Yet it exhibits a remarkable thermal stability up to about  $150^\circ\text{C}$  on expulsion of the accommodated solvent guest, reflecting on robustness of the cooperative interaction synthons applied in this case.

## V. FINAL REMARKS

The network structures described above represent several unique examples of deliberately designed solids that are fully sustained by specific and directional synthons of intermolecular interaction, and not by virtue of van der Waals forces, as is commonly observed in organic crystals. It confirms that targeted solid state synthesis based on suitable molecular recognition algorithms is an effective approach in the design of multiporphyrin networks. With the fast development of supramolecular chemistry, such systems provide an increasingly important class of materials for a variety of possible scientific and technological applications. They could be useful in the areas of molecular separation and transport, heterogeneous catalysis, and as functional solid state receptors and reactors.<sup>49</sup> Further studies will focus also on the design of related building blocks with asymmetric substitutions with different functions, in an effort to explore other interaction synthons and to design chiral arrays (e.g., for asymmetric catalysis), nanosized supramolecular particles of technological significance, extended systems with

metal atoms at different oxidation states (e.g., for charge-transfer applications), and so forth. The rapidly developing techniques of supramolecular chemistry and crystal engineering will undoubtedly lead to future formulations of new attractive materials with useful properties.

### ACKNOWLEDGMENTS

The author would like to acknowledge the invaluable contribution of his coworkers and graduate students to the results reviewed above which originate from this laboratory: Dr. Helena Krupitsky, Dr. Parthasarathi Dastidar, Dr. Srinivasan Balasubramanian, Dr. Krishna Kumar Ramanathan, Dr. Yael Diskin-Posner, Dr. Sanjay Dahal, Dr. Gutam Patra, Dr. Mikki Vinodu, Mrs. Michaela Shmilovits and Mrs. Zafra Stein. He is also grateful for the financial support granted by The Israel Science Foundation (Grant No. 68/01 and Grant No. 254/04), as well as by the US-Israel Binational Science Foundation (BSF), Jerusalem, Israel (Grant No. 1999082).

### REFERENCES

1. Lehn, J.-M. *Supramolecular Chemistry*, VCH, Weinheim, **1995**.
2. For recent reviews on noncovalent assembly of porphyrin arrays and their potential applications see: (a) Chambron, J.-C.; Heitz, V.; Sauvage, J.-P. *The Porphyrin Handbook*, Vol. 6, Academic Press, Orlando FL, **2000**, ch. 40, 1–42. (b) Chou, J.-H.; Nalwa, H. S.; Kosal, M. E.; Rakow, N. A.; Suslick, K. S. *The Porphyrin Handbook*, Vol. 6, Academic Press, Orlando, FL, **2000**, ch. 41, pp. 43–132. (c) Sanders, J. K. M.; Bampas, N.; Clyde-Watson, Z.; Darling, S. L.; Hawley, J. C.; Kim, H.-J.; Mak, C. C.; Webb, S. J. In *The Porphyrin Handbook*, Vol. 3, Kadish, K. M.; Smith, K. M.; Guillard, R. eds. Academic Press, London, **2000**, pp. 1–48.
3. (a) Hunter, C. A.; Meah, M. N.; Sanders, J. K. M. *J. Am. Chem. Soc.* **1990**, *112*, 5773–5780. (b) Hunter, C. A.; Sanders, J. K. M. *J. Am. Chem. Soc.* **1990**, *112*, 5525–5534.
4. Scheidt, W. R.; Lee, Y. J. *Structure and Bonding* **1987**, *64*, 1–72.
5. (a) Byrn, M. P.; Curtis, C. J.; Hsiou, Y.; Khan, S. I.; Sawin, P. A.; Tendick, S. K.; Terzis, A.; Strouse, C. E. *J. Am. Chem. Soc.* **1993**, *115*, 9480–9497. (b) Byrn, M. P.; Curtis, C. J.; Goldberg, I.; Hsiou, Y.; Khan, S. I.; Sawin, P. A.; Tendick, S. K.; Strouse, C. E. *J. Am. Chem. Soc.* **1991**, *113*, 6549–6557. (c) Byrn, M. P.; Curtis, C. J.; Khan, S. I.; Sawin, P. A.; Tsurumi, R.; Strouse, C. E. *J. Am. Chem. Soc.* **1990**, *112*, 1865–1874.
6. Byrn, M. P.; Curtis, C. J.; Hsiou, Y.; Khan, S. I.; Sawin, P. A.; Terzis, A.; Strouse, C. E. In *Comprehensive Supramolecular Chemistry*, Vol. 6, MacNicol, D. D.; Toda, F.; Bishop, R., eds., Elsevier Science, New York, **1996**, pp. 715–732.
7. (a) Goldberg, I. *Cryst. Eng. Comm.* **2002**, *4*, 109–116. (b) Goldberg, I. *Chem. Eur. J.* **2000**, *6*, 3863–3870. (c) Goldberg, I. *Chem. Commun.* **2005**, 1243–1254.
8. Goldberg, I.; Krupitsky, H.; Stein, Z.; Hsiou, Y.; Strouse, C. E. *Supramol. Chem.* **1995**, *4*, 203–221.

9. (a) Dastidar, P.; Krupitsky, H.; Stein, Z.; Goldberg, I. *J. Incl. Phenom.* **1996**, *24*, 241–262. (b) Krupitsky, H.; Stein, Z.; Goldberg, I. *J. Incl. Phenom.* **1995**, *20*, 211–232.
10. (a) Krishna Kumar, R.; Balasubramanian, S.; Goldberg, I. *Inorg. Chem.* **1998**, *37*, 541–552. (b) Krishna Kumar, R.; Balasubramanian, S.; Goldberg, I. *Mol. Cryst. Liq. Cryst.* **1998**, *313*, 105–114.
11. Krishna Kumar, R.; Balasubramanian, S.; Goldberg, I. *Chem. Commun.* **1998**, 1435–1436.
12. Dastidar, P.; Stein, Z.; Goldberg, I.; Strouse, C. E. *J. Supramol. Chem.* **1996**, *7*, 257–270.
13. Dahal, S.; Goldberg, I. *J. Phys. Org. Chem.* **2000**, *13*, 382–387.
14. (a) Jeffrey, G. A. In *An Introduction to Hydrogen Bonding*. Oxford University Press, New York, **1997**, p. 56. (b) Whitesides, G. M.; Simanek, E. E.; Matias, J. P.; Seto, C. T.; Chin, D. N.; Mammen, M.; Gordon, D. M. *Acc. Chem. Res.* **1995**, *28*, 37–44.
15. (a) Kobayashi, K.; Koyanagi, M.; Endo, K.; Masuda, H.; Aoyama, Y. *Chem. Eur. J.* **1998**, *4*, 417–424. (b) Bhryappa, P.; Wilson, S. R.; Suslick, K. S. *J. Am. Chem. Soc.* **1997**, *119*, 8492–8502.
16. Diskin-Posner, Y.; Krishna Kumar, R.; Goldberg, I. *New J. Chem.* **1999**, *23*, 885–890.
17. (a) Diskin-Posner, Y.; Goldberg, I. *Chem. Commun.* **1999**, 1961–1962. (b) Schareina, T.; Kempe, R. Z. *Annorg. Allg. Chem.* **2000**, *626*, 1279–1281.
18. See, for example: (a) Anderson, S.; Anderson, H. L.; Sanders, J. K. M. *Acc. Chem. Res.* **1993**, *26*, 469–475. (b) Danks, I. P.; Sutherland, I. O.; Yap, C. H. *J. Chem. Soc., Perkin Trans* **1990**, *1*, 421–422.
19. (a) Fleischer, E. B.; Shachter, A. M. *Inorg. Chem.* **1991**, *30*, 3763–3769. (b) Shachter, A. M.; Fleischer, E. B.; Haltiwanger, R. C. *J. Chem. Soc., Chem. Comm.* **1988**, 960–961. (c) Fleischer, E. B. *Inorg. Chem.* **1962**, *1*, 493–495.
20. Krupitsky, H.; Stein, Z.; Goldberg, I.; Strouse, C. E. *J. Incl. Phenom.* **1994**, *18*, 177–192.
21. Gunter, M. J.; McLaughlin, G. M.; Berry, K. J.; Murray, K. S.; Irving, M.; Declercq, P. E. *Inorg. Chem.* **1984**, *23*, 283–300.
22. (a) Abrahams, B. F.; Hoskins, B. F.; Robson, R. *J. Am. Chem. Soc.* **1991**, *113*, 3606–3607. (b) Abrahams, B. F.; Hoskins, B. F.; Michail, D. M.; Robson, R. *Nature (London)* **1994**, *369*, 727–729.
23. Lin, K.-J. *Angew. Chem. Int. Ed.* **1999**, *38*, 2730–2732. See also: Deiters, E.; Bulach, V.; Hosseini, W. *Chem. Commun.* **2005**, 3906–3908.
24. Diskin-Posner, Y.; Patra, G. K.; Goldberg, I. *Dalton Trans.* **2001**, 2775–2782.
25. Pan, L.; Kelly, S.; Huang, X.; Li, J. *Chem. Commun.* **2002**, 2334–2335.
26. Barkigia, K. M.; Battioni, P.; Riou, V.; Mansuy, D.; Fajer, J. *Chem. Commun.* **2002**, 956–957.
27. Shmilovits, M.; Vinodu, M.; Goldberg, I. *New J. Chem.* **2004**, *28*, 223–227.
28. Hagman, D.; Hagman, P. J.; Zubietta, J. *Angew. Chem. Int. Ed.* **1999**, *38*, 3165–3168.
29. Sharma, C. V. K.; Broker, G. A.; Huddleston, J. G.; Baldwin, J. W.; Metzger, R. M.; Rogers, R. D. *J. Am. Chem. Soc.* **1999**, *121*, 1137–1144.
30. Pan, L.; Noll, B. C.; Wang, X. *Chem. Commun.* **1999**, 157–158.
31. Carlucci, L.; Ciani, G.; Proserpio, D. M.; Porta, F. *Angew. Chem. Int. Ed.* **2003**, *42*, 317–322.
32. Kondo, M.; Kimura, Y.; Wada, K.; Mizutani, T.; Ito, Y.; Kitagawa, S. *Chem. Lett.* **2000**, 818–819.
33. (a) Fujita, N.; Biradha, K.; Fujita, M.; Sakamoto, S.; Yamaguchi, K. *Angew. Chem. Int. Ed.* **2001**, *40*, 1718–1721. (b) Ikeda, A.; Ayabe, M.; Shinkai, S.; Sakamoto, S.; Yamaguchi, K. *Org. Lett.* **2000**, *2*, 3707–3710.

34. (a) Lengo, E.; Zangrando, E.; Minatel, R.; Alessio, E. *J. Am. Chem. Soc.* **2002**, *124*, 1003–1012.  
(b) Lengo, E.; Milani, B.; Zangrando, E.; Geremia, S.; Alessio, E. *Angew. Chem. Int. Ed.* **2000**, *39*, 1096–1099.
35. (a) Chichak, K.; Branda, N. R. *Chem. Commun.* **1999**, 523–524. (b) Wilson, G. S.; Anderson, H. L. *Chem. Commun.* **1999**, 1539–1540.
36. (a) Stang, P. J.; Fan, J.; Olenyuk, B. *Chem. Commun.* **1997**, 1453–1454. (b) Slone, R. V.; Hupp, J. T. *Inorg. Chem.* **1997**, *36*, 5422–5437.
37. (a) Drain, C. M.; Nifiatis, F.; Vasenko, A.; Batteas, J. D. *Angew. Chem. Int. Ed.* **1998**, *37*, 2344–2347. (b) Drain, C. M.; Lehn, J.-M. *Chem. Commun.* **1994**, 2313–2315.
38. Vinodu, M.; Stein, Z.; Goldberg, I. *Inorg. Chem.* **2004**, *43*, 7582–7584.
39. Diskin-Posner, Y.; Dahal, S.; Goldberg, I. *Chem. Commun.* **2000**, 585–586.
40. Diskin-Posner, Y.; Dahal, S.; Goldberg, I. *Angew. Chem. Int. Ed.* **2000**, *39*, 1288–1292.
41. (a) Diskin-Posner, Y.; Goldberg, I. *New J. Chem.* **2001**, *25*, 899–904. (b) Diskin-Posner, Y.; Patra, G. K.; Goldberg, I. *Eur. J. Inorg. Chem.* **2001**, 2515–2523.
42. Shmilovits, M.; Vinodu, M.; Goldberg, I. *Cryst. Growth Des.* **2003**, *3*, 855–863.
43. Kosal, M. E.; Chou, J.-H.; Suslick, K. S. *J. Porphyrins Phthalocyanines* **2002**, *6*, 377–381.
44. Kosal, M. E.; Chou, J.-H.; Wilson, S. R.; Suslick, K. S. *Nat. Mater.* **2002**, *1*, 118–121. See also: Suslick, K. S.; Bhyrappa, P.; Chou, J.-H.; Kosal, M. E.; Nakagaki, S.; Smitherney, D. W.; Wilson, S. R. *Acc. Chem. Res.* **2005**, *38*, 283–291.
45. Shmilovits, M.; Vinodu, M.; Goldberg, I. *Cryst. Growth Des.* **2004**, *4*, 633–638.
46. (a) Krishna Kumar, R.; Diskin-Posner, Y.; Goldberg, I. *J. Incl. Phenom.* **2000**, *37*, 219–230. (b) Diskin-Posner, Y.; Patra, G. K.; Goldberg, I. *Dalton Trans.* **2001**, 2775–2782. (c) Shukla, A. D.; Dave, P. C.; Suresh, E.; Das, A.; Dastidar, P. *Dalton Trans.* **2000**, 4459–4463.
47. (a) Brandon, E. J.; Rogers, R. D.; Burkhart, B. M.; Miller, J. S. *Chem. Eur. J.* **1998**, *4*, 1938–1943.  
(b) Brandon, E. J.; Rittenberg, D. K.; Arif, A. M.; Miller, J. S. *Inorg. Chem.* **1998**, *37*, 3376–3384.  
(c) Miller, J. S.; Calabrese, J. C.; McLean, R. S.; Epstein, A. J. *Adv. Mater.* **1992**, *4*, 498–501.
48. (a) Diskin-Posner, Y.; Patra, G. K.; Goldberg, I. *Chem. Commun.* **2002**, 1420–1421.  
(b) Diskin-Posner, Y.; Patra, G. K.; Goldberg, I. *Cryst. Eng. Comm.* **2002**, *4*, 296–301.
- 49 Drain, C. M.; Goldberg, I.; Sylvain, I.; Falber, A. *Top. Curr. Chem.* **2005**, *245*, 55–88.

# Chapter 4

## Homo- and Heterochirality in Crystals

PAVEL A. LEVKIN, VLADIMIR YU. TORBEEV, DENIS A. LENEV,  
and REMIR G. KOSTYANOVSKY

*N.N. Semenov Institute of Chemical Physics, Russian Academy of Sciences,  
119991 Moscow, Russian Federation*

- I. Introduction
- II. Symmetry Space Groups of Homo- and Heterochiral Crystals
- III. Recognition of Homo- and Heterochiral Crystals
- IV. “Switching” between Homo- and Heterochiral Crystallizations
  - A. Racemic Conglomerate versus Racemic Compound of the Same Chemical Composition
  - B. Racemic Conglomerate versus Racemic Compound of Different Chemical Compositions
    - 1. Formation of Racemic Conglomerate versus Racemic Compound among Solvates and Host–Guest Inclusion Compounds
    - 2. Formation of Racemic Conglomerate versus Racemic Compound Depending on Counter Ions, Central Metal Atoms, Ligands
    - 3. Formation of Racemic Conglomerate versus Racemic Compound Depending on Covalently Bound Substituents
- V. Transformations between Homo- and Heterochiral Crystals
- VI. Homo- and Heterochiral Crystal Engineering
- VII. Concluding Remarks
- References

### I. INTRODUCTION

Homochiral crystallization in the racemic conglomerates appears to be Fortune’s gift. Homochiral crystallization provides the simplest route to enantiopure compounds.<sup>1,2</sup> Recently the relevance of homochiral crystallization to producing biological homochirality has been discussed.<sup>3</sup> In this chapter we review some



Maybe the first true image  
of homochirality in art.  
Nefertari (the queen-wife  
of Ramses II) and goddess  
Izida. From Valley of the  
Queens in Thebes -  
tomb of Nefertari - XIXth  
Dynasty, Egypt (1255 BC).

Heterochirality in art. Natalia  
Goncharova (1881-1962),  
“Two spanish women in a  
garden” (1920s-early 1930s).  
From the State Treliakov  
gallery (Moscow, Russia).



features of homo- and heterochiral crystallization and the ways these modes can switch between each other.

Chiral molecules are packed in crystals in four different ways:<sup>4,5a</sup> (1) as a racemic compound (achiral, in most cases crystals in which the two enantiomers are present in equal amounts in a well-defined arrangement within the lattice), such as racemic tartaric acid, (2) as a conglomerate (racemic mixture of homochiral enantiopure enantiomorphous crystals, each of which contains only one of the two enantiomers) such as sodium ammonium tartrate tetrahydrate (Pasteur's salt), (3) as a solid solution (a crystal containing two enantiomers that can replace each other in the asymmetric unit) such as camphor, or (4) as an anomalous "unbalanced" racemate (a crystalline species, in which the ratio of ordered enantiomers is not unity).<sup>6</sup> A special case of crystalline mixtures is the chiral quasi-racemate. Chiral quasi-racemates are usually obtained by cocrystallization of nonenantiomeric chiral molecules which are nearly mirror images.<sup>4,7</sup>

Disregarding the last-mentioned special case, solid enantiomeric mixtures of chiral molecules obtained in nonenantioselective syntheses are in most cases racemic compounds (type 1), rarely (<10 % cases<sup>4</sup>) conglomerates (type 2), and in few cases racemates of type 3 or 4. Wallach's rule<sup>9</sup>, which assumes higher densities and higher thermodynamic stabilities for racemates compared to the corresponding enantiomers and their conglomerates,<sup>10</sup> has been criticized.<sup>11</sup> The most probable reason for the low frequency of the conglomerate formation is the presence of additional second-order symmetry elements and their combinations with the first-order elements in the space groups of symmetry (or simply, space groups) of racemic crystals. This increases the statistical probability of more effective packing and crystallization of racemic compounds.<sup>11</sup> By enantioselective synthesis, enantiomeric resolution, or from a natural source, one can obtain a chiral compound of interest in enantiomerically pure form from the necessary chiral crystals. The crystallographic relation of enantiomorphic crystals to racemic crystals, for resolvable enantiomers of a chiral compound, is not polymorphic, since the liquid and vapor phase compositions for such crystals are different. We will treat this relation as *diastereomorphic*. As defined by the IUPAC, "diastereomorphism" is a relationship between objects—or models—that is analogous to that between diastereomeric molecular entities.<sup>8</sup> We will regard the behavior of chiral compounds that exist as both racemic compound and conglomerate as *diastereomorphism*, and the crystals formed will be termed *diastereomorphs*.

## II. SYMMETRY SPACE GROUPS OF HOMO- AND HETEROCHIRAL CRYSTALS

Homochiral crystallization occurs in 65 space groups of symmetry with first-order elements (translations, rotations, and screw axes), whereas heterochiral is

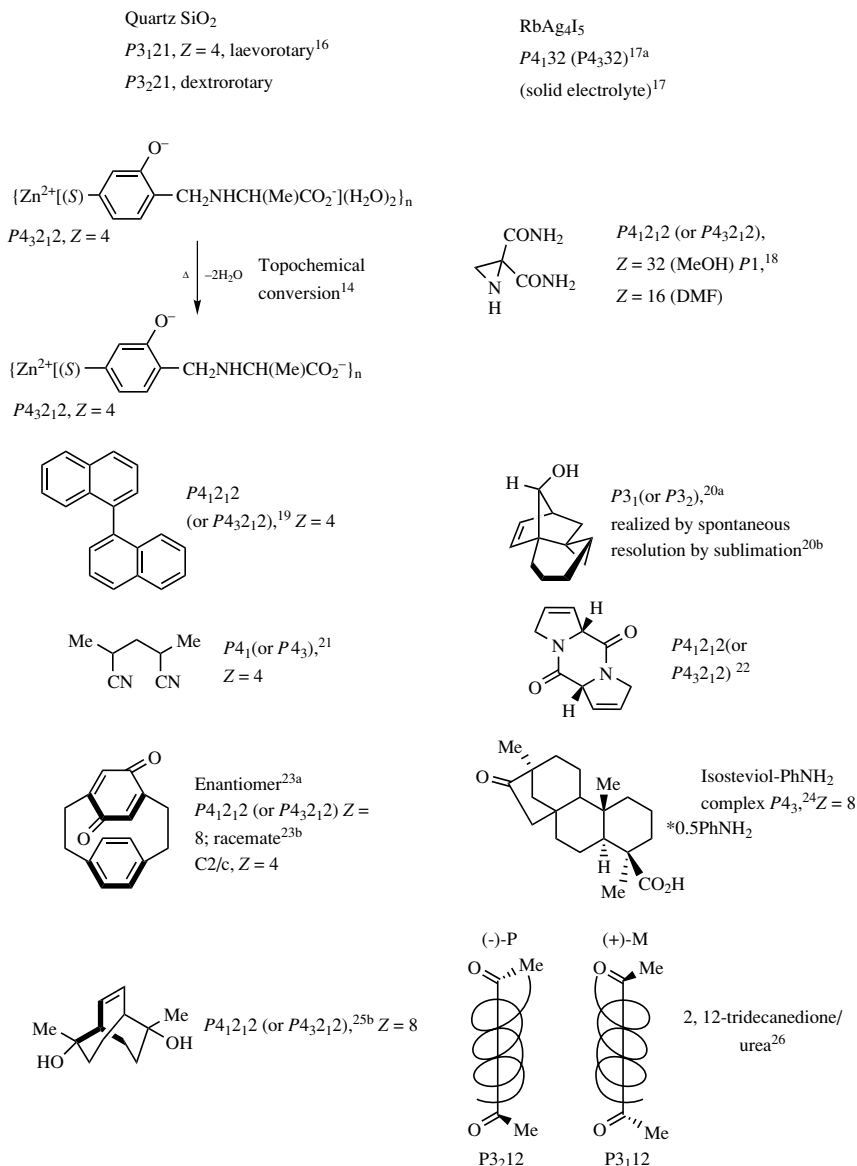
Table 4.1  
Space Groups of Homochiral Crystals

Crystal Class	Chiral	Achiral
Cubic	$P4_132; P4_332$	$P23; P2_13; I23; I2_13; F23;$ $P432; P4_232; I432; I4_132;$ $F432; F4_132$
Tetragonal	$P4_1; P4_3; P4_122;$ $P4_322; P4_12_12; P4_32_12$	$P4; P4_2; I4; I4_1; P422;$ $P42_12; P4_222; P4_22_12;$ $I422; I4_122$
Monoclinic		$P2; P2_1; C2$
Orthorhombic		$P222; P222_1; P2_12_12;$ $P2_12_12_1; C222; C222_1; I222;$ $I2_12_12_1; F222$
Triclinic		$P1$
Trigonal	$P3_1; P3_2; P3_112; P3_212;$ $P3_121; P3_21$	$P3; P312; P321; R3; R32$
Hexagonal	$P6_1; P6_5; P6_2; P6_4; P6_122;$ $P6_522; P6_222; P6_422$	$P6; P6_3; P622; P6_322$

observed for the rest 165 Fedorov groups. Until recently all 65 groups (Table 4.1) were considered chiral.<sup>5</sup> However, there are only 11 pairs of truly chiral enantiomorphous<sup>12</sup> space groups for which each of two enantiomorphous crystals can be described by an individual space group of the pair. In the remaining 43 space groups both enantiomorphous crystals belong to the same space group. The distribution of organic crystals among different space groups and subgroups has been analyzed statistically.<sup>13</sup>

Some interesting cases of crystallization in chiral space groups are presented in Scheme 4.1. The isosteviol-aniline complex forms an *M* left-handed double helix (space group  $P4_3$ ,  $Z = 8$ ) of isosteviol molecules located around the crystallographic axis  $4_3$  cross-linked by the amino groups of aniline (Figure 4.1). One can similarly expect formation of diastereomeric complexes of isosteviol with chiral amines: *M*-isosteviol/(*S*)-amine and *M*-isosteviol/(*R*)-amine. Crystallizations in chiral space groups are also known for their helicate forms ( $P4_32_12$  and  $P6_1$ ).<sup>15</sup>

An intriguing problem is finding the existence of diastereomorphs (*R*)-guest/( $P6_122$ )-host and (*S*)-guest/( $P6_122$ )-host among the urea inclusion compounds.<sup>27</sup> Computational analysis predicts a strong preference of the first diastereomer for (*R*)-2-bromotridecane- and 2-bromotetradecane-urea clathrates.<sup>27</sup> Recently Hollingsworth et al.<sup>26</sup> found two polymorphs of achiral guest tridecane-2,12-dione/urea clathrate: (+)-[guest/right-handed urea] ( $P3_12$ ) and (-)-[guest/left-handed urea] ( $P3_2$ ). But it is not yet clear whether Schlenk's resolution of



Scheme 4.1. Examples of crystallization in 11 pairs of chiral space groups.

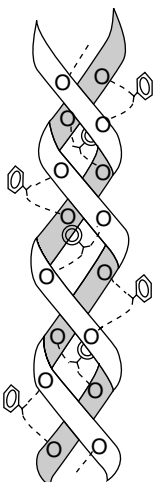


*Figure 4.1.* Double helix of isosteviol molecules cross-linked by amino groups of aniline. Reproduced with the permission of the authors.<sup>24</sup>

racemic terminally substituted alkanes (see Refs. 26, 27) takes place through the diastereomeric complexes or through the spontaneous resolution of a conglomerate of the enantiomorphous complexes.

There are a number of compounds that are racemic conglomerates (in particular, space group  $P2_12_12_1$ ). However, their crystal lattices actually consist of many domains (lamellae) of both of the enantiomers instead of containing only one enantiomer.<sup>28</sup> The origin of lamellar racemic twinning (or polyepitaxy) is the low rate of the mass transport phenomena. Once the first enantiomorph of the conglomerate has nucleated and begins to grow, the solution in close proximity gradually becomes supersaturated with the opposite enantiomer. If structural prerequisites are satisfied, at some critical point the second enantiomorph nucleates on the surface of the first one. During the next cycle the solution becomes locally supersaturated with the first enantiomer and a new lamella of the corresponding enantiomorph starts to grow. Finally, it leads to the crystal consisting of alternating lamellae of opposite enantiomorphs, and thus a racemic composition. Such a phenomenon has represented an obstacle in resolution of enantiomers by crystallization. Since 1950 several methods for overcoming this obstacle have been proposed: use of enantiopure “tailor-made” additives,<sup>28f-h</sup> wetting reagents,<sup>28i</sup> gentle stirring,<sup>28j</sup> and suppression of growth along twinning direction.<sup>28k</sup> We suspect that by varying the mass transport conditions, a crystal engineer can increase or reduce the thickness of

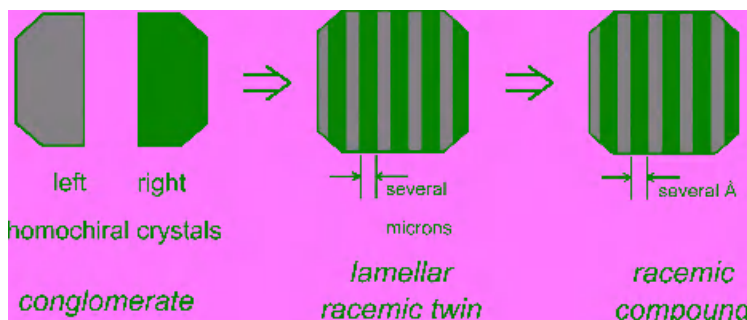


*Figure 4.2.* Crystallization behavior of racemate. (a) As separate left- and right-handed homochiral crystals (conglomerate); (b) as racemic twin consisting of domains of opposite chirality with micron dimensions; (c) as a racemic compound whose “domains” have molecular dimensions. See color insert.

each lamella and, finally, obtain metastable crystals of a racemic compound by reducing convection and diffusion processes (e.g. by crystallization in gels) (Figure 4.2).

### III. RECOGNITION OF HOMO- AND HETEROCHIRAL CRYSTALS

Apart from X-ray diffraction the well-known techniques for detection and visualization of differences between homo- and heterochiral crystal structures include solid state IR (ss IR),<sup>29,30</sup> Raman,<sup>29,30,31</sup> solid state NMR (ss NMR) (especially CP-MAS  $^{13}\text{C}$  NMR),<sup>32,31a</sup> and solid state UV-VIS.<sup>31a</sup> Solid state ESR spectra of radicals provide valuable information on crystal structures, magnetic properties, local environment, and spatial distribution in the lattice.<sup>33</sup> Recently we showed a way to differentiate between homo- and heterochiral crystal structures by ESR spectroscopy.<sup>34</sup> Conglomerate formation may be confirmed if the solid state spectrum of the crystalline racemic form is identical to that of the enantiomerically pure substance.

All the mentioned methods are suitable for qualitative differentiation among the different crystalline modifications. However, in the literature, until now only CP-MAS  $^{13}\text{C}$  NMR, PXRD, and DSC have been used for the quantitative analyses of different crystalline samples.<sup>31a,35</sup> Single crystals of a conglomerate and a racemic compound have enantiomeric and racemic compositions, respectively. Consequently they can be differentiated by analysis of the separate crystals of the two forms by solid state circular dichroism or solid state optical rotation methods. Furthermore, solutions of single crystals of a conglomerate must be optically

active, in contrast to the crystals of the racemic compound, for optical methods to be utilized in the solution.

So far the most convenient and effective method for recognition of homo- or heterochiral composition appears to be chiral chromatography. The advantages of this method consist in its high sensitivity and directness compared with the ss NMR, PXRD, ss IR, and other methods that require the solid state spectra of a racemic sample to be compared with an enantiomerically pure one. Chiral stationary phase chromatography has successfully been used to detect conglomerate formation and lamellar racemic twinning.<sup>36</sup>

Melting point diagrams and ternary solubility diagrams are often convenient ways to detect, surprisingly, the formation of racemic compounds or conglomerates.<sup>4</sup> However, they require corroboration by another method because transformations may occur between racemic compounds and conglomerates in a solution or upon heating (Section V). An observation of hemihedry (presence of hemihedral faces) may be an indication of conglomerate formation, yet the absence of hemihedry is not proof of a racemic compound formation. Excess of one of the enantiomers in a crystal and consequently conglomerate formation can be proved by formation of the cholesteric phase upon dissolution of the crystal in a nematic liquid crystal.

Nonsolubility of one enantiomer in a saturated solution of the racemate is another test for conglomerate formation,<sup>37</sup> demonstrated for the first time on the salts of 2,6-diaminospiro[3.3]heptane (see Section B.3).<sup>38</sup> The resolution of a racemate by crystallization from an optically active solvent may also indicate conglomerate formation.<sup>4</sup> However, we have observed that compounds capable of enantiomerization under crystallization conditions do not follow this trend because their solutions are enriched with the more solvated enantiomer. Therefore crystallization takes place in a nonracemic mixture. Kostyanovsky et al. have shown that many compounds with a three-coordinated nitrogen-forming racemic compounds are enriched in one of the enantiomers by crystallization from optically active solvents (see Ref. 39).

As early as 1910 Ostrovskii proposed triboluminescence “as a criterion for distinguishing between racemic compounds and conglomerates.”<sup>40a</sup> Studies that followed confirmed the triboluminescence response to be characteristic of acentric crystals. Indeed, the same response was observed for centrosymmetric materials.<sup>40b</sup>

Pasteur was first to describe quasi-racemic compounds<sup>41</sup> as a mixture (1:1) of chiral compounds that have similar structures but are opposite in their absolute configurations. Isotopomeric quasi-racemates (IQR), meaning mixtures of enantiomers (1:1)—one of which contains an isotopic label—are especially useful in studies of chiral recognition. The formation of homochiral protonated or metallated enantiomers, or their oligomers, in gas phase can be detected by

electrospray mass spectrometry. In the case of ion-cyclotron resonance the species with different  $m/z$  values can be sequentially retained in the ion trap by Pasteur-like manual sorting.<sup>42a</sup> We studied the above-mentioned properties of IQR using the following conglomerates: (+)-Asn/(-)-Asn ( $^{15}\text{N}$ -amide), (+)-C<sub>5</sub>H<sub>5</sub>N<sup>+</sup>CH(CO<sub>2</sub><sup>-</sup>)CH<sub>2</sub>CO<sub>2</sub>H/(-)- C<sub>5</sub>D<sub>5</sub>N<sup>+</sup>CH(CO<sub>2</sub><sup>-</sup>)CH<sub>2</sub>CO<sub>2</sub>H as well as racemic compounds such as (+)-dimethyl tartrate/(-)-dimethyl tartrate-d<sub>6</sub>, (+)-tartaric diamide/(-)-tartaric diamide( $^{2}\text{H}$ ), and (+)-1,2-diethyl-4,8-dimethylglycoluril/(-)-1,2-diethyl-4,8-dimethylglycoluril-d<sub>6</sub>[42]. With “achiral” methods (MS, NMR, IR, etc.) we found that crystallization followed by dissolution of one of the crystals of the IQR can be used for the identification of conglomerate formation, racemic twinning, and unbalanced packing of the chiral molecules in anomalous racemates.<sup>6</sup>

A well-known sign of conglomerate formation is a large difference in the melting points of the enantiomers and the corresponding racemate ( $\Delta m_{\text{p}_{\text{e-r}}}$   $\geq 25^\circ\text{C}$ ).<sup>4,37</sup> Nevertheless, because of the possible phase transformations, this sign of conglomerate formation may be only reliable near the melting point of a chiral compound.

#### IV. “SWITCHING” BETWEEN HOMO- AND HETEROCHIRAL CRYSTALLIZATIONS

In 1991 the “European pharmacopeia” consisted of a number of pharmaceuticals, of which 58% were polymorphic, 57% were capable of forming hydrates and 20% solvates.<sup>43</sup> These figures show that a greater part of organic compounds are capable of forming polymorphs and pseudopolymorphs. There should be examples of diastereomorphs (homo/heterochiral pairs) among the polymorphs and pseudopolymorphs. Analysis of 163 pairs of polymorphic crystal structures showed that 24% of the pairs had one centrosymmetric member and one noncentrosymmetric member.<sup>44</sup> The detailed investigations of these examples have provided us with the factors that govern racemic compound over conglomerate formation.<sup>4,10,45</sup> If the conditions leading to conglomerate formation by a certain compound are known, the enantiomers can be resolved by direct crystallization with an enantiomerically pure seed.<sup>4,5a</sup>

It should be pointed out that formation of a racemic compound can be successfully used for increasing the optical purity of non-racemic mixtures. Thus, precipitation of an insoluble racemic complex of 1,1'-binaphthol with diethyl ether from a non-racemic solution made possible isolation of R-(+)-1,1'-binaphthol with 99% ee from the mother liquor.<sup>46</sup> Crystallization of the racemic compound of sodium ammonium tartrate from a non-racemic solution above 27°C (conditions of the formation of the racemic compound) led to increase in the optical purity of the mother liquor from 65% to 80%.<sup>5c</sup>

### A. Racemic Conglomerate versus Racemic Compound of the Same Chemical Composition

Compounds **1–5** (Table 4.2) are found to form both the racemic compound and conglomerate. The two forms have different melting points  $T_r$  (racemic compound) and  $T_c$  (enantiomer), and similarly a transition temperature  $T_i$  above which one form is more stable and below which the other form is more stable. Formation of a compound (by crystallization or sublimation) below and above the intermediate temperature can lead to the two different crystal structures. Although according to Ostwald's rule of stages,<sup>47</sup> a metastable form can be formed at any temperature, the lifetime of the metastable phase depends on the rate of the transformation into the more stable form. The metastable phase lifetime may be very long (infinite in the limit), or it may be so short that detection of the metastable form is not possible.

1,1'-Binaphthyl **1** (Table 4.2) is the most extensively studied example that forms both racemic compound and conglomerate. The latter is more stable at the temperatures above 76°C and melts at 158°C; the racemic compound melts at 145°C, and it is more stable below 76°C.<sup>48a</sup> Similar temperature-dependent conglomerate formation is evident in naphthidine **2** (Table 4.2). Its racemic compound is stable below 197°C and metastable above 197°C up to the melting at 202°C. The conglomerate of **2** is stable above 197°C (melting point 204°C) and undergoes solid state transformation into the racemic compound below 197°C. Crystallization below 197°C gives the racemic compound, whereas the conglomerate is obtained by sublimation of the racemic sample at the temperature between 197°C and 203°C.<sup>48b</sup>

Labianca et al.<sup>51</sup> showed a crystalline mixture of racemic compound and racemic conglomerate of acid **3** to be precipitated from its solution in water (Table 4.2) above 35°C. However, below 35°C the only form obtained is the racemic compound.

The medicine nimodipine **5**<sup>52</sup> (Table 4.2) forms a mixture of racemic compound (mp 124°C) and a conglomerate (mp 116°C) upon crystallization. Although the two forms can coexist at room temperature, the conglomerate is more stable at temperatures below 88°C and the racemic compound is thermodynamically more stable above 88°C, up to a melting point of 124°C. The transformation of the conglomerate into the racemic compound occurs as the mixture melts, at the intermediate temperature of 116°C.

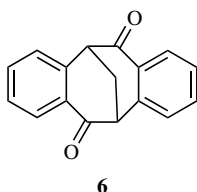
Unlike **1** and **2**, in the case of the related compound **4** (Table 4.2), the conglomerate is stable below 186°C, and the racemic compound is stable above this temperature up to its melting point at 191°C.<sup>53</sup>

Compound **6** was first described by Stetter and Reischl<sup>54a</sup> and prepared in enantiomerically pure forms by Naemura et al.<sup>54b</sup> According to Naemura and et al. the melting point of the enantiomerically pure **6** was much higher than

Table 4.2  
Racemates Forming Both Racemic Compound and Conglomerate

Name	Formula	$T_r$ (°C)	$T_e$ (°C)	$T_i$ (°C)	Reference
1,1'-Binaphthyl ( <b>1</b> )		145	158 <sup>a</sup>	76	45b
Naphthidine(4,4'-diamino-1,1'-binaphthyl) ( <b>2</b> )		202	204 <sup>a</sup>	197	48b
4,4'-Azo-bis-4-cyanopentanoic acid ( <b>3</b> )		118	130	35	51
2,2'-Diamino-1,1'-binaphthyl ( <b>4</b> )		191	242	186	53
Nimodipine [isopropyl (2-methoxyethyl)-1,4-dihydro-2,6-dimethyl-4-(3-nitrophenyl)-3,5-pyridinedi carboxylate] ( <b>5</b> )		124	116	88	52

<sup>a</sup> The stated temperature corresponds to the melting point of the eutectic mixture because of rapid racemization above this point, and hence melting points of the enantiomers are unknown.



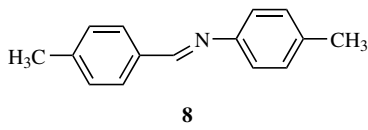
that of its racemate ( $\Delta\text{mp}$  46 °C!). A difference in melting points between the racemic compound and the enantiomer larger than 30 °C is an indicator of conglomerate formation.<sup>4</sup> However, the large (up to 43 mg) and well-formed crystals (colorless needles) of **6** (Figure 4.3a) obtained by crystallization at room temperature are not optically active and their melting point corresponds to that of the racemate (mp 146–148 °C).<sup>36b</sup> The racemic nature of the crystals was confirmed by enantioselective analytical gas chromatography (GC) of solutions of separate single crystals and by X-ray crystallographic data: the compound had the space group  $P\bar{1}$ ,  $Z = 4$ . Crystallization was attempted with various solvents and at different rates of cooling as well as at lower temperatures but gave the same racemic compound (the *ee* of separate single crystals was equal to zero). Only when crystallization was attempted at elevated temperatures (100 °C and above) from a number of solvents (e.g., *n*-octane, toluene) did the expected conglomerate (mp of single crystal, crystal, 188–190 °C) arise, as was confirmed by GC (the *ee* of a single crystal was not equal to zero) and X-ray study (space group  $P2_12_12_1, Z = 4$ ). Single crystals obtained at these conditions have different morphologies (colorless plates) (Figure 4.3b), and their solutions are optically active.



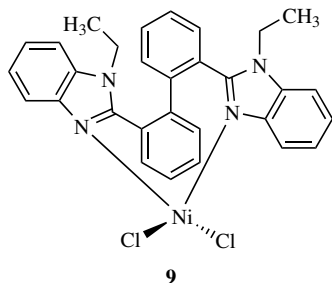
*Figure 4.3.* (a) Single crystals of the racemic compound of **6**; (b) single crystals of the conglomerate of **6**.

The influence of a solvent on the “switching” that occurs between homo- and heterochiral packing can be seen in the example of 1,3-diphenylpropane-1,3-diol **7**, which forms a mixture of crystals of racemic compound and racemic conglomerate when crystallized from benzene or ethyl acetate;<sup>55</sup> slow evaporation of **7** in a methanol solution gives rise only to the conglomerate form.

Unresolvable 4-methyl-*N*-(4-methylbenzylidene)aniline **8** can make three crystalline modifications and it is an example of concomitant<sup>56a</sup> and disappearing polymorphs.<sup>56b</sup> Bernstein et al. found that form I (racemic compound, space group  $P2_1/c$ )<sup>56c</sup> obtained during the first synthesis “disappears” after formation of the diastereomorphs II and III. Subsequently form I is no longer unachievable, whereas forms II and III can be precipitated simultaneously. Form II has chiral crystal structure (space group  $P2_1$ ),<sup>56d</sup> whereas form III crystallizes as a racemic compound (space group  $P2_1/c$ ).<sup>56e</sup> It is worth mentioning that despite the “disappearance” of form I, lattice energy calculations performed on the three polymorphs show that the energies of the forms I and III are comparable but considerably lower than the energy of form II.<sup>56f</sup>

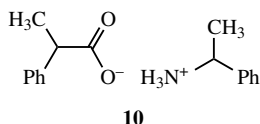


Compound **9** is a precatalyst for oligomerization of ethylene or for polymerization of norbornene. By crystallization of **9** from acetonitrile, a mixture of blue and purple crystals is obtained. The purple crystals are a racemic compound, whereas the blue crystals are a racemic conglomerate.<sup>57a</sup> This case constitutes another example of chirodichroism.\*<sup>57b</sup>



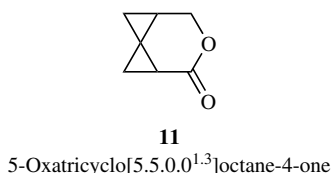
\*We use the existing terminology,<sup>57b</sup> but a more appropriate term may be *chirodichromism*, which is analogous to thermochromism, photochromism, and so forth.

Formation of a metastable racemic compound by a compound forming the conglomerate (diastereomorphism) can be an insuperable obstacle on the way to resolution of this compound into enantiomers by preferential crystallization. Thus Dufour et al.<sup>58a,b</sup> have observed a poor entrainment effect in the case of preferential crystallization of 1-phenylethylammonium hydratropate salt (**10**), which forms a stable conglomerate upon crystallization.



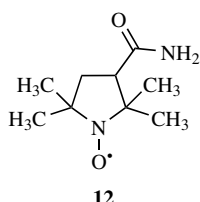
By systematic optimization of different crystallization parameters unstable racemic compound could be detected and then could be reproducibly obtained by fast crystallization of the supersaturated solution of **10**. This racemic compound was irreversibly transformed into the more stable conglomerate upon heating.<sup>58b</sup> Growth of the unstable racemic compound on the surface of the conglomerate crystals on reaching a certain local supersaturation of the counterenantiomer at the mother liquor–crystal interface was attributed to a low maximum value of enantiomeric excess ( $ee_{max} = 5\text{--}6\%$ ) of the final mother liquor.

In case of preferential crystallization of the system ( $\pm$ )-ephedrine (eph)-( $\pm$ )-mandelic acid (ma), which crystallizes as racemic conglomerate of (+)-eph-(+)-ma and (-)-eph-(-)-ma, no metastable racemic compound could be detected. Consequently, the *ee* of the final mother liquor increased up to 10.6%.<sup>58b</sup> Interestingly, crystallization of the ephedrine base<sup>59</sup> and mandelic acid<sup>60</sup> in free form gave rise to stable racemic compounds.



Tricyclic lactone **11** is an interesting compound, discovered recently by de Meijere et al.,<sup>61</sup> that forms composite crystals, with each separate crystal composed of two different crystalline modifications, namely racemic compound (space group  $P2_1/c$ ) and racemic conglomerate (space group  $P2_12_12_1$ ). The building blocks in the crystals of the racemic compound and the conglomerate are homochiral layers,

and the only difference in their crystal structures is whether the packing of the layers is homo- or heterochiral.



In 1975 Chion and Lajzerowicz investigated the crystal structure of 2,2,5,5-tetramethylpyrrolidine-3-carboxamide-1-oxyl **12** and detected the simultaneous formation of two crystalline modifications: racemic compound (space groups  $P2_1/c$ ) and conglomerate ( $P2_1$ ).<sup>62</sup> Their finding led us to investigate differences between hetero- and homochiral structures (using compound **12**) by means of ESR spectroscopy. ESR spectra of nitroxyl radicals provided valuable information about their crystal structure, magnetic properties, local environment, and spatial distribution in the lattice.<sup>33</sup> Moreover this technique appears to be the most sensitive yet, and it gives good information about the arrangements of molecules in close environment.

The typical ESR spectra for the three different orientations of the conglomerate crystal **12** in a magnetic field are given in Figure 4.4. The crystals of the racemic

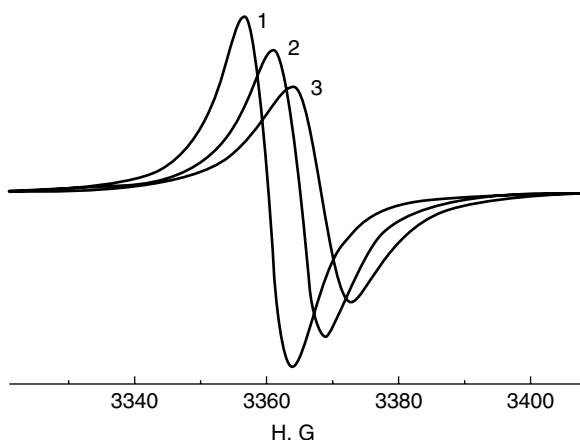


*Figure 4.4.* ESR response from a single crystal of the racemic conglomerate at the three relative orientations  $\theta$  of the crystal in magnetic field:  $0^\circ$  (1),  $60^\circ$  (2), and  $90^\circ$  (3).

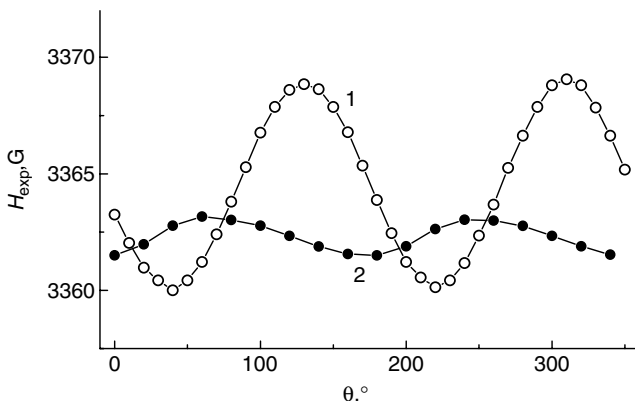


Figure 4.5. Variation of the resonance magnetic field  $H_{\text{exp}}$  value with  $\theta$ , turning angle of the enantiomeric (1) and racemic (2) crystals around the axis perpendicular to  $\mathbf{B}_0$  (magnetic field) and parallel to  $\mathbf{B}_1$  (electric field).

compound show analogous ESR single lines with similar  $g$  and  $\Delta H$  values. Figure 4.5 shows the variation of the resonance magnetic field value  $H_{\text{exp}}$  with  $\theta$ , the angle of rotation of the crystals, for enantiomeric and racemic crystals. The crystals were rotated around the axis perpendicular to  $\mathbf{B}_0$  (the magnetic field) and parallel to  $\mathbf{B}_1$  (the electric field).

Figure 4.5 shows the essential difference between the enantiomeric crystal and the crystal of the racemic compound: the variation of the signal position ( $H_{\text{exp}}$ ) of the first case is much more pronounced than that of the second case. This difference depends on the crystal structures of the two samples, and it easily allows one to distinguish experimentally between racemic and enantiomorphous crystals of **12** using the ESR method.

In the course of our search for the desired formation of a conglomerate, we discovered two more crystalline modifications in addition to the known forms. All four modifications crystallized simultaneously from an acetone solution. Among them the ratios were slightly dependent on the solvent and the rate of the crystallization. The racemic compound (form I in Figure 4.6a) and the conglomerate (form II in Figure 4.6b) can only be formed by crystallization. Conversely, the stable form III (Figure 4.6c) along with crystallization from the solution is formed by solvent-mediated transformation.<sup>63</sup> Form IV is obtained by melting followed by solidification, by quenching, or by fast evaporation of the radical solution and then by sublimation. All the four forms show different solid state IR and powder X-ray diffraction spectra, according to the different crystal structures.<sup>34</sup> Unfortunately, we were not able to obtain suitable crystals of forms III and IV for the single-crystal X-ray analysis.

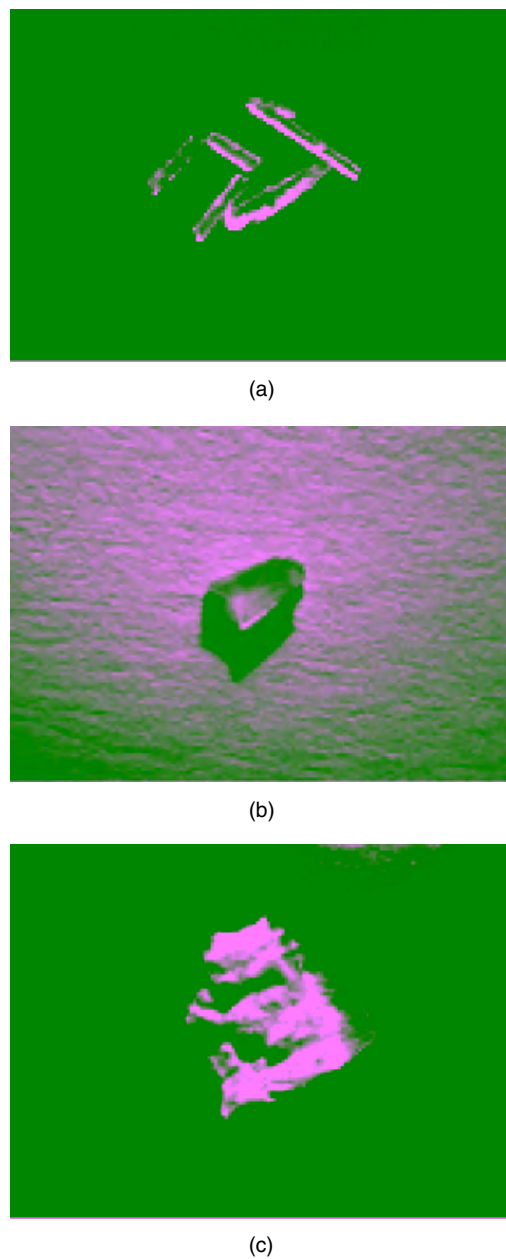
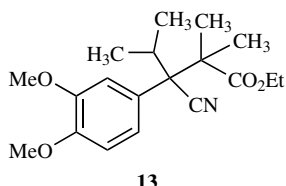


Figure 4.6. Photographs of crystals 12: (a) racemic compound (form I), space group  $P2_1/c$ ; (b) conglomerate (form II), space group  $P2_1$ ; (c) form III.

In the investigation of branched chain organic compounds, Ros et al.<sup>64</sup> found another example of simultaneous formation of a metastable racemic compound and a stable conglomerate by compound **13**. The racemic compound was found to melt at 82–84 °C, while the conglomerate melted at 90–92 °C.” The racemic compound can be transformed into a conglomerate by melting and resolidification or by heating the sample of the racemic compound at 70 °C for 20 h. Crystallization of **13** from solution led to the mixture of the two forms at all conditions examined by Ros et al., and only crystallization of **13** from the melt with addition of a seed of the racemic compound, was found to be a satisfactory way for the directional formation of the metastable racemic compound.



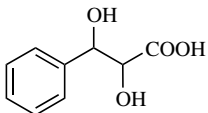
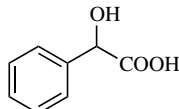
Seeding a solution or a melt with a particular crystalline modification will often give the same modification, but crystallization without seeding can furnish more than one crystalline phase. Unlike seeding, carefully designed, or “tailor-made,” additives can selectively inhibit growth of certain crystal forms. The role of tailor-made additives in crystal nucleation has been explained by the Weizmann Institute group<sup>65</sup> as due to molecules that assemble to form coexisting clusters adapting a variety of arrangements and shapes in supersaturated solutions, some of which resemble the crystals into which they eventually develop. The Weizmann Institute hypothesis has been used to explain the ability of “tailor-made” additives to inhibit precipitation of targeted crystal phases.<sup>65b</sup> It is assumed that the additive stereoselectively binds to the appropriate surfaces of the targeted crystal nuclei and inhibits their growth. The additive will interact weakly, if at all, with nuclei of the other phases, leaving them to grow without meddling. Thus, in choosing the racemic nuclei as the target, we can expect crystallization of the metastable conglomerate.

A brilliant demonstration of this principle is the crystallization of racemic histidine hydrochloride with polymers serving as the “tailor-made” additives.<sup>65c</sup> Histidine hydrochloride crystallizes from aqueous solution in the centrosymmetric form ( $\text{His}\cdot\text{HCl}\cdot 2\text{H}_2\text{O}$ ; phase  $\alpha$ ) below 45 °C, but above 45 °C it precipitates as racemic conglomerate of enantiomorphous crystals of  $\text{His}\cdot\text{HCl}\cdot \text{H}_2\text{O}$  (phase  $\beta$ ). This implies that the two phases are relatively close energetically, and we can expect crystallization of the metastable conglomerate to occur below 45 °C. Addition of a small amount (1–2 wt%) of different enantiopure polymers (e.g., poly(*p*-(acryla mido)phenylalanine) led to the selective crystallization of only one enantiomorph

of the unstable  $\beta$  phase at 25 °C. “Tailor-made” additives were able to adsorb enantiospecifically on certain faces of the racemic  $\alpha$  phase and corresponding enantiomorph of the  $\beta$  phase, blocking their growth and thereby leading to the crystallization of the opposite enantiomorph of  $\beta$  phase unaffected.

The same result was obtained in the case of glutamic acid and valine hydrochloride. Crystallization of Val·HCl from a racemic aqueous solution yielded two major phases in varying ratios depending on the conditions of crystallization: racemic compound (space group  $P2_1/c$ ) and conglomerate (space group  $P2_12_12_1$ ). Conversely, crystallization of Val·HCl in the presence of 1 wt% of the chiral polymer (*S*-lysine attached to polymethacrylic acid) produced only (*R*)-Val·HCl.<sup>65a</sup>

By the principle of Le Chatelier and the modified equation of Schröder-Van Laar-Prigogine-Defay, the stability of the racemic compound and conglomerate depends on pressure.<sup>4,45b</sup> Enantiomers become more stable at higher pressures if their density is greater than that of the racemic compound. Therefore a conglomerate can be obtained by crystallization at higher pressure, though it is not possible at the normal pressure. Collet<sup>45b</sup> showed that the melting point phase diagrams of enantiomer mixtures can be calculated as a function of temperature and pressure. He calculated such diagrams for the two compounds: phenylglyceric acid **14** and mandelic acid **15**. The former acid was found to form a conglomerate at pressures higher than 12 Kbar, while the latter transformed into the conglomerate at pressures higher than 7 Kbar.

**14****15**

## B. Racemic Conglomerate versus Racemic Compound of Different Chemical Compositions

The arrangement of molecules in a crystal structure depends on the number and nature of solvate molecules introduced into its lattice and on guest molecules in the host-guest inclusion compounds. Change of the counter ions or central metal atoms in salts and metal complex compounds often also leads to the alteration of crystal packing and possibly to a switch from hetero- to homochiral packing. Clearly alteration of covalently bound substituents in molecules can result in their different packing. The point is that even minor changes of substituents, not leading to considerable conformational deflections, can radically alter the crystal packing of molecules.

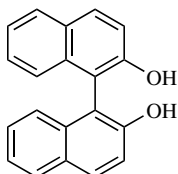
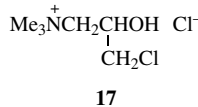
The formation of a different crystal structure with a different composition can be effected not only “from within” by changing the packing molecules or their

composition but also by changing crystallization conditions (temperature, pressure, humidity, additives, etc.) or by mechanical processing (grinding, pressing, etc).

The influence of temperature on the stability of crystal forms solvated to a various degree is in agreement with Van't Hoff's rule ("the least solvated compound is the most stable at high temperature").<sup>4</sup> For instance, sodium-ammonium tartrate tetrahydrate (Pasteur's conglomerate) is formed below 28 °C, whereas less hydrated racemic salt (Scacchi's monohydrated salt) is formed above 28 °C.<sup>4</sup> Recently a similar phenomenon was described for an inclusion compound: conglomerate is formed at the lower temperature (0 °C), and the racemic compound of a different guest/host composition is formed at room temperature.<sup>25f</sup> In the case of solvates, the driving force of the temperature-dependent racemic compound—conglomerate crystallization—is the enthalpy of solvate formation, which is usually exothermic, and consequently the stability of the more solvated form decreases with increasing temperature. Desolvation and solvation processes are often accompanied by phase transformations and depend very much on the solvent.<sup>66</sup> The solubility of compounds solvated to a variable degree varies greatly when passing from one to another modification, in contrast to crystalline modifications which are not solvated. Thus, in solvates and inclusion compounds the solvent of the crystallization is an important factor in controlling the formation of different crystalline modifications.

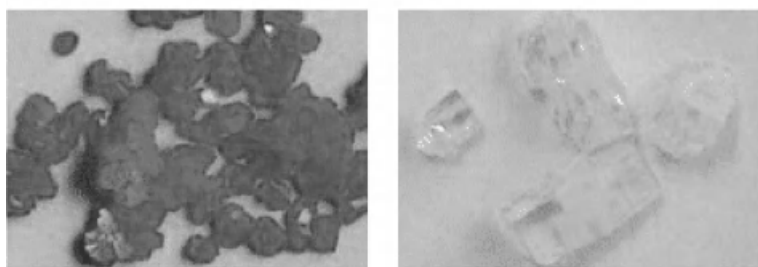
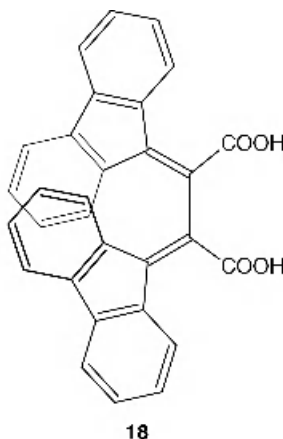
### *1. Formation of Racemic Conglomerate versus Racemic Compound among Solvates and Host–Guest Inclusion Compounds*

Several compounds that form both a racemic compound and a conglomerate differing in a number of solvate molecules have been reported.<sup>4</sup> Here some examples will be discussed and developed to show the influence of guest molecules on the racemic compound versus the conglomerate formation. Conglomerate formation by an inclusion compound opens up possibilities of resolution of both the host and the guest molecules simultaneously by preferential crystallization. This has been recently illustrated by Toda et al.<sup>67</sup> with the example of the inclusion compound of 2,2'-dihydroxy-1,1'-binaphthyl **16** with *N*-(3-chloro-2-hydroxypropyl)-*N,N,N*-trimethylammonium chloride **17** crystallizing as a conglomerate.

**16**

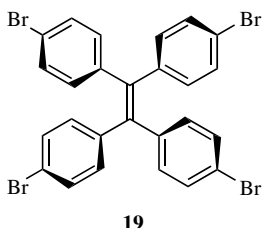
2,3-Bis-9-fluoren lidenesuccinic acid **18** has the ability to form stable inclusion compounds with a wide variety of guest molecules. Eight guests (EtOH, 2-butanone, cyclohexanone, ethylacetate, THF, dioxane, DMF, and DMSO) promote crystals of racemic compounds, whereas three other guests (acetone, cyclopentanone, THF) promote conglomerates. When using THF as a guest molecule, both a racemic compound (**18**:THF = 1:2) and a conglomerate (**18**:THF = 1:1) are formed. Nevertheless, **18** itself forms a racemic compound. (Figure 4.7) The inclusion compounds were obtained by crystallization from the guests. Thus one can alternate between hetero- and homochiral crystallizations by varying the solvent of crystallization.<sup>68</sup> In the case of **18**, acetone and cyclopentanone may be considered conglomerators.<sup>5c</sup>

An interesting case of the transformation of a racemic compound into a conglomerate, and vice versa, depending on the guest molecule and exposure to

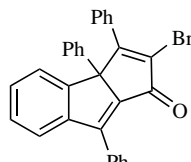
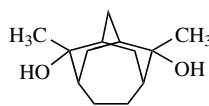


*Figure 4.7.* Photographs of racemic compound crystals of free host **18** (*left*) and conglomerate crystals of the 1:1 inclusion complex of **18** with acetone (*right*). An example of chirodichro(m)ism (for the first case, see Schurig<sup>57b</sup>). Reproduced with the permission of the authors.<sup>68</sup> See color insert.

vapors of the guest was investigated by Toda et al.<sup>70</sup> The crystallization solvent determines whether tetra(4-bromophenyl)ethylene **19** forms a metastable racemic or a thermodynamically more stable chiral host–guest inclusion complex. For example, a conglomerate is formed with *p*-xylene, and a racemic compound is formed with toluene. Also solid phase transformation of the racemic compound into the chiral complex occurred upon the exposure of the compound to vapors of the achiral guest (THF, *p*-xylene, benzene, dioxane, etc.). Lower stability of the racemic compound was evident by the fact that the transformation always occurred toward the chiral inclusion compound. Surprisingly, the formation of chiral inclusion complexes from the racemic host was also caused by the action of vapors of tetrahydrofuran and  $\beta$ -picoline, even though crystallization of **19** in these solvents led to the racemic form.<sup>70</sup> The behavior could be explained by the kinetically controlled formation of a metastable racemic compound upon crystallization that preceded the phase transformation into the more stable conglomerate upon the compound’s interaction with the solvent’s vapors. Analogous transformations of unstable conglomerates into the more stable racemic compounds were observed in malic acid and serine (Section V).<sup>71</sup> Transformations caused by high humidity are akin to the solvent-mediated transformations,<sup>63b</sup> which take place in intermediate solutions.

**19**

Bishop and coworkers developed a “helical tubulate family”<sup>25</sup> of the compounds that form stable inclusion complexes with a great number of small molecules incorporated into channels of crystal lattices formed by the H-bonded molecules. Compound **20** is a helical tubulate family member, and it crystallizes as a conglomerate in the same chiral space group  $P3_121$  with large guest molecules (e.g.,  $\text{CCl}_4$  or fluorocyclohexane).<sup>25c,j</sup> In the case of complexes of **20** with smaller molecules (e.g., dichlormethane or cyclohexane), the helical tubulate lattice transforms into the ellipsoidal clathrate lattice (achiral space group  $I4/acd$ )<sup>[25c,j]</sup> so it becomes a racemic compound. However, the cavity is not maintained without an included molecule.<sup>25g</sup> Enantiomerically pure **20** has been shown recently to have dramatically different inclusion properties: the helical tubulate lattice has remained for both small guest molecules and bulk guest molecules which do not form inclusion compounds with racemic **20**.<sup>25c</sup>



Toda and Tanaka<sup>72</sup> investigated inclusion compounds of **21** with 30 different guests. They showed that **21** forms racemic compounds with 15 different guest molecules (Table 4.3) and conglomerates with the other 15 (Table 4.4).

Table 4.3

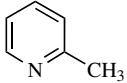
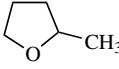
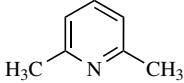
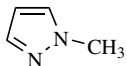
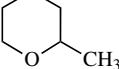
Formation of Racemic Compound Inclusion Crystals of **21** with Different Solvents (Guests)

Solvent (Guest)	Melting Point <sup>a</sup> (°C)	Solvent (Guest)	Melting Point (°C)
	112–115		100–102
	nd <sup>b</sup>		59–61
	nd <sup>b</sup>		145–149
	109–112		177–179
CHCl <sub>3</sub>	101–105		159–165
CHBr <sub>3</sub>	129–135	PhCl	88–90
CH <sub>2</sub> Cl <sub>2</sub>	nd <sup>b</sup>		132–138
PhOMe	127–131		

<sup>a</sup>Melting point of pure racemic **21** is between 185 °C and 186 °C.

<sup>b</sup>Not distinct.

Table 4.4  
Formation of Conglomerate Inclusion Crystals of **21** with Different Solvents (Guests)

Solvent (Guest)	Melting Point <sup>a</sup> (°C)	Solvent (Guest)	Melting Point (°C)
	112–114		135–139
	nd <sup>b</sup>		98–102
	120–125		119–123
	nd	MeI	nd
	122–128	EtBr	nd
	nd	EtI	nd
	nd	CCl <sub>4</sub>	127–130
		CBr <sub>4</sub>	129–134

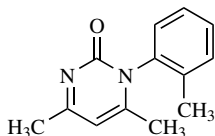
<sup>a</sup>Melting point of pure racemic **21** is 185–186°C.

<sup>b</sup>Not distinct.

A surprisingly high percentage of the conglomerates (50%) accounts for the inclination of this particular compound to homochiral crystallization. Most of the 30 compounds are isomorphous, so they should not properly be considered individually. Nevertheless, there are some compounds that are prone to the conglomerate formation. For instance, there are only two racemic compounds among the 13 chiral quinoneimines studied by Kostyanovsky and Avdeenko.<sup>73</sup>

*N*-Aryl-2(1*H*)-pyrimidinone **22** furnishes a mixture of two crystalline modifications by crystallization from ethanol: conglomerate (monoclinic, space group *P*2<sub>1</sub>) and racemic compound (monohydrated **22**·H<sub>2</sub>O; tetragonal, space group *I*4<sub>1</sub>/*a*).<sup>36c</sup> In the case of the related pyrimidones, enantiomerization at

high temperatures together with conglomerate formation was used to break the symmetry upon spontaneous resolution and to produce a number of optically active compounds in high chemical and enantiomeric yields.<sup>36c</sup>



22

In 1919, Jaeger<sup>74a</sup> first reported that optically active crystals of potassium tris(oxalato)cobaltate(III) ( $K_3[Co(ox)_3]*nH_2O$ , ox =  $(C_2O_4)^{2-}$ ) **23** can be obtained at 13.2°C and higher temperatures, while racemic ones are deposited below this temperature. However, Okazaki et al.<sup>74b</sup> reported that the real behavior of **23** upon crystallization is much more complicated. Two racemic compounds, form I ( $K_3[Co(ox)_3]\cdot 3.5H_2O$ , space group  $P\bar{1}$ ) and form II ( $K_3[Co(ox)_3]\cdot 2H_2O$ , space group  $C2/c$ ), were deposited below 5°C; the form II and conglomerate form III ( $K_3[Co(ox)_3]\cdot 2H_2O$ , space group  $P3_121$ ) were deposited above 20°C. Between 5°C and 20°C all the three forms were precipitated simultaneously (Figure 4.8).

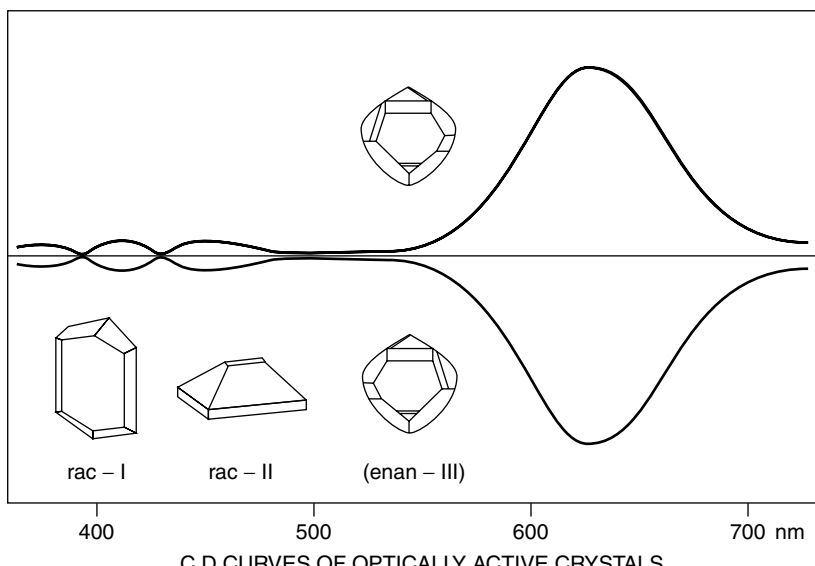


*Figure 4.8.* Sketches of enantiomorphous crystals of the form III ( $K_3[Co(ox)_3]\cdot 2H_2O$ , space group  $P3_121$ ) with their CD curves and the sketches of racemic-I ( $K_3[Co(ox)_3]\cdot 3.5H_2O$ , space group  $P\bar{1}$ ), and racemic-II ( $K_3[Co(ox)_3]\cdot 2H_2O$ , space group  $C2/c$ ) crystals.<sup>74b</sup> Reproduced with the permission of the American Chemical Society ©.

## 2. Formation of Racemic Conglomerate versus Racemic Compound Depending on Counter Ions, Central Metal Atoms, or Ligands

Over the last decade extensive studies were made of the influence of counter ions on conglomerate and racemic compound formation. In particular, many such studies concentrated on the structural investigations of salts of various carboxylic acids with amines. Most supposed the resolution of racemic amines and carboxylic acids by the diastereomeric salt method to be the easiest way. However, Saigo et al.<sup>75</sup> demonstrated that a great number of chiral amines forming racemic compound can be transformed into a conglomerate by a salt formation with a particular carboxylic acid. On the basis of his investigation some empirical rules for the selection of the “derivatizing reagent for conglomerate formation” were proposed: (1) the derivatizing reagent should be rigid and flat, (2) it should be able to form a helical column by forming hydrogen bonds with the molecule of the achiral amines and (3) the sizes of the derivatizing reagent and the racemate should be complementary.<sup>75b,c</sup> These rules were not applicable to conglomerate formation by the salts of chiral amines and dicarboxylic acids for which the more important factor was the existence of  $-\text{CH}_2-\text{CH}_2-$  units between the two carboxylic groups.<sup>75d</sup> Nevertheless, the rules were reasonably reliable for the salts of chiral primary monoamines and achiral monocarboxylic acids.<sup>75a</sup>

Studies of crystal structures of salts of chiral amines with achiral carboxylic acids have shown that all the conglomerate crystals consist of characteristic H-bonded  $2_1$ -columns. However, racemic compounds can be composed of achiral columns and planar networks in addition to the  $2_1$ -columns. In the achiral columns the amines are related by a center of symmetry, and they rarely can form planar networks. The percentage of the formation of the homochiral supramolecular units over the heterochiral ones (inverse center columns and planar networks) is surprisingly about 60%. Hetero- or homochiral spatial arrangements of such chiral  $2_1$ -columns by means of the weak interactions give rise to racemic or enantiomorphous crystals, respectively.<sup>75a</sup>

“Switching” behavior from hetero- to homochiral crystallization after the counter ion change has been shown in the case of *erythro* 2-amino-1,2-diphenyl ethanol **24**. The free base forms a racemic compound, while its salt with cinnamic acid crystallizes as the conglomerate.<sup>75e</sup>  $\alpha$ -Phenylethylamine ( $\alpha$ -PEA) forms conglomerates with two (itaconic acid **25** and succinic acid **26**) out of nine salts with various achiral amino acids.<sup>75d</sup> Crystallization of (*R,S*)-2-amino-3-chloropropanoic acid hydrochloride **27** as a conglomerate, in contrast to the corresponding free acid, was used for its resolution into enantiomers by preferential crystallization.<sup>76</sup>

Compounds such as  $[(3,2,3\text{-tet})\text{Co}(\text{N}_3)_2]^+\text{X}^-$ , ( $\text{X} = \text{Cl}, \text{Br}, \text{F}, \text{NO}_3$ ; 3,2,3-tet = 1,5,8,12-tetraazadodecane) crystallize as racemic compounds, but when turning to

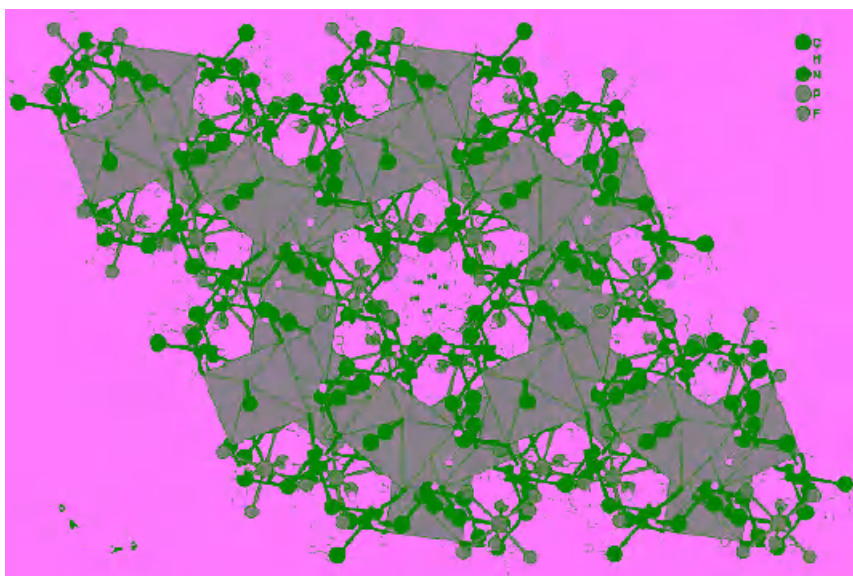
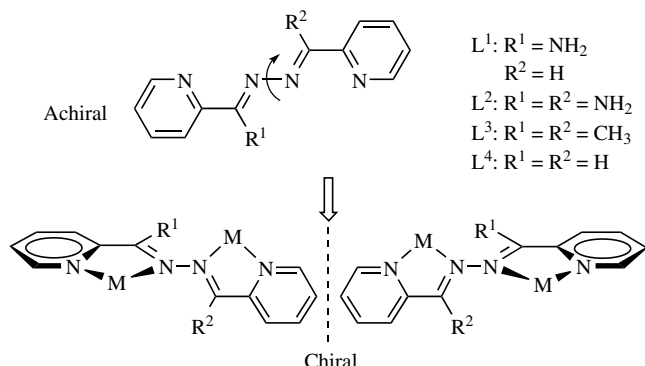


*Figure 4.9.* View of the cavities along *c*-axis for compound  $[(3,2,3\text{-tet})\text{Co}(\text{N}_3)_2]\text{PF}_6$ . For clarity, P–F bonds are indicated by a purple color, and other bonds are in black. Clusters of cations are packed in a spiral array generated by the  $6_1$  screw as regular, hexagonal cavities parallel to the *c*-axis. Adjacent helices are held together by the  $\text{PF}_6^-$ -anions.<sup>77</sup> Reproduced with the permission of the American Chemical Society ©. See color insert.

the  $\text{PF}_6^-$  counter ion, the precipitate becomes a conglomerate of enantiomorphous crystals (space group  $P6_1$ ) (Figure 4.9).<sup>77</sup>

Kaki et al.<sup>78</sup> investigated the solubility diagrams of bis(ethylenediamine) glycinatocobalt (III) salts  $[\text{Co}(\text{gly})(\text{en})_2]\text{X}_2$ , where  $\text{X}_2 = \text{SO}_4^{\text{2-}}$ ,  $\text{S}_2\text{O}_3^{\text{2-}}$ ,  $(\text{NO}_3)_2$ ,  $(\text{SCN})_2$ ,  $(\text{CH}_3\text{CO}_2)_2$ ,  $(\text{ClO}_4)_2$ ,  $(\text{CH}_3\text{CO}_2)\text{ClO}_4$ . Their studies revealed that the thiosulfate, nitrate, thiocyanate, acetate, and perchlorate salts crystallize as racemic compounds, while sulphate salt forms a 3,5-hydrated racemic compound upon crystallization below 39 °C and monohydrated conglomerate above 39 °C. In addition they found out that the double salt  $[\text{Co}(\text{gly})(\text{en})_2](\text{CH}_3\text{CO}_2)\text{ClO}_4$  crystallizes as a conglomerate within all the temperature range (5–50 °C) in contrast to the acetate and the perchlorate salts forming racemic compounds.

$[\text{Cis-}\alpha\text{-dinitro}(1,8\text{-diamino-3,6-diazaoctane})\text{Co(III)}]\text{Cl}$  **28** forms a conglomerate, although the change of chlorine anion to the stronger hydrogen-bonding counter anions such as  $\text{NO}_2^-$  and  $\text{NO}_3^-$ , or even the replacement of Co by Rh in the molecule, alters the hydrogen-bonding pattern and results in the racemic compound. An analogous conglomerate–racemic compound transformation



Scheme 4.2. Diazine ligands and generation of conformational chirality. Reproduced with the permission of the authors.<sup>81</sup>

occurs upon “switching” from the secondary  $-NH-$  groups to sulfur in such a compound as [cis- $\alpha$ -dinitro(1,8-diamino-3,6-dithiaoctane)Co(III)]Cl.<sup>79</sup>

Compound  $[M(bpy)_3](PF_6)_2$  with  $M=Ru$  crystallizes as a racemic compound of  $\beta$ -type (space group  $P\bar{3}c1$ ), while for  $M=Zn$  the heterochiral structure changes for the homochiral one, and a crystal of  $\gamma$ -type (space group  $P3_1$ ) is formed. For  $M=Ni$ , crystals of both structural types can be obtained concomitantly from the same crystallization batch. These compounds constitute another case where small changes in molecular geometry induce the alteration of hetero- to homochiral structures.<sup>80</sup>

Ligands  $L^1$ ,  $L^2$ ,  $L^3$ , and  $L^4$  (Scheme 4.2) in compounds  $[Mn_3(L^1)_2(N_3)_6]n$  (**29**),  $[Mn_2(L^2)_2(N_3)_3]n(ClO_4)n \cdot nH_2O$  (**30**),  $[Mn_2(L^3)(N_3)_4]n$  (**31**),  $[Mn_2(L^3)(N_3)_4]n \cdot nMeOH$  (**32**), and  $[Mn_2(L^4)(N_3)_4]n$  (**33**) are achiral. Nevertheless, they possess conformational chirality, which is hidden within the coordination polymers (Scheme 4.2).<sup>81</sup> Compounds **29** and **30** are found to form chiral one-dimensional (1D) chains. These are packed in a homochiral manner thus leading to conglomerate formation. Compound **32** crystallizes in the achiral space group  $P\bar{1}$ , and the structure consists of two-dimensional (2D) achiral layers. Compound **31** can form simultaneously both homo- (**31b**) and heterochiral (**31a**) coordination polymers, with the crystals of both structures consisting of homochiral layers (Figure 4.10) being related by the  $3_1$  screw axis and by inversion centers, respectively. So the entire crystals are homo- (**31b**) and heterochiral (**31a**). These coordination polymers can function as chiral magnets that combine both magnetism and optical activity. Their ability to form conglomerates along with racemic compounds allows one to examine the differences in chiromagnetic properties for the racemic and the

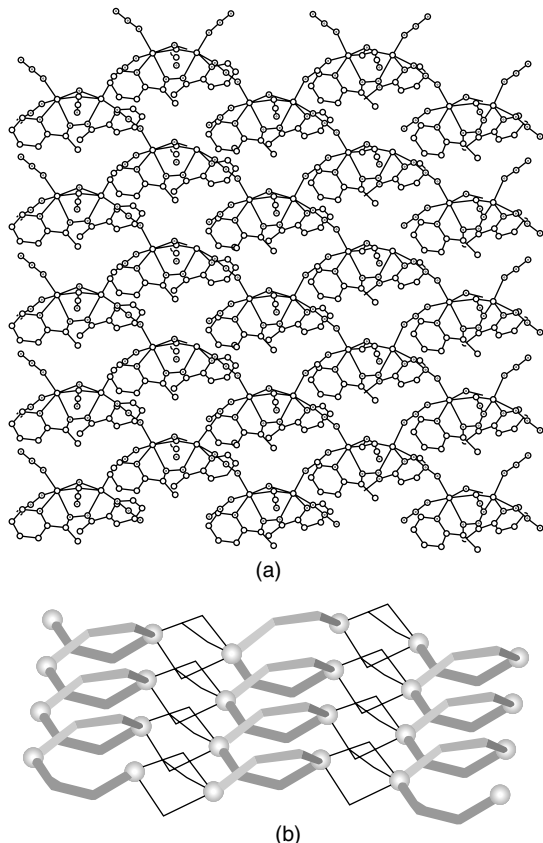
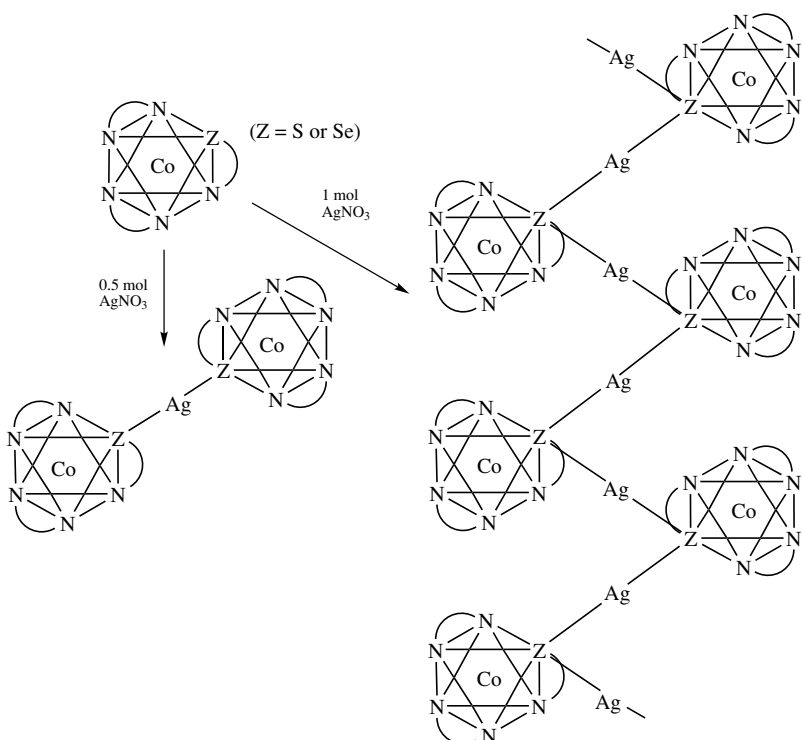


*Figure 4.10.* View of coscading homochiral chains (a), and detail of the helical chains formed by Mn atoms and azido bridges (b) in **31a**. The arrangement of **31b** is similar. Reproduced with the permission of the authors.<sup>81</sup>

chiral structures without encountering difficulties in the resolution of racemates into enantiomers.<sup>81</sup>

An interesting case of a chiral coordination polymer was recently reported by Konno et al.<sup>82</sup> A reaction of  $[\text{Co}(\text{X})(\text{en})_2](\text{NO}_3)_2$  ( $\text{X}=2\text{-aminoethanethiolate or 2-aminoethaneselenoate}$ ) **34** with  $\text{AgNO}_3$  in a 2:1 ratio in water produced a racemic compound whose crystals consisted of S- or Se-bridged  $\text{Co}^{\text{III}}\text{Ag}^{\text{I}}\text{Co}^{\text{III}}$  trinuclear heterochiral units (Scheme 4.3, Figure 4.11) whereas, corresponding 1:1 reaction leads to the conglomerate of homochiral crystals consisting of S- or Se-bridged  $(\text{Co}^{\text{III}}\text{Ag}^{\text{I}})_n$  homochiral chains (Scheme 4.3).



*Scheme 4.3.* Left: Heterochiral units making up the racemic compound crystals. Right: Homochiral chains making up the conglomerate crystals.

### 3. Formation of Racemic Conglomerate versus Racemic Compound Depending on Covalently Bound Substituents

The next issue of interest is whether the conglomerate formation of a certain compound will remain so after substitution of its atoms for those of adjacent groups or periods of the periodic table. Attempts at such replacements reveal (Table 4.5) that in the cases of A-D the substitution results in a dramatic change of crystal structure because the replaced atoms participate in strong interactions. However, the crystals of methanesulfinic and methaneseleninic acids (compounds E) are isomorphous, probably due to the lack of short contacts for the central atoms (S and Se). Some such cases are represented in Scheme 4.4. From the data of Scheme 4.4 and Table 4.5 we can expect conglomerate formation to occur among the phosphorus analogues of the chiral ammonium salts (Table 4.6).

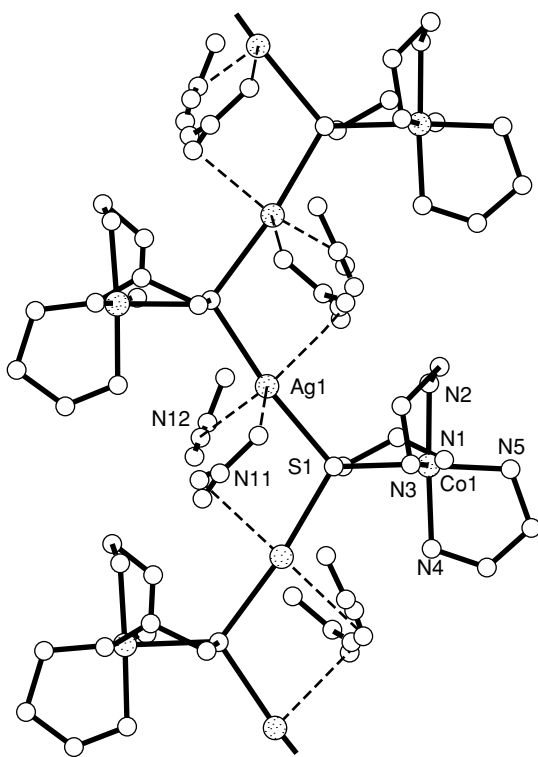
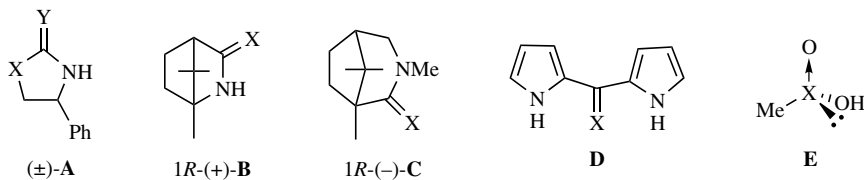


Figure 4.11. Perspective view of  $-(\text{NO}_3)_3$  [34a]. H atoms are omitted for clarity. The nitrate anions, do not contact with the  $\text{Ag}^{\text{I}}$  atom. Reproduced with the permission of the authors.

From the frequency of occurrence of different crystal modifications for the same molecules, even under the same conditions (concomitant polymorphs)<sup>56</sup> and with minor, if any, conformational variations upon switching from one crystal structure to another, we can expect the change of a covalently bound substituent to radically affect crystal packing. For example, replacement of one halogen in a molecule with another can alter the crystal packing, and also change the packing mode from hetero- to homochiral, although the geometry of the molecules in the crystals remains the same. The latter occurrence shows the importance of the intermolecular interactions in crystal structure formation. For instance, hexa-tert-butyl-1,3-dibromotrigerman **35**, which lacks any stereogenic center with chirality based on the helical arrangements of the germanium halogen atoms, crystallizes as a racemic compound, whereas replacement of the bromine atoms with iodine ones shows negligible variations in the molecular geometry but gives rise to a compound crystallizing as a conglomerate.<sup>90</sup>

Table 4.5  
Space Groups for Oxygen, Sulphur, and Selenium Analogues A–E



Type	X	Y	Space Group	Z	Reference
<b>A</b>	S	O	<i>P</i> 2 <sub>1</sub> 2 <sub>1</sub> 2 <sub>1</sub>	4	29a
	O	O	<i>Pna</i> 2 <sub>1</sub>	4	29b
	O	S	<i>P</i> 2 <sub>1</sub> / <i>n</i>	4	29c
	S	S	<i>P</i> 2 <sub>1</sub> / <i>n</i>	4	29d
<b>B</b>	O	—	<i>P</i> 4 <sub>3</sub> ( <i>P</i> 4 <sub>1</sub> )	8	83
	S	—	<i>P</i> 2 <sub>1</sub>	4	83
<b>C</b>	O	—	<i>P</i> 2 <sub>1</sub>	4	83
	S	—	<i>P</i> 2 <sub>1</sub> 2 <sub>1</sub> 2 <sub>1</sub>	4	83
<b>D</b>	O <sup>a</sup>	—	<i>P</i> 2 <sub>1</sub> 2 <sub>1</sub> 2 <sub>1</sub>	4	84
	S <sup>b</sup>	—	<i>Pbca</i>	8	84
<b>E</b>	S <sup>c</sup>	—	<i>P</i> 2 <sub>1</sub> 2 <sub>1</sub> 2 <sub>1</sub>	4	85, 86
	Se <sup>c</sup>	—	<i>P</i> 2 <sub>1</sub> 2 <sub>1</sub> 2 <sub>1</sub>	4	86

<sup>a</sup>Left-handed helices.

<sup>b</sup>Layers.

<sup>c</sup>Prepared by spontaneous resolution

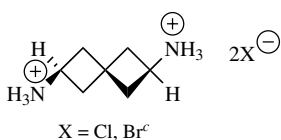
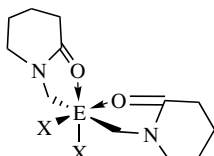
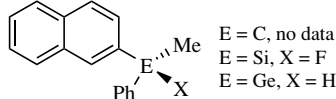
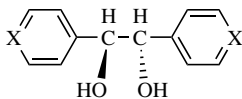
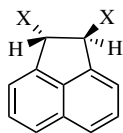
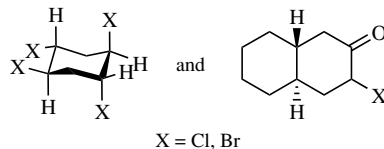
Another example we can cite is halogen-substituted 3-hydroxy-3-phenylpropionic acids. The racemic unsubstituted acid was shown to form a conglomerate.<sup>91a,b</sup> The para-fluoro acid formed racemic compounds.<sup>91c,d</sup> The para-chloro and para-bromo- substituted acids were found to form conglomerates,<sup>91e,f</sup>

Table 4.6  
Crystallographic Data for Chiral Ammonium and Phosphonium Salts

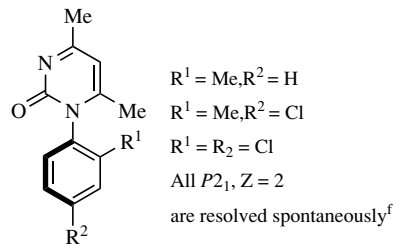
Compound	X	Space Group	Z	Reference
( $\pm$ )-Me(Et)N <sup>+</sup> (All)Ph X <sup>-</sup>	I (CHCl <sub>3</sub> )	P2 <sub>1</sub> 2 <sub>1</sub> 2 <sub>1</sub>	4	88
( $\pm$ )-Me(Bn)N <sup>+</sup> (All)Ph X <sup>-</sup>	Cl	P2 <sub>1</sub> 2 <sub>1</sub> 2 <sub>1</sub>	4	<sup>a</sup>
	Br	P2 <sub>1</sub> 2 <sub>1</sub> 2 <sub>1</sub>	4	28k
	I	P2 <sub>1</sub> 2 <sub>1</sub> 2 <sub>1</sub>	4	28k
	Br	P2 <sub>1</sub> 2 <sub>1</sub> 2 <sub>1</sub>	4	28k
(S)-(+)-Me-(n-Pr)P <sup>+</sup> (Bn)Ph X <sup>-</sup>	Br	P2 <sub>1</sub> 2 <sub>1</sub> 2 <sub>1</sub>	4	28k
( $\pm$ )-Me(n-Pr)N <sup>+</sup> (Bn)Ph X <sup>-</sup>	Br	P2 <sub>1</sub> 2 <sub>1</sub> 2 <sub>1</sub>	4	<sup>a</sup>

<sup>a</sup>Not published.

K and Rb acid tartrates

 $[\text{Co(III})(\text{NO}_2)_2(\text{en})_2]\text{X}$ , X = Cl, Br<sup>b</sup> $\text{Na}_3[\text{M(III)}(\text{ox})_3]$ , M = Co, Rh $[\text{Co(III)}(\text{edta})](\text{H}_2\text{O})_2$ , X = K,  $\text{NH}_4^b$ 

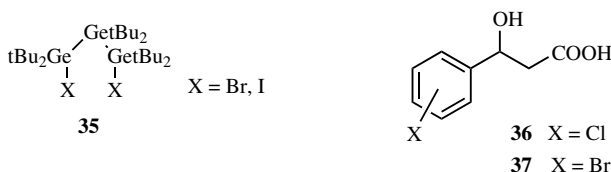
$\text{E} = \text{Sn}$   
 $\text{X} = \text{Br, P}6_1 (\text{Z} = 6)d$   
 $\text{X} = \text{I, P}6_5 (\text{Z} = 6)d$   
 $\text{E} = \text{Ge}$   
 $\text{X} = \text{Br, P}6_1 (\text{Z} = 6)e$



*Scheme 4.4* Examples of compounds retaining homochiral mode of crystallization after changing one of their atoms on another. Notes: (a) see Jacques et al.<sup>4</sup>; (b) see also Kostyanovsky et al.<sup>69</sup>; (c) see Janson and Pose.<sup>38</sup>; (d) see Ovchinnikov et al.<sup>87a</sup>; (e) see Ovchinnikov et al.<sup>87b</sup>; (f) see Sakamoto et al.<sup>36c</sup>

but the equivalent meta-chloro- and meta-bromo-substituted acids were reported to crystallize as racemic compounds.<sup>91a</sup> More insight into the structural differences between conglomerates and racemic compounds formed by closely related compounds comes from Larsen and Marthi.<sup>92a,b</sup> They performed crystal structure determinations of optically active and racemic meta-chloro- (**36**) and meta-bromo- (**37**) substituted 3-phenyl-3-hydroxy propionic acids.

X-ray diffraction data have revealed that racemic **36** and **37** are isostructural (monoclinic,  $P2_1/c$ ). The enantiopure and racemic crystals only differ in the orientation of hydrogen-bonded chains. The results from these structural studies, together with those of other halogen-substituted 3-hydroxy-3-phenylpropionic acids, show that the O–H···O hydrogen bonds are formed between identical donor and acceptor atoms in two distinct motifs. In their analyses of crystal structures Larsen and Marthi<sup>92a,b</sup> therefore concluded that the crystallization of racemates as either racemic compounds or conglomerates can only be rationalized if weak intermolecular interactions are taken into account. The close resemblance



of packing modes of racemates and corresponding enantiomers for significant number of such pairs was first discussed by Pedone and coworkers<sup>93</sup> and theoretical basis for this was provided by the Kitaigorodkii Aufbau principle<sup>94</sup> developed by Zorkii.<sup>95</sup> Saigo's X-ray crystallographic studies of the chiral salts provide additional experimental evidence.<sup>75</sup> However, in primarily achiral aggregates, any packing mode can lead to racemic structures (see Section VI).

## V. TRANSFORMATIONS BETWEEN HOMO- AND HETEROCHIRAL CRYSTALS

In 1897 Kipping and Pope<sup>96</sup> reported the first examples of possible transformations between a racemic compound and a racemic conglomerate. Thermodynamic aspects of this phenomenon were discussed by Jacques et al.<sup>4</sup> Recently Coquerel<sup>5b</sup> reviewed possible binary melting diagrams of enantiomers that, together with ternary solubility and Gibbs free energy versus temperature diagrams, are simple and informative means for describing both relative thermodynamic stabilities of racemic compound/racemic conglomerate pairs and possible phase transformations between them.<sup>4,56a</sup> Some examples of transformations occurring directly in solid state or through an intermediate solution, liquid, or vapor phase, in addition to a few examples mentioned in the previous sections, are given in the following section.

One of the most extensively studied compounds capable of solid phase transformation between homo- and heterochiral crystals is 1,1'-binaphthyl.<sup>48</sup> It was shown that its racemic compound can be transformed into a racemic conglomerate above 76°C. 1,1'-Binaphthyl is capable of enantiomerization (half-time of racemization in solution is about 10 h at 25°C),<sup>49</sup> and consequently above 76°C (under conditions of conglomerate formation) it can convert from a racemic mixture to a single enantiomer. Recently a full transformation of this racemate into one of the enantiomers was carried out under conditions of fast enantiomerization (absolute asymmetric synthesis).<sup>50</sup>

2,3:6,7-Dibenzobicyclo[3.3.1]nona-2,6-diene-4,8-dione **6** is the latest example of a compound forming both a racemic compound **R** (by crystallization below

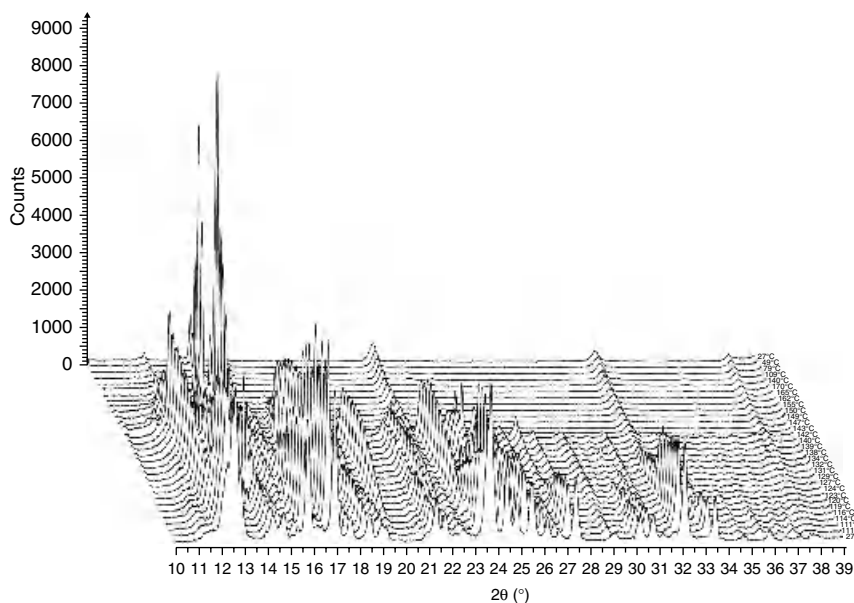
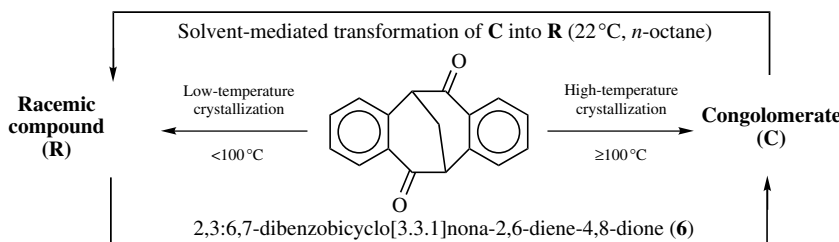
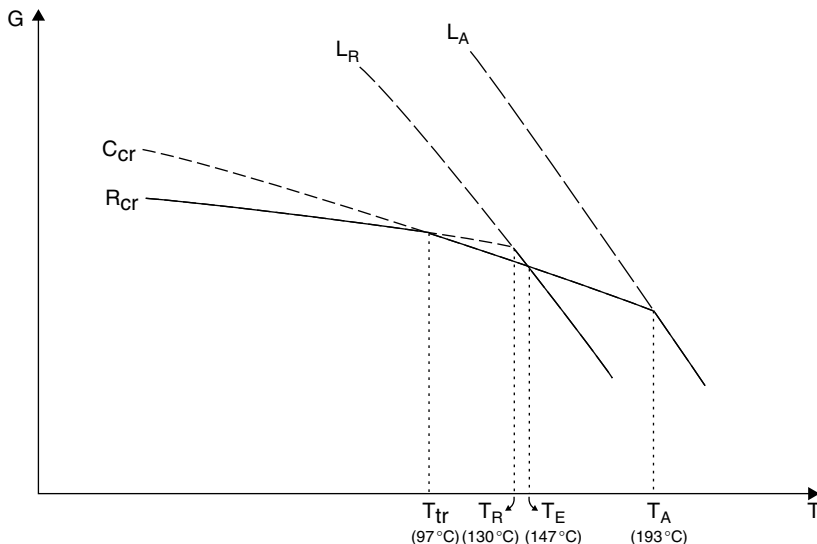


Figure 4.12. Variable temperature powder X-ray diffraction analysis of **R**. Solid phase transformation of **R** into **C** occurs upon heating within the temperature range of 116–129°C.

100°C) and a racemic conglomerate **C** (by crystallization above 100°C).<sup>36b</sup> We have investigated the thermodynamic aspects of this phenomenon, namely the relative stabilities of the two forms and possibility of the transformations.<sup>63a</sup> A solid phase transformation of **R** into **C** upon heating above 97°C has been detected by DSC and PXRD analyses (Figure 4.12). At the same time the homochiral form **C** was converted into **R** by solvent mediated transformation at room temperature (Scheme 4.5).



Scheme 4.5. Schematic representation of the racemic compound-conglomerate transformations of **6**.



*Figure 4.13.* Schematic representation of the dependence of  $G$  (Gibbs's free energy) on  $T$  (temperature);  $R_{cr}$  and  $C_{cr}$  characterize the free energies of the crystalline racemic compound **R** and the conglomerate **C**, respectively;  $L_R$  and  $L_A$  describe the free energy of the melts of hetero- and homochiral compositions. The dashed lines show a metastable phase capable of spontaneous conversion to the corresponding more stable state.

The ease of mutual transmutations between **R** and **C** can be explained by their virtually the same densities,<sup>36b</sup> and thus the closeness of their thermodynamic stabilities despite the large difference in melting points.

With the data thus obtained, we plotted Gibbs free energy against temperature ( $G$  vs.  $T$ ) for the two modifications of the diketone (Figure 4.13). As the figure shows,  $T = 97^\circ\text{C}$  is the critical temperature below which **R** is more stable and above which **C** is more stable,  $130^\circ\text{C}$  is the melting point of **R**, and  $147^\circ\text{C}$  is the melting temperature of the eutectic mixture of the enantiomers. Knowing the range of the stability of **C** consequently opens the way for the resolution of **6** into enantiomers by direct crystallization.

Racemic 3-(3-chlorophenyl)-3-hydroxypropanoic acid **36** was described by Collet and Jacques.<sup>91a</sup> Formation of a racemic compound on crystallization (space group  $P2_1/c$ ) was reported. Although its transformation into conglomerate on melting was considered as very probable, the only evidence of this was the identity of the melting points of the racemic compound and the calculated melting point of the conglomerate.<sup>91a</sup> Later, Larsen and Marthi<sup>92</sup> studied halogen-substituted 3-hydroxy-3-phenylpropionic acids in order to gain insight into their

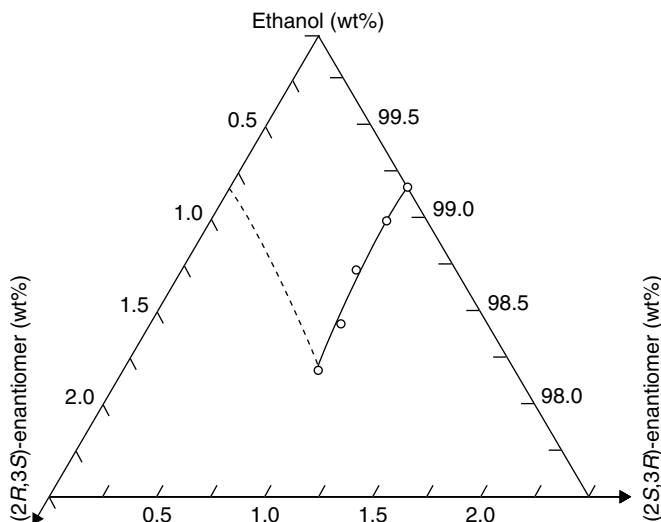


Figure 4.14. Standard representation of a ternary solubility diagram of a compound crystallizing as a conglomerate (the case of **38**).<sup>97d</sup>

conglomerate with regard to racemic compound formation. They investigated **36** by DSC analysis and did not observe any solid–solid transitions upon heating the sample racemic compound. Nevertheless, after two years they discovered that the sample of **36** had transformed into a conglomerate during storage. Thermodynamic measurements of **36** showed that the conglomerate and the racemic compound were in equilibrium.<sup>92b</sup>

Benzylammonium salt of (*2RS,3SR*)-2-benzoylamino-3-hydroxy-3-phenyl propionic acid **38** exists as a conglomerate around room temperature but forms a racemic compound in the vicinity of its melting point.<sup>97d</sup> This fact was confirmed by a ternary solubility diagram of this salt which corresponds to the conglomerate (Figure 4.14), although the binary melting point diagram corresponds to the racemic compound (Figure 4.15). Similar behavior of conglomerate–racemic compound transformation has been observed by Shiraiwa et al.<sup>97e</sup> for several compounds: *R,S*-2-benzoylamino-2-benzyl-3-hydroxypropanoic acid **39**, *R,S*-1,1,3,3-tetramethylbutylammonium hydrogen malate **40**,<sup>97b</sup> *R,S*-cysteine salt of benzenesulfonic acid **41**,<sup>97c</sup> and ammonium salt of *R,S*-*N*-acetyl-2-aminobutyric acid.<sup>97a</sup> It should be noted that compounds **38** and **39** have relatively small differences between melting points of the enantiomers and the racemic compound 13 °C and 12 °C, respectively, and they crystallize from solutions as conglomerates. Usually conglomerates are expected to be formed if the corresponding enantiomers

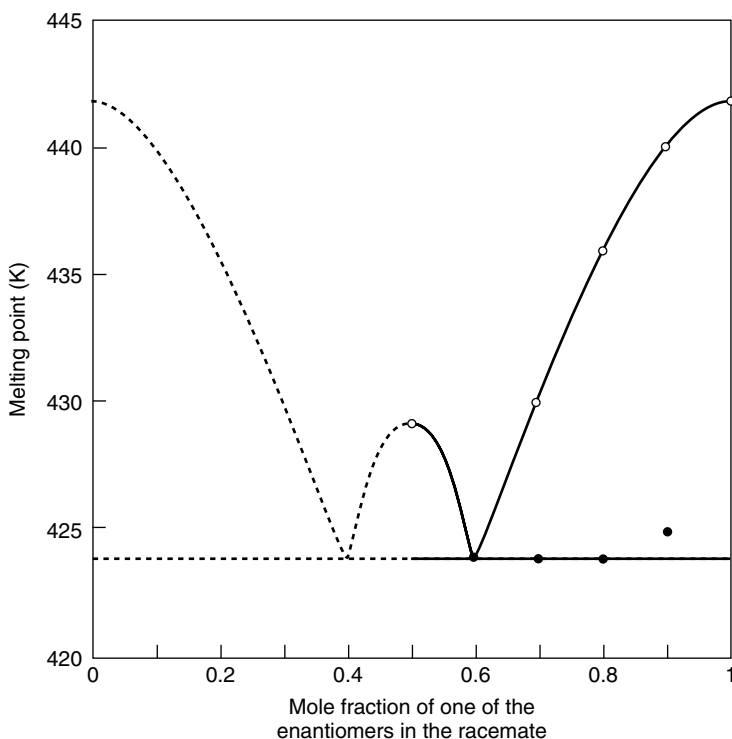
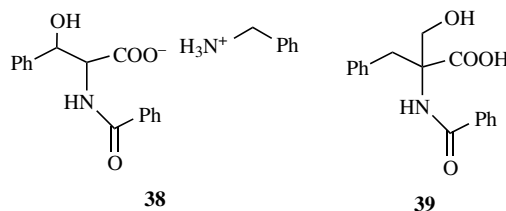
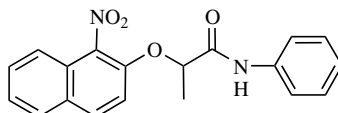


Figure 4.15. Standard representation of a binary melting diagram of a compound existing as a racemic compound upon melting (the case of **38**).<sup>97d</sup>

melt approximately by 20 to 30 degrees higher than the racemates do. Collet et al.<sup>4</sup> used this relation to evaluate the frequency of conglomerate formation at 5% to 10%. However, as we have recently shown,<sup>63a,36a</sup> the temperature difference is only reliable in close proximity to the melting point of the racemate, as is evident in compounds **38**, **39**, and **6**.



In the case of anilide of 2-(1-nitro-2-naphthoxy)propionic acid **55**, the temperature of transformation of the racemic compound obtained by crystallization into the corresponding conglomerate has been determined to be equal to 173 °C. The transformation was detected by solid state IR spectroscopy.<sup>98</sup>

**43**

Racemic zopiclone crystallizes simultaneously as a mixture of two forms: racemic compound (form I) (monoclinic dihydrate; space group  $P2_1/c$ ) and conglomerate (form III) (orthorombic anhydrous form, space group  $P2_12_12_1$ ). Form I loses water molecules when heated and transforms into an anhydrous form II (space group  $P2_1/c$ ). Following heating of form II, a spontaneous resolution in the solid phase gives rise to form III. Interestingly, unlike the irreversible transformation  $\text{II} \rightarrow \text{III}$ , the transformation  $\text{I} \rightarrow \text{II}$  is reversible, and form II can revert to form I upon exposure to high relative humidity at room temperature. Crystal packing and the zopiclone molecular conformations in forms I and II are essentially the same, whereas transformation  $\text{II} \rightarrow \text{III}$  is accompanied by considerable changes in molecular conformation and crystal packing.

Conglomerate formation is a rather rare (<10%) phenomenon.<sup>4</sup> Nevertheless, if one considers a physical mixture of enantiomers as the conglomerate, it is possible to investigate the stability of the latter with respect to the racemic compound even if the conglomerate cannot be attained by crystallization. Such a strategy has been employed by Yamamoto et al. in the study of conglomerate stability of some organic acids.<sup>71</sup> They have studied the transformations of conglomerates of malic acid **44**, tartaric acid **45**, serine **46**, valine **47**, leucine **48**, and norleucine **49** into corresponding racemic compounds under milling action and humidification. Conglomerates of **44**, **45**, and **46** readily transformed into racemic compounds upon grinding and humidification, whereas the solid phase transformations of **47**, **48**, and **49** only occurred after humidification. The differences in solid phase transformation have been attributed to differences in the hydrogen bonding patterns of the crystal structures. The solid phase transformations were detected by PXRD, ss IR, and DSC.<sup>71</sup>

In the case of the conglomerate of the ephedrine base, its transformation into the racemic compound was observed not only in the solid state but also in the liquid, as a solution (solvent mediated transformation), and in the vapor state. The reaction in the solid appeared to proceed via the vapor phase as indicated by



Figure 4.16. Photograph showing the growth of the racemic compound of ephedrine, consisting of needles at the center of a glass Petri dish, from vapors of the individual enantiomers kept diametrically separated. The crystals on the left are of *L*-ephedrine; those on the right are of *D*-ephedrine.<sup>59</sup>

the growth of crystals of the racemic compound between separated crystals of the two enantiomers in a glass Petri dish (Figure 4.16).<sup>59</sup>

A similar example of racemic compound formation from two opposite enantiomers in the solid state was accidentally discovered by Schurig.<sup>57b</sup> When mixing crystals of the two enantiomers of dicarbonyl-rhodium(I)-3-TFA-camphorate **50** he noticed a change of color from yellow to deep red-green. The yellow color would correspond to the enantiopure material, and the red-green to the racemic compound crystals (Figure 4.17). Thus, it was possible to observe solid state transformation of a conglomerate into a racemic compound by the naked eye. The phenomenon of differently colored racemic and enantiopure material was termed chirodichro(m)ism.<sup>57b</sup>

Recently an interesting experiment of phase transformation between homo- and heterochiral structures was reported by Bernal et al.<sup>99</sup> Centrosymmetric crystals of [(tren) $\text{Co}(\text{N}_3)_2\text{I}$ ] **51** (tren = tris(2-aminoethyl)amine =  $(\text{H}_2\text{N}-\text{CH}_2-\text{CH}_2)_3\text{N}$ ) (space group  $P2_1/n$ ) obtained by crystallization at room temperature were found to transform into noncentrosymmetric crystals (space group  $P2_1$ ) upon cooling. Bernal et al. showed that upon cooling, one of the two molecules related by the



*Figure 4.17.* Chirodichro(m)ism in the solid state of dicarbonyl-rhodium(I) 3-(trifluoroacetyl)-(1R)-camphorate. *Left:* Crystals of the pure enantiomer (1R)-**50**. *Right:* Crystals of the racemate (1R/1S)-**50**.<sup>57b</sup> Reproduced with the permission of the author. See color insert.

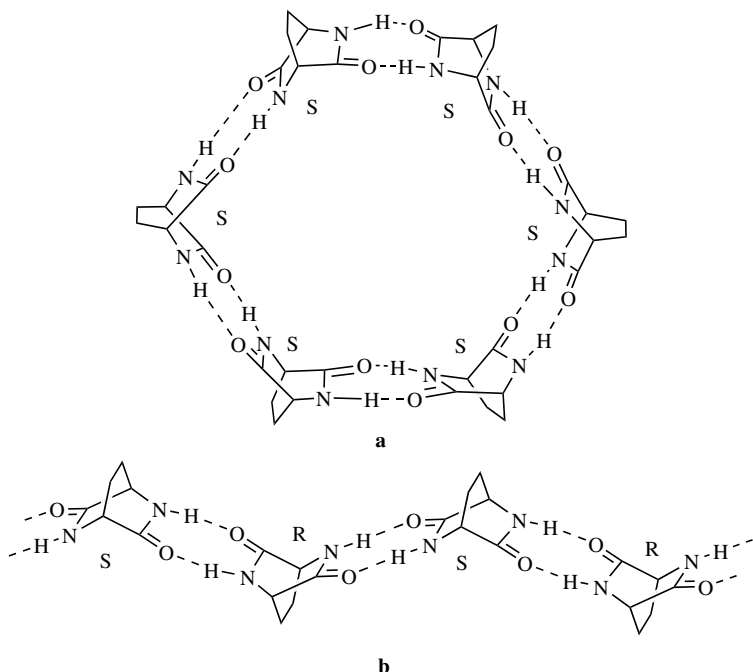
inversion center alternated its torsion angles, resulting in loss of the center of symmetry. Consequently the space group changed from centrosymmetric  $P2_1/n$  to the noncentrosymmetric  $P2_1$ , but the crystal on the whole remained racemic. Heating of the same sample resulted in recovery of the center of inversion. It should be noted that changing the counter ion from iodine to bromine resulted in the formation of a conglomerate (space group  $P2_12_12_1$ ) that was stable over the whole temperature range.<sup>99</sup>

Crystallization of 1,1'-bis-2-naphthol **52** from methanol solution with addition of tetramethylammonium chloride **53** leads either to a racemic compound **52:53**:MeOH (from concentrated solution) or to a racemic conglomerate **52:53** (from diluted solution). However, the MeOH molecule is liberated upon heating of the racemic complex up to 120°C, which is accompanied by transformation of the racemic complex into the conglomerate complex. The same transformation can occur just by contact of the racemic compound with MeOH vapor in the solid state. Surprisingly, contact of a mixture of powdered **52** and **53** with MeOH vapor for 30 min leads to the conglomerate complex **52:53**, although simple mixing of powdered **52** and equimolar amount of **53** by mortar and pestle for 30 min does not give the complex.<sup>67</sup>

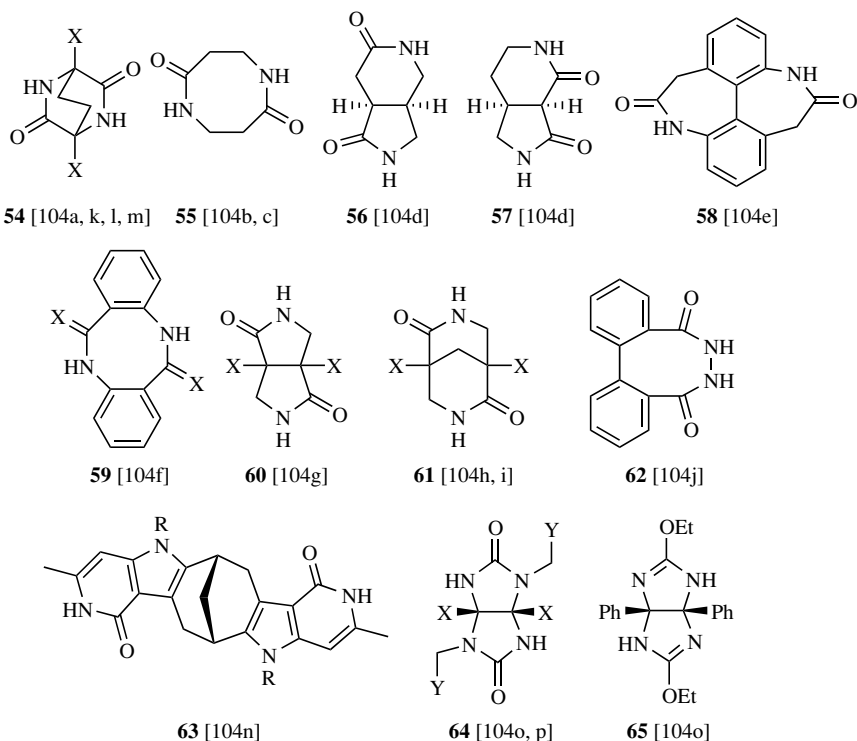
## VI. HOMO- AND HETEROCHIRAL CRYSTAL ENGINEERING

The concept of the supramolecular synthon is a key point in crystal engineering.<sup>100</sup> Most synthons are based on two-point or planar three-point interactions and do not carry any three-dimensional (including chiral) stereochemical information. Only the conformation of an organic molecule that contains the synthons, a three-dimensional coordination of the synthons by the tetrahedral carbon atom<sup>101</sup> or metal ion (Section IV.B.), or a chiral environment of supramolecular

synthons can encode such information.<sup>102</sup> Nevertheless, even in simple cases the encoding is ambiguous. For instance, in the spiral structures of diastereomeric supramolecular complexes of enantiopure 1,2-*trans*-diaminocyclohexane and enantiopure 1,2-*trans*-cyclohexanediol (supraminols) the spiral direction is determined only by the amine chirality.<sup>103</sup> The first chiral supramolecular synthon (**54**, X = H) with defined homo- and heterochiral types of self-assembly (Schemes 4.7 and 4.8) was proposed by Lehn et al.<sup>102,104a</sup> The chiral information in this molecule is defined by its rigid conformation and hexagonal dihedral angle between the mean planes of amidic groups. Amidic H-bonding in the homochiral case results in a so-called hexameric bracelet (Scheme 4.7a). We studied this structure in gas phase (RHF/STO-3G) theoretically (Figure 4.18) as it converged to a minimum. Efficient packing of such a bracelet is difficult. Therefore in the enantiopure crystal, homochiral self-assembly occurs via the formation of H-bonded layers.<sup>104a</sup> In crystals of the racemic compound<sup>104a</sup> heterochiral zigzag tapes are observed (Scheme 4.6).



*Scheme 4.6.* Chiral information expressed by **54** (X = H). (a) Hypothetical homochiral bracelet; (b) real heterochiral zigzag tape.



Racemic compounds outnumber the racemates of similar chiral supramolecular synthons **54–65** that are capable of forming heterochiral tapes via amidic H-bonding.<sup>104</sup>

We utilized the heterochiral motif suggested by Lehn (Scheme 4.6) in designing racemic “molecular brick walls with both organic and inorganic coatings” of alkyl,<sup>104i</sup> metal,<sup>104m</sup> and alkylammonium<sup>105</sup> **54**-dicarboxylates (Figure 4.19). The brick wall motif can also be used to engineer chiral crystals<sup>106,104i</sup> by way of quasi-racemate methodology<sup>7,106a</sup> or simply by introducing chiral enantiopure substituents.<sup>106b</sup> The **54**-diacid ( $X = \text{CO}_2\text{H}$ ) has the common feature mentioned above (Section IV.B.3): packing of enantiomers in enantiopure and racemic crystals is very similar and in both cases homochiral layers are realized.<sup>104i</sup>

In crystal engineering it is very important to remember that the crystal structure of an organic molecule is a delicate balance of directionally strong and anisotropically weak interactions, and any peripheral changes can break the balance. For **64**,  $X = Y = \text{Ph}$ , the molecules pack in heterochiral tapes,<sup>104o</sup>

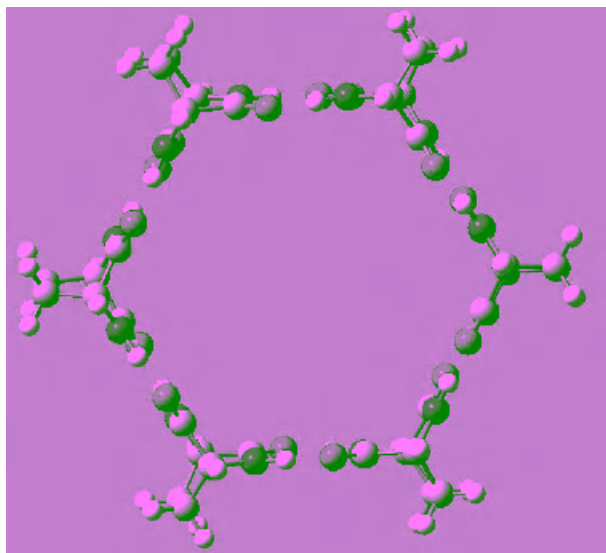


Figure 4.18. *Ab initio* RHF/STO-3G optimized structure of  $D_6$ -symmetric Lehn's bracelet.<sup>104a</sup> See color insert.

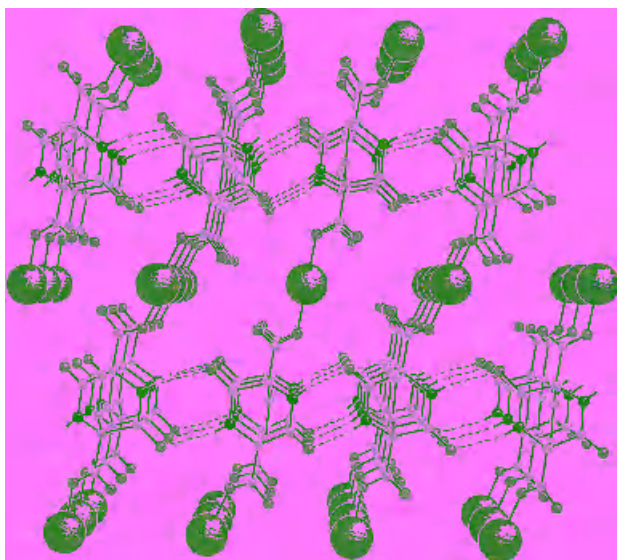
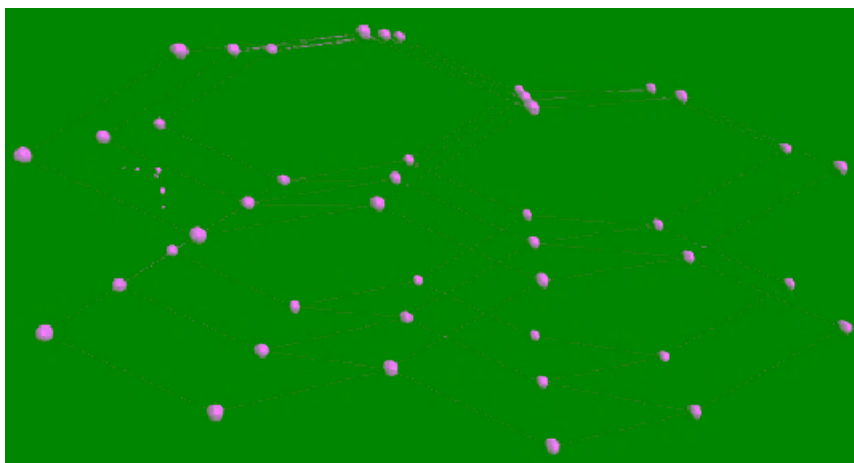
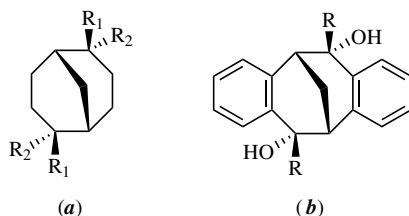


Figure 4.19. Molecular brick walls with inorganic coating in the crystal structures of metal **54**-dicarboxylates.<sup>104m</sup> See color insert.



*Figure 4.20.* Diamondoid H-bonding network in the crystal structure of **64** ( $X = \text{H}$ ,  $Y = \text{Me}$ ).<sup>104p</sup> The balls denote centers of the molecules, and the lines unite molecules by  $\text{NH}\cdots\text{OH}$ -bonding pathways. See color insert.

whereas in the case of glycoluril, with  $X = \text{H}$  and  $Y = \text{Me}$ , molecules form a conglomerate<sup>104p</sup> with a three-dimensional diamondoid structure (Figure 4.20). This conglomerate was spontaneously resolved and used as an enantiopure precursor of the drug Albicar.<sup>45d,107</sup> When passing from  $\text{H}$  to  $\text{Me}$  and  $\text{Et}$  in *exo*-, *exo*-diols **66**, **67**, and **68**, respectively, (Scheme 4.7) the H-bonding pattern changes fundamentally and gives rise to different crystal packing. **66** and **68** have achiral crystal structures consisting of H-bonded 3D networks (space groups  $P2_1/c$  and  $Fdd2$ , respectively),<sup>25q</sup> while **67** has a chiral tubular structure based on tight spiral spines of H-bonds (space group  $P3_121$ ).<sup>25q,r</sup> Crystals structures of the related *endo*-,*endo*-diols **69**, **70**, and **71** (Scheme 4.7) are also achiral and not isomorphous. *Endo*-,*endo*-dimethyldiol **69** forms H-bonded layers (space group



*Scheme 4.7.* (a) **66** ( $R_1 = \text{OH}$ ,  $R_2 = \text{H}$ ), **67** ( $R_1 = \text{OH}$ ,  $R_2 = \text{Me}$ ), **68** ( $R_1 = \text{OH}$ ,  $R_2 = \text{Et}$ ), **69** ( $R_1 = \text{Me}$ ,  $R_2 = \text{OH}$ ); (b) **70** ( $R = \text{Me}$ ), **71** ( $R = \text{H}$ ).

*Pc*),<sup>25s</sup> while *endo*-,*endo*-dibenzodimethyldiol **70** does not form cooperative O–H···O hydrogen bonds at all and the molecules are joined into heterochiral chains by means of weak C–H···O contacts.<sup>25p</sup> Surprisingly, molecules of *endo*-,*endo*-dibenzodiol **71** produce cooperative O–H···O hydrogen bonds that bind them into heterochiral hexamers. The hexamers themselves are packed one over another, creating a porous crystal structure (Figure 4.21).<sup>25p</sup>

Examples of fundamental changes in crystal packing due to disruption of the main structure-determining contacts are numerous. One such case is the

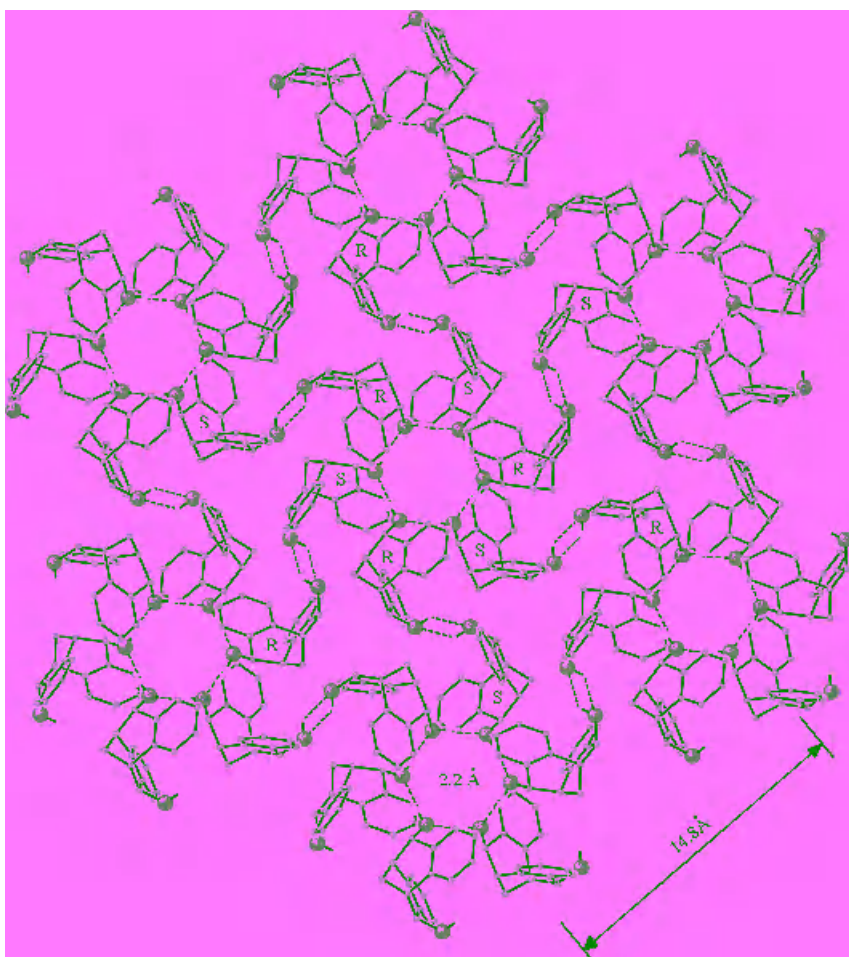


Figure 4.21. View of porous crystal structure of **71** along the crystallographic *c*-axis. The diameter of the canals, 2.2 Å, given here takes into account atomic van der Waals radii. See color insert.

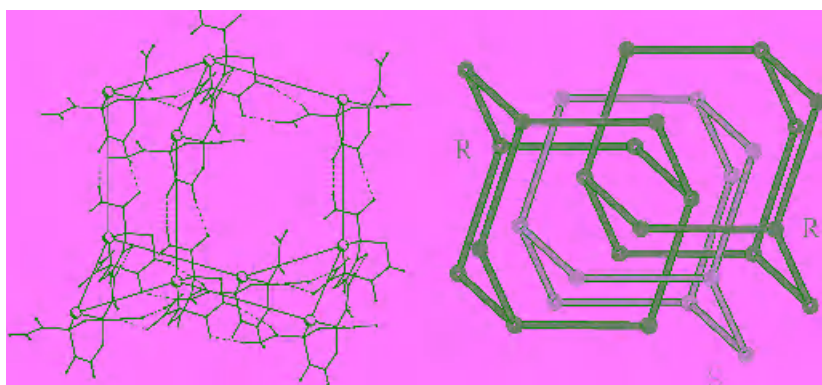


Figure 4.22. Homochiral threefold interpenetrated H-bonded diamondoid networks in the crystal structure of **61** ( $X = \text{CONH}_2$ ).<sup>6</sup> See color insert.

change from heterochiral tapes in **61** ( $X = \text{CO}_2\text{Alk}$ )<sup>104h,i</sup> to homochiral threefold interpenetrated diamondoid networks as competitive H-bonding substituents ( $X = \text{CONH}_2$ ) are introduced (Figure 4.22).<sup>6</sup> Interestingly, the homochiral hexamers resembling Lehn's bracelet could be separated in the crystal structure (Figure 4.23).<sup>6</sup>

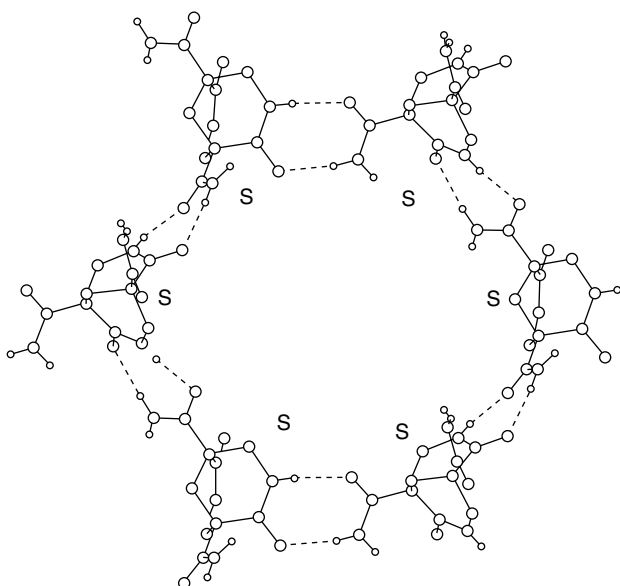


Figure 4.23. Homochiral H-bonded hexamers in the crystal structure of **61** ( $X = \text{CONH}_2$ ).<sup>6</sup>

## VII. CONCLUDING REMARKS

At the present time there are, at our disposal, some effective methods for searching and studying homochiral crystals. The numerous examples presented in this chapter of transformations between racemic compounds and conglomerates, of isomorphism of structural analogs and of approaches for directed engineering of homochiral crystals, show promise for significant progress in the analysis and understanding of the formation of racemic conglomerates. Therefore, resolution by crystallization using established and forthcoming methods suggests an alternative to chiral stationary phase chromatography and biotechnology in the industrial production of enantiopure drugs and other materials.<sup>108a</sup>

Homochiral crystallization seems to be the easiest way of obtaining enantiopure compounds from their racemates. A possible origin of prebiotic homochirality is the breaking of symmetry by spontaneous resolution during homochiral crystallization in conjunction with such amplifying conditions as autocatalysis by secondary nucleation in conditions of a deficiency of achiral derivatizing reagents.<sup>3,5c,69,73,88,108b</sup>

## REFERENCES

1. (a) Collins, A. N.; Sheldrake, G. N.; Crosby, J. eds., *Chirality in Industry* Wiley, Chichester, **1992**. (b) Collins, A. N.; Sheldrake, G. N.; Crosby, J. eds., *Chirality in Industry. II: Developments in the Commercial Manufacture and Applications of Optically Active Compounds*, (Wiley, Chichester, **1997**).
2. Green, M. M.; Nolte, R. J. M.; Meijer, E. W., eds., *Materials-Chirality: Topics in Stereochemistry*, vol. 24, Denmark, S. E., Siegel J., series eds., Wiley, Hoboken, **2003**.
3. (a) Cintas, P. *Angew. Chem. Int. Ed.* **2002**, *41*, 1139–1145. (b) Avalos, M.; Babiano, R.; Cintas, P.; Jimenez, J. L.; Palcios, J. C. *Orig. Life Evol. Biosph.* **2004**, *34*, 391–405.
4. Jacques, J.; Collet, A.; Wilen, S. H. Enantiomers, Racemates and Resolutions, Krieger, Malabar, FL, **1994**.
5. (a) Perez-Garcia, L.; Amabilino, D. B. *Chem. Soc. Rev.* **2002**, *31*, 342–356. (b) Coquerel, G. *Enantiomer* **2000**, *5*, 481. (c) Kostyanovsky, R. G.; Kostyanovsky, V. R.; Kadorkina, G. K.; Torbeev, V. Yu. *Mendeleev Commun.* **2000**, 83–84.
6. Kostyanovsky, R. G.; Lyssenko, K. A.; Lenev, D. A.; Bronzova, I. A. *Tetrahedron: Asymmetry* **2002**, *13*, 2697–2701, and references therein.
7. (a) Fredga, A. *Tetrahedron*, 1960, **8**, 126–144. (b) Davis, R. E.; Whitesell, J.K.; Wong, M.-S.; Chang, N.-L. in *The Crystal as a Supramolecular Entity*, Desiraju, G. R., ed., Wiley, Chichester, England, **1996**, pp. 63–106. (c) Hendi, M. S.; Hooter, P.; Davis, R. E.; Lynch, V. M.; Wheeler, K. A. *Cryst. Growth Des.* **2004**, *4*, 95–101.
8. IUPAC Compendium of Chemical Terminology, available at <http://iupac.org/publications/compendium/>.
9. Wallach, O. *Liebigs Ann. Chem.* **1895**, 286, 90–143.

10. (a) Collet, A.; Ziminski, L.; Garcia, C.; Vigne-Maeder, F. *Chiral discrimination in Crystalline Enantiomer Systems: Facts, Interpretations, and Speculations*, Siegel, J. C. ed. Supramolecular Stereochemistry. NATO ASI Series. Kluwer Academic, Dordrecht, **1995**; pp. 91–110. (b) Collet, A. *Optical Resolution*, Vol. 10, Reinhoudt, D. N., ed. Comprehensive supramolecular chemistry, Pergamon, London, **1996**, pp. 113–149. (c) Collet, A. *Enantiomer* **1999**, *4*, 157–172.
11. Brock, C. P.; Schweizer, W. B.; Dunitz, J. D. *J. Am. Chem. Soc.* **1991**, *113*, 9811–9820.
12. (a) Flack, H. D. *Helv. Chim. Acta* **2003**, *86*, 905–921. (b) Flack, H. D.; Bernardinelli, G. *Cryst. Eng.* **2003**, *6*, 213–223.
13. (a) Kuleshova, L. N.; Antipin, M. Yu. *Crystallogr. Rep.* **2003**, *48*, 259–279. (b) Kuleshova, L. N.; Antipin, M. Yu. *Crystallogr. Rep.* **2002**, *47*, 268–280. (c) Kuleshova, L. N.; Antipin, M. Yu. *Russ. Chem. Rev.* **1999**, *68*, 1–18. (d) Belsky, V. K.; Zorkaya, O. N.; Zorky, P. M. *Acta Cryst., Sect. A* **1995**, *51*, 473–481. (e) Baur, W. H.; Kassner, D. *Acta Cryst.* **1992**, *B48*, 356–369.
14. Ranford, J. D.; Vittal, J. J.; Wu, D. *Angew. Chem. Int. Ed.* **1998**, *37*, 1114–1116.
15. Piguet, C.; Bernardinelli, G.; Hopfgartner, G. *Chem. Rev.* **1997**, *97*, 2005–2062.
16. (a) Kaminsky, W. *Rep. Prog. Phys.* **2000**, *63*, 1575–1640. (b) Haussuehl, S. Kristallphysik, Physik Verlag, Verlag Chemie, Weinheim, 1983. (c) LePage, Y. and Donnay, G. *Acta Cryst.* **1976**, *B32*, 2456–2459.
17. (a) Geller, S. *Science* **1967**, *157*, 310–312. (b) Owens, B. B.; Argue, G. R. *Science* **1967**, *157*, 308–309. (c) Geller, S. *Phys. Rev.* **1976**, *B14*, 4345–4355.
18. Brückner, S. *Acta Cryst.* **1982**, *B38*, 2405–2408.
19. (a) Kress, R. B.; Duesler, E. N.; Etter, M. C.; Paul, I. C.; Curtin, D. Y. *J. Am. Chem. Soc.* **1980**, *102*, 7709–7714. (b) Kuroda, R.; Mason, S. F. *J. Chem. Soc. Perkin Trans. 2* **1981**, 167–170.
20. (a) Paquette, L. A.; Lau, C. J.; Browne, A. R.; O'Brien, M. E. *J. Am. Chem. Soc.* **1986**, *108*, 8111–8112. (b) Paquette, L. A.; Lau, C. J. *J. Org. Chem.* **1987**, *52*, 1634–1635. (c) Paquette, L. A.; Lau, C. J. *J. Org. Chem.* **1987**, *52*, 1635–1637.
21. Alexander, L. E.; Engmann, R.; Clark, H. G. *J. Phys. Chem.* **1966**, *70*, 252–259.
22. Karle, I. L.; Ottenheyen, H. C. J.; Witkop, B. *J. Am. Chem. Soc.* **1974**, *96*, 539–543.
23. (a) Fedyanin, I. V.; Lyssenko, K. A.; Vorontsova, N. V.; Rozenberg, V. I.; Antipin, M. Yu. *Mendeleev Commun.* **2003**, 15–16. (b) Vorontsova, N. V.; Rozenberg, V. I.; Vorontsov, E. V.; Antonov, D. Yu.; Bubnov, Yu. N. *Russ. Chem. Bull.* **2002**, *51*, 1369.
24. Alfonsov, V. A.; Bakaleynik, G. A.; Gubaidullin, A. T.; Kataev, V. E.; Kovyljaeva, G. I.; Konovalov, A. I.; Litvinov, I. A.; Strobykina, I. Ju.; Andreeva, O. V.; Korochkina, M. G. *Mendeleev Commun.* **1999**, 227–228.
25. (a) Alshahateet, S. F.; Nakano, K.; Bishop, R.; Craig, D. C.; Harris, K. D. M.; Scudder, M. L. *Cryst. Eng. Comm.* **2004**, *6*, 5–10. (b) Kim, S.; Bishop, R.; Craig, D. C.; Dance, I. G.; Scudder, M. L. *J. Org. Chem.* **2002**, *67*, 3221–3230. (c) Alshahateet, S. F.; Bishop, R.; Craig, D. C.; Scudder, M. L. *Cryst. Eng. Comm.* **2002**, *8*, 1–4. (d) Alshahateet, S. F.; Bishop, R.; Craig, D. C.; Scudder, M. L. *Cryst. Eng. Comm.* **2002**, *4*, 42–45. (e) Yue, W.; Bishop, R.; Craig, D. C.; Scudder, M. L. *Cryst. Eng. Comm.* **2002**, *4*, 591–595. (f) Yue, W.; Bishop, R.; Craig, D. C.; Scudder, M. L. *Tetrahedron* **2000**, *56*, 6667–6673. (g) Yue, W.; Bishop, R.; Scudder, M. L.; Craig, D. C. *J. Chem. Soc. Perkin Trans. 1* **1997**, 2937–2946. (h) Ahn, P. D.; Bishop, R.; Craig, D. C.; Downing, G. A.; Scudder, M. L. *Aust. J. Chem.* **1997**, *50*, 1053–1059. (i) Ung, A. T.; Gisachev, D.; Bishop, R.; Scudder, M.; Dance, I. G.; Craig, D. C. *J. Am. Chem. Soc.* **1995**, *117*, 8745–8756. (j) Bishop, R.; Craig, D. C.; Scudder, M. L.; Marchand, A. P.; Liu, Z. *J. Chem. Soc., Perkin Trans. 2* **1995**, 1295–1300. (k) Ung, A. T.; Bishop, R.; Craig, D. C.; Dance, I. G.; Scudder, M. L. *Tetrahedron* **1993**, *49*, 639–648. (l) Ung, A. T.; Bishop, R.; Craig, D. C.; Dance, I. G.; Scudder, M. L. *J. Chem. Soc., Chem.*

- Commun.* **1991**, 1012–1014. (m) Bishop, R. in: *Comprehensive Supramolecular Chemistry*, Vol. 6: *Solid-State Supramolecular Chemistry: Crystal Engineering*, MacNicol, D.; Toda, F.; Bishop, R. eds., Pergamon, Oxford, **1996**, ch. 4, pp. 85–115. (n) Bishop, R.; Dance, I. G. *Top. Curr. Chem.* **1988**, *149*, 137–188. (o) Hawkins, S. C.; Bishop, R.; Dance, I. G.; Lipari, T.; Craig, D.; Scudder, M. L. *J. Chem. Soc., Perkin Trans.* **1993**, *2*, 1729–1735. (p) Kostyanovsky, R. G.; Levkin, P. A.; Lyssenko, K. A.; Strelenko, Yu. A.; Golovanov, D. G. *Mendeleev Commun.* **2002**, 220–222. (q) Bishop, R.; Choudhury, S.; Dance, I. *J. Chem. Soc. Perkin Trans.* **1982**, *2*, 1159–1168. (r) Bishop, R.; Dance, I. *J. Chem. Soc., Chem. Commun.* **1979**, 992–993. (s) Hawkins, S. C.; Scudder, M. L.; Craig, D. C.; Rae, A. D.; Abdul Raof, R. B.; Bishop, R.; Dance, I. G. *J. Chem. Soc. Perkin Trans.* **1990**, *2*, 855–870.
26. Hollingsworth, M. D.; Brown, M. E.; Dudley, M.; Chung, H.; Peterson, M. L.; Hillier, A. C. *Angew. Chem. Int. Ed.* **2002**, *41*, 965–969.
27. (a) Harris, K. D. M. *Phase Transitions* **2003**, *76*, 205–218. (b) Harris, K. D. M. *Chem. Soc. Rev.* **1997**, *26*, 279–289. (c) Yeo, L.; Harris, K. D. M. *J. Chem. Soc., Faraday Trans.* **1998**, *94*, 1633–1639. (d) Hollingsworth, M. D.; Harris, K. D. M. in: *Comprehensive Supramolecular Chemistry*, Vol. 6, MacNicol, D. D.; Toda, F.; Bishop, R. eds., Pergamon Press, Oxford, **1996**, ch. 7, pp. 177–237.
28. (a) Furberg, S.; Hassel, O. *Acta Chem. Scand.* **1950**, *4*, 1020–1023. (b) Martin, R. H.; Marchant, M. J. *Tetrahedron* **1974**, *30*, 343–345. (c) Green, B. S.; Knossow, M. *Science* **1981**, *214*, 795–797. (d) Davey, R. J.; Black, S. N.; Williams, L. J.; McEwan, D.; Sadler, D. E.; *J. Cryst. Growth* **1990**, *102*, 97–102. (e) Potter, G. A.; Garcia, C.; McCague, R.; Adger, B.; Collet, A. *Angew. Chem., Int. Ed. Eng.* **1996**, *35*, 1666–1668. (f) Berfeld, M.; Zbaida, D.; Leiserowitz, L.; Lahav, M. *Adv. Mater.* **1999**, *11*, 328–331. (g) Zbaida, D.; Lahav, M.; Drauz, K.; Knaup, G.; Kottenhahn, M. *Tetrahedron* **2000**, *56*, 6645–6649. (h) Addadi, L.; Weinstein, S.; Gati, E.; Weissbuch, I.; Lahav, M. *J. Am. Chem. Soc.* **1982**, *104*, 4610–4617. (i) Beilles, S.; Cardinael, P.; Ndzie, E.; Petit, S.; Coquerel, G. *Chem. Eng. Sci.* **2001**, *56*, 2281–2294. (j) Gervais, C.; Beilles, S.; Cardinael, P.; Petit, S.; Coquerel, G. *J. Phys. Chem. B* **2002**, *106*, 646–652. (k) Torbeev, V. Yu.; Lyssenko, K. A.; Kharybin, O. N.; Antipin, M. Yu.; Kostyanovsky, R. G. *J. Phys. Chem. B* **2003**, *107*, 13523–13531.
29. (a) Kitoh, S.; Kubota, A.; Senda, H.; Kunimoto, K.-K. 15th International Symposium on Chirality, October 20–23, **2003**, Shizuoka, Japan, Abstracts, PA-44, p. 155. (b) Kitoh, S.; Senda, H.; Kunimoto, K.-K.; Maeda, S.; Hanai, K. *Cryst. Res. Technol.* **2004**, *39*, 375–381. (c) Kitoh, S.; Kunimoto, K.-K.; Funaki, N.; Senda, H.; Kumae, A.; Hanai, K. *J. Chem. Crystallogr.* **2002**, *32*, 547–553. (d) Kunimoto, K.-K.; Kitoh, S.; Ichitani, M.; Funaki, N.; Kuwae, A.; Hanai, K. *Heterocycles* **2002**, *57*, 2011–2019.
30. Lutz, H. D.; Haeuseler, H. *J. Mol. Struct.*, **1999**, *511–512*, 69–75.
31. (a) Stockton, G. W.; Godfrey, R.; Hitchcock, P.; Mendelsohn, R.; Mowery, P. C.; Rajan, S.; Walker, A. F. *J. Chem. Soc., Perkin Trans. 2*, **1998**, 2061–2072. (b) Taylor, L. S. *Am. Pharm. Rev.* **2001**, *4*, 60–67.
32. Potrzebowski, M. *J. Eur. J. Org. Chem.* **2003**, *8*, 1367–1376.
33. (a) Carrington, A.; McLachlan, A. D. *Introduction to Magnetic Resonance with Applications to Chemistry and Chemical Physics*. Harper and Row, New York, **1967**. (b) Wetrz, J. E.; Bolton, J. R. *Electron Spin Resonance*, McGraw-Hill, New York, **1972**.
34. Levkin, P. A.; Kokorin, A.; Schurig, V.; Kostyanovsky, R. G. *Chirality*, **2006**, in press.
35. Stahly, G. P.; McKenzie, A. T.; Andres, M. C.; Russell, C. A.; Byrn, S. R.; Johnson, P. *J. Pharm. Sci.* **1997**, *86*, 970–971
36. (a) Zbaida, D.; Lahav, M.; Drauz, K.; Knaup, G.; Kottenhahn, M. *Tetrahedron* **2000**, *56*, 6645–6649. (b) Levkin, P. A.; Strelenko, Yu. A.; Lyssenko, K. A.; Schurig, V.; Kostyanovsky, R. G. *Tetrahedron Asymm.* **2003**, *14*, 2059–2066. (c) Sakamoto, M.; Utsumi, N.; Ando, M.;

- Saeki, M.; Mino, T.; Fujita, T.; Katoh, A.; Nishio, T.; Kashima, C. *Angew. Chem. Int. Ed.* **2003**, *42*, 4360–4363.
37. Eliel, E. L.; Wilen, S. H.; Doyle, M. P. *Basic Organic Chemistry*. Wiley Interscience, New York, **2001**, p. 200.
38. Janson, S. E.; Pope, W. J. *Proc. Roy. Soc., London* **1936**, *A154*, 53–60.
39. (a) Kostyanovsky, R. G.; Schurig, V.; Trapp, O.; Lyssenko, K. A.; Averkiev, B. B.; Kadorkina, G. K.; Prosyannik, A. V.; Kostyanovsky, V. R. *Mendeleev Commun.* **2002**, 137–140. (b) Kostyanovsky, R. G.; Schurig, V.; Lyssenko, K. A.; Trapp, O.; Kadorkina, G. K.; Kostyanovsky, V. R.; Averkiev, B. *Mendeleev Commun.* **2004**, 306–309.
40. (a) Ostromissenskii, I. *Zh. Russ. Fiz.-Khim. Obsh.* **1911**, *42*, 606–609. (b) Sweeting, L. M. *Chem. Mater.* **2001**, *13*, 854–870.
41. Pasteur, L. *Ann. Chim. (Paris)* **1853**, *38*, 437.
42. (a) Kostyanovsky, R. G.; Nikolaev, E. N.; Kharybin, O. N.; Kadorkina, G. K.; Kostyanovsky, V. R. *Mendeleev Commun.* **2003**, 97–99, and references therein. (b) Kostyanovsky, R. G.; Kharybin, O. N.; Kadorkina, G. K. *Mendeleev Commun.* **2004**, in press. (c) Kostyanovsky, R. G.; Nikolaev, E. N.; Kharybin, O. N.; Kadorkina, G. K.; Bakulin, D. A. *Mendeleev Commun.* **2006**, in press.
43. (a) Henck, J.-O.; Griesser, U. J.; Burger, A. *Pharm. Ind.* **1997**, *59*, 165–169; (b) Cairra, M. R. *Top. Curr. Chem.* **1998**, *198*, 163–208.
44. Gavezzotti, A.; Filippini, G. *J. Am. Chem. Soc.* **1995**, *117*, 12299–12305.
45. (a) Tamura, R.; Fujimoto, D.; Lepp, Z.; Misaki, K.; Miura, H.; Takahashi, H.; Ushio, T.; Nakai, T.; Hirotsu, K. *J. Am. Chem. Soc.* **2002**, *124*, 13139–13153. (b) Collet, A.; Vigne-Maeder, F. *New J. Chem.* **1995**, *19*, 877–880. (c) Collet, A.; Brienne, M.-J.; Jacques, J. *Bull. Soc. Chim. France* **1972**, 127–142. (d) Kostyanovsky, R. G.; Kadorkina, G. K.; Lyssenko, K. A.; Torbeev, V. Yu.; Kravchenko, A. N.; Lebedev, O. V.; Grintselev-Knyazev, G. V.; Kostyanovsky, V. R. *Mendeleev Commun.* **2002**, 6–8. (e) Kostyanovsky, R. G.; Lakhvich, F. A.; Philipchenko, P. M.; Lenev, D. A.; Torbeev, V. Yu.; Lyssenko, K. A. *Mendeleev Commun.* **2002**, *4*, 147–149. (f) Li, Z. J.; Zell, M. T.; Munson, E. J.; Grant, D. J. *W. J. Pharm. Sciences* **1999**, *88*(3), 337–346.
46. Toda, F.; Yoshizawa, K.; Hyoda, S.; Toyota, S.; Chatziefthimiou, S.; Mavridis, I. M. *Org. Biomol. Chem.* **2004**, *2*, 449–451.
47. van Santen, R. A. *J. Phys. Chem.* **1984**, *88*, 5768–5769.
48. (a) Wilson, K. R.; Pincock, R. E. *J. Am. Chem. Soc.*, **1975**, *97*, 1474–1478. (b) May D.-M.; Lu Pincock, R. E. *J. Org. Chem.* **1978**, *43*(4), 601–604.
49. (a) Cooke, A. S.; Harris, M. M. *J. Chem. Soc. B* **1963**, 2365–2373. (b) Colter, A. K.; Clemens, L. M. *J. Am. Chem. Soc.* **1965**, *87*, 846. (c) Wilson, K. R.; Pincock, R. E.; *Canad. J. Chem.* **1977**, *55*, 889–894.
50. (a) Kondepudi, D. K.; Laudadio, J.; Asakura, K. *J. Am. Chem. Soc.*, **1999**, *121*, 1448–1451 (b) Asakura, K.; Soda, T.; Uchida, T.; Osanai, Sh.; Kondepudi, D. K. *Chirality*, **2002**, *14*, 85–89.
51. Labianca, D. A. *J. Chem. Educ.* **1975**, *52*(3), 156.
52. Grundenberg, A.; Keil, B.; Henck, J. O. *Int. J. Pharm.* **1995**, *118*, 11–21.
53. Jacques, J.; Fouquey, C.; Gabard, J.; Douglas, W. C. R. *Acad. Sci.* **1967**, *265*, 260–262.
54. (a) Stetter H.; Reischl A. *Chem. Ber.* **1960**, *93*, 791–795. (b) Tatemitsu H.; Ogura, F.; Nakagawa Y.; Nakagawa M.; Naemura K.; Nakazaki, M. *Bull. Chem. Soc. Jpn.* **1975**, *48*, 2473–2483.
55. Dale, J. *J. Chem. Soc.* **1961**, 910–922.
56. (a) Bernstein, J.; Davey, R. J.; Henck, J.-O. *Angew. Chem., Int. Ed.* **1999**, *38*, 3441–3461. (b) Dunitz, J. D.; Bernstein, J. *Acc. Chem. Res.* **1995**, *28*, 193–200. (c) Bar, I.; Bernstein, J. *Acta Cryst.* **1982**, *B38*, 121–125. (d) Bar, I.; Bernstein, J., *Acta Cryst.* **1977**, *B33*, 1738–1744.

- (e) Bernstein, J.; Bar I., et al. *Acta Cryst.* **1976**, *B32*, 1609–1611. (f) Bar, I.; Berrstein, J. *J. Phys. Chem.* **1982**, *86*, 3223–3231.
57. (a) Stibrany, R. T.; Matturro, M. G.; Zushma, S.; Patil, A. O. *Acta Cryst.* **2004**, *E60*, m188–m189. (b) Schurig, V. *Angew. Chem. Int. Ed.* **1981**, *20*, 807.
58. (a) Dufour, F.; Perez, G.; Coquerel, G. *Bull. Chem. Soc. Jpn.* **2004**, *77*, 79–86. (b) Dufour, F.; Gervais, C.; Petit, M.-N.; Perez, G.; Coquerel, G. *J. Chem. Soc., Perkin Trans. 2* **2001**, 2022–2036.
59. Duddu S. P.; Grant D. *J. Pharm. Res.* **1992**, *9*, 1083–1091.
60. (a) Profir, V. M.; Rasmuson, A. C. *Cryst. Growth Des.* **2004**, *4*, 315–323. (b) Profir, V. M.; Furusjoe, E.; Danielsson, L.-G.; Rasmuson, A. C. *Cryst. Growth Des.* **2002**, *2*, 273–279.
61. (a) Yufit, D. S.; Kozhushkov, S. I.; Howard, J. A. K.; de Meijere, A. *Acta Cryst.* **2002**, *B58*, 673–676. (b) Herbstein, F. H. *Acta Cryst.* **2003**, *B59*, 303–304.
62. Chion, B.; Lajzerowicz, J. *Acta Cryst.* **1975**, *B31*, 1430–1435.
63. (a) Levkin, P. A.; Schweda, E.; Kolb, H.-J.; Schurig, V.; Kostyanovsky, R. G. *Tetrahedron: Asymm.* **2004**, *15*, 1445–1450. (b) Gu, C.-H.; Young, V. Jr.; Grant, D. J. W. *J. Pharm. Sci.* **2001**, *90*(11), 1878–1890.
64. (a) Roux, M. V.; Jimenez, P.; Vacas, A.; Cano, F. H.; Apreda-Rojas, M. C.; Ros, F. *Eur. J. Org. Chem.* **2003**, *11*, 2084–2091. (b) Ros, F.; Molina, M. T. *Eur. J. Org. Chem.* **1999**, *11*, 3179–3183.
65. (a) Weissbuch, I.; Lahav, M.; Leiserowitz, L. *Cryst. Growth Des.* **2003**, *3*, 125–150. (b) Weissbuch, I.; Addadi, L.; Lahav, M.; Leiserowitz, L. *Science* **1991**, *253*, 637–645. (c) Weissbuch, I.; Zbaida, D.; Addadi, L.; Leiserowitz, L.; Lahav; M. *J. Am. Chem. Soc.* **1987**, *109*, 1869–1871.
66. Bechtloff, B.; Nordhoff, S.; Ulrich, J. *Cryst. Res. Technol.* **2001**, *36*, 1315–1328.
67. Yoshizawa, K.; Toyota, S.; Toda, F. *Tetrahedron* **2004**, *60*, 7767–7774.
68. Tanaka, K.; Iwamoto, T.; Caira, M. R. *New J. Chem.* **2004**, *28*, 329–331.
69. Kostyanovsky, R. G.; Torbeev, V. Yu.; Lyssenko, K. A. *Tetrahedron: Asymmetry* **2001**, *12*, 2721–2726.
70. Tanaka, K.; Fujimoto, D.; Altreuther, A.; Oeser, T.; Irngartinger, H.; Toda, F. *J. Chem. Soc., Perkin Trans. 2* **2000**, *2*(10), 2115–2120.
71. Piayrom, S.; Yonemochi, E.; Oguchi, T.; Yamamoto, K. *J. Pharm. Pharmacol.* **1997**, *49*, 384–389.
72. Toda, F.; Tanaka, K. *Tetrahedron: Asymmetry* **1990**, *1*, 359–362.
73. Kostyanovsky, R. G.; Avdeenko, A. P.; Konovalova, S. A.; Kadorkina, G. K.; Prosyannik, A. V. *Mendeleev Commun.* **2000**, *16*–18.
74. (a) Jaeger, F. M. *Recl. Trav. Chim. Pays-Bas Belg.* **1919**, *38*, 249. (b) Okazaki, H.; Kushi, Y.; Yoneda, H. *J. Am. Chem. Soc.* **1985**, *107*, 4183–4189.
75. (a) Kinbara, K.; Hashimoto, Y.; Sukegawa, M.; Nohira, H.; Saigo, K. *J. Am. Chem. Soc.* **1996**, *118*, 3441–3449. (b) Kimoto, H.; Saigo, K.; Ohashi, Y.; Hasegawa, M. *Bull. Chem. Soc. Jpn.* **1989**, *62*, 2189–2195. (c) Saigo, K.; Kimoto, H.; Nohira, H.; Yanagi, K.; Hasegawa, M. *Bull. Chem. Soc. Jpn.* **1987**, *60*, 3655–3658. (d) Bocskei, Z.; Kassai, C.; Simon, K.; Fogassy, E.; Kozma, D. *J. Chem. Soc., Perkin Trans. 1* **1996**, *2*, 1511–1515. (e) Saigo, K.; Ogawa, S.; Kikuchi, S.; Kasahara, A.; Nohira, H. *Bull. Chem. Soc. Jpn.* **1982**, *55*, 1568–1573.
76. Shiraiwa, T.; Miyazaki, H.; Ohkubo, M.; Ohta, A.; Yoshioka, A.; Yamane, T.; Kurokawa, H. *Chirality* **1996**, *8*, 197–200.
77. Saha, M. K.; Ramanujam, R.; Bernal, I.; Fronczek, F. R. *Cryst. Growth Des.* **2002**, *2*, 205–212.

78. Kaki, S.; Yamanari, K.; Shimura, Y. *Bull. Chem. Soc. Jpn.* **1982**, *55*, 769–774.
79. Bernal, I.; Cetrullo, J.; Worrell, J. H.; Li, T. *Polyhedron* **1994**, *13*, 463–468.
80. (a) Breu, J.; Domel, H.; Stoll, A. *Eur. J. Inorg. Chem.* **2000**, 2401–2408. (b) Breu, J.; Domel, H.; Norrby, P.-O. *Eur. J. Inorg. Chem.* **2000**, 2409–2419.
81. Gao, E.-Q.; Yue, Y.-F.; Bai, S.-Q.; He, Z.; Yan, C.-H. *J. Am. Chem. Soc.* **2004**, *126*, 1419–1429.
82. Konno, T.; Yoshimura, T.; Masuyama, G.; Hirotsu, M. *Bull. Chem. Soc. Jpn.* **2002**, *75*, 2185–2193.
83. Polonski, T.; Milewska, M. J.; Konitz, A.; Gdaniec, M. *Tetrahedron: Asymm.* **1999**, *10*, 2591–2604.
84. Norsten, T. B.; McDonald, R.; Branda, N. R. *Chem. Commun.* **1999**, 719–720.
85. Seff, K.; Heidner, E. G.; Meyers, M.; Trueblood, K. N. *Acta Cryst.* **1969**, *B25*, 350–354.
86. Nakashima, Y.; Shimizu, T.; Hirabayashi, K.; Kamigata, N.; Yasui, M.; Nakazato, M.; Iwasaki, F. *Tetrahedron Lett.* **2004**, *45*, 2301–2303.
87. (a) Ovchinnikov, Yu. E.; Pogozikh, S. A.; Razumovskaya, I. V.; Bylikin, S. Yu.; Shipov, A. G.; Smirnova, L. I.; Negrebetsky, V. V.; Baukov, Yu. I. *Russ. Chem. Bull.* **1999**, *48*, 1964–1974. (b) Ovchinnikov, Yu. E.; Pogozikh, S. A.; Khrustalev, V. N.; Bylikin, S. Yu.; Negrebetsky, V. V.; Shipov, A. G.; Baukov, Yu. I. *Russ. Chem. Bull.* **2000**, *49*, 1775–1781.
88. Kostyanovsky, R. G.; Kostyanovsky, V. R.; Kadorkina, G. K.; Lyssenko, K. A.; *Mendeleev Commun.* **2001**, 1–4.
89. Peerdeman, A. F.; Holst, J. P. C.; Horner, L.; Winkler, H. *Tetrahedron Lett.* **1965**, 811–815.
90. Weidenbruch, M.; Hagedorn, A.; Peters, K.; von Schnering, H. G. *Chem. Ber.* **1996**, *129*, 401–404.
91. (a) Collet, A.; Jacques, J. *Bull. Soc. Chim. Fr.* **1972**, *10*, 3857–3862. (b) Cesario, M.; Guilhem, J. *Cryst. Struct. Comm.* **1974**, *3*, 123–126. (c) Cesario, M.; Guilhem, J. *Cryst. Struct. Comm.* **1974**, *3*, 127–130. (d) Cesario, M.; Guilhem, J. *Cryst. Struct. Comm.* **1974**, *3*, 131–134. (e) Cesario, M.; Guilhem, J. *Cryst. Struct. Comm.* **1974**, *3*, 179–182. (f) Cesario, M.; Guilhem, J. *Cryst. Struct. Comm.* **1974**, *3*, 183–186.
92. (a) Larsen, S.; Marthi, K. *Acta Cryst.* **1995**, *B51*, 338–346. (b) Larsen, S.; Marthi, K. *Acta Cryst.* **1997**, *B53*, 803–811.
93. DiBlasio, B.; Napolitano, G.; Pedone, C. *Acta Crystallogr.* **1977**, *B33*, 542–545.
94. Kitaigorodsky, A. I. *Molecular Crystals and Molecules*; Academic Press, New York, **1973**.
95. Zorkii, P. M. *Kristallografia*, **1968**, *13*, 26–32 [in Russian].
96. Kipping, F. S.; Pope, W. J. *J. Chem. Soc. Trans.* **1897**, *71*, 989–1001.
97. (a) Shiraiwa, T.; Yoshida, H.; Tsuda, M.; Kurokawa, H. *Bull. Chem. Soc. Jpn.* **1987**, *60*, 947–952. (b) Shiraiwa, T.; Sado, Y.; Inoue, M.; Sakamoto, K.; Miyazaki, H.; Kurokawa, H. *Bull. Chem. Soc. Jpn.* **1988**, *61*, 899–903. (c) Shiraiwa, T.; Tazoh, H.; Sunami, M.; Sado, Y.; Kurokawa, H. *Bull. Chem. Soc. Jpn.*, **1987**, *60*, 3985–3990. (d) Shiraiwa, T.; Saijoh, R.; Suzuki, M.; Yoshida, K.; Nishimura, S.; Nagasawa, H. *Chem. Pharm. Bull.* **2003**, *51*, 1363–1367. (e) Shiraiwa, T.; Suzuki, M.; Sakai, Y.; Nagasawa, H.; Takatani, K.; Noshi, D.; Yamanashi, K. *Chem. Pharm. Bull.* **2002**, *50*, 1362–1366.
98. (a) Collet, A.; Brienne, M.-J.; Jacques, J. *Bull. Soc. Chim. France*, **1972**, 127–142. (b) Jacques, J.; Fouquey, C.; Gabard, J.; Douglas, W. C. R. Acad. Sci. **1967**, *265*, 260–262.
99. Saha, M. K.; Fronczek, F. R.; Rees, L. H.; Bernal, I. *Inorg. Chem. Comm.* **2003**, *6*, 983–988.
100. (a) Desiraju, G. R. *Crystal Engineering: The Design of Organic Solids*. Elsevier, Amsterdam, **1989**. (b) Seddon, K. R.; Zaworotko, M., eds. *Crystal Engineering: The Design and Applications*

- of Functional Solids. Kluwer Academic, Dordrecht, **1999**. (c) Whitesell, J. K., ed. *Organised Molecular Assemblies in the Solid State*. Wiley, Chichester, England, 1999, and literature cited in all above.
101. Fur, E. L.; Demers, E.; Maris, T.; Wuest, J. D. *Chem. Commun.* **2003**, 2966–2967, and references therein.
  102. Lehn, J.-M. *Supramolecular Chemistry*; VCH, Weinheim, Germany, **1995**.
  103. Hanessian, S.; Simard, M.; Roelens, S. *J. Am. Chem. Soc.* **1995**, *117*, 7630–7645.
  104. (a) Brienne, M.-J.; Gabard, J.; Leclercq, M.; Lehn, J.-M.; Cesario, M.; Pascard, C.; Cheve, M.; Dutruc-Rosset, G. *Tetrahedron Lett.* **1994**, *35*, 8157–8160. (b) MacDonald, J. C. Whitesides, G. M. *Chem. Rev.* **1994**, *94*, 2383–2420. (c) White, D. N. J.; Dunitz, J. D. *Isr. J. Chem.* **1972**, *10*, 249–256. (d) Altomare, C.; Cellamare, S.; Carotti, A.; Casini, G.; Ferappi, M.; Gavuzzo, E.; Mazza, F.; Canupt, P.-M.; Gaillard, P.; Testa, B. *J. Med. Chem.* **1995**, *38*, 170–179. (e) Tichy, M.; Ridvan, L.; Holy, P.; Zavadá, J.; Cisarova, I.; Podlaha, J. *Tetrahedron: Asymmetry* **1998**, *9*, 227–234. (f) Olszewska, T.; Gdaniec, M.; Polonski, T. *J. Org. Chem.* **2004**, *69*, 1248–1255. (g) Kostyanovsky, R. G.; El'natanov, Yu. I.; Krutius, O. N.; Lyssenko, K. A.; Strelenko, Yu. A. *Mendeleev Commun.* **1999**, 70–73. (h) Kostyanovsky, R. G.; Lyssenko, K. A.; El'natanov, Yu. I.; Krutius, O. N.; Bronzova, I. A.; Strelenko, Yu. A.; Kostyanovsky V. R. *Mendeleev, Commun.* **1999**, 106–108. (i) Kostyanovsky, R. G.; Lyssenko, K. A.; Bronzova, I. A.; Krutius, O. N.; Strelenko, Yu. A.; Korlyukov, A. A. *Mendeleev Commun.* **2000**, 106–107. (j) Lenev, D. A.; Lyssenko, K. A.; Golovanov, D. G.; Weingart, O.; Buß, V.; Kostyanovsky, R. G. *Tetrahedron: Asymmetry* **2004**, *15*, 537–543. (k) Kostyanovsky, R. G.; El'natanov, Yu. I.; Krutius, O. N.; Chervin, I. I.; Lyssenko, K. A. *Mendeleev Commun.* **1998**, 228–230. (l) Lyssenko, K. A.; Lenev, D. A.; Kostyanovsky, R. G. *Tetrahedron* **2002**, *58*(42), 8525–8537. (m) Lenev, D. A.; Lyssenko, K. A.; Kostyanovsky, R. G. *Eur. J. Inorg. Chem.* **2003**, 2979–2985. (n) Stoncius, S.; Butkus, E.; Zilinskas, A.; Larsson, K.; Oehrstroem, L.; Berg, U.; Waernmark, K. *J. Org. Chem.* **2004**, *69*, 5196–5203. (o) Wu, A.; Fettinger, J. C.; Isaacs, L. *Tetrahedron* **2002**, *58*, 9769–9777. (p) Samuratov, E. B.; Batsanov, A. S.; Struchkov, Yu. T.; Tsividze, A. Yu.; Tsintadze, M. G.; Khmel'nitskii, L. I.; Simonov, Yu. A.; Dvorkin, A. A.; Lebedev, O. V.; Merkova, T. B. *Khim. Geterotsikl. Soedin.* **1991**, 937–942 [*Chem. Heterocycl. Comp. (Engl. Transl.)* **1991**, *27*, 745–750].
  105. Lenev, D. A.; Lyssenko, K. A.; Kostyanovsky, R. G. *Mendeleev Commun.* **2004**, 312–314.
  106. (a) Kostyanovsky, R. G.; Lyssenko, K. A.; Lenev, D. A.; *Mendeleev Commun.* **1999**, 154–156. (b) Kostyanovsky, R. G.; Krutius, O. N.; Bronzova, I. A.; Lenev, D. A.; Lyssenko, K. A.; Averkiev, B. B. *Mendeleev Commun.* **2001**, 6–8.
  107. (a) Kravchenko, A. N.; Kadorkina, G. K.; Sigachev, A. S.; Maksareva, E. Yu.; Lyssenko, K. A.; Belyakov, P. A.; Lebedev, O. V.; Kharybin, O. N.; Makhova, N. N.; Kostyanovsky, R. G. *Mendeleev Commun.* **2003**, 114. (b) Kostyanovsky, R. G.; Lyssenko, K. A.; Kadorkina, G. K.; Lebedev, O. V.; Kravchenko, A. N.; Kostyanovsky, V. R. *Mendeleev Commun.* **1998**, 231–233; (c) Kostyanovsky, R. G.; Lyssenko, K. A.; Kravchenko, A. N.; Lebedev, O. V.; Kadorkina, G. K.; Kostyanovsky, V. R. *Mendeleev Commun.* **2001**, 134–136.
  108. (a) Kostyanovsky, R. G.; *Mendeleev Commun.* **2003**, 85–90; (b) Kostyanovsky, R. G.; Lakhvich, F. A., Philipchenko, P. M., Lenev, D. A.; Torbeev, V. Yu.; Lyssenko, K. A.; *Mendeleev Commun.* **2002**, 147–149.

## Chapter 5

# Supramolecular Synthesis of 1D Chains and 2D Layers in Hydrogen Bond Networks of Ureas and 2-Pyrimidinones

ASHWINI NANGIA

*School of Chemistry, University of Hyderabad,  
Hyderabad 500 046, India*

- I. Introduction
    - A. Molecular and Supramolecular Chemistry
    - B. Crystal Engineering
  - II. Hydrogen Bond Mimicry
    - A. Hydrogen Bonding in Ureas
    - B. From Ureas to 2-Pyrimidinones
  - III. Hydrogen Bond Networks in 2-Pyrimidinones
    - A. Proof of Concept
    - B. C—H···O Chain Synthon in *N*-Arylpyrimidinone Salts
    - C. Recurring 2D Polar Layer Arrangement
    - D. Model for 2D Polar Layer Assembly
  - IV. Design of SHG Active Unsymmetrical Ureas
  - V. Conclusion and Future Directions
- Acknowledgments  
References

The constructing of Nature's molecules in the laboratory from atoms and/or simple molecules, a process often known as total synthesis, is one of the most demanding human practices.

K. C. Nicolaou<sup>1</sup>

---

*Topics in Stereochemistry, Volume 25*, edited by Scott E. Denmark and Jay S. Siegel  
Copyright © 2006 John Wiley & Sons, Inc.

The chemist's drive towards the synthesis of nanoscale composites, employing the noncovalent bond, has led to the birth of a highly interdisciplinary field of chemical research—viz., supramolecular chemistry—in recent years.

J. F. Stoddart<sup>8</sup>

## I. INTRODUCTION

### A. Molecular and Supramolecular Chemistry

One of the goals of modern-day chemistry is the construction of larger and larger molecular assemblies. In the area of covalent chemistry these large structures are the numerous synthetic targets and complex natural product syntheses being pursued in research laboratories around the world.<sup>1,2</sup> Starting in the 1950s, from the synthesis of quinine, cortisone, strychnine, cedrol, and reserpine, modern organic synthesis has flourished in the last five decades, culminating in the total synthesis of complex natural products like palytoxin, taxol, epothilones, calicheamycins, and brevetoxin B, to name but a few examples.<sup>3,4</sup> However these triumphs have come at a great price. Even when total synthesis is performed in a convergent manner, the complex multistep reactions are not only time-consuming but also expensive in terms of materials required and persons employed. For example, to conquer the total synthesis of complex and challenging CP-molecules, a team of graduate and postdoctoral researchers would have to synthesize and pass on starting materials and intermediates in a relay race round the clock for several years.<sup>5</sup>

A parallel stream of thought started emerging at the turn of the millennium when it became clear that the synthesis of large mesoscale assemblies and nanostructures for materials science would be increasingly difficult with the covalent bond used as the glue.<sup>6–8</sup> This realization prompted chemists to seek other strategies for the construction of extended structures, leading to the chemistry of noncovalent synthesis, namely supramolecular chemistry. J.-M. Lehn defined supramolecular chemistry as “chemistry beyond the molecule”.<sup>9</sup> In the same way that molecular chemistry deals with atomic structures held together by covalent bonds, supramolecular chemistry is about molecular assemblies held together by noncovalent intermolecular bonds. A proper knowledge of the molecular recognition process permits the design of small, relatively simple building blocks that have the information inbuilt to self-assemble into larger structures. This idea is illustrated from the elegant work of Stoddart<sup>8</sup> (Figure 5.1). The dicarboxylic acid **1**, which possesses a  $\pi$ -excessive hydroquinone ring, can thread through the macrocyclic cavity of the  $\pi$ -deficient tetra cationic cyclophane **2**, stabilized by aryl–aryl interactions, to form the pseudorotaxane  $[1.2]^{4+}$ . The pseudorotaxane thus formed further self-assembles to supramolecular arrays through carboxylic

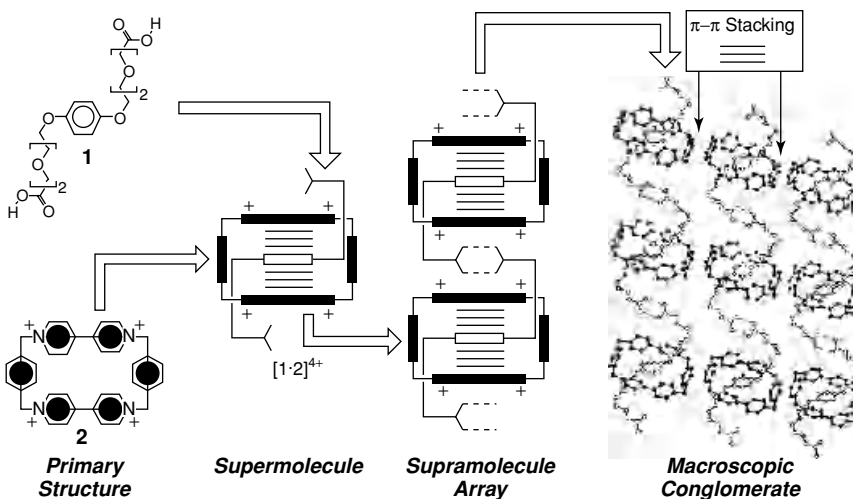


*Figure 5.1.* Supramolecular hierarchy illustrated using the pseudorotaxane  $[1.2]^{4+}$  complex. Simple molecular building blocks have the information inbuilt to self-assemble into larger supramolecular structures.

acid dimer O—H $\cdots$ O hydrogen bonds and then into a conglomerate through van der Waals and extended  $\pi\cdots\pi$  stacking interactions.

## B. Crystal Engineering

Today crystal engineering<sup>10</sup> is viewed as supramolecular synthesis in the solid state, namely the construction of crystalline materials from molecules and/or ions using noncovalent interactions, hydrogen bonds, and/or metal–ligand bonds.<sup>11–13</sup> An important goal in crystal engineering is the design of solids with specific structures and tunable properties. One can design materials that have nonlinear optical, magnetic, or catalytic function. In order to obtain NLO materials the molecules or ions must be organized in a noncentrosymmetric arrangement, for magnetic materials they must be positioned so that communication between the spins is facilitated, and for chemical separations the porous materials must be able to house volatile liquids or ions. To build functional materials, one must be able to control the assembly of molecular building blocks into supramolecular architectures and the nature of intermolecular interactions between them. This exercise is facilitated by the identification of repetitive or robust structural units that may be associated with a particular functional group, preferably across families of crystal structures. Desiraju<sup>14</sup> coined the term “supramolecular synthons” for intermolecular interactions and hydrogen bond patterns that are economical in

size and encode maximum structural information about crystallization.<sup>15</sup> The development of organic solid state chemistry requires a proper theory of crystal packing. Crystal structures are mediated by intermolecular interactions and the most accurate method of obtaining precise information on hydrogen bonds is through X-ray crystallography. With an exponential increase in the number of accurate X-ray crystal structures that are being reported,<sup>16</sup> thanks to CCD (charged-coupled device) area detector technology, structural chemists are looking for organic crystals that can act as catalysts, microporous materials, and frequency doublers, and also toward applications in molecular modeling and drug design.<sup>17</sup> The realization that a crystal is a supermolecule *par excellence*, with atoms and covalent bonds being replaced by molecules and intermolecular interactions, has added recognition to crystal engineering<sup>18</sup> as the supramolecular equivalent of organic synthesis and brought it to the main stream of chemical sciences.<sup>19</sup> The hydrogen bond is a cornerstone in crystal engineering, supramolecular chemistry, biological recognition and enzymatic catalysis. The reader is referred to excellent books and reviews on the nature, properties, and applications of hydrogen bonds.<sup>20–23</sup>

## II. HYDROGEN BOND MIMICRY

### A. Hydrogen Bonding in Ureas

The urea functionality is a reliable and popular building block to assemble persistent one-dimensional hydrogen bond chains through N–H···O hydrogen bonds. The  $\alpha$ -network in urea crystal structures, with the anti–NH protons donating to the carbonyl oxygen in a bifurcated motif, has a repeat distance of 4.7 Å. Lauher and Fowler<sup>24</sup> have designed two-dimensional networks with

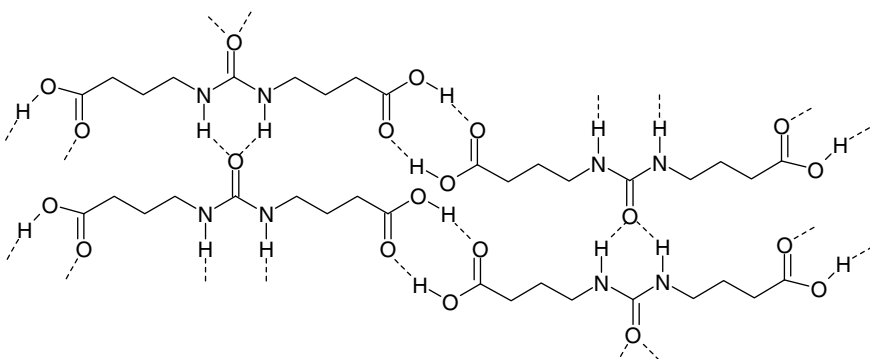


*Figure 5.2.* Schematic layered structure in urylenedicarboxylic acid formed by the two self-complementary functional groups urea and COOH.

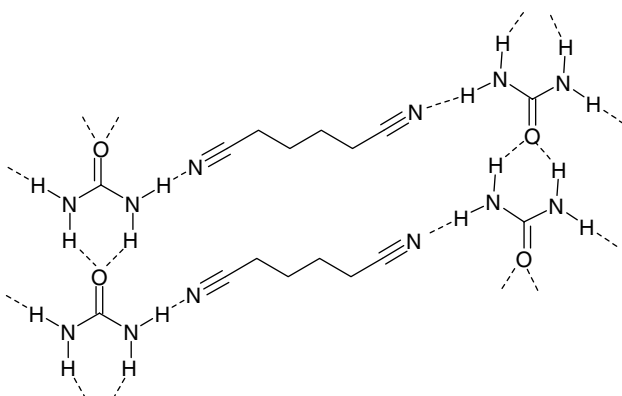
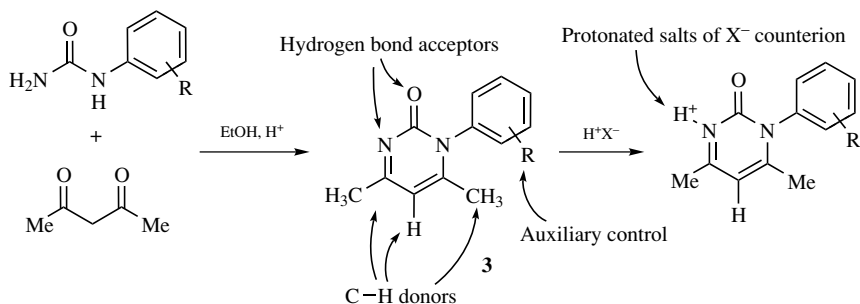


Figure 5.3. Two-dimensional layer in urea and  $\alpha,\omega$ -alkanedinitrile complex.

urylenedicarboxylic acids (Figure 5.2), which form two independent sets of 1D self-complementary hydrogen-bonded chains oriented in orthogonal arrays. The urea portion of these molecules forms the  $\alpha$ -network that is cross-linked by a second hydrogen bond chain between the carboxylic acid groups. An advantage with such a modular approach is that the 1D networks generate predictable 2D patterns. Hollingsworth et al.<sup>25</sup> have used the urea scaffold to control molecular aggregation in the third dimension. Cocrystals of urea and  $\alpha,\omega$ -dinitrile spacer molecules contain the robust  $\alpha$ -network through urea *anti*-NH protons and the *syn* NH protons form heteromeric chains with the terminal cyano groups (Figure 5.3). These  $\text{CN}(\text{CH}_2)_n\text{CN}$ /urea cocrystals offer the flexibility that the orientation of adjacent urea chains can be controlled to give an anti-parallel arrangement when  $n = 4$  or a parallel arrangement when  $n = 3, 5$ . Urea channel inclusion complexes are obtained for  $n > 5$ . In addition to crystal structure engineering, macrocyclic molecules with the urea moiety can generate capsules and nanotubes for trapping small guest molecules.<sup>26–28</sup>

## B. From Ureas to 2-Pyrimidinones

The pyrimidinone **3** was used in our group as a precursor for the synthesis of nonnatural  $\beta$ -lactam analogues.<sup>29</sup> The ease of synthesizing pyrimidinones, obtained by the condensation of acetylacetone with *N*-phenyl urea, together with the ability to make phenyl derivatives and also various salts with inorganic acids, makes it a versatile substrate for structural studies (Scheme 5.1). The pyrimidinone skeleton is rich in activated C–H donors and strong acceptors like oxygen and nitrogen. For crystallization these conjugated molecules are readily soluble in common organic solvents like chloroform, methanol, ethyl acetate, and hexane. On the basis of



Scheme 5.1. 2-Pyrimidinones (3) as a novel scaffold for crystal engineering.

hydrogen bonding and close-packing arguments, we reasoned that pyrimidinones would self-assemble in a manner similar to the  $\alpha$ -network in urea crystal structures (Figure 5.4). One or both of the two N–H···O hydrogen bonds in urea would be replaced by a C–H···O interaction in 2-pyrimidinone and their salts. Our interest

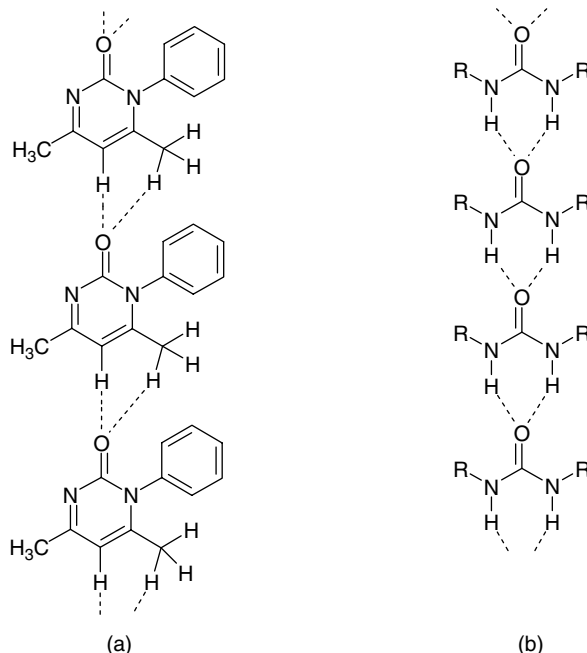
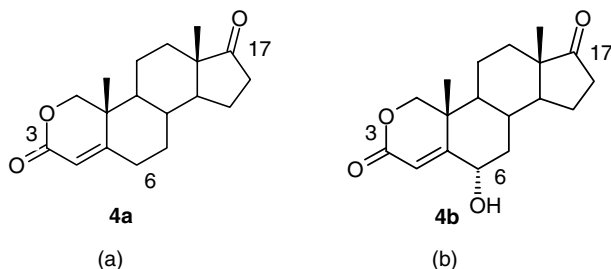


Figure 5.4. (a) The C–H···O hydrogen bond tape expected in 2-pyrimidinone (3). (b) The  $\alpha$ -network of N–H···O hydrogen bonds in urea. Comparison of these structures shows that pyrimidinones, a category of masked ureas, would self-assemble in the same manner using weak hydrogen bonds.

in studying strong and weak hydrogen bond mimicry was initiated by recent observations on isostructurality and hydrogen bond equivalence in 2-oxasteroids, a class of anabolic drugs and hormones. The C–H $\cdots$ O interaction in the crystal structure of 2-oxa-4-androstene-3,17-dione (**4a**) is replaced by a C–O–H $\cdots$ O hydrogen bond in the  $6\alpha$ -hydroxy analogue (**4b**) (Figure 5.5).<sup>30</sup> After identifying 1D isostructurality in steroids, we have extended it to 2D layers and finally for the comparison of complete crystal structures. Androst-4-ene-3,6,17-trione,



(a)

(b)

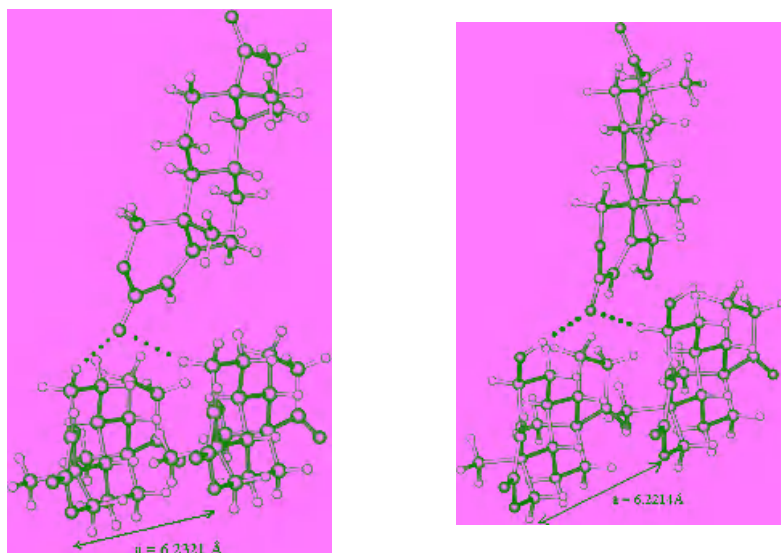


*Figure 5.5.* (a) Crystal structure 2-oxa-4-androstene-3,17-dione (**4a**) and (b)  $6\alpha$ -hydroxy-2-oxa-4-androstene-3,17-dione (**4b**). Note the near identity of  $a$ -axis and the similarity in hydrogen bonding and arrangement of molecule in both these structures. The C–O–H $\cdots$ O hydrogen bond in (b) is replaced by C–H $\cdots$ O interaction in (a).

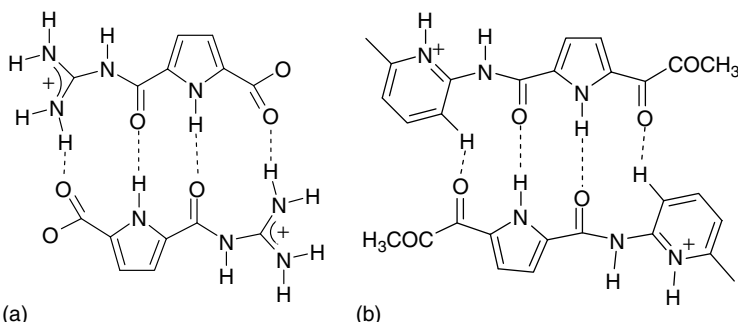


*Figure 5.6.* (a) Schematic representation of the dimer formed by the chloride salt of 5-(guanidino-carbonyl)pyrrole-2-carboxylic acid. (b) The chloride salt of 5-amidopyridinium-pyrrole-2-carboxylate. Chloride ions are not shown for clarity. The N–H···O hydrogen bond in (a) is replaced by C–H···O interaction in (b).

a potent inhibitor of the cytochrome P<sub>450</sub> enzyme aromatase, is isostructural to the substrate of the same enzyme, androst-4-ene-3,17-dione.<sup>31</sup> Such observations form the basis for structure-based drug design and in the application of small-molecule crystal structures toward understanding drug–receptor binding.<sup>17</sup> A recent example of strong and weak hydrogen-bond mimicry is that N–H···O hydrogen bond in the dimer of 5-(guanidinocarbonyl)pyrrole-2-carboxylate is isofunctionally replaced by a C–H···O interaction in 5-amidopyridinium-pyrrole-2-carboxylate (Figure 5.6).<sup>32</sup> The recurrence and consistent packing is due to the limited number of donors and acceptors. Whitesides and coworkers<sup>7</sup> synthesized linear tape, crinkled tape and rosette motifs of N–H···O hydrogen bonds in cyanuric acid and melamine complexes, CA·M. The C–H···O surrogate of the linear tape structure was engineered by us in organic clay-type host–guest architectures of 4,4-bis(4'-biphenyl)cyclohexa-2,5-dienone **5** (Figure 5.7).<sup>33</sup> The occurrence of chain and layer hydrogen bond networks in 2-pyrimidinones analogous to ureas will reinforce hydrogen bond mimicry in crystal engineering.

In addition to hydrogen bond mimicry, shape and size similarity have also been employed as design criteria in crystal engineering. Davis and Whitesell<sup>34</sup> control the orientation of molecules in noncentrosymmetric crystal structures of quasiracemates by group replacement in enantiomers, (*R*)-A and (*S*)-A'. A and A' are identical molecules differing by a small group replacement with similar volumes, such as S/CH<sub>2</sub>, phenyl/thienyl, naphthalene/indole, methyl/chloro/bromo, and dimethylamino/isopropylidene. For example, crystal structures of isopropylidene *rac*-(**6a**) and dimethylamino *rac*-(**6b**) are virtually identical in terms of space group ( $P2_1/c$ ), metric constants, and molecular packing

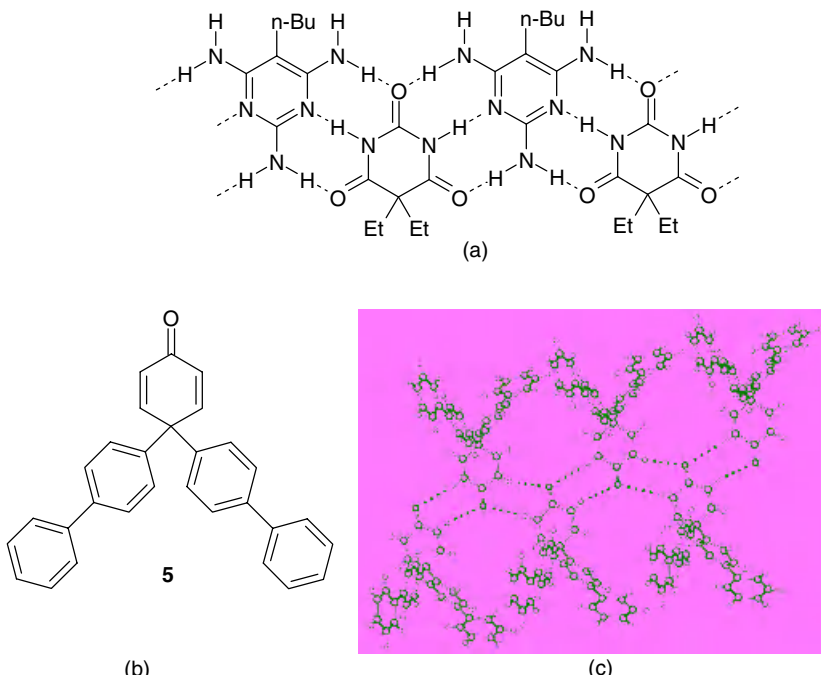


*Figure 5.7.* (a) Linear N–H···O tape in CA·M complex. (b) 4,4'-bis(4'-biphenyl) cyclohexa-2,5-dienone (**5**). (c) C–H···O benzoquinone tape in the *bc*-plane of the crystal structure. The included guest molecules between the hydrophobic aryl groups are not shown for clarity.

(Figure 5.8). The structure of quasi-racemate (*S*)-(**6a**)–(*R*)-(**6b**) is similar to the racemic components but in noncentrosymmetric space group  $P2_1$ . Similarly quasi-centrosymmetric molecules, *rac*-(**6c**) and (*S*)-(**6c**), have identical crystal packing in  $P2_1/c$  and  $P2_1$  space groups.

### III. HYDROGEN BOND NETWORKS IN 2-PYRIMIDINONES

#### A. Proof of Concept

The crystal structures of simple *N*-arylpyrimidinones **7**–**9** (Scheme 5.2) confirm the hypothesis of Figure 5.4.<sup>35</sup> Phenylpyrimidinone **7** (space group *Pbcm*) shows a linear chain of C–H···O hydrogen bonds (2.11 Å, 171.5°, interaction *i*) between translation-related molecules along the *a*-axis (Figure 5.9). This hydrogen-bonded

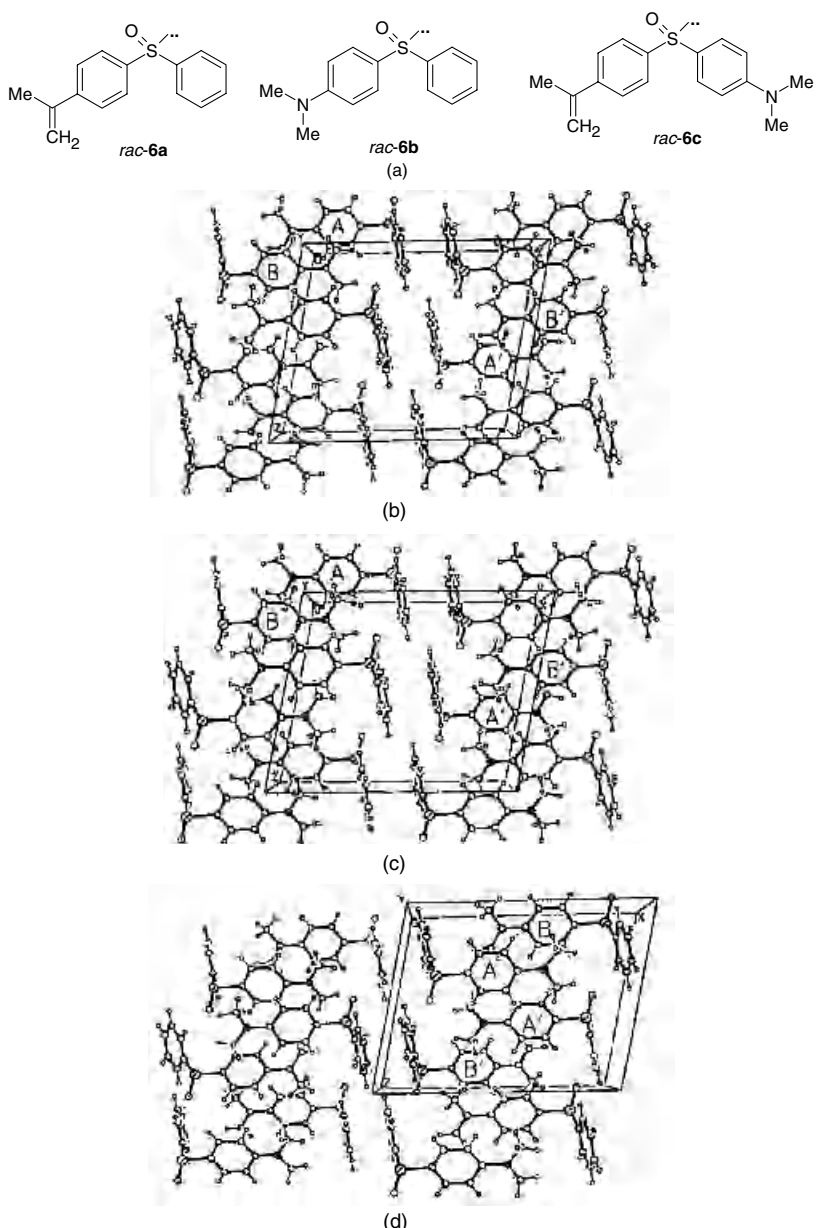
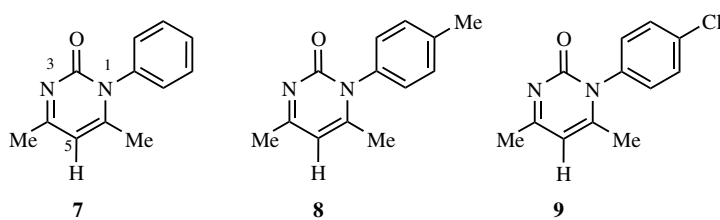
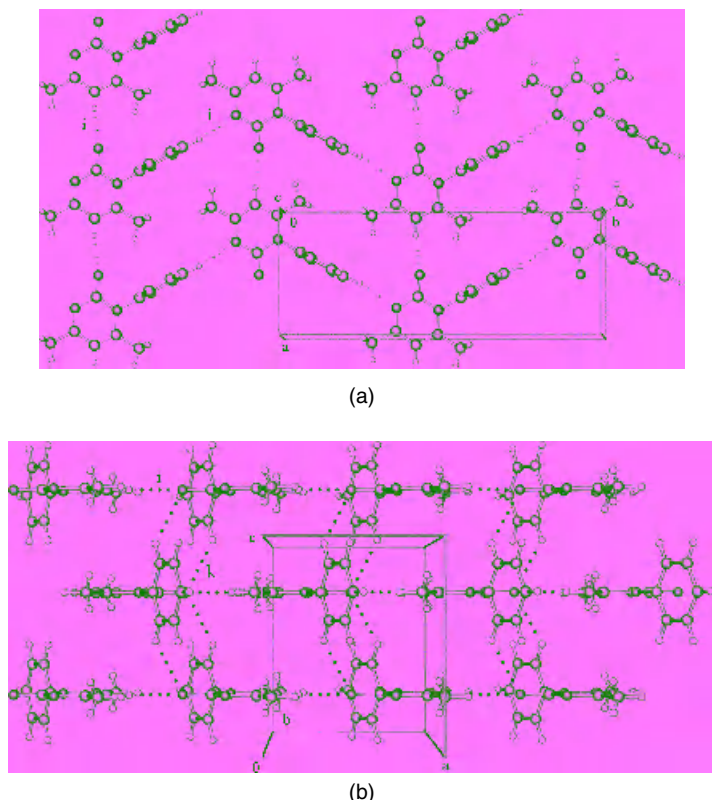


Figure 5.8. (a) Diaryl sulfoxides (**6a**), (**6b**), and (**6c**) with isosteric groups. (b) and (c) Crystal structures of *rac*-(**6a**) and *rac*-(**6b**) in centrosymmetric  $P2_1/c$  space group. (d) Crystal structure of quasi-racemate *S*-(**6a**)-*R*-(**6b**) with similar packing in chiral space group  $P2_1$ .



*Scheme 5.2.* Neutral pyrimidinones (7–9) to test the hydrogen bond mimicry hypothesis.



*Figure 5.9.* Crystal structure of phenyl pyrimidinone (7). (a) View of the ab-layer to show the C–H···O and C–H···N hydrogen bond chains (interactions *i* and *j*). Molecules in adjacent chains run anti-parallel along the  $\alpha$ -axis. (b) View of interlayer interactions.

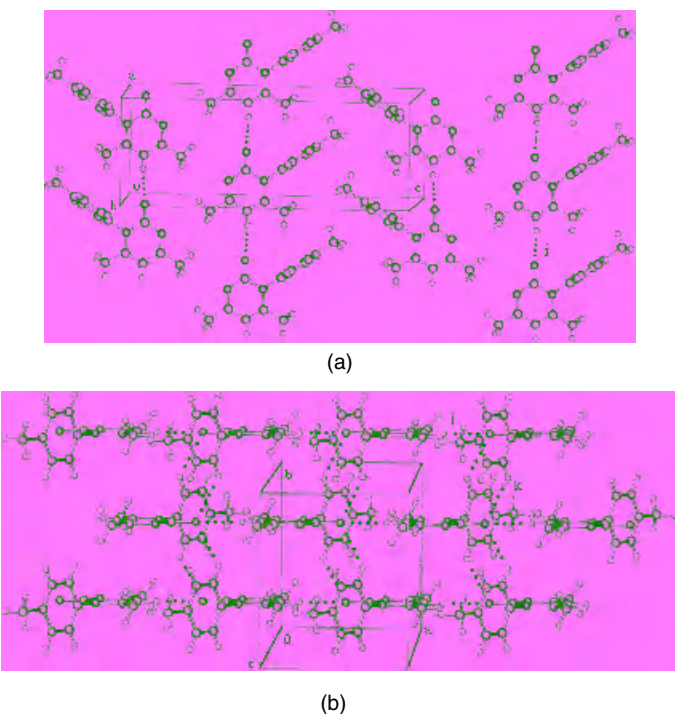


*Figure 5.10.* Crystal structure of tolyl pyrimidinone (**8**). (a) View of the ac-layer to show the C–H···O chain (interaction *i*) and the T-shaped approach of the tolyl methyl group to the phenyl ring centroid (CH<sub>3</sub>···π 3.78 Å). Note the parallel arrangement of molecules along the *a*-axis. (b) Interlayer packing viewed down the *c*-axis. The chloro derivative (**9**) is isostructural.

chain is connected to *b*-glide-related neighboring molecules through a zigzag motif of C–H···N hydrogen bonds (2.42 Å, 168.5°, interaction *j*), resulting in the two-dimensional network of C–H···O and C–H···N hydrogen bonds in the mirror plane. The short C–H···O hydrogen bond directs self-assembly along the one-dimensional chain and other interactions (*k*, 2.51 Å, 123.6°) complete the crystal packing.

The tolyl derivative **8** (space group *Pnma*) has linear chains of C–H···O hydrogen bonds (2.22 Å, 173.9°, interaction *i*) connecting translation-related molecules along [100] (Figure 5.10a). Adjacent *a*-glide-related chains pack in a parallel orientation to produce 2D layers, which are connected through C–H···O interactions from the *o*- and *m*-phenyl hydrogens to the carbonyl acceptor (2.48 Å, 125°, interaction *k*; Figure 5.10b). The tolyl methyl group points toward the phenyl ring π-cloud centroid of an adjacent molecule (C···π 3.78 Å). The chloro

derivative **9** is isostructural to **8**, with the tolyl CH<sub>3</sub>···π interaction in the former structure being replaced by the isofunctional and isosteric Cl···π interaction in the chlorophenyl derivative.

Methyl and chloro groups not only play a space filling role (van der Waals volume 24 and 20 Å<sup>3</sup>) in crystal structures, referred to as chloro–methyl exchange, but also provide electrostatic stabilization because the C–H and C–Cl groups point toward the π-electron cloud of the phenyl ring. Crystallographic studies on C–H···π,<sup>36,37</sup> and C–Cl···π,<sup>38,39</sup> interactions show that these weak intermolecular interactions are directional and stabilizing. The isostructural Me/Cl pair **8** and **9** may be contrasted with tetraphenylporphyrin crystal structures wherein the 4-chlorophenylporphyrin contains the unusual C–Cl···π contact, but the 4-tolyl derivative<sup>40</sup> (Figure 5.11) has different crystal packing through stacks of C–H···π interactions.

Pyrimidinones **7–9** contain the C–H···O hydrogen bond chain analogous to the α-network in ureas. The crystallographic repeat distance along the α-network in pyrimidinones is 7.1 to 7.3 Å, compared to 4.6 to 4.7 Å in ureas. A difference between the crystal structures of phenylpyrimidinone **7** and methyl/chloro derivatives **8, 9** is that the chains of molecules are aligned antiparallel within a layer in **7**, whereas the molecular dipoles are oriented in the same direction in **8** and **9**. The parallel alignment of carbonyl groups in **8** and **9** is referred to as 2D polar layer arrangement. Having established the recurrence of C–H···O tape in pyrimidinones, crystal engineering of 2D polar layers and attempts to induce noncentrosymmetric crystal packing based on the chain synthon are discussed. For a discussion on building supramolecular networks with metal–ligand and hydrogen bonds in porphyrins, see Chapter 3 by I. Goldberg in this volume.

## B. C–H···O Chain Synthon in *N*-Arylpyrimidinone Salts

Organic salts are preferred over neutral molecules as synthons because of their high thermal and mechanical stability, better crystallinity, and less volatility. Another advantage with salts is that the counter ions can be varied easily, and this makes the approach highly successful toward engineering of novel materials. Salts can give rise to efficient physical properties by combining functionalized organic scaffolds with appropriate counter ions. The use of ionic compounds should further improve the chance of achieving a noncentrosymmetric crystal structure because the counter ions separate and screen the dipolar chromophores from one another, thereby reducing the dipole–dipole interactions, which tend to give centrosymmetric packing (Figure 5.12). 4-Amino-1-methylpyridinium benzene-sulfonates crystallize in noncentrosymmetric space groups, and many of them exhibit useful physical properties, like second harmonic generation

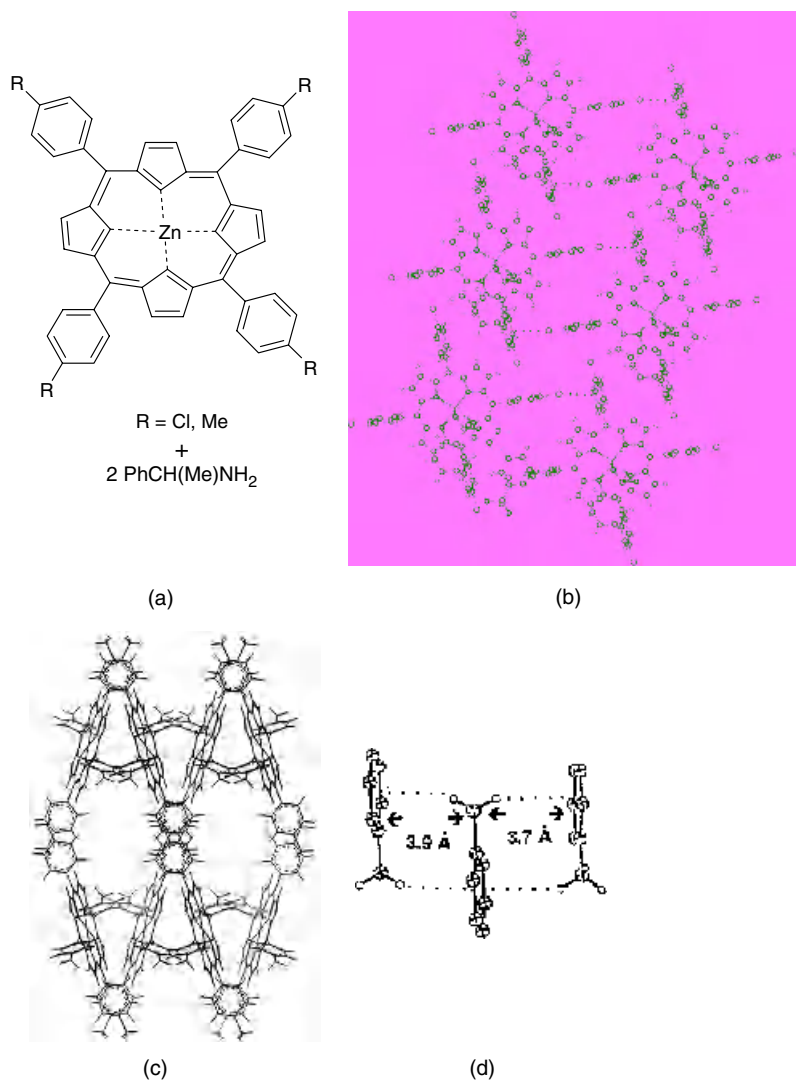
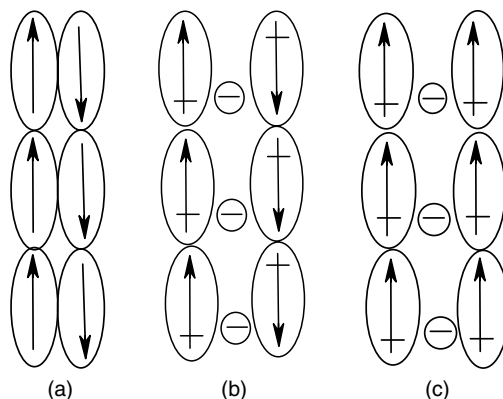


Figure 5.11. (a) Zn-tetra(4-chloro/methyl-phenyl)porphyrin L- $\alpha$ -methylbenzylamine complex. (b) The T-shaped C–Cl $\cdots$ π interaction ( $3.57\text{\AA}$ ,  $166.7^\circ$ ) between the chlorophenyl rings of adjacent molecules. (c) Tolyl porphyrin host lattice viewed down the *c*-axis. (d) The stacking geometry of tolyl residues to show the interplanar distances and C–H $\cdots$ π contacts.



*Figure 5.12.* (a) Anti-parallel arrangement of molecular dipoles typical for a covalent compound. (b) Anti-parallel arrangement of molecular dipoles in a salt. (c) Parallel alignment of molecular dipoles in a salt. The probability for parallel arrangement is higher in salts because counter ions shield the dipolar molecules.

(SHG).<sup>41</sup> Noncentrosymmetric cocrystals prepared from 2-amino-5-nitropyridine and achiral benzenesulfonic acids are colorless, have high melting points, and good molecular hyperpolarisability.<sup>42</sup> In general, the large molecular hyperpolarizability ( $\beta$ ) and dipole moment ( $\mu$ ) of conjugated ionic species arises from strong electron-acceptor and electron-donor characteristics of the cation and anion parts. Masse et al.<sup>43</sup> show that tetra(4-methoxyphenyl)phosphonium iodide, an organic salt built with quasi octupolar tetrahedral chromophores and having quadratic NLO properties, can be used as a flexible and neutral building block in crystal engineering. The hydrothermal reaction between trimesic acid and 1,2-bis(4-pyridyl)ethane in the presence of cadmium(II) ions<sup>44</sup> results in trimesate anion sheets intercalated with bipyridinium cations and solvent molecules (Figure 5.13). Ward et al.<sup>45</sup> have exploited two-dimensional hydrogen-bonded sheets generated from guanidinium cations and organosulfonate anions. The 2D layers when connected with aromatic pillars form bricklike molecular architectures or discrete double layers that can accommodate various guests.

Crystallization of pyrimidinones **7–9** from aqueous HCl and HNO<sub>3</sub> afforded diffraction quality crystals of **10** (H·HCl), **12** (Me·HCl), **13** (Cl·HCl), **14** (Cl·HNO<sub>3</sub>), and **15** (Me·HNO<sub>3</sub>) salts at room temperature (Scheme 5.3).<sup>46</sup> The structure of **11** (H·HNO<sub>3</sub>) could not be solved and refined because of heavy distortion of the phenyl ring. *N*-protonation occurs at the more basic imine nitrogen in all structures. The molecules of salt **10** (H·HCl) arrange in hydrogen-bonded chains along [001] through a V-shaped bifurcated motif of C—H···O hydrogen bonds, from vinyl and methyl C—H donors (2.77 Å, 146°; 2.31 Å, 169°; *i* and *ii*) to the

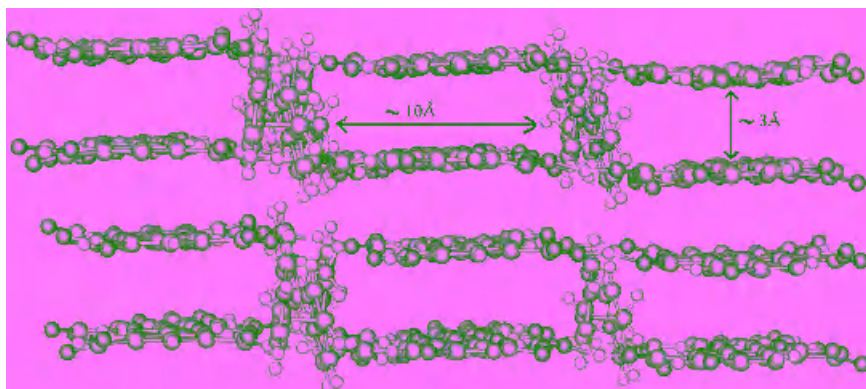
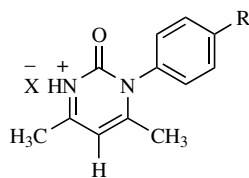


*Figure 5.13.* The layered structure of trimesate anion in a Cd(II) complex. Bipyridinium cations and solvent molecules occupy the interlayer space.

carbonyl O acceptor (Figure 5.14). Such chains further interact with the  $\text{Cl}^-$  ion via  $\text{N}^+ - \text{H}\cdots\text{Cl}^-$  ( $2.01 \text{ \AA}$ ,  $158^\circ$ , *iii*) and  $\text{C}-\text{H}\cdots\text{Cl}^-$  ( $3.03 \text{ \AA}$ ,  $168^\circ$ , *iv*) hydrogen bonds<sup>47</sup> to produce a lamellar structure stabilized by pyrimidinone cations and chloride anions. The polar layers of phenyl pyrimidinone molecules pack in a noncentrosymmetric fashion (space group  $Pmn2_1$ ) such that the phenyl ring projects out of the  $bc$ -plane above and below the pyrimidinone ring of adjacent  $2_1$  related molecules. The  $\text{C}-\text{H}\cdots\text{O}$  hydrogen bond chain is intact in the salt, which shows that this robust synthon can tolerate interference from other strong hydrogen bonding and ionic groups.



**10:**  $\text{R} = \text{H}$ ,  $\text{X} = \text{Cl}^-$  ( $\text{H}\cdot\text{HCl}$ )

**11:**  $\text{R} = \text{H}$ ,  $\text{X} = \text{NO}_3^-$  ( $\text{H}\cdot\text{HNO}_3$ )

**12:**  $\text{R} = \text{CH}_3$ ,  $\text{X} = \text{Cl}^-$  ( $\text{Me}\cdot\text{HCl}$ )

**13:**  $\text{R} = \text{Cl}$ ,  $\text{X} = \text{Cl}^-$  ( $\text{Cl}\cdot\text{HCl}$ )

**14:**  $\text{R} = \text{Cl}$ ,  $\text{X} = \text{NO}_3^-$  ( $\text{Cl}\cdot\text{HNO}_3$ )

**15:**  $\text{R} = \text{CH}_3$ ,  $\text{X} = \text{NO}_3^-$  ( $\text{Me}\cdot\text{HNO}_3$ )

*Scheme 5.3.* Salts of 2-pyrimidinones crystallized from  $\text{HCl}$  and  $\text{HNO}_3$  (**10–15**).

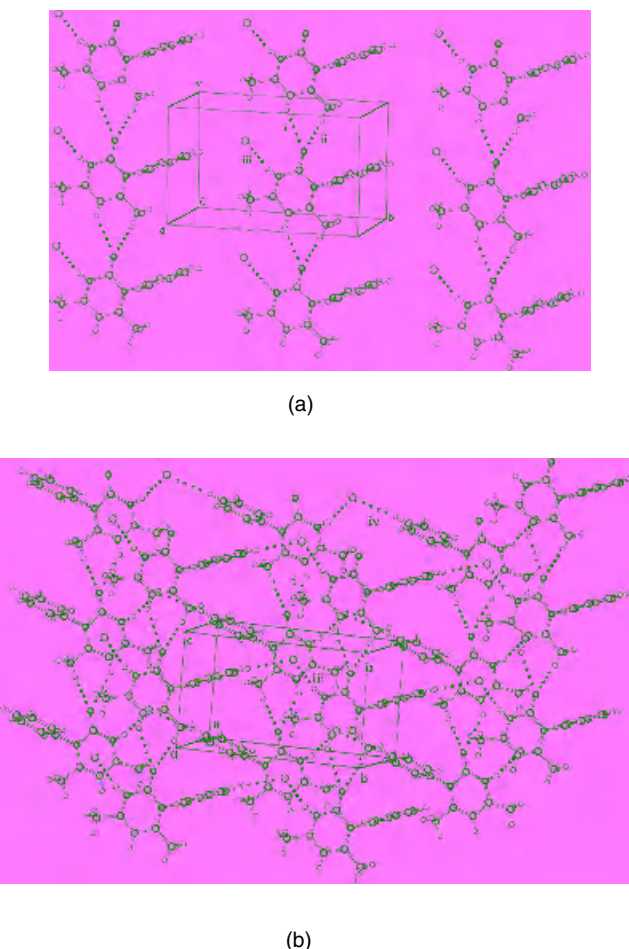


*Figure 5.14.* (a) Linear array of phenylpyrimidinone molecules in the crystal structure of **10** ( $\text{H}\cdot\text{HCl}$ ) mediated by the V-shaped  $\text{C}-\text{H}\cdots\text{O}$  synthon. (b)  $\text{N}^+-\text{H}\cdots\text{Cl}^-$ ,  $\text{C}-\text{H}\cdots\text{O}$  and  $\text{C}-\text{H}\cdots\text{Cl}^-$  hydrogen bonds stabilise the  $bc$ -layer. Note the parallel stacking of 2D polar layers.

The hydrochloride salts **12** and **13** ( $\text{Me}\cdot\text{HCl}$ ,  $\text{Cl}\cdot\text{HCl}$ ) are stabilized by cation–anion association via  $\text{N}^+-\text{H}\cdots\text{Cl}^-$  interaction ( $2.15\text{\AA}$ ,  $176^\circ$ , *iii*) and the V-shaped  $\text{C}-\text{H}\cdots\text{O}$  chain synthon ( $2.75\text{\AA}$ ,  $146^\circ$ ;  $2.39\text{\AA}$ ,  $170^\circ$ ; *i* and *ii*). The pyrimidinone rings of **12** are aligned parallel in the *ac* layer with the carbonyl groups pointing in the same direction (2D polarity, Figure 5.15), but the overall structure is centrosymmetric because adjacent layers are inversion-related. The unit cell

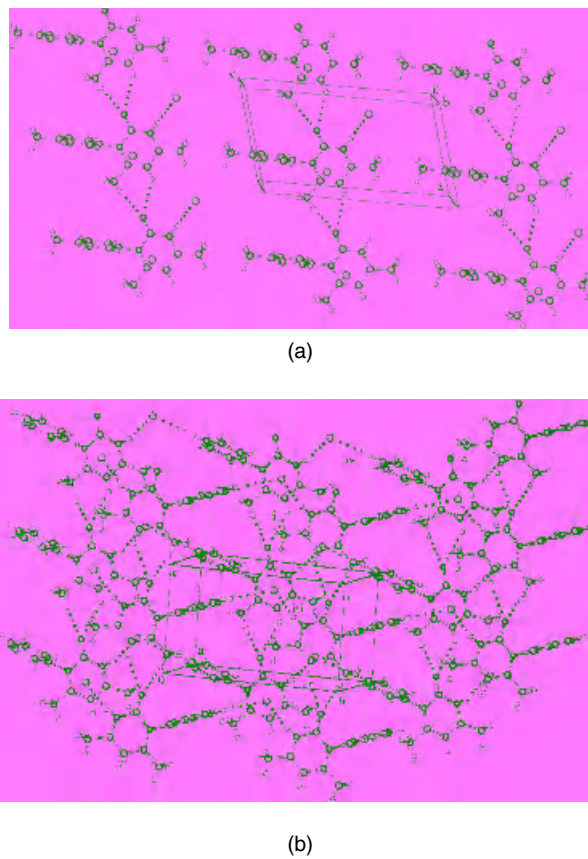


*Figure 5.15.* (a) Lamellar structure of tolylpyrimidinone molecules in **12** ( $\text{Me}\cdot\text{HCl}$ ) stabilized by the V-shaped  $\text{C}-\text{H}\cdots\text{O}$  synthon and  $\text{N}^+-\text{H}\cdots\text{Cl}^-$  hydrogen bonds. Note the 2D polar arrangement. (b) Molecules in adjacent layers pack in opposite directions, giving a centrosymmetric arrangement. The chloro derivative (**13**) is isostructural.

similarity index (II)<sup>48</sup> of **12** and **13** (space group  $P2_1/m$ ) is 0.0043, implying close identity in these crystal structures.

The two-dimensional polar sheets in **12** and **13** may be compared with hydrogen-bonded layers in uronium sulfonate crystal structures. Uronium and sulfonate ions self assemble into hydrogen-bonded polar sheets. The cation and anion moieties are mismatched in terms of the number of hydrogen bonding groups, which results in the formation of chains (Figure 5.16*b*), similar to the ribbon motif of guanidinium ions (Figure 5.16*a*). The hydrogen bond donors and acceptors not used in the formation of chains connect to form the

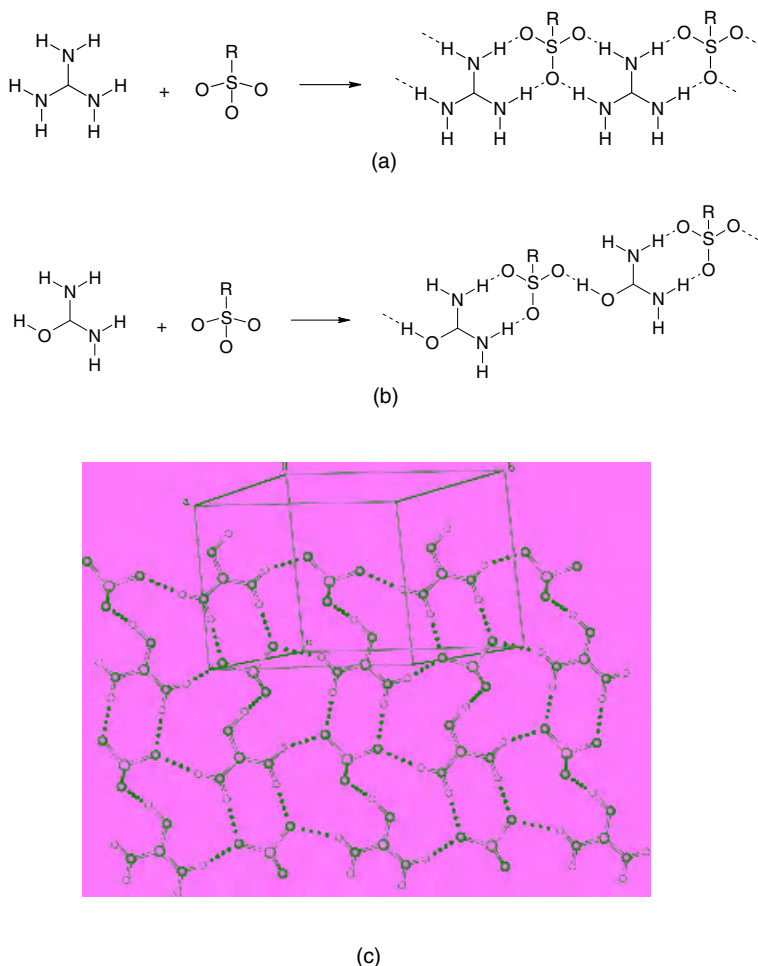


Figure 5.16. Hydrogen bonding in (a) guanidinium sulfonates and (b) uronium sulfonates. (c) The organization of the uronium and sulfonate ions in 2D polar layer. Note that the uronium ions point in the same direction. The crystal structure is centrosymmetric.

uronium sulfonate sheet of Figure 5.16c. The 2D polar layers observed in the chloride structures above are similar to the layered structures of isoleucinamide hydrochloride and valinamide hydrochloride, both in chiral space group  $P2_1$ .<sup>49</sup> In isoleucinamide hydrochloride, translation-related molecules are connected through  $\text{N}-\text{H}\cdots\text{O}$  and  $\text{C}-\text{H}\cdots\text{O}$  hydrogen bonds such that the carbonyl oxygen acts as a bifurcated acceptor (Figure 5.17). The chains are cross-linked through  $\text{N}-\text{H}\cdots\text{Cl}^-$  hydrogen bonds in a 2D polar layer arrangement. The  $\alpha$ -network

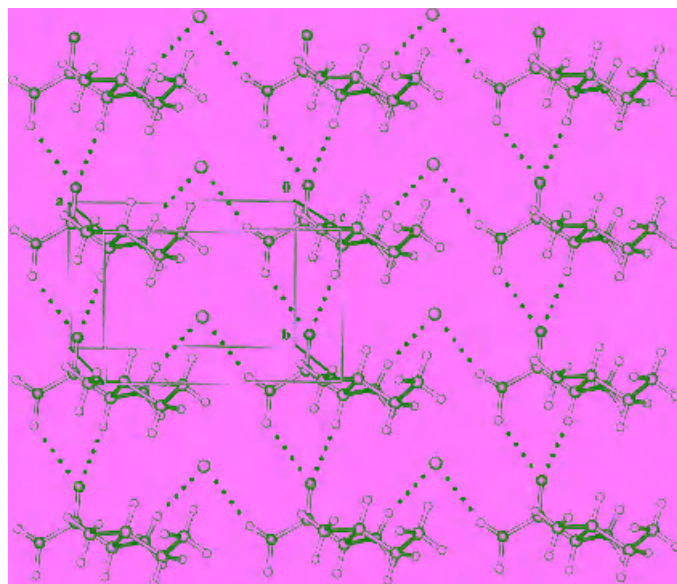
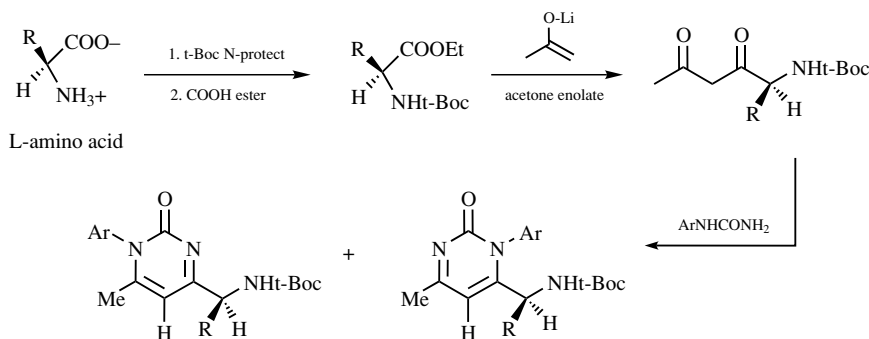


Figure 5.17. 2D polar layer structure of isoleucinamide hydrochloride. Note the similarity of the V-shaped synthon with that in the tolyl hydrochloride (**12**) shown in Figure 5.15.

of bifurcated N–H···O and C–H···O hydrogen bonds in isoleucinamide hydrochloride serves as a guide in designing noncentrosymmetric layer structures of chiral 2-pyrimidinones synthesized from optically active amino acids and *N*-phenylurea (Scheme 5.4). We predict that these structures will have polar layers in enantiomorphous space groups.



Scheme 5.4. Proposed synthesis of 2-pyrimidinones from L-amino acids for self-assembly to layered chiral crystal structures.

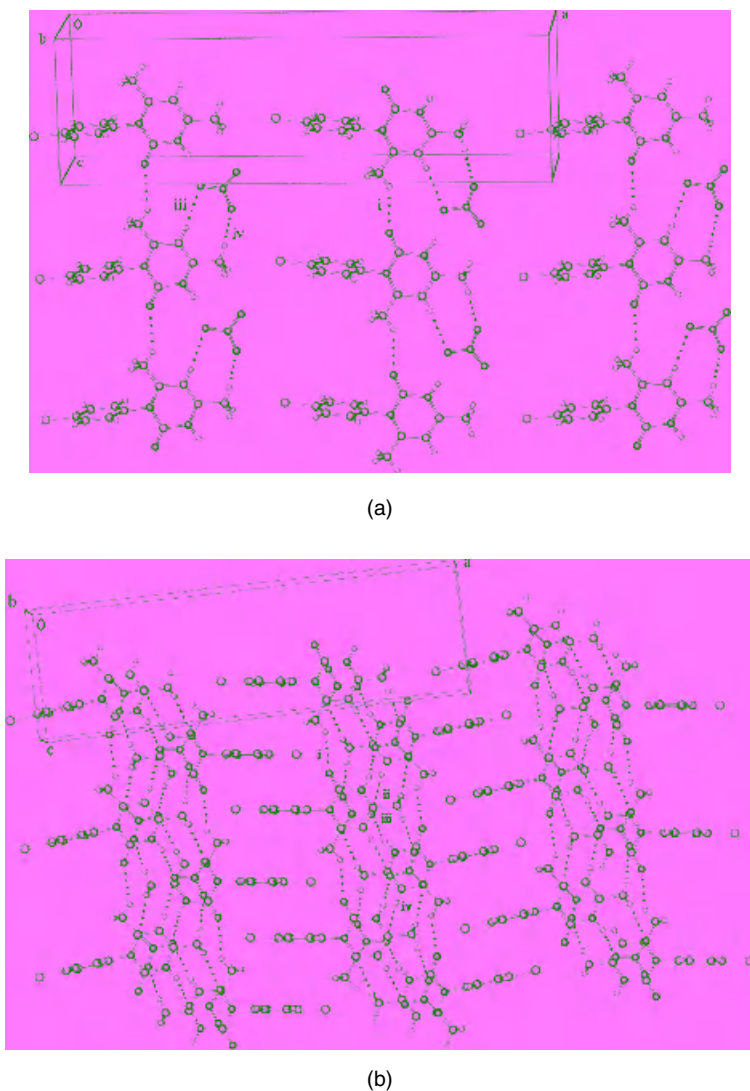


Figure 5.18. (a) Lamellar structure of **14** ( $\text{Cl}\text{-HNO}_3$ ) mediated via  $\text{C}-\text{H} \cdots \text{O}$  hydrogen bonds along the *c*-axis. Molecules are aligned anti-parallel within the *ac* plane. (b) The  $\text{N}^+ - \text{H} \cdots \text{O}^-$  and  $\text{C}-\text{H} \cdots \text{O}$  hydrogen bonds in the intra- and inter-layer region and the interdigitation of aryl groups between hydrogen-bonded columns.

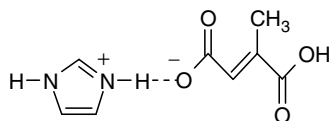
The isostructural nitrate salts **14** and **15** ( $\text{Cl}\cdot\text{HNO}_3$ ,  $\text{Me}\cdot\text{HNO}_3$ ) crystallize in *Pnma* space group. The C–H…O chain in **14** (2.61 Å, 143°, *i*) originates from the methyl hydrogen donor and the acceptor is not bifurcated as in the chloride salt structures (Figure 5.18). This difference from the chloride salts could be to accommodate the relatively larger  $\text{NO}_3^-$  counterion without too much alteration in the rest of the packing seen in the pyrimidinone family.  $\text{NO}_3^-$  ions connect molecules along [001] through an elaborate network of N–H…O (1.90 Å, 163°, *ii*) and C–H…O hydrogen bonds (2.54 Å, 174°; 2.15 Å, 174°; *iii* and *iv*). The aryl rings of inversion related molecules interdigitate between hydrogen-bonded domains to give centrosymmetric layers. The close packing of the aryl rings prevents the formation of voids, which could have been occupied by solvent molecules.

The chloride and nitrate salts of 2-pyrimidinones illustrate polar and centrosymmetric layer motifs, respectively. To summarize, the pyrimidinone salts self-assemble via weak, neutral C–H…O, and strong ionic  $\text{N}^+ - \text{H}\cdots\text{X}^-$  hydrogen bonds. The C–H…O chain synthon with a periodicity of around 7.3 Å persists in the chloride salts **10**, **12**, and **13**, and moreover, it favors crystallization of 2D polar layer structures. The frequency of 2D polarity increases in *meta*-phenylpyrimidinone derivatives.

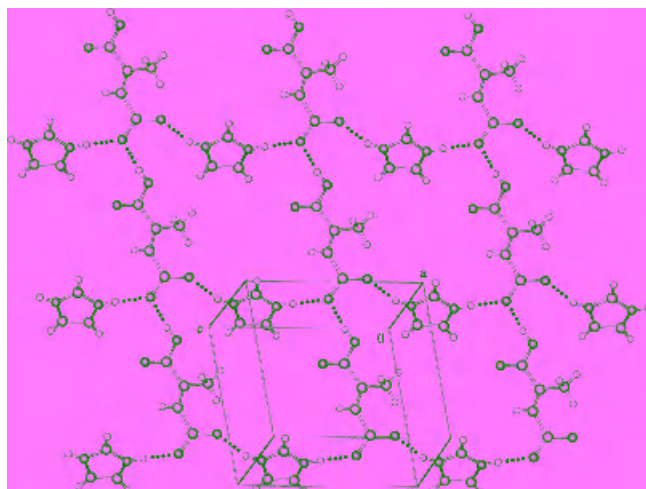
### C. Recurring 2D Polar Layer Arrangement

The problem of predicting or controlling crystallization of organic molecules in crystal structures with desired architecture or symmetry is still largely unsolved.<sup>50–52</sup> Despite the enormous potential of chiral or polar hydrogen-bonded solids in materials science (e.g., ferroelectric, nonlinear optics),<sup>12</sup> there are no general solutions for inducing the self-assembly of achiral molecules into space groups that lack an inversion center. Using chiral molecules appears to be an obvious approach, since the absence of crystallographic inversion center is guaranteed. However, difficulties in synthesizing chiral molecules together with issues such as phase matching and the distance of the chiral center from the chromophore, which must be addressed for efficient NLO solids, makes this simple route ineffective for materials scientists. Moreover the most common space group for chiral molecules,  $P2_12_12_1$ , is of little utility in inducing SHG effects because the three polar axes are mutually orthogonal and cancel out any molecular SHG properties. Although the chiral handle guarantees noncentrosymmetric space groups the crystal packing does not necessarily give high SHG efficiency.<sup>10,53,54</sup> It is estimated that only 10% of achiral, nonpolar organic molecules crystallize in space groups that lack the inversion center, while the probability is higher (25%) for all structures.<sup>55</sup> Molecular dipoles generally tend towards anti-parallel alignment (Figure 5.12). The correlation between the magnitude of the dipole

moment and centrosymmetry has been studied.<sup>56</sup> Hollingsworth<sup>12,57</sup> and Hulliger<sup>58</sup> have engineered the parallel alignment of dipolar molecules in channel inclusion compounds for NLO applications. Two-dimensional host frameworks have been used to produce polar crystallographic symmetry through banana-shaped pillars intercalated between flexible hydrogen-bonded sheets.<sup>59</sup> MacDonald<sup>60</sup> reported polar layers of ionic O—H···O<sup>−</sup> and N<sup>+</sup>—H···O<sup>−</sup> hydrogen bonds in imidazole carboxylates (Figure 5.19). However, these crystal structures are centrosymmetric because adjacent layers are inversion related. Diamondoid networks couple high thermal stability with efficient SHG activity.<sup>61</sup> These networks characterize an interesting structural motif for the construction of noncentrosymmetric solids because they are not inclined to pack in centrosymmetric space groups without an inversion center at each tetrahedral node. The optical and electronic properties of helical structures<sup>62–64</sup> are of added interest. The inherent chirality of helical

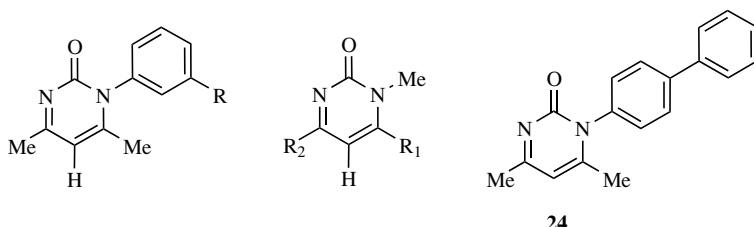


(a)



(b)

Figure 5.19. (a) Imidazolium hydrogen mesaconate. (b) Crystal structure to show the 2D polar layer sustained by strong O—H···O and N—H···O hydrogen bonds. Adjacent layers are inversion related.



- 16:** R = Br  
**17:** R = I  
**18:** R = NO<sub>2</sub>  
**19:** R = CH<sub>3</sub>  
**20:** R = OCH<sub>3</sub>  
**21:** R = F  
**22:** R = Cl
- 23a:** R<sub>1</sub> = Me, R<sub>2</sub> = Ph  
**23b:** R<sub>1</sub> = Ph, R<sub>2</sub> = Me

*Scheme 5.5.* *meta*-Phenylpyrimidinones (**16–22**) and miscellaneous compounds (**23, 24**).

networks comes from the chiral spatial arrangement of the lattice rather than the presence of chiral building blocks. The approaches above illustrate different methods of generating chiral (polar) crystals. Our solution to the problem of engineering chiral self-assembly is modular: the 3D structure is dissected into 2D polar layers that must stack in a parallel fashion. This simplifies the difficult task of steering parallel alignment of dipolar layers to the third dimension.

The crystal structures of *meta*-phenyl pyrimidinones **16m-Br**, **17m-I**, **18m-NO<sub>2</sub>**, **19m-Me**, **20m-OMe**, **21m-F** are discussed (Scheme 5.5).<sup>65</sup> Single crystals of **22m-Cl** could not be obtained despite several attempts. Translation-related molecules of *m*-Br (**16**) (space group *P*  $\bar{1}$ ) are connected by the now familiar C–H…O hydrogen bond synthon (2.47 Å, 154°, *i*) along the *a*-axis. C–H…Br interaction (3.12 Å, 121°, *ii*) connects such chains in the lateral direction to produce a rectangular grid in the (0 1  $\bar{1}$ ) plane (Figure 5.20). The carbonyl groups of **16m-Br** point in the same direction within a layer; that is, they form the 2D-polar layer structure. Linear chains of C–H…O and C–H…Br interactions run across to produce the polar sheet structure. The interlayer region has an abundance of C–H…O/C–H…Br interactions and an overall fit from close packing. Adjacent layers are inversion related.

The *N*-phenyl ring in **16m-Br** is tilted with respect to the pyrimidinone ring at an angle of 74.8°. In symmetrical phenyl derivatives **7–9** (e.g., Ph, *para*-tolyl, *para*-chlorophenyl), the aryl and heterocyclic ring are exactly perpendicular to each other such that the pyrimidinone ring lies in the mirror plane and the *m* plane bisects the phenyl ring. The orthogonal orientation of aryl and pyrimidinone rings in symmetrical derivatives of pyrimidinone is understood by calculating the energy of the isolated molecule as a function of the interplanar dihedral angle

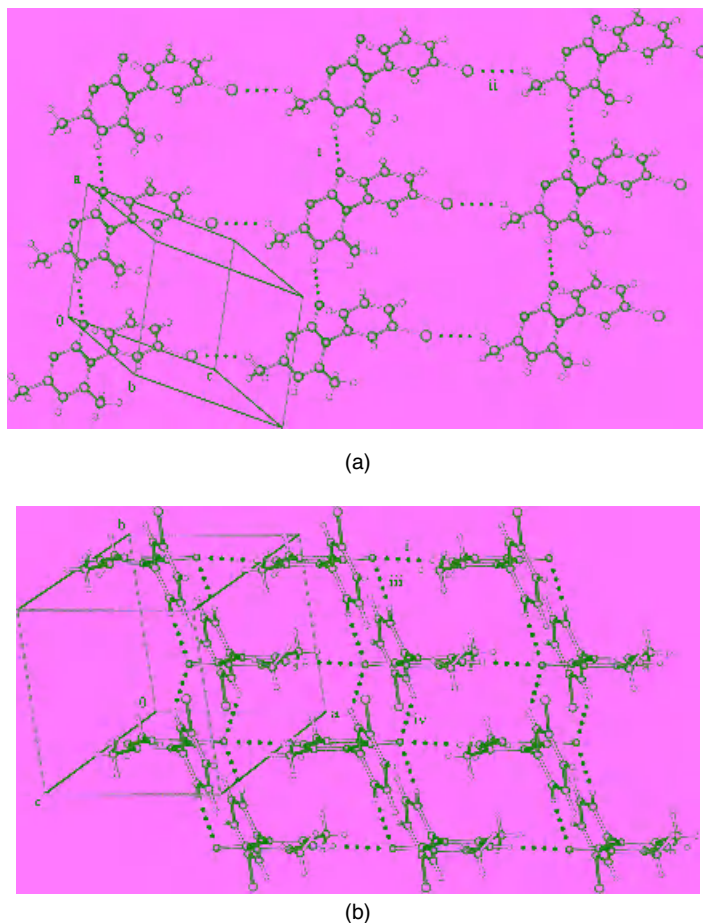


Figure 5.20. (a) C–H···O hydrogen-bonded 1D chain and C–H···Br interaction in the crystal structure of *m*-Br (**16**). Note the parallel alignment of molecules in the 2D layer. (b) Centrosymmetric arrangement of adjacent layers through interactions *iii* and *iv*.

( $\tau/^\circ$ ) (Spartan, RHF 3-21G\*).<sup>46</sup> The energy plotted in a dihedral angle graph, with a minimum at  $\tau = 90^\circ$ , is very shallow in the region  $80^\circ < \tau < 100^\circ$  (Figure 5.21). A slight deviation from the perpendicular conformation, and hence departure from mirror crystal symmetry, is tolerated if this tilt results in a stabilizing interaction elsewhere in the structure. The weak C–H···Br interaction in **16m**-Br (Figure 5.20, *ii*) is optimized as a result of the slight tilt of the phenyl ring. Despite these minor changes the robust C–H···O linear synthon is preserved, and this is important from a crystal engineering perspective. In **16m**-Br and other *meta*-phenyl

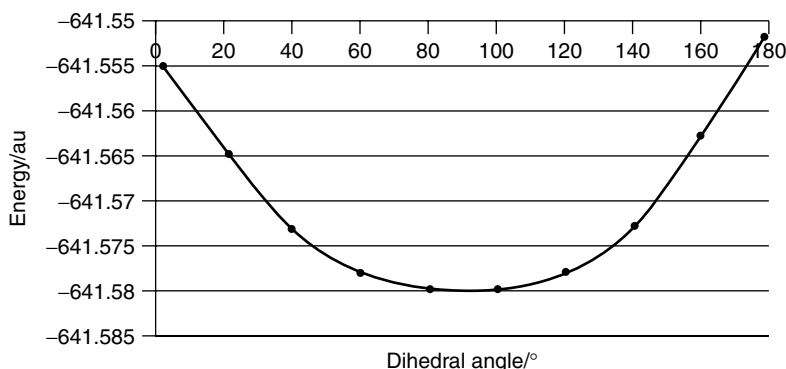


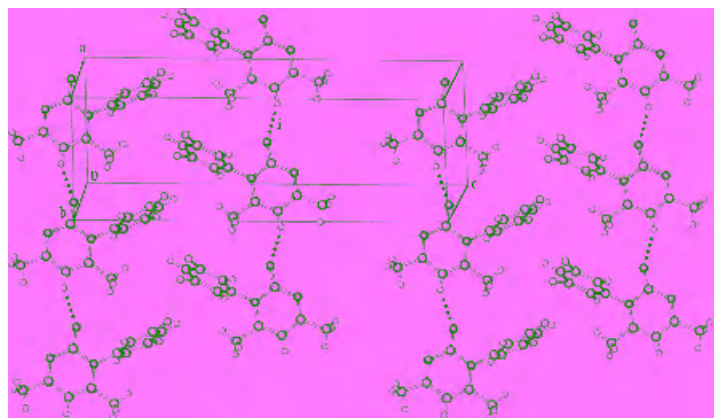
Figure 5.21. Molecular energy versus  $(\text{O})\text{C}-\text{N}-\text{C}-\text{C}-(\text{Ph})$  torsion angle in phenylpyrimidinone (7) calculated in Spartan (RHF 3-21G\*).

derivatives, the molecular and the crystal symmetry are lower (space group  $P\bar{1}$ ) compared to the *para*-phenyl derivatives ( $Pnma$ ,  $P2_1/m$ ).<sup>35,46</sup>

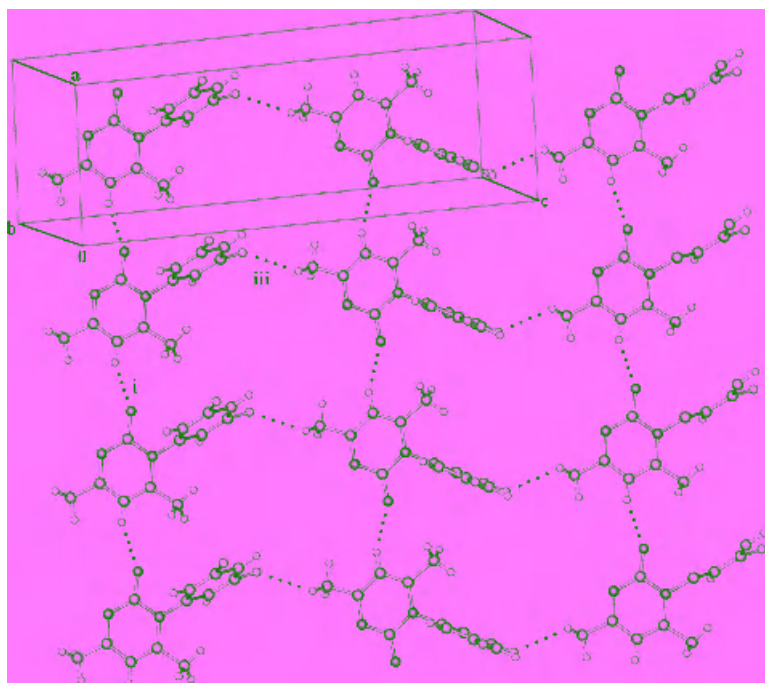
X-ray crystal structures of **17m-I** and **18m-NO<sub>2</sub>** are identical to **16m-Br**. The calculated volume of Br, I, and NO<sub>2</sub> groups is similar (26, 32, 29 Å<sup>3</sup>), and so is the arrangement of molecules in these crystal structures. The structure of the tolyl derivative **19m-Me** contains the robust C–H···O hydrogen bond chain but the tolyl ring rotates about the C–N bond such that its Me group moves away from a neighboring pyrimidinone Me group. This is due to the absence of stabilizing C–H···X interaction in the lateral direction. The *m*-OMe derivative (**20**) has the C–H···O chain synthon with OMe groups participating in centrosymmetric (Ph)C–H···O dimer. The 2D polar layer motif persists in these *meta*-phenyl pyrimidinones.

The structures, thus far, signify the robustness of the recurring C–H···O hydrogen-bonded chain synthon in directing the arrangement of pyrimidinone molecules. While the individual C–H···O interactions may be weak (2–3 kcal/mol), the chain synthon constructed with these weak hydrogen bonds is robust enough to sustain self-assembly in a number of structures. There is thus a hierarchy of interactions even within the weak hydrogen bond category. The 1D chain and the 2D layer interactions are predictable, but the factors that control the stacking of layers are not fully understood.

The crystal structure of **21m-F** is interesting because it crystallizes in a mirror-containing space group ( $Pnma$ ), like the *para*-phenyl derivatives, even though it is a *meta*-phenyl pyrimidinone. The pyrimidinone molecule resides in the mirror plane and this plane bisects the *N*-*m*-fluorophenyl ring (Figure 5.22a). This structure is isomorphous with *p*-Me (**8**) and *p*-Cl (**9**) ( $Pnma$ ) in that the 1D chains are oriented parallel within the 2D-polar layer. However, it



(a)



(b)

Figure 5.22. (a) Parallel alignment of 1D chains sustained by  $\text{C}-\text{H}\cdots\text{O}$  interaction *i* in the crystal structure of 21m-F. (b) Interlayer  $\text{C}-\text{H}\cdots\text{F}$  interaction *iii*. The F atom is disordered with 0.5 occupancy in each location.

is different from the structure of H (**7**) (*Pbcm*) in which 1D chains are aligned antiparallel within the layer. Normally replacement of H with F in a molecule does not result in significant structural differences<sup>66</sup> because the van der Waals radius of these atoms is similar ( $H_{vdW}$  1.20 Å,  $F_{vdW}$  1.47 Å). However, when the H and F structures are different, specific C–H…F interactions may be involved.<sup>67</sup> Analysis of the interlayer packing in **21m**-F shows that there is a (Me)C–H…F interaction (2.59 Å, 125°, *iii*) (Figure 5.22*b*) between inversion-related molecules. The F atom is refined with a site occupancy of 0.5. The pyrimidinone ring atoms reside on the mirror plane and are fully ordered. A possible reason for the 50% occupancy of fluorine could be that in this way the unsymmetrical phenyl ring conforms to the higher mirror symmetry in the crystal. The mirror plane *m* in 2-pyrimidinone crystal structures is perhaps directed by the stable bisected-phenyl conformation (Figure 5.21).<sup>46</sup> Normally, molecules do not reside on the *m* plane because it decreases packing efficiency by 2% to 3%.<sup>68</sup> However, retention of *m* or twofold symmetry is thermodynamically advantageous because the molecules are symmetrically arranged.

Last, we note that the recurring C–H…O chain synthon and the polar layer structure persist when one of the pyrimidinone Me groups is successively replaced by a Ph group, as in **23a** and **23b**,<sup>65</sup> or the *N*-phenyl is replaced with *N*-biphenyl group **24** (Scheme 5.5).<sup>46</sup> We show that 2D polar layers may be engineered via the robust pyrimidinone tape synthon. The molecules can tolerate large variations in molecular structure, such as *para*- to *meta*-phenyl, electron-withdrawing and electron-donating groups, and furthermore groups with a similar volume (Cl, Me, Br, I, NO<sub>2</sub>) that give isostructural crystals. The challenge of controlling the parallel alignment of 1D dipoles or 2D polar layers in space groups that lack the inversion center, such as *P2*<sub>1</sub>, *Fdd2*, *Pna2*<sub>1</sub>, and *Imm2*, is still a daunting task with no general solution in the foreseeable future.

#### D. Model for 2D Polar Layer Assembly

The persistent occurrence of 2D polar layers in 2-pyrimidinone crystal structures survives changes in molecular structure ranging from the simple exchange of groups to the replacement of phenyl with methyl or biphenyl groups to the structures of ionic salts. Notwithstanding that the space groups and detailed crystal-packing motifs are different, the 1D chain of C–H…O hydrogen bonds and the 2D polar layer assembly are recurring structural features. Understanding 2D polarity in the dozen or so pyrimidinone structures<sup>65</sup> begins from the robust C–H…O hydrogen bond chain synthon. Such chains may align parallel (2D polarity) or anti-parallel (centrosymmetric layer motif). Four possible arrangements of hydrogen-bonded chains of pyrimidinone molecules in 2D layers are shown in Figure 5.23. Motifs (*a*, *b*) are 2D polar while the chains are aligned antiparallel in (*c*, *d*). The most

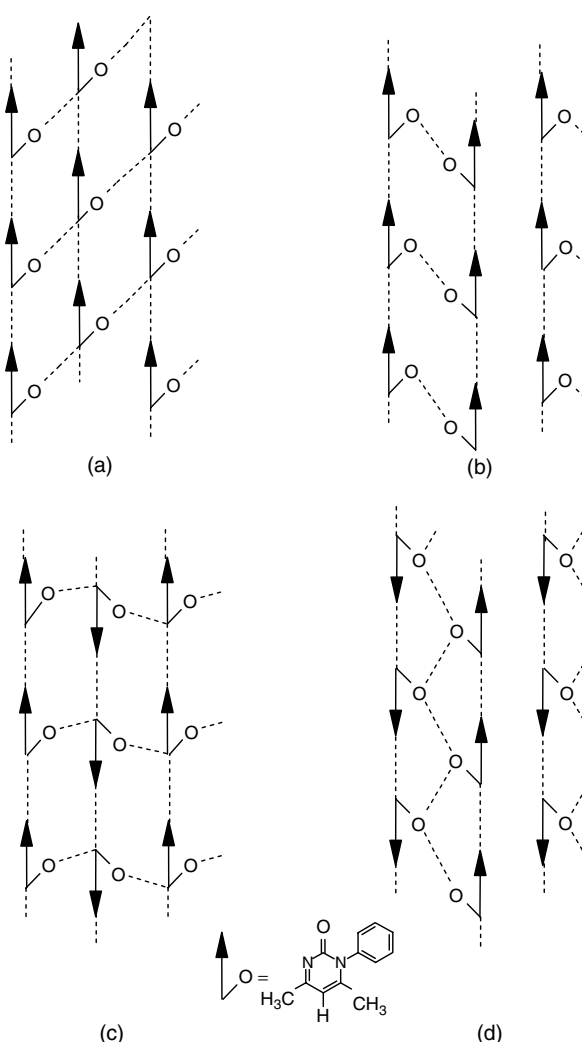


*Figure 5.23.* Model to explain the recurrence of 2D polar layer arrangement in arylpyrimidinones. The 1D chain is constructed with C–H···O interactions in all cases while the lateral interactions in the layer are different. (a) Parallel alignment of 1D chains and the lateral C–H···X interactions are simultaneously optimized. (b) Parallel alignment of 1D chains and the herringbone motif between phenyl groups. (c) In anti-parallel alignment of 1D chains, the lateral C–H···X interaction is bent. (d) Anti-parallel alignment of 1D chains with neighboring phenyl groups being inversion-related. Motif (a) is present in over half the structures (8/15), motif (b) in four structures, and motif (c) in three structures. Motif (d) is not found in any structure.

common pattern in pyrimidinone crystals is depicted in (a). Translation-related molecules form the C–H $\cdots$ O hydrogen-bonded chain (in the direction of the arrow) and such chains are further connected through weak hydrogen bonds or van der Waals interactions involving the phenyl ring. This 2D-polar motif is present in eight structures: H·HCl (**10**), *p*-Me·HCl (**12**), *p*-Cl·HCl (**13**), *m*-Br (**16**), *m*-I (**17**), *m*-NO<sub>2</sub> (**18**), *m*-Me (**19**), and *m*-OMe (**20**). In motif (b), a twofold screw axis or glide plane parallel to the polar (arrow) direction relates molecules in adjacent chains. These symmetry operations are favored because they result in the stable herringbone geometry between phenyl rings, and furthermore the methyl groups close-pack on the other side of the chain. The 2D-polar motif (b) is present in four structures: *p*-Me (**8**), *p*-Cl (**9**), *p*-Ph (**24**), and *m*-F (**21**). In the anti-parallel arrangement (c), the interactions are similar to (a) but the symmetry operation that relates the hydrogen-bonded molecules is different. A 2<sub>1</sub>-screw axis or glide-plane perpendicular to the polar (arrow) direction relates adjacent chains that now run in opposite directions within a layer. Three structures belong to this centrosymmetric layer category, H (**7**), *p*-Me·HNO<sub>3</sub> (**15**), and *p*-Cl·HNO<sub>3</sub> (**14**). Motif (c) is not preferred, even though it has similar interactions and void size compared to (a), because the methyl group of pyrimidinone is not correctly placed within the molecular tape for lateral interaction with an acceptor group on the phenyl group (dotted lines). A hydrogen bond between the phenyl ring and pyrimidinone heterocycle in the lateral direction would be bent in (c). The centrosymmetric layer (d), with adjacent chains related by the inversion center, is not observed in any structure. This is because inversion symmetry is not compatible with the ubiquitous herringbone T-geometry between phenyl rings in the solid state.<sup>69,70</sup> Even though inversion-related phenyl rings can engage in  $\pi$ – $\pi$  stacking, this motif is not favored in the present case because quadrupole-quadrupole interaction (charge-transfer component) between like phenyl rings is minimal. Thus the dominant 2D polar layer arrangement in 2-pyrimidinones is rationalized through motifs (a) and (b) that account for 12 of the 15 crystal structures.

The primary condition for frequency doubling, a noncentrosymmetric crystal structure, is not yet achieved in the pyrimidinone family. Notwithstanding the high percentage of centrosymmetric crystals, further work is justified on these materials because the condition for phase matching<sup>53</sup> is properly fulfilled in these structures. The optimum angle for the alignment of the chromophore charge transfer axis with the crystallographic polar axis in point group *mm2* is 54.7° for a phase-matched crystal like NPP (Figure 5.24). This value is 56.9° for neutral pyrimidinones (**8**) and (**9**), which have 2D polar layers but in centrosymmetric space group. If these polar layers can be arranged in parallel arrays to obtain a noncentrosymmetric crystal lattice (e.g., amino acid derived pyrimidinones, Scheme 5.4), then an SHG active solid is likely to result.

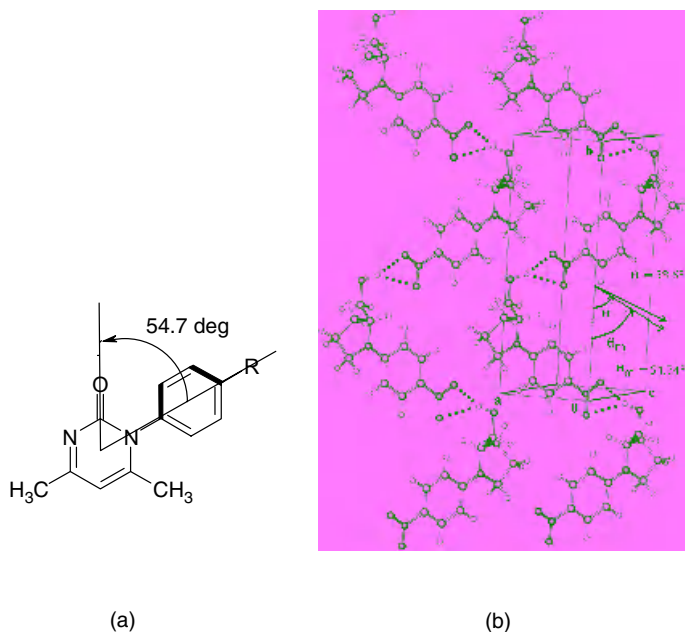
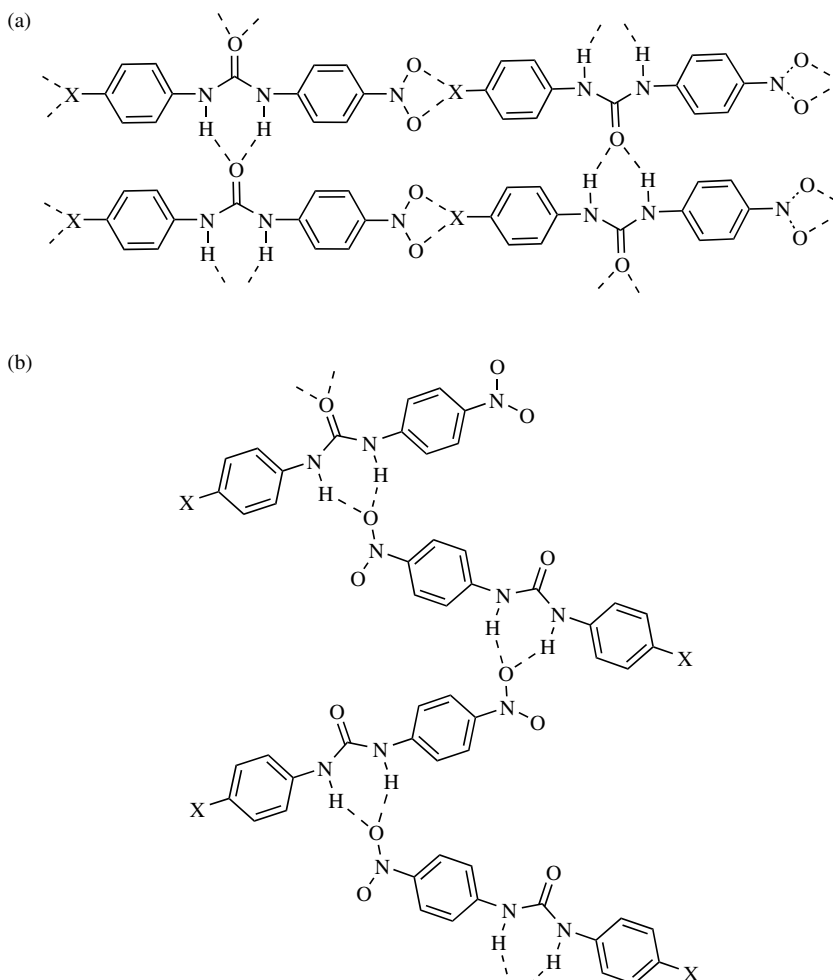


*Figure 5.24.* (a) Orientation of a potential chromophoric aryl group with the carbonyl axis in the crystal structure of 2-pyrimidinone. (b) The angle made by the molecular dipole with the polar axis in the crystal structure of *N*-(4-nitrophenyl)-(L)-prolinol, NPP, a SHG active compound. Note that the angle in 8 and 9 is 56.9°, close to the optically ideal value is 54.7°.

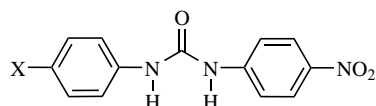
#### IV. DESIGN OF SHG ACTIVE UNSYMMETRICAL UREAS

So far we have discussed the structures of 2-pyrimidinones, which are masked ureas, to construct supramolecular architectures. Lauher and Fowler<sup>24,71</sup> have published 2D sheet structures of urea tape  $\alpha$ -networks and COOH/COOH and CONH<sub>2</sub>/CONH<sub>2</sub> hydrogen bonding in the lateral direction. We show how the urea  $\alpha$ -network together with X···NO<sub>2</sub> interaction in the lateral direction (Scheme 5.6) may be exploited to assemble 2D layers and noncentrosymmetric crystal structure for NLO applications. The ureas used as potential candidates for this crystal engineering exercise are listed in Scheme 5.7. The combination of the urea and nitro functionality in the same molecule appeared favorable at the outset toward our end goal of noncentrosymmetric crystal. The nitro group is introduced in several organic NLO chromophores because it favors crystallization in space groups that lack the inversion center and the donor– $\pi$ –acceptor conjugated system has a strong dipole moment.<sup>54</sup> Recently, single crystals in the polar space group *Fdd2* have been



*Scheme 5.6.* Some possible hydrogen bond synthons in the crystal structures of nitro diphenyl ureas: (a) Urea···urea and (b) urea···nitro hydrogen bonding.

engineered via the I···O<sub>2</sub>N synthon,<sup>72</sup> an interaction that connects urea molecules in the lateral direction as shown in Scheme 5.6a. Crystal structures of some closely related nitrodiphenylureas are reported. *N*-3-nitrophenyl-*N'*-3'-nitrophenylurea crystallizes in two polymorphic modifications:<sup>73</sup> a centrosymmetric  $\alpha$ -polymorph in  $P2_1/c$  space group and a noncentrosymmetric  $\beta$ -polymorph in  $C2$  space group. The  $\beta$ -polymorph of *N*-3-nitrophenyl-*N'*-3'-nitrophenylurea (Figure 5.25) and *N*-4-nitrophenyl-*N'*-4'-nitrophenylurea have powder SHG efficiency of 1.5 and



- |                     |                   |
|---------------------|-------------------|
| <b>25:</b> X = I    | <b>30:</b> X = CN |
| <b>26:</b> X = C≡CH | <b>31:</b> X = Ac |
| <b>27:</b> X = Br   | <b>32:</b> X = Me |
| <b>28:</b> X = Cl   | <b>33:</b> X = H  |
| <b>29:</b> X = F    |                   |

Scheme 5.7. Some nitro diphenyl urea molecules (25–33) for crystal engineering.

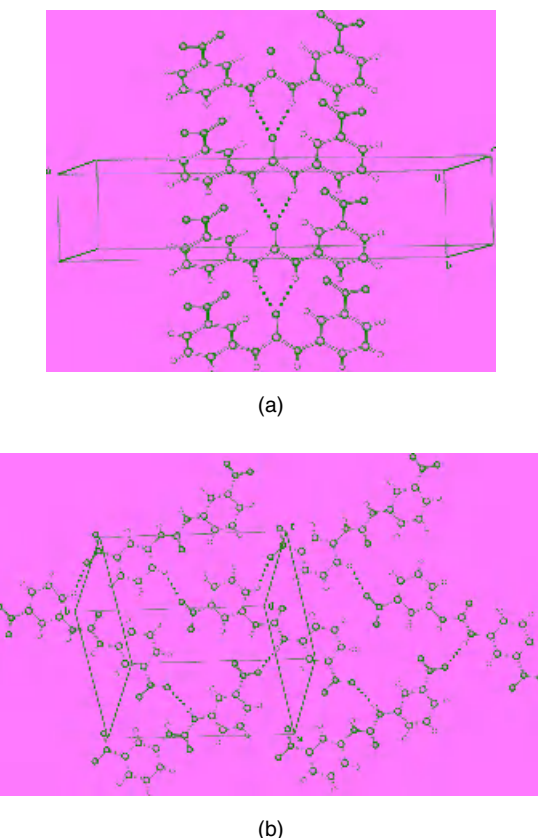
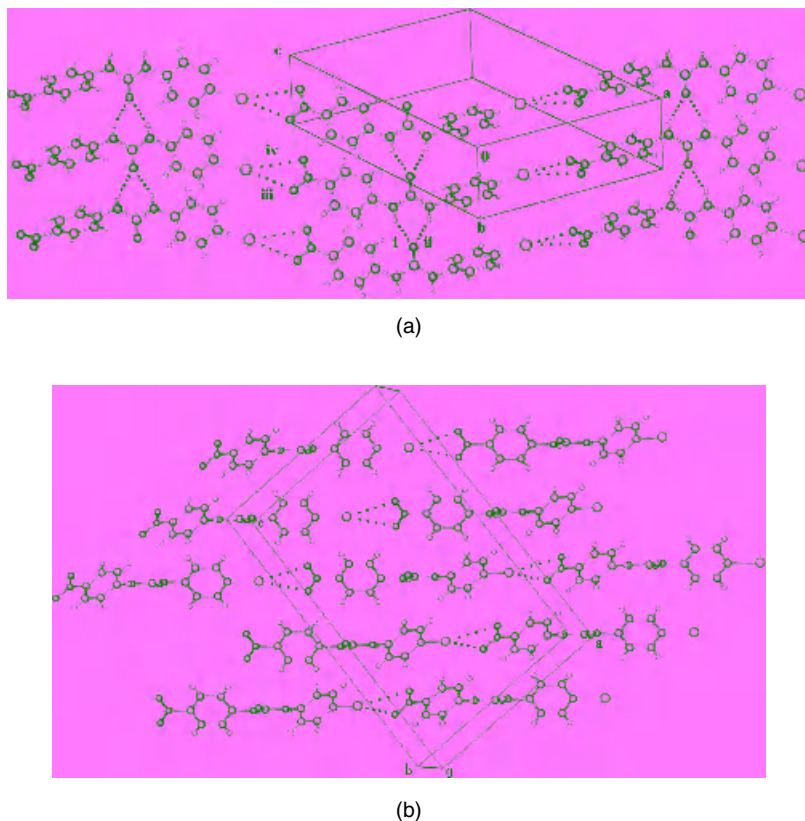


Figure 5.25. (a) N–H···O hydrogen-bonded tape ( $\alpha$ -network) in the  $\beta$ -polymorph of *N*-3-nitrophenyl-*N'*-3'-nitrophenylurea in space group  $C2$ . The phenyl ring is twisted with respect to the urea plane by  $46.8^\circ$ . (b)  $\alpha$ -Polymorph of *N*-3-nitrophenyl-*N'*-3'-nitrophenylurea with different hydrogen bonding pattern in space group  $P2_1/c$ .

8.8 times that of urea respectively.<sup>74</sup> The crystal structure of *N*-4-nitrophenyl-*N'*-4'-nitrophenylurea is not reported. The nitro-substituted diphenylurea molecules with X = halogen, C≡C—H, N(CH<sub>3</sub>)<sub>2</sub>, CH<sub>3</sub>, COCH<sub>3</sub>, and H, on one side and NO<sub>2</sub> on the other side were systematically screened to engineer their crystallization in noncentrosymmetric space group.

The iodo-nitro urea (**25**) crystallizes in the polar space group *Cc* via the urea N—H···O tape synthon and I···O<sub>2</sub>N interaction in the lateral direction.<sup>75</sup> The carbonyl group is aligned along the short *b*-axis (4.67 Å) of the unit cell. The aryl groups are twisted out of the urea plane (49.1, 45.6°) to adjust to the robust  $\alpha$ -network. N—H···O hydrogen bonds are 2.128 Å, 153.3°, and 2.131 Å, 155° (*i* and *ii*) and the I···O<sub>2</sub>N bifurcated motif is 3.28 Å, 169.6°, and 3.61 Å, 154.3°



*Figure 5.26.* (a) N—H···O  $\alpha$ -network along the *b*-axis in the crystal structure of iodo-nitro urea (**25**). (b) Polar assembly of phase-matched chromophores mediated by the I···NO<sub>2</sub> synthon resulting in the intense SHG signal. The dominant orientation of the disordered iodo/nitro atoms is shown.

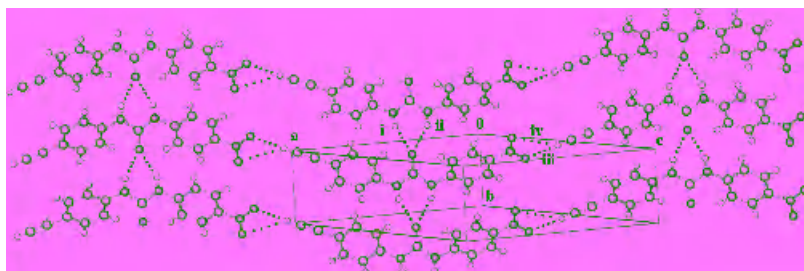
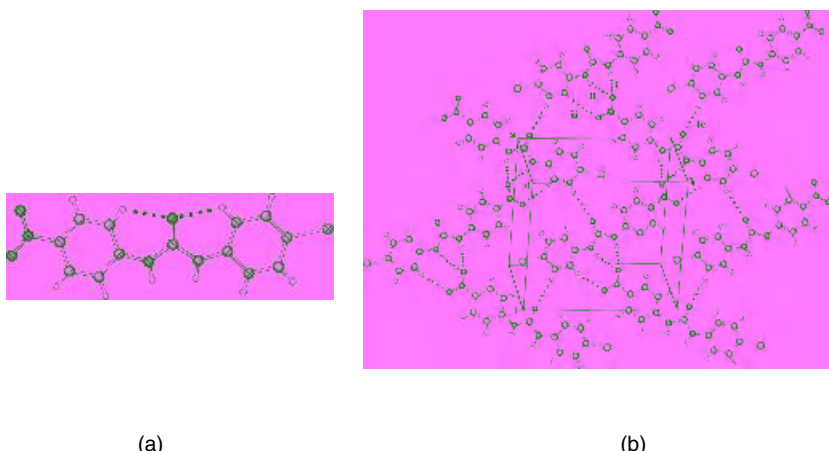


Figure 5.27. Urea tape network in the polar crystal of ethynyl-nitro urea (**26**).

(*iii* and *iv*) (Figure 5.26). From the prospect of engineering macroscopic polarity in the crystal, although molecules of (**25**) are aligned antiparallel along the carbonyl axis, the inclined, parallel orientation of NH–π–NO<sub>2</sub> chromophores will result in a net dipole moment. The polar chains along [2 0 –1] connect glide-related molecules via the I···O<sub>2</sub>N synthon. The iodo and nitro groups are disordered with site occupancy factor of 0.9 and 0.1. The structure is solved and refined with *R*-factor of 0.028. SHG measurement on a microcrystalline sample of (**25**) with Nd<sup>3+</sup>-YAG laser at 1064 nm yielded a strong quadratic nonlinear response, with an intense green signal at 532 nm equal to that of the benchmark compound 3-methyl-4-nitropyridine1-oxide (POM).<sup>76</sup> The possible phase matching in the polar crystal (**25**) is in agreement with an SHG signal over 13 times stronger than that of urea.

The crystalline ethynylurea (**26**) is isostructural to (**25**), confirming recent observations that iodo to ethynyl exchange does not generally disturb the crystal packing.<sup>77</sup> Figure 5.27 shows translation related molecules connected through N–H···O (2.11, 2.10 Å; 154.6°, 156.3°; *i* and *ii*) hydrogen bonds resulting in the  $\alpha$ -network, and such glide-related tapes are in turn connected laterally through C≡C–H···O<sub>2</sub>N (2.40, 3.05 Å; 167.8°, 142.9°; *iii* and *iv*) interactions. The C≡C–H···NO<sub>2</sub> chains viewed down the *b*-axis shows that all the chains are aligned in the same direction, resulting in the net dipole moment that is crucial for developing materials with useful properties. The aryl rings are twisted out of the urea plane by 48.8° and 47.3°.

In contrast to the polar crystals of iodo and ethynylureas, the bromo compound (**27**) crystallizes in the centrosymmetric space group *P*2<sub>1</sub>/*n*. This structure was determined to evaluate the robustness of the N–H···O urea tape synthon. The X···O<sub>2</sub>N interaction is stabilized by the Lewis acid–Lewis base or donor–acceptor pairing or *n*→σ\* electron donation, with the polar electropositive portion of halogen pointing to the electronegative oxygen of NO<sub>2</sub>. The strength of the X···O<sub>2</sub>N interaction decreases in the order I>Br>Cl (as –10 to –6 kJ/mol)<sup>78</sup>



*Figure 5.28.* (a) ORTEP diagram of bromo-nitro urea (**27**) to show the intramolecular C–H…O interaction. (b) Layered structure of (**27**) stabilized by N–H…O<sub>nitro</sub> hydrogen bonds and C–H…O<sub>urea</sub> interaction. The Br atom is not involved in any short intermolecular contacts.

because of the greater polarizability of the heavier halogen. The crystal structure of bromo compound (**27**) is different from the iodo derivative (**25**). It adopts a flat planar molecular conformation stabilized by an intramolecular C–H…O hydrogen bond (2.3 Å, 121°; Figure 5.28a). The molecules are arranged in a herringbone fashion such that glide-related molecules are connected via N–H…O hydrogen bonds (2.10 Å, 2.25 Å; 161.3°, 157.0°, *i* and *ii*) with the nitro oxygen acceptor in a bifurcated motif (Figure 5.28b). The second oxygen of the NO<sub>2</sub> group accepts a C–H…O hydrogen bond from the *o*-Ph donor (2.74 Å, 162.1°, *iii*). The *m*-Ph group makes C–H…O hydrogen bond with the urea carbonyl oxygen (2.97 Å, 164.1°, *iv*). The layered structure of (**27**) has no short Br…Br contacts. The chloro derivative (**28**) is isostructural with  $\Pi = 0.008$ .<sup>48</sup> Single-crystal X-ray diffraction and packing analysis of remaining structures will be reported in due course.

Two conclusions may be drawn from this study:<sup>75</sup> (1) that the weak I…O<sub>2</sub>N or C≡C–H…O<sub>2</sub>N synthon can direct the robust N–H…O tape  $\alpha$ -network in diphenyl ureas; (2) that these weak interactions can induce crystallization in noncentrosymmetric, polar space group. Thus the weak I…O<sub>2</sub>N interaction is the “discriminator synthon” even in the presence of strong N–H…O hydrogen-bonding groups. We not only show the engineering of a crystal structure but also of macroscopic property in the same material.

Some recent examples of noncentrosymmetric crystal design for NLO are summarized to place our results in context. 4-(4'-Ethynylphenyl)ethynylpyridine (**34**) crystallizes in the polar space group *Fdd2* through linear chains of C–H…N

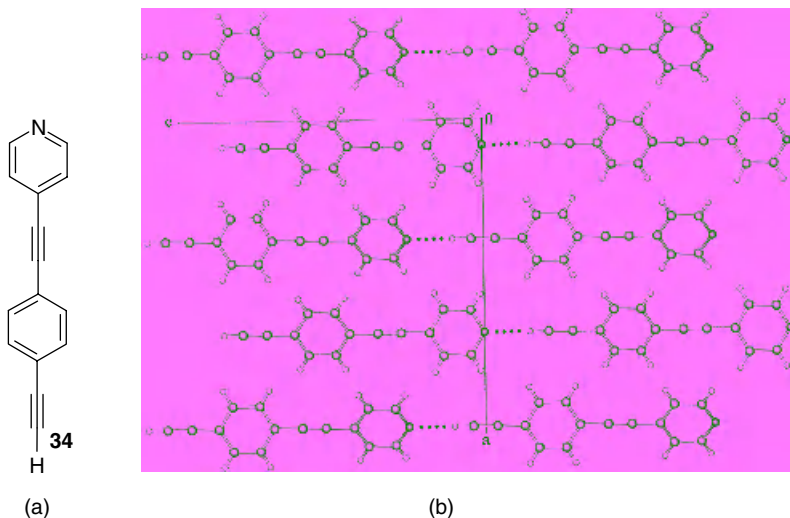


Figure 5.29. (a) 4-(4'-Ethynylphenyl)ethynylpyridine. (b) Parallel alignment of linear chains of chromophores mediated by C–H···N hydrogen bonds, which play a role in constructing the polar crystal for bulk SHG property.

hydrogen bonds (Figure 5.29).<sup>79</sup> In 1,3-dibromo-2,4,6-trinitrobenzene (**35**), the perfect polar alignment of hyperpolarizable chromophores in hexagonal networks (Figure 5.30) results in SHG response of over 15 times that of urea.<sup>80</sup> The weak hydrogen bonds avoid anti-parallel alignment of large dipole moments arising from strong hydrogen bonding groups.<sup>56</sup> Octupolar molecules derived from the boroxine framework **36** (Figure 5.31) combine excellent transparency in the near UV-visible region ( $\lambda < 280\text{ nm}$ ) and significant first-order hyperpolarizabilities ( $\beta(0) = 56 \times 10^{-30}\text{ esu}$ ) to optimize efficiency–transparency trade-off in molecular NLOs.<sup>81</sup>

Because the theme of this book is about stereochemistry of molecules in a crystal we briefly mention the rare, yet pharmaceutically important phenomenon of conglomerate crystallization,<sup>82</sup> namely the spontaneous formation of homochiral supramolecular architectures.<sup>83</sup> Toda<sup>84</sup> has reviewed examples of achiral molecules organized in a chiral crystal lattice of the same molecule<sup>29b,85</sup> or of a host compound.<sup>39,86</sup> For example, it was recently shown that *ortho*-substituted *N*-phenyl 2-pyrimidinones **37** (Scheme 5.8) exhibit C–N axial chirality and some derivatives (**37a**, **37c**, **37d**) can be spontaneously resolved<sup>85</sup> by conglomerate crystallization without an outside chiral agent. These atropisomeric pyrimidinones are stable at room temperature for several days but racemize above 170 °C.

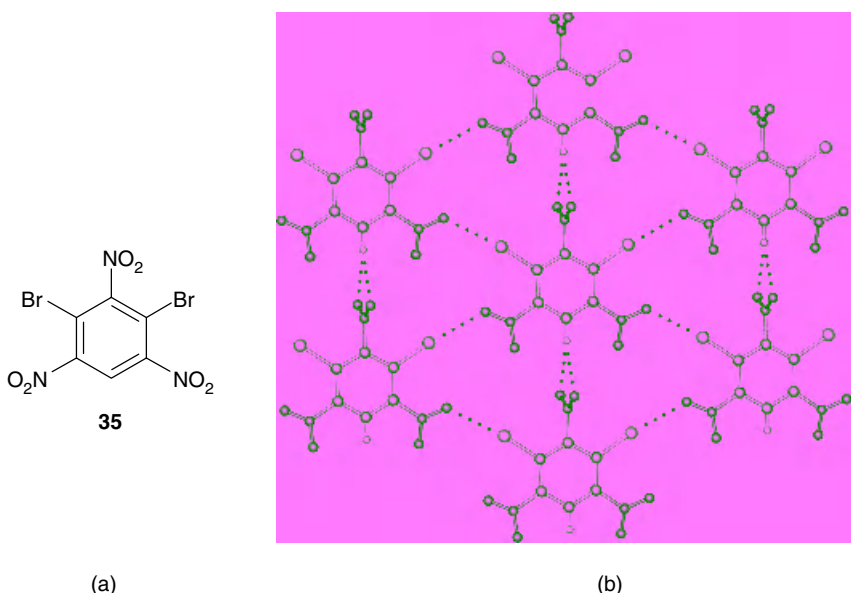


Figure 5.30. The hexagonal network structure of 1,3-dibromo-2,4,6-trinitrobenzene (35). The C–H···O hydrogen bonds point along the polar axis.

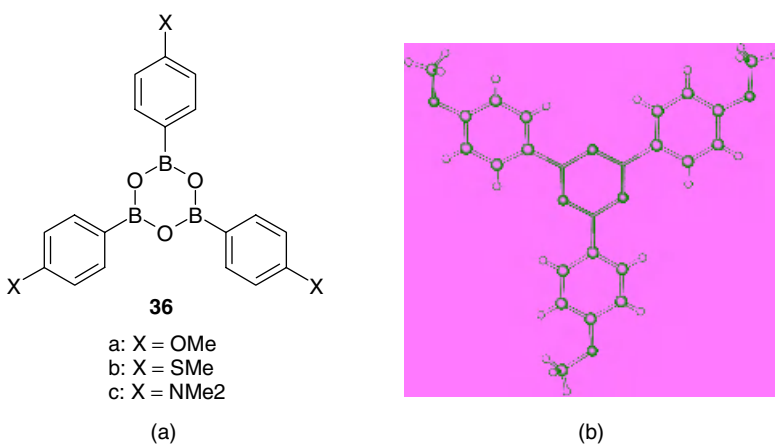
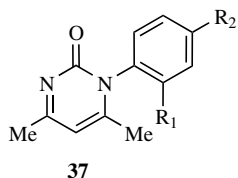


Figure 5.31. (a) The boroxine framework (36) and (b) the X-ray crystal structure of (36a). These molecules are transparent in the near UV-visible spectrum because the central core is not aromatic.



- a: R1 = Me, R2 = H
- b: R1 = Cl, R2 = H
- c: R1 = Me, R2 = Cl
- d: R1 = Cl, R2 = Cl

*Scheme 5.8.* Resolution of *ortho*-phenyl pyrimidinones (**37**) by conglomerate crystallization.

## V. CONCLUSION AND FUTURE DIRECTIONS

This study was started with the urea  $\alpha$ -network to engineer 2-pyrimidinone crystal structures using the concept of hydrogen bond mimicry. The robust C–H…O chain synthon in pyrimidinones is exploited for the construction of 1D chain and 2D layer structures. Strong N–H…O and O–H…O hydrogen bonds in urea networks are faithfully replaced by weak C–H…O, C–H…N, and C–H…halogen interactions in pyrimidinone structures. Notably several of the pyrimidinone layer structures have polar alignment of molecular dipoles in the 2D network, though in a centrosymmetric environment, leaving structural control in the third dimension as a goal for ongoing studies. We predict that 2-pyrimidinones synthesized from 1,3-diketone derivatives of optically active amino acids will not only retain the tape and layer synthons but also pack in chiral space groups. Crystal engineering of a polar crystal for NLO devices is elegantly addressed in the iodo-nitro diphenyl urea. Both the urea and the pyrimidinone systems are at the stage where further research will bear fruitful results.

A method for predicting crystal structures from just molecular formulae has eluded scientists for more than 50 years. The problem is currently being addressed by two very different approaches. But which one is more likely to succeed?

G. R. Desiraju<sup>51</sup>

Are crystal structures predictable? The one-word answer to the title question is still “No,” although at certain levels of discussion a “Maybe” or even a conditional “Yes,” may be entertained as possible responses.

J. D. Dunitz<sup>52</sup>

## ACKNOWLEDGMENTS

I thank my students and research collaborators whose names appear in the cited works. Financial support from the Indo-French Center for the Promotion of Advanced Research (1708-1) and the Department of Science and Technology (SR/S5/OC-02/2002) is acknowledged.

## REFERENCES

1. Nicolaou, K. C.; Sorensen, E. J. *Classics in Total Synthesis*. Wiley-VCH, Weinheim, **1996**.
2. Nicolaou, K. C.; Vourloumis, D.; Wissinger, N.; Baran, P. S. *Angew. Chem. Int. Ed.* **2000**, *39*, 44.
3. Corey, E. J.; Cheng, X.-M. *The Logic of Chemical Synthesis*, Wiley, New York, **1989**.
4. Ng, F. W.; Lin, H.; Chiu, P.; Danishefsky, S. J. *J. Am. Chem. Soc.* **2002**, *124*, 9812.
5. Nicolaou, K. C.; Baran, P. S. *Angew. Chem. Int.* **2002**, *41*, 2678.
6. Seebach, D. *Angew. Chem., Int. Ed. Engl.* **1990**, *29*, 1320.
7. Whitesides, G. M.; Simanek, E. E.; Mathias, J. P.; Seto, C. T.; Chin, D. N.; Mammen, M.; Gordon, D. M. *Acc. Chem. Res.* **1995**, *28*, 37.
8. Fyfe, M. C. T.; Stoddart, J. F. *Acc. Chem. Res.* **1997**, *30*, 393.
9. Lehn, J.-M. *Supramolecular Chemistry*, VCH, Weinheim, **1995**.
10. Desiraju, G. R. *Crystal Engineering: The Design of Organic Solids*. Elsevier, Amsterdam, 1989.
11. Braga, D.; Desiraju, G. R.; Miller, J. S.; Orpen, A. G.; Price, S. L. *CrystEngComm* **2002**, *4*, 500.
12. Hollingsworth, M. D. *Science* **2002**, *295*, 2410.
13. Braga, D. *Chem. Commun.* **2003**, 2751.
14. Desiraju, G. R. *Angew. Chem., Int. Ed. Engl.* **1995**, *34*, 2311.
15. Nangia, A.; Desiraju, G. R. *Top. Curr. Chem.* **1998**, *198*, 57.
16. Allen, F. H. *Acta Cryst.* **2002**, *B58*, 380.
17. Nangia, A. *CrystEngComm* **2002**, *4*, 93.
18. Nangia, A. In *Encyclopedia of Supramolecular Chemistry*, Atwood, J. L.; Steed, J. W., eds. Dekker, New York, **2004**, p. 967.
19. Steed, J. W.; Atwood, J. L. *Supramolecular Chemistry*. Wiley, Chichester, **2000**.
20. Jeffery, G. A. *An Introduction to Hydrogen Bonding*. Oxford University Press, New York, **1997**.
21. Desiraju, G. R.; Steiner, T. *The Weak Hydrogen Bond in Structural Chemistry and Biology*. Oxford University Press, Oxford, **1999**.
22. Steiner, T. *Angew. Chem., Int. Ed.* **2002**, *41*, 48.
23. Desiraju, G. R. *Acc. Chem. Res.* **2002**, *35*, 565.
24. (a) Zhao, X.; Chang, Y.-L.; Fowler, F. W.; Lauher, J. W. *J. Am. Chem. Soc.* **1990**, *112*, 6627.  
(b) Fowler, F. W.; Lauher, J. W. *J. Phys. Org. Chem.* **2000**, *13*, 850.
25. (a) Hollingsworth, M. D.; Santarsiero, B. D.; Oumar-Mahamat, H.; Nicholas, C. J. *Chem. Mater.* **1991**, *3*, 23. (b) Hollingsworth, M. D.; Brown, M. E.; Santarsiero, B. D.; Huffman, J. C.; Goss, C. C. *Chem. Mater.* **1994**, *6*, 1227.
26. Rebek, J. Jr. *Chem Commun.* **2000**, 637.
27. Shimizu, L. S.; Hughes, A. D.; Smith, M. K.; Davis, M. J.; Zhang, B. P.; Hans-Conrad L. Z.; Shimizu, K. D. *J. Am. Chem. Soc.* **2003**, *125*, 14972.

28. Choi, H.-J.; Park, Y. S.; Cho, C. S.; Koh, K.; Kim, S.-H.; Paek, K. *Org. Lett.* **2004**, *5*, 4431.
29. (a) Nangia, A.; Chandrakala, P. S. *Tetrahedron Lett.* **1995**, *36*, 7771. (b) Chandrakala, P. S.; Katz, A. K.; Carrell, H. L.; Sailaja, P. R.; Podile, A. R.; Nangia, A.; Desiraju, G. R. *J. Chem. Soc., Perkin Trans.* **1998**, *1*, 2597.
30. Anthony, A.; Jáskolski, M.; Nangia, A.; Desiraju, G. R. *Chem. Commun.* **1998**, 2537.
31. Anthony, A.; Jáskolski, M.; Nangia, A. *Acta Cryst.* **2000**, *B56*, 512.
32. Schmuck, C.; Lex, J. *Eur. J. Org. Chem.* **2001**, 1519.
33. Kumar, V. S. S.; Nangia, A. *Chem. Commun.* **2001**, 2392.
34. Davis, R. E.; Whitesell, J. K.; Wong, M.-S.; Chang, N.-L. In *The Crystal as a Supramolecular Entity, Perspectives in Supramolecular Chemistry*, Vol. 2, Desiraju, G. R., ed. Wiley, Chichester, **1995**, p. 63.
35. Muthuraman, M.; Fur, Y. L.; Bagieu-Beucher, M.; Masse, R.; Nicoud, J.-F.; George, S.; Nangia, A.; Desiraju, G. R. *J. Solid State Chem.* **2000**, *152*, 221.
36. Madhavi, N. N. L.; Katz, A. K.; Carrell, H. L.; Nangia, A.; Desiraju, G. R. *Chem Commun.* **1997**, 1953.
37. (a) Nishio, M.; Hirota, M.; Umezawa, Y. *The CH/π Interaction. Evidence, Nature and Consequences*. Wiley-VCH, New York, **1998**. (b) Nishio, M. *CrystEngCom* **2003**, *6*, 130.
38. Csorégh, I.; Weber, E.; Hens, T.; Czugler, M. *J. Chem. Soc., Perkin Trans.* **1996**, *2*, 2733.
39. Jetti, R. K. R.; Nangia, A.; Xue, F.; Mak, T. C. W. *Chem. Commun.* **2001**, 919.
40. (a) Krupitsky, H.; Stein, Z.; Goldberg, I. *J. Incl. Phenom. Mol. Recognit.* **1995**, *20*, 211. (b) Dastidar, P.; Goldberg, I. *Acta Cryst.* **1996**, *C52*, 1976.
41. Anwar, Okada, S.; Oikawa, H.; Nakanishi, H. *Chem. Mater.* **2000**, *12*, 1162.
42. Koshima, H.; Hamada, M.; Yagi, I.; Uosaki, K. *Cryst. Growth Des.* **2001**, *1*, 467.
43. Bourgogne, C.; Fur, Y. L.; Juen, P.; Masson, P.; Nicoud, J.-F.; Masse, R. *Chem. Mater.* **2000**, *12*, 1025.
44. Almeida, F. A.; Bond, A. D.; Khimyak, Y. Z.; Klinowski, J. *New J. Chem.* **2002**, *26*, 381.
45. Holman, K. T.; Privovar, A. M.; Swift, J. A.; Ward, M. D. *Acc. Chem. Res.* **2001**, *34*, 107.
46. George, S.; Nangia, A.; Muthuraman, M.; Bagieu-Beucher, M.; Masse, R.; Nicoud, J.-F. *New J. Chem.* **2001**, *25*, 1520.
47. (a) Aakeröy, C. B.; Evans, T. A.; Seddon, K. R.; Pálinkó, I. *New J. Chem.* **1999**, *23*, 145. (b) Thallapally, P. K.; Nangia, A. *CrystEngComm* **2001**, *27*, 114. (c) Brammer, L.; Bruton, E. A.; Sherwood, P. *Cryst. Growth Des.* **2001**, *1*, 277. (d) Balamurugan, V.; Hundal, M. S.; Mukerji, R. *Chem. Eur. J.* **2004**, *10*, 1683.
48. Fábián, L.; Kálmann, A. *Acta Cryst.* **1999**, *B55*, 1099.
49. In, Y.; Fujii, M.; Sasada, Y.; Ishida, T. *Acta Cryst.* **2001**, *B57*, 72.
50. Gordon-Wylie, S. W.; Clark, G. R. *Cryst. Growth Des.* **2003**, *3*, 453.
51. Desiraju, G. R. *Nat. Mat.* **2002**, *1*, 77.
52. Dunitz, J. D. *Chem. Commun.* **2003**, 545.
53. Zyss, J.; Nicoud, J.-F. *Curr. Opin. Solid State Mater. Sci.* **1996**, *1*, 533.
54. Wong, M. S.; Bosshard, C.; Günter, P. *Adv. Mater.* **1997**, *9*, 837.
55. Brock, C. P.; Dunitz, J. D. *Chem. Mater.* **1994**, *6*, 1118.
56. Whitesell, J. K.; Davis, R. E.; Saunders, L. L.; Wilson, R. J.; Feagins, J. P. *J. Am. Chem. Soc.* **1991**, *113*, 3267.
57. Hollingsworth, M. D. *Curr. Opin. Solid State Mater. Sci.* **1996**, *1*, 514.
58. Hulliger, J. *Chem. Eur. J.* **2002**, *8*, 4579.

59. Holman, K. T.; Pivovar, A. M.; Ward, M. D. *Science* **2001**, *294*, 1907.
60. MacDonald, J. C.; Dorresteijn, P. C.; Pilley, M. M. *Cryst. Growth Des.* **2001**, *1*, 29.
61. Evans, O. R.; Lin, W. *Acc. Chem. Res.* **2002**, *35*, 511.
62. Moulton, B.; Zaworotko, M. J. *Chem. Rev.* **2001**, *101*, 1629.
63. Schmuck, C. *Angew. Chem. Int. Ed.* **2003**, *42*, 2448.
64. Grosshans, P.; Jouaiti, A.; Bulach, V.; Planeix, J.-M.; Hosseini, M. W.; Nicoud, J.-F. *Chem. Commun.* **2003**, 1336.
65. George, S.; Nangia, A.; Bagieu Beucher, M.; Masse, R.; Nicoud, J.-F. *New J. Chem.* **2003**, *27*, 568.
66. Nangia, A. *New J. Chem.* **2000**, *24*, 1049.
67. Choudhury, A. R.; Guru Row, T. N. *Cryst. Growth Des.* **2004**, *4*, 47.
68. Kitaigorodsky, A. I. *Molecular Crystals and Molecules*. Academic Press, New York, **1973**.
69. Janiak, C. *J. Chem. Soc., Dalton Trans.* **2000**, 3885.
70. Jennings, W. B.; Farrell, B. M.; Malone, J. F. *Acc. Chem. Res.* **2001**, *34*, 885.
71. Chang, Y.-L.; West, M.-A.; Fowler, F. W.; Lauher, J. W. *J. Am. Chem. Soc.* **1993**, *115*, 5991.
72. (a) Sarma, J. A. R. P.; Allen, F. H.; Hoy, V. J.; Howard, J. A. K.; Thaimattam, R.; Biradha, K.; Desiraju, G. R. *Chem. Commun.* **1997**, *101*. (b) Masciocchi, N.; Bergamo, M.; Sironi, A. *Chem. Commun.* **1997**, *1347*. (c) Thaimattam, R.; Sharma, C. V. K.; Clearfield, A.; Desiraju, G. R. *Cryst. Growth Des.* **2001**, *1*, 103.
73. Huang, K. S.; Britton, D.; Etter, M. C.; Byrn, S. R. *J. Mater. Chem.* **1995**, *5*, 379.
74. Nicoud, J.-F.; Twieg, R. J. In *Nonlinear Optical Properties of Organic Molecules and Crystals*, Vol. 1, Chemla, D. S.; Zyss, J. eds. Academic Press, Orlando, **1987**, p. 221.
75. George, S.; Nangia, A.; Lam, C.-K.; Mak, T. C. W.; Nicoud, J.-F. *Chem. Commun.* **2004**, 1202.
76. Zyss, J.; Chemla, D. S.; Nicoud, J.-F. *J. Chem. Phys.* **1981**, *74*, 4800.
77. (a) Weiss, H.-C.; Boese, R.; Smith, H. L.; Haley, M. H. *Chem. Commun.* **1997**, 2403. (b) Robinson, J. M. A.; Kariuki, B. M.; Harris, K. D. M.; Philp, D. J. *J. Chem. Soc., Perkin Trans.* **1998**, *2*, 2459. (c) Langley, P. J.; Hulliger, J.; Thaimattam, R.; Desiraju, G. R. *New J. Chem.* **1998**, *1307*. (d) Robinson, J. M. A.; Kariuki, B. M.; Harris, K. D. M. *Chem. Commun.* **1999**, 329.
78. (a) Lommerse, J. P. M.; Stone, A. J.; Taylor, R.; Allen, F. H. *J. Am. Chem. Soc.* **1996**, *118*, 3108. (b) Allen, F. H.; Lommerse, J. P. M.; Hoy, V. J.; Howard, J. A. K.; Desiraju, G. R. *Acta Cryst.* **1997**, *B53*, 1006.
79. Ohkita, M.; Suzuki, T.; Nakatani, K.; Tsuji, T. *Chem. Commun.* **2001**, 1454.
80. Thallapally, P. K.; Desiraju, G. R.; Bagieu-Beucher, M.; Massé, R.; Bourgogne, C.; Nicoud, J.-F. *Chem. Commun.* **2002**, 1052.
81. Alcaraz, G.; Euzenat, L.; Mongin, O.; Katan, C.; Ledoux, I.; Zyss, J.; Blanchard-Desce, M.; Vaultier, M. *Chem. Commun.* **2003**, 2766.
82. Jacques, J.; Collet, A.; Wilen, S. H. *Enantiomers, Racemates and Resolution*. Wiley-Interscience, New York, **1981**.
83. Ishida, Y. In *Encyclopedia of Supramolecular Chemistry*, Atwood, J. L.; Steed, J. W. eds. Dekker, New York, **2004**, p. 1349.
84. Toda, F. *Cryst. Eng. Comm.* **2002**, *4*, 215.
85. Sakamoto, M.; Utsumi, N.; Ando, M.; Saeki, M.; Mino, T.; Fujita, T.; Katoh, A.; Nishio, T.; Kashima, C. *Angew. Chem. Int. Ed.* **2003**, *42*, 4360.
86. Tanaka, K.; Fujimoto, D.; Oeser, T.; Irngartinger, H.; Toda, F. *Chem. Commun.* **2000**, 413.

# **Chapter 6**

## **Chiral Auxiliaries Powerful for Both Enantiomer Resolution and Determination of Absolute Configuration by X-Ray Crystallography**

**NOBUYUKI HARADA**

*Institute of Multidisciplinary Research for Advanced Materials,  
Tohoku University, 2-1-1 Katahira, Aoba, Sendai 980-8577 Japan*

- I. Introduction
- II. Methods for Determining Absolute Configuration and Their Evaluation
- III. Methods for Chiral Synthesis and Their Evaluation
  - A. Resolution of Racemates
  - B. Asymmetric Syntheses
- IV. Chiral Auxiliary for HPLC Resolution and X-ray Crystallography: Application to Carboxylic Acids
- V. Design of Chiral Auxiliaries for Resolution of Alcohols by HPLC and X-ray Crystallographic Analysis
- VI. Camphorsultam Dichlorophthalic Acid (CSDP Acid) ( $-$ )-2 for Both HPLC Resolution of Alcohols and X-ray Crystallographic Analysis: Development and Applications
- VII. Conclusions
  - Acknowledgments
  - References

### **I. INTRODUCTION**

It is well recognized that the molecular chirality is essential to life processes, and most biologically active compounds controlling physiological functions of living organisms are chiral. Hence in the structural study of biologically active compounds, including natural products, determination of absolute configuration

becomes a major issue. Another issue is the enantioselective synthesis of natural products and biologically active compounds that become pharmaceutical targets and how efficiently desired enantiomers can be synthesized with high enantiopurity. Furthermore, studies on chiral functional molecules and molecular machines, such as the light-powered chiral molecular motor developed in our laboratory, have been progressing in recent years. Therefore the unambiguous determination of absolute configuration of chiral compounds as well as their enantioselective synthesis are of vital importance in the field of material science.

We have recently developed chiral carboxylic acids as novel chiral auxiliaries that are powerful molecular tools for resolution and unambiguous determination of absolute configuration of various alcohols. Those chiral acids are very useful for the facile synthesis of enantiomers with high enantiomeric purity and also for the absolute configurational assignment. The resolution of various compounds using these chiral acids has been successfully implemented as detailed throughout this chapter.

## II. METHODS FOR DETERMINING ABSOLUTE CONFIGURATION AND THEIR EVALUATION

The methods to determine the absolute configuration of chiral compounds are classified into the following two categories.

1. *Nonempirical methods for determining absolute configuration of chiral compounds.* The main methods of this category are the Bijvoet method, which depends on X-ray crystallography,<sup>1</sup> and the circular dichroism (CD) exciton chirality method.<sup>2</sup> These two powerful methods allow for nonempirical determination of the configuration of a target molecule but without information on the absolute configuration of the reference compounds. In X-ray crystallography, the anomalous dispersion effect of heavy atoms can be measured very accurately under proper conditions and the absolute stereostructure obtained is clear and unambiguous. In addition, the molecule can be projected as a three-dimensional structure, and therefore the method has been employed extensively. However, the X-ray method needs single crystals of suitable size for good X-ray diffraction, and so the critical problem is how to obtain such single crystals. As a consequence a study using this method often becomes a lengthy trial and error search for ideal single crystals.

The CD exciton chirality method<sup>2</sup> is also useful because the absolute configuration can be determined in a nonempirical manner, and it does not require crystallization. Furthermore chiral chemical and biological reactions are traceable by CD, and even the absolute configurations and conformations of unstable compounds can be obtained by this method. However, because

some compounds are not ideal targets for this method, the results must be interpreted carefully.

2. *Relative methods for determining the absolute configuration using an internal reference with a known absolute configuration.* Absolute configuration can be obtained by determining the relative configuration at the position of interest against a reference compound or substituent with a known absolute configuration. A typical example is the X-ray crystallography taken after the introduction of a chiral auxiliary with a known absolute configuration.<sup>3–6</sup> In this case the absolute configuration of the point in question can be automatically determined by the configuration of the auxiliary introduced as an internal reference. Consequently, the samples do not need to contain heavy atoms for the anomalous dispersion effect. The result obtained is very clear, even when the final *R*-value is not small due to poor quality of the single crystal. The absolute configuration can be determined with certainty when only the relative configuration is obtained. A variety of methods have been developed to link the internal reference to the target molecule. Some examples are ionic bonding such as conventional acid-base salts, covalent bonding such as esters or amides, and the use of recently developed inclusion complexes.<sup>7–9</sup> These relative X-ray diffraction methods find widespread application.

Proton nuclear magnetic resonance (<sup>1</sup>H NMR) anisotropy is today the method most often employed for the study of the absolute configuration of natural products. In particular, the absolute configurations of secondary alcohols are frequently determined by an advanced Mosher method developed by Kusumi et al.<sup>10–13</sup> In this case the absolute configurations of chiral auxiliaries, such as Mosher's reagent [ $\alpha$ -methoxy- $\alpha$ -(trifluoromethyl) phenylacetic acid (MTPA)] and Trost's reagent [ $\alpha$ -methoxyphenylacetic acid (MPA)], are known, and the preferred conformation of the esters formed with chiral secondary alcohols and MTPA or MPA acid is rationalized. In addition the aromatic substituent (phenyl group) generates a magnetic anisotropy effect due to the ring current induced under the external magnetic field, and so the proton NMR signals of the alcohol moiety facing to the phenyl group in the preferred conformation are moved to a higher magnetic field (high field shift). By observing the <sup>1</sup>H NMR anisotropy effect, one can determine the absolute configuration of the alcohol part. This method is particularly convenient because it does not require crystallization of compounds and NMR spectrometers are ubiquitous. One problem with this method is that it is based on the assumption of preferred conformation of molecules in solution. Nevertheless, the method is highly reliable because it has a self-diagnostic function. Further, besides its wide application to secondary alcohols, the <sup>1</sup>H NMR method can be extended to other kinds of compounds.

Absolute configuration can also be determined relatively by chemical correlation or comparison of optical rotation,  $[\alpha]_D$ , and/or the CD spectrum with that of reference compounds with the known absolute configuration. Although this method is frequently employed, a careful selection of reference compounds is necessary for reliable analysis.

### III. METHODS FOR CHIRAL SYNTHESIS AND THEIR EVALUATION

After determination of the absolute configuration, the synthesis of the chiral compound is commonly pursued. The methods used to synthesize chiral compounds can be roughly divided into two categories, each of which can be further divided and has advantages and disadvantages as described below. In this chapter the term "enantioselective synthesis" is used in a broad sense to include not only so-called asymmetric synthesis but also resolution. In addition the method by which covalently bonded diastereomers are formed via a chiral auxiliary, followed by HPLC separation and recovery of the target compound, is also treated more broadly as resolution.

#### A. Resolution of Racemates

- Type 1. By this method a chiral auxiliary is ionically bonded to racemates, and the mixture of diastereomers formed is subjected to fractional recrystallization to obtain enantiopure compounds. This method is also applicable to inclusion complexes such as those formed by hydrogen bonding.<sup>7-9</sup> The critical point is whether or not one diastereomer can be obtained with diastereomeric purity through fractional recrystallization. It should be noted that recrystallization does not always afford a pure diastereomer. This method is most suitable for mass preparation of the chiral compounds.
- Type 2. By this method a chiral auxiliary is covalently bonded to racemates to produce a diastereomeric mixture, which is separated by conventional HPLC on silica gel or other methods to obtain pure diastereomers, and then the chiral auxiliary is cleaved off (Figure 6.1). The critical point of this method is whether or not the diastereomers can be clearly separated by HPLC. If a clean separation is achieved, the target compound, after cleavage of the chiral auxiliary, will be enantiopure. It is advisable to use a chiral auxiliary that can be cleaved off easily.
- Type 3. By this method, racemates are directly separated by HPLC or GC using columns made of chiral stationary phases. A number of

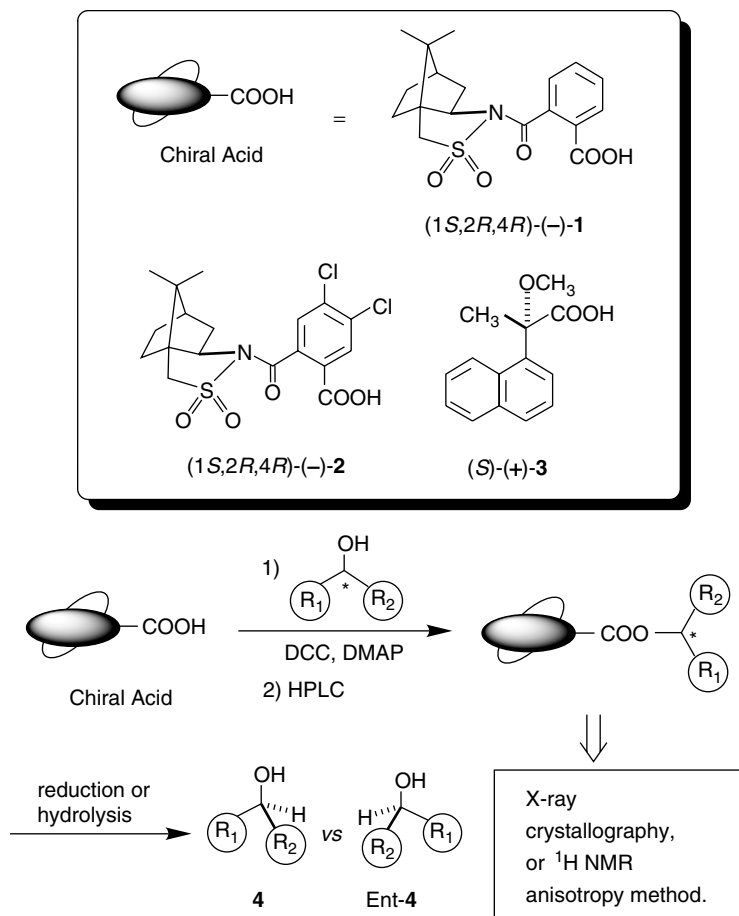


Figure 6.1. Resolution and determination of absolute configuration of alcohols using chiral carboxylic acids.

reports have been published with excellent results.<sup>14</sup> The question is nevertheless whether or not racemates are cleanly separated into enantiomers. If a clean separation is achieved, pure enantiomers can be obtained by this method. The method is also convenient and suitable for analytical separation because it does not require derivatization. However, since chiral stationary phase columns are expensive, they are mostly used for analytical purposes. In some applications such as for pharmaceutical materials, separation is conducted on a large scale to obtain the chiral compound. Careful analysis is required

when determining absolute configuration by the elution order, as there are many exceptions.

- Type 4. By this method racemates undergo an enzymatic or asymmetric reaction to yield enantiomers by kinetic resolution. High stereoselectivity of the enzymatic reaction leads to high enantiopurity.<sup>15</sup> However, care should be taken because enantiopurity is related to substrate conversion.

## B. Asymmetric Syntheses

Type 1. By this method, enantiomerically enriched products are obtained by the action of a chiral reagent or chiral catalyst on achiral compounds. This is a highly efficient and powerful method and is well known, from the many eminent reviews published on asymmetric syntheses, so no further explanation is required here. The problem with this method is that the products obtained are not always enantiopure. Furthermore it is generally difficult to determine the absolute configuration of the products based on the reaction mechanism. Accordingly an independent determination of the absolute configuration by the methods described above is suggested.

Type 2. By this method, enantiomerically enriched compounds are obtained, such as by enzymatic reaction on achiral or meso compounds. The asymmetric reaction of a meso compound by an enzyme is a particularly interesting case and is referred to as desymmetrization. Likewise in this case the enantiopurity is not always 100%, and the absolute configuration must be determined separately.

## IV. CHIRAL AUXILIARY FOR HPLC RESOLUTION AND X-RAY CRYSTALLOGRAPHY: APPLICATIONS TO CARBOXYLIC ACIDS

As illustrated in Figure 6.1, resolution of type A2 is considered to be a highly efficient method to prepare appropriate amounts of various chiral compounds on a laboratory scale with high enantiopurity. In the type A2 method, a chiral auxiliary is covalently bonded to a racemic mixture and the obtained diastereomeric mixture is separated by conventional HPLC on silica gel. By this method an efficient separation is possible even with a small amount of sample, compared to the fractional recrystallization method described in type A1.

Diastereomers of nitrogen-containing compounds such as hydrazones<sup>16</sup> and amide derivatives<sup>17</sup> can be separated well by HPLC on silica gel. In particular, HPLC on silica gel is very effective for the separation of diastereomers of amides that are formed with chiral amines and racemic carboxylic acids. However, recovery of carboxylic acids is a problem, because amides are not easily hydrolyzed. Some extra reactions such as nitrosation prior to hydrolysis are needed.<sup>17</sup>

(1*S*,2*R*,4*R*)(*-*)-2,10-Camphorsultam (**5**), which has been successfully employed as a chiral auxiliary in asymmetric syntheses, is very useful for resolution of various carboxylic acids. The obtained diastereomeric mixture of camphorsultam amides is separated by HPLC on silica gel. In addition, the camphorsultam amides of the separated diastereomers can be readily cleaved by LiAlH<sub>4</sub> reduction to yield a primary alcohol, and then subsequently converted to enantiopure carboxylic acids by oxidation.

Amides made with 2,10-camphorsultam (**5**) generally have excellent crystallinity and are obtained as large single crystals needed for X-ray crystallography.<sup>3-6</sup> By this resolution method, two kinds of diastereomers are obtained simultaneously, doubling the possibility of obtaining single crystals. If the X-ray crystallographic analysis of one diastereomer is successful, the absolute configuration of the other is automatically determined.

The absolute configuration of the chiral auxiliary, (1*S*,2*R*,4*R*)(*-*)-2,10-camphorsultam (**5**), is known, because it is synthesized from naturally occurring (1*R*,4*R*)(*+*)-camphor.<sup>18</sup> Consequently the auxiliary configuration can be used as an internal reference for the determination of the absolute configuration by X-ray crystallography, leading to the absolute configuration of a carboxylic acid moiety. Moreover 2,10-camphorsultam (**5**) contains a sulfur as the heavy atom, making it possible to determine the absolute configuration by the Bijvoet method also.

A typical example is illustrated in Figure 6.2.<sup>3</sup> (1*S*,2*R*,4*R*)(*-*)-2,10-Camphorsultam (**5**) was treated with NaH to make an anion, which was then allowed to react with the acid chloride of ( $\pm$ )-2,6-bis(benzyloxymethyl)spiro[3.3]heptane-2,6-dicarboxylic acid (**6**). The resulting diastereomeric amides **7a** and **7b** showed good separation and appeared as two spots ( $\Delta R_f = 0.12$ ) even on a 5 cm TLC plate of silica gel. Nearly 100 mg was separated by a single HPLC run on silica gel (22Φ × 300 mm: benzene/ethyl acetate (EtOAc) = 20:1):  $R_s = 2.9$ .

The first eluted fraction (*-*)-**7a** gave prismatic crystals by recrystallization from EtOAc; a single crystal was subjected to X-ray crystallography. The absolute configuration was unambiguously determined as *S* using the camphor moiety as an internal reference. In addition, the absolute configuration determined by the anomalous dispersion effect of the heavy atom was consistent with that by the internal reference method. After reduction of amide (*S*)-(*-*)-**7a** with LiAlH<sub>4</sub> to

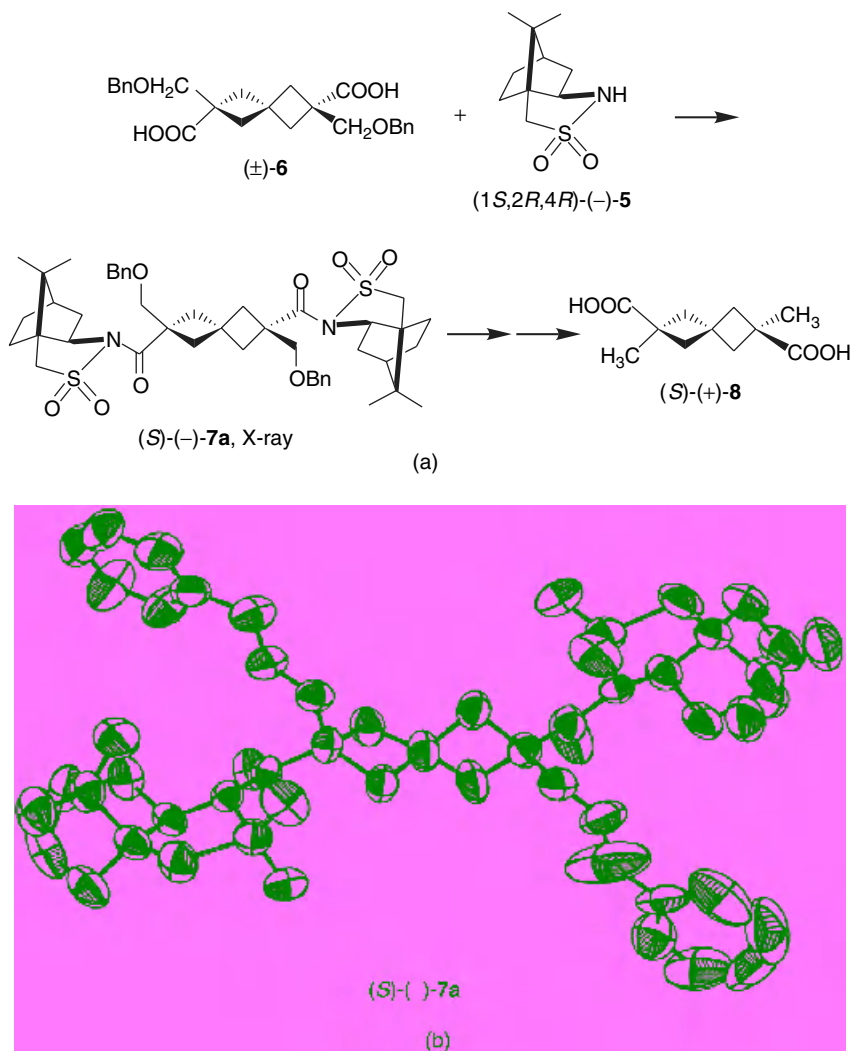
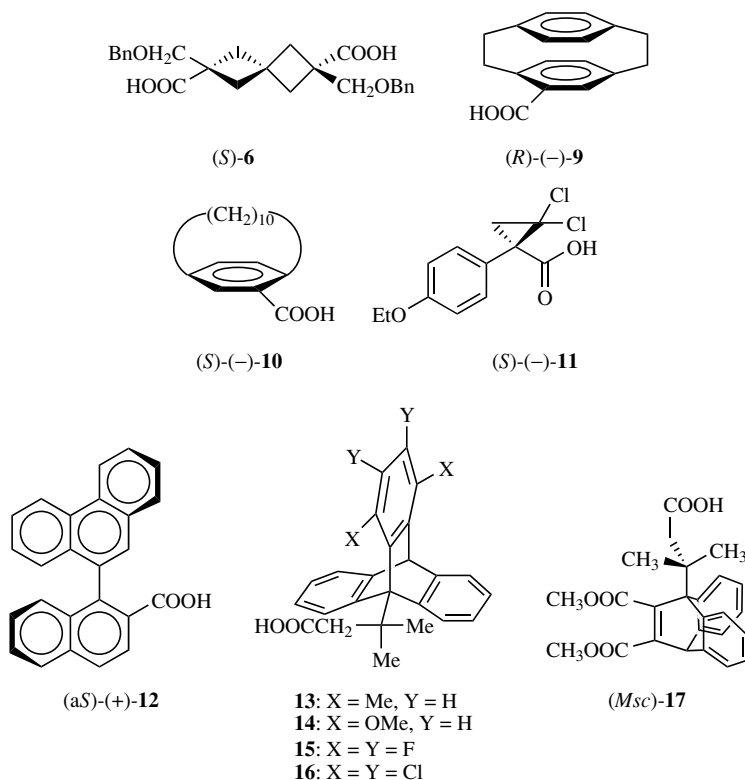


*Figure 6.2.* (a) Resolution of carboxylic acid **6**, determination of its absolute configuration by X-ray crystallography, and synthesis of the enantiopure Fecht acid analogue *(S)*-*(+)*-**8**. (b) ORTEP drawing of amide *(S)*-*(-)*-**7a**.

cleave the chiral auxiliary, it was converted to *(S)*-*(+)*-2,6-dimethylspiro[3.3]heptane-2,6-dicarboxylic acid (**8**) via several reactions. This way we have synthesized nonracemizing and enantiopure Fecht acid analogue **8** and determined its absolute configuration.<sup>3</sup>



Other examples are shown in Table 6.1. The auxiliary configuration method is thus applicable to the resolution of carboxylic acids in various structures, their absolute configurations can be determined by X-ray analysis because of their excellent crystallinity. The absolute configurational studies of individual compounds listed in Table 6.1 reveal some interesting facts. For example, the absolute configuration of [8]paracyclophane-10-carboxylic acid had been previously determined as  $(S)(+)$  by chemical correlation to an authentic compound with known absolute configuration. Nevertheless, this configuration was proved wrong<sup>4</sup> so the absolute configuration of compound **10** should be revised.

Compounds **13–17** are interesting examples of atropisomeric and optically active substances studied by Toyota et al. In general, it is very difficult to determine the absolute configuration of chiral compounds of atropisomerism. However, Toyota et al. successfully solved this problem by application of the 2,10-camphorsultam method described above.<sup>20–22</sup>

Table 6.1  
Resolution of Carboxylic Acids by Separation of (1*S*,2*R*,4*R*)(*-*)-2,10-Camphorsultam Amides Using HPLC on Silica Gel, and Determination of Their Absolute Configurations by X-ray Crystallography

Entry	Solvent <sup>a</sup>	$\alpha$	$R_s$	X-ray	Absolute Configuration of First Fraction	Reference
<b>6</b>	Bz/EA = 20/1	—	2.87	○ (1st, Fr.)	<i>S</i>	3
<b>9</b>	H/EA = 5/1	—	1.60	○ (1st, Fr.) ○ (2nd Fr.)	<i>R</i>	3,4
<b>10</b>	H/EA = 5/1	—	0.70	○ (1st, Fr.)	<i>S</i>	4
<b>11</b>	H/EA = 5/1	1.20	2.87	○ (1st, Fr.)	<i>S</i>	19
<b>12</b>	H/EA = 4/1	—	—	○ (2nd, Fr.)	a <i>S</i>	5
<b>13</b>	H/ET = 2/1	—	—	○ (1st, Fr.)	<i>Psc</i>	20, 22
<b>14</b>	— (recry.)	—	—	○	—	20, 22
<b>15</b>	— (recry.)	—	—	○	—	20, 22
<b>16</b>	CH <sub>2</sub> Cl <sub>2</sub>	—	—	○ (1st, Fr.)	<i>Psc</i>	20, 22
<b>17</b>	H/ET = 1/2	—	—	○ (1st, Fr.)	<i>Msc</i>	21

<sup>a</sup>Bz = benzene, EA = ethyl acetate, H = *n*-hexane, ET = diethyl ether.

## V. DESIGN OF CHIRAL AUXILIARIES FOR RESOLUTION OF ALCOHOLS BY HPLC AND X-RAY CRYSTALLOGRAPHIC ANALYSIS

The chiral auxiliary 2,10-camphorsultam (**5**) described above was useful for the resolution and determination of absolute configuration of carboxylic acids. However, the demand for the syntheses of chiral alcohols and determination of their absolute configurations is greater than that of carboxylic acids. What kind of auxiliary is applicable to alcohols, which also retains the above-mentioned characteristics of chiral auxiliaries?

This problem was approached by introducing linkers in our molecular design that connect the 2,10-camphorsultam and the alcohol (Figure 6.3).<sup>23</sup> We selected an amide bond for 2,10-camphorsultam and an ester bond for alcohols to bond with the linker. The amide bond was retained because of its good affinity with silica gel whereas the ester bond was employed for alcohols because it can be readily formed and cleaved. We therefore began with phthalic acid as a linker molecule.<sup>23</sup> Whereas in terephthalic acid and succinic acid the two chiral moieties are separated spatially, in phthalic acid they are close enough and are expected to result in a stronger interaction (Figure 6.3).

The desired chiral phthalic acid (camphorsultam phthalic acid: CSP acid) (*-*)-**1** was synthesized by reacting (1*S*,2*R*,4*R*)(*-*)-2,10-camphorsultam (**5**) anion with

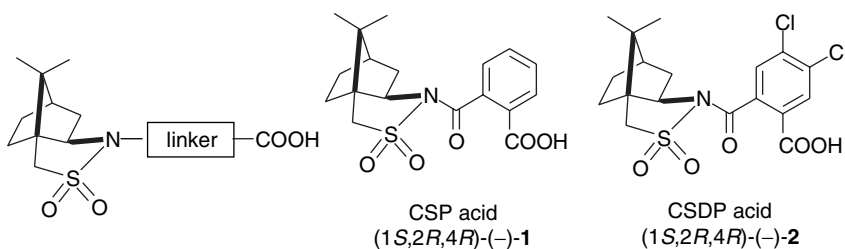


Figure 6.3. Design of chiral carboxylic acids containing 2,10-camphorsultam moiety.

phthalic anhydride: mp 184–187 °C from CHCl<sub>3</sub>;  $[\alpha]_D^{20} -134.7$  (*c* 2.218, MeOH). The compound **1** should be formally called phthalic acid amide. However, here we adopted its common name, CSP acid. This carboxylic acid was condensed with alcohol under the conditions of DCC and DMAP.<sup>23</sup>

The following exemplifies this method: The CSP acid (−)**1** was allowed to react with (±)-α-methyl-(4-bromobenzyl)methanol (**18**) (Table 6.2), followed by separation of the obtained diastereomeric mixture by HPLC on silica gel: hexane/EtOAc = 3:1;  $\alpha = 1.1$ ,  $R_s = 1.3$ . In general, two chemical components are fully separable if the separation factor  $\alpha$  is 1.1 or more. Ester **19b** obtained as

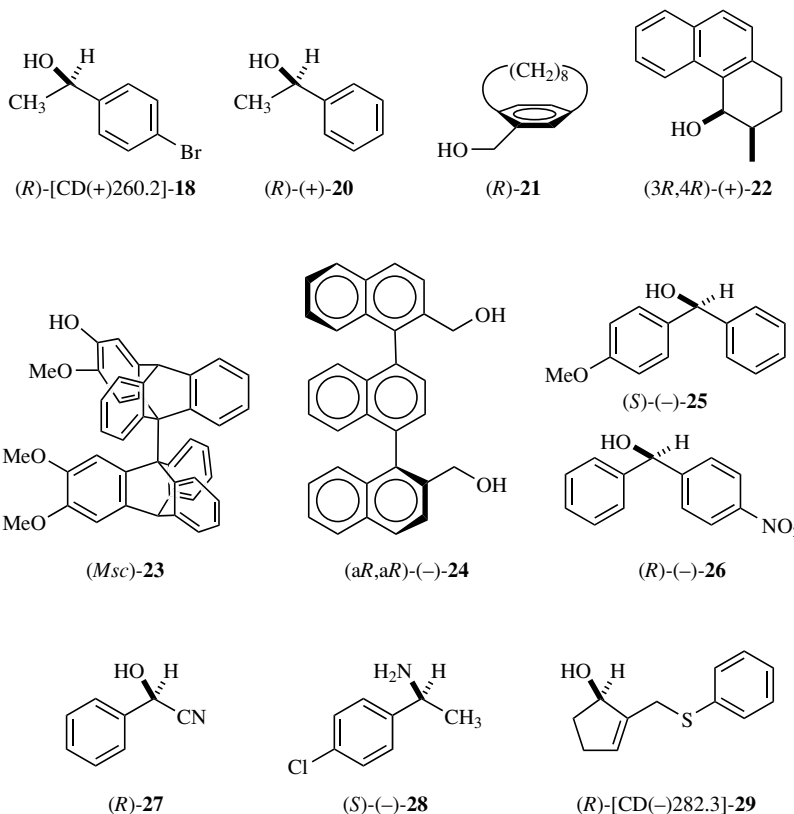
Table 6.2  
Resolution of Alcohols by HPLC on Silica Gel Using (1S,2R,4R)(−)-CSP Acid, and  
Determination of Their Absolute Configurations by X-ray Crystallography

Entry	Solvent <sup>a</sup>	$\alpha$	$R_s$	X-ray	Absolute Configuration of First Fraction	Reference
<b>18</b>	H/EA=3/1	1.1	1.3	○ (2nd, Fr.)	<i>R</i>	23
<b>20</b>	H/EA=5/1	1.1	1.3	○ (1st, Fr.)	<i>R</i>	23
<b>21</b>	H/EA=4/1	—	0.73	—	<i>R</i>	4
<b>22</b>	H/EA=7/1	1.1	0.8	—	3 <i>R</i> ,4 <i>R</i>	24, 25
<b>23</b>	CH <sub>2</sub> Cl <sub>2</sub> /EA=50/1	—	—	○ (1st, Fr.)	<i>Msc</i>	26
<b>24</b>	H/EA=2/1	1.2	1.3	—	<i>aR,aR</i>	27, 28
<b>25</b>	H/EA=4/1	1.1	1.3	○ (1st, Fr.)	<i>S</i>	29
<b>26</b>	H/EA=5/1	1.1	1.6	○ (1st, Fr.)	<i>R</i>	29
<b>27</b>	H/EA=3/1	1.3	2.8	○ (1st, Fr.)	<i>R</i>	19
<b>28</b>	H/EA=2/1	1.1	1.0	○ (1st, Fr.)	<i>S</i>	19
<b>29</b>	H/EA=3/1	1.1	1.6	○ (2nd, Fr.)	<i>R</i>	23

<sup>a</sup>H = *n*-hexane, EA = ethyl acetate.

the second eluted fraction had a good crystallinity, which led to single crystals suitable for X-ray crystallographic analysis by recrystallization from MeOH. From the ORTEP drawing the absolute configuration of the alcohol unit was unambiguously determined to be *S*, by using the 2,10-camphorsultam moiety as the internal reference and also by the heavy atom effect. Enantiopure alcohol (*S*)-(-)-**18** was recovered from ester **19b**.<sup>23</sup>

Other examples are shown in Table 6.2. The successful resolution of various alcohols, determination of their absolute configurations by X-ray analysis, and recovery of enantiopure alcohols listed in the table proved the effectiveness of this method. In cyanohydrin **27** and amine **28**, the diastereomeric separation and determination of absolute configurations are possible; nevertheless, recovery of enantiopure compounds **27** and **28** remains a problem because the amides are not easily hydrolyzed. Amine **28** can be resolved as the salt of (2*R*,3*R*)-(+) -tartaric



acid,<sup>19</sup> and its absolute configuration was established as (*S*)-(*-*) by this method. For compound **29**, the absolute configuration was unambiguously determined by this internal reference method, despite the large *R*-value owing to its poor crystallinity.

Esters of CSP acid (*-*)-**1** generally have low solubility, possibly due because of high crystallinity, resulting in longer elution time by HPLC on silica gel. In addition, crystals were often obtained in the form of fine needles and these were unsuitable for X-ray crystallography. Since these results indicate that the use of CSP acid esters with low solubility can be counterproductive, a variety of compounds were investigated with the expectation of higher solubility.

## VI. CAMPHORSULTAM DICHLOROPHTHALIC ACID (CSDP ACID) (*-*)-**2** FOR BOTH HPLC RESOLUTION OF ALCOHOLS AND X-RAY CRYSTALLOGRAPHIC ANALYSIS: DEVELOPMENT AND APPLICATIONS

Camphorsultam dichlorophthalic acid (CSDP acid) (*-*)-**2** [mp 221°C from EtOH;  $[\alpha]_D^{20}$ -101.1 (c. 1.375, MeOH); Figure 6.3], with 4,5-dichlorophthalic acid as a linker, was found to be effective for solving the problem discussed above. Namely it has higher solubility and has a shorter elution time on HPLC. In addition, it tends to provide prismatic crystals suitable for X-ray crystallographic analysis. For instance, for ( $\pm$ )-*cis*-1,2,3,4-tetrahydro-3-methyl-4-phenanthrenol (**22**) shown in Table 6.2 and Figure 6.4, the elution times of two diastereomers using CSP acid were 27.6 and 31.0 min, respectively, whereas the times using CSDP acid under the same conditions were 14.6 and 16.7 min, respectively, almost half the time required for CSP acid. Furthermore, the separation and resolution factors were also improved.<sup>24</sup>

The chiral auxiliary, dichlorophthalic acid (*-*)-**2**, is very useful as an internal reference in determining absolute configuration by X-ray analysis, as in the case of phthalic acid (*-*)-**1**. Moreover carboxylic acid **2** contains two chlorines as the heavy atoms in addition to a sulfur atom, which leads to efficient determination of absolute configuration by the anomalous dispersion effect.

For example, alcohol ( $\pm$ )-**22** was condensed with chiral dichlorophthalic acid (*-*)-**2** in the presence of DCC and DMAP (Figure 6.4). The diastereomeric mixture of two esters obtained was subjected to HPLC on silica gel: hexane/EtOAc = 7:1,  $\alpha$  = 1.18,  $R_s$  = 1.06. Whereas ester **30a**, obtained as the first eluted fraction, afforded fine needle like crystals which were unsuitable for X-ray analysis when recrystallized from MeOH, the second eluted fraction

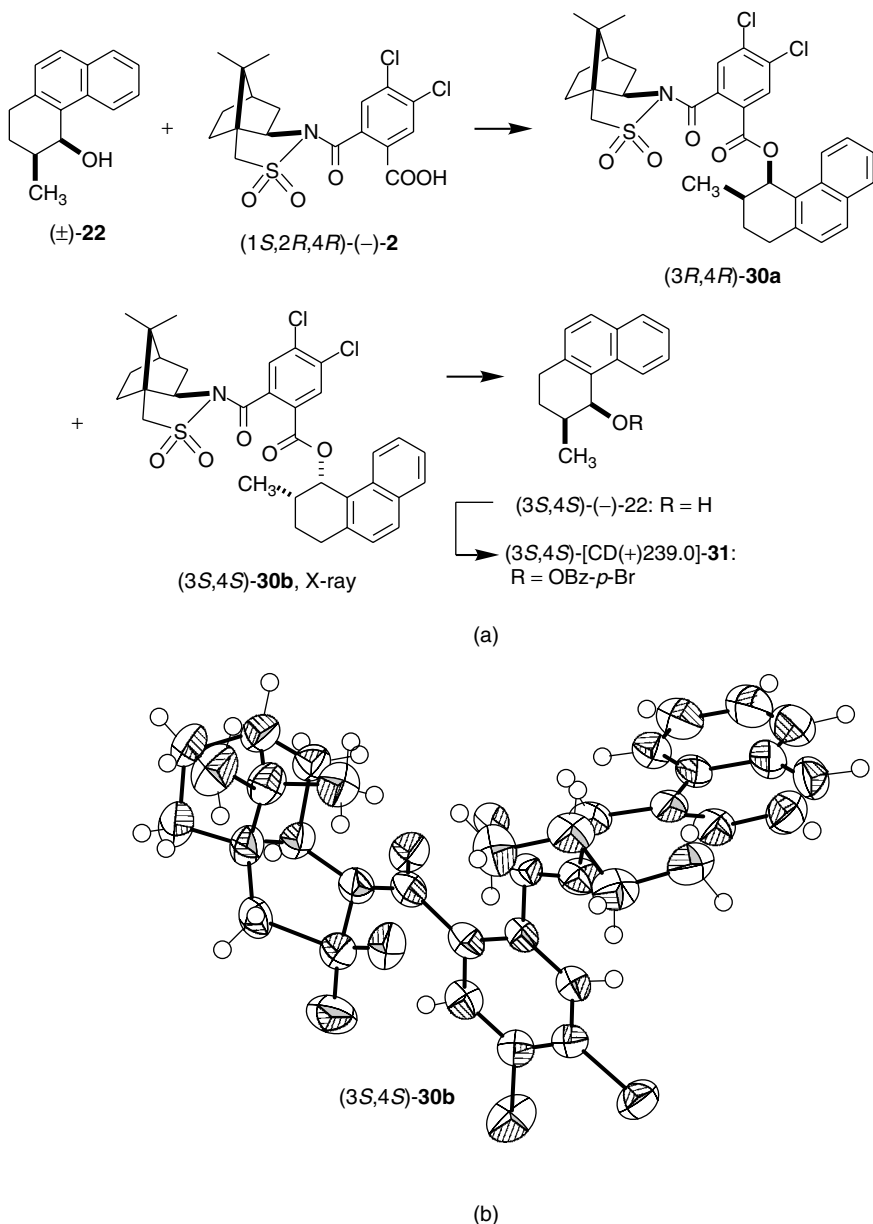


Figure 6.4. (a) Resolution of alcohol **(±)-22** using chiral dichlorophthalic acid **(-)-2** and determination of its absolute configuration by X-ray crystallography. (b) ORTEP drawing of ester **(3S,4S)-30b**.

**30b** gave larger prisms, suitable for X-ray analysis when recrystallized from EtOAc. The absolute configuration of **30b** was unambiguously determined to be (3*S*,4*S*) using the 2,10-camphorsultam part as an internal reference and also by the heavy atom effect. Ester **30b** was reduced with LiAlH<sub>4</sub> to remove the chiral auxiliary, yielding enantiopure alcohol (3*S*,4*S*)-(−)-**22**.<sup>24,25</sup> This absolute configuration was consistent with the result obtained by the CD exciton chirality method applied to the corresponding 4-bromobenzoate (**31**).<sup>24</sup> Recently it was found that the solvolysis with K<sub>2</sub>CO<sub>3</sub>/MeOH was very effective in the recovery of enantiopure alcohols from chiral dichlorophthalic acid esters in high yield.

Table 6.3 lists many other examples. Chiral dichlorophthalic acid esters of *para*-substituted diphenylmethanols **25**, **26**, and **34–38** were cleanly separated by HPLC on silica gel, although the *para*-substituents governing the chirality of molecule are apart from the stereogenic center, namely the carbon atom with the hydroxyl group.<sup>29,30,32</sup> These results indicate that the chiral dichlorophthalic acid recognizes the molecular chirality.

The chirality recognition of (4-methylphenyl)phenylmethanol (**36**) as a dichlorophthalic acid ester was impossible; in alcohol **36**, the difference between hydrogen and methyl group constitutes the molecular chirality, and it is generally difficult to recognize such a small difference. Therefore the diastereomeric separation by HPLC on silica gel failed.<sup>29</sup> Then the following strategy was adopted; first, (4-bromophenyl)(4'-methylphenyl)methanol (**37**) was selected as the precursor, which was resolved as the chiral dichlorophthalates, and their absolute configurations were determined by X-ray crystallography. The removal of the bromine atom led to the desired and enantiopure alcohol (*S*)-(−)-**36**.<sup>29</sup> This strategy was also useful for the synthesis and determination of absolute configuration of isotopically-substituted chiral diphenylmethanols as described below.

The molecular chirality is also generated by substitution with isotopes as shown in <sup>2</sup>H-substituted diphenylmethanol **39** and <sup>13</sup>C-substituted diphenyl methanol **43**.<sup>32,33</sup> It is almost impossible to directly resolve these isotopically substituted chiral compounds by HPLC with a chiral stationary phase or by HPLC on silica gel using a chiral auxiliary. In such a case a precursor such as (±)-(4-bromophenyl)(phenyl-2,3,4,5,6-*d*<sub>5</sub>)methanol (**40**) should be selected, and then resolution as a chiral dichlorophthalate and determination of absolute configuration can be carried out. Subsequently, the bromine atom is removed to yield the desired and enantiopure (phenyl-2,3,4,5,6-*d*<sub>5</sub>)phenylmethanol (**39**).<sup>32</sup>

The preparation of (phenyl-2,3,4,5,6-*d*<sub>5</sub>)phenylmethanol (**39**) was carried out as follows: racemic alcohol (±)-**40** was condensed with chiral dichlorophthalic acid, and then the formed esters were separated by HPLC on silica gel. Both

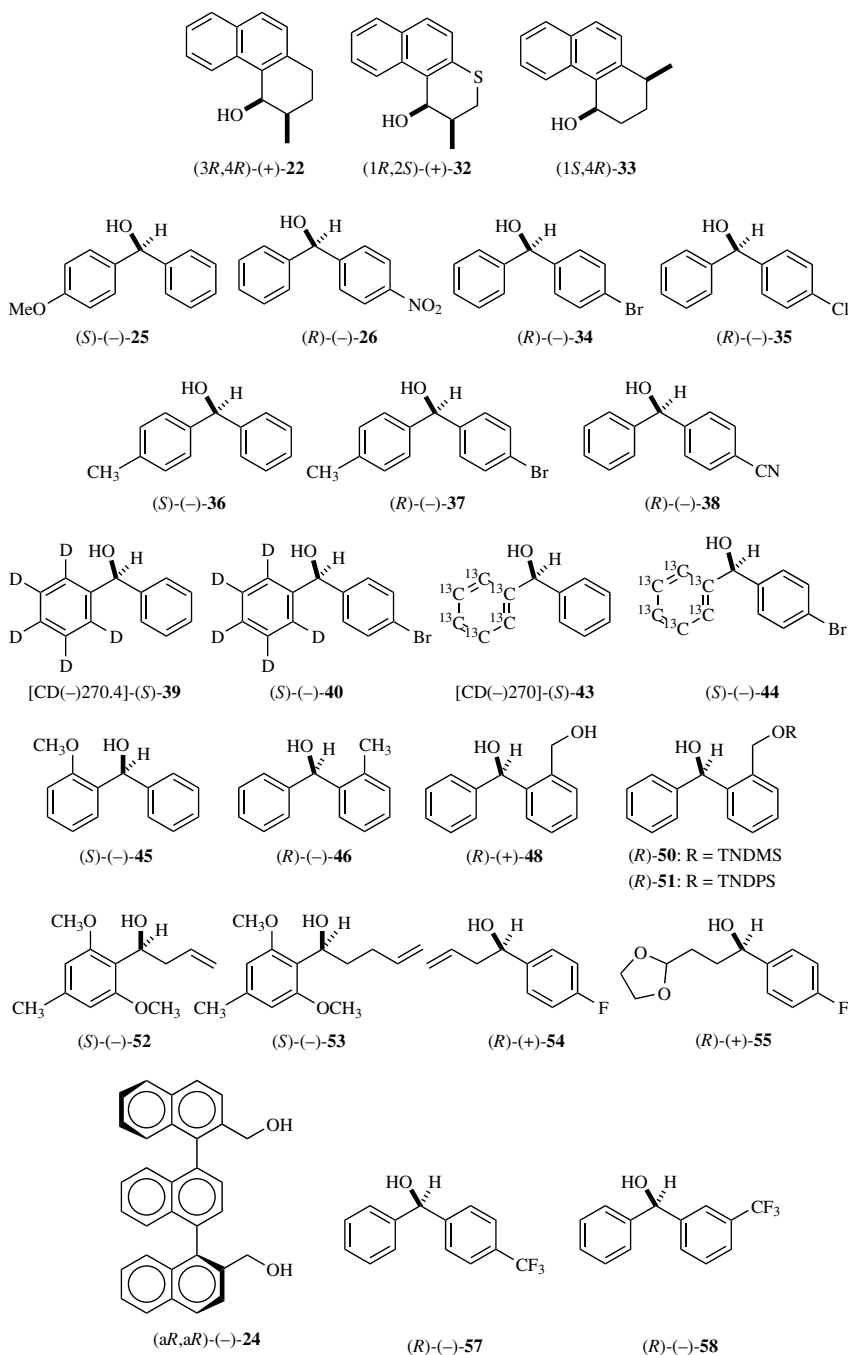
Table 6.3  
Resolution of Alcohols by HPLC on Silica Gel Using (1*S*,2*R*,4*R*)-(−)-CSDP Acid, and  
Determination of Their Absolute Configurations by X-ray Crystallography

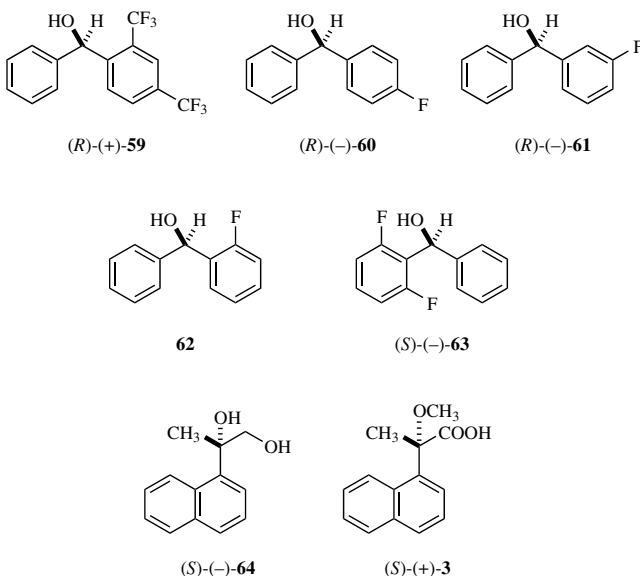
Entry	Solvent <sup>a</sup>	$\alpha$	$R_s$	X-ray	Absolute Configuration of First Fraction	Reference
22	H/EA=7/1	1.18	1.06	○ (2nd, Fr.)	3 <i>R</i> ,4 <i>R</i>	24, 25
32	H/EA=7/1	1.23	1.27	○ (1st, Fr.) ○ (2nd, Fr.)	1 <i>R</i> ,2 <i>S</i>	31
33	H/EA=10/1	1.30	1.74	○ (1st, Fr.)	1 <i>S</i> ,4 <i>R</i>	24
25	H/EA=4/1	1.20	0.91	—	<i>S</i>	29
26	H/EA=5/1	1.26	1.37	—	<i>R</i>	29
34	H/EA=8/1	1.17	0.80	○ <sup>b</sup>	<i>R</i>	32
35	H/EA=6/1	1.17	0.95	—	<i>R</i>	30
36	H/EA=7/1	—	—	—	—	29
37	H/EA=8/1	1.18	0.83	○ (1st, Fr.)	<i>R</i>	29
38	H/EA=4/1	1.1	1.0	—	<i>R</i>	30
40	H/EA=8/1	1.21	1.07	○ <sup>b</sup>	<i>S</i>	32
44	H/EA=4/1	1.27	1.20	○ <sup>b</sup>	<i>S</i>	33
45	H/EA=5/1	1.12	1.01	○ (1st, Fr.)	<i>S</i>	34
48	H/EA=4/1	1.14	0.91	○ (2nd, Fr.)	<i>R</i>	34, 35
50	H/EA=10/1	1.26	1.03	—	<i>R</i>	34
51	H/EA=6/1	1.26	1.29	—	<i>R</i>	36
52	H/EA=5/1	1.16	1.11	○ (1st, Fr.)	<i>S</i>	37
53	H/EA=5/1	1.12	0.87	○ (1st, Fr.)	<i>S</i>	37
54	H/EA=2/1	1.11	0.88	—	<i>R</i>	37
55	H/EA=2/1	1.38	1.19	○ (1st, Fr.)	<i>R</i>	37
24	H/EA=3/1	1.2	1.6	○ (2nd, Fr.)	<i>aR</i> , <i>aR</i>	27, 28
57	H/EA=5/1	1.34	2.37	○ (1st, Fr.)	<i>R</i>	38
58	H/EA=5/1	1.16	1.22	○ (1st, Fr.) ○ (2nd, Fr.)	<i>R</i>	38
59	H/EA=4/1	1.00	—	—	—	38
60	H/EA=5/1	1.11	1.33	—	<i>R</i>	38
61	H/EA=5/1	1.05	0.77	—	—	38
62	H/EA=4/1	1.00	—	—	—	38
63	H/EA=4/1	1.21	2.50	○ (1st, Fr.)	<i>S</i>	38
64	H/EA=4/1	1.27	1.14	○ <sup>c</sup>	<i>S</i>	40

<sup>a</sup>H=n-hexane, EA=ethyl acetate.

<sup>b</sup>X-ray analysis of camphanate ester.

<sup>c</sup>X-ray analysis of 4-bromobenzoate.





diastereomeric esters separated but gave fine, needle-like crystals after a series of recrystallizations. Accordingly, after recovering the enantiopure alcohol  $(-)$ -40 from the first-eluted fraction 41a, a part of  $(-)$ -40 was converted to ester 42 using  $(-)$ -camphanic acid chloride. Ester 42 showed good crystallinity, yielding prismatic crystals suitable for X-ray analysis, and the absolute configuration of the alcohol moiety was determined as *S*, using the absolute configuration of  $(-)$ -camphanic acid part as an internal reference. Subsequently, alcohol  $(S)$ - $(-)$ -40 was reduced with  $\text{H}_2\text{NNH}_2/\text{H}_2\text{O}$  in the presence of Pd-C to yield the isotopically substituted chiral and enantiopure  $(\text{phenyl}-2,3,4,5,6-d_5)\text{phenylmethanol}$  [ $\text{CD}(-)270.4$ ]- $(S)$ -39, the absolute configuration of which was unambiguously determined. The specific rotation  $[\alpha]_D$  measured at the wavelength of the sodium D-line (589 nm) is usually used to distinguish enantiomers, but it is difficult to measure  $[\alpha]_D$  value of compounds with isotope-substitution chirality. We have therefore proposed a new definition of configuration of enantiomers that uses CD data because CD is much more sensitive than  $[\alpha]_D$  and so accurately measurable even with small samples. For example,  $[\text{CD}(-)270.4]$ - $(S)$ -39 stands for the enantiomer with negative CD at 270.4 nm and *S* absolute configuration.<sup>32</sup>

It would be even more advantageous if  $(-)$ -camphanic acid could be used from the beginning as the chiral auxiliary for resolution. However, the resolving power

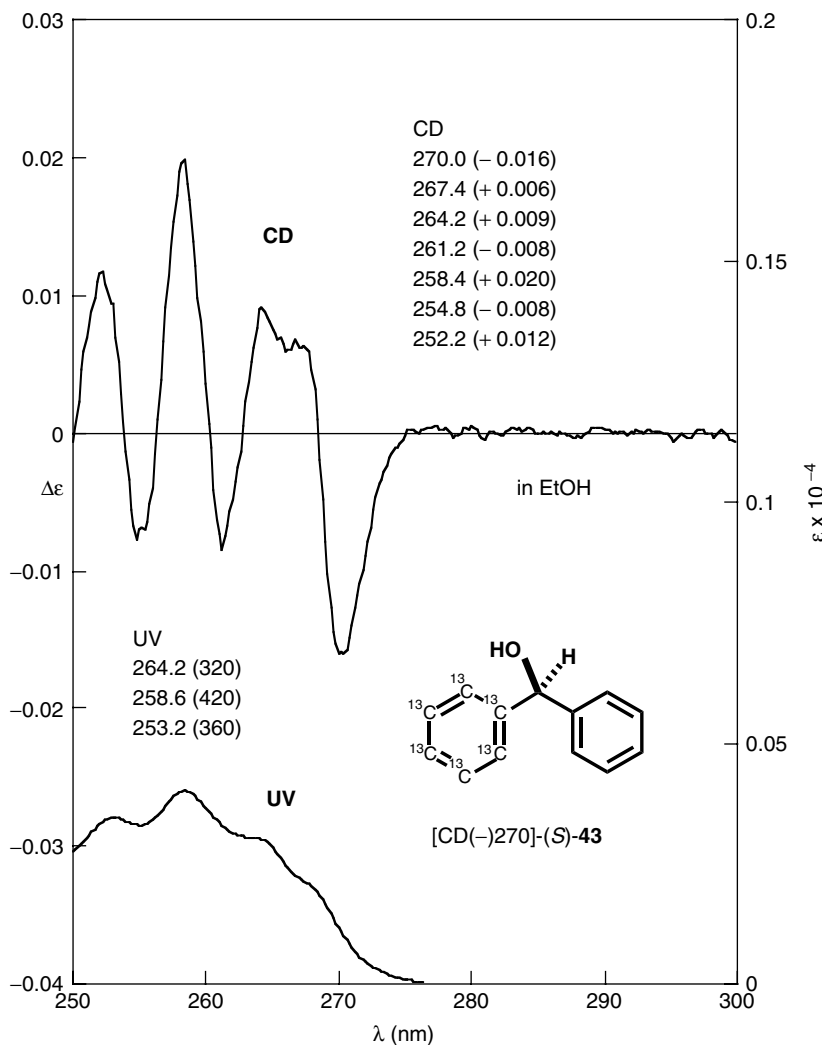


Figure 6.5. UV and CD spectra of (phenyl-1,2,3,4,5,6-<sup>13</sup>C<sub>6</sub>)phenylmethanol (**43**) in EtOH.

of (–)-camphanic acid is generally weak. For example, camphanic acid esters of alcohol **40** cannot be separated by HPLC on silica gel.

A similar scheme can be applied to synthesize <sup>13</sup>C-substituted chiral diphenylmethanol (**43**).<sup>33</sup> Namely (4-bromophenyl)(phenyl-1,2,3,4,5,6-<sup>13</sup>C<sub>6</sub>)methanol

( $\pm$ )-(44) is chosen, and then resolution and determination of the absolute configuration are carried out as described above. Subsequently the bromine atom is removed to yield the  $^{13}\text{C}$ -substituted chiral (phenyl-1,2,3,4,5,6- $^{13}\text{C}_6$ )phenylmethanol [CD(-)-270]-(S)-43. Despite the very slight difference between isotopes  $^{12}\text{C}$  and  $^{13}\text{C}$ , the CD spectrum of  $^{13}\text{C}$  substituted chiral diphenylmethanol (S)-43 is clearly observable as illustrated in Figure 6.5.<sup>33</sup>

Interesting results can also be obtained in the case of *ortho*-substituted diphenylmethanols. By the method described above, enantiopure (2-methoxyphenyl)phenylmethanol (–)-(45) is prepared and its absolute configuration determined as S.<sup>34</sup> Chiral (2-methylphenyl)phenylmethanol (46) had previously been synthesized by asymmetric catalytic reaction, and its absolute configuration had been assigned based on the reaction mechanism. But such absolute configurational assignment based solely on the reaction mechanism is not reliable. To settle such a case, independent and unambiguous determination of the absolute configuration is necessary. Although direct resolution of 46 as a chiral dichlorophthalate failed the indirect method was successful.<sup>34-36</sup> This strategy consists of enantio-resolution of (2-hydroxymethylphenyl)phenylmethanol (48) as the chiral dichlorophthalate, determination of absolute configuration by X-ray analysis, and further conversion of the enantiopure derivative of 48 to the desired alcohol 46. The chiral dichlorophthalic acid (–)-2 (1 equiv.) is allowed to react with diol ( $\pm$ )-48 to yield a diastereomeric mixture of esters, in which the primary alcohol group is selectively esterified. In this case, although the chiral auxiliary bonded to the primary alcohol is remote from the stereogenic center of 48, the diastereomeric esters can be cleanly separated. Single crystals are obtained from the second-eluted fraction (–)-49b, leading to the determination of its absolute configuration as S by X-ray analysis. The first-eluted fraction (R)-(–)-49a can be converted to the desired enantiopure alcohol (R)-(–)-46 via several reaction steps. The result above indicates that the absolute configuration of 46 as previously assigned on the basis of an asymmetric reaction mechanism is incorrect.<sup>35</sup>

This method is also effective for preparation of a variety of benzyl alcohols 52–55.<sup>37</sup> Benzyl alcohols are useful as chiral synthons for the total synthesis of natural products because of their unambiguous absolute configurations and high enantiopurity.

Atropisomer 24 is a unique chiral compound containing three naphthalene rings. Its resolution and determination of absolute configuration were carried out by this method.<sup>27,28</sup> Racemic diol, ( $\pm$ )-1,1'-4',1''-ternaphthalene-2,2''-dimethanol (24), was combined with chiral dichlorophthalic acid 2 forming diesters. The diesters are separated by HPLC on the silica gel: hexane/EtOAc = 2:1,  $\alpha$  = 1.18. Whereas the first-eluted fraction (–)-56a yielded fine needle-like crystals by recrystallization from hexane/EtOAc, the second-eluted fraction (+)-56b yielded large crystals.

In general, single crystals suitable for X-ray analysis take prismatic or columnar forms with definite surfaces and edges, or have thick plate-like forms. The second-eluted ester (+)-**56b** gave clusters that did not look like single crystals. However, after dissection of the clusters the central part was subjected to X-ray analysis, revealing a single crystal. More interesting, the formula weight of an asymmetric unit estimated from the preliminary lattice constant did not agree with the molecular weight of (+)-**56b**. However, careful investigation of the data revealed that half of the molecule **56b** was equivalent to one asymmetric unit. Namely ester (+)-**56b** has a C<sub>2</sub> symmetric structure even in crystals, despite the fact that the molecule contains complex chiral dichlorophthalic acid moieties. The absolute configuration, meaning torsion among three naphthalene chromophores, was unambiguously determined as (aS,aS) on the basis of internal reference. The chiral auxiliaries were removed from ester (aS,aS)-(+)-**56b** to yield enantiopure diol (aS,aS)-(+)-**24**. The absolute configuration obtained from this X-ray crystallographic analysis was consistent with that by application of the CD exciton chirality method to (+)-**24**.<sup>27,28</sup>

Recently much attention has been directed toward chiral fluorinated organic compounds, as some chiral synthetic drugs consist of fluorinated aromatic moieties. To prepare chiral fluorinated diphenylmethanols and to determine their absolute configurations by X-ray crystallography, the CSDP acid method was employed.<sup>38</sup> For example, (4-trifluoromethylphenyl)phenylmethanol **57** was esterified with CSDP acid (-)-**2** yielding a diastereomeric mixture of esters, which was cleanly separated by HPLC on silica gel: separation factor  $\alpha = 1.34$ ; resolution factor  $R_s = 2.37$  (Table 6.3). The first-eluted ester was recrystallized from EtOH, giving prisms, one of which was subjected to X-ray crystallography. Although the trifluoromethyl moiety took a disordered structure, the absolute configuration of the first-eluted ester was unambiguously determined as *R* by the internal reference method using the (1*S*,2*R*,4*R*) absolute configuration of the camphor part and also by the heavy atom effect. Enantiopure (4-trifluoromethyl phenyl)phenylmethanol (*R*)-(-)-**57** was easily recovered by treating the first-eluted CSDP ester with K<sub>2</sub>CO<sub>3</sub> in MeOH. Although the absolute configuration of (+)-**4** had previously been estimated as *S* by the Horeau's method, the abnormality of its application had been pointed out.<sup>39</sup> The absolute configuration of (4-trifluoromethylphenyl)phenylmethanol (*R*)-(-)-**57** was thus determined by X-ray crystallography.

Other fluorinated diphenylmethanols were similarly esterified with CSDP acid (-)-**2**, and the diastereosmeric mixtures obtained were subjected to HPLC on silica gel. As shown in Table 6.3, diastereosmeric CSDP esters of (3-trifluoromethyl phenyl)phenylmethanol **58**, (4-fluorophenyl)phenylmethanol **60**, and (2,6-difluorophenyl)phenylmethanol **63** were separated well with  $\alpha$ -values of

more than 1.1. In the case of (3-fluorophenyl)phenylmethanol **61**, its CSDP esters were partially separated:  $\alpha = 1.05$ , but it was not suitable for separation of preparative scale. The CSDP esters of the remaining alcohols, (2-trifluoromethylphenyl)phenylmethanol **59** and (2-fluorophenyl)phenylmethanol **62**, appeared as single peaks in HPLC on silica gel, indicating no separation at all (Table 6.3). As listed in Table 6.3, the resolution method using CSDP acid was thus applicable to four fluorinated diphenylmethanols among seven compounds.<sup>38</sup>

In the case of (3-trifluoromethylphenyl)phenylmethanol **58**, the final *R*-value of the first-eluted CSDP ester remained higher because of low crystallinity. However, even in such a case, its absolute configuration was clearly determined based on the internal reference of absolute configuration of the camphor moiety. The second eluted CSDP ester also crystallized as prisms, allowing the X-ray crystallographic determination of absolute configuration (Table 6.3). In the case of (4-fluorophenyl)phenylmethanol **60**, no single crystals suitable for X-ray analysis were obtained from both CSDP esters, and therefore their absolute configurations could not be determined by X-ray crystallography. However, the absolute configuration of (4-fluorophenyl)phenylmethanol **60** was determined by the <sup>1</sup>H NMR anisotropy method.<sup>38</sup> The first-eluted CSDP ester of (2,6-difluorophenyl)phenylmethanol **63** was recrystallized from EtOH giving prisms; the X-ray analysis led to the unambiguous assignment of an *S* absolute configuration to (−)-**63** (Table 6.3).

The compound, 2-(1-naphthyl)propane-1,2-diol (**64**), was isolated as a chiral metabolite of 1-isopropynaphthalene in rabbits. The metabolite, however, was not enantiopure, and its absolute configuration had been only empirically estimated based on the reaction mechanism. To obtain the enantiopure diol **64** and to determine its absolute configuration in an unambiguous way, the CSDP acid method was applied to (±)-**64**.<sup>40</sup> In this case only the primary alcohol part was esterified, and a diastereomeric mixture obtained was clearly separated by HPLC on silica gel: hexane/EtOAc = 4:1,  $\alpha = 1.3$ ,  $R_s = 1.1$ . In this HPLC the presence of free tertiary hydroxyl group proved to be important; protection of the tertiary alcohol group led to poor separation.

Despite many recrystallizations, both diastereomers were obtained only as amorphous solids. Therefore, the first-eluted fraction (−)-**65a** was reduced with LiAlH<sub>4</sub> to yield enantiopure glycol (−)-**64**, which was further converted to 4-bromobenzoate (−)-**66** (Figure 6.6). By recrystallization from EtOH, (−)-**66** gave single crystals suitable for X-ray analysis, and consequently its absolute configuration was determined as *S* by Bijvoet pair measurement of the anomalous dispersion effect from the bromine atom (Table 6.4).<sup>40</sup>

Furthermore enantiopure 2-methoxy-2-(1-naphthyl)propionic acid (MαNP acid) (*S*)-(+)-(**3**) was obtained after several reactions from diol (*S*)-(−)-**64** (Figure 6.7).<sup>40</sup> This novel carboxylic acid, MαNP acid (**3**), was also

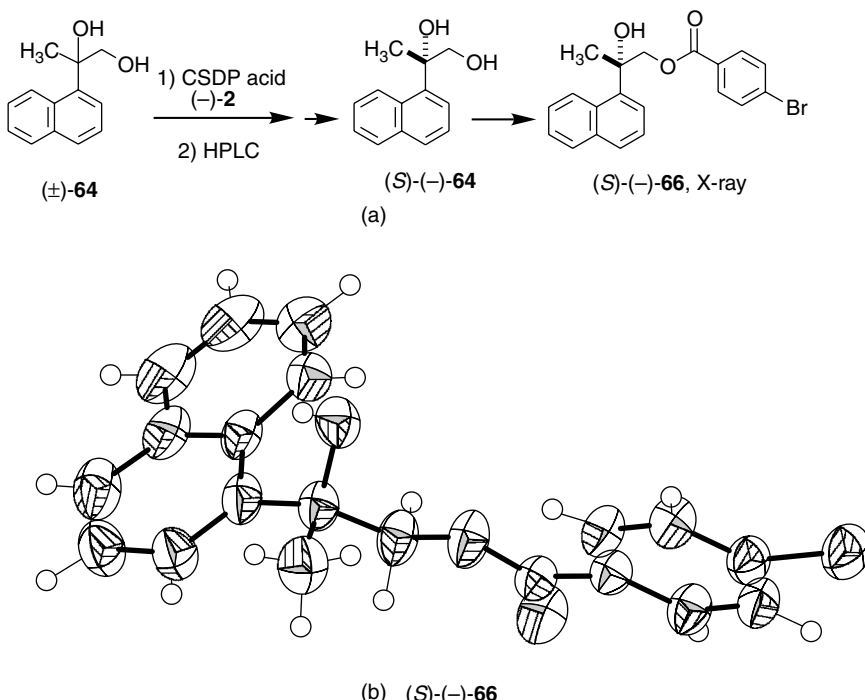


Figure 6.6. (a) Resolution and determination of the absolute configuration of 2-(1-naphthyl)-propane-1,2-diol (**64**). (b) ORTEP drawing of ester (S)-(-)-**66**.

powerful for the resolution and determination of the absolute configuration of various secondary alcohols by the  $^1\text{H}$  NMR anisotropy method.<sup>41–47</sup> The absolute configurations of most alcohols listed in Table 6.3, for which the X-ray crystallographic method could not be applied, were determined by this  $^1\text{H}$  NMR anisotropy method using  $\text{M}\alpha\text{NP}$  acid (**3**). The results obtained by the  $^1\text{H}$  NMR anisotropy method are, of course, consistent with those by the X-ray method. Therefore, the methods of CSDP and  $\text{M}\alpha\text{NP}$  acids are useful as complementary molecular tools.

## VII. CONCLUSIONS

Several novel chiral auxiliaries, in particular, chiral carboxylic acids have been developed. *These CDAs (chiral derivatizing agents) have been applied to the*

Table 6.4  
Bijvoet Pairs of (*S*)-(−)-2-(1-Naphthyl)propane-1,2-diol 1-*p*-Bromobenzoate (**66**):  
Observed and Calculated Values of the Structural Factors for (h, k, l) and (h, k, −l)  
Reflections, and Their Ratios

h	k	l	$ F_o(hkl) $	$ F_o(hk-l) $	$ F_o(hkl) / F_o(hk-l) $
			$[ F_c(hkl) ]$	$[ F_c(hk-l) ]$	$[ F_c(hkl) ]/[ F_c(hk-l) ]$
1	4	1	39.4 [35.4]	32.1 [27.9]	1.23 [1.26]
1	5	1	39.3 [37.7]	46.2 [42.2]	0.85 [0.89]
2	8	1	78.4 [74.1]	73.8 [68.4]	1.06 [1.08]
4	1	1	102.6 [91.1]	92.8 [84.6]	1.11 [1.08]
5	5	1	10.1 [11.3]	20.2 [19.0]	0.50 [0.59]
2	1	2	162.2 [154.3]	149.3 [143.6]	1.09 [1.07]
4	4	2	83.0 [81.0]	90.7 [87.6]	0.92 [0.92]
5	6	2	71.0 [68.1]	66.4 [62.6]	1.07 [1.09]
1	3	3	76.0 [74.9]	83.6 [79.6]	0.91 [0.94]
2	1	3	75.8 [72.8]	69.5 [66.6]	1.09 [1.09]
2	3	3	89.7 [86.5]	99.6 [94.5]	0.90 [0.90]
2	5	3	80.9 [77.3]	73.8 [69.4]	1.10 [1.11]
3	7	3	66.8 [63.6]	73.2 [69.1]	0.91 [0.92]
5	4	3	40.0 [40.1]	46.4 [45.6]	0.86 [0.88]
2	1	4	104.6 [99.5]	98.0 [92.6]	1.07 [1.07]
2	10	3	49.4 [49.7]	45.0 [43.7]	1.10 [1.07]
7	5	3	42.2 [40.9]	36.3 [35.3]	1.16 [1.16]
4	4	4	80.9 [75.5]	87.0 [80.7]	0.93 [0.94]

<sup>a</sup> Reflections satisfying  $||F_o(hkl)| - |F_o(hk-l)|| > 10 \sigma(F_o)$  were selected, where  $\sigma(F_o) = [\sigma_{\text{count}}^2 + (0.007|F_o|)^2]^{0.5}$ .

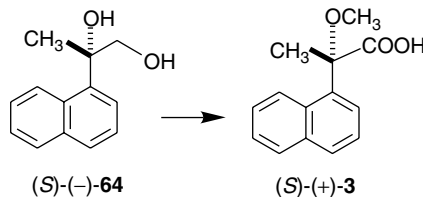


Figure 6.7. Synthesis of the novel chiral carboxylic acid, (*S*)-(+)2-methoxy-2-(1-naphthyl)propionic acid (**3**), and determination of its absolute configuration.

*resolution of alcohols by the diastereomeric HPLC method and the determination of absolute configuration by X-ray crystallography.* The X-ray crystallographic method using an internal reference proved to be reliable for determining absolute configuration. The CSDP acid method described above is particularly powerful for the preparation of enantiomeric alcohols with high enantiopurity on a laboratory scale and also for the simultaneous determination of their absolute configurations.

### ACKNOWLEDGMENTS

The author thanks the graduate students and colleagues in his laboratory for their contributions and all the collaborators for their efforts and cooperation, whose names are listed in references cited. This project has been supported by grants from the Ministry of Education, Science, Sports, Culture, and Technology, Japan, and the Japan Society for the Promotion of Science.

### REFERENCES

1. Bijvoet, J. M.; Peerdeman, A. F.; Van Bommel, A. J. *Nature* **1951**, *168*, 271.
2. Harada, N.; Nakanishi, K. *Circular Dichroic Spectroscopy—Exciton Coupling in Organic Stereochemistry*. University Science Books, Mill Valley, CA and Oxford University Press, Oxford, 1983.
3. Harada, N.; Soutome, T.; Murai, S.; Uda, H. *Tetrahedron: Asymmetry* **1993**, *4*, 1755.
4. Harada, N.; Soutome, T.; Nehira, T.; Uda, H.; Oi, S.; Okamura, A.; Miyano, S. *J. Am. Chem. Soc.* **1993**, *115*, 7547.
5. Harada, N.; Hattori, T.; Suzuki, T.; Okamura, A.; Ono, H.; Miyano, S.; Uda, H. *Tetrahedron: Asymmetry* **1993**, *4*, 1789.
6. Hattori, T.; Harada, N.; Oi, S.; Abe, H.; Miyano, S. *Tetrahedron: Asymmetry* **1995**, *6*, 1043.
7. Toda, F. *Top. Curr. Chem.* **1987**, *140*, 43. Toda, F. *Inclusion Compounds*, Vol. 4, Atwood, J. L.; Davis, J. E.; MacNicol, D. D., eds. Oxford University Press, Oxford, **1991**, pp. 126–187. Toda, F. *Advances in Supramolecular Chemistry*, Vol. 2, Gokel, G. W. ed. JAI Press, London, **1992**, pp. 141–191.
8. Toda, F.; Tanaka, K.; Miyahara, I.; Akutsu, S.; Hirotsu, K. *J. Chem. Soc., Chem. Commun.* **1994**, 1795. Toda, F.; Tanaka, K.; Leung, C. W.; Meetsma, A.; Feringa, B. L. *J. Chem. Soc., Chem. Commun.* **1994**, 2371. Toda, F.; Tanaka, K.; Watanabe, M.; Abe, T.; Harada, N. *Tetrahedron: Asymmetry* **1995**, *6*, 1495–1498.
9. Toda, F. *J. Synth. Org. Chem. Jpn.* **1990**, *47*, 1118.
10. Ohtani, I.; Kusumi, T.; Kashman, Y.; Kakisawa, H. *J. Am. Chem. Soc.* **1991**, *113*, 4092. Kusumi, T.; Takahashi, H.; Ping, X.; Fukushima, T.; Asakawa, Y.; Hashimoto, T.; Kan, Y.; Inouye, Y. *Tetrahedron Lett.* **1994**, *35*, 4397. Kusumi, T.; Takahashi, H.; Hashimoto, T.; Kan, Y.; Asakawa, Y. *Chem. Lett.* **1994**, 1093.

11. Seco, J. M.; Latypov, Sh. K.; Quinoa, E.; Riguera, R. *Tetrahedron Lett.* **1994**, *35*, 2921. Latypov, Sh. K.; Seco, J. M.; Quinoa, E.; Riguera, R. *J. Org. Chem.* **1995**, *60*, 504. Seco, J. M.; Latypov, Sh. K.; Quinoa, E.; Riguera, R. *Tetrahedron* **1997**, *53*, 8541.
12. Trost, B. M.; Belletire, J. L.; Godleski, S.; McDougal, P. G.; Balkovec, J. M.; Baldwin, J. J.; Christy, M. E.; Ponticello, G. S.; Varga, S. L.; Springer, J. P. *J. Org. Chem.* **1986**, *51*, 2370.
13. Ohrui, H. *J. Synth. Org. Chem. Jpn.* **1998**, *56*, 591. Fukushi, K. *Nippon Nogeikagaku Kaishi* **1998**, *72*, 1345.
14. Review articles: *J. Chromatogr. A* **2001**, *906*, 1–482. Yamamoto, C.; Okamoto, Y. *Maku* **2000**, *25*, 277. Kobayashi, Y.; Matsuyama, A.; Onishi, A. *Fine Chemicals* **2000**, *29*, 59.
15. Patel, R. N. ed. *Stereoselective Biocatalysis*. Dekker, New York, **2000**.
16. Harada, N.; Ochiai, N.; Takada, K.; Uda, H. *J. Chem. Soc., Chem. Commun.* **1977**, 495.
17. Harada, N.; Ono, H.; Nishiwaki, T.; Uda, H. *J. Chem. Soc., Chem. Commun.* **1991**, 1753.
18. Weismiller, M. C.; Towson, J. C.; Davis, F. A. *Organic Syntheses* **1990**, *69*, 154.
19. Nehira, T.; Harada, N. To be published.
20. Toyota, S.; Miyasaka, T.; Matsumoto, Y.; Matsuo, T.; Oki, M. *Bull. Chem. Soc. Jpn.* **1994**, *67*, 1680.
21. Toyota, S.; Akinaga, T.; Kojima, H.; Aki, M.; Oki, M. *J. Am. Chem. Soc.* **1996**, *118*, 11460.
22. Toyota, S. *Enantiomer* **1999**, *4*, 25.
23. Harada, N.; Nehira, T.; Soutome, T.; Hiyoshi, N.; Kido, F. *Enantiomer* **1996**, *1*, 35.
24. Harada, N.; Koumura, N.; Robillard, M. *Enantiomer* **1997**, *2*, 303.
25. Harada, N.; Koumura, N.; Feringa, B. L. *J. Am. Chem. Soc.* **1997**, *119*, 7256.
26. Toyota, S.; Yasutomi, A.; Kojima, H.; Igarashi, Y.; Asakura, M.; Oki, M. *Bull. Chem. Soc. Jpn.* **1998**, *71*, 2715.
27. Harada, N.; Vassilev, V. P.; Hiyoshi, N. *Enantiomer* **1997**, *2*, 123.
28. Harada, N.; Hiyoshi, N.; Vassilev, V. P.; Hayashi, T. *Chirality* **1997**, *9*, 623.
29. Harada, N.; Fujita, K.; Watanabe, M. *Enantiomer* **1997**, *2*, 359.
30. Fujita, K.; Harada, N. To be published.
31. Koumura, N.; Harada, N. To be published.
32. Harada, N.; Fujita, K.; Watanabe, M. *Enantiomer* **1998**, *3*, 64.
33. Harada, N.; Fujita, K.; Watanabe, M. *J. Phys. Org. Chem.* **2000**, *13*, 422.
34. Kuwahara, S.; Watanabe, M.; Harada, N.; Koizumi, M.; Ohkuma, T. *Enantiomer* **2000**, *5*, 109.
35. Watanabe, M.; Kuwahara, S.; Harada, N.; Koizumi, M.; Ohkuma, T. *Tetrahedron: Asymmetry* **1999**, *10*, 2075.
36. Taji, H.; Harada, N. To be published.
37. Kosaka, M.; Watanabe, M.; Harada, N. *Chirality* **2000**, *12*, 362.
38. Naito, J.; Kosaka, M.; Sugito, T.; Watanabe, M.; Harada, N.; Pirkle, W. H. *Chirality* **2004**, *16*, 22.
39. Wu, B.; Mosher, H. S. *J. Org. Chem.* **1986**, *51*, 1904.
40. Kuwahara, S.; Fujita, K.; Watanabe, M.; Harada, N.; Ishida, T. *Enantiomer* **1999**, *4*, 141.
41. Ichikawa, A.; Hiradate, S.; Sugio, A.; Kuwahara, S.; Watanabe, M.; Harada, N. *Tetrahedron: Asymmetry* **1999**, *10*, 4075.

42. Harada, N.; Watanabe, M.; Kuwahara, S.; Sugio, A.; Kasai, Y.; Ichikawa, A. *Tetrahedron: Asymmetry* **2000**, *11*, 1249.
43. Taji, H.; Kasai, Y.; Sugio, A.; Kuwahara, S.; Watanabe, M.; Harada, N.; Ichikawa, A. *Chirality* **2002**, *14*, 81.
44. Harada, N.; Watanabe, M.; Kuwahara, S.; Kosaka, M. *J. Synth. Org. Chem. Jpn* **2001**, *59*, 985.
45. Taji, H.; Watanabe, M.; Harada, N.; Naoki, N.; Ueda, Y. *Org. Lett.* **2002**, *4*, 2699.
46. Naito, J.; Kosaka, M.; Sugito, T.; Watanabe, M.; Harada, N.; Pirkle, W. H. *Chirality* **2004**, *16*, 22.
47. Kasai, Y.; Taji, H.; Fujita, T.; Yamamoto, Y.; Akagi, M.; Sugio, A.; Kuwahara, S.; Watanabe, M.; Harada, N.; Ichikawa, A.; Schurig, V. *Chirality* **2004**, *16*, 569.

## Chapter 7

# Engineering Stereospecific Reactions in Crystals: Synthesis of Compounds with Adjacent Stereogenic Quaternary Centers by Photodecarbonylation of Crystalline Ketones

CHRISTOPHER J. MORTKO and MIGUEL A. GARCIA-GARIBAY

*University of California, Los Angeles, Department of Chemistry and Biochemistry, 607 Charles E. Young Drive East, Los Angeles, CA 90095-1569*

- I. Introduction
- II. Photodecarbonylation Reactions
  - A. Photodecarbonylation Reactions in Crystals: Early Observations
- III. Reactions in Crystals
  - A. Structural Considerations: The Topochemical Postulate and Reaction Cavity Concepts
  - B. Molecularity
  - C. Energetic Considerations
  - D. Molecular Structure as a Source of Information to “Engineer” Reactions in Crystals
- IV. From Molecular Information to Reactive Crystals
  - A. Predicting Solid State Reactivity from Thermochemical Parameters
  - B. Ranking Reactivity as a Function of  $\alpha$ -Substituents: Phenyl-Substituted Cyclohexanones
  - C. Testing the Effects of Phenyl and Alkyl Groups in Cyclopentanones
  - D. Experimental and Computational Results with  $\alpha$ -Alkyls and  $\alpha$ -Carbonyl Ketones
- V. Subtle (but Predictable) Aspects of the Solid State Photodecarbonylation Reaction
  - A. Stereoelectronic Effects on Benzylic Stabilization
  - B. Ultrafast Competing Reactions:  $\gamma$ -Hydrogen Abstraction
  - C. Quenching by  $\beta$ -Phenyl Groups
  - D. Quenching by Electron Transfer
- VI. Stereochemistry of the Photodecarbonylations Reaction in Crystals
  - A. Stereospecificity and Scale Up
  - B. Diastereo- and Enantiospecific Syntheses of Vicinal Tertiary and Quaternary Centers
  - C. Total Synthesis of ( $\pm$ )-Herbertenolide by Photodecarbonylation of a Crystalline Ketone

VII. Final Comments  
 Acknowledgments  
 References

## I. INTRODUCTION

Although most chemists in academic and industrial laboratories routinely deal with chemical transformations in a wide variety of solid materials and crystalline compounds, chemical reactivity in the solid state remains counterintuitive. However, with the advent of green chemistry,<sup>1</sup> the potential of reactions with no solvent is increasingly appreciated, and many chemists are engaged in systematic efforts to study the factors that control reactions in organic solids.<sup>2</sup> In recent times, a large number of transformations have been carried out in the absence of solvents, from pure crystalline reactants to pure crystalline products, in close to 100% chemical yields.<sup>3</sup> In this chapter we discuss our efforts on a general engineering approach to reactions in crystals, emphasizing an emerging application in one of the most challenging problems in organic synthesis: the stereoselective construction of adjacent stereogenic quaternary centers (Figure 7.1).<sup>4</sup>

The stereoselective construction of adjacent stereogenic quaternary centers addressed in this chapter challenges notions of reactivity and stereochemical control acquired from the study of reactions in fluid media. As illustrated in Figure 7.1, *the chemo- and stereoselective formation of the sigma bond between adjacent stereogenic quaternary centers can be obtained by a combination of tri-substituted, carbon-centered radicals generated by decarbonylation of hexasubstituted crystalline ketones.* Some apparent conflicts arise from this statement. First of all, our experience indicates that radical centers should lose their configurational identity shortly after they are generated by cleavage of the ketone  $\alpha$ -bonds as they become solvent-separated and on their way to becoming free radicals (Scheme 7.1). In addition bond-forming reactions involving prochiral  $sp^2$ -radical centers should generate two pairs of diastereomers (*RR*, *SS* and *SR*, *RS*). Third, experience from solution studies indicates that radical reactions are

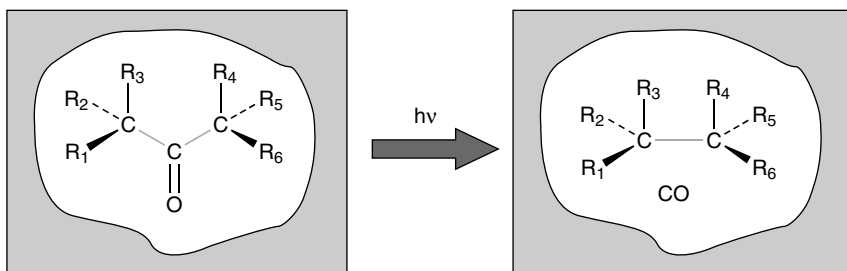
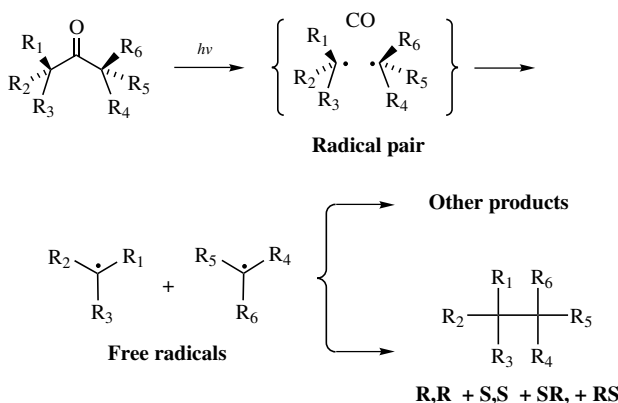


Figure 7.1. Stereospecific decarbonylation of a hexasubstituted ketone in the crystalline solid state.



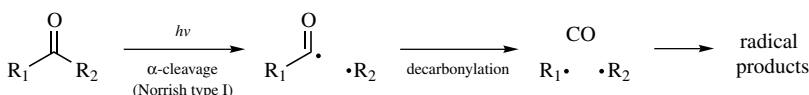
Scheme 7.1.

difficult to control and that they tend to give many products thus of questionable practical value for the suggested reaction.

If preconceptions about radical reactions are not enough to dissuade one from pursuing the suggested transformation, a major conflict arises when one considers the generation of radical pairs in a crystalline ketone. Influenced by ORTEP diagrams and other representations of molecules in crystals, our intuition suggests that static molecules in crystals should not be able to break bonds and undergo chemical reactions. In the following two sections, we describe the earliest examples of decarbonylation reactions in crystals and give a brief analysis of the general factors that influence reactions in crystals. After brief coverage of structural, energetic, and entropic factors, we elaborate a working model designed to engineer decarbonylation reactions in crystals in a reliable manner.

## II. PHOTODECARBOXYLATION REACTIONS

Reports on the photochemical decarbonylation of ketones date back to 1910 when Bowen and Watts reported that photolysis of acetone yielded ethane and carbon monoxide.<sup>5</sup> Later, Norrish suggested that photodecarbonylation is a radical process involving a photochemical  $\alpha$ -cleavage,<sup>6</sup> now known as the Norrish type-I reaction, followed by loss of CO (decarbonylation)<sup>7</sup> from the acyl radical fragment (Scheme 7.2).<sup>8</sup>



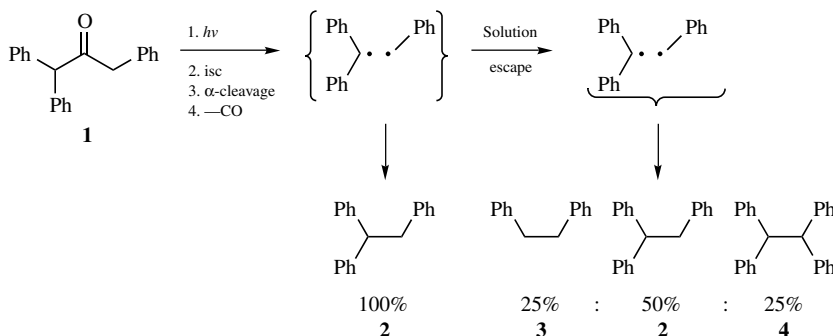
Scheme 7.2.

The two reactions in Scheme 7.2 are general, both in the gas phase and in solution, and have been covered in several excellent reviews.<sup>9,10,11</sup>  $\alpha$ -Cleavage and decarbonylation are favored when the radicals formed after each step are relatively stable. For simple aliphatic ketones, the rate constants and activation energies for  $\alpha$ -cleavage and decarbonylation correlate with the stability of the radicals formed. Although  $\alpha$ -cleavage is known to occur from both singlet and triplet states, singlet state reactions are subject to internal decay by an avoided crossing along the reaction coordinate, and they have lower pre-exponential factors than those reacting from the triplet state. Notably the loss of CO is independent of spin multiplicity and relatively insensitive to medium effects.<sup>12</sup>

#### A. Photodecarbonylation Reactions in Crystals: Early Observations

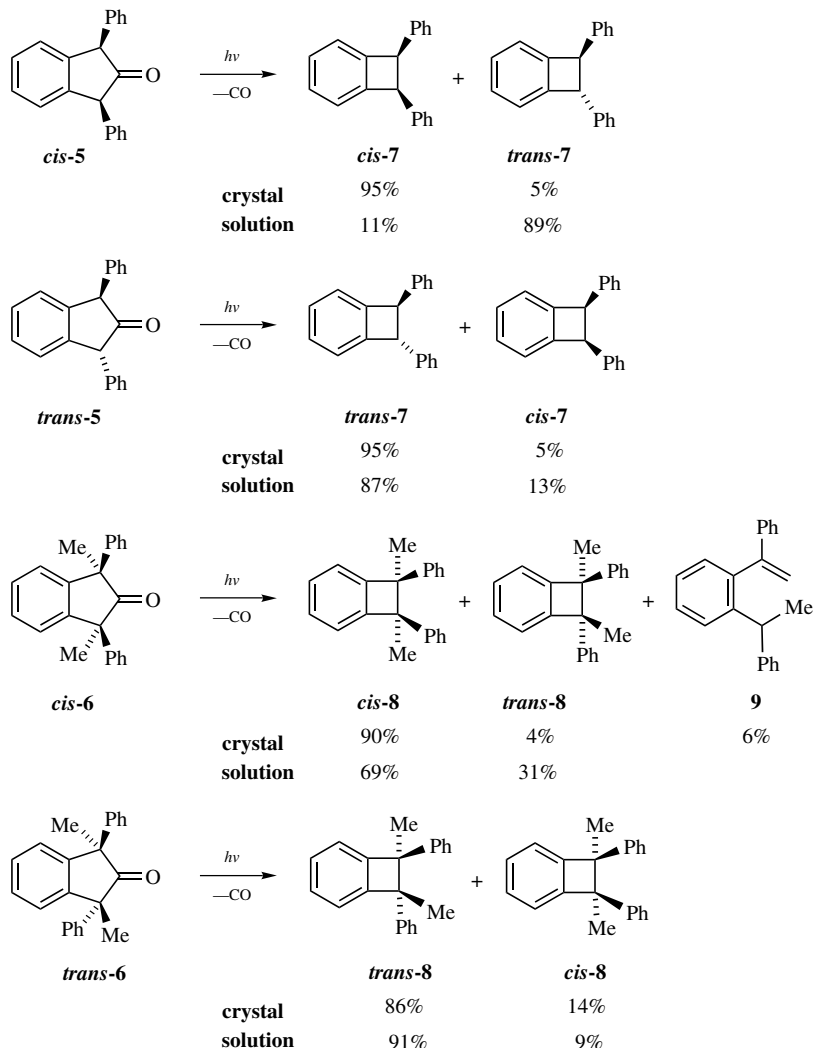
Photochemical decarbonylations in crystals were first documented by Quinkert et al. in the 1960s while exploring the effects of viscosity on the recombination of radical pairs. The remarkable control exerted by crystals was first illustrated with 1,1,3-triphenyl-2-propanone **1** (Scheme 7.3).<sup>13</sup> It was shown that photolysis of **1** in benzene conforms to the expected  $\alpha$ -cleavage and decarbonylation reactions to form diphenylmethyl and benzyl radicals, which are free to diffuse apart in solution. Combination of the two radicals in solvents occurs by random encounters, giving statistical mixtures of products **2**, **3**, and **4**. Interestingly, when irradiations were carried out in the crystalline phase, the radical pair was unable to diffuse, leading to the exclusive formation of **2** by combination of the original, or *geminate* radical pair, with a 100% cage effect. A very similar observation, with a nearly perfect control of the cage effect in radical pairs generated by decarbonylation of crystalline 1,3,4-triphenyl-2-butanone, was reported by Turro et al. in 1983.<sup>14</sup>

A remarkably high stereospecificity was subsequently reported by Quinkert et al. for several crystalline 2-indanone derivatives. Experiments were carried out in

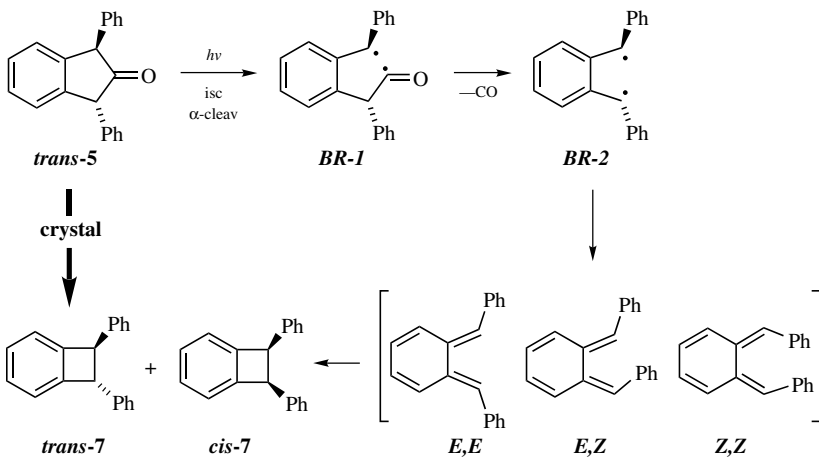


*Scheme 7.3.* Cage effect in crystal.

benzene solutions and in crystalline samples of *cis*- and *trans*-diphenyl-2-indanones **5** and **6**.<sup>15</sup> Photodecarbonylation in solution led to diphenylbenzocyclobutanes **7** and **8**, respectively, both with a very similar selectivity (*cis* : *trans* ≈ 10:90), which suggests that reactions may occur with equilibration of a common intermediate. In contrast, reactions in crystals proceeded with stereospecificity values of 95% and with excellent conversions (Scheme 7.4).



Scheme 7.4.



Scheme 7.5.

Subsequent experiments have shown that photodecarbonylation of analogous indanones in solution proceeds through 1,4-biradical intermediates that close to short-lived *ortho*-quinodimethanes, before undergoing an electrocyclic ring closure to the final benzocyclobutane products.<sup>16</sup> The suggested solution mechanism is summarized in Scheme 7.5 with *trans*-5 as an example. The results in the solid state can be understood in terms of a similar process, where the 1,4-biradical intermediates (BR2) are configurationally locked, and unable to undergo bond rotations to form the *ortho*-quinodimethane within the restricted environment of the crystal. The stereospecific formation of benzocyclobutane is likely to occur by a least motion pathway by direct bond formation from the 1,4-biradical.<sup>17</sup>

### III. REACTIONS IN CRYSTALS

#### A. Structural Considerations: The Topochemical Postulate and Reaction Cavity Concepts

The structural constraints determining the feasibility of reactions in crystals were first suggested by Kohlshutter in 1918. He proposed that reactions in crystals are controlled by the rigidity and topology of the crystal lattice, in what is now known as the topochemical postulate.<sup>18</sup> Qualitatively stated, the topochemical postulate indicates that *reactions in crystals can only occur with minimal atomic and molecular motion*.<sup>19</sup> In the mid-1960s the postulate was corroborated rigorously by Schmidt and coworkers when they correlated the photochemical  $2\pi + 2\pi$  reactivity of several cinnamic acid derivatives with their X-ray crystal structures.<sup>20</sup> They

confirmed that the configuration of the photochemically generated cyclobutanes is determined by the relative orientation of the double bonds within the crystal. Schmidt suggested that metric considerations determine the limits over which a  $2\pi + 2\pi$  reaction may or may not occur in the solid state. Heraldng the importance of pre-organization, he showed that photodimerizations require the two double bonds to crystallize parallel to each other with a center-to-center distance no longer than 4.2 Å.<sup>20,21</sup> He also showed that reactions in crystals tend to proceed with greater chemo- and stereoselectivity than analogous reactions in solution, which led him to suggest the possibility of “engineering” crystals to control the relative orientation of molecules for reactivity purposes.<sup>21</sup> Interestingly, Schmidt’s work on solid state chemistry has had the strongest influence in this discipline. Propelled by the recent maturity of supramolecular chemistry, crystal engineering has become a major research activity in many laboratories around the world.<sup>22</sup>

A few years after Schmidts’s pioneering work, Cohen offered a more general and intuitive suggestion that encompasses the principles behind the topochemical postulate.<sup>23,24</sup> He suggested that reactions in crystals can be thought of as occurring within a cavity, whose size and shape is determined by its own structure and the van der Waals surface of the surrounding close-neighboring molecules.<sup>25</sup> He suggested that attempts to distort the reaction cavity by a reacting molecule should be resisted by the nonbonding crystal potential, since close neighbors cannot move out of the way. He suggested that only those reactions capable of proceeding with minimal structural changes be allowed while all others are disfavored. Computational studies carried out in the last few years using current computational methods strongly support the reaction cavity model for several types of solid state reactions.<sup>26</sup> An idealized model representing the reaction cavity of *trans*-diphenyl-2-indanone **5** is shown in Figure 7.2. Note the loss of CO and the

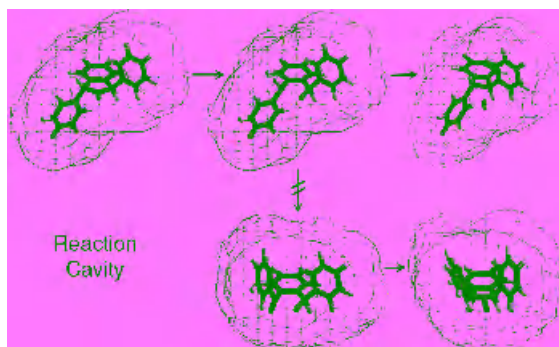


Figure 7.2. Idealized representation of the reaction cavity for the photodecarbonylation of *trans*-diphenyl-2-indanone **5** illustrating the reactant, the acyl-alkyl biradicals, and the final product with the molecules of CO trapped near its original lattice site. The excited states, biradical intermediates, and final products must fit within the space originally reserved for the ground state reactant. See color insert.

formation of *trans*-benzocyclobutane **7** by a shape- and volume-conserving, least motion pathway. A structure illustrating the changes in shape required to form the *cis*-biradical and *cis*-benzocyclobutane **7** highlights the forbidden nature of large amplitude conformational motions within the crystal.

### B. Molecularity

Elementary reactions in crystals can be unimolecular or bimolecular. Since most crystals are pure substances, solid state bimolecular reactions generally occur between identical partners.<sup>27</sup> As indicated by Schmidt, the main challenge in the reliable design of bimolecular reactions is that they require precise distances and orientations between potential reaction centers. In contrast, unimolecular reactions rely less on specific packing structures and more on conformational factors and the geometry and rigidity of the environment. Since it is difficult to predict packing motifs for bimolecular reactions in a reliable manner,<sup>28</sup> it should be more productive to focus on the design of unimolecular reactions.

### C. Energetic Considerations

While the topochemical postulate and reaction cavity concepts stress the importance of pre-organization and the forbidden nature of large amplitude motions, it is difficult to design viable chemical reactions in crystals with no insight into the driving forces required. To address this problem, an energetic formulation of the topochemical postulate is desirable:<sup>29</sup>

Since reactions in crystals can only occur under conditions where translational, rotational, and conformational forms of kinetic energy are kept at a minimum, viable reagents must not only be pre-organized, but they must have a high energy content. Molecules with high potential energy should be able to undergo spontaneous bond-breaking and bond-making processes despite the severe structural constraints that limits their atomic and molecular movement.

In search of general strategies, dissociative reactions are particularly promising as they require minimal pre-organization, tend to be determined mainly by enthalpic factors, and have positive reaction entropies. As illustrated in Figure 7.3a, reactants with high-energy content tend to have access to highly exothermic processes, which, as suggested by the Hammond postulate, have early transition states and low activation barriers. The main consequence of crystallizing the reactant in Figure 7.3a is that its motion becomes highly restricted by the nonbonding potentials of the reaction cavity—represented by parabolas over the reactant and the product coordinates in Figure 7.3b. As molecular motion within the crystal becomes more difficult, the transition state is primarily associated with the amount of work required to cause structural deformations to the reactant and

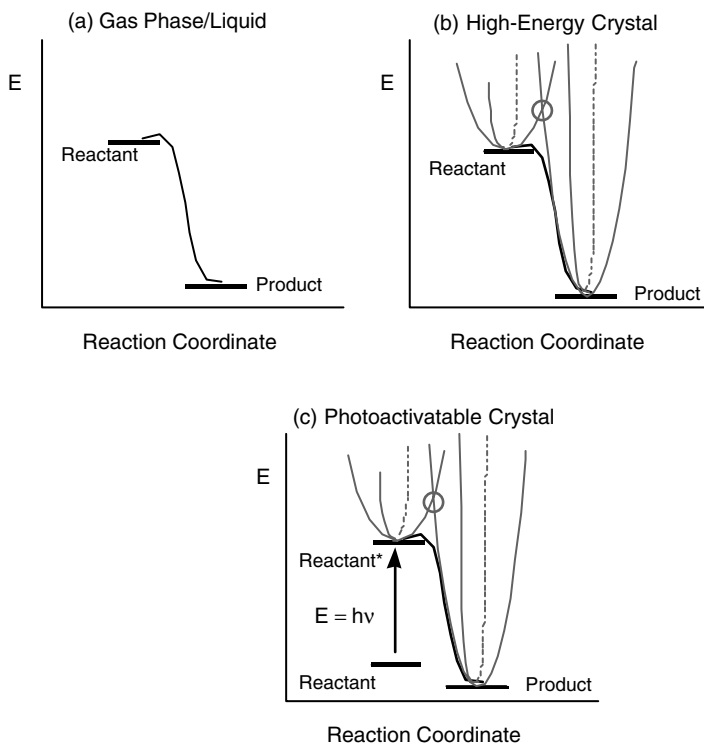


Figure 7.3. (a) Gas phase reaction coordinate for a high-energy reactant illustrating a highly exothermic reaction with a very early transition state. (b) The same reaction in a crystalline solid will be influenced by the crystal potential consisting of nonbonding interactions with close neighboring molecules. (c) Reaching a high-energy reactant within a crystal with photochemical excitation.

the lattice, represented by the point of intersection of the potentials corresponding to the reactant and the prospective product.

The situation depicted in Figure 7.3b represents the energetic profile of explosive materials. Obvious concerns can be avoided by selecting photochemical reactions where electronic excitation can add as much as 80 to 90 kcal/mol and one photon at a time (Figure 7.3c). Not surprisingly, the most documented solid state reactions are photochemically initiated: these include the  $2\pi + 2\pi$  photodimerization of olefins,<sup>20,21</sup> the intramolecular abstraction of  $\gamma$ -hydrogens by excited carbonyls,<sup>30</sup> and the di- $\pi$ -methane rearrangement.<sup>31</sup>

There may be many thermal and bimolecular solid state reactions amenable to synthetic applications. However, we have chosen to restrict our own research to unimolecular photochemical processes. Although this may seem too strong of a restriction, there is a wide variety of readily available crystalline compounds

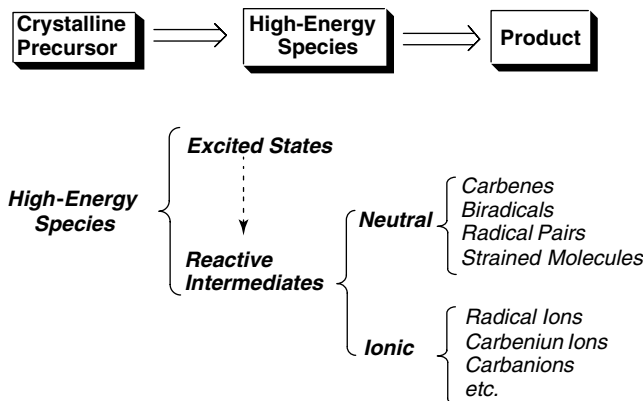
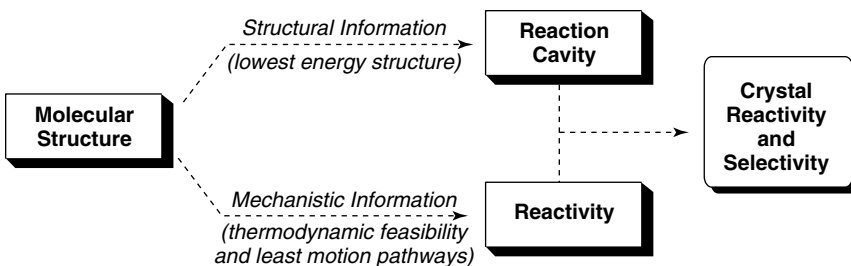


Figure 7.4. From stable crystals to selective product formation through high-energy species.

that can be photochemically activated to generate neutral and ionic high-energy species. We have recently studied the generation and reactivity of carbenes,<sup>25,29</sup> of oxonium ylides,<sup>32</sup> and of many radical pairs, and biradicals, which are the subject of this chapter (Figure 7.4). The appeal of these high-energy species is that their chemistry has been well characterized and their reactivity is reasonably predictable.

#### D. Molecular Structure as a Source of Information to “Engineer” Reactions in Crystals<sup>33</sup>

For reactions in crystals to be selective, their reaction cavities must be pre-arranged to favor the formation of one product significantly more than others. Many crystals favor no reaction at all, and render potential reactants kinetically stabilized. Efficient reactions in crystals also require the reactant and the product to have a similar size and shape. This way they can coexist within the same crystal lattice without perturbing other reaction cavities, which may change the outcome of the solid state reaction. As a general strategy to “engineer” reactions in crystals, one may postulate that molecular structures contain much of the information that determines solid state reactivity and crystallization properties (Figure 7.5). In fact, with today’s mechanistic knowledge and the power of computational chemistry, one can make reasonable predictions of chemical reactivity for a large number of structures and many chemical processes. In addition it is well known that most organic molecules crystallize in their lowest energy conformation so that molecular structure determines the size and shape of the reaction cavity, which can be determined with a high level of confidence using quantum mechanical



*Figure 7.5.* Molecular structure contains the information that determines crystallization properties and reaction cavity (top arrow) as well as the thermodynamic and mechanistic feasibility of reactions in solids (bottom arrow). The kinetic feasibility and selectivity are determined by the selection imposed by reaction cavity on potential reaction pathways.

and force-field methods. Ultimately unimolecular reactivity and selectivity are determined by whether a chosen structure possesses thermodynamically viable reaction pathways, and whether the reaction cavity is organized to make a given reaction kinetically feasible.

Ideally, with mechanistic information, simple conformational analyses, and chemical intuition, one is able to predict the feasibility of reactions in crystals by following the steps in Figure 7.5. Starting with a hand-drawn structure and some mechanistic knowledge, one can estimate the energy content of the ground state and chemical reactions likely to occur in the excited state. Concurrently, it is reasonable to assume that the lowest energy conformation predicted by a suitable computational method is the most likely to be represented in the crystal. With the lowest energy conformation available, one obtains some insight into the size and shape of the reaction cavity. Knowing that activated species such as excited state and reactive intermediates will be forced to exist within the confines of the reaction cavity, one can analyze the least motion pathways available, and predict the most likely product knowing that atomic and molecular displacements are usually kept at a minimum.

#### IV. FROM MOLECULAR INFORMATION TO REACTIVE CRYSTALS<sup>34</sup>

Although the work of Quinkert demonstrates the feasibility of the solid state photodecarbonylation reaction and illustrates its potential in terms of stereochemical control,<sup>13,15,17</sup> it does not provide a general approach that can be used to plan and design synthetic applications. As indicated in the previous section, to engineer reactions in crystals in a reliable manner, one must learn how to decipher the solid state reactivity and selectivity contained at the molecular structure level.

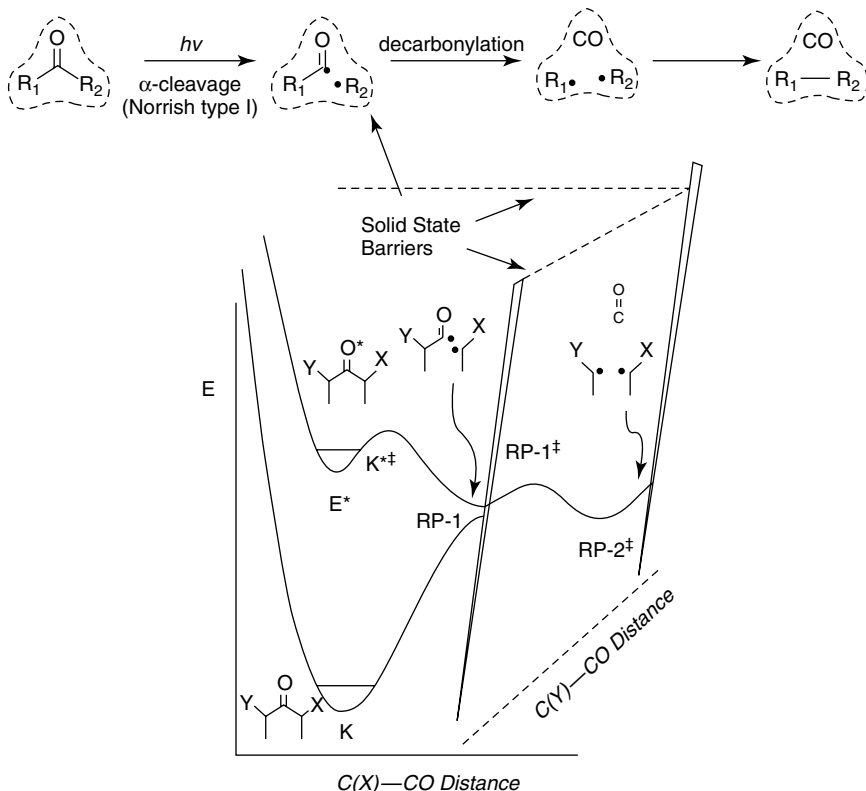


Figure 7.6. Reaction coordinates for  $\alpha$ -cleavage and decarbonylation from an excited crystalline ketone stressing how inter-radical distances are limited by the boundaries of the reaction cavity. The presence of small energy barriers for the two steps ( $K^{*\ddagger}$  and  $RP1^{\ddagger}$ ) is also illustrated in the Figure.

Molecular factors playing a role on the solid state decarbonylation reaction of crystalline ketones (K) can be analyzed with the help of the idealized energy surface in Figure 7.6.<sup>34</sup> Represented in this figure are the coordinates for the  $\alpha$ -cleavage [ $C(X)-COC(Y)$  distance] and decarbonylation steps [ $\bullet CO-C(Y)$  distance] that produce the alky-acyl (RP-1) and alkyl-alkyl (RP-2) radical pairs, respectively. The steric boundaries imposed by the reaction cavity form a reaction cage, which is represented by the dashed-lines in the figure. The reaction cavity restricts the separation of the two radical centers and inhibits large atomic and molecular displacements.

In the figure, the absorption of a photon introduces up to around 80 kcal/mol of energy to form the  $n, \pi^*$  excited state of the starting ketone ( $K + h\nu \rightarrow K^*$ ).<sup>10</sup> It is well known that both singlet and triplet  $n, \pi^*$  surfaces are dissociative and that

the energy of the transition state ( $K^{*\dagger}$ ) correlates with the stability of the radicals formed. If the energy content of RP-1 is lower than that of  $K^*$ , separation of the two fragments within the lifetime of the excited state to give the radical pair ( $K^* \rightarrow RP-1$ ) may be kinetically feasible. However, since the two radical centers cannot separate far from each other within the confines of the reaction cavity, they may easily go back to the ground state ( $RP1 \rightarrow K$ ), effectively wasting the energy of the photon. In fact, while this is probably true for most reactions occurring along the singlet state surface, those that occur along the triplet surface produce triplet radical pairs that may live long enough for decarbonylation to occur by stretching the  $C(Y)-CO$  bond along the other reaction coordinate. If this analysis is correct, one should expect the efficiency of the solid state reaction to increase for ketones (K) with high triplet energies, large triplet yields, and strongly exothermic  $\alpha$ -cleavage and decarbonylation reactions.

### A. Predicting Solid State Reactivity from Thermochemical Parameters

To be useful, the model in Figure 7.5 must have predictive power. Given that two bonds are broken and a new bond is made during the desired reaction, a structure-activity relation should be based on the effect of substituents on the two bond-cleavage reactions. Since most of the thermal energy within crystals exists in the form of many low-energy lattice vibrations and a few normal modes (rather than collisions, rotations, and conformational motions), it is reasonable to assume that thermal population of transition states and higher energy products should be very unlikely. For that reason, as suggested in Figure 7.3, bond-cleavage reactions in crystals should only be feasible when they have very low barriers and they are exothermic. With this assumption, a model can be formulated in terms of the energy content available within a molecule after photochemical excitation ( $E^*$ ), and the effect of  $\alpha$ -substituents (X and Y) on the bond dissociation enthalpies of the  $C(Y)-CO-C(X)$   $\alpha$ -bonds. Key to this model is a well-known correlation between reaction exothermicity and activation energies for  $\alpha$ -cleavage<sup>10</sup> and decarbonylation reactions,<sup>35</sup> the well-documented bond dissociation and radical stabilizing energies of a wide variety of substituents,<sup>36</sup> and the potential of calculating these parameters with reasonable accuracy.

As indicated in Figure 7.7, one may use thermochemical values for the decarbonylation acetone (X, Y=H) as a reference to evaluate the radical stabilizing effects of the  $\alpha$ -substituents and determine whether or not a bond-cleavage reaction will be exothermic. If the excitation energies remain fairly constant when X and Y are not conjugated with the carbonyl group, absorption of a photon introduces around 88 kcal/mol to form the singlet excited state.<sup>10</sup> Intersystem crossing to the triplet very rapidly releases about 8 kcal/mol, leaving roughly 80 kcal/mol available to break the two  $\alpha$ -bonds.  $\alpha$ -Cleavage in acetone

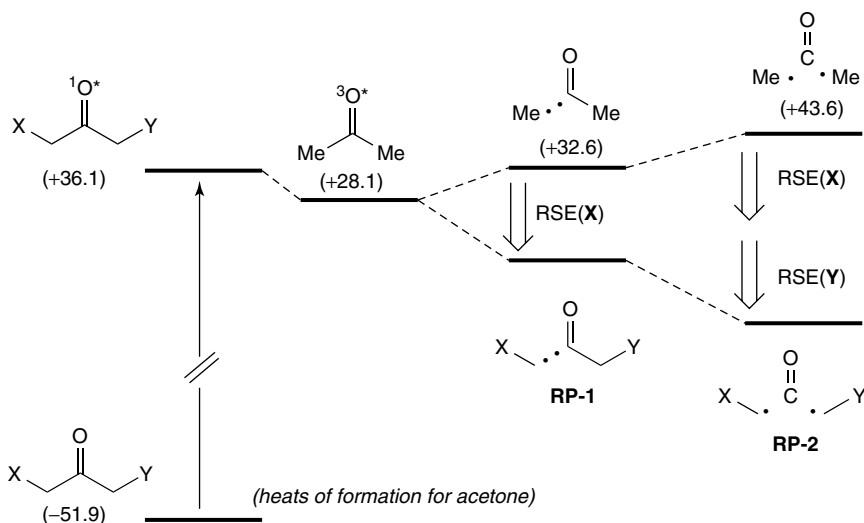


Figure 7.7. Thermochemical diagram for an excited state photodecarbonylation reaction comparing acetone ( $X=Y=H$ ) with an acetone derivative possessing radical stabilizing substituents  $X$  and  $Y$ .

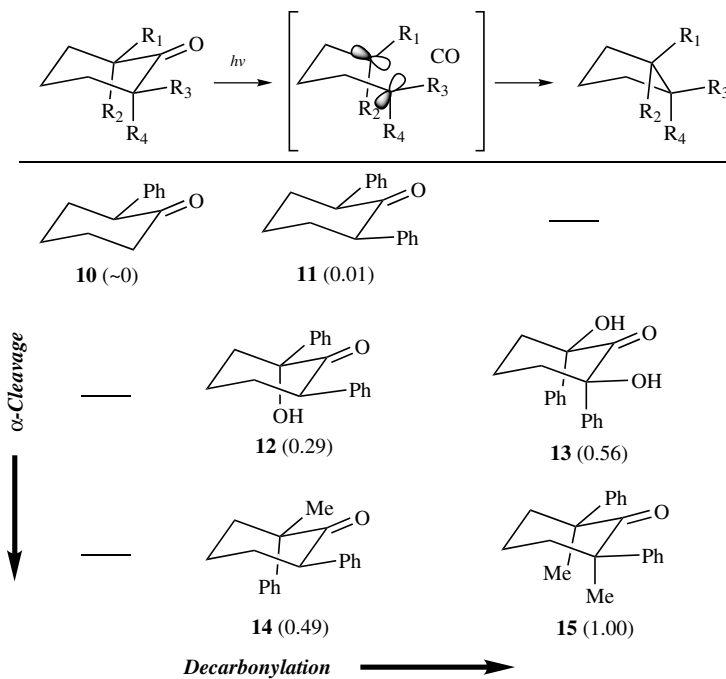
is endothermic by 4.5 kcal/mol and the loss of CO from acetyl radical requires an additional 11 kcal/mol. Not surprisingly, acetone can react in the gas phase and in solution (with low quantum yields), but alkanones are known to be stable in solid state polymers.<sup>37</sup> It is reasonable to postulate that analogues of acetone must have  $\alpha$ -cleavage and decarbonylation reactions that are exothermic in order to become reactive in the solid state. Since large changes in excitation energies for simply substituted ketones are unlikely, one can take advantage of substituents with large radical stabilization energies,  $RSE(X)$  and  $RSE(Y)$ , that will lower the bond dissociation energies of the two  $\alpha$ -bonds in a predictable manner. Radical stabilization energies of the substituents  $X$  and  $Y$  are defined as the difference between the bond dissociation energy of  $CH_3X$  (or  $CH_3Y$ ) and  $CH_4$  as  $RSE(X,Y) = [DH^\circ(X,Y-CH_2-H)] - [DH^\circ(H-CH_2-H)]$ .

Assuming that the weakest bond cleaves first, and knowing that the reaction is limited by the loss of CO, we may expect that groups with  $RSE$  greater than 11 kcal/mol will be required on both  $\alpha$ -carbons to make the reaction feasible. In agreement with this simple hypothesis, the examples from Quinkert et al. in Schemes 7.2 and 7.3 involve ketones with one or more phenyl groups on the  $\alpha$ -carbons. Published thermochemical data show that  $\alpha$ -phenyl,  $\alpha,\alpha$ -diphenyl, and  $\alpha$ -methyl- $\alpha,\alpha$ -diphenyl groups have  $RSE$  values of 16.5, 20.5, and 22.5 kcal/mol,<sup>36</sup> all of which exceed the suggested minimum of 11 kcal/mol.

### B. Ranking Reactivity as a Function of $\alpha$ -Substituents: Phenyl-Substituted Cyclohexanones

In one of the earlier trials and qualitative confirmations of our model, we tested the relative solid state efficiencies of 2-phenyl- and 2,6-diphenylcyclohexanones with 2-hydroxy, 2-methyl, 2,6-dihydroxy, or 2,6-dimethyl substituents (Scheme 7.6).<sup>38</sup> The selection of compounds **10–14** was based on the expected radical stabilizing effects of their  $\alpha$ -substituents, and their ability to form good crystals. In addition, since compounds **10–14** are all known to have very similar solution quantum yields ( $\Phi > 0.6$ ), we could correlate differences in their solid state reactivity to the effects of substituents.

To rank compounds **10–15** in order of their solid state photochemical reactivity, photochemical studies were carried out in side-by-side irradiations with polycrystalline samples dispersed in KBr matrices. The extent of reaction was conveniently determined with FT-IR by measuring changes in the absorbance of the CO stretch as a function of irradiation time. Although the solution photochemistry of **10–15** was very similar, the relative efficiencies of the solid



Scheme 7.6.

state reactions, shown in parentheses in Scheme 7.6, were remarkably large. The photostability of **10** and variations in quantum yields that span nearly 100-fold (e.g., **11** vs. **15**) can be understood in terms of the energy surface in Figure 7.5 if we assume that the efficiency of  $\alpha$ -cleavage is determined by substituents at C2 and the dissociation of CO bond by substituents at C6. Comparing the reactivity of **10** and **11**, we see that they both have phenyl substituents at C2 and can be expected to have similarly efficient  $\alpha$ -cleavage reactions. However, because the loss of CO from **10** would give a relatively unstable primary radical, the reaction is too slow to compete with intersystem crossing, so the singlet state of RP1 returns to the ground state ketone, rendering crystals of **10** unreactive. A small set of bond dissociation and radical stabilization energies is collected in Table 7.1. As shown in the table, the radical stabilization energy of an alkyl group is 4.5 kcal/mol, well below the suggested minimum of 11 kcal/mol, which reflects the relatively low stability of primary radicals. In contrast, the loss of CO in the case of **11** produces a resonance-stabilized secondary benzylic radical with a RSE = 19.6 kcal/mol, which makes decarbonylation possible.

Table 7.1  
C–H Bond Dissociation Energies and Radical Stabilization Energies  
of Selected Substituents

Radical Descriptor	Substituent(s)	BDE (kcal/mol)	RSE (kcal/mol)	SS Reactivity
Methyl	$-\text{CH}_3$	105.0	—	No
1ry alkyl	$-\text{CH}_2-\text{CH}_3$	100.5	4.5	No
2ry alkyl	$-\text{CH}(\text{CH}_3)_2$	98.1	6.9	No
3ry alkyl	$-\text{C}(\text{CH}_3)_3$	95.7	9.3	No
1ry benzylic	$-\text{CH}_2-\text{Ph}$	88.5	16.5	Yes
2ry benzylic	$-\text{CH}(\text{CH}_3)\text{Ph}$	85.4	19.6	Yes
3ry benzylic	$-\text{C}(\text{CH}_3)_2\text{Ph}$	83.5	21.5	Yes
2ry-hydroxy -benzylic	$-\text{CH}(\text{OH})\text{Ph}$	87.5	17.5	Yes
3ry-hydroxy -benzilic	$-\text{C}(\text{CH}_3)\text{OHPH}$	88.3	16.7	Yes
2ry bisbenzylic	$-\text{CH}(\text{Ph})_2$	84.5	20.5	Yes
3ry bisbenzylic	$-\text{C}(\text{CH}_3)\text{Ph}$	82.8	22.2	Yes
1ry enol (ester)	$-\text{CH}_2-\text{COOR}$	97.1	7.9 (8.9)	No
2ry enol (ester)	$-\text{CH}(\text{Me})\text{COOR}$	94.0	11.0 (15.07)	Yes
3ry enol (ester)	$-\text{C}(\text{Me})_2\text{COOR}$	92.6	12.4 (19.79)	Yes

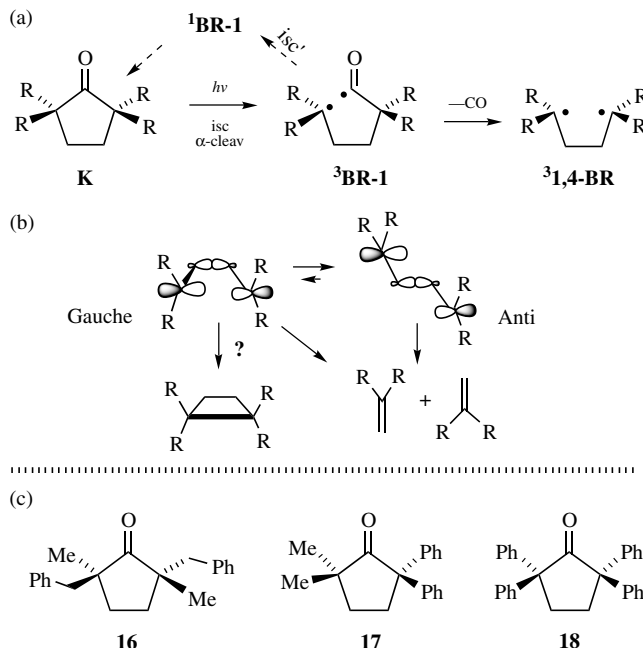
Source: Data from Luo.<sup>36</sup>

Note: Solid state reactivity is assumed to require RSE values greater than 11 kcal/mol. Values in parentheses were obtained from B3LYP/6-31G\*\* calculations in Campos and Garcia-Garibay.<sup>34</sup>

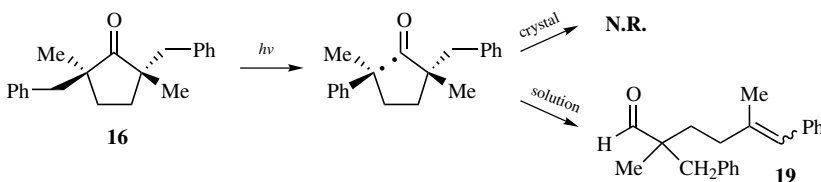
The relative solid state reaction efficiencies of compounds **11**, **12**, and **14** in the central column in Scheme 7.6 reach values of 0.01, 0.29, and 0.49, while those of **13** and **15** have relative values of 0.56 and 1.0. The effects of phenyl, hydroxy, and alkyl substituents in **12** and **13** can be estimated as RSE = 16.7 kcal/mol, and that of one phenyl and two alkyl groups in **14** and **15** as RSE = 21.5 kcal/mol (Table 7.1). If the weakest bond cleaves first, variations down a given column in Scheme 7.6 should reflect the effect of substituents on the efficiency of the  $\alpha$ -cleavage reaction and variation from left to right on each row the effect of substituents of the decarbonylation step. With the largest variations from **10** to **11** (0 to 0.001) and from **11** to **12** (0.001 to 0.29), it is clear that both steps must be optimized for the overall reaction to be efficient in the crystal. As expected, the highest solid state reactivities were observed in compounds **13** and **15**, which have the most radical stabilizing  $\alpha$ -substituents of the set.

### C. Testing the Effects of Phenyl and Alkyl Groups in Cyclopentanones

The effects of  $\alpha$ -alkyl and  $\alpha$ -phenyl substituents are documented in Peterfy et al. for the set of crystalline cyclopentanones **16–18** (Scheme 7.7).<sup>39</sup> The solid state photochemistry of cyclopentanones **16–18** can be used to analyze the effect of



Scheme 7.7.



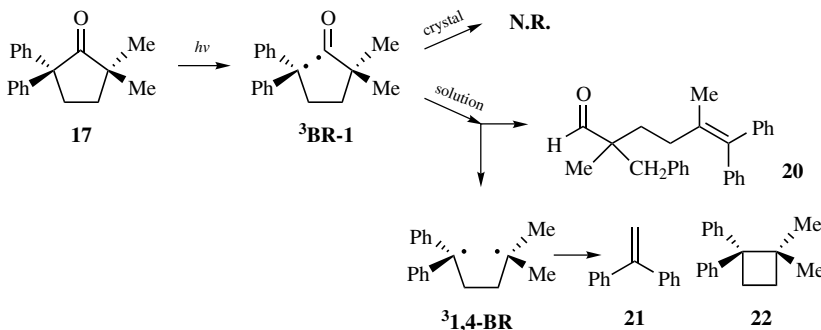
Scheme 7.8.

alkyl groups on the solid state photodecarbonylation reaction and the effect of the solid state on the chemoselectivity of 1,4-biradicals.<sup>40</sup>

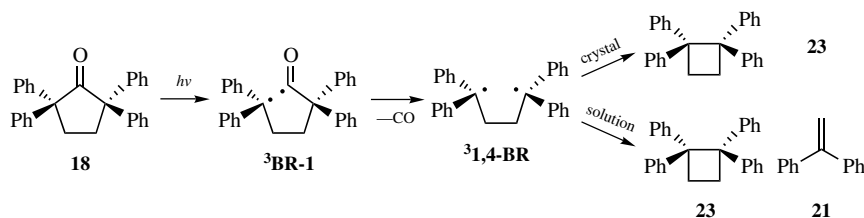
With *trans*-benzyl substituents ( $\text{Ph}-\text{CH}_2-$ ) only to improve its crystallinity, cyclopentanone **16** was analyzed to test the effect of two alkyl groups at each C2 and C5. The tetraphenyl derivative **18** was chosen as the most likely to undergo decarbonylation and thus ensured the formation of the 1,4-biradical in the solid state (Scheme 7.10). With two phenyl substituents at C2 and two methyl groups at C5, cyclopentanone **17** was prepared with the hope of ensuring  $\alpha$ -cleavage to test the effect of the methyl groups at C5 on the loss of CO.

The solution photochemistry of **16** in benzene gave enal **19** as a *trans:cis* = 2:1 mixture in a 0.9 quantum yield. It is worth noting that no cyclobutanes or alkenes that could be formed by decarbonylation were observed, strongly suggesting that decarbonylation is not a favored process, even in solution, for acyl radicals with alkyl substituents. As expected from this observation, no reaction was observed upon long irradiation in the solid state: the RSE value for two alkyl substituents is only 9.3 kcal/mol, slightly below the suggested 11.0 kcal/mol cut off.

The photochemistry of ketone **17** differs from that of **16** in that there is a low quantum yield of reaction ( $\Phi = 0.04$ ). At low conversion (10–20%), enal **20** is formed by disproportionation, indicating that  $\alpha$ -cleavage occurs on the weakest  $\alpha$ -bond, involving the carbon bearing the two phenyl substituents. Decarbonylation in solution leads to 1,1-diphenylethylene **21** and cyclobutane **22** to give a total product distribution of  $\mathbf{20}:\mathbf{21}:\mathbf{22} \approx 5:2:3$  (Scheme 7.9). In agreement with



Scheme 7.9.



Scheme 7.10.

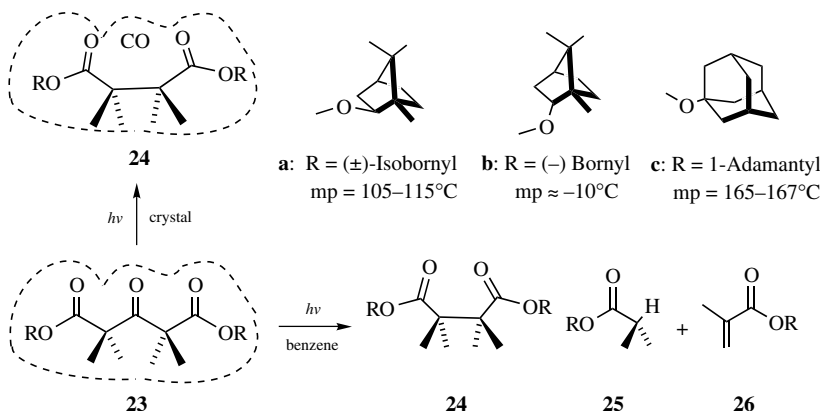
experiments carried out with crystals of **16**, there were no products formed upon photolysis in the solid state. With a RSE = 20 kcal/mol for two phenyl groups  $\alpha$ -cleavage is more than likely to occur in the crystal. However, if decarbonylation requires RSE > 11 kcal/mol, two methyl groups at C5 in ketone **17** only provide RSE = 9.5 kcal/mol, which is insufficient to enable the second reaction.

Not only was tetraphenylcyclopentanone **18** the only compound that reacted in the solid state, but reaction times for similar amount of reactant were as short in the crystal as in dilute benzene solution. Irradiation of polycrystalline samples of **18** (mp = 180–182 °C) gave cyclobutane **23** as the only product in >95% yield. This was an unprecedented degree of chemical control on the selectivity of cyclization against the cleavage reactions for 1,4-biradicals.<sup>41</sup> Although preferential formation alkene **21** with small amounts of **23** in solution reflects the formation of *anti* and *gauche* conformers, the *syn*-relation about the C3-C4 of the reactant is retained in the crystal by both the intermediate biradical and the product (Scheme 7.10).

#### D. Experimental and Computational Results with $\alpha$ -Alkyl- and $\alpha$ -Carbonyl ketones

Results from the literature analyzed in the previous sections indicate that crystalline ketones with at least one phenyl group on each of the two  $\alpha$ -carbons are photoreactive, while those with only an alkyl group at either or both  $\alpha$ -carbons are photostable. The RSE values of  $\alpha$ -substituents in reactive crystals (ketones **1**, *cis*- and *trans*-**5**, *cis*- and *trans*-**6**, **10–15**, and **18**) are all above 16.5 kcal/mol ( $\alpha$ -phenyl groups) and those of stable crystals of **16** and **17** are below 9.6 kcal/mol (tertiary alkyl). To narrow the limits of reactivity and to challenge the simple thermochemical model, the solid state reactivity of crystalline ketones with carbonyl groups in the  $\alpha$ -position was investigated by Yang et al. As indicated in Table 7.1, the of RSE values for primary, secondary, and tertiary  $\alpha$ -alkoxycarbonyl groups go from 7.9 to 11, to 12.4 kcal/mol.<sup>42</sup>

Keto diesters **23a–23c** (Scheme 7.11) were selected as the starting point to study solid state reaction.<sup>43</sup> The *iso*-bornyl diester **23a** was obtained as a diastereomeric mixture of four compounds and the bornyl diester **23b** as single enantiomer. The adamantyl compound **23c** was selected for its higher melting point.

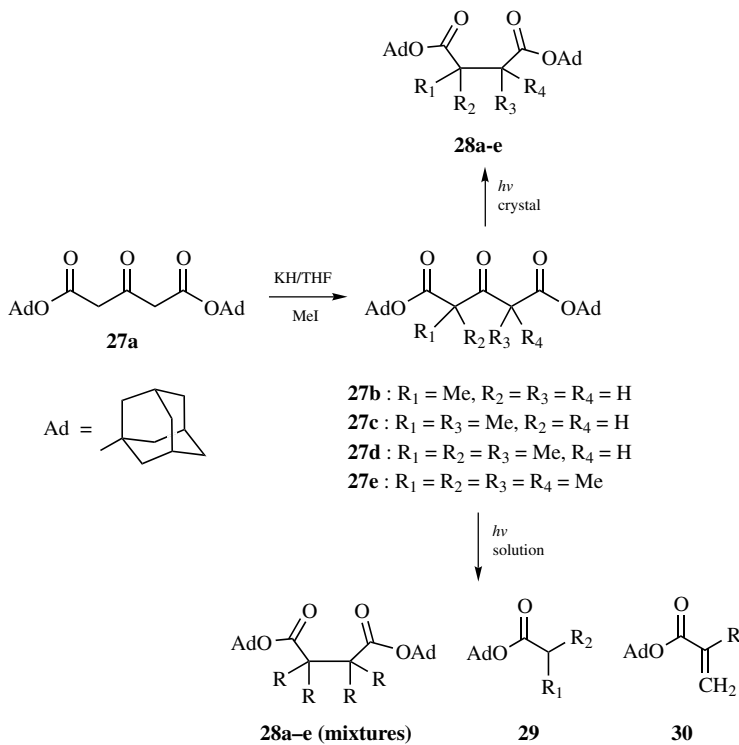


*Scheme 7.11.*

Irradiation of compounds **23a**–**23c** in benzene at room temperature gave diesters **24a**–**24c** along with  $\alpha$ -methylpropionates **25a**–**25c** and methacrylates **26a**–**26c**. As was predicted from the RSE values provided by the methyl and ester groups, the irradiations in the solid proceeded smoothly. Crystals of diester **23a** reacted to 70% conversion and gave compound **24a** as the sole product with 100% selectivity. The photochemistry of crystalline **23c** was also 100% selective toward **24c** at 88% conversion. Importantly, irradiation beyond these values at ambient temperature resulted in crystal melting and formation of propionates **25** and **26**. The solid state photochemistry of **23b** was complicated by the low melting points (m.p. = –10 °C) of the starting material and product. When photolyzed at –70 °C, crystals of **23b** gave a mixture of products even at 35% conversion. Diester **24b** was formed with 75% selectivity, with the remainder being propionate **25b**. Notably, the intermediate tertiary enol radicals undergo bond formation so long as the integrity of the solid phase is not compromised.<sup>43</sup>

The level of alkyl stabilization required to enable the solid state reaction was subsequently tested with compounds **27a–27e** (Scheme 7.12).<sup>44</sup> It was determined that the keto form was the tautomer present in all the compounds by solid state FT-IR and <sup>13</sup>C CPMAS NMR analysis, and it was shown that **27c** crystallized as a solid solution of *meso*: *d,l*-diastereomers in a 1:4 diastereomeric ratio (m.p. = 55–59 °C).

Irradiation of **27a**–**27e** in dilute benzene solutions gave mixtures of succinates **28a**–**28e**, acetates **29** and acrylates **30** after 4 h of irradiation. Photolysis conducted side-by-side to determine differences in decarbonylation efficiencies in the solid state (Figure 7.8) indicated that higher degrees of alkyl substitutions increase the efficiency of the decarbonylation reaction. With a limiting value of RSE = 7.9 kcal/mol for a single carbonyl at one or both  $\alpha$ -carbons, crystals of **27a** and **27b** were photostable (reaction was only observed in partially melted samples).<sup>44</sup>



Scheme 7.12.

The solid state photochemistry of *meso*- and *d,l*-27c was rather inefficient and melting was observed after around 8% conversion, as expected for the four-component mixture (*meso* and *d,l*) of starting material and products. Despite its limiting melting point, we were able to conclude that secondary enol radicals with RSE = 11 kcal/mol can be formed in crystals. Accordingly, irradiation of 27d proceeded more efficiently, and 27e was the most reactive sample of the set with reactions proceeding to high conversion values with an ideal chemoselectivity toward 28e. Notably the more heavily substituted ketones display the highest reactivity, with intermediate radicals that have a clear tendency to make a C–C bond between two adjacent quaternary centers.<sup>44</sup>

Because experimental thermochemical parameters from model compounds are not always available from published data, it is up to the chemist to ascertain the utility of quantum mechanical calculations that predict the feasibility of solid state reactions. To evaluate this approach, Campos et al. determined the RSE for all the methyl ester analogues of the compounds in Scheme 7.12 using B3LYP/6-31G\*\* methods.<sup>45</sup> Heats of formation at 298 K for acetone, and all the

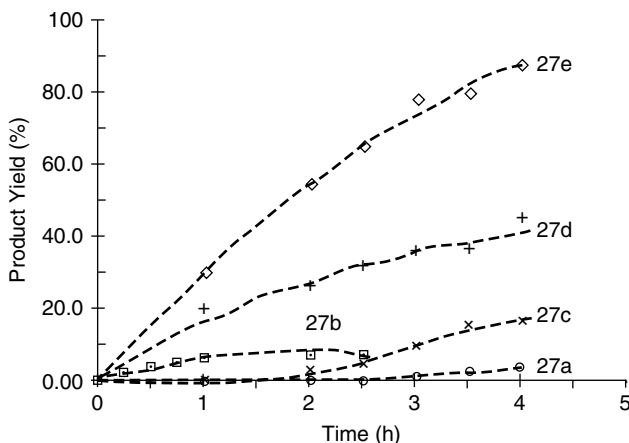
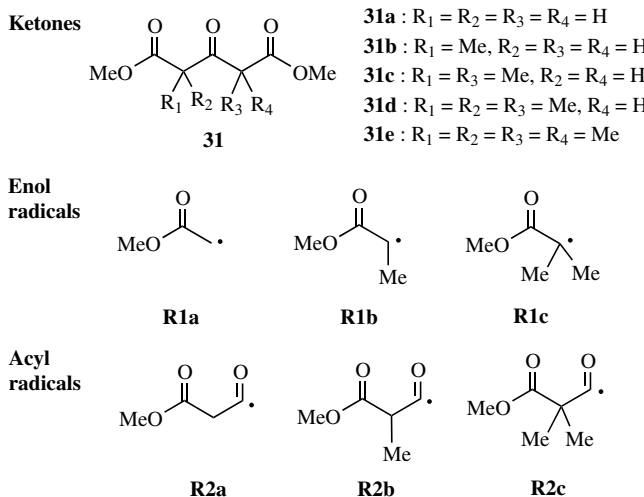


Figure 7.8. Relative rates for the photodecarbonylation of ketones **27a–27e** in the solid state as a function of irradiation time. Ketones **27a** and **27b** display sigmoidal behavior and begin to react after around 2 h. Mixtures of *meso*- and *d,l*-**27c** melted at ambient temperature after reaching about 10% conversion.

ketones, enol radicals, and acyl radicals in Scheme 7.13, were used to determine bond dissociation energies and reaction enthalpies. The results obtained are summarized in Table 7.2 and Figure 7.9. The radical stabilizing energies of a carbonyl ester alone and with one or two methyl groups were also obtained and



Scheme 7.13.

Table 7.2

Calculated Bond Dissociation Energies (BDE in kcal/mol) for the First and Second Bond Cleavage Reactions in the Decarbonylation of Acetone and the Keto diesters (**31a–31f**)

Reactant	BDE-1	Radicals (BDE-1)	BDE-2	Radicals + CO (BDE-2)
CH <sub>3</sub> COCH <sub>3</sub>	81.14	CH <sub>3</sub> , CH <sub>3</sub> CO	9.58	2 CH <sub>3</sub>
<b>31a</b>	72.38	<b>R1a, R2a</b>	-1.02	<b>2R2a</b>
<b>31b</b>	67.10	<b>R1a, R2b</b>	-1.02	<b>R2a, R2b</b>
<b>31c</b>	62.08	<b>R1a, R2c</b>	-1.02	<b>R2a, R2c</b>
<b>31d</b>	65.90	<b>R1b, R2b</b>	-6.49	2 R2b
<b>31e</b>	61.64	<b>R1b, R2c</b>	-6.49	<b>R2b, R2c</b>
<b>31f</b>	55.48	<b>R1c, R2c</b>	-9.48	2 R2c

are included in parentheses in Table 7.1. The B3LYP/6-31G\*\*-derived RSE value for the formation of a primary enol radical (8.9 kcal/mol) is in reasonable agreement with that obtained from the literature (7.9 kcal/mol). In contrast, the RSE values calculated for the formation of secondary and tertiary enol radicals are significantly greater than those reported in the literature. Instead of 11.0 and 12.4 kcal/mol, respectively, the calculated values are 15.07 and 19.89 kcal/mol.

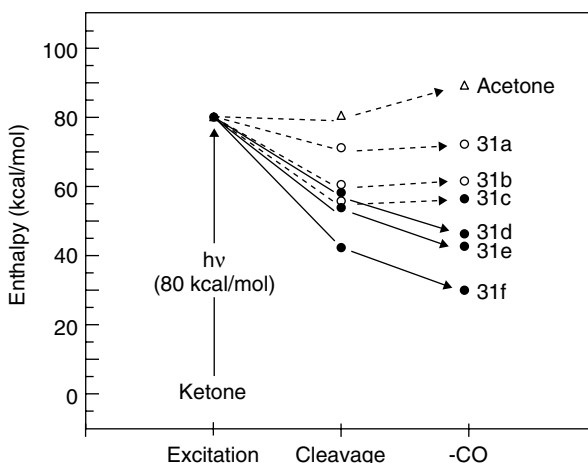


Figure 7.9. Calculated enthalpy changes upon electronic excitation (assumed 80 kcal/mol),  $\alpha$ -cleavage, and decarbonylation of acetone and keto diesters **31a–31f**. Acetone and **31a** react in solution with very low quantum yields. Compounds **31b–31f** react efficiently in solution. Compounds **31a** and **31b** are photostable in the solid state. Compound **31c** has not been investigated experimentally but is predicted to be reactive in solution and photostable in the solid state. Only **31d–31f** (black dots and solid arrows) react efficiently in the solid state.

While the results are quantitatively different, they are consistent with the solid state results and the postulated RSE>11 kcal/mol cutoff. A graphic summary of the computational results in Figure 7.9 shows a very good correlation between thermochemical parameters and reaction efficiencies.<sup>45</sup>

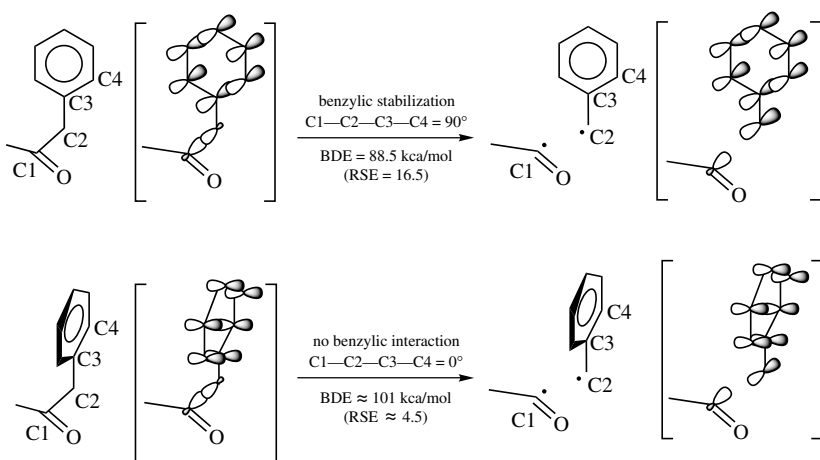
## V. SUBTLE (BUT PREDICTABLE) ASPECTS OF THE SOLID STATE PHOTODECARBOXYLATION REACTION

Several structural factors can lower the bond dissociation energies of ketone  $\alpha$ -bonds in a predictable manner. In principle, all one needs is a structure to consult the radical stabilizing effects (RSE) of the  $\alpha$ -substituents. Fortunately the RSE values of a large number of substituents can be frequently found in tables, or calculated with reasonable accuracy. However, it should be also realized that other factors play a role in determining the efficiency of the solid state reaction. Among these factors we have recently analyzed examples that highlight role of stereoelectronic effects, competing reactions, and internal quenchers.

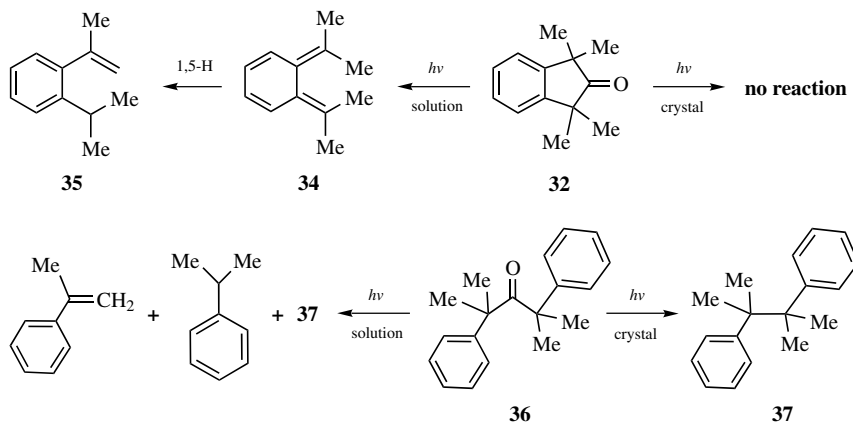
### A. Stereoelectronic Effects on Benzylic Stabilization

Stabilization of a radical center by resonance requires the singly occupied orbital to be aligned in a parallel fashion with its interacting  $\pi$ -system. Knowing that conformational motions in crystals are severely restricted, one should expect that crystallization of the reactant in a suitable conformation should be essential for the effects of resonance delocalization to be expressed. With regard to benzylic stabilization by an  $\alpha$ -phenyl group, it has been suggested that full conjugation and resonance account for 12.5 kcal/mol of the total stabilization energy provided by a phenyl group. The expected stereoelectronic requirement for benzylic interactions are illustrated in Scheme 7.14 for  $\alpha$ -cleavage reactions, but similar analysis should apply to decarbonylations.<sup>46</sup> Because the C1–C2 bond is broken and C2 rehybridizes from  $sp^3$  to  $sp^2$ , full resonance delocalization requires a C1–C2–C3–C4 dihedral angle of 90°, and no advantage can be drawn when the  $\alpha$ -phenyl group has a dihedral angle of 0°.

Crystals of 1,1,3,3-tetramethyl-2-indanone **32** have been used to demonstrate that crystalline ketones with  $\alpha$ -phenyl groups unable to adopt a dihedral angle C1–C2–C3–C4 = 90° cannot react efficiently in the solid state.<sup>47</sup> Compound **32** was investigated along with two others bearing ketal and thioketal groups in their  $\alpha$ -positions, which will be analyzed below. Unlike the  $\alpha,\alpha'$ -diphenylsubstituted 2-indanones studied by Quinkert et al. (Scheme 7.4),  $\alpha$ -cleavage and decarbonylation in **32** can only benefit from the effect of the benzene group within the ring system and the four  $\alpha$ -methyl groups. Since **32** is substituted with one phenyl group and two methyls in each  $\alpha$ -carbon, inspection of Table 7.1 will



suggest a RSE  $\approx 21.5$  kcal/mol for the formation of a tertiary benzylic radical. However, the perpendicular orientation between the C1–C2 bond undergoing cleavage and the plane of the aromatic  $\pi$ -system deprives it from the benefits of resonance stabilization, estimated at 12.5 kcal/mol. In fact, while solution photolysis of **32** proceeds smoothly to give the unstable *ortho*-quinodimethane **34**, which converts to styrene **35**, crystalline samples (m.p. = 75–76 °C) are completely photostable (Scheme 7.15). An interesting comparison can be drawn between



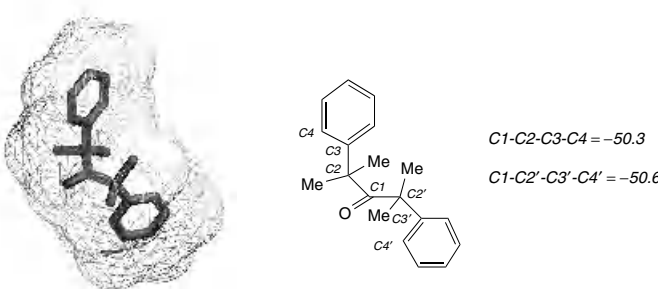
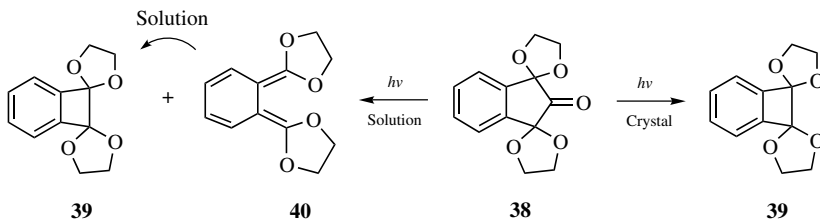


*Figure 7.10.* Reaction cavity of ketone **36** derived from its X-ray crystal structure with the equivalent line formula illustrating the dihedral angles that determine the extent of benzylic stabilization. See color insert.

ketones **32** and **36**, since the latter reacts efficiently in solution and in crystals. The conformation present in crystals of **36** has dihedral angles of 50.3° and -50.6° between bonds being broken and the plane of the phenyl groups (Figure 7.10). Although not very close to the ideal 90°, small amplitude librations of the phenyl group should facilitate the solid state reaction. As it is the case, in most solid state reactions analyzed so far, the chemoselectivity of **36** is ideal toward the formation of adjacent quaternary centers, up to >95% conversion.

A comparison of the results with crystals of **32** and **36** indicates that the benzene ring of 2-indanones is not stereochemically suited in the solid state reaction. With that observation, and motivated by a report by Leinweber et al.,<sup>48</sup> we decide to analyze the effect of *gem*-dialkoxy groups on the  $\alpha$ -positions of 2-indanone. Although there is limited information on the RSE of *gem*-dialkoxy groups, available data for dimethoxymethane show that the two oxygen atoms stabilize a C-centered radical by around 17 kcal/mol,<sup>49</sup> thus making ketals and acetals attractive functional groups for the solid state reaction. As reported by Leinweber et al., photolysis of the bis(ethylenedioxy) derivative of ninhydrin **38** in solution provides the bisketal **39** in about 48% yield at 100% conversion.<sup>1</sup>H NMR analysis of photolyzed samples showed the formation of the thermally and

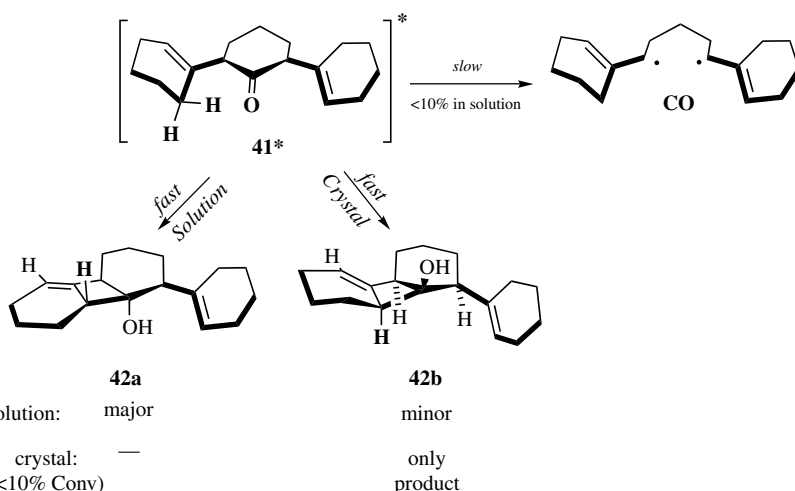


*Scheme 7.16.*

photochemically labile of *o*-xylylene **40** (Scheme 7.16), which may account for the low yield of **39** in solution. In contrast, photolysis of **38** in the solid state (m.p. = 115 °C) led to **39** as the only product after 25% conversion. Extended photolysis at ambient temperature resulted in melting and the formation of additional products suggesting the need of lower photolysis temperatures. It is interesting to note that the *o*-xylylene **40** was not detected in the solid state, which suggests that its formation is not topochemically allowed.

### B. Ultrafast Competing Reactions: $\gamma$ -Hydrogen Abstraction

The quantum and chemical yield of photochemical reactions depends on the rate of the reaction of interest as compared to those of other competing processes that deplete the excited state. Based on  $RSE \approx 15 - 18 \text{ kcal/mol}^{50}$   $\alpha$ -vinyl groups are predicted to make  $\alpha$ -cleavage and decarbonylation exothermic and viable in the solid state.<sup>51</sup> Crystals of *cis*-2,6-di(1-cyclohexenyl)cyclohexanone **41** (Scheme 7.17) were chosen as a test of this hypothesis based on their simple preparation from cyclohexanone and known crystallinity (m.p. = 79 °C).<sup>52</sup> Additional interest in the study of  $\beta,\gamma$ -unsaturated ketones comes from their rich photochemical possibilities, which included 1,3-acyl shifts, oxa-di- $\pi$ -methane rearrangements,  $2\pi + 2\pi$  cycloadditions, and  $\gamma$ -hydrogen abstraction.<sup>53</sup> Ketone **41** can exist in several rotamers with the equatorial cyclohexenyl groups having their alkenes either *syn* or *anti* to the carbonyl. In the latter case, an allylic  $\gamma$ -hydrogen is very close to the carbonyl *n*-orbital opening the possibility of a fast H-transfer reaction.



Scheme 7.17.

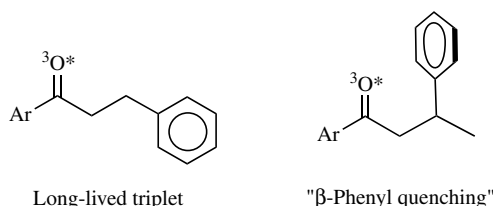
Photochemical experiments carried out in benzene solutions with  $\lambda > 300\text{ nm}$  revealed a complex product mixture that was constant as a function of conversion, suggesting that all products were stable under the reaction conditions. Analysis of the crude mixture by GC/MS showed that there were three minor products that had loss of CO ( $M^+ - 28$ ), which accounted for less than 10% of the total. The major products were isomeric with the starting ketone, and their mass spectra were characterized by an  $M^+ - 18$  peak, indicating that their structures had a tendency to lose water. The major products were confirmed by FTIR and rigorously characterized by 2D NMR, and were assigned as cyclobutanols **42a** and **42b**.<sup>54</sup> The products were formed in the ratio of 4:1 in solution.

Large needles of **41** from saturated methanol solutions required prolonged irradiation times (ca. 48 h) to achieve the accumulation of products. At less than 10% conversion at 300 K, the reaction yielded cyclobutanol **42b** with >90% selectivity. At higher conversions, the solid began to degrade, resulting in lower selectivities. An X-ray crystal structure of **41** revealed the origin for the preference of  $\gamma$ -hydrogen abstraction over  $\alpha$ -cleavage as one of allylic hydrogens is only 2.651 Å from the carbonyl oxygen, and therefore close to the carbonyl *n*-orbital. This distance is within the optimum value of 2.7 Å suggested by Scheffer,<sup>55</sup> thus explaining the dominant nature of the H-atom transfer reaction. The relatively sluggish solid state reactivity may be due to a singlet state reaction, which allows for relaxation back to the ground state by a well-known avoided crossing mechanism.<sup>56</sup> It is important to note out that the major cyclobutanol in the solid state is different from that observed in solution and that it correlates well with a topochemically allowed pathway. A conclusion drawn from these experiments is that  $\beta,\gamma$ -unsaturated ketones with allylic hydrogens positioned near the carbonyl oxygen are more likely to undergo  $\gamma$ -hydrogen abstraction than  $\alpha$ -cleavage and decarbonylation.

### C. Quenching by $\beta$ -Phenyl Groups<sup>57</sup>

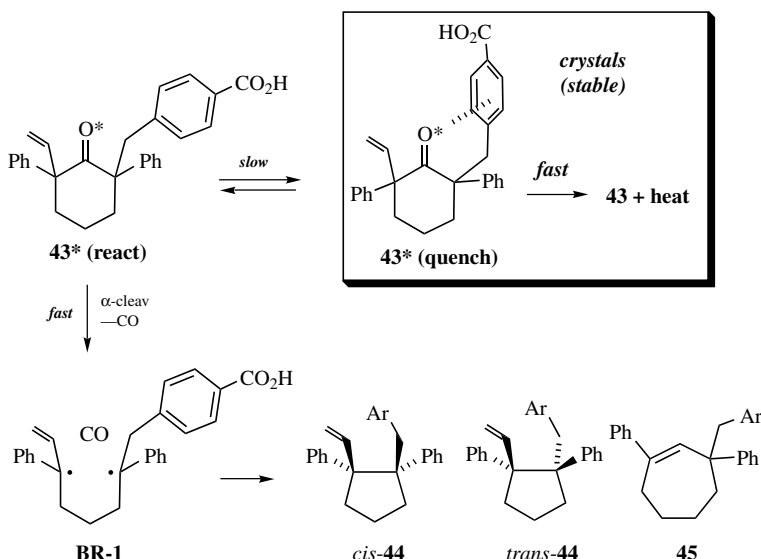
It is well known that ketones with  $\beta$ -phenyl substituents display conformation-dependent quenching. This interaction is thought to occur by a charge transfer interaction between the carbonyl *n,π\** excited state and the  $\beta$ -phenyl substituent (Scheme 7.18).<sup>58–61</sup> It had been shown that  $\beta$ -phenyl quenching may reduce triplet lifetime of crystalline propiophenones from 8  $\mu\text{s}$ , when they have no  $\beta$ -phenyl group, down to 0.7 and 0.4  $\mu\text{s}$ , depending on the proximity of the aryl substituent to the carbonyl in racemic and chiral crystals.<sup>62</sup>

To test the importance of this effect on solid state photodecarbonylation, we synthesized *cis*- and *trans*-2-(4-carboxybenzyl)-2,6-diphenyl-6-vinylcyclohexanone (Scheme 7.19) *cis*-**43** and *trans*-**43** from 2,6-diphenylcyclohexanone. Solution photolysis gave mixtures of both *cis* and *trans* cyclopentanes **44** as



Scheme 7.18.

well as cycloheptene **45**. The look of stereospecificity in the formation of **44** was expected as biradicals are free to explore many different conformations before forming the bond in the product. The three products were formed in a 10:5:1 ratio of *trans*-**44**:*cis*-**44**:**45**. Although solution experiments were relatively clean up to >95% conversion, UV light exposure of crystalline samples led to no reaction despite  $\alpha$ -carbon substituents expected to facilitate the reaction. Even at prolonged reaction times (12 h), crystals of *cis*-**43** (m.p. = 219–220 °C) and *trans*-**43** (m.p. = 200–202 °C) were photostable. Examination of their X-ray crystal structures showed that both compounds adopt twist-boat conformations with the benzyl group in a pseudoequatorial position. The presumed quenching interaction involves the carbonyl oxygen n-orbital pointing toward the edge of the



Scheme 7.19.

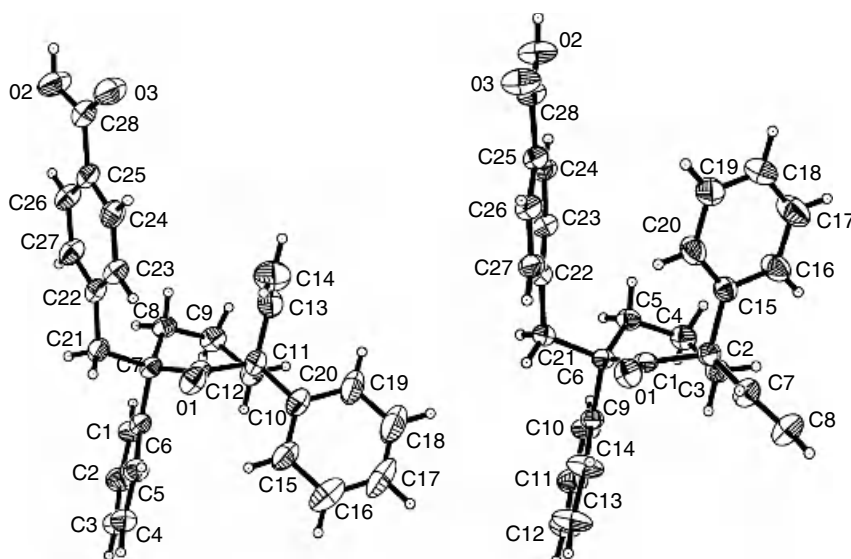
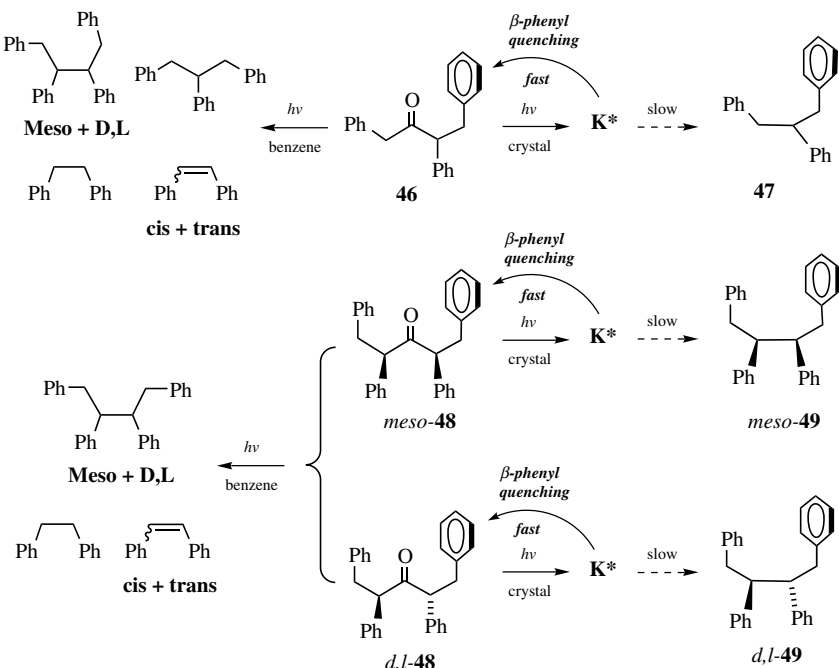


*Figure 7.11.* Ortep views of compounds *cis*-43 (left) and *trans*-43 (right) illustrating their twist-boat conformations and the disposition of the benzyl group with respect to the ketone carbonyl.

$\beta$ -phenyl ring. The distance between the oxygen and an *ortho*-carbon is 3.19 Å and 3.13 Å, for *cis*-43 and *trans*-43, and the two structures are such that the C=O bond is nearly eclipsed with respect to the  $\alpha,\beta$  sigma bond bearing the benzyl group (Figure 7.11). Notably, those distances are slightly less than the sum of the van der Waals radii of carbon and oxygen of 3.2 Å. We propose that this interaction is responsible for the deactivation of the excited state in crystals. In conclusion, while conformational equilibration may allow for the reaction to proceed in solution, the conformation and reaction cavity in crystals of *cis*-43 and *trans*-43 are predisposed toward  $\beta$ -phenyl quenching, so decarbonylation is not observed in the crystalline state.

Additional examples of  $\beta$ -phenyl quenching in crystals have been recently documented by comparing the relative solid state efficiency of  $\beta$ -phenyl-containing compounds with analogous structures lacking the quenching motif (Scheme 7.20). Recent studies from our group showed that photochemical reactions in crystals of triphenylbutanone **46** and *meso*- and *d,l*-**48** proceeded in very low yields after long irradiation periods (e.g., less than 5% conversion in 12 h). Notably reactions in crystals were highly chemoselective and stereospecific. As indicated in Scheme 7.20, the only products detected in crystals were those

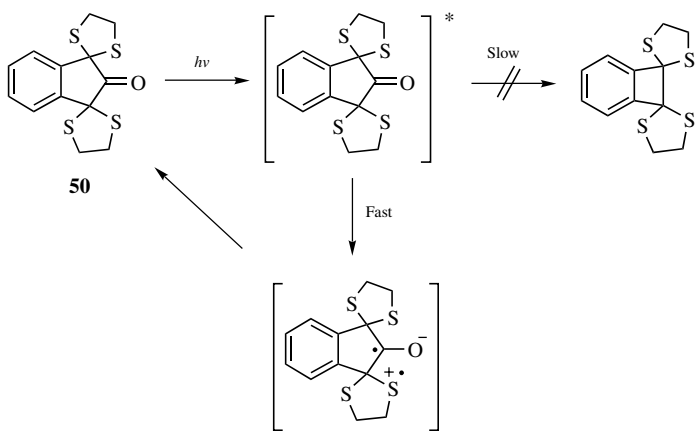


Scheme 7.20.

formed by decarbonylation and stereospecific radical-radical combination. The *meso*- and *d,l*-diastereomers of ketone **48** reacted to give diphenylethanes *meso*-**49** and *d,l*-**49**, respectively, as the only solid state products.<sup>63</sup>

#### D. Quenching by Electron Transfer<sup>47</sup>

When the photochemistry of 1,3-bis-(ethylenedithioxy)-2-indanone **50** was investigated to determine whether  $\alpha$ -thioketal substituents would facilitate the reaction in the solid state, crystals of **50** turned out to be completely stable.<sup>47</sup> Although there are no experimental or calculated RSE values for 1,3-dithianes, a single  $\alpha$ -sulfur atom in dimethyl sulfide has RSE = 11 kcal/mol,<sup>64</sup> suggesting that a thioketal with two sulfur atoms might make a crystalline ketone reactive. However, it is also known that sulfur atoms in thiols and sulfides have the ability to quench ketone excited states by electron transfer (Scheme 7.21).<sup>65</sup> In agreement with this expectation, the photochemical reactivity of **50** in solution was very inefficient, giving complex mixtures of uncharacterized products.



Scheme 7.21.

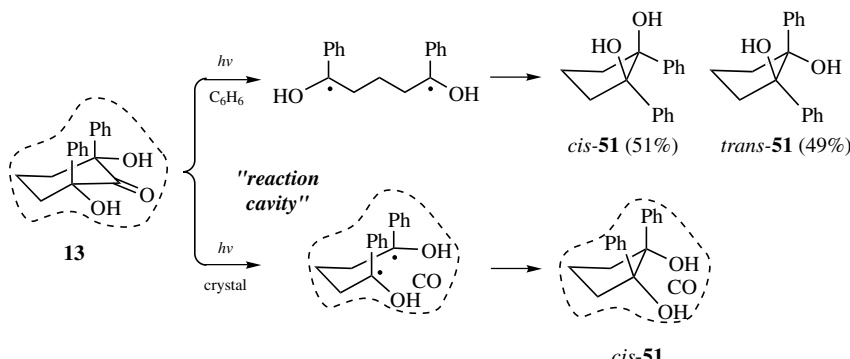
Crystals of **50** (m.p. = 197–198°C) were photostable under all photolysis conditions.<sup>47</sup>

We predict that analogous results should be expected with ketones possessing amines and electron-rich aromatic groups with low ionization potential, which may quench triplet ketones by electron transfer. In essence, one should expect that efficient quenching interactions identified in solution should carry on to the solid state.

## VI. STEREOCHEMISTRY OF THE PHOTODECARBOXYLATIONS REACTION IN CRYSTALS

### A. Stereospecificity and Scale Up

All the examples discussed in previous sections illustrate the controlling effect of the reaction cavity on the dynamics of biradicals and radical pairs. While a clear preference for “in-cage” radical-radical combination over disproportionation and fragmentation was observed in all cases, many studies were done in a relatively small scale and sometimes to limited conversion, primarily in search of mechanistic insight on the solid state reaction. Under those conditions, radical combination reactions were shown to proceed with excellent stereospecificity, as expected from size and shape similarities between reactant and product. In several cases the role of rigidity and homogeneity on the stereoselectivity of the reaction, and changes in reaction selectivity as a function of conversion, sample size, and temperature, have also been investigated. One of our earliest studies with



Scheme 7.22.

*cis*-2,6-dihydroxy-2,6-diphenylcyclohexanone **13** (Schemes 7.6 and 7.22)<sup>66</sup> is also one of the more detailed ones.

As expected for sequential  $\alpha$ -cleavage and decarbonylation steps where the intermediates biradicals are allowed to explore their most stable extended conformations (Scheme 7.22, top), excitation of **13** in dilute benzene solutions led to cyclopentanes *cis*-**51** and *trans*-**51**. Although no other products were formed and the solution reaction was remarkably clean, radical combination occurred with no stereochemical preference, yielding nearly identical amounts of the *cis* and *trans* products. When photochemical reactions were carried out with 2 to 5 mg samples of finely powdered crystals dispersed between two microscope slides at 298 K with  $\lambda > 350$  nm, *cis*-**51** was the only product observed up to around 95% to 98% conversion. Satisfyingly, when reactions were scaled up to nearly 1 g using a finely powdered solid, a 19:1 ratio of *cis*-**51** to *trans*-**51** was obtained with conversion values to greater than 95%. Dissolution and recrystallization of the product mixture provided pure samples of *cis*-**51** in an overall excellent chemical process. The selectivity of the reaction was easily explained from expectations of the size and shape of the reaction cavity of the starting ketone in its own crystal lattice. X-ray crystallographic analysis showed compound **13** to crystallize in a chair conformation with both phenyl groups in an axial orientation while the equatorial hydroxyl groups were involved in extended hydrogen-bonding chains. X-ray analysis also showed that the structure of the major product has a high degree of geometric congruence with that of the reactant, thus explaining their ability to coexist within the same crystal lattice (Figure 7.12).

Reactions monitored as a function of conversion by solid state  $^{13}\text{C}$  NMR with cross polarization and magic angle spinning (CPMAS), and by solid state FT-IR with microcrystalline samples in KBr matrices, revealed a clean conversion of the reactant to the crystalline product with no intermediate solid phases and no

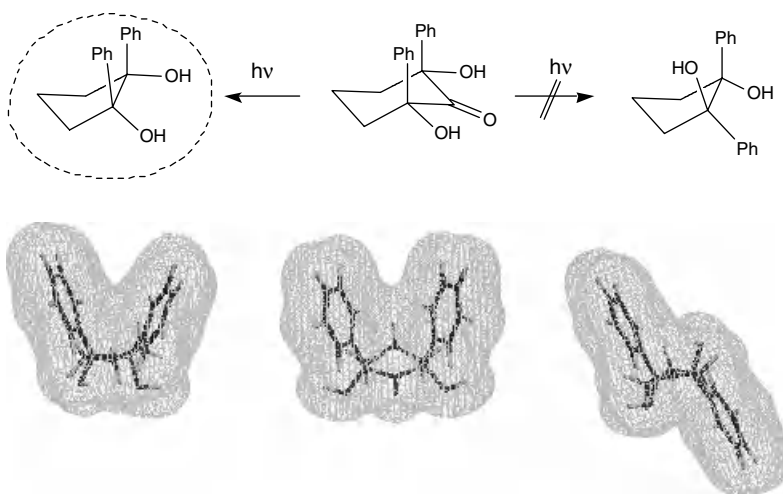


*Figure 7.12.* A comparison of the X-ray crystal structure of ketone **13** with those of its two combination products (*cis*-**51** on the left and *trans*-**51** on the right) helps rationalize the high selectivity observed when reactions are carried out in crystals. A van der Waals surface is shown to help visualize the size and shape of the reaction cavity.

detectable byproducts. It was shown that the spectra of “as-formed” products were identical to those of recrystallized samples, even though the packing structures of the reactant and the product were quite different. This observation indicated that a phase transition had occurred along with reaction. Thermal analysis by differential scanning calorimetry (DSC) showed the expected depression of the melting point of the reactant as a function of reaction progress, and revealed the coexistence of two solid phases with a eutectic temperature of 85 °C. The importance of the eutectic temperature comes from the fact that there can be no liquid phases below that point, indicating that experiments at 25 °C occur in the solid state. A series of experiments using alcohols and an amorphous sucrose glass (caramel) as reaction media showed that viscosity changes over eight orders of magnitude are not enough to achieve the selectivity observed in the crystal (Figure 7.13.).

Experiments also showed that high reaction selectivities in crystals require control of excitation wavelength. Given that crystalline solids are very strongly absorbing media, irradiations carried out at the tail of the UV-Vis absorption spectrum must be used to facilitate penetration of light deep into the bulk of the solid. It is frequently observed that microcrystalline samples retain the selectivity observed in large single crystals while minimizing the problems associated with the limited penetration of light into the large single crystals. Excitation into the lowest energy levels of the excited state also limits local heating from internal

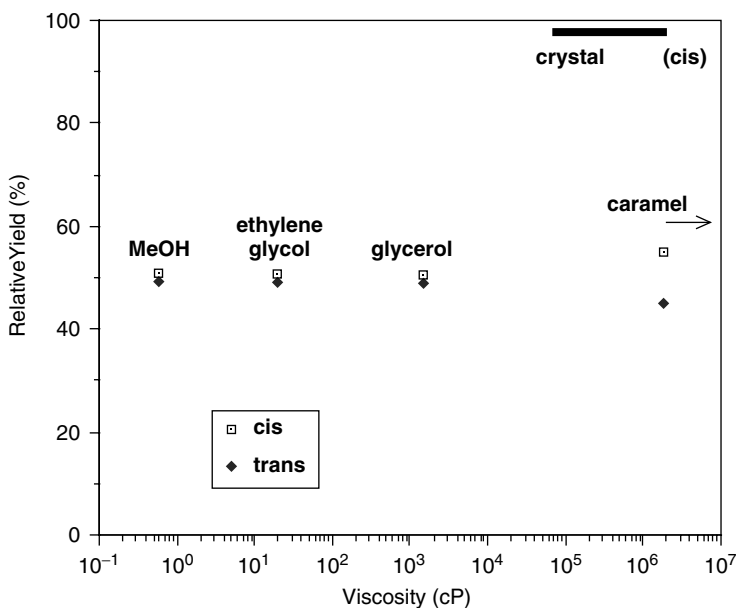
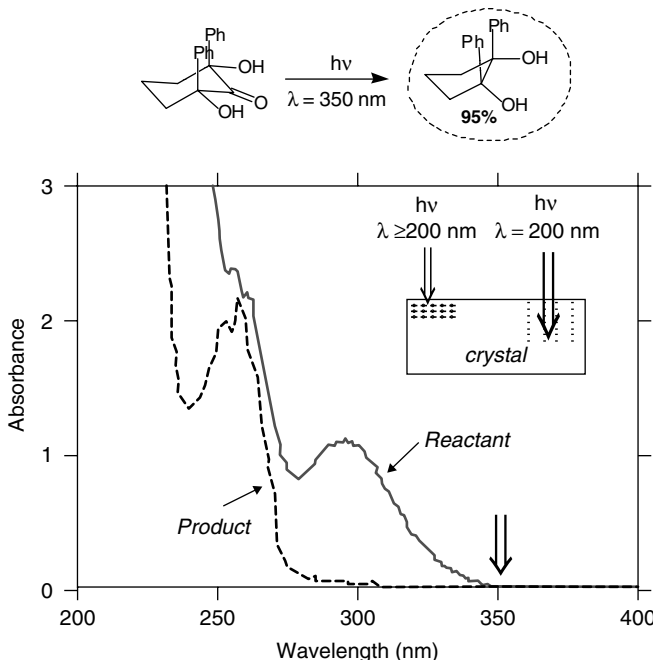


Figure 7.13. Effect of viscosity on the selectivity of product formation upon decarbonylation of *cis*-2,6-diphenyl-2,6-dihydroxycyclohexanone **13**. The viscosity of sucrose glasses (caramel) noted in the plot is the value reported value at 100 °C.<sup>67</sup>

conversion and helps prevent local melting. Furthermore, light absorption by the photoproduct should be completely avoided. In the case of ketone **13**, irradiation was carried out with monochromatic light at  $\lambda = 350\text{ nm}$  or with a  $\lambda > 350\text{ nm}$  using a cutoff filter (Figure 7.14).

We have suggested that photochemical reactions in solids occur heterogeneously with a reaction front determined by exposure to light. When product molecules begin to form, they go into a solid solution in the crystal lattice of the reactant until the solubility limit is attained (mixed crystals, Figure 7.15). As the mole fraction of product molecules continues to increase, a new crystal phase begins to nucleate with a composition that may include both the product and the reactant. The coexistence of two solid phases and two components causes the formation of a eutectic point, and this determines the lowest temperature at which liquid phases can exist. Several examples of eutectic transitions in reacting crystal have been documented in the literature by differential scanning calorimetry (DSC). It has been suggested that reactions in crystals are more likely to proceed with the desired control when carried out at temperatures that are below the eutectic transition.



*Figure 7.14.* UV absorption spectra of ketone **13** and its solid state photoproduct *cis*-**51** illustrating the wavelength selected for excitation in the solid state ( $\lambda \geq 350$  nm). Irradiation at this wavelength allows for deeper penetration in the crystal and reduces local heating from excess photon energy.

## B. Diastereo- and Enantiospecific Syntheses of Vicinal Tertiary and Quaternary Centers

The need for a robust method for the generation of diastereomerically and enantiomerically pure compounds with adjacent tertiary and quaternary centers has been discussed in several reviews.<sup>68</sup> To that effect, crystalline samples of 2-carbomethoxy-4-cyano-2,4-diphenyl-3-butanone **53** were prepared in enantiomerically pure and racemic forms.<sup>69</sup> From a survey of the literature data it appears that the phenyl, carbomethoxy, and methyl groups at C2 should lower the BDE of the C2–C3 bond by around 25 kcal/mol, making the  $\alpha$ -cleavage reaction highly exothermic and efficient.<sup>70</sup> Similarly, decarbonylation of the acyl radical should be facilitated by the phenyl and cyano substituents at C4, which are expected to provide RSE values of around 22.7 kcal/mol.<sup>36</sup> Enantiomerically pure and racemic (2*R*, 4*S*)-2-carbomethoxy-4-cyano-2,4-diphenyl-3-butanone **53** were synthesized from methyl malonates **52a** and **52b** as illustrated in Scheme 7.23.

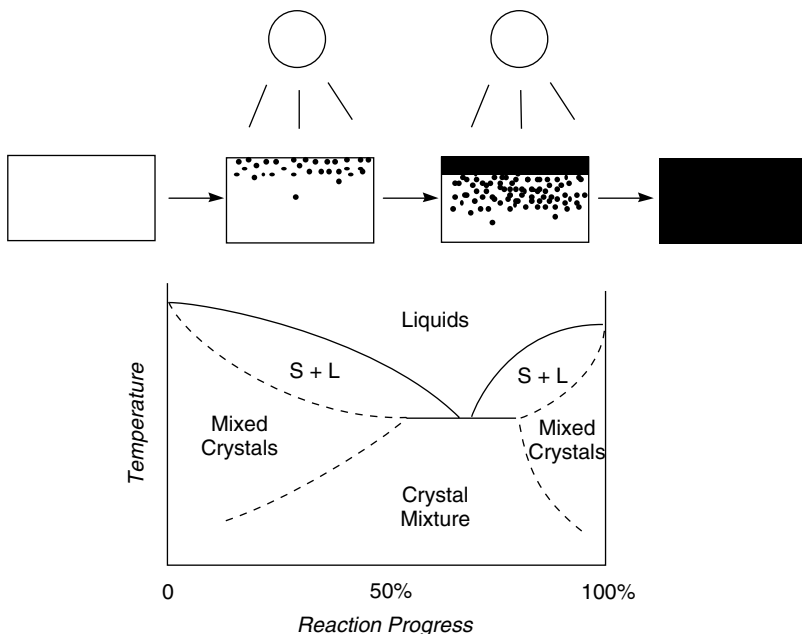
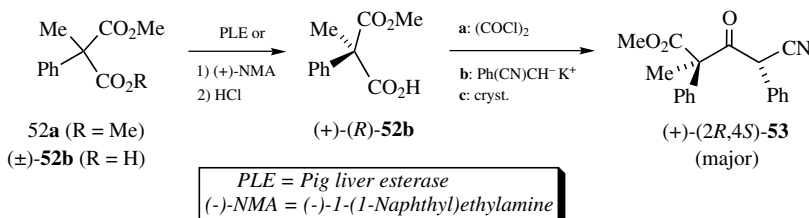


*Figure 7.15.* Schematic representation of the phase diagram for a solid state reaction that occurs by formation of a solid solution and separation of the product phase. Reactions in crystals must be carried out at temperatures below the eutectic of the two-component phase diagram to ensure that reaction occurs in the solid phase.

Enantiomerically pure samples of monoacid **52b** were prepared by enzymatic kinetic resolution of diester **52a** with pig liver esterase or by classic kinetic resolution with enantiomerically pure  $\alpha$ -methylnaphthylamine followed by recrystallization. Ketone **53** was obtained by nucleophilic substitution of the acyl chloride of acid **52b** with the anion of benzyl cyanide followed by recrystallization.



*Scheme 7.23.*

Irradiation of  $(+)-(2R,4S)$ -**53** and  $(\pm)-(2R,4S)$ -**53** in oxygen-free 0.1 M benzene solutions with a medium pressure mercury Hanovia lamp using a Pyrex filter ( $\lambda > 290$  nm) at 298 K gave complex product mixtures. In contrast, solid state reactions were highly selective with only one product being formed by combination of the intermediate radical pair. Finely powdered crystals (50 mg) of  $(+)-(2R,4S)$ -**53** and  $(\pm)-(2R,4S)$ -**53** irradiated to 40–60% conversion gave the expected radical combination products **54** with  $>95\%$  stereospecificity. The relative configuration of the products, determined by X-ray diffraction analyses, confirmed the stereospecificity of the solid state reaction (Figure 7.16). Compound

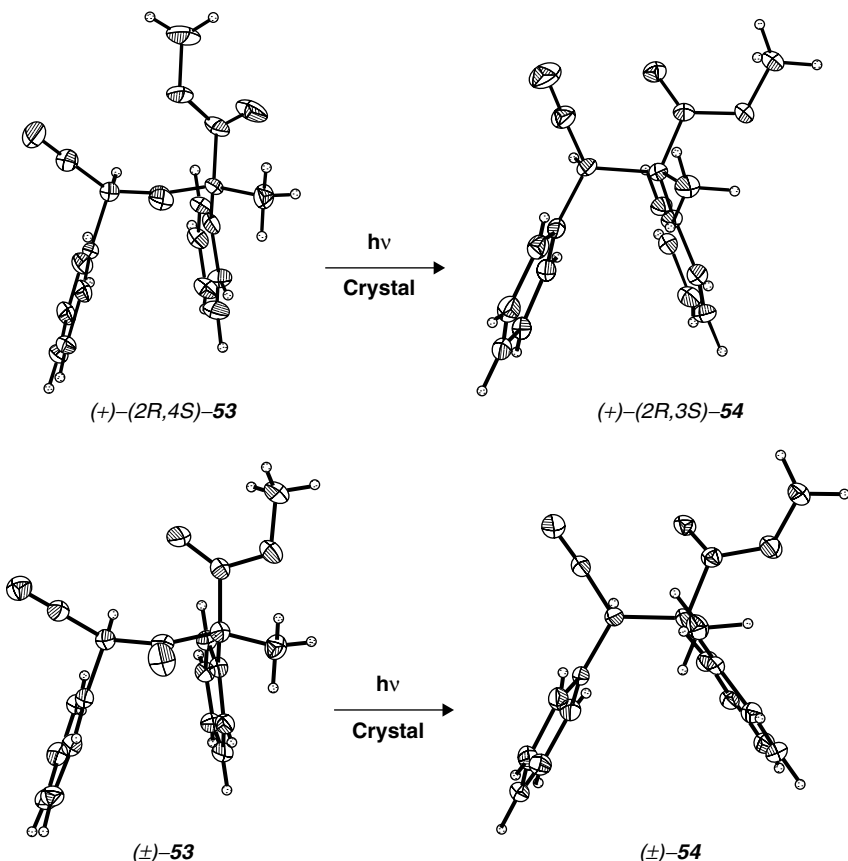


Figure 7.16. ORTEP diagrams of (top)  $(+)-(2R,4S)$ -**53** and its solid state product  $(+)-(2R,3S)$ -**54**, and (bottom) ORTEP diagrams of  $(\pm)-(2RS,4SR)$ -**53** and the racemic solid state photoproduct  $(\pm)-(2R,3S,3R)$ -**54**. Of the racemic crystals only the  $(2R,4S)$ -**1** and  $(2R,3R)$ -**2** enantiomers are illustrated.

(+)-(2*R*,4*S*)-**53** (m.p. = 66–68 °C) crystallizes in the hexagonal space group *P*6<sub>5</sub> with six ketones and one disordered hexane molecule per unit cell. Compound (±)-(2*R*,4*S*)-**43** (m.p. = 97–100 °C) crystallizes in space group *P*2<sub>1</sub>/*c* with four molecules per unit cell and no solvent of crystallization.

The X-ray structures of both ketones are typified by a conformation in which the 2-methyl and 4-cyano groups are eclipsed with the carbonyl group of the ketone and the 4-phenyl groups in a staggered conformation. The difference between the racemic crystals and the optically active crystals is in the ester carbonyl. The ester carbonyl points away from the cyano substituent in the crystals in the enantio-enriched material, and toward the cyano substituent in the racemic compound.

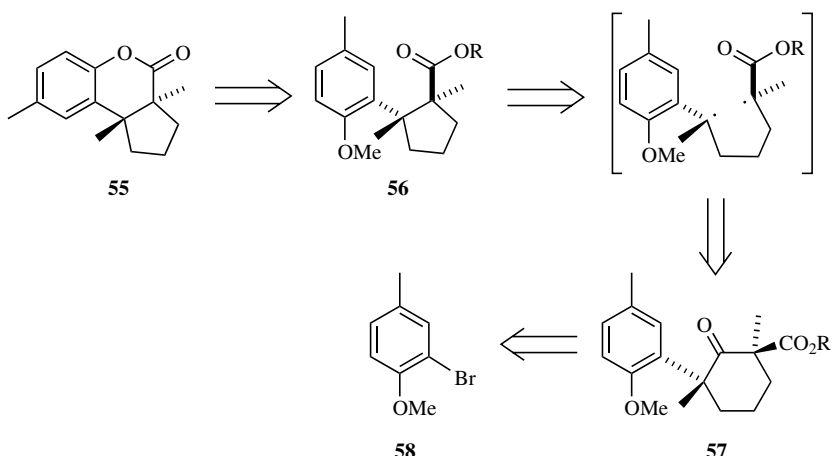
The X-ray crystal structures of (+)- and (±)-**54** were also obtained after dissolving crystals of reacted (+)- and (±)-**53**, respectively (Figure 7.16). DSC analysis of (±)-(2*R*,4*S*)-**53** before and during the reaction showed the formation of a broad eutectic point centered at 60 °C, which indicates that the reaction proceeds by a phase separation mechanism. The solvent of crystallization makes the phase diagram more complicated in the case of (+)-(2*R*,4*S*)-**53**.

### C. Total Synthesis of (±)-Herbertenolide by Stereospecific Decarbonylation of a Crystalline Ketone

With a promising working model to recognize the criteria that determine the structural, energetic, and entropic demands of the solid state decarbonylation reaction, it only remained to test it in the synthesis of a natural product with a nontrivial structure. As a test case we selected the sesquiterpene natural product herbertenolide **55**.<sup>71</sup>

Herbertenolide was first isolated and characterized by Matsuo et al.<sup>72</sup> from the leafy liverwort *Herberta adunca*, whose extract has been shown to exhibit a remarkable growth suppression of certain plant pathogenic fungi. To date, there have been only two reported syntheses by Eicher et al.<sup>73</sup> and Fukuyama et al.<sup>74</sup> Its structure is characterized by a tricyclic cyclopentabenzopyranone base system with a five-six ring junction that included two adjacent quaternary centers with a *trans*-dimethyl motif (Scheme 7.24). The retrosynthetic analysis outlined in Scheme 7.24 suggests that formation of the lactone ring might proceed spontaneously after hydrolysis of the ester and deprotection of the ether group in **56**. The preparation of ester **56**, which contains the target vicinal quaternary centers, is formulated by the key stereospecific solid state photodecarbonylation of the cyclohexanone precursor **57**, which was prepared by conventional methods from bromoanisole **58**.

When planning the solid state reaction, the nature of the groups at the quaternary carbons should be evaluated in terms of their potential as radical stabilizing substituents, their involvement in side reactions and quenching processes, as well



Scheme 7.24.

as their effect on the crystallinity of the precursor. In the case of ketone **3** the formation of tertiary benzylic and tertiary enol radicals bode well for the excited state  $\alpha$ -cleavage and acyl radical decarbonylation reactions. The electron-rich nature of the *para*-methylanisole group could be a matter of concern in terms of its potential quenching abilities by intramolecular electron transfer to the  $n,\pi^*$ excited state. Fortunately this potential complication did not occur in the case of **57**. Although the melting point of the novel ketone **57** could not be anticipated, we had confidence that both ester and aryl-ether groups would be amenable to the preparation of a wide variety of derivatives, which would make it possible to find a crystalline compound with relative ease. The preparation of the simple methyl ester derivative **57** was selected as a test to develop a concise synthetic strategy (Scheme 7.25).

As illustrated in Scheme 7.25, the synthesis of ketone **57** began with commercial 2-bromo-4-methylanisole **58**. Lithium halogen exchange and treatment with cyclohexene oxide and  $\text{BF}_3\text{OEt}_2$  gave *trans*-cyclohexanol **59**, which was submitted to Swern oxidation to the corresponding cyclohexanone **60**. Ketone **60** was then methylated stepwise to produce the 2,6-dimethyl derivative **61**, which reacted with Mander's reagent to give the desired ketone **57** with the *trans*-dimethyl configuration controlled by acylation of the enolate on the face opposite to the bulky aryl group. Ketone **57** turned out to be highly crystalline (*m.p.* = 96–97 °C) and its relative configuration was confirmed by a single-crystal X-ray diffraction analysis (Figure 7.17). The conformation of **57** is such that the methyl ester is axial and the aryl group equatorial, both with torsion angles that

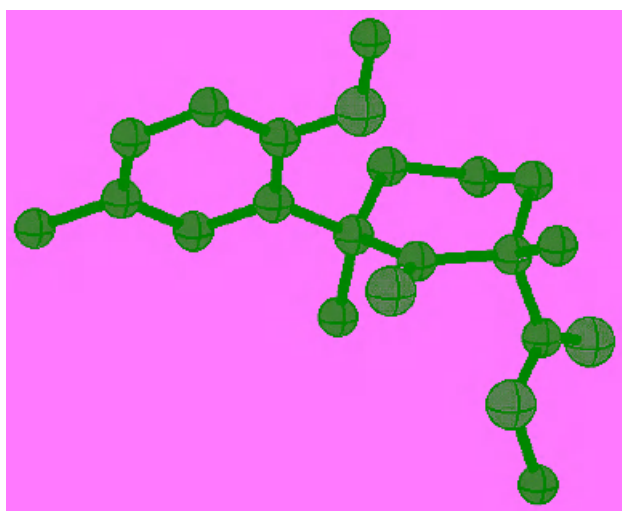
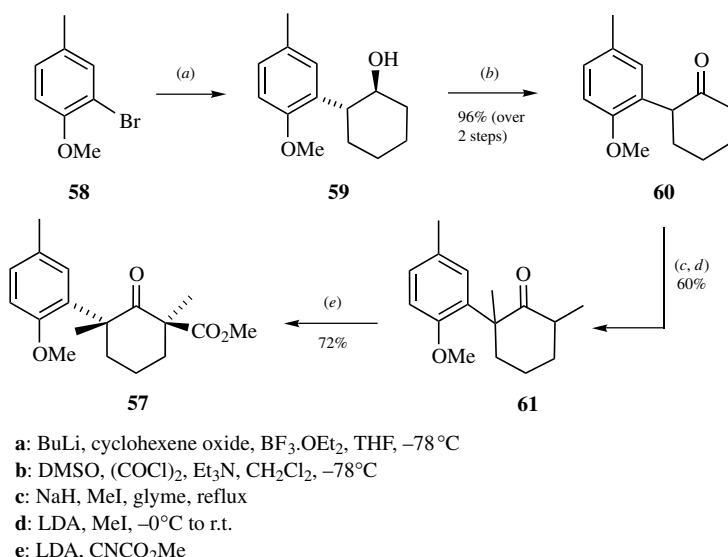
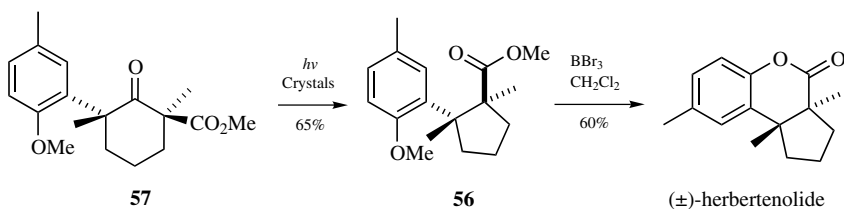


**Figure 7.17.** Molecular structure of ketone **57**. A crystalline precursor for the synthesis of Herberatenolide. See color insert.



Scheme 7.26.

allow for resonance delocalization of the postulated intermediate radicals with little rotation or displacement (Figure 7.17).

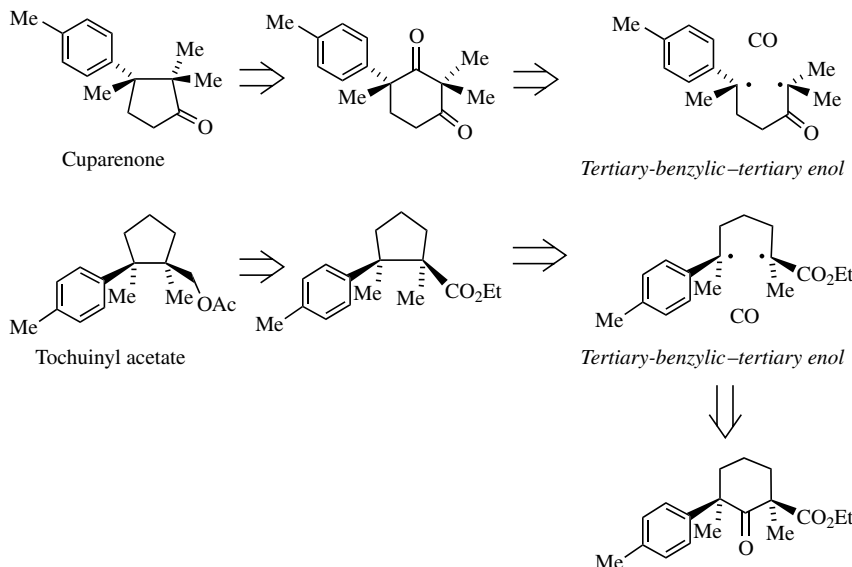
Irradiation of ketone **57** in the solid state with  $\lambda \geq 310\text{ nm}$  proceeded with ideal stereospecificity to the *trans*-dimethylcyclopentane **56** up to 20–35% conversion, after which the sample began to melt. Separation of the unreacted starting material and product could be achieved by dissolution and recrystallization such that higher yields could be achieved after several cycles. Subsequent treatment of compound **56** with  $\text{BBr}_3$  in  $\text{CH}_2\text{Cl}_2$  led to concurrent hydrolysis of the ether and ester groups, and *in situ* cyclization to give the racemic form of the natural product ( $\pm$ )-herbertenolide in high yield (Scheme 7.26).

The synthesis of herbertenolide represents the first case where a solid state reaction is reported as the key step in the synthesis of a natural product. At the time this chapter is being prepared, early reports on the synthesis of two more natural products with key solid-to-solid reactions have been accomplished and publications are in preparation. These targets are the sesquiterpenes  $\alpha$ -cuparenone and tochuanyl acetate, which have been prepared according to the retrosynthetic Schemes illustrated in Scheme 7.27.

## VII. FINAL COMMENTS

While, in general, numerous constraints make solid state reactions challenging, they can be used advantageously. Here we have shown the viability of the solid state photo-decarbonylation reaction as a general method for the construction of adjacent quaternary stereogenic centers. We have also analyzed many of the factors that affect the reaction in a predictable manner. The most important requirements and the experimental parameters required to optimize the quantum and chemical yields are listed below:

- Ketones should have large triplet yields, high triplet energies.* The formation of two radical centers within van der Waals distance should make it



Scheme 7.27.

very easy for ketones to form the bond that was broken to make the two radicals in the first place. Because singlet radical pairs can recombine within the time scale of a single bond vibration, reactions in crystals are more likely when they occur from the triplet excited state. Fortunately most ketones have reasonably large triplet yields and their triplet energies tend to be reasonably high.

- Ketones should have radical stabilizing substituents at the  $\alpha$ -and  $\alpha'$ -carbons.* Radical stabilizing substituents lower the bond dissociation energy of the sigma bonds that break during reaction. In order for decarbonylation to occur, unstrained ketones must be flanked by radical stabilizing groups on each  $\alpha$ -carbon. We established that simple alkyl radicals are not sufficient for the solid state reaction, whereas the formation of secondary and tertiary radicals with resonance stabilizing groups is conducive to its occurrence. We reported that phenyl,<sup>38,39</sup> carbonyl,<sup>43–45</sup> alkoxy,<sup>47</sup> and alkenyl<sup>75</sup> substituents enable decarbonylation in the solid state. This list is not exhaustive, and there may be many other radical stabilizing groups that should be investigated.
- There must be no competing reactions or internal quenchers.* From solution studies we have the mechanistic knowledge of unimolecular excited state processes likely to apply in the solid state. Here we showed that competing

$\gamma$ -hydrogen abstraction,<sup>51</sup>  $\beta$ -phenyl quenching,<sup>57,63</sup> and electron transfer quenching<sup>47</sup> can prevent a reaction from occurring in the solid state even when other favorable factors are present.

4. *The ketone precursor must be a crystalline solid.* While crystals are not necessary for a reaction to proceed, reactions in amorphous solids are generally not as selective.<sup>66</sup>
5. *Light should reach every molecule in the crystal.* To ensure that every molecule within a crystal can be reached by a photon, one must select the proper excitation wavelength and crystal size.<sup>2a,b</sup> The high optical density of pure crystals requires the use of filters or monochromators to select weakly absorbing wavelengths near the tail of the absorption spectrum. In general, large crystalline specimens are not suitable for preparative purposes because they become highly scattering as the reaction proceeds along an excitation front. The use of microcrystalline samples is ideal because of their larger surface area and smaller cross section. The mechanical mixing of both dry and fluid-suspended powders can ensure homogeneous exposure.
6. *The product should not absorb at the excitation wavelength.*<sup>76</sup> Ideally reactions in crystals should proceed in such a way that the absorption of the reactant is bleached to make a reaction front. As in solution photochemistry, products that compete for light with the reactant can undergo secondary photochemical processes and can act as filters that prevent light from reaching the inner portions of the optically dense crystal.
7. *The reactant and the product must coexist (be co-soluble) in the same crystal lattice.* This requirement will be satisfied for reactions that proceed by pathways of least motion.
8. *The reaction must be carried out at temperatures well below the solid line of the two component phase diagram.* Photolysis temperatures should be controlled to avoid the formation of liquid phases at and above the eutectic point. The eutectic point can be determined by analyzing partially reacted samples with differential scanning calorimetry (DSC).<sup>2a,b</sup>
9. *The product should be a solid.* The product must also be a solid. If the product of the reaction is a liquid, the reactant will be dissolved as the reaction proceeds. Melting will cause a loss of the selectivity during the reaction. Reactants can be selected so that they can be derivatized with groups that increase the melting of the reactant and the product.

Our hope is that these guidelines will motivate readers to explore other cases that may contribute to the development of solid state organic chemistry.

## ACKNOWLEDGMENTS

The authors thankfully acknowledge support from the National Science Foundation. We would like to dedicate this manuscript to Prof. Gerhard Quinkert whose studies at Johann Wolfgang Goethe-University in Frankfurt, Germany Institute of Organic Chemistry and Chemical Biology inspired much of the aforementioned research.

## REFERENCES

1. (a) Poliakoff, M.; Fitzpatrick, J. M.; Farren, T. R. A.; Anastas, P. T. *Science* **2002**, *297*, 807–810.  
(b) Anastas, P. T. *Green Chemistry: Theory and Practice*, Oxford University Press, Oxford, 1998.
2. For recent reviews and monographs on solid state chemistry, see: (a) Keating, A. E.; Garcia-Garibay, M. A. *Molecular and Supramolecular Photochemistry*, Vol. 2, Ramamurthy, V.; Schanze, K., eds. Dekker, New York, **1998**, pp. 195–248. (b) Garcia-Garibay, M. A.; Constable, A. E.; Jernelius, J.; Choi, T.; Cizmeciyani, D.; Shin, S. H. *Physical Supramolecular Chemistry*. Kluwer Academic, Dordrecht, **1996**. (c) Gamlin, J. N.; Jones, R.; Leibovitch, M.; Patrick, B.; Scheffer, J. R.; Trotter, J. *Acc. Chem. Res.* **1996**, *29*, 203–209. (d) Toda, F. *Acc. Chem. Res.* **1995**, *28*, 480–486. (e) Singh, N. B.; Singh, R. J.; Singh, N. P. *Tetrahedron* **1994**, *50*, 6441–6493. (f) Gabarskcyk, J. B.; Jones, D. W. *Organic Crystal Chemistry*. Oxford University Press, Oxford, **1991**. (g) Hollingsworth, M. D.; McBride, J. M. *Adv. Photochem.* **1990**, *15*, 279–379. (h) Lamartine, R. *Bull. Soc. Chim. Fr.* **1989**, 237–246. (i) Scheffer, J. R.; Garcia-Garibay, M. A.; Nalamasu, O. *Org. Photochem.* **1987**, *8*, 249–347. (j) Desiraju, G. R. *Organic Solid State Chemistry*. Elsevier: Amsterdam, **1987**. (k) Ramamurthy, V.; Venkatesan, K. *Chem. Rev.* **1987**, *87*, 433–481. (l) Desiraju, G. R. *Endeavour* **1984**, *8*, 201. (m) Paul, I. C.; Curtin, D. Y. *Science* **1975**, *187*, 19–26.
3. (a) Varshney, D. B.; Papaefstathiou, G. S.; MacGillivray, L. R. *Chem. Commun.* **2002**, 1964–1965.  
(b) Papaefstathiou, G. S.; Kipp, A. J.; MacGillivray, L. R. *Chem. Commun.* **2001**, 2462–2463.  
(c) Kaupp, G.; Boy, J.; Schmeyers, J. *Chem. Eur. J.* **1998**, *4*, 2467–2474; (d) Schmeyers, J.; Toda, F.; Boy, J.; Kaupp, G. *J. Chem. Soc. Perkin Trans.* **1998**, *2*, 989–993.
4. For leading references and reviews, see: (a) Overman, L. E.; Paone, D. V.; Stearns, B. A. *J. Am. Chem. Soc.* **1999**, *121*, 7702–7703. (b) Corey, E. J.; Guzman-Perez, A. *Angew. Chem. Int. Ed.* **1998**, *37*, 388–401. (c) Fuji, K. *Chem. Rev.* **1993**, *93*, 2037–2066. (d) Martin, S. F. *Tetrahedron*, **1980**, *36*, 419–460. (e) Christoffers, J.; Mann, A. *Angew. Chem. Int. Ed.* **2001**, *40*, 4591–4597.  
(f) Christoffers, J.; Baro, A. *Angew. Chem. Int. Ed.* **2003**, *42*, 1688–1690.
5. Bowen, E. J.; Watts H. G. *J. Chem. Soc.* **1926**, 1607, and references therein.
6. (a) Norrish, R. G. W. *Trans. Faraday Soc.* **1937**, *33*, 1521. (b) Norrish, R. G. W. *Trans. Faraday Soc.* **1934**, *30*, 103. (c) Norrish, R. G. W.; Crone, H. G.; Saltmarsh, O. D. J. *Chem. Soc.* **1934**, 1456; Bamford, C. H.; Norrish, R. G. W. *J. Chem. Soc.* **1935**, 1504.
7. (a) Chatgilialoglu, C.; Crich, D.; Komatsu, M.; Ryu, I. *Chem. Rev.* **1999**, *99*, 1991. (b) Vinogradov, M. G.; Nikishin, G. I. *Russ. Chem. Rev.* **1971**, *40*, 916.
8. Turro, N. J. *Modern Molecular Photochemistry*. University Science Books, Sausalito, **1991**.

9. Norrish, R. G. W.; Appleyard, M. E. S. *J. Chem. Soc.* **1934**, 874.
10. (a) Weiss, D. *Organic Photochemistry*, Vol. 5, Padwa, A., ed. Dekker, New York, **1981**, pp 347 ff.  
(b) Noyes, W. A. Jr. *Photochemistry and Reaction Kinetics*, Ashmore, P. G.; Dainton, F. S.; Sugden, T. M., eds. Cambridge University Press, Cambridge, **1967**, p. 1. (c) Wagner, P. J.; Hammond, G. S. *Adv. Photochem.* **1968**, *5*, 21. (d) Schaffner, K. *Pure Appl. Chem.* **1968**, *16*, 75. (e) Dalton, J. C.; Turro, N. J. *Annu. Rev. Phys. Chem.* **1970**, *21*, 499. (f) Horspool, W. M. *Photochemistry* **1985**, *16*, 215.
11. (a) Bohne, C. *CRC Handbook of Organic Photochemistry and Photobiology*; Horspool, W. M.; Song, P.S., eds. CRC Press, Boca Raton, **1995**, p. 423. (b) Turro, N. J.; Schuster, G. *Science* **1975**, *187*, 303.
12. (a) Lipscher, J.; Fischer, H. *J. Phys. Chem.* **1984**, *88*, 2555–2559. (b) Tsentalovich, Y. P.; Fischer, H. *J. Chem. Soc., Perkin Trans.* **1994**, *2*, 729–733. (c) Kurnyshewva, O. A.; Gritsan, N. P.; Tsentalovich, Y. P. *Phys. Chem. Chem. Phys.* **2001**, *3*, 3677–3682.
13. Quinkert, G.; Opitz, K.; Wiersdorff, W. W.; Weinlich, J. *Tetrahedron Lett.* **1963**, *27*, 1863–1886.
14. Baretz, B. H.; Turro, N. J. *J. Am. Chem. Soc.* **1983**, *105*, 1309–1316.
15. (a) Quinkert, G.; Cimbollek, G.; Buhr, G. *Tetrahedron Lett.* **1966**, *38*, 4573–4578. (b) Quinkert, G.; Opitz, K.; Wiersdorff, W. W.; Finke, M. *Liebigs Ann. Chem.* **1966**, *693*, 44–75. (c) Quinkert, G.; Wiersdorff, W. W.; Finke, M.; Opitz, K. *Tetrahedron Lett.* **1966**, *20*, 2193–2200.
16. 2-Indanones: (a) Paul, T.; Hassan, M. A.; Korth, H.-G.; Sustmann, R.; Avila, D. V. *J. Org. Chem.* **1996**, *61*, 6835–6848. (b) Netto-Ferreira, J. C.; Wintgens, V.; Scaiano, J. C. *Tetrahedron Lett.* **1989**, *30*, 6851–6854. (c) Keeffe, J. R.; Kresge, A. J.; Yin, Y. *J. Am. Chem. Soc.* **1988**, *110*, 8201–8206. (d) Starr, C. R.; Eastman, R. H. *J. Org. Chem.* **1966**, *31*, 1393–1402.
17. Quinkert, G.; Lorenz, H.-P.; Wiersdorff, W.-W. *Chem. Ber.* **1969**, *102*, 1517–1605.
18. Kohlshutter, H. W. *Anorg. Allg. Chem.* **1918**, *105*, 121.
19. M. D. Cohen, G. M. Schmidt. *J. Chem. Soc.* **1964**, 1996.
20. Schmidt, G. M. *Solid State Photochemistry*. Verlg Chemie, New York, **1976**.
21. Schmidt, G. M. *J. Pur Appl. Chem.* **1971**, *27*, 647.
22. Crystal engineering: (a) Nangia, A. *Cryst. Eng. Comm.* **2002**, *4*, 93–101. (b) Hollingsworth, M. D. *Science* **2002**, *295*, 2410–2413. (c) Desiraju, G. R. *Current Science* **2001**, *81*, 1038–1042. (d) Desiraju, G. R. *Crystal Engineering: The Design of Organic Solids*. Elsevier, Amsterdam, **1989**. (e) Braga, D.; Desiraju, G. R.; Miller, J. S.; Orpen, A. G.; Price, S. L. *Cryst. Eng. Comm.* **2002**, *4*, 500–509. (f) Desiraju, G. R. Designing Organic Crystals, *Prog. Solid St. Chem.* **1987**, *17*, 295–353. (7) Thomas, J. M. *Nature* **1981**, *289*, 633.
23. Cohen, M. D. *Angew. Chem. Int. Ed.* **1975**, *14*, 386–393.
24. Weiss, R. G.; Ramamurthy, V.; Hammond, G. S. *Acc. Chem. Res.* **1993**, *26*, 530.
25. Garcia-Garibay, M. A.; Houk, K. N.; Keating, A. E.; Cheer, C. J.; Leibovitch, M.; Scheffer, J. R.; Wu, L.-C. *Org. Lett.* **1999**, *1*, 1279–1281.
26. (a) Keating, A. E.; Shin, S. H.; Houk, K. N.; Garcia-Garibay, M. A. *J. Am. Chem. Soc.* **1997**, *119*, 1474–1475. (b) Keating, A. E.; Shin, S. H.; Huang, F. K.; Garrell, R. L.; Garcia-Garibay, M. A. *Tetrahedron Lett.* **1999**, *40*, 261–264. (c) Garcia-Garibay, M. A.; Houk, K. N.; Keating, A. E.; Cheer, C. J.; Leibovitch, M.; Scheffer, J. R.; Wu, L.-C. *Org. Lett.* **1999**, *1*, 1279–1281. (d) Zimmerman, H. E.; Zhu, Z. *J. Am. Chem. Soc.* **1994**, *116*, 9757–9758. (e) Zimmerman, H. E.; Zuraw, M. J. *J. Am. Chem. Soc.* **1989**, *111*, 2358–2361. (f) Gavezzotti, A.; Simonetta, M. *Chem. Rev.* **1982**, *82*, 5220.

27. The preparation of crystals for hetero-bimolecular solid state reactions has been addressed with some success: (a) Koshima, H.; Ding, K.; Chisaka, Y.; Matsuura, T. *J. Am. Chem. Soc.* **1996**, *118*, 12059–12065. (b) Ito, Y. *Synthesis-Stuttgart* **1998**, *1*, 1.
28. Promising strategies for the alignment of potential reaction partners have begun to emerge in the last few years: (a) MacGillivray, L. R.; Reid, J. L.; Ripmeester, J. A. *J. Am. Chem. Soc.* **2000**, *122*, 7817–7818. (b) Amirsakis, D. G.; Garcia-Garibay, M. A.; Rowan, S. J.; Stoddart, J. F.; White, A. J. P.; Williams, D. *J. Angew. Chem. Int. Ed.* **2001**, *40*, 4256–4261.
29. (a) Garcia-Garibay, M. A.; Shin, S. H.; Sanrame, C. *Tetrahedron* **2000**, *56*, 6729–6737. (b) Garcia-Garibay, M. A. *Acc. Chem. Res.* **2003**, *36*, 491–498.
30. (a) Scheffer, J. R. *Solid State Organic Chemistry*; Desiraju, G. R., ed. VCH, Amsterdam, **1987**, pp 1–45. (b) Ihmels, H.; Scheffer, J. R. *Tetrahedron* **1999**, *55*, 885–907. (c) Gudmundsdottir, A. D.; Lewis, T. J.; Randall, L. H.; Scheffer, J. R.; Rettig, S. J.; Trotter, J.; Wu, C.-H. *J. Am. Chem. Soc.* **1996**, *118*, 6167–6184.
31. (a) Casswell, L.; Garcia-Garibay, M. A.; Scheffer, J. R.; Trotter, J. *J. Chem. Ed.* **1993**, *70*, 785. (b) Garcia-Garibay, M.; Scheffer, J. R.; Trotter, J.; Wireko, F. *Tetrahedron Lett.* **1987**, *28*, 4789–4792. (c) Scheffer, J. R.; Trotter, J.; Garcia-Garibay, M.; Wireko, F. *Mol. Cryst. Liq. Cryst.* **1988**, *156* (Pt. A), 63–84. (d) Garcia-Garibay, M.; Scheffer, J. R.; Trotter, J.; Wireko, F. *J. Am. Chem. Soc.* **1989**, *111*, 4985–4986. (e) Pokkuluri, P. R.; Scheffer, J. R.; Trotter, J. *J. Am. Chem. Soc.* **1990**, *112*, 3676–3677.
32. Dang, H.; Suhrada, C. P.; Garcia-Garibay, M. A. Unpublished work.
33. Garcia-Garibay, M. A. *Curr. Opin. Sol. St. Mater. Sci.* **1998**, *3/4*, 399–406.
34. Campos, L. M.; Garcia-Garibay, M. A. In *CRC Handbook of Organic Photochemistry and Photobiology*, Horspool, W.; Leni, F. eds. CRC Press, Boca Raton, **2004**, pp. 1–41.
35. Fisher, H.; Paul, H. *Acc. Chem. Res.* **1987**, *20*, 200–206.
36. Luo, Y.-R. *Handbook of Bond Dissociation Energies in Organic Compound*. CRC Press, Boca Raton, **2003**.
37. Slivinskas, J. A.; Guillette, J. E. *J. Polym. Sci., Polym. Chem. Ed.* **1973**, *11*, 3043–3056.
38. Choi, T.; Peterfy, K.; Khan, S. I.; Garcia-Garibay, M. A. *J. Am. Chem. Soc.* **1996**, *118*, 12477–12478.
39. Peterfy, K.; Garcia-Garibay, M. A. *J. Am. Chem. Soc.* **1998**, *120*, 4540–4541.
40. (a) Schuster, D. I. In *The Photochemistry of Enones*, Patai, S.; Pappoport, Z., eds. Wiley, New York, **1989**, pp. 623–756. (b) Andrew, D.; Weedon, A. C. *J. Am. Chem. Soc.* **1995**, *117*, 5647–5663. (c) Sciano, J. C. *Acc. Chem. Res.* **1982**, *15*, 252–258. (d) Wagner, P.; Park, B.-S. *Org. Photochem.* **1991**, *11*, 227–366.
41. Bartlett, P. D.; Porter, N. A. *J. Am. Chem. Soc.* **1968**, *90*, 5317–5319.
42. Adam, W.; Emmert, O.; Heidenfelder, T. *J. Org. Chem.* **1999**, *64*, 3417–3421.
43. Yang, Z.; Garcia-Garibay, M. A. *Org. Lett.* **2000**, *2*, 1963–1965.
44. Yang, Z.; Ng, D.; Garcia-Garibay, M. A. *J. Org. Chem.* **2001**, *66*, 4468–4475.
45. Campos, L. M.; Ng, D.; Yang, Z.; Dang, H.; Martinez, H. L.; Garcia-Garibay, M. A. *J. Org. Chem.* **2002**, *67*, 3749–3754.
46. (a) Hrovat, D. A.; Borden, W. T. *J. Phys. Chem.* **1994**, *98*, 10460–10464, (b) Dorigo, A. E.; Li, Y.; Houk, K. N. *J. Am. Chem. Soc.* **1989**, *111*, 6942–6948.
47. Ng, D.; Yang, Z.; Garcia-Garibay, M. A. *Tetrahedron Lett.* **2002**, *43*, 7063–7066.
48. Leinweber, D; Butenschon, H. *Tetrahedron Lett.* **1997**, *38*, 6385–6386.
49. Denisov, E. T.; Denosova, T. G. *Handbook of Antioxidants* CRC Press, Boca Raton **200**.

50. Brocks, J. J.; Beckhaus, H.-D. Beckwith, A. L. J.; Ruechardt, C. *J. Org. Chem.* **1998**, *63*, 1935–1943.
51. Morko, C. J.; Dang, H.; Campos, L. M.; Garcia-Garibay, M. A. *Tetrahedron Lett.* **2003**, *44*, 6133–6136.
52. Bell, Thomas W.; Vargas, J. R.; Crispino, G. A. *J. Org. Chem.* **1989**, *54*, 1978–1987.
53. Houk, K. N. *Chem. Rev.* **1976**, *76*, 1–74.
54. Formation of this product is in agreement with the photochemistry of 2-(1-cyclohexenyl)-cyclohexanone: (a) Cookson, R. C.; Rogers, N. R. *J. Chem. Soc., Chem. Comm.* **1972**, *13*, 809–810. (b) Cookson, R. C.; Rogers, N. R. *J. Chem. Soc. Perkin Trans. I.* **1974**, *10*, 1037–1043.
55. Ihmels, H.; Scheffer, J. R. *Tetrahedron* **1999**, *55*, 885–907.
56. Salem, L.; Leforestier, C.; Segal, G.; Wetmore, R. *J. Am. Chem. Soc.* **1975**, *97*, 479–487.
57. Ng, D.; Yang, Z.; Garcia-Garibay, M. A. *Tetrahedron Lett.* **2001**, *42*, 9113–9116.
58. (a) Carlson, G. L. B.; Quina, F. H.; Zarnegar, B. M.; Whitten, D. G. *J. Am. Chem. Soc.* **1975**, *97*, 347–354. (b) Wagner, P. J.; Kelso, P. A.; Kemppainen, A. E.; Haug, A.; Gruber, D. R. *Mol. Photochem.* **1970**, *2*, 81–85. (c) Netto-Ferreira, J. C.; Leigh, W. J.; Scaiano, J. C. *J. Am. Chem. Soc.* **1985**, *107*, 2617–2622. (d) Boch, R.; Bohne, C.; Netto-Ferreira, J. C.; Scaiano, J. C. *Can. J. Chem.* **1991**, *69*, 2053. (e) Leigh, W. J.; Banisch, J. H.; Workentin, M. S. *J. Chem. Soc. Chem. Commun.* **1983**, 988–990.
59. (a) Whitten, D. G.; Punch, W. E. *Mol. Photochem.* **1970**, *2*, 77–80. (b) Wagner, P. J.; Kelso, P. A.; Kemppainen, A. E.; Haug, A.; Gruber, D. R. *Mol. Photochem.* **1970**, *2*, 81–85. (c) Netto-Ferreira, J. C.; Leigh, W. J.; Scaiano, J. C. *J. Am. Chem. Soc.* **1985**, *107*, 2617–2622. (d) Boch, R.; Bohne, C.; Netto-Ferreira, J. C.; Scaiano, J. C. *Can. J. Chem.* **1991**, *69*, 2053. (e) Leigh, W. J.; Banisch, J. H.; Workentin, M. S. *J. Chem. Soc., Chem. Commun.* **1983**, 988.
60. Scaiano, J. C.; Perkins, M. J.; Sheppard, J. W.; Platz, M. S.; Barcus, R. L. *J. Photochem.* **1983**, *21*, 137–147.
61. (a) Moorthy, J. N.; Peterson, W. S.; Bohne, C. *J. Am. Chem. Soc.* **1997**, *119*, 11094–11095. (b) Moorthy, J. N.; Monahan, S. L.; Sunoj, R. B.; Chandrasekhar, J.; Bohne, C. *J. Am. Chem. Soc.* **1999**, *121*, 3093–3103.
62. Boch, R.; Bohne, C.; Scaiano, J. C. *J. Org. Chem.* **1996**, *61*, 1423–1428.
63. Dang, H.; Yang, Z.; Ng, D.; Garcia-Garibay, M. A. Unpublished results.
64. Jefferson, A.; Nicovich, J. M.; Wine, P. H. *J. Phys. Chem.* **1994**, *98*, 7128–7135.
65. (a) Guttenplan, J. B.; Cohen, S. G. *J. Org. Chem.* **1973**, *38*, 2001–2007. (b) Inbar, S.; Linschitz, H.; Cohen, S. G. *J. Am. Chem. Soc.* **1982**, *104*, 1679–1682. (c) Marciniak, B.; Bobrowski, K.; Hug, G. L. *J. Phys. Chem.* **1993**, *97*, 11937–11943. (d) Bobrowski, K.; Marciniak, B.; Hug, G. L. *J. Potochem. Photobio. Chem.* **1994**, *A1*, 159–168.
66. Choi, T.; Cizmeciyani, D.; Khan, S. I.; Garcia-Garibay, M. A. *J. Am. Chem. Soc.* **1995**, *118*, 12893–12894.
67. CRC *Handbook of Chemistry and Physics*. CRC Press, Boca Raton, **1984**.
68. Ellison, M. E.; Ng, D.; Dang, H.; Garcia-Garibay, M. A. *Org. Lett.* **2003**, *5*, 2531–2534.
69. Jacques, J.; Collet, A.; Wilen, S. H. *Enantiomers, Racemates, and Resolutions*. Wiley, New York, **1981**.
70. Luo, Y.-R. *Handbook of Bond Dissociation Energies in Organic Compounds*. CRC Press, Boca Raton, **2003**.
71. Ng, D.; Yang, Z.; Garcia-Garibay, M. A. *Org. Lett.* **2004**, *6*, 645–647.
72. (a) Matsuo, A.; Yuki, S.; Nakayama, M. *Chem. Lett.* **1983**, *7*, 1041–1042. (b) Matsuo, A.; Yuki, S.; Nakayama, M. *J. Chem. Soc. Perkin Trans.* **1986**, *41*, 701–710.

73. Eicher, T.; Servet, F.; Speicher, A. *Synthesis* **1996**, 7, 863–870.
74. Fukuyama, Y.; Yuasa, H.; Tono, Y.; Harada, K.; Wada, M.; Asakawa, Y.; Hashimoto, T. *Tetrahedron* **2001**, 57, 9299–9307.
75. Mortko, C. J.; Garcia-Garibay, M. A. Abstracts of Papers. 227th ACS National Meeting, Anaheim, CA, March 28–April 1, 2004.
76. For an example where the selectivity of a solid state reaction varies as a function of wavelength please, see Ref. 26a.

## Chapter 8

# The CH/π Hydrogen Bond: An Important Molecular Force in Controlling the Crystal Conformation of Organic Compounds and Three-Dimensional Structure of Biopolymers

MOTOHIRO NISHIO and YOJI UMEZAWA

*The CHPI Institute 3-10-7 Narusedai Machida, Tokyo 194-0043, Japan*

- I. Introduction
    - A. Four Types of Hydrogen Bonds
    - B. The CH/π Hydrogen Bond
    - C. Characteristics of the CH/π Hydrogen Bond
  - II. Conformation of Organic Compounds
    - A. Organic Compounds
    - B. Peptides
      - 1. Cyclic Peptides
      - 2. Acyclic Peptides
  - III. Interligand Interactions in Coordination and Organometallic Compounds
    - A. Coordination Compounds
    - B. Transition Metal Compounds
    - C. CH/π Hydrogen Bond Implicated in the Mechanism of Enantioselective Catalytic Reactions
  - IV. Three-dimensional Structure of Biopolymers
    - A. Proteins
    - B. Nucleic Acids
  - V. Database Studies
    - A. Compounds of Small Molecular Weight
    - B. Biopolymers
  - VI. Conclusions
- Acknowledgments  
References

## I. INTRODUCTION

### A. Four Types of Hydrogen Bonds

The shape or conformation of molecules is determined by a combination of various noncovalent forces, attractive as well as repulsive. These weak molecular forces are important in controlling the process of self-assembly and the specificity in supramolecular or host/guest chemistry. To be effective in a dynamically interacting system, the energy of a one-unit interaction should not be too large. Strong forces are incompatible with the dynamic process of molecular recognition; there, weaker and flexible interactions play the central part. The weak molecular forces include the London dispersion force, various electrostatic forces, and hydrogen bonds.

The conventional hydrogen bond<sup>1</sup> is the interaction occurring between hard acids and hard bases ( $\text{XH}/\text{Y}$ ; X, Y = O, N, halogen:  $3\sim 7 \text{ kcal mol}^{-1}$ ). Evidence has gradually accumulated to show that weaker hydrogen bonds<sup>2</sup> are also ubiquitous, including  $\text{XH}/\pi^3$  (X = O, N, halogen:  $2\sim 4 \text{ kcal mol}^{-1}$ ) and  $\text{CH}/n$  ( $n$  as contrasted to  $\pi$ ) or  $\text{CH}/\text{X}$  interactions (X = O, N, halogen:  $2\sim 4 \text{ kcal mol}^{-1}$ ). The former are hydrogen bonds occurring between hard acids and soft bases, while the latter are hydrogen bonds between soft acids and hard bases. In recent years a still weaker molecular force, the  $\text{CH}/\pi$  hydrogen bond ( $0.5\sim 2 \text{ kcal mol}^{-1}$ ),<sup>4,5</sup> has become recognized to play an important role in various chemical and biochemical phenomena.

### B. The $\text{CH}/\pi$ Hydrogen Bond

The recognition that the interaction between CHs and  $\pi$ -systems is attractive first came from thermochemical and spectral observations. In 1952, Tamres showed that benzene and analogues dissolve in chloroform exothermically.<sup>6</sup> In 1955, Huggins and Pimentel reported that the C-D stretching frequency of  $\text{CDCl}_3$  red-shifted in benzene by around  $5 \text{ cm}^{-1}$ ; the infrared data were consistent with the criteria for hydrogen bond systems.<sup>7</sup> Many workers have since demonstrated, by measurement of IR<sup>8</sup> or NMR<sup>9</sup> spectra, that the interaction of CH with  $\pi$ -bases is attractive.

In 1974, Itaka et al. reported crystallographic results that the *t*-butyl group in a pair of sulfoxide diastereomers ( $\text{C}_6\text{H}_5\text{CHCH}_3\text{SO}-t\text{-C}_4\text{H}_9$ ) is close to a phenyl group in the other terminus of the molecule (Figure 8.1).<sup>10</sup> In these sulfoxides, the distance between one of the three carbons in the *t*-butyl group to  $\text{C}_6\text{H}_5$  was found to be very short. They considered, at the outset of the study, that the *t*-butyl/phenyl congested conformation is a result of the unfavorable steric interaction between the *t*-butyl and benzylic methyl groups. Subsequent findings that an alkyl group R is often in the folded  $\text{R}/\text{C}_6\text{H}_5$  conformation in compounds  $\text{C}_6\text{H}_5\text{CHCH}_3\text{X}-\text{R}^{11}$  and  $\text{C}_6\text{H}_5\text{CHCH}_3\text{X}-\text{Ar}^{12}$  led the authors to suggest an attractive force to operate between the alkyl and phenyl groups.<sup>13</sup> A hypothesis was presented that a weak

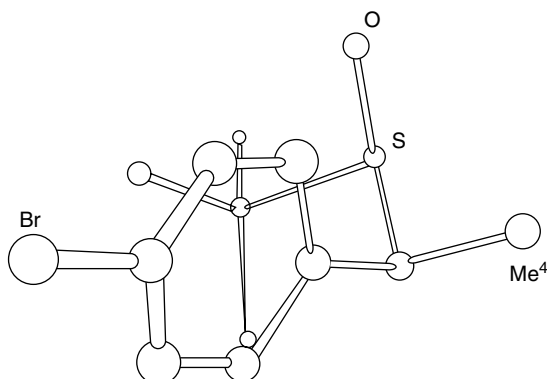


Figure 8.1. Crystal conformation of 1-phenylethyl *t*-butyl sulfoxide  $C_6H_5CHCH_3SO-t-C_4H_9$ .  
Source: Kodama et al. (*J. Chem. Soc., Perkin Trans. 2* **1976**, 1490–1495, Fig. 1).

attractive force, the CH/ $\pi$  interaction, plays important roles in various fields of chemistry and biochemistry.<sup>14</sup> Theoretical calculations supporting the CH/ $\pi$  concept followed.<sup>15,16</sup>

Stabilization of the CH/ $\pi$  hydrogen bond comes largely from the dispersion force.<sup>17</sup> Evidence for the hydrogen-bond nature of this interaction has been provided by comparative database<sup>18</sup> and MO studies of various intermolecular<sup>19</sup> and intramolecular<sup>20</sup> systems. Consistent with this conclusion, activation of either the donor<sup>21</sup> or the acceptor<sup>22</sup> component of the CH/ $\pi$  bond leads to its strengthening.<sup>23</sup> Though the electrostatic nature is not large, this is effective at a distance longer than the sum of the van der Waals radii. Contribution from the charge–transfer interaction has also been suggested;<sup>25</sup> this remains a matter of current debate, however.

### C. Characteristics of the CH/ $\pi$ Hydrogen Bond

Before discussing the individual topics, it seems appropriate to summarize the characteristics of the CH/ $\pi$  hydrogen bond.

One of the unique characteristics of the CH/ $\pi$  hydrogen bond is that many CH and  $\pi$  groups may cooperatively participate in the interaction. The donor CH is present in every organic group. Compounds bearing  $\pi$ -electrons are also abundant in nature. The enthalpy of the total interaction may become appreciable as a result of the interplay among many interactions, though the stabilization from a one-unit CH/ $\pi$  hydrogen bond is very small.<sup>24</sup> Another point is that the CH/ $\pi$  hydrogen bond is favorable with respect to entropy. Groups bearing CHs or aromatic moieties are often symmetric. Therefore the CH and  $\pi$  groups have many chances to interact (Figure 8.2). Stabilization ( $\Delta G = \Delta H - T\Delta S$ ) of the CH/ $\pi$ -interacted system

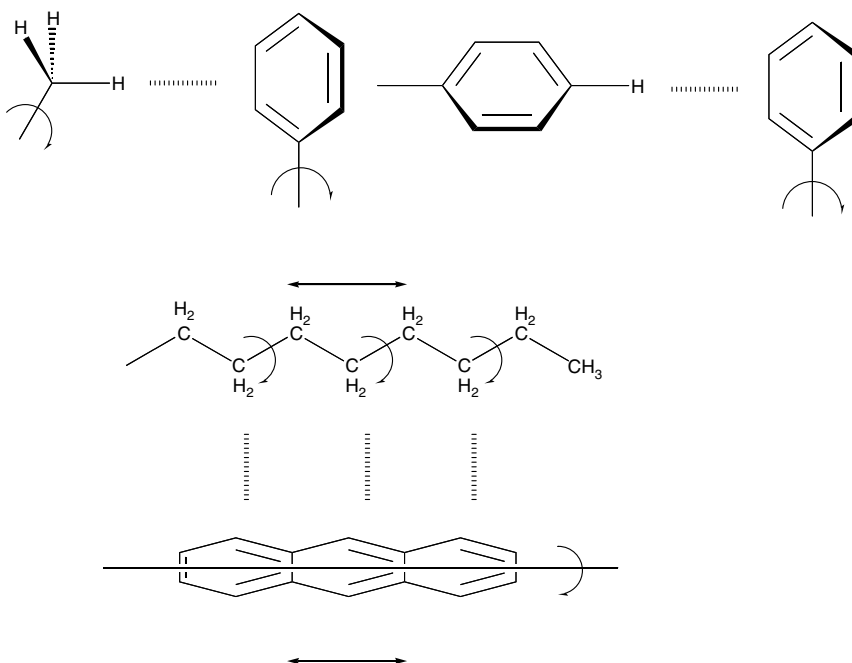


Figure 8.2. Schematic drawings illustrating the characteristics of the CH/π hydrogen bonds.

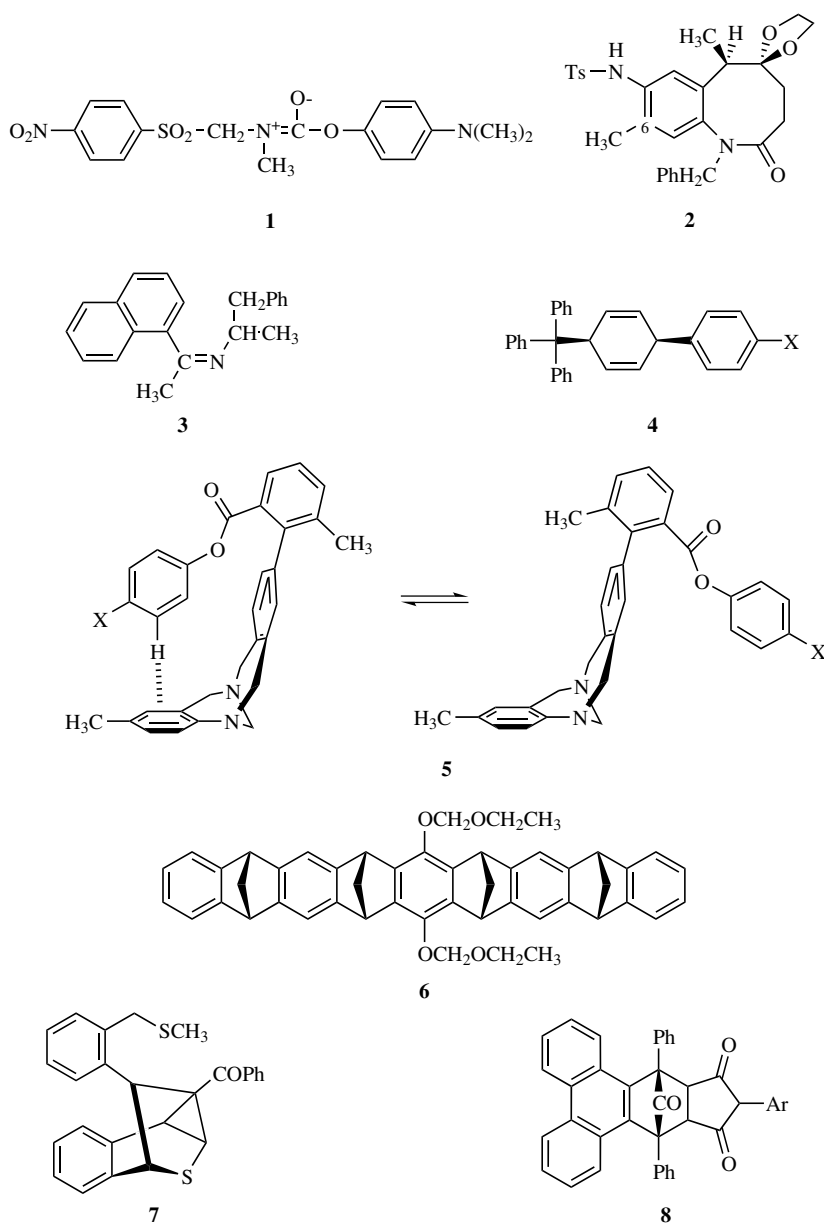
consequently increases. Finally, the CH/π hydrogen bond plays its role in polar protic solvents such as water. This is because stabilization of the CH/π hydrogen bond comes mostly from the dispersion force. The Coulombic interaction and the ordinary hydrogen bond, on the contrary, are not effective in polar protic media.

Here we confine ourselves to intramolecular interactions in chemistry and structural biology. A more general outlook on the CH/π hydrogen bond in crystals is available in another treatise by one of the authors.<sup>25</sup> There, intermolecular interactions such as crystal packing, self-assembly, host/guest chemistry, enantioselection, etc. are largely dealt with.

## II. CONFORMATION OF ORGANIC COMPOUNDS

### A. Organic Compounds

Early in the 1970s, Engberts reported that several organic compounds bearing at least an aromatic group at the terminus of the molecule favor the folded



Scheme 8.1.

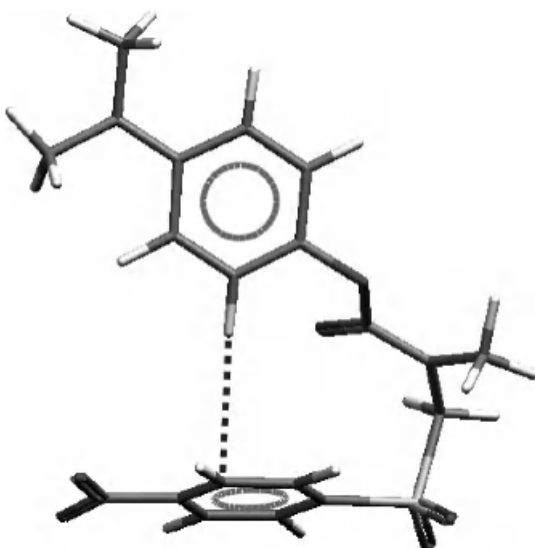


Figure 8.3. X-ray crystal conformation of *p*-dimethylaminophenyl *N*-methyl-*N*-(*p*-nitrophenylsulfonylmethyl)carbamate **1** (CSD refcode APSMCB).

conformation in solution.<sup>26</sup> The proximity of the aromatic rings was suggested on the ground of UV and NMR spectral data. Later the crystal structures of these compounds were shown to be similar to the solution conformations for ethyl *N*-methyl-*N*-(*p*-tolylsulfonylmethyl)carbamate,<sup>27</sup> *N,N'*[bis( $\alpha$ -tosylbenzyl)]urea,<sup>28</sup> substituted benzyl phenyl sulfones,<sup>29</sup> and *p*-dimethylaminophenyl *N*-methyl-*N*-(*p*-nitrophenylsulfonylmethyl) carbamate **1** (Scheme 8.1, **1–8**).<sup>30</sup> An example is given in Figure 8.3.

Ban studied the solution and crystal structure of a 1-benzazocinone derivative **2**.<sup>31</sup> The methyl group in the benzazocinone moiety was reported to be close to the aromatic ring of the *N*-benzyl group. Figure 8.4 shows that the methyl and methylene groups are in contact with phenyl groups in the vicinity. That the folded conformation maintains in solution was shown by  $^1\text{H}$ -NMR ( $\delta$  0.68 for  $6\text{-CH}_3$ ) and NOE (23% enhancement) measurements. They explained the result in terms of the CH/π interaction.

Hamor et al. studied the conformation of *N*-[1-(1-naphthyl)ethylidene]-1-phenyl-2-propylamine **3**.<sup>32</sup> The more stable Z-isomer, which was isolated in crystalline form, exhibits an NMR signal at  $\delta$  5.91 ppm assignable to a naphthyl proton  $\alpha$  to the imino group. The X-ray crystal structure (Figure 8.5) revealed that this hydrogen is situated close to the phenyl ring (H/centriod distance 2.68 Å). These authors attributed the result to the attractive interaction occurring between

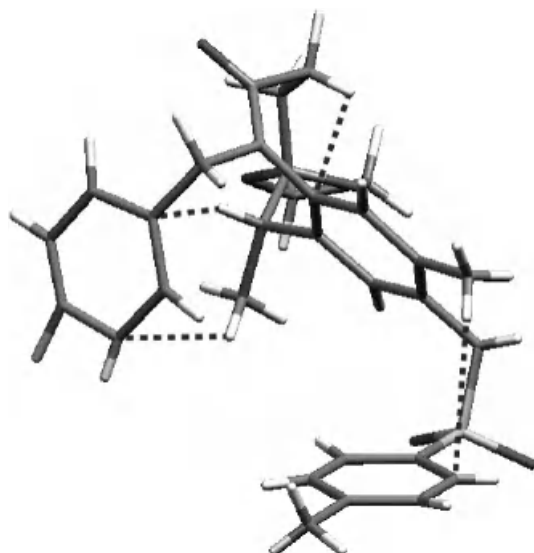


Figure 8.4. X-ray crystal conformation of a 1-benzazocinone derivative **2** (CSD refcode COPTOQ).

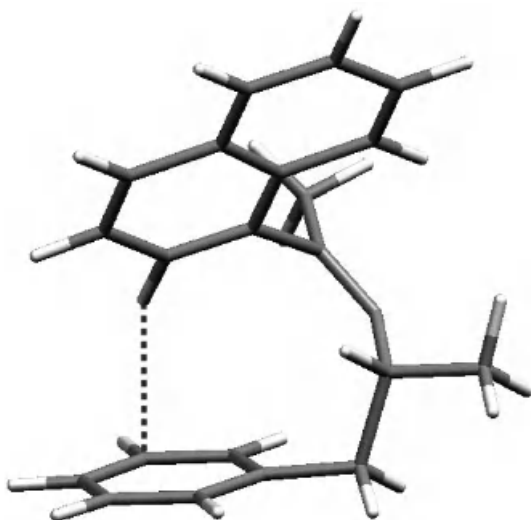


Figure 8.5. X-ray crystal conformation of *N*-[1-(1-naphthyl)ethylidene]-1-phenyl-2-propylamine **3** (CSD refcode JEBHIH).

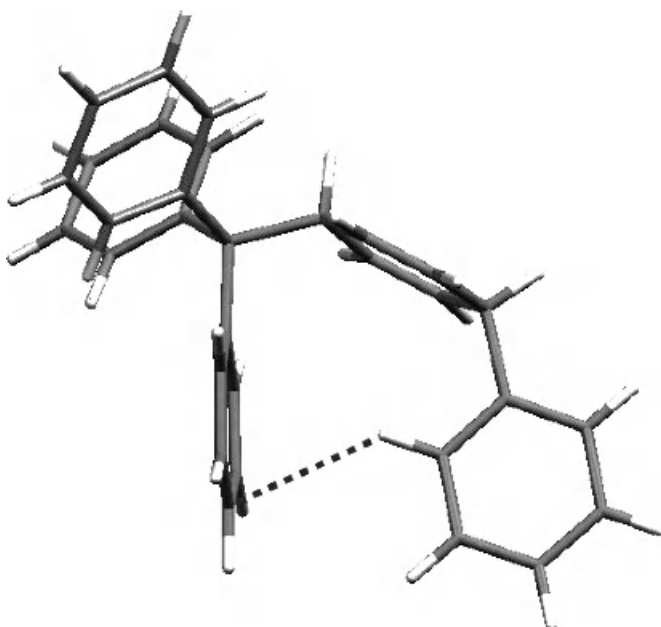


Figure 8.6. X-ray crystal conformation of *cis*-1,4-dihydro-4-tritylbiphenyl **4** (CSD refcode DHTRBP10).

the two aromatic rings. They reported similar phenomena for structurally related alkenes, nitrones, and imines.<sup>33</sup> This type of interaction is often referred to as an “edge-to-face  $\pi/\pi$ <sup>34</sup> or a T-type aromatic<sup>35</sup> interaction”, etc. We prefer the term “aromatic CH/π hydrogen bond” in view of its nature.

Grossel determined the X-ray crystal structure of *cis*-1,4-dihydro-4-tritylbiphenyl and its 4-bromo analogue **4** (Figure 8.6).<sup>36</sup> The distance between an aromatic CH and a nearby phenyl ring was found to be shorter in the 4-Br derivative (2.48 Å) than in the nonsubstituted one (2.55 Å). <sup>1</sup>H-NMR data were consistent with the observation above to show that the crystal conformation is kept in solution.

Wilcox studied the atropisomerism of a series of dibenzodiazocine esters **5**. These compounds are in two conformations that interconvert to each other by slow rotation of the C–C single bond.<sup>37</sup> The X-ray crystal structure of the more stable folded conformer (Figure 8.7) demonstrated that the two rings in the termini of the molecule are in a nearly perfect T-relationship. The <sup>1</sup>H NMR data suggest that the conformation above maintains in solution.

Klärner et al. reported on the conformation of a molecular tweezer of rigid-ribbon type **6**.<sup>38</sup> The upfield <sup>1</sup>H NMR chemical shift of the peak assignable to

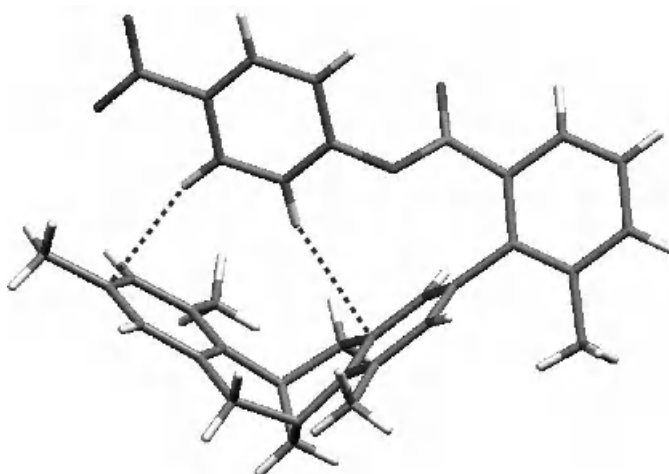


Figure 8.7. X-ray crystal conformation of a dibenzodiazocine ester **5**,  $\text{X} = \text{NO}_2$  (CSD refcode PIWYEZ).

the methyl group ( $\delta -0.53$ ) led them to suggest that this is a consequence of the anisotropy of the arene unit of **6**. By the crystallographic determination, one of the side-chain ethoxy groups was found to be folded and its terminal methyl group centered in the cavity (Figure 8.8).

Shimizu studied the solution and solid conformation of a benzothiopyran derivative **7**.<sup>39</sup> The X-ray crystal structure of **7** showed that the *S*-methyl group is located just above the benzene ring (Figure 8.9). The unusual high-field  $^1\text{H}$  NMR chemical shift ( $\delta 1.69$  ppm) of the relevant signal was interpreted on this basis.

Harano and coworkers determined the solid structure of Diels-Alder adducts of phencyclane **8**. Close CH/ $\pi$  contacts were observed between aromatic CHs of these derivatives and nearby aromatic rings (Figure 8.10).<sup>40</sup> The  $^1\text{H}$  NMR signal of the relevant protons was found to be at a high magnetic field.

Stoddart and his associates synthesized compounds bearing a 2,2'-bis(amino)diphenyl ether unit **9** (Scheme 8.2, **9–15**).<sup>41</sup> They found that CH/ $\pi$  and ordinary hydrogen bonds cooperate in bringing the whole molecule into a coiled conformation (Figure 8.11). Notice that the terminal methyl and methylene groups are both involved in CH/ $\pi$  bonds to bring about this peculiar structure. It is certain that such a conformation maintains in solution because **9** failed to produce a pseudorotaxane by penetrating into the cavity of the host macrocycle.

Another interesting case was provided by Miyake et al. in the self-assembly of a podand derived from ferulic acid **10**.<sup>42</sup> On treatment with an alkali metal cation,

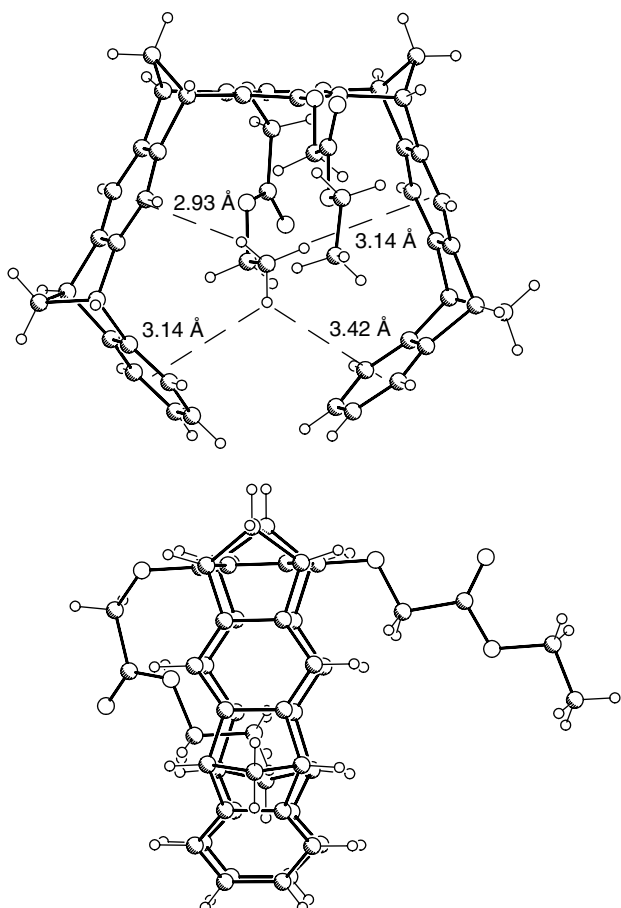


Figure 8.8. X-ray crystal conformation of a molecular tweezer **6**. Adapted from Klärner et al. (*Angew. Chem., Int. Ed. Engl.* **1996**, *35*, 1130–1132, Fig. 2).

compound **10** gave a dimeric complex. The “U” shape of the product dimer has been rationalized to be tightly held by four hydrogen bonds and four OCH<sub>3</sub>/π interactions (Figure 8.12); one of the hydrogens of a CH<sub>3</sub>O group was found close (2.70 Å) to the nearby phenyl ring.

Short CH/π distances are often reported in the solid state conformation of macrocyclic polyethers incorporating aromatic rings.<sup>43</sup> Csöregh et al. determined the X-ray crystal structure of 9,10-dihidro-9,10-ethaneoanthracenedicarboximide **11**.<sup>44</sup> A CH unit in the *ortho* methyl group of the xylyl moiety points to the center of the phenyl group close to it. The CH/π (center) distance was 2.57 Å. Kuwatani

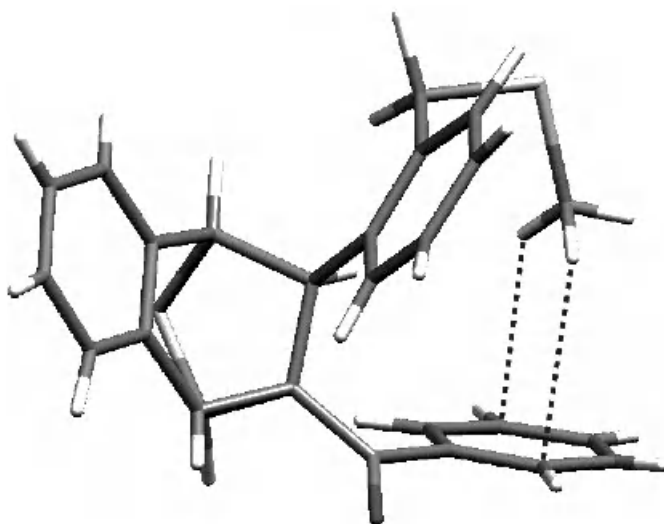


Figure 8.9. X-ray crystal conformation of a benzothiopyran derivative **7** (CSD refcode TOCSIN).

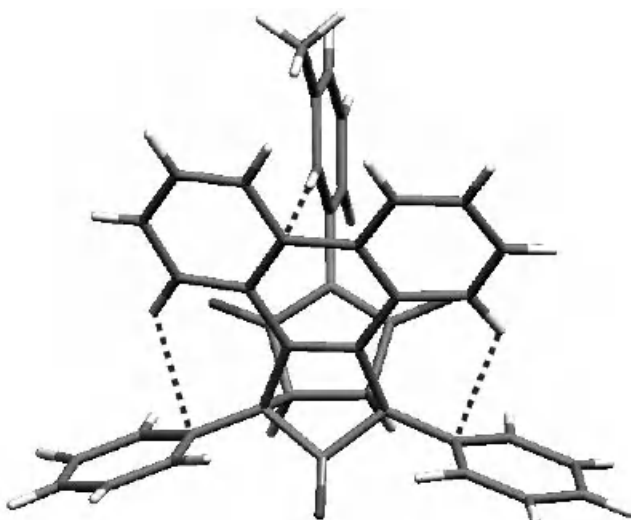
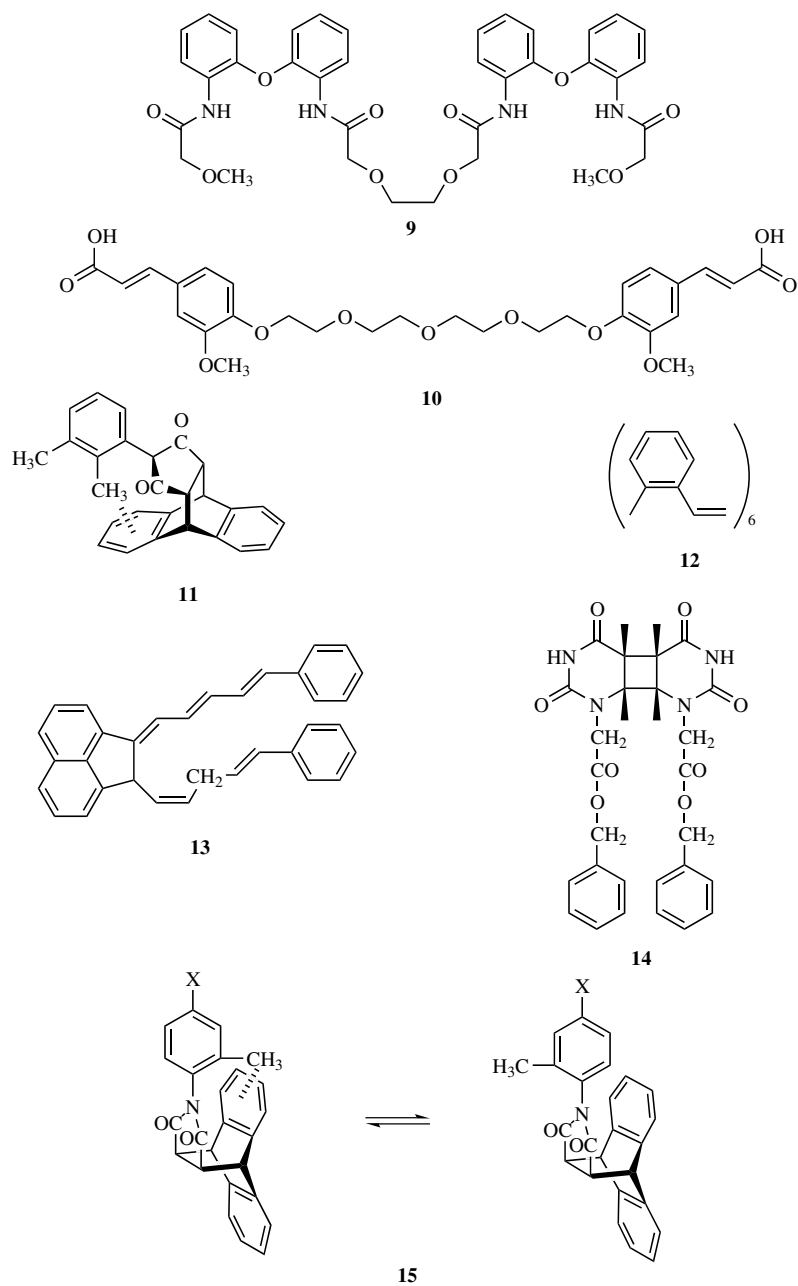


Figure 8.10. X-ray crystal conformation of a Diels-Alder adducts of phencyclone **8** ( $\text{Ar} = 1\text{-naphthyl}$ ) (CSD refcode LUBGOE).



Scheme 8.2.

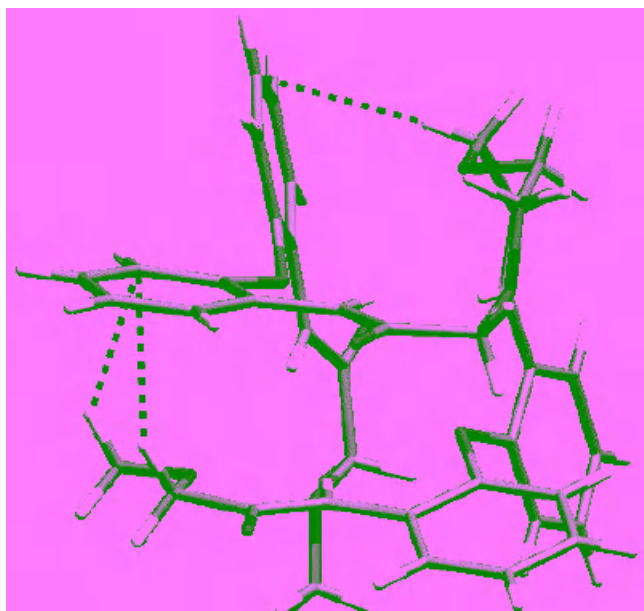


Figure 8.11. X-ray crystal conformation of a 2,2'-(bisamino)diphenyl ether **9** (CSD refcode TOJQUE).

et al. studied *all-Z*-hexabenzoc annulene **12** with a triangular benzene cluster substructure.<sup>45</sup> The X-ray crystal structure of **12** has  $C_3$  symmetry. Complementary CH/ $\pi$  interactions among these rings suggest a sustained intramolecular assembly of the inner benzene rings. The solution conformation of **12** was studied by temperature-dependent NMR spectroscopy. The signal attributed to the *ortho*-hydrogen appeared at  $\delta$  4.4 ppm, demonstrating the proximity of the CH unit to the benzene  $\pi$ -ring, as was found in the crystal structure.

Short intramolecular CH/C(arene) distances have also been reported in many crystal structures. Examples include procatechol,<sup>46</sup> a parallel preorganized polyene **13** (Figure 8.13),<sup>47</sup> a benzazepin-2-one,<sup>48</sup> *cis-syn*-bis((1-benzyloxycarbonyl)-5,6-dihydro-uracil-5,6-diyl) **14** (Figure 8.14),<sup>49</sup> pyridinocalix[4]arene,<sup>50</sup> *N*-tigloylbenzoformamides,<sup>51</sup> hydroxy(phenyl)methylcyclohexanone, 1-*n*-butyl-3-methylimidazolium salt,<sup>52</sup> 3-ethyl-2-hydroxy(phenyl)methylcyclopentanone,<sup>53</sup> heterohelicenes,<sup>54</sup> a diosgenyl glucopyranoside,<sup>55</sup> and so on.<sup>56</sup> In every case when determined, the relevant  $^1\text{H}$  NMR peaks are considerably shielded relative to the standard values to show that the crystal conformation is kept in solution. Prevalence of the alkyl/aryl-congested conformation in these compounds has become clear also from solution<sup>57</sup> and gas-phase<sup>58</sup> studies.

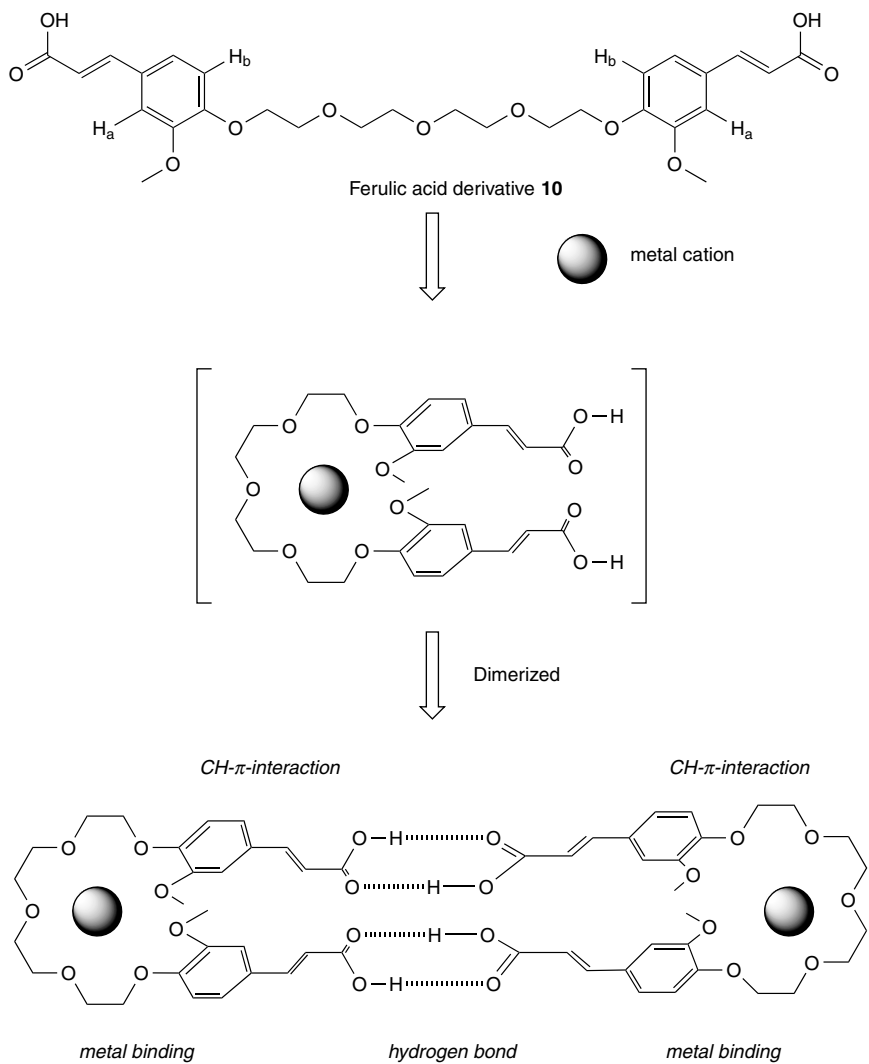


Figure 8.12. Self-assembly of a podand **10** to a dimer complex. Adapted from Miyake et al. (*Chem. Commun.* **2002**, 132–133, Fig.1).

Kishikawa studied the conformer distribution of *N*-(4-substituted-2'-methylphenyl)-9,10-dihydro-9,10-ethanoanthracene-11,12-carboximides **15**.<sup>59</sup> <sup>1</sup>H-NMR data suggest that a methyl group in the amide ring is close to an aromatic ring in the *syn*-rotamer. However, the *anti*-conformation was found in the X-ray

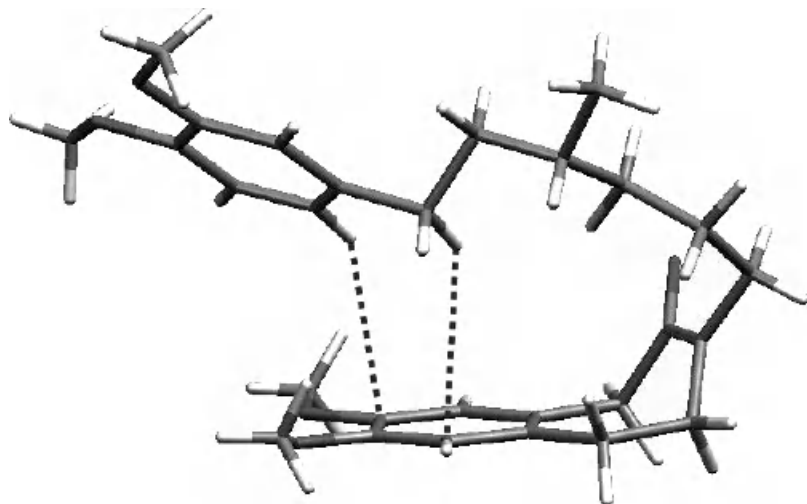


Figure 8.13. X-ray crystal conformation of a parallel preorganized polyene **13** (CSD refcode JENHAL).

crystal structure (Figure 8.15). The result can be ascribed to the intermolecular CH/π interactions between the methyl group and aromatic rings of an adjacent molecule in the crystal. To our knowledge, the result above is one of the rare cases where the conformations in crystals and solution significantly differ. Interestingly

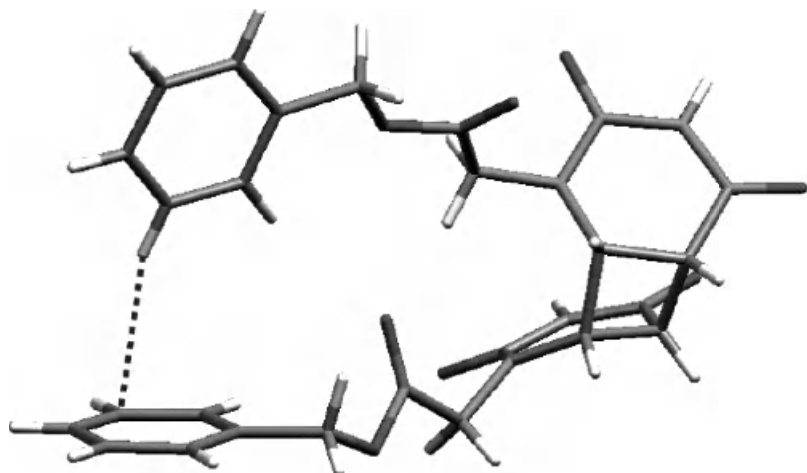


Figure 8.14. X-ray crystal conformation of *cis*-*syn*-bis((1-benzyloxycarbonyl)-5,6-dihydro-uracil-5,6-diyl) **14** (CSD refcode ZUDFEJ).

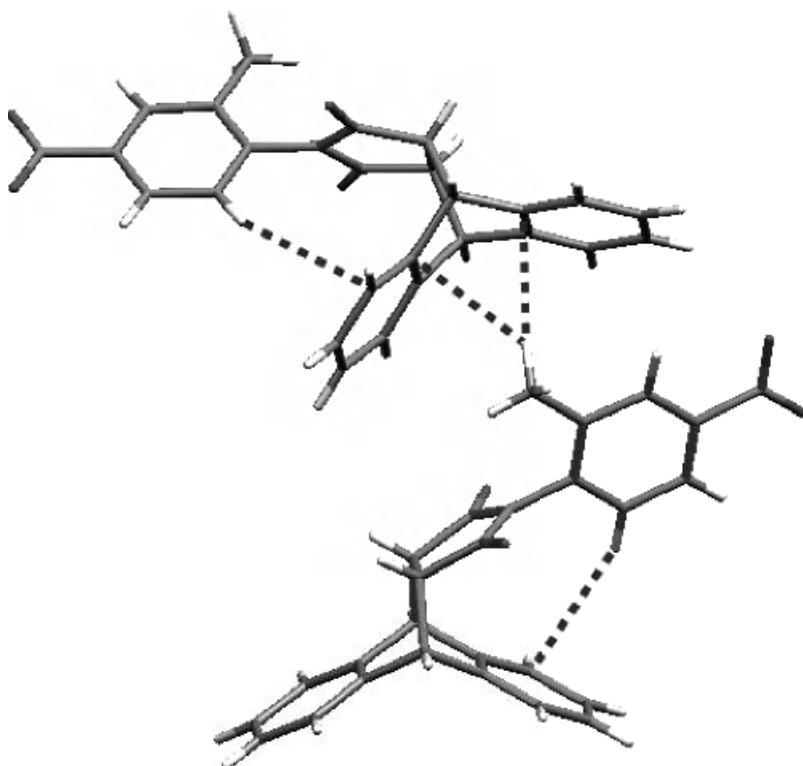


Figure 8.15. X-ray crystal conformation of *N*-(4-substituted-2'-methylphenyl)-9,10-dihydro-9,10-ethanoanthracene-11,12-carboximides **15** (CSD refcode RIZCOS).

in the solid and the solution state, the conformation is controlled by CH/π hydrogen bonds.

## B. Peptides

### *I. Cyclic Peptides*

In 1967, Kopple reported the preference of folded conformations for a series of cyclic dipeptides *cyclo*(Gly-L-Tyr), *cyclo*(L-Ala-L-Tyr) and *cyclo*(L-His-L-Tyr).<sup>60</sup> Later, the solid state structure of *cyclo*(Gly-L-Tyr) and *cyclo*(L-Ser-L-Tyr), was found to be the same as in solution.<sup>61</sup> Figure 8.16 gives the X-ray crystal structure of *cyclo*(L-Phe-L-Phe). It appears that the CH/π interaction has an important role in maintaining the compact structure. A folded structure was suggested also for

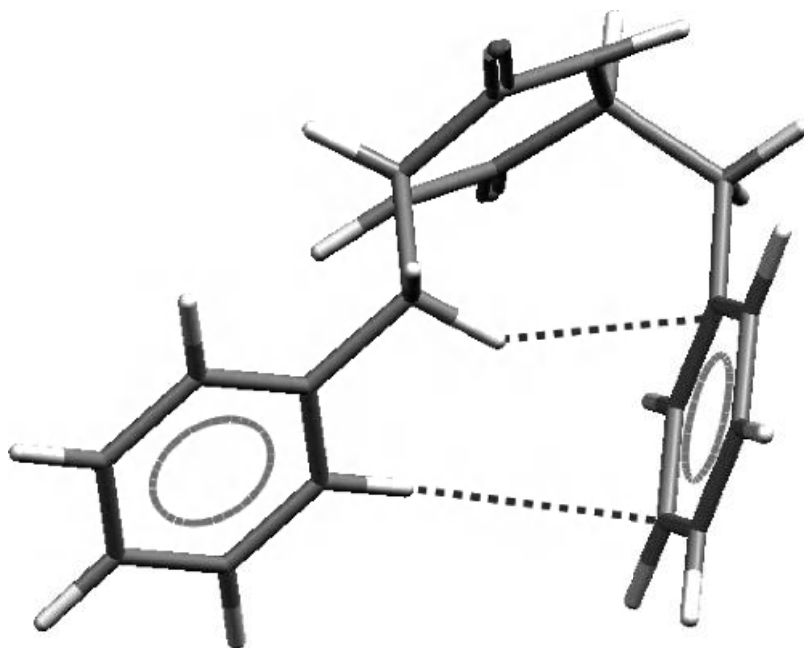


Figure 8.16. X-ray crystal structure of *cyclo*(L-Phe-L-Phe) (CSD refcode DUZDUX).

the solution<sup>62</sup> and solid<sup>63</sup> state conformation of a cyclic heptapeptide antibiotic ilamycin B<sub>1</sub>.

The tendency of the aromatic side chain of a residue to fold over the diketopiperazine ring has since been shown in a number of solution<sup>64</sup> and crystal structures of cyclic dipeptides: *cyclo*(L-Pro-D-Phe),<sup>65</sup> *cyclo*(N-Me-L-Phe-N-Me-L-Phe), *cyclo*(N-Me-L-Phe-N-Me-D-Phe),<sup>66</sup> *cyclo*(D-Phe-L-γ-thiaPro),<sup>67</sup> *cyclo*(L-Leu-L-Tyr),<sup>68</sup> *cyclo*(aminoisobutyryl-L-Phe),<sup>69</sup> *cyclo*(L-Phe-L-Phe),<sup>70</sup> *cyclo*(N-Me-L-Phe-L-Phe),<sup>71</sup> and *cyclo*(N-Me-L-α-aminobutyryl-L-Phe).<sup>72</sup> Figure 8.17 shows the crystal structure of *cyclo*(L-Phe-D-Leu-Gly-L-Phe-L-Leu-Gly) tetrahydrate.<sup>73</sup> Short CH/Aryl-distances are shown between the leucine and phenylalanine side chains. Similar conformations are found for its analogues *cyclo*(L-Phe-D-Leu-Gly-D-Phe-L-Leu-Gly) and *cyclo*(L-Phe-L-Leu-Gly-D-Phe-L-Leu-Gly).

## 2. Acyclic Peptides

With regard to linear peptides, folded conformations have long been known for peptides with one aromatic and another aliphatic residue.<sup>74</sup> Examples include the solution conformation of flavinyl peptides,<sup>75</sup> somatostatin,<sup>76</sup> and bradykinin

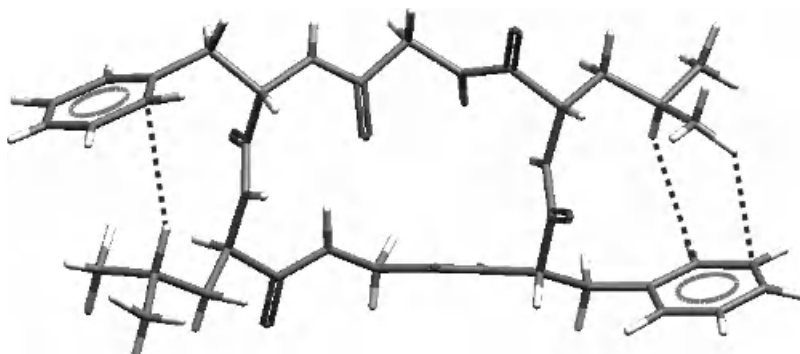


Figure 8.17. X-ray crystal conformation of *cyclo*(L-Phe-d-Leu-Gly-L-Phe-d-Leu-Gly) (CSD refcode PHLEGL10).

analogues.<sup>77</sup> In 1972, Deber and Joshua reported that the folded conformation prevails in solution for a series of dipeptides bearing phenylalanine as a component (L-Phe-d-aa; aa = Asn, Asp, Gln, Glu, Arg, Lys,  $\alpha$ -amino butyric acid, norvaline), on the basis of a systematic  $^1\text{H}$  NMR study.<sup>78</sup> They observed significant upfield shifts for methylene protons of the residue aa, as compared to those in dipeptides with only aliphatic residues: L-Ala-d-aa. It is noteworthy that more pronounced upfield shifts were observed for the methylene hydrogens of polar residues (Asp, Glu, Arg, Lys).<sup>79</sup> They explained the results in terms of an attractive interaction that may operate between the phenylalanine aromatic ring and the CH groups of the other residue. Shimohigashi showed the preference of alkyl/Ar proximate geometry in solution for a series of dipeptide derivatives d-aa-L-Phe-BzI (aa = Leu, Val, Ala; BzI =  $\text{CH}_2\text{C}_6\text{H}_5$ ), d-Arg-L-Phe-NHBzI<sup>80</sup> and chymotrypsin inhibitors d-Leu-L-Phe-NHBzI and d-Thr-L-Phe-NHBzI.<sup>81</sup> They interpreted the result in terms of the CH/π interaction. Kim et al.<sup>82</sup> reported the folded conformation of a chymotrypsin inhibitory peptidomimetic 2-allyl-3-benzenepropanoate and attributed the result to the CH/π interaction.

Short CH/Ar distances have in fact been reported in the crystal structure of dipeptides L-Asp-L-Phe and L-Phe-L-Pro.<sup>83</sup> Smith and Griffith provided evidence for the folded crystal conformation in enkephalin.<sup>84</sup> Figure 8.18 gives the X-ray crystal conformation of leucine-enkephalin Tyr-Gly-Gly-Phe-Leu.<sup>85</sup> We see an aromatic CH/π bond (2.67 Å) between the side chains of Tyr and Phe. The folded structure is assisted by two hydrogen bonds. The compact shape of the peptides may correlate with their biological activity.<sup>86</sup> The extended crystal conformation, however, was reported in two enkephalin fragments Tyr-Gly-Gly-Phe and Gly-Gly-Phe-Leu.<sup>87</sup>

Burley et al. reported on the Aryl/Aryl proximate crystal structure for L-Lys-L-Phe-L-Phe, L-Phe-Gly-Gly-d-Phe, L-phenylalanyl benzyl ester and *N*-L-phenyl-acetyl-L-Phe.<sup>88</sup> Figure 8.19 shows the crystal structure of L-Phe-Gly-Gly-d-Phe

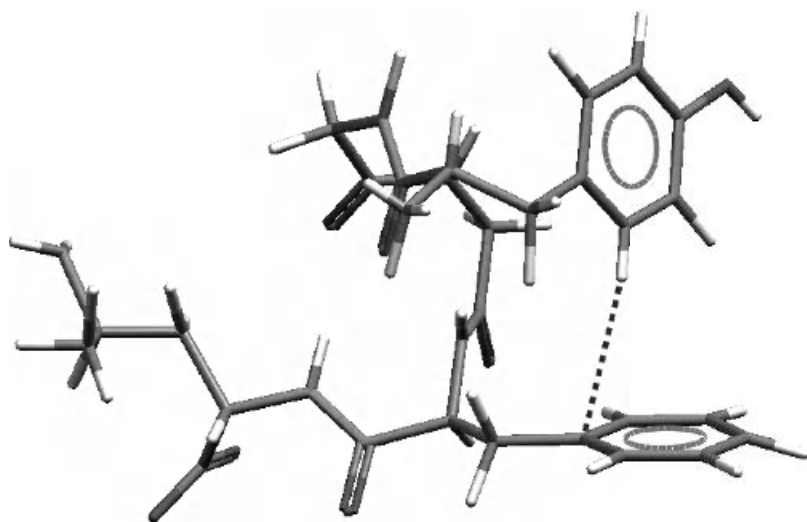


Figure 8.18. X-ray crystal conformation of leucine-enkephalin (CSD refcode GEWWAG).

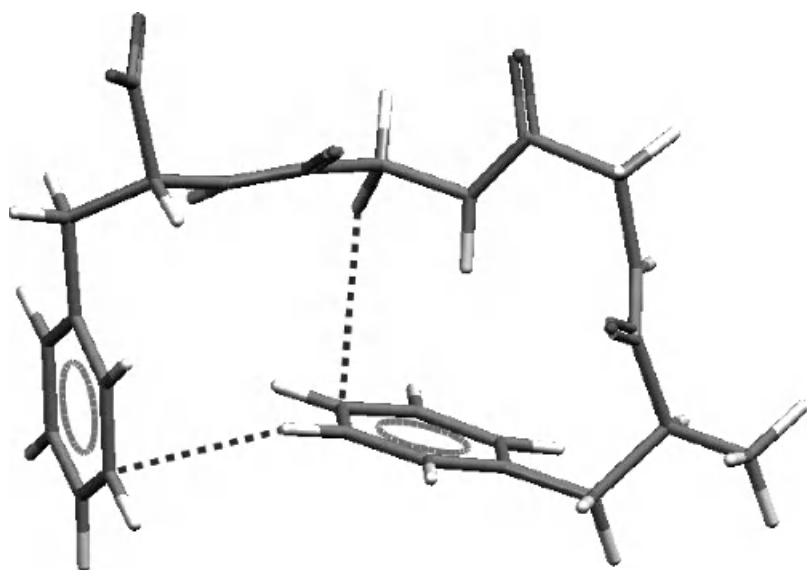


Figure 8.19. X-ray crystal conformation of L-Phe-Gly-Gly-d-Phe (CSD refcode FEYZEO).

trihydrate.<sup>89</sup> Short intramolecular CH/Aryl distances are noted between a glycine and an aromatic carbon of a phenylalanine (3.06 Å) and between aromatic rings of the phenylalanines (2.76 Å). NH/π contact is also shown between NH of Gly and the aromatic rings of Phe. It is remarkable that the molecule adopts the compact structure without any intramolecular hydrogen bonds. They speculated that a stabilizing interaction is working between the relevant groups. The results are now understood in the context of the CH/π and NH/π hydrogen bonds.

A number of CH/π associated folded conformations have also been unveiled in the X-ray crystal structures of higher peptide analogues. Examples include Gly-Phe-Phe, Phe-Gly-Gly, formyl-Met-Leu-Phe, Lys-Phe-Phe, Leu-Leu-Tyr, Pro-Tyr-Ile-Leu, Tyr-D-Thr-Gly-Phe-Leu-Thr, and Val-Phe-Phe-Ala-Phe-Phe-Val-Phe-Gly. A similar folded conformation was reported for Boc-Gly-Gly-Gly benzyl ester (Figure 8.20).<sup>90</sup> It is remarkable that the terminal *t*-butyl group is curled over the aromatic group at the other terminus of the peptide. Toniolo and coworkers found the folded X-ray crystal conformation in longer synthetic peptides.<sup>91</sup>

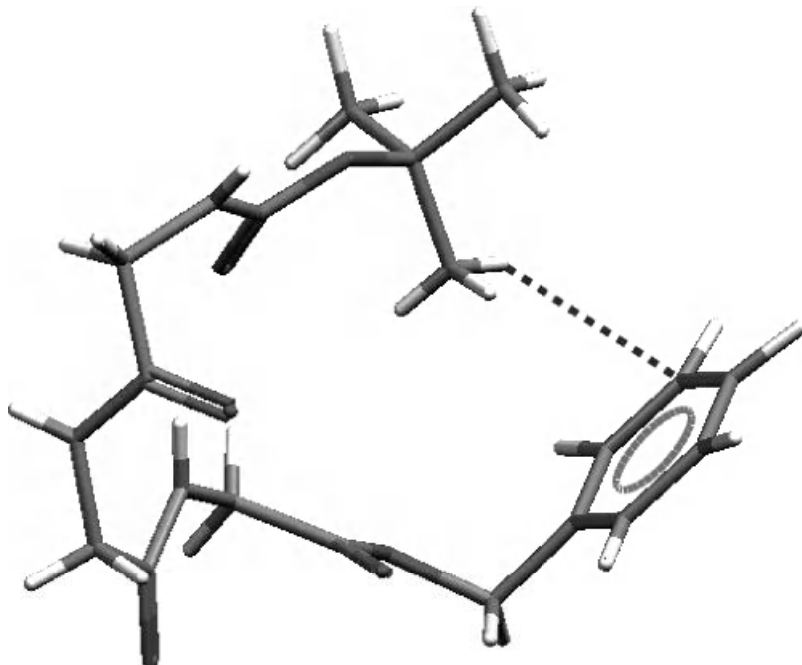


Figure 8.20. X-ray crystal conformation of Boc-Gly-Gly-Gly benzyl ester (CSD refcode GEGLOT).

### III. INTERLIGAND INTERACTIONS IN COORDINATION AND ORGANOMETALLIC COMPOUNDS

#### A. Coordination Compounds

In 1974 Sigel pointed out that ternary metal complexes with ligands bearing at least one aromatic group such as 2,2'-bipyridyl, 1,10-phenanthroline, aromatic amino acids, and nucleic acid bases are in the folded conformation.<sup>92,93</sup> This was substantiated later by their own crystallographic determinations of  $[\text{Cu}(1,10\text{-phenanthroline})(\text{L-phenylpropionate})]$ ,<sup>94</sup>  $[\text{Cu}(\text{histamine})(\text{L-Phe})]$ , and  $[\text{Cu}(\text{histamine})(\text{L-Tyr})]$ .<sup>95</sup>

Okawa first recognized the importance of CH/π interactions in the stereoselectivity of the formation of coordination compounds.<sup>96,97</sup> Later the folded structure was reported for the X-ray crystal conformation of bis[N-(R)-1-phenylethylsalicylideneiminato]-zinc.<sup>98</sup> Masuda reported on the importance of CH/π bonds in cobalt complexes of *N*-pyridoxy-L-amino acids.<sup>99</sup> They also reported on the indispensable role of intramolecular CH/π bonding in ternary metal complexes involving methyl-substituted phenylalanines as ligand.<sup>100</sup>

The role of CH/π hydrogen bonds has been shown in intramolecular interactions of porphyrin coordination systems in solution.<sup>101</sup> For instance, Inoue et al. showed, by <sup>1</sup>H NMR analysis, CH/π interactions between alkyl groups coordinated to the central metal and aromatic rings at the *ortho*-positions of a *meso* phenyl substituent.<sup>102</sup> Mizutani found intramolecular short CH/π distances in a zinc porphyrin derivative in a complex with various amines and amino esters.<sup>103</sup> Venkatraman et al. observed CH/π interactions between a pyrrole-CH and a mesityl ring of 10,15-*meso* aryl azuliporphyrins.<sup>104</sup>

#### B. Transition Metal Compounds

Colquhoun et al. reported that CH/π interactions are important in rhodium complexes with dibenzo-3*n*-crown-*n* ethers and cycloocta-1,5-diene or norbornadiene.<sup>105</sup> In every case the diene ligands were found to be sandwiched between the two aromatic rings of the dibenzo-crown so that a number of allylic and vinylic CH groups are brought about into close proximity with the π-arene systems. An example is shown in Figure 8.21. They argued that stabilizing interactions occur between these ligands, which are oriented with their planes orthogonal to each other.

Onaka studied the structure of  $[(\eta^5\text{-CH}_3\text{C}_5\text{H}_4)\text{Mn}(\text{CO})1,1'\text{-bis}(\text{diphenylphosphino})\text{ferrocene}]$ .<sup>106</sup> This compound crystallized in two crystal forms with slightly different colors; they exhibited IR (C≡O) peaks at 1835 and 1810 cm<sup>-1</sup>, respectively. Figure 8.22 shows the X-ray crystal structure of the more stable isomer. The distance between one of the hydrogens on the methyl group to the

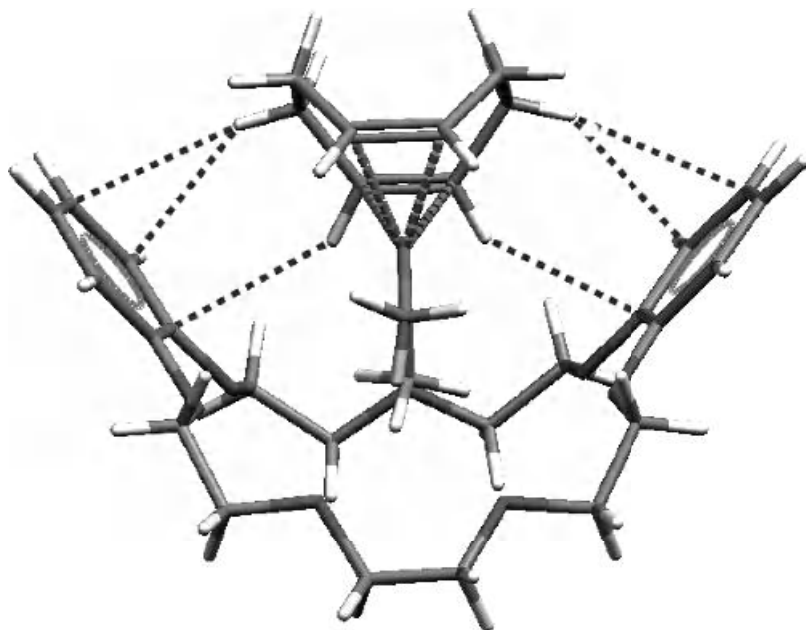


Figure 8.21. X-ray crystal conformation of rhodium complexes with dibenzo- $3n$ -crown- $n$  ethers and cycloocta-1,5-diene (CSD refcode DUDSUQ).

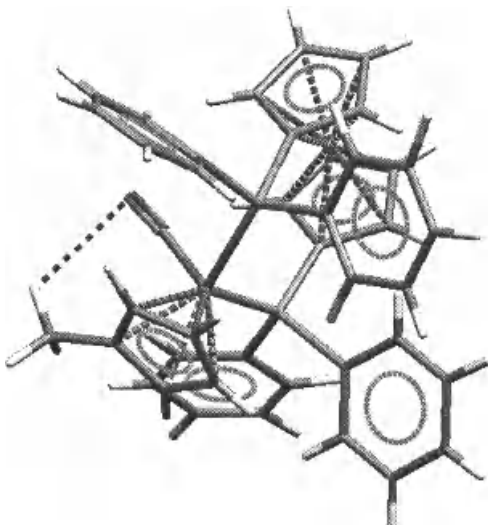


Figure 8.22. X-ray crystal conformation of  $[(\eta^5\text{-CH}_3\text{C}_5\text{H}_4)\text{Mn}(\text{CO})1,1'\text{-bis(diphenylphosphino)}\text{ferrocene}]$  (CSD refcode YALLEC).

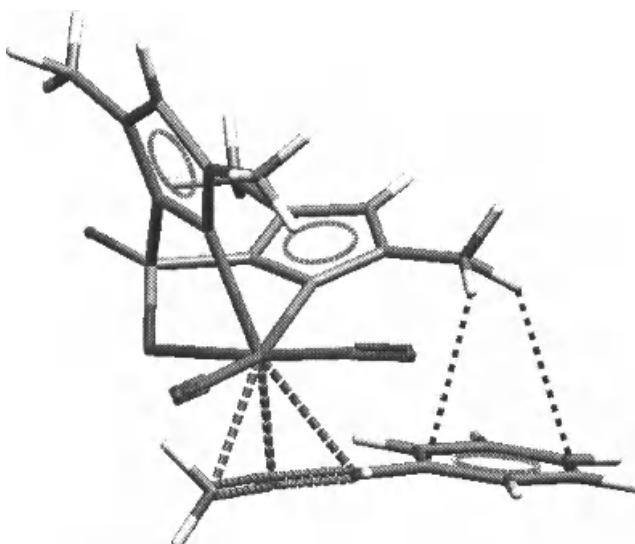


Figure 8.23. X-ray crystal conformation of  $\text{LMo}(\text{CO})_2(\eta^3\text{-H}_2\text{C}=\text{CHCHC}_6\text{H}_4\text{X})$ :  $\text{L} = \text{bis}(3,5\text{-dimethyl-1-pyrazolyl})\text{phosphate}$  (CSD refcode POMJUW).

midpoint of the  $\text{C}\equiv\text{O}$  bond was reported to be very short ( $2.70\text{\AA}$ ). The IR data are consistent with the expectation that the  $\text{CH}_3/\text{C}\equiv\text{O}$  eclipsed conformation is kept also in solution. They argued the findings on the basis of the  $\text{CH}/\pi$  hydrogen bond.

Sarkar studied the crystal and solution conformation of a series of molybdenum complexes  $\text{LMo}(\text{CO})_2(\eta^3\text{-H}_2\text{C}=\text{CHCHC}_6\text{H}_4\text{X})$ :  $\text{L} = \text{bis}(3,5\text{-dimethyl-1-pyrazolyl})\text{phosphate}$ .<sup>107</sup> A methyl group in the 3,5-dimethyl-1-pyrazolyl moieties in a stable conformation was found to place itself just above the phenyl ring (Figure 8.23). Replacement of the *para*-hydrogen with an electron-donating  $\text{OCH}_3$  and an electron-withdrawing  $\text{NO}_2$  was accompanied, respectively, by an increase and decrease of the ratio of the folded conformer. This shows that increase of the  $\pi$ -electron density of the aromatic ring will favor the  $\text{CH}/\pi$  associated structure.

Yamanari reported on the stabilizing role of a methyl group on the basis of stereoselectivity of the formation of linkage isomers, *fac* and *mer*, in cobalt and ruthenium complexes containing pyrimidine-2-thione derivatives and 2,2'-bipyridyl.<sup>108</sup> The X-ray crystal structure of linkage isomers of  $[\text{Ru}(4\text{-methyl-pyrimidine-2-thione})(2,2'\text{-bipyridyl})_2]$  was determined (Figure 8.24).<sup>109</sup> The difference in the stability of the adjacent and remote isomers has been attributed to  $\text{CH}_3/\pi$  hydrogen bonds occurring between the ligands. Schmidt also showed the stabilizing role of the  $\text{CH}_3/\pi$  bond in the crystal and solution conformation of several antimony complexes (Figure 8.25).<sup>110</sup>

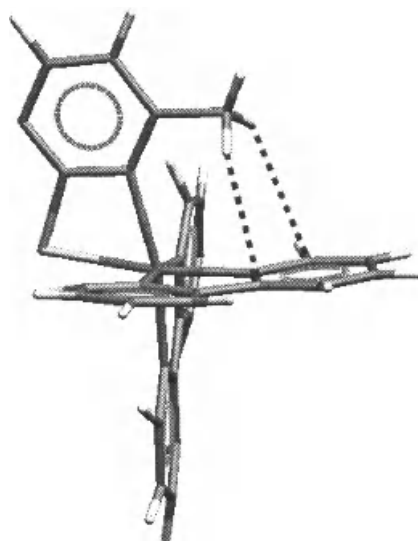


Figure 8.24. X-ray crystal conformation of a ruthenium complex containing 4-methyl-pyrimidine-2-thione and 2,2'-bipyridyl (CSD refcode TISHOS).

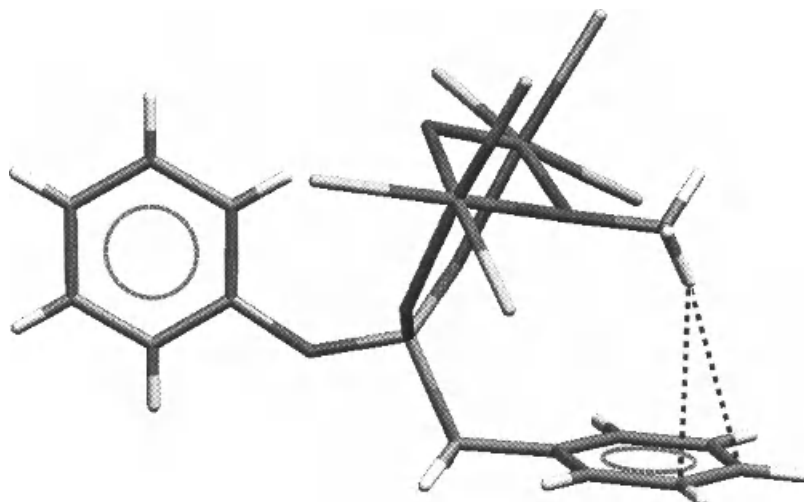


Figure 8.25. X-ray crystal conformation of  $\mu$ -methoxy- $\mu$ -oxo- $\mu$ -phenyl-benzylphosphonato- $\kappa$ -O,  $\kappa$ -O'-bis[trichloro-antimon(V)] (CSD refcode GUGDAN).

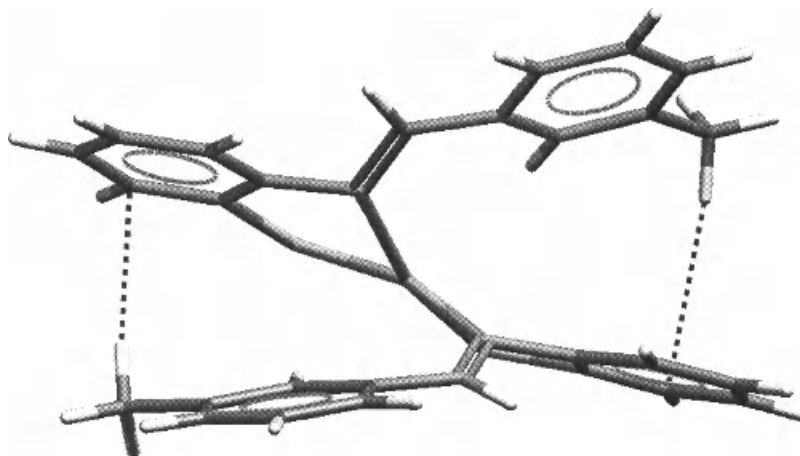


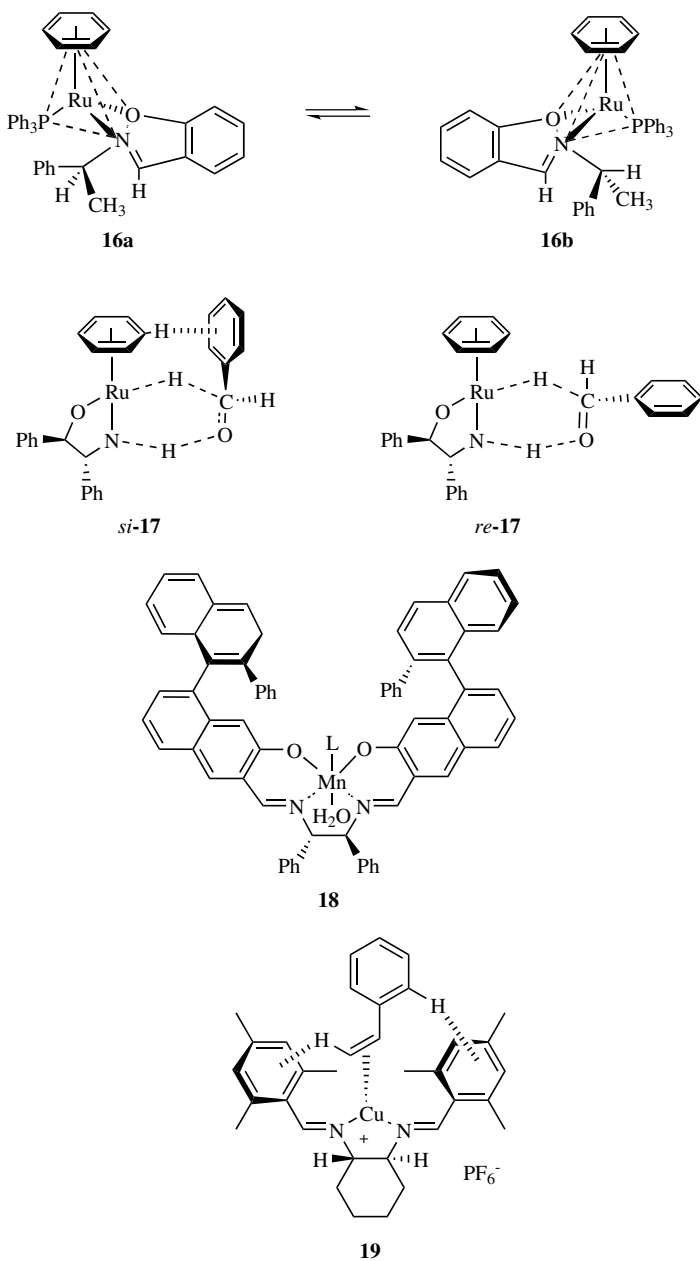
Figure 8.26. X-ray crystal conformation of bis[2-(*m*-tolylmethylenamino)-benzenethiolato]nickel(II) (CSD refcode LOPMEI).

Cini et al. studied the crystal structure of transition metal complexes of purine-6-thione and triphenylstibine.<sup>111</sup> There they found short distances (2.43, 2.59 Å) between an aromatic CH of the purine ligand and a phenyl group of Ph<sub>3</sub>Sb adjacent to it. They also noted a close contact of an aromatic CH to another aromatic ring in a neighboring ligand in 1,9-dimethylpurine-6-thione, 3,5-dimethylpyridine, and 1,4-pyrazine.<sup>112</sup> Methyl groups in the pentamethylcyclopentadienyl moiety were found, in a rhodium<sup>113</sup> and a ruthenium complex,<sup>114</sup> to be just over the phenyl ring in the phenyl-substituted pentadienyl ligand.

Kawamoto determined the crystal structure of bis[2-(*m*-tolylmethylenamino)-benzenethiolato]nickel(II). The methyl group of the pendant arm was found close to the 2-amino-benzenethiol moiety (Figure 8.26).<sup>115</sup> Variable temperature <sup>1</sup>H NMR studies indicated that the restriction of rotation of the pendant arm is attributable to the effect of CH/π bonds. There are many other papers reporting on the CH/π hydrogen bond in metal complexes.<sup>116</sup>

### C. CH/π Hydrogen Bonds Implicated in the Mechanism of Enantioselective Catalytic Reactions<sup>117</sup>

In 1983, Brunner first reported that a ruthenium complex with arene ligands might exist in a pair of diastereomers.<sup>118</sup> By <sup>1</sup>H-NMR determinations, one of the diastereomers in a half-sandwich complex [ $\eta^6$ C<sub>6</sub>H<sub>6</sub>Ru(1-phenylethylsalicylaldehyde)PPh<sub>3</sub>]PF<sub>6</sub> **16a** has been shown to be more stable than the diastereoisomeric congener **16b** (Scheme 8.3, **16–19**). In the X-ray crystal structure of the more



Scheme 8.3

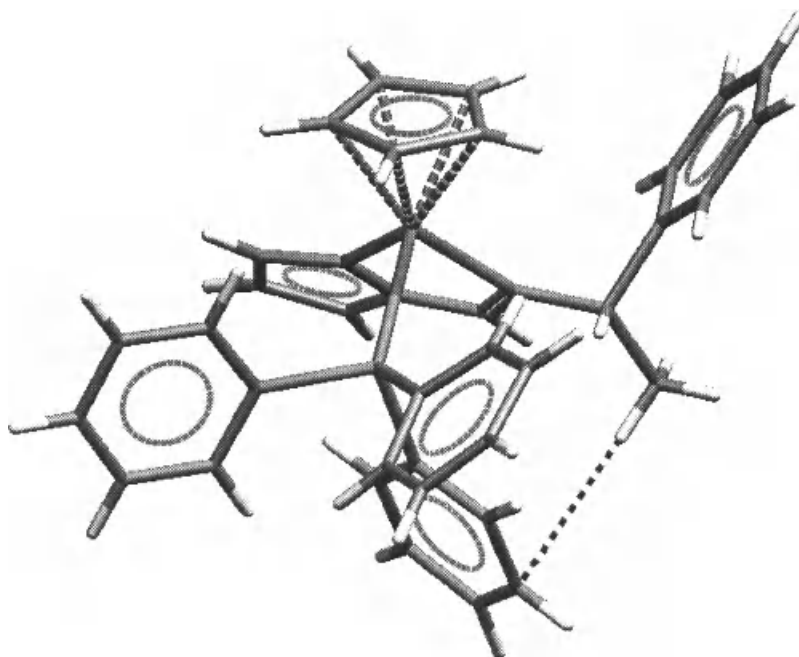
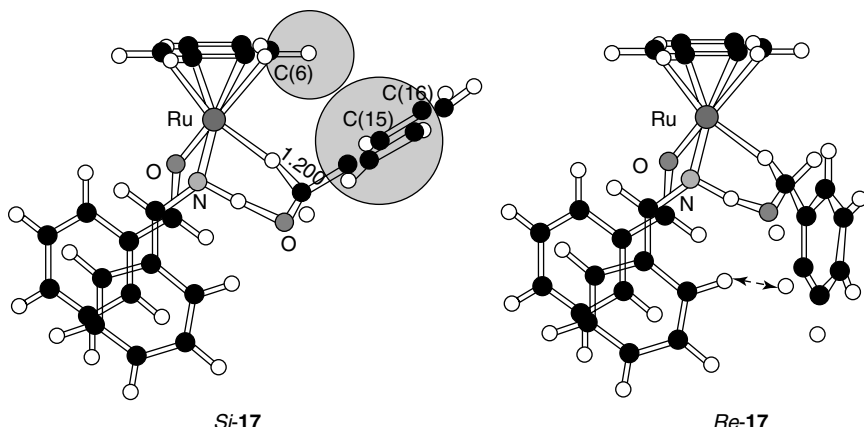


Figure 8.27. X-ray crystal conformation of the more stable diastereoisomer of  $[\eta^6\text{C}_6\text{H}_6\text{Ru}(1\text{-phenylethylsalicylaldimine})\text{PPh}_3]$  (CSD refcode JUFQAC).

stable isomer **16a**, a CH group of the  $\eta^6$ -benzene ligand was found to point to the aromatic ring in the neighboring 1-phenylethylsalicylaldimine group. Brunner termed this phenomenon the “ $\beta$ -phenyl effect”<sup>119</sup> and suggested that the transition metal complexes that are configurationally stable at the central metal atom can be used as optically active auxiliaries in enantioselective synthesis. The mechanism is now understood in terms of the CH/π hydrogen bond.<sup>120</sup> Figure 8.27 gives the crystal structure of another complex showing an interesting case of the new isomerism, propeller isomerism.<sup>121</sup> The configuration of the three phenyl rings in the crystal is primarily determined by intramolecular CH/π interactions and not by packing forces.<sup>122</sup>

Noyori studied by MO calculations, the ruthenium-catalyzed hydrogen transfer between alcohols and carbonyl compounds **17** (Figure 8.28). A short CH/π contact [C(6)H/C(15) distance 2.993 Å] was shown in the more favored transition structure of the asymmetric transfer.<sup>123</sup> The origin of the enantioselectivity in the transfer hydrogenation of aromatic carbonyl compounds, catalyzed by chiral  $\eta^6$ -arene-ruthenium complexes, was attributed to the CH/π hydrogen bonds.<sup>124</sup>



*Figure 8.28.* Diastereomeric transition structures, *Si-17* (favored) and *Re-17* (less favored). The geometries were optimized at the B3LYP/LAN2DZ level. Adapted from Yamakawa et al. (*Angew. Chem., Int. Ed. Engl.* **2001**, *40*, 2818–2821, Fig. 1).

To accommodate the remarkable enantioselectivity of an osmium-catalyzed reaction, Sharpless suggested that the edge-to-face relationship between two aromatic ligands in the osmium complex is important in stabilizing the transition-state leading to the preferred dihydroxylation product.<sup>125</sup> Importance of CH/π interactions in stabilizing the structure of transition metal complexes has in fact been demonstrated in a number of crystallographic determinations of enantioselective catalysts. Gladysz studied the crystal structure of a chiral rhenium complex  $[(\eta^5\text{-C}_5\text{H}_5)\text{Re}(\text{NO})(\text{PPh}_3)(\text{S}(\text{CH}_2\text{Ph})_2)]^+\text{TfO}^-$ .<sup>126</sup> The remarkable selectivity observed in the [1,3]-hydrogen migration was attributed to the attractive force operating between the cyclopentyl and a phenyl group in the triphenylphosphane ligand. Katsuki analyzed the crystal structure of a (salen)manganese(III) complex **18** with axial chirality (Figure 8.29).<sup>127</sup> There they presented an explanation, based on OH/π and CH/π interactions, for the effect of apical ligand on the catalytic asymmetric epoxidation.

Jacobsen found that  $C_2$ -symmetric 1,2-diimines are effective ligands for copper-catalyzed enantioselective aziridination<sup>128</sup> and cyclopropanation.<sup>129</sup> The crystal structure of a Cu(I) complex **19** bound to styrene was determined (Figure 8.30). Two 1,3,5-tri-*t*-butylphenyl groups in the ligand are orthogonal to each other, with the phenyl group of styrene lying squarely in the resulting cleft. CH/π bonds of the *cis*-β-hydrogen and an aromatic CH of styrene with the arene moiety of the complex stabilize the binding of the prochiral substrate. Preferential binding, in solution, of one enantioface of the alkene to the chiral complex is apparent from inspection of relevant proton and carbon NMR signals at low temperature. Implication for the design of ligands based on chiral diaryldiamines

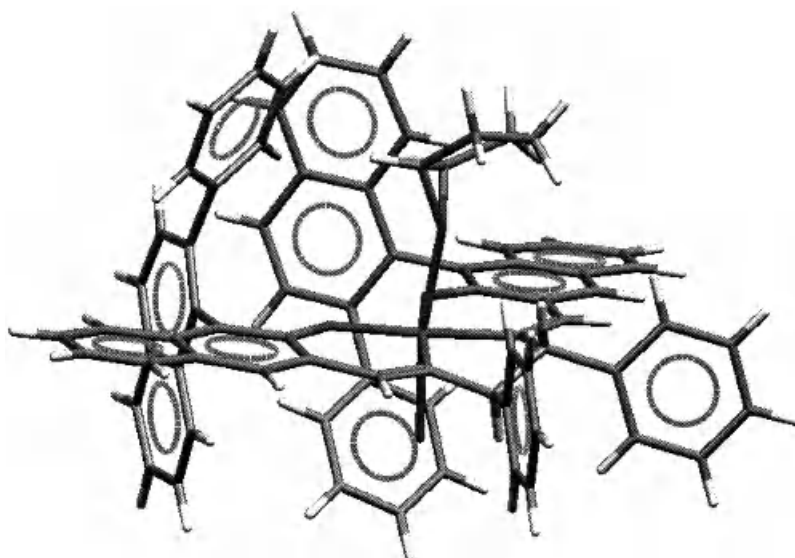


Figure 8.29. X-ray crystal conformation of a (salen)manganese(III) complex **18**, L = cyclopentene oxide (CSD refcode RORXEB).

has been suggested. Scott discussed on the structural origin of a variation in the catalyst efficiency in enantioselective aziridination reactions of alkenes.<sup>130</sup> Such an effect was found also in the crystal structure of ( $\eta^6$ -arene)ruthenium complexes bearing *p*-cymene as a ligand.<sup>131</sup>

To summarize this section, CH/ $\pi$  hydrogen bonds can reduce the conformational degree of freedom of a prochiral substrate in the transition metal catalyst. The decrease of freedom enhances the difference in the Gibbs energies ( $\Delta\Delta G^\ddagger$ ) of the rate-determining step of enantioselective reactions.

#### IV. THREE-DIMENSIONAL STRUCTURE OF BIOPOLYMERS

In this section CH/ $\pi$  interactions implicated in the three-dimensional (3D) structure of proteins and nucleic acids are briefly reviewed. Readers interested in these issues are referred also to other review articles.<sup>132,133,134</sup>

##### A. Proteins

In 1978, one of the authors of this chapter pointed out that a CH/ $\pi$  hydrogen bond could play a role in biochemistry on the grounds that protein structural data

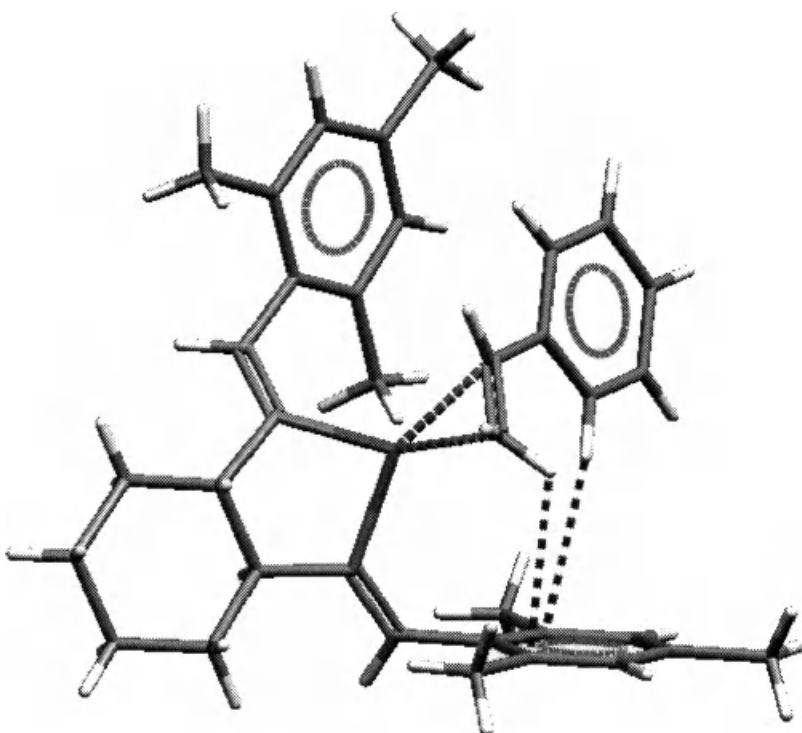


Figure 8.30. X-ray crystal structure of **19** bound to styrene (CSD refcode TIZZIL).

scatters, as was noted in the literature.<sup>135</sup> Perutz first recognized the importance of the  $\pi$ -hydrogen bond in structural biology.<sup>136</sup> A number of studies have since appeared demonstrating the importance of CH/ $\pi$  interaction in the 3D structure of biopolymers.

Kim and coworkers determined the X-ray structure of a carboxypeptidase/inhibitor complex.<sup>137</sup> They found short distances between Leu203 and Ile243 of the protein and the phenyl group of the inhibitor 2-benzyl-2,4-epoxybutanoic acid and attributed the result to the CH/ $\pi$  interaction. Hirama determined the structure of an antitumor antibiotic neocarzinostatin by  $^1\text{H}$  NMR analysis and explained the result in terms of the CH/ $\pi$  interaction.<sup>138</sup> Kim determined the crystal structure of neocarzinostatin;<sup>139</sup> the aromatic rings of two phenylalanine residues were found in the edge-to-face relationship.

Quirocho and Vyas studied the crystal structure of several carbohydrate-binding protein/carbohydrate complexes. Specific substrate such as L-arabinose<sup>140</sup> and D-glucose<sup>141</sup> was found sandwiched by aromatic side chains of Phe and Trp in

the proteins. It is noteworthy that axial CHs of the carbohydrates point to the surface of the aromatic ring of these residues. Harata and Muraki determined a number of X-ray crystal structures of proteins specific to carbohydrates such as lysozyme,<sup>142</sup> hevein domains,<sup>143</sup> and wheat-germ agglutinin in complex with specific substrates;<sup>144</sup> there they found a number of short distances between CHs of the ligands and aromatic residues of the proteins. Muraki reviewed the importance of CH/π hydrogen bonds in proteins specific to carbohydrates.<sup>145</sup> Fantini reviewed the possibility of aromatic residues of bacterial adhesins and toxins to interact with carbohydrates of glycosphingolipids.<sup>146</sup>

A number of crystallographic studies pointed out also the importance of CH/π hydrogen bonds, including Tet repressor/tetracycline complex,<sup>147</sup> glycogen phosphorylase b,<sup>148</sup> chymotrypsin,<sup>149</sup> porcine pancreatic elastase,<sup>150</sup> dienolactone hydrolase,<sup>151</sup> aldose reductase,<sup>152</sup> β-lactoglobulin,<sup>153</sup> squalene cyclase,<sup>154</sup> adenosine deaminase,<sup>155</sup> lectins,<sup>156</sup> estrogen receptor,<sup>157</sup> pheromone-binding protein,<sup>158</sup> and human poly(ADP-ribose) polymerase, etc.<sup>159</sup> Use of the CH/π hydrogen bond in the drug design has been suggested.<sup>160</sup>

Umezawa and Nishio retrieved coordinates of several proteins from the Protein Data Bank (PDB) and analyzed the structures by using a program composed for the survey of XH/π contacts in biopolymers.<sup>161</sup> The proteins examined include hemoglobin, lysozyme, D-xylene isomerase, carp parvalbumin,<sup>162</sup> GTP specific proteins, SH2 domains,<sup>163</sup> major histocompatibility antigens,<sup>164</sup> and TATA-box binding proteins,<sup>165</sup> etc.<sup>166</sup> Figure 8.31 gives the global view of the parvarlbumin crystal structure. Notice that the structure of this small protein (109 residues) is tightly held by many phenylalanines buried in the interior of the molecule.

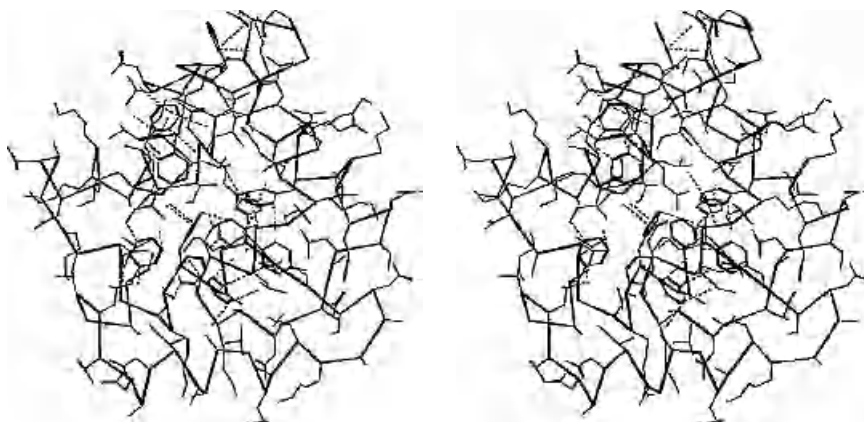


Figure 8.31. Stereoview of carp parvalbumin (PDB code 5CPV). Dotted lines indicate short CH/π contacts. Source: Nishio et al. (*Kagaku to Seibutsu* **1995**, 33, 311–318, Fig. 7).

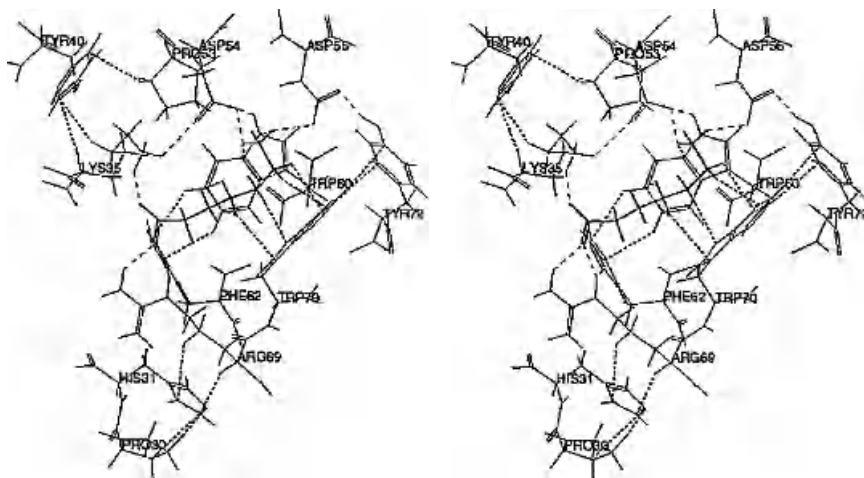


Figure 8.32. Stereoview of the substrate-binding region of human plasminogen kringle (PDB code 2PK4). CH/π interactions (dotted lines) and hydrogen bonds (dashed lines). Source: Nishio et al. (*Yuki Gosei Kagaku Kyokaishi* 1997, 55, 18–28, Fig. 20).

Figure 8.32 shows the substrate-binding region of human plasminogen kringle. Notice that aromatic as well as aliphatic CHs in the side chain are involved in the binding of the specific substrate  $\epsilon$ -aminocaproic acid (a lysine analogue), in cooperation with hydrogen bonds.

A remarkable fact is that not only nonpolar residues such as valine and leucine but the side chains of lysine and arginine are often involved in CH/π bonds by using their methylene CHs. The present author termed this the “lysine-arginine CH/π interaction”.<sup>167</sup> The energetic contribution from this kind interaction is considerable.<sup>168</sup> It is certain that these residues are effective, with the use of the linearly arranged CHs and the terminal NH group, in stabilizing the 3D structure of proteins. Figures 8.33 and 8.34 illustrate such interactions that were unveiled in human growth hormone-binding protein.

The active-site gorge of acetylcholine esterase (AchE) is lined with a number of aromatic residues,<sup>169</sup> and it was believed for long to bind only cationic molecules such as acetylcholine [Ach:  $(\text{CH}_3)_3\text{N}^+\text{CH}_2\text{CH}_2\text{OCOCH}_3$ ]. This phenomenon, however, is better accommodated in the context of the CH/π interaction. To be effective, CH hydrogens do not need to be polarized much. Cohen et al. studied the kinetics of the binding of Ach analogues such as 3,3-dimethylbutyl acetate, 4-*t*-butylthio-2-butanone, and 3,3-dimethylbutanol with AchE.<sup>170</sup> These neutral compounds were found to bind as effectively as Ach to the so-called anionic site of the enzyme.<sup>171</sup> This demonstrates that the positive charge makes little contribution if any to the binding.<sup>172</sup> Comparisons of quaternary compounds  $(\text{CH}_3)_3\text{N}^+ - \text{R}$  and

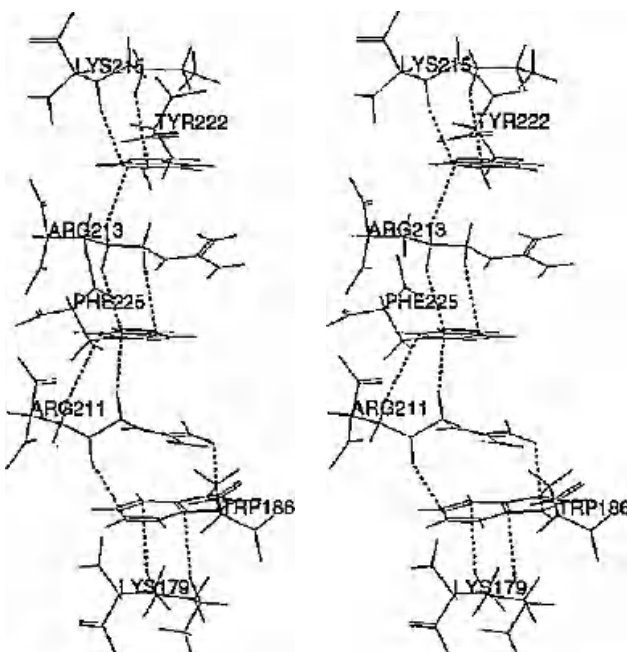


Figure 8.33. A lysine-arginine CH/π interaction network disclosed in human growth hormone-binding protein (PDB code 3HHR). Source: Nishio et al. (*Yuki Gosei Kagaku Kyokaishi* **1997**, 55, 18–28, Fig. 23).

$(CH_3)_3C-R$  as ligands with their corresponding lower analogues  $(CH_3)_2N^+H-R$  and  $(CH_3)_2CH-R$  showed the latter to be much less effective than the former with regard to its binding capabilities to AchE. It is apparent that the number and probability of the CHs participating in the interaction lend more intense effect in stabilizing the structures of the complex.<sup>173</sup> Our survey of CH/π interactions involved in the X-ray crystal structures of various AchE/substrate complexes supports this suggestion.<sup>174</sup> Recently an uncharged inhibitor polyethylene glycol derivative  $HS(CH_2CH_2O)_5CH_2CH_2OH$  has been shown to bind the active site of AchE.<sup>175</sup>

## B. Nucleic Acids

In 1978, Kennard and coworkers determined the crystal structure of a deoxytetranucleotide 5'-*P*-adenylyl-3',5'-thymidylyl-3',5'-adenylyl-3',5'-thymidine (pATAT; A, adenine; T, thymine). There they found the structure of the sugar-phosphate backbone to be very different from the canonical structure of *B*-DNA; the

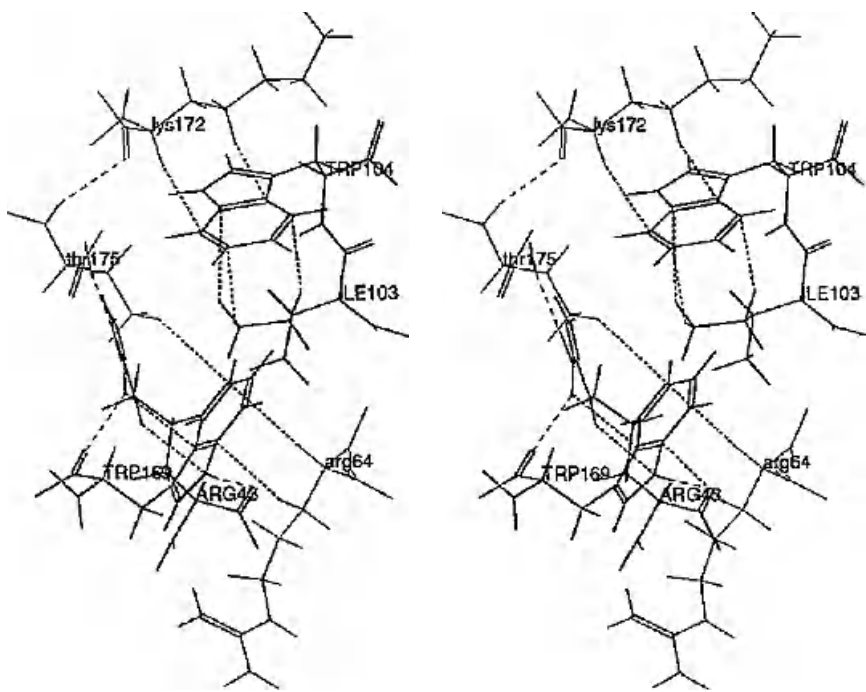


Figure 8.34. CH/π interactions (dotted lines) and hydrogen bonds (dashed lines) involved in the high-affinity binding site of human growth hormone-binding protein complexed with human growth hormone (PDB code 3HHR). Source: Nishio et al. (*Yuki Gosei Kagaku Kyokaishi* **1997**, *55*, 18–28, Fig. 22).

conformation of the phosphodiester-bridge changes between the A-T and T-A steps (Figure 8.35). Thus the first two bases A and T pair with the complementary bases from another molecule, but then the phosphate backbone swings away from the helical orientation.<sup>176</sup> Klug et al. reported an unusual conformation of a DNA polymer with repeating A-T sequences.<sup>177</sup> T is stacked with the preceding adenine base, but there is no interaction of T with A next to it. They noticed the methyl group of thymine in an A-T step to place itself over the ring of A, whereas in the T-A step there was no such an interaction. This was argued as the primary cause of the DNA structure and suggested importance of CH<sub>3</sub> in T.

Umezawa and Nishio found, by the analysis of DNA structures in the Nucleic Acid Database (NDB), the important role of T-methyl group in stabilizing the DNA 3D structure.<sup>178</sup> Figure 8.36 shows an illustrative example for the ATAT portion of a DNA CGCGATATCGCG (C, cytosine; G, guanine). Since an A-T sequence is lined with another A-T in the complementary strand, this makes up

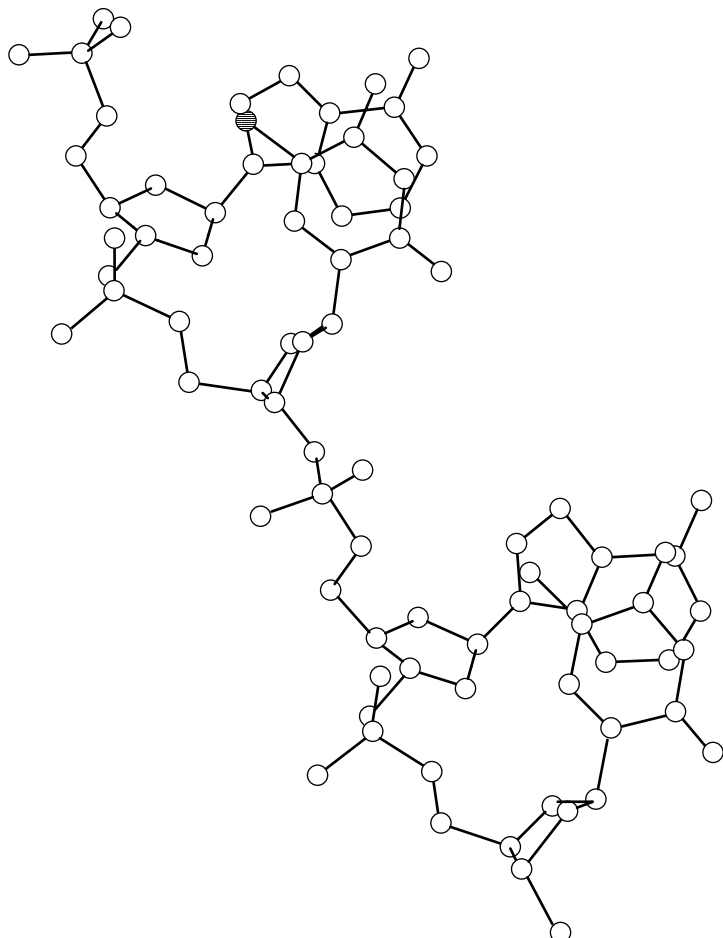


Figure 8.35. Crystal conformation of 5'-P-adenylyl-3',5'-thymidylyl-3',5'-adenylyl-3',5'-thymidine. Adapted from Viswamitra et al. (*Biopolymers* **1982**, *21*, 513–533, Fig. 2).

two sets of CH/π interactions. Such a “twin T-methyl/π interaction” brings this part of the DNA robust and sticky. A repeated A-T sequence often appears at the upstream of a gene. This is implicated in the sequence-dependent deformability of the DNA double helix and thus may modulate various biochemical events such as duplication and transcription. Chou et al. reported on a remarkable stabilizing effect of thymine CH<sub>3</sub> group by an NMR study of the d(TTG) loop structure.<sup>179</sup>

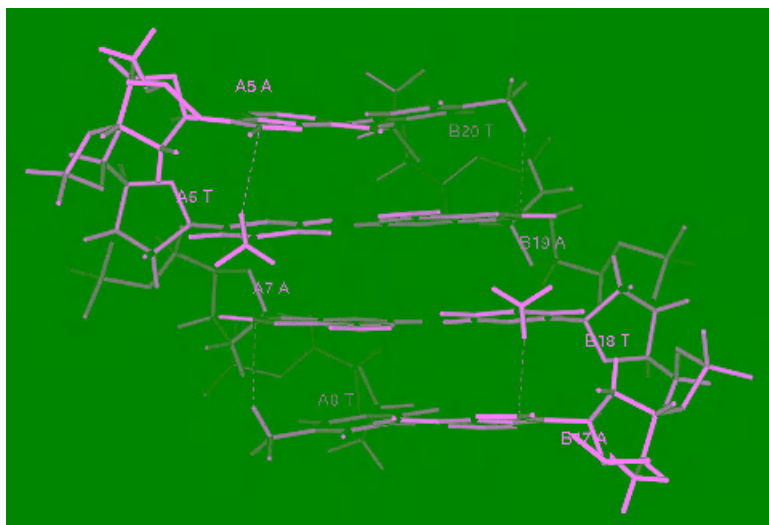


Figure 8.36. Crystal structure of the ATAT portion of a DNA CGCGATATCGCG (NDB code BDL078). T in white and A in yellow. Red sticks indicate CH/π contacts. See color insert.

Methylation at C(5) of cytosine or N(6) of adenine is interesting with regard to important biochemical events such as transcription and resistance to restriction enzymes, since such a modification may result in the change in the robustness of DNA.<sup>180</sup> Our analysis of the crystal data retrieved from the NDB gave conclusion consistent with this hypothesis: the CH<sub>3</sub> group in the modified DNA was found to form an additional contact with the π-base preceding it.

To summarize this section, the CH/π hydrogen bond has been shown to play an indispensable role in determining the 3D structure and the substrate specificity of biopolymers.

## V. DATABASE STUDIES

### A. Compounds of Small Molecular Weight

Takahashi et al. analyzed crystallographic data retrieved from the Cambridge Structural Database (CSD) and showed that a considerable fraction (>29%) of aromatic compounds involved CH/π intramolecular distances shorter than 3.05 Å.<sup>181</sup> Umezawa et al. reported that short intramolecular CH/π distances were found in 42% peptide structures (55/130) bearing at least one aromatic residue.<sup>182</sup> The proportion of hit entries was 94% when intermolecular CH/π contacts

were surveyed in the same database subset. Janiak examined the interaction in organometallic entries in the CSD and reported that the complete stacking of planar ligands was rare; offset  $\pi/\pi$  stacks or aromatic CH/ $\pi$  interactions dominate.<sup>183</sup> Suezawa et al. examined the crystal structure of transition metal compound and found short intramolecular CH/ $\pi$  contacts in more than 50% of the CSD entries.<sup>184</sup> Zaric and coworkers found many CH/ $\pi$  contacts involved in the planar chelate ring of transition metal compounds.<sup>185</sup> Reger reported that the offset  $\pi/\pi$  stacking and CH/ $\pi$  hydrogen bond are commonly observed in metal complexes of 1,1',3,3'-tetrakis(pyrazol-1-yl)propane.<sup>186</sup>

By a systematic search of the CSD and comparison of the results obtained by the MO method, Allen, Harris and Taylor have presented evidence that the effect of the so-called packing forces is neither large nor systematic for controlling the crystal conformation of organic compounds.<sup>187</sup> Suezawa et al. carried out a combined database and MO study for organic compounds with substructure ArylCH<sub>2</sub>XCH<sub>2</sub> and ArylCHCH<sub>3</sub>XCH.<sup>188</sup> The proportion of crystal structures bearing an alkyl (R) and aromatic (Aryl) group in the *syn* relationship relative to the *anti*-conformation  $r_{syn/anti}$  was found to depend on the nature of the group R and X. A linear correlation has been shown to exist between  $\ln r_{syn/anti}$  and  $\Delta G_{syn-anti}$ . Thus the CH/ $\pi$  interaction is important in controlling the R/Aryl-folded structure of aralkyl compounds. Recent ab initio MO calculations give results consistent with this suggestion.<sup>189</sup>

## B. Biopolymers

In 1985 Burley and Petsko,<sup>190</sup> and Singh and Thornton,<sup>191</sup> examined the orientation of phenylalanine side chains in proteins and found that the edge-to-face interaction is generally favored over the face-to-face orientation. The result is now understandable in the context of the aromatic CH/ $\pi$  hydrogen bond. By analyzing 19 adenine-cofactor specific enzymes, Chakrabarti and Samanta found that CH/ $\pi$  interactions play a vital role in the binding of substrates.<sup>192</sup> Weiss et al. retrieved 1154 protein structures from the PDB and examined close contacts between CH and  $\pi$ -groups.<sup>193</sup> On the donor side, a preference for aromatic CH groups was found, but also for the aliphatic side chains of the amino acid residues. CH/ $\pi$  interactions involving aromatic groups, either as donor or as acceptor groups, are found mostly in the interior of the protein. It is likely that CH/ $\pi$  interactions contribute to the process of folding and the overall stability of the protein 3D structure. Many workers discussed the relevance of CH/ $\pi$  hydrogen bonds<sup>194</sup> and  $\pi/\pi$  stackings<sup>195</sup> in the protein local structure. As for the X-ray crystal structure of *B*-DNA, twin T-methyl/ $\pi$  interaction has been found in every structure that bears (AT)<sub>n</sub> ( $n > 2$ ) and T<sub>n</sub> ( $n > 4$ ) sequence.<sup>174</sup>

To cite the other weak hydrogen bonds in biopolymers, database studies demonstrated the importance of CH/O hydrogen bonds in protein structures.<sup>196</sup>

Steiner and Koellner examined the NH/π and OH/π hydrogen bonds in protein X-ray crystal data and commented on the role of these interactions.<sup>197</sup> NH/π interactions were found more frequently than OH/π interactions,<sup>198</sup> this is reasonable since NH is softer than OH as an acid.

## VI. CONCLUSION

Crystallographic studies, including database analyses, have revealed that the CH/π hydrogen bond plays a critical role in determining the three-dimensional structure of molecules. A considerable part of the interactions, broadly ascribed in the past to the nonspecific interaction, should be reexamined in the context of *specific* weak forces. Nonspecific effects such as the “hydrophobic effect”<sup>199</sup> and the so-called packing forces by no means constitute the origin of specific interactions in chemistry and biochemistry.<sup>200</sup>

## ACKNOWLEDGMENTS

This study is dedicated to the memory of the late Professor Derek H. R. Barton and the late Professor Max F. Perutz.

## REFERENCES

1. Pimentel, G. C.; McClellan, A. L. *The Hydrogen Bond*. Freeman, San Francisco, **1960**. Jeffrey, G. A. *An Introduction to Hydrogen Bonding*. Oxford University Press, Oxford, **1997**. Scheiner, S. *Hydrogen Bonding: A Theoretical Perspective*, Oxford University Press, Oxford, **1997**.
2. Desiraju, G. R.; Steiner, T. *The Weak Hydrogen Bond in Structural Chemistry and Biology*, Oxford University Press, Oxford, **1999**. Desiraju, G. R. *Acc. Chem. Res.* **2002**, *35*, 565–573. Nishio, M. *Weak Hydrogen Bonds in Encyclopedia of Supramolecular Chemistry*, Atwood, J. L.; Steed, J. W., eds. Dekker, New York, **2004**, pp. 1576–1585.
3. Review: Josien, M.-L.; Sourisseau, G. *Hydrogen Bonding*, Hadzi, D. ed. Pergamon Press, London, **1959**, pp. 129–137. Oki, M. *Kagaku no Ryoiki*, **1959**, *13*, 839–847. Yoshida, Z.; Osawa, E. *Kagaku no Ryoiki* **1960**, *14*, 163–173; 248–254. Iwamura, H. *Kagaku to Kogyo* **1964**, *17*, 617–625.
4. Nishio, M.; Hirota, M.; Umezawa, Y. *The CH/π Interaction. Evidence, Nature, and Consequences*. Wiley-VCH, New York, **1998**.
5. A comprehensive literature list of the CH/π interaction is available in the author’s Web site <<http://www.tim.hi-ho.ne.jp/dionisio>>.
6. Tamres, M. *J. Am. Chem. Soc.* **1952**, *74*, 3375–3378.
7. Huggins, C. M.; Pimentel, G. C. *J. Chem. Phys.* **1955**, *23*, 896–898. Huggins, C. M.; Pimentel, G. C. *J. Phys. Chem.* **1956**, *60*, 1615–1619.

8. Brand, J. C. D.; Eglinton, G.; Tyrrell, J. *J. Chem. Soc.* **1965**, 5914–5919. West, R.; Krahanzel, C. S.; *J. Am. Chem. Soc.* **1961**, 83, 765–768. Yoshida, Z.; Osawa, E. *Nippon Kagaku Zasshi*, **1966**, 87, 509–535.
9. Reeves, L. W.; Schneider, W. G. *Can. J. Chem.* **1957**, 35, 251–261. Hatton, J. V.; Richards, R. E. *Trans. Faraday Soc.* **1961**, 57, 28–33.
10. Iitaka, Y.; Kodama, Y.; Nishihata, K.; Nishio, M. *Chem. Commun.* **1974**, 389–390. Kodama, Y.; Nishihata, K.; Nishio, M.; Iitaka, Y. *J. Chem. Soc., Perkin Trans. 2* **1976**, 1490–1495.
11. Kodama, Y.; Nishihata, K.; Zushi, S.; Nishio, M.; Uzawa, J.; Sakamoto, K.; Iwamura, H. *Bull. Chem. Soc. Jpn.* **1979**, 52, 2661–2669. Zushi, S.; Kodama, Y.; Nishihata, K.; Umemura, K.; Nishio, M.; Uzawa, J.; Hirota, M. *Bull. Chem. Soc. Jpn.* **1980**, 53, 3631–3640. Kodama, Y.; Zushi, S.; Nishihata, K.; Nishio, M. *J. Chem. Soc., Perkin Trans. 2* **1980**, 1306–1312. Uzawa, J.; Zushi, S.; Kodama, Y.; Fukuda, Y.; Nishihata, K.; Umemura, K.; Nishio, M.; Hirota, M. *Bull. Chem. Soc. Jpn.* **1980**, 53, 3623–3630.
12. Kobayashi, K.; Kodama, Y.; Nishio, M.; Sugawara, T.; Iwamura, H. *Bull. Chem. Soc. Jpn.* **1982**, 55, 3560–3564; Kunieda, N.; Endo, H.; Hirota, M.; Kodama, Y.; Nishio, M. *Bull. Chem. Soc. Jpn.* **1983**, 56, 3110–3117.
13. One of the present authors reported that *t*-butyl benzyl sulfoxide  $C_6H_5CH_2SO-tBu$  has the same conformation in solution: Kodama, Y.; Nishihata, K.; Nishio, M.; Nakagawa, N. *Tetrahedron Lett.* **1977**, 2105–2108. Later the conclusion was shown to be erroneous, due to the incorrect configuration assignment of deuterated benzylic sulfoxide: Iitaka, Y.; Itai, A.; Tomioka, N.; Kodama, Y.; Ichikawa, K.; Nishihata, K.; Nishio, M.; Izumi, M.; Doi, K. *Bull. Chem. Soc. Jpn.* **1986**, 59, 2801–2806. The “finding,” nevertheless, prompted the authors to speculate on the possibility that the interaction between an alkyl group and a  $\pi$ -system is attractive.
14. Nishio, M. *Kagaku no Ryoiki*, **1977**, 31, 834–842; 998–1006; **1979**, 33, 422–432; **1983**, 37, 243–249.
15. Aoyama, T.; Matsuoka, O.; Nakagawa, N. *Chem. Phys. Lett.* **1979**, 67, 508–509. Takagi, T.; Tanaka, A.; Matsuo, S.; Maezaki, H.; Tani, M.; Fujiwara, H.; Sasaki, Y. *J. Chem. Soc., Perkin Trans. 2* **1987**, 1015–1018.
16. Recent high-level MO calculations include: Samanta, U.; Chakrabarti, P.; Chandrasekhar, J. *J. Phys. Chem. A* **1998**, 102, 8964–8969. Tsuzuki, S.; Honda, K.; Uchimaru, T.; Mikami, M.; Tanabe, K. *J. Phys. Chem. A* **1999**, 103, 8265–8271. Oki, M.; Takano, S.; Toyota, S. *Bull. Chem. Soc. Jpn.* **2000**, 73, 2221–2230. Scheiner, S.; Grabowski, S. *J. J. Molec. Struct.* **2002**, 615, 209–218.
17. Sakaki, S.; Kato, K.; Miyazaki, T.; Musashi, Y.; Ohkubo, K.; Ihara, H.; Hirayama, C. *J. Chem. Soc., Faraday Trans.* **1993**, 89, 659–664. Tsuzuki, S.; Honda, K.; Uchimaru, T.; Mikami, M.; Tanabe, K. *J. Am. Chem. Soc.* **2000**, 122, 3746–3753.
18. Umezawa, Y.; Tsuboyama, S.; Honda, K.; Uzawa, J.; Nishio, M. *Bull. Chem. Soc. Jpn.* **1998**, 71, 1207–1213. Takahashi, O.; Kohno, Y.; Iwasaki, S.; Saito, K.; Iwaoka, M.; Tomoda, S.; Umezawa, Y.; Tsuboyama, S.; Nishio, M. *Bull. Chem. Soc. Jpn.* **2001**, 74, 2421–2430.
19. Novoa, J. J.; Mota, F. *Chem. Phys. Lett.* **2000**, 318, 345–354. Uguzzoli, F.; Arduini, A.; Massera, C.; Pochini, A.; Secchi, A. *New J. Chem.* **2002**, 26, 1718–1723. Takahashi, O.; Kohno, Y.; Saito, K. *Chem. Phys. Lett.* **2003**, 378, 509–515.
20. Abe, K.; Hirota, M.; Morokuma, K. *Bull. Chem. Soc. Jpn.* **1985**, 58, 2713–2714. Gung, B. J.; Zhu, Z.; Fouch, R. A. *J. Am. Chem. Soc.* **1995**, 117, 1783–1788. Hirota, M.; Sakakibara, K.; Suezawa, H.; Yuzuri, T.; Ankai, E.; Nishio, M. *J. Phys. Org. Chem.* **2000**, 13, 620–623. Bagno, A.; Saielli, G.; Scorrano, G. *Chem. Eur. J.* **2002**, 8, 2047–2056. Ribas, J.; Cubero, E.; Luque, F. J.; Orozco, M. *J. Org. Chem.* **2002**, 67, 7057–7065.

21. Fan, M.-F.; Lin, Z.; McGrady, J. E.; Mingos, D. M. P. *J. Chem. Soc., Perkin Trans. 2* **1996**, 563–568. Tsuzuki, S.; Honda, K.; Uchimaru, T.; Mikami, M.; Tanabe, K. *J. Phys. Chem. A* **2002**, *106*, 4423–4428.
22. Ehama, R.; Yokoo, A.; Tsushima, M.; Yuzuri, T.; Suezawa, H.; Hirota, M. *Bull. Chem. Soc. Jpn.* **1993**, *66*, 814–818. Kobayashi, K.; Asakawa, Y.; Aoyama, Y. *Supramolec. Chem.* **1993**, *2*, 133–135. Cozzi, F.; Sigel, J. S. *Pure Appl. Chem.* **1995**, *67*, 683–689. Carver, F. J.; Hunter, C. A.; Seward, E. M. *Chem. Commun.* **1998**, 775–776.
23. Lee E.-C.; Hong, B.-H.; Lee, J.-Y.; Kim, J.-C.; Kim, D.; Kim, Y.; Tarakeshwar, P.; Kim, K.-S. *J. Am. Chem. Soc.* **2005**, *127*, 4530–4537.
24. It may be pointed out that 100 to 1 selectivity results from difference in the Gibbs energy ( $\Delta G$ ) of only ca. 2.8 kcal mol<sup>-1</sup> at ambient temperature.
25. Nishio, M. *Cryst. Eng. Comm.* **2004**, *6*, 130–158.
26. van Est-Stammer, R.; Engberts, J. B. F. N. *Tetrahedron Lett.* **1971**, 3215–3218. van Est-Stammer, R.; Engberts, J. B. F. N. *Rec. Trav. Chim.* **1972**, *91*, 1298–1308. van Est-Stammer, R.; Engberts, J. B. F. N. *Can. J. Chem.* **1973**, *51*, 1187–1191. Tel, R. M.; Engberts, J. B. F. N. *Rec. Trav. Chim.* **1974**, *93*, 37–39.
27. Tickle, J.; Engberts, J. B. F. N. *J. Chem. Soc., Perkin Trans. 2* **1973**, 2031–2035.
28. Tel, R. M.; Engberts, J. B. F. N. *J. Chem. Soc., Perkin Trans. 2* **1976**, 483–488.
29. Tickle, J.; Hess, J.; Vos, A.; Engberts, J. B. F. N. *J. Chem. Soc., Perkin Trans. 2* **1978**, 460–465.
30. Visser, R. J. J.; Vos, A.; Engberts, J. B. F. N. *J. Chem. Soc., Perkin Trans. 2* **1978**, 634–639.
31. Oda, K.; Ohnuma, T.; Ban, Y. *J. Am. Chem. Soc.* **1984**, *106*, 5378–5379.
32. Hamor, T. A.; Jennings, W. B.; Procter, L. D.; Tolley, M. S.; Boyd, D. R.; Mullan, T. *J. Chem. Soc., Perkin Trans. 2* **1990**, 25–30.
33. Boyd, D. R.; Evans, T. A.; Jennings, W. B.; Malone, J. F.; O'Sullivan, W.; Smith, A. *J. Chem. Soc., Chem. Commun.* **1996**, 2269–2270.
34. Hunter, C. A.; Sanders, J. K. M. *J. Am. Chem. Soc.* **1990**, *112*, 5525–5534. Hunter, C. A. *Chem. Soc. Rev.* **1994**, 101–109.
35. Jennings, W. B.; Farrel, B. M.; Malone, J. M. *Acc. Chem. Res.* **2001**, *34*, 885–894.
36. Grossel, M. C.; Cheetham, A. K.; Hope, D. A. O.; Weston, S. C. *J. Org. Chem.* **1993**, *58*, 6654–6661.
37. Paliwal, S.; Geib, S.; Wilcox, C. S. *J. Am. Chem. Soc.* **1994**, *116*, 4497–4498. Kim, E.-I.; Paliwal, S.; Wilcox, C. S. *J. Am. Chem. Soc.* **1998**, *120*, 11192–11193.
38. Klärner, F.-G.; Benkhoff, J.; Boese, R.; Burkert, U.; Kamieth, M.; Naatz, U. *Angew. Chem., Int. Ed. Engl.* **1996**, *35*, 1130–1132. Klärner, F.-G.; Kahlert, B. *Acc. Chem. Res.* **2003**, *36*, 916–932.
39. Shimizu, H.; Yonezawa, T.; Watanabe, T.; Kobayashi, K. *J. Chem. Soc., Chem. Commun.* **1996**, 1659–1660.
40. Yoshitake, Y.; Misaka, J.; Setoguchi, K.; Abe, M.; Kwaji, T.; Eto, M.; Harano, K. *J. Chem. Soc., Perkin Trans. 2* **2002**, 1611–1619.
41. Ashton, P. R.; Hörner, B.; Kocian, O.; Menzer, S.; White, A. J. P.; Stoddart, J. F.; Williams, D. J. *Synthesis* **1996**, *8*, 930–940.
42. Miyake, Y.; Hosoda, A.; Takagaki, M.; Nomura, E.; Taniguchi, H. *Chem. Commun.* **2002**, 132–133.
43. Slawin, A. M. Z.; Spencer, N.; Stoddart, J. F.; Williams, D. J. *J. Chem. Soc. Chem. Commun.* **1987**, 1070–1072. Ashton, P. R.; Chrystal, E. J. T.; Mathias, J. P.; Parry, K. P.; Slawin, A. M.

- Z.; Spencer, N.; Stoddart, J. F.; Williams, D. J. *Tetrahedron Lett.* **1987**, 6367–6370. Anelli, P. L.; Crystal, E. J. T.; Mathias, J. P.; Parry, K. P.; Slawin, A. M. Z.; Spencer, N.; Stoddart, J. F.; Williams, D. J. *Tetrahedron Lett.* **1988**, 1575–1576. Anelli, P. L.; Slawin, A. M. Z.; Stoddart, J. F.; Williams, D. J. *Acta Crystallogr.* **1990**, 46C, 1468–1470. Hinze, B.; Marquis, D.; Marsau, P.; Cotrait, M.; Desvergne, J. P. *Tetrahedron Lett.* **1996**, 37, 5499–5502. Baxter, I.; Ben-Haida, A.; Colquhoun, H. M.; Hodge, P.; Kohnke, F. H.; Williams, D. J. *Chem. Commun.* **1998**, 2213–2214. Bryan, J. C.; Bunick, G. J.; Sachleben, R. A. *Acta Crystallogr.* **1999**, 55C, 250–252. Evans, D. J.; Junk, P. C.; Smith, M. K. *New J. Chem.* **2002**, 26, 1043–1048.
44. Csöregi, I.; Finge, S.; Weber, E. *Supramolec. Chem.* **2003**, 14, 241–246.
45. Kuwatani, Y.; Igarashi, J.; Iyoda, M. *Tetrahedron Lett.* **2004**, 45, 359–362.
46. Kido, M.; Miura, I.; Manabe, Y.; Nakagawa, K. *Chem. Pharm. Bull.* **1982**, 30, 44–50.
47. Vögtle, F.; Schmohel, E.; Nieger, M. *J. Chem. Soc., Chem. Commun.* **1993**, 760–762.
48. Reiffen, M.; Eberlein, W.; Muller, P.; Psiorz, M.; Noll, K.; Heider, J.; Lillie, C.; Kobinger, W.; Luger, P. *J. Med. Chem.* **1990**, 33, 1496–1504.
49. Carell, T.; Epple, R.; Gramlich, V. *Angew. Chem., Int. Ed. Engl.* **1996**, 35, 620–623.
50. Pappalardo, S. *New J. Chem.* **1996**, 20, 465–472.
51. Sakamoto, M.; Takahashi, M.; Fujita, T.; Watanabe, S.; Nishio, T.; Iida, I.; Aoyama, H. *J. Org. Chem.* **1997**, 62, 6298–6308.
52. Dupont, J.; Suarez, P. A. Z.; De Souza, R. F.; Burrow, R. A.; Kintzinger, J.-P. *Chem. Eur. J.* **2000**, 6, 2377–2381.
53. Kitamura, M.; Nakano, K.; Miki, T.; Okada, M.; Noyori, R. *J. Am. Chem. Soc.* **2001**, 123, 8939–8950.
54. Kitahara, Y.; Tanaka, K. *Chem. Commun.* **2002**, 932–933.
55. Myszka, H.; Bednarczyk, D.; Ciunik, Z.; Kaca, W. *Magn. Reson. Chem.* **2002**, 40, 231–236.
56. Vögtle, F.; Schmohel, E.; Nieger, M. *J. Chem. Soc., Chem. Commun.* **1993**, 760–762. Raj, S. S. S.; Fun, H.-K.; Wu, J.; Tian, Y.-P.; Xie, F.-X.; Shao, Z.-H.; Li, S.-L. *Acta Crystallogr. Sect. C* **2000**, 56, 1321–1322. Moriguchi, T.; Inoue, M.; Yasutake, M.; Synmyozu, T.; Sakata, K.; Tsuge, A. *J. Chem. Soc., Perkin Trans. 2* **2001**, 2084–2088. Schulte, J. H.; Werz, D. B.; Rominger, F.; Gleiter, R. *Org. Biomol. Chem.* **2003**, 2788–2794. Muktha, B.; Srinivas, O.; Amresh, M. R.; Guru Row, T. N.; Jayaraman, N.; Sekar, K. *Carbohydrate Res.* **2003**, 338, 2005–2011. Wachsmann, C.; Weber, E.; Czugler, M.; Seichter, W. *Eur. J. Org. Chem.* **2003**, 2863–2876. Azumaya, I.; Kato, T.; Okamoto, I.; Yamasaki, R.; Tanatani, A.; Yamaguchi, K.; Kagechika, H.; Takayanagi, H. *Org. Lett.* **2003**, 3939–3942. Lee, B.-W.; Lee, J.-H.; Jang, K.-C.; Kang, J.-E.; Kim, J.-H.; Park, K.-M.; Park, K.-H. *Tetrahedron Lett.* **2003**, 44, 5905–5907. Lhoták, P.; Himl, M.; Stibor, I.; Sykora, J.; Dvoráková, H.; Lang, J.; Petřícková, H. *Tetrahedron* **2003**, 59, 7581–7585. Nishinaga, T.; Miyata, Y.; Nodera, N.; Komatsu, K. *Tetrahedron* **2004**, 60, 3375–3382.
57. Examples: van Duynhoven, J. P. M.; Janssen, R. G.; Verboom, W.; Franken, S. M.; Casnati, A.; Pochini, A.; Ungaro, R.; de Mendoza, J.; Nieto, P. M.; Prados, P.; Reinhoudt, D. N. *J. Am. Chem. Soc.* **1994**, 116, 5814–5822. Matsugi, M.; Itoh, K.; Nojima, M.; Hagimoto, Y.; Kita, Y. *Chem. Eur. J.* **2002**, 8, 5551–5564. Wolf, C.; Pranatharthiharan, L.; Ramagos, R. B. *Tetrahedron Lett.* **2002**, 43, 8563–8567.
58. Breen, P. J.; Warren, J. A.; Bernstein, E. R.; Seeman, J. I. *J. Am. Chem. Soc.* **1987**, 109, 3453–3455. Dickinson, J. A.; Joireman, P. W.; Kroemer, R. T.; Robertson, E. G.; Simons, J. P. *J. Chem. Soc., Faraday Trans.* **1997**, 93, 1467–1472.
59. Kishikawa, K.; Yoshizaki, K.; Kohmoto, S.; Yamamoto, M.; Yamaguchi, K.; Yamada, K. *J. Chem. Soc., Perkin Trans. 1* **1997**, 1233–1239.

60. Kopple, K. D.; Marr, D. H. *J. Am. Chem. Soc.* **1967**, *89*, 6193–6200. Kopple, K. D.; Ohnishi, M. *J. Am. Chem. Soc.* **1969**, *91*, 962–970.
61. Webb, L. E.; Lin, C.-F. *J. Am. Chem. Soc.* **1971**, *93*, 3818–3819. Lin, C.-F.; Webb, L. E. *J. Am. Chem. Soc.* **1973**, *95*, 6803–6811.
62. Cary, L. W.; Takita, T.; Ohnishi, M. *FEBS Lett.* **1971**, *17*, 145–148.
63. Itaka, Y.; Nakamura, H.; Takada, K.; Takita, T. *Acta Crystallogr.* **1974**, *B30*, 2817–2825.
64. Edelhoch, H.; Bernstein, R. S.; Wilchek, M. *J. Biol. Chem.* **1968**, *243*, 5985–5992. Strickland, E. H.; Wilchek, M.; Horwitz, J.; Billups, C. *J. Biol. Chem.* **1970**, *245*, 4168–4177. Deslauriers, R.; Grzonka, Z. Schaumburg, K.; Shiba, T.; Walter, R. *J. Am. Chem. Soc.* **1975**, *97*, 5093–5100.
65. Ramani, R.; Venkatesan, K.; Marsh, R. E., Hu Kung, W.-J. *Acta Crystallogr.* **1976**, *B32*, 1051–1056.
66. Benedetti, E.; Marsh, R. E.; Goodman, M. *J. Am. Chem. Soc.* **1976**, *98*, 6676–6684.
67. van Poucke, M.; Geise, H. J.; Lenstra, A. T. H. *Acta Crystallogr.* **1983**, *C39*, 227–230.
68. Suguna, K.; Ramakumar, S.; Kopple, K. D. *Acta Crystallogr.* **1984**, *C40*, 2053–2056.
69. Suguna, K.; Ramakumar, S.; Nagaraj, R.; Balaram, P. *Acta Crystallogr.* **1985**, *C41*, 284–286.
70. Gdaniec, M.; Liberek, B. *Acta Crystallogr.* **1986**, *C42*, 1343–1345.
71. Gdaniec, M.; Liberek, B. *Acta Crystallogr.* **1987**, *C43*, 982–985.
72. Gdaniec, M. *Acta Crystallogr.* **1988**, *C44*, 1042–1044.
73. Barnes, C. L.; van der Helm, D. *Acta Crystallogr.* **1982**, *B38*, 2589–2595.
74. Lemieux, R. U.; Barton, M. A. *Can. J. Chem.* **1971**, *49*, 767–776.
75. McKenzie, R. E.; Föry, W.; McCormick, D. B. *Biochemistry* **1969**, *8*, 1839–1844.
76. Holladay, L. A.; Puett, D. *Proc. Natl. Acad. Sci., USA* **1976**, *73*, 1199–1202. Veber, D. F.; Holly, F. W.; Paleveda, W. J.; Nutt, R. F.; Bergstrand, S. J.; Torchiana, M.; Glitzer, M. S.; Saperstein, R.; Hirschmann, R. *Proc. Natl. Acad. Sci., USA* **1978**, *75*, 2636–2640. Arison, B. H.; Hirschmann, R.; Paleveda, W. J.; Brady, S. F.; Veber, D. F. *Biochem. Biophys. Res. Commun.* **1981**, *100*, 1148–1153.
77. London, R. E.; Stewart, J. M.; Williams, R.; Cann, J. R.; Matwiyoff, N. A. *J. Am. Chem. Soc.* **1979**, *101*, 2455–2462. Anteunis, M. J. O.; Borremans, F. A. M.; Stewart, J. M.; London, R. E. *J. Am. Chem. Soc.* **1981**, *103*, 2187–2191.
78. Deber, C. M.; Joshua, H. *Biopolymers* **1972**, *11*, 2493–2503.
79. The so-called hydrophobic effect does not explain these phenomena.
80. Sakamoto, H.; Shimohigashi, Y.; Maeda, I.; Nose, T.; Nakashima, K.; Nakamura, I.; Ogawa, T.; Kawano, K.; Ohno, M. *J. Molec. Recogn.* **1993**, *6*, 95–100. Maeda, I.; Shimohigashi, Y.; Nakamura, I.; Sakamoto, H.; Kawano, K.; Ohno, M. *Biochem. Biophys. Res. Commun.* **1993**, *193*, 428–433.
81. Shimohigashi, Y.; Maeda, I.; Nose, T.; Ikesue, K.; Sakamoto, H.; Ogawa, T.; Ide, Y.; Kawahara, M.; Nezu, T.; Terada, Y.; Kawano, K.; Ohno, M. *J. Chem. Soc., Perkin Trans. 1* **1996**, 2479–2485. Maeda, I.; Shimohigashi, Y.; Ikesue, K.; Nose, T.; Ide, Y.; Kawano, K.; Ohno, M. *J. Biochem.* **1996**, *119*, 870–877.
82. Kim, D. H.; Li, Z.-H.; Soo, S. L.; Park, J.; Chung, S. J. *Bioorg. Med. Chem.* **1998**, *6*, 239–249.
83. Gorbitz, C. H.; Etter, M. C. *Acta Crystallogr.* **1993**, *C49*, 1673–1676.
84. Smith, G. D.; Griffith, J. F. *Science* **1978**, *199*, 1214–1216.
85. Aubry, A.; Birlirakis, N.; Sakarellos-Daitsiotis, M.; Sakarellos, C.; Marraud, M. *J. Chem. Soc., Chem. Commun.* **1988**, 963–964.
86. Cotrait, M.; Geofre, S.; Hospital, M.; Prigoux, G. *Acta Crystallogr.* **1979**, *B35*, 114–118. Prigoux, G.; Cotrait, M.; Geofre, S. *Acta Crystallogr.* **1986**, *C42*, 315–317. Deletré, J.;

- Berthou, J.; Lifchitz, A. *Acta Crystallogr.* **1988**, *C44*, 902–904. Nikiforovich, G. V.; Kövér, K. E.; Kolodziej, S. A.; Nock, B.; George, C.; Deschamps, J. R.; Flippen-Anderson, J. L.; Marchall, G. R. *J. Am. Chem. Soc.* **1996**, *118*, 959–969.
87. Prangé, P. T.; Pascard, C. *Acta Crystallogr.* **1979**, *B35*, 1812–1819.
88. Wang, A. H.-J.; Burley, S. K. *Acta Crystallogr.* **1987**, *C43*, 1635–1636. Burley, S. K.; Wang, A. H.-J.; Votano, J. R.; Rich, A. *Biochemistry* **1987**, *26*, 5091–5099.
89. Fujii, S.; Burley, S. K.; Wang, A. H.-J. *Acta Crystallogr.* **1987**, *C43*, 1008–1009.
90. Hiyama, Y.; Niu, C.-H.; Silverton, J. V.; Bavoso, A.; Torchia, D. A. *J. Am. Chem. Soc.* **1988**, *110*, 2378–2383. See Table 1 of Ref. 182 for a more complete list of peptide crystal conformations bearing short intramolecular CH/π distances.
91. Formaggio, F.; Peggion, C.; Crisma, M.; Toniolo, C.; Tchertanov, L.; Guilhem, J.; Mazaleyrat, J.-P.; Goubard, Y.; Wakselman, M. *Helv. Chim. Acta* **2001**, *84*, 481–501. Saviano, M.; Benedetti, E.; Vitale, R. M.; Kaptein, B.; Broxterman, Q. B.; Crisma, M.; Formaggio, F.; Toniolo, C. *Macromolecules* **2002**, *35*, 4204–4209.
92. Naumann, C. F.; Sigel, H. *J. Am. Chem. Soc.* **1974**, *96*, 2750–2756.
93. Review: Sigel, H. *Pure Appl. Chem.* **1989**, *61*, 923–932. Yamauchi, O.; Odani, A.; Masuda, H.; Sigel, H. Eds. Sigel, A.; Sigel, H. *Stacking Interactions Involving Nucleotides and Metal Ion Complexes*, Dekker, Basle, **1996**, *32*, 207–270. Sigel, H.; Griesser, R. *Chem. Soc. Rev.* **2005**, *34*, 875–900.
94. Dubler, E.; Haring, U. K.; Scheller, H.; Baltzer, P.; Sigel, H. *Inorg. Chem.* **1984**, *23*, 3785–3792.
95. Sigel, H.; Triboulet, R.; Yamauchi, O. *Comments Inorg. Chem.* **1990**, *9*, 305–330.
96. Okawa, H.; Numata, Y.; Mio, A.; Kida, S. *Bull. Chem. Soc. Jpn.* **1980**, *53*, 2248–2251.
97. Review: Okawa, H. *Coord. Chem. Rev.* **1988**, *92*, 1–28.
98. Sakiyama, H.; Okawa, H.; Matsumoto, N.; Kida, S. *J. Chem. Soc., Dalton Trans.* **1990**, 2935–2939.
99. Jitsukawa, K.; Iwai, K.; Masuda, H.; Ogoshi, H.; Einaga, H. *J. Chem. Soc., Dalton Trans.* **1997**, 3691–3698.
100. Mizutani, M.; Tomosue, S.; Kinoshita, H.; Jitsukawa, K.; Masuda, H.; Einaga, H. *Bull. Chem. Soc. Jpn.* **1999**, *72*, 981–988.
101. Nakamura, M. *Inorg. Chim. Acta* **1989**, *161*, 73–80. Nakamura, M.; Nakamura, N. *Chem. Lett.* **1990**, 181–184. Nakamura, M. *Bull. Chem. Soc. Jpn.* **1995**, *68*, 197–203.
102. Sugimoto, H.; Aida, T.; Inoue, S. *J. Chem. Soc., Chem. Commun.* **1995**, 1411–1412.
103. Mizutani, T.; Wada, K.; Kitagawa, S. *J. Org. Chem.* **2000**, *65*, 6097–6106.
104. Venkatraman, S.; Anand, V. G.; Raja, V. P.; Rath, H.; Sankar, J.; Chandarashekhar, T. K.; Teng, W.; Ruhlandt, K. *Chem. Commun.* **2002**, 1660–1661.
105. Colquhoun, H. M.; Stoddart, J. F.; Williams, D. J. *Angew. Chem., Int. Ed. Engl.* **1986**, *25*, 487–507. Colquhoun, H. M.; Doughty, S. M.; Stoddart, J. F.; Slawin, A. M. Z.; Williams, D. J. *J. Chem. Soc., Dalton Trans.* **1986**, 1639–1652.
106. Onaka, S.; Furuta, H.; Takagi, S. *Angew. Chem., Int. Ed. Engl.* **1993**, *32*, 87–88.
107. Chowdhury, S. K.; Joshi, V. S.; Samuel, A. G.; Puranik, V. G.; Tavale, S. S.; Sarkar, A. *Organometallics* **1994**, *13*, 4092–4096.
108. Yamanari, K.; Dogi, S.; Okubo, K.; Fujihara, T.; Fuyuhiro, A.; Kaizaki, S. *Bull. Chem. Soc. Jpn.* **1994**, *67*, 3004–3008. Yamanari, K.; Nozaki, T.; Fuyuhiro, A.; Kaizaki, S. *Chem. Lett.* **1996**, 35–36.
109. Yamanari, K.; Nozaki, T.; Fuyuhiro, A.; Kushi, Y.; Kaizaki, S. *J. Chem. Soc., Dalton Trans.* **1996**, 2851–2856.

110. Hornung, H.-D.; Klinkhammer, K. W.; Schmidt, A. *Main Group Metal Chem.* **1997**, *20*, 157–167. Burchardt, A.; Klinkhammer, K. W.; Schmidt, A. *Main Group Metal Chem.* **1999**, *22*, 301–309.
111. Cavaglioni, A.; Cini, R. *J. Chem. Soc., Dalton Trans.* **1997**, 1149–1158. Cini, R.; Corcini, M.; Cavaglioni, A. *Inorg. Chem.* **2000**, *39*, 5874–5898.
112. Bellucci, C.; Cini, R. *J. Inorg. Biochem.* **1999**, *76*, 243–250.
113. Yamanari, K.; Fukuda, Y.; Yamamoto, S.; Kushi, Y.; Fuyuhiro, A.; Kubota, N.; Fukuo, T.; Arakawa, R. *J. Chem. Soc., Dalton Trans.* **2000**, 2131–2136.
114. Kul somphob, V.; Turpin, G. C.; Lam, K.-C.; Youngkin, C.; Trakarnpruk, W.; Carroll, P.; Rheingold, A. L.; Ernst, R. D. *J. Chem. Soc., Dalton Trans.* **2000**, 3086–3093.
115. Kawamoto, T.; Kushi, Y. *J. Chem. Soc., Dalton Trans.* **2000**, 3022–3026. Kawamoto, T.; Konno, T. *Bull. Chem. Soc. Jpn.* **2003**, *76*, 127–132.
116. Archibald, S. J.; Blake, A. J.; Schröder, M.; Winpenny, R. E. P. *J. Chem. Soc., Chem. Commun.* **1994**, 1669–1670. Colbert, M. C. B.; Lewis, J.; Long, N. J.; Raithby, P. R.; White, A. J. P.; Williams, D. *J. Chem. Commun.* **1997**, 1091–1092. Yoshida, N.; Oshio, H.; Shiro, M. *J. Chem. Soc., Perkin Trans. 2* **1999**, 975–983. McNelis, B. J.; Nathan, L. C.; Clark, C. J. *J. Chem. Soc., Dalton Trans.* **1999**, 1831–1834. Yoshida, N.; Ichikawa, K.; Shiro, M. *J. Chem. Soc., Perkin Trans. 2* **2000**, 17–26. Kobayashi, K.; Takahashi, H.; Nishio, M.; Umezawa, Y.; Tsu boyama, K.; Tsu boyama, S. *Anal. Sci.* **2000**, *16*, 1103–1104. Bonar-Law, R. P.; McGrath, T. D.; Singh, N.; Bickley, J. F.; Femoni, C.; Steiner, A. *J. Chem. Soc., Dalton Trans.* **2000**, 4343–4347. Baar, C. R.; Carbray, L. P.; Jennings, M. C.; Puddephatt, R. J. *Organometallics* **2001**, *20*, 408–417. Cross, W. J.; Godfrey, S. M.; McAuliffe, C. A.; Pritchard, R. G. *Chem. Commun.* **2001**, 1764–1765. Allred, R. A.; Arif, A. M.; Berreau, L. M. *J. Chem. Soc., Dalton Trans.* **2002**, 300–301. de Cian, A.; Djukic, J.-P.; Fischer, J.; Pfeffer, M.; Dötz, K. H. *Chem. Commun.* **2002**, 638–639. Yajima, T.; Shimazaki, Y.; Ishigami, N.; Odani, A.; Yamauchi, O. *Inorg. Chim. Acta* **2002**, *337*, 193–202. Yajima, T.; Okajima, M.; Odani, A.; Yamauchi, O. *Inorg. Chim. Acta* **2002**, *339*, 445–454. Onishi, M.; Yamaguchi, M.; Nishimoto, E.; Itoh, Y.; Nagaoka, J.; Umakoshi, K.; Kawano, H. *Inorg. Chim. Acta* **2002**, *343*, 111–118. García-Raso, A.; Fiol, J. J.; Adrover, B.; Moreno, V.; Mata, I.; Espinosa, E.; Molins, E. *J. Inorg. Biochem.* **2003**, *95*, 77–86. Elduque, A.; Carmona, D.; Oro, L. A.; Eisenstein, M.; Fish, R. H. *J. Organomet. Chem.* **2003**, *668*, 123–127. Sreekanth, A.; Sivakumar, S.; Kurup, M. R. *P. J. Molec. Struct.* **2003**, *655*, 47–58. García-Raso, A.; Fiol, J. J.; Adrover, B.; Tauler, P.; Pons, A.; Moreno, V.; Mata, I.; Espinosa, E.; Molins, E. *Polyhedron* **2003**, *22*, 3255–3264. Sreekanth, A.; Kurup, M. R. *P. Polyhedron* **2003**, *22*, 3321–3332. Ciunik, Z.; Ruman, T.; Lukasiewicz, M.; Wolowiec, S. *J. Molec. Struct.* **2004**, *690*, 175–180. Herradón, B.; Montero, A.; Mann, E.; Maestro, M. A. *CrystEngComm* **2004**, *6*, 512–521. Reger, D. L.; Gardinier, J. R.; Smith, M. D. *Inorg. Chem.* **2004**, *43*, 3825–3832. Kojima, T.; Miyazaki, S.; Hayashi, K.; Shimazaki, Y.; Tani, F.; Naruta, Y.; Matsuda, Y. *Chem. Eur. J.* **2004**, *10*, 6402–6410. Johansson, A.; Hakansson, M. *Chem. Eur. J.* **2005**, *11*, 5238–5248. Miodragovic, Dj. U.; Miodragovic, Z. M.; Skara, D.; Malinar, M. J.; Minic, D. M.; Andjelkovic, K. *Thermochim. Acta* **2005**, *436*, 90–95. Tsubaki, H.; Tohyama, S.; Koike, K.; Saitoh, H.; Ishitani, O. *Dalton Trans.* **2005**, 385–395. Jiang, Y.-F.; Xi, C.-J.; Liu, Y.-Z.; Nicolos-Gutierrez, J.; Choquesillo-Lazarte, D. *Eur. J. Inorg. Chem.* **2005**, 1585–1588. Dilman, A. D.; Arkhipov, D. E.; Korlyukov, A. A.; Ananikov, V. P.; Danilenko, V. M.; Tartakovsky, V. A. *J. Organomet. Chem.* **2005**, *690*, 3680–3689. Matsumoto, K.; Jitsukawa, K.; Masuda, H.; *Tetrahedron Lett.* **2005**, *46*, 5687–5690. Cordes, D. B.; Hanton, L. R. *Inorg. Chem. Commun.* **2005**, *8*, 967–970. Ma, C.; Zhang, J.; Tian, G.; Zhang, J. *J. Organomet. Chem.* **2005**, *690*, 519–533.
117. Nishio, M. *Tetrahedron* **2005**, *61*, 6923–6950.
118. Brunner, H. *Angew. Chem., Int. Ed. Engl.* **1983**, *22*, 987–1012.

119. For recent examples of the  $\beta$ -phenyl effect, see: Brunner, H.; Oeschey, R.; Nuber, B. *J. Chem., Soc., Dalton Trans.* **1996**, 1499–1508. Brunner, H.; Oeschey, R.; Nuber, B. *Organometallics* **1996**, *15*, 3616.
120. Brunner, H. *Angew. Chem., Int. Ed. Engl.* **1999**, *38*, 1194–1208.
121. Brunner, H.; Neuhierl, T.; Nuber, B. *J. Organomet. Chem.* **1998**, *563*, 173.
122. Brunner, H.; Oeschey, R.; Nuber, B. *Angew. Chem., Int. Ed. Engl.* **1994**, *33*, 866–868.
123. Yamakawa, M.; Ito, H.; Noyori, R. *J. Am. Chem. Soc.* **2000**, *122*, 1466–1478. Yamakawa, M.; Yamada, I.; Noyori, R. *Angew. Chem., Int. Ed. Engl.* **2001**, *40*, 2818–2821.
124. Noyori, R.; Yamakawa, M.; Hashiguchi, S. *J. Org. Chem.* **2001**, *66*, 7931–7944. Zhou, Y.-B.; Tang, F.-Y.; Xu, H.-D.; Wu, X.-Y.; Ma, J.-A.; Zhou, Q.-L. *Tetrahedron: Asymmetry* **2002**, *13*, 469–473.
125. Becker, H.; Hou, P.-T.; Kolb, H. C.; Loren, S.; Norrby, P.-O.; Sharpless, K. B. *Tetrahedron Lett.* **1994**, *35*, 7315–7318.
126. Cagle, P. C.; Meyer, O.; Vichard, D.; Weickhardt, K.; Arif, A. M.; Gladysz, J. A. *Organometallics* **1996**, *15*, 194–204.
127. Irie, R.; Hashihayata, T.; Katsuki, T.; Akita, M.; Morooka, Y. *Chem. Lett.* **1998**, 1041–1042. Hashihayata, T.; Punniyamurthy, T.; Irie, R.; Katsuki, T.; Akita, M.; Morooka, Y. *Tetrahedron* **1999**, *55*, 14599–14610.
128. Li, Z.; Conser, K. R.; Jacobsen, E. N. *J. Am. Chem. Soc.* **1993**, *115*, 5326–5327. Li, Z.; Quan, R. W.; Jacobsen, E. N. *J. Am. Chem. Soc.* **1995**, *117*, 5889–5890.
129. Quan, R. W.; Li, Z.; Jacobsen, E. N. *J. Am. Chem. Soc.* **1996**, *118*, 8156–8157.
130. Sanders, C. J.; Gillespie, K. M.; Bell, D.; Scott, P. *J. Am. Chem. Soc.* **2000**, *122*, 7132–7133. Gillespie, K. M.; Sanders, C. J.; O'Shaughnessy, P.; Westmoreland, I.; Thickitt, C. P.; Scott, P. *J. Org. Chem.* **2002**, *67*, 3450–3458.
131. Arena, C. G.; Calamia, S.; Faraone, F.; Graiff, C.; Tiripicchio, A. *J. Chem. Soc., Dalton Trans.* **2000**, 3149–3157. Rath, R. K.; Nethaji, M.; Chakravarty, A. R. *Polyhedron* **2002**, *21*, 1929–1934.
132. Nishio, M.; Hirota, M.; Umezawa, Y. *The CH/ $\pi$  Interaction. Evidence, Nature, and Consequences*. Wiley-VCH, New York, **1998**, ch. 11.
133. Desiraju, G. R.; Steiner, T. *The Weak Hydrogen Bond in Structural Chemistry and Biology*. Oxford University Press, Oxford, **1999**, ch. 5.
134. Weiss, M. S.; Brandi, M.; Sühnel, J.; Pal, D.; Hilgenfeld, R. *Trends Biochem. Sci.* **2001**, *26*, 521–523.
135. Nishio, M. *29th Symposium on Protein Structures, Osaka*, **1978**, Abstract, pp. 161–164.
136. Levitt, M.; Perutz, M. F. *J. Mol. Biol.* **1988**, *201*, 751–754. Perutz, M. F. *Phil. Trans. R. Soc. A* **1993**, *A345*, 105–112.
137. Yun, M.; Pak, C.; Kim, S.; Nam, D.; Kim, S. C.; Kim, D. H. *J. Am. Chem. Soc.* **1992**, *114*, 2281–2282.
138. Tanaka, T.; Hirama, M.; Fujita, K.; Imajo, S.; Ishiguro, M. *J. Chem. Soc., Chem. Commun.* **1993**, 1205–1207. Takahashi, K.; Tanaka, T.; Suzuki, T.; Hirama, M. *Tetrahedron* **1994**, *50*, 1327–1340.
139. Kim, K.-H.; Kwon, B.-M.; Myers, A. G.; Rees, D. C. *Science* **1993**, *262*, 1042–1046.
140. Quiocho, F. A.; Vyas, N. K. *Nature* **1984**, *310*, 381–386.
141. Vyas, N. K.; Vyas, M. N.; Quiocho, F. A. *Science* **1988**, *242*, 1290–1295.
142. Harata, K.; Muraki, M. *Acta Crystallogr.* **1997**, *D53*, 650–657. Muraki, M.; Harata, K.; Sugita, N.; Sato, K. *Acta Crystallogr.* **1998**, *D54*, 834–843. Muraki, M.; Harata, K.; Sugita, N.; Sato, K. *Biochemistry* **2000**, *39*, 292–299. Muraki, M.; Harata, K. *J. Molec. Recogn.* **2003**, *16*, 72–82.

143. Muraki, M.; Morii, H.; Harata, K. *Protein Eng.* **2000**, *13*, 385–389.
144. Muraki, M.; Ishimura, M.; Harata, K. *Biochim. Biophys. Acta* **2002**, *1569*, 10–20.
145. Review: Muraki, M. *Prot. Peptide Lett.* **2002**, *9*, 195–209. See also Bernardi, A.; Arosio, D.; Potenza, D.; Sánchez-Medina, I.; Mari, S.; Cañada, F. J.; Jiménez-Barbero, J. *Chem. Eur. J.* **2005**, *10*, 4395–4406. Chávez, M. I.; Andreu, C.; Vidal, P.; Aboitiz, N.; Freire, F.; Groves, P.; Asensio, J. L.; Asensio, G.; Muraki, M.; Cañada, F. J.; Jiménez-Barbero, J. *Chem. Eur. J.* **2005**, *11*, 7060–7074. Blundell, C. D.; Almond, A.; Mahoney, D. J.; DeAngelis, P. L.; Campbell, I. D.; Day, A. J.; *J. Biol. Chem.* **2005**, *280*, 18189–18201. Support for the importance of Ch/π hydrogen bonds in carbohydrate-binding proteins has recently been provided by hight-level *ab initio* MO calculations: Spiwok, V.; Lipovova, P.; Skalova, T.; Buchtelova, E.; Hasek, J.; Kralova, B. *Carbohydr. Res.* **2004**, *339*, 2275–2280. Sujatha, M. S.; Sasidhar, Y. U.; Balaji, P. V. *Biochemistry* **2005**, *44*, 8554–8562. Fernandez-Alonso, M.; Cañada, F. J. Jiménez-Barbero, J.; Cuevas, G. *J. Am. Chem. Soc.* **2005**, *127*, 7379–7386.
146. Taieb, N.; Yahi, N.; Fantini, J. *Adv. Drug Delivery Rev.* **2004**, *56*, 779–794.
147. Hinrichs, W.; Kisker, C.; Düvel, M.; Müller, A.; Tovar, K.; Hillen, W.; Saenger, W. *Science* **1994**, *264*, 418–420.
148. Zographos, S. E.; Oikonomakos, N. G.; Tsitsanou, K. E.; Leonidas, D. D.; Chrysina, E. D.; Skamnaki, V. T.; Bischoff, H.; Goldmann, S.; Watson K. A.; Johnson, L. N. *Structure* **1997**, *5*, 1413–1425.
149. Kashima, A.; Inoue, Y.; Sugio, S.; Maeda, I.; Shimohigashi, Y. *Eur. J. Biochem.* **1998**, *255*, 12–23.
150. Nakanishi, I.; Kinoshita, T.; Sato, A.; Tada, T. *Biopolymers* **2000**, *53*, 434–445.
151. Robinson, A.; Edwards, K. J.; Carr, P. D.; Barton, J. D.; Ewart, G. D.; Ollis, D. L. *Acta Crystallogr.* **2000**, *D56*, 1376–1384.
152. Kinoshita, T.; Miyake, H.; Fujii, T.; Takakura, S.; Goto, T. *Acta Crystallogr.* **2002**, *D58*, 622–626.
153. Zsila, F.; Bikdi, Z.; Simonyi, M. *Biochem. Pharmacol.* **2002**, *7421*, 1–10.
154. Lehnhart, A.; Weihofen, W. A.; Pleschke, A. E. W.; Schulz, G. E. *Chem. Biol.* **2002**, *9*, 639–645. See also Sato, T.; Kanai, Y.; Hoshino, T. *Biosci. Biotechnol. Biochem.* **1998**, *62*, 407–411.
155. Kinoshita, T.; Nishio, N.; Nakanishi, I.; Sato, A.; Fujii, T. *Acta Crystallogr.* **2003**, *D59*, 299–303.
156. Hayashida, M.; Fujii, T.; Hamasu, M.; Ishigura, M.; Hata, Y. *J. Mol. Biol.* **2003**, *334*, 551–565.
157. Fish, R. H.; Jaouen, G. *Organometallics* **2003**, *22*, 2166–2177.
158. Klusak, V.; Havlas, Z.; Rulsek, L.; Vondrasek, J. V.; Svatos, A. *Chem. Biol.* **2003**, *10*, 331–340. Mohanty, S.; Zubkov, S.; Gronenborn, A. M. *J. Mol. Biol.* **2004**, *337*, 434–451.
159. Kinoshita, T.; Nakanishi, I.; Warizawa, M.; Iwashita, A.; Kido, Y.; Hattori, K.; Fujii, T. *FEBS Lett.* **2004**, *556*, 43–46.
160. Schoepfer, J.; Gay, B.; Caravatti, G.; García-Echeverria, C.; Fretz, H.; Rahuel, J.; Furet, P. *Bioorg. Med. Chem. Lett.* **1998**, *8*, 2865–2870. Schoepfer, J.; Fretz, H.; Gay, B.; Furet, P.; García-Echeverria, C.; End, N.; Caravatti, G. *Bioorg. Med. Chem. Lett.* **1999**, *9*, 221–226. Barreka, M. L.; Carotti, A.; Carrieri, A.; Chimirri, A.; Monforte, A. M.; Calace, M. P.; Rao, A. *Bioorg. Med. Chem.* **1999**, *7*, 2283–2292. Chen, L.; Trilles, R.; Miklowski, D.; Huang, T.-N.; Fry, D.; Campbell, R.; Rowan, K.; Schwinge, V.; Tilley, J. W. *Bioorg. Med. Chem. Lett.* **2002**, *12*, 1679–1682. Umezawa, K.; Kawakami, M.; Watanabe, T. *Pharmacol. Therapeut.* **2003**, *99*, 15–24. Nakagawa, Y.; Irie, K.; Yanagita, R. C.; Ogihashi, H.; Tsuda, K. *J. Am. Chem. Soc.* **2005**, *127*, 5746–5747. Irie, K.; Nakagawa, Y.; Ogihashi, H. *Chem. Record* **2005**, *5*, 185–195.
161. The crystal data of biopolymers do not bear hydrogen coordinates except for those determined by the neutron diffraction method. Hydrogens are generated and the position optimized before the analysis. The CH/π distances within a cut-off value were then collected and the results

- compared with those obtained by use of the neutron diffraction data of bovine pancreatic trypsin inhibitor and ribonuclease. Agreement between the two sets of data was satisfactory in the two cases above. See Nishio, M.; Hirota, M.; Umezawa, Y. *The CH/π Interaction. Evidence, Nature, and Consequences*. Wiley-VCH, New York, **1998**, pp. 178–181, tab. 11.1 and 11.2.
162. Nishio, M.; Umezawa, Y.; Hirota, M.; Takeuchi, Y. *Tetrahedron* **1995**, *51*, 8665–8701. Nishio, M.; Hirota, M.; Umezawa, Y. *The CH/π Interaction. Evidence, Nature, and Consequences*. Wiley-VCH, New York, **1998**, ch. 11.
  163. Umezawa, Y.; Nishio, M. *Bioorg. Med. Chem.* **1998**, *6*, 493–504.
  164. Umezawa, Y.; Nishio, M. *Bioorg. Med. Chem.* **1998**, *6*, 2507–2515.
  165. Umezawa, Y.; Nishio, M. *Bioorg. Med. Chem.* **2000**, *8*, 2643–2650.
  166. Nishio, M.; Umezawa, Y.; Hirota, M. *Kagaku to Seibutsu* **1995**, *33*, 311–318. Nishio, M.; Umezawa, Y.; Hirota, M. *Yuki Gosei Kagaku Kyokaishi* **1997**, *55*, 18–28.
  167. Nishio, M.; Hirota, M.; Umezawa, Y. *The CH/π Interaction. Evidence, Nature, and Consequences*. Wiley-VCH, New York, **1998**, pp. 192–194. Umezawa, Y.; Nishio, M. *Bioorg. Med. Chem.* **1998**, *6*, pp. 501–502.
  168. de Vos, A. M.; Ultsch, M. H.; Kossiakoff, A. A. *Science* **1992**, *255*, 306–312. Clackson, T.; Wells, J. A. *Science* **1995**, *267*, 383–386. Wells, J. A. *Proc. Natl. Acad. Sci., USA* **1996**, *93*, 1–6. Clackson, T.; Ultsch, M. H.; Wells, J. A.; de Vos, A. M. *J. Mol. Biol.* **1998**, *277*, 1111–1128. Butterfield, A. M.; Sweeney, M. M.; Waters, M. L. *J. Org. Chem.* **2005**, *70*, 1105–1114.
  169. Sussman, J. L.; Harel, M.; Frolov, F.; Oefner, C.; Goldman, A.; Toker, L.; Silman, I. *Science* **1991**, *253*, 872–879.
  170. Hasan, F. B.; Cohen, S. G.; Cohen, J. B. *J. Biol. Chem.* **1980**, *255*, 3898–3904. Cohen, S. G.; Lieberman, D. L.; Hasan, F. B.; Cohen, J. B. *J. Biol. Chem.* **1982**, *257*, 14087–14092.
  171. The term “anionic site” is misleading. Cohen proposed a more reasonable term “trimethyl site”. The term “CH/π site” may be more adequate in view of its nature.
  172. The hydrogens in  $(\text{CH}_3)_3\text{N}^+$  are positively charged relative to those in normal methyl groups and therefore are more prone to the CH/π bonding. Approximately an eightfold increase in the binding ability of  $(\text{CH}_3)_3\text{N}^+\text{H}$  relative to  $(\text{CH}_3)_3\text{COH}$  was reported for a series of calixarene complexes: Kobayashi, K.; Asakawa, Y.; Aoyama, Y. *Supramolec. Chem.* **1993**, *2*, 133–135. See also: Table 5 of Nishio, M.; Umezawa, Y.; Hirota, M.; Takeuchi, Y. *Tetrahedron* **1995**, *51*, 8665–8701.
  173. See discussions raised in Section 11.6 of Nishio, M.; Hirota, M.; Umezawa, Y. *The CH/π Interaction. Evidence, Nature, and Consequences*. Wiley-VCH, New York, **1998**.
  174. Umezawa, Y.; Nishio, M. *Biopolymers* **2005**, *79*, 248–258.
  175. Koellner, G.; Steiner, T.; Millard, C. B.; Silman, I.; Sussman, L. J. *J. Mol. Biol.* **2002**, *320*, 721–725.
  176. Viswamitra, M. A.; Kennard, O.; Jones, P. G.; Sheldrick, G. M.; Salisbury, G. M.; Falvello, L.; Shakked, Z. *Nature* **1978**, *273*, 687–688. Viswamitra, M. A.; Shakked, Z.; Jones, P. G.; Sheldrick, G. M.; Salisbury, S. A.; Kennard, O. *Biopolymers* **1982**, *21*, 513–533.
  177. Klug, A.; Jack, A.; Viswamitra, M. A.; Kennard, O.; Shakked, Z.; Steitz, T. A. *J. Mol. Biol.* **1979**, *131*, 669–680.
  178. Umezawa, Y.; Nishio, M. *Nucleic Acids Res.* **2002**, *30*, 2183–2192.
  179. Chou, S.-H.; Chin, K. H.; Chen, C. W. *J. Biomolec. NMR* **2001**, *19*, 33–48.
  180. Hodges-Garcia, Y.; Hagerman, P. J. *Biochemistry* **1992**, *31*, 7595–7599.
  181. Takahashi, H.; Umezawa, Y.; Tsuboyama, S.; Uzawa, J.; Nishio, M. *Tetrahedron* **1999**, *55*, 10047–10056.

182. Umezawa, Y.; Tsuboyama, S.; Takahashi, H.; Uzawa, J.; Nishio, M. *Bioorg. Med. Chem.* **1999**, 7, 2021–2026.
183. Janiak, C. *J. Chem. Soc., Dalton Trans.* **2000**, 3885–3896.
184. Suezawa, H.; Yoshida, T.; Umezawa, Y.; Tsuboyama, S.; Nishio, M. *Eur. J. Inorg. Chem.* **2002**, 3148–3155.
185. Bogdanovic, G. A.; Spasojevic-de Brie, A.; Zaric, S. D. *Eur. J. Inorg. Chem.* **2002**, 1599–1602.
186. Reger, D. L.; Gardinier, J. R.; Semenuic, R. F.; Smith, M. D. *Dalton Trans.* **2003**, 1712–1718.
187. Allen, F. H.; Harris, S. E.; Taylor, R. *J. Computer-Aided Mol. Design* **1996**, 10, 247–254.
188. Suezawa, H.; Ishihara, S.; Takahashi, O.; Saito, K.; Kohno, Y.; Nishio, M. *New J. Chem.* **2003**, 27, 1609–1613.
189. Tsuzuki, S.; Houjou, H.; Nagawa, Y.; Hiratani, K. *J. Chem. Soc., Perkin Trans. 2* **2001**, 1951–1955. Takahashi, O.; Kohno, Y.; Gondoh, Y.; Saito, K.; Nishio, M. *Chem. Eur. J.* **2003**, 9, 756–762. Takahashi, O.; Saito, K.; Kohno, Y.; Suezawa, H.; Ishihara, S.; Nishio, M. *Bull. Chem. Soc. Jpn.* **2003**, 76, 2167–2173. Takahashi, O.; Saito, K.; Kohno, Y.; Suezawa, H.; Ishihara, S.; Nishio, M. *New J. Chem.* **2004**, 28, 355–360.
190. Burley, S. K.; Petsko, G. A. *Science* **1985**, 229, 23–28. Burley, S. K.; Petsko, G. A. *Adv. Protein Chem.* **1988**, 39, 125–189.
191. Singh, J.; Thornton, J. M. *FEBS Lett.* **1985**, 191, 1–6.
192. Chakrabarti, P.; Samanta, U. *J. Mol. Biol.* **1995**, 251, 9–14.
193. Brandi, M.; Weiss, M. S.; Jabs, A.; Sühnel J.; Hilgenfeld, R. *J. Mol. Biol.* **2001**, 307, 357–377.
194. Jabs, A.; Weiss, M. S.; Hilgenfeld, R. *J. Mol. Biol.* **1999**, 286, 291–304. Pal, D.; Chakrabarti, P. *J. Mol. Biol.* **1999**, 294, 271–288. Samanta, U.; Pal, D.; Chakrabarti, P. *Proteins* **2000**, 38, 288–300. Toth, G.; Watts, C. R.; Murphy, R. F.; Lovas, S. *Proteins* **2001**, 47, 373–381. Toth, G.; Watts, C. R.; Murphy, R. F.; Lovas, S. *Protein Eng.* **2001**, 14, 543–547. Bhattacharyya, R.; Samanta, U.; Chakrabarti, P. *Protein Eng.* **2002**, 15, 91–100. Thomas, A.; Meurisse, R.; Charlotteaux, B.; Brasseur, R. *Proteins* **2002**, 48, 628–634, 635–644. Meurisse, R.; Brasseur, R.; Thomas, A. *Biochem. Biophys. Acta* **2003**, 1649, 85–96.
195. Waters, M. L. *Curr. Opinion Chem. Biol.* **2002**, 6, 736–741; Gazit, E. *Bioinformatics Discovery Note* **2002**, 18, 880–883. Gazit, E. *FASEB J.* **2002**, 16, 77–83. Boehr, D. D.; Farley, A. R. R.; Wright, G. D.; Cox, J. R. *Chem. Biol.* **2002**, 9, 1209–1217.
196. Derewenda, Z. S.; Lee, L.; Derewenda, U. *J. Mol. Biol.* **1995**, 252, 248–262. Chakrabarti, P.; Chakrabarti, S. *J. Mol. Biol.* **1998**, 284, 867–873. Fabiola, G. F.; Krishnaswamy, S.; Nagarajan, V.; Pattabhi, V. *Acta Crystallogr.* **1997**, A53, 316–320.
197. Steiner, T.; Koellner, G. *J. Mol. Biol.* **2001**, 305, 535–557.
198. Flocco, M. M.; Mowbray, S. L. *J. Mol. Biol.* **1994**, 235, 709–717. Mitchell, J. B. O.; Nandi, C. L.; McDonald, I. K.; Thornton, J. M.; Price, S. L. *J. Mol. Biol.* **1994**, 239, 315–331.
199. The “concept of hydrophobic effect” is a subject of controversy among physical chemists. See, for example: Patterson, D.; Barbe, M. *J. Phys. Chem.* **1976**, 80, 2435–2436. Shinoda, K. *J. Phys. Chem.* **1977**, 81, 1300–1302. Cramer, R. D. III. *J. Am. Chem. Soc.* **1977**, 99, 5408–5411. Murphy, K. P.; Privalov, P. L.; Gill, S. J. *Science* **1990**, 247, 559–561. Dill, K. *Science* **1990**, 250, 297.
200. The logical consequence is that a specific structure is brought about by forces of an enthalpic nature, attractive or repulsive. See: Shinoda, K. *Kagaku to Kogyo* **1967**, 21, 1400–1405. Hildebrand, J. H. *Proc. Natl. Acad. Sci., USA* **1979**, 76, 194. Privalov, P. L.; Gill, S. J. *Adv. Protein Chem.* **1988**, 39, 191–234.

# Chapter 9

## Stereoselective Thermal Solid State Reactions

GERD KAUPP

*University of Oldenburg, P.O. Box 2503, D-26111 Oldenburg, Germany*

- I. Introduction
- II. Techniques in Organic Solid State Chemistry
- III. Halogen Additions
- IV. Hydrohalogen Additions
- V. HCl Additions with Rearrangement
- VI. Eliminations
- VII. Nucleophilic Substitutions
- VIII. Carbonyl Condensation Reactions
- IX. Wittig Reactions
- X. Michael and Enolate Additions
- XI. Grignard Reactions
- XII. Cycloadditions
- XIII. Reductions
- XIV. Oxidations
- XV. Protonations (Ligand Conformations)
- XVI. Thermal Rearrangements
- XVII. Solid State Geometrical Isomerizations
- XVIII. Linear Dimerizations and Polymerizations
- XIX. Conclusions
- References

### I. INTRODUCTION

The scope of this article is the stereochemistry of organic (including organometallic) gas-solid, solid-solid, and thermal, but not photochemical or radiolytical solid state reactions. This coverage excludes thermal phase transitions between crystal

modifications or the thermal interconversions of high- and low-spin isomers of transition-metal complexes as related but separate subjects.<sup>1</sup> Also important solvent-free solid–liquid reactions or the formation of liquid organic products from solids are not treated here, since they follow different mechanistic rules. Solid state reactions profit from crystal structure packing. The molecules pack in largely unpredictable ways; however, empirical crystal engineering is advancing. From the beginning there was the idea that the well-arranged molecules may be so confined that stereospecificity will ensue upon reaction with gases. For example, it was claimed in 1972 that *trans*-stilbene and chlorine gas reacted by exclusive *cis*-addition to form *dl*-dichlorostilbene while the solution reaction gave a 2:1 mixture of the *dl*- and *meso*-stereoisomers. However, scrutiny of the experiment in the light of the new reactivity theory—that is (1) phase rebuilding, (2) phase transformation, and (3) crystal disintegration<sup>2,3</sup>—gave totally different results. Although the earlier hypotheses, since 1964, assumed minimal atomic and molecular movements in solid state reactions, atomic force microscopy (AFM), scanning near-field optical microscopy (SNOM), and depth-dependent grazing-incidence diffraction (GID) experiments enforced a paradigmatic change with the indispensable requirement of long-range anisotropic molecular migrations. These were found to be essential in the phase rebuilding stage (with gradually increasing disorder of the crystal) followed by phase transformations into the product phase and disintegration of the crystal (thermal or photochemical) or detachment in the >100 nm reaction zone (gas–solid or solid–solid). The new molecules with different shape must immediately accommodate the crystal lattice upon their formation rather than residing in a so-called reaction cavity where they would build up enormous pressure.<sup>4,5</sup> The new reactivity scheme provides an experimentally founded understanding of solid state and, in particular, gas–solid and solid–solid reactions that was not available to the so-called topochemistry principle. Furthermore the new mechanistic evidence urges scrutiny of claims for “complete stereospecificity” if undue extrapolations of enantiomeric purities were executed from reactions with (very) low conversions.

## II. TECHNIQUES IN ORGANIC SOLID STATE CHEMISTRY

Gas–solid reactions that run to completion require vacuum-tight glassware. In laboratory-scale syntheses the flask containing the crystals is evacuated and the reactive gases let in at the desired pressure or speed at room temperature or with cooling or heating of the flask. Stirring or shaking is necessary if a reactant gas is liberated in order to mix the gases. The crystals must not be finely ground or milled in most cases in order to avoid violent reaction. Larger scale gas–solid reactions use loosely packed columns and gas flow. Heat is removed or added by

admixed air or inert gas at the appropriate ratio as the reacting gas proportion is increased toward the end. However, improperly diluted reactive gases can create a sharp reaction front through the column. The stream bed and the suspension or fluidized beds can be chosen. In addition, volume increase during reaction has to be taken into account.<sup>2,3</sup>

Solid–solid reactions require contacts between reacting crystals over and over again (we do not consider here “contacts” through liquids; short-range sublimation is considered a gas–solid reaction). Toda's group most often mixed powdered reactants, which were left to react upon standing, sometimes with sonication or occasional grinding.<sup>6</sup> This technique is time-consuming, and the reactions are rarely complete. Continuous cogrinding and a final sonication should only be used if milling is not available.

For complete solid–solid reactions with 100% yield in stoichiometric mixtures, ball-milling is by far the first choice.<sup>2,3,7</sup> Because ball-milling of molecular crystals does not induce “mechanochemistry” (breaking of regular molecular bonds cannot occur, with the exception of weak bonds of explosives, but intermolecular interactions between ion-pairs or H-bonds and van der Waals attractions can be broken, and the surface is increased by crystal disintegration), the moderate efficiency of swing-mills with cooling/heating device is sufficient.<sup>2,3</sup> High milling efficiency in rotor-mills for larger scale milling (up to kg scale and beyond)<sup>8</sup> increases the contact rate and is essential for tribochemistry (mechanochemistry if strong σ-bonds in polymers or infinite covalent crystals are broken with formation of local plasma at the freshly broken crystal surfaces, e.g., at silica or silicon) with totally different reactivities in plasma chemistry with virtually all kinds of organic additives,<sup>9</sup> but it is a subject beyond the scope of this review as is mechanical alloying.<sup>9</sup> Furthermore even highly coordinated salts (e.g., KI) do not experience significant charge separation upon breakage of the crystal, and their grinding or milling is therefore not tribo- or mechanochemical in nature.<sup>10</sup>

Mechanistic investigations of gas–solid and solid–solid reactions as well as their proper engineering require identifiable crystal surfaces for atomic force microscopy (AFM) and scanning near-field optical microscopy (SNOM)<sup>2,11</sup> in combination with X-ray diffraction data, which are the basis of crystal packing analyses.<sup>2,3,12</sup> It has been shown that contact-AFM is a powerful tool to differentiate solid state from intermediate nano or micro liquid phase reactions.

Clearly, submicroscopic liquid phases would destroy any advantage of the crystal structure. It is hoped that all reactions selected from the literature (also with regard to the melting points) are real solid state reactions without intermediate liquids below the (usually not reported) eutectic temperatures. It had also to be assumed that visual inspection by the authors did not indicate liquefaction in reactions with ground solids. Fortunately, due to lack of solvation, the solid state reactions occur at considerably lower temperatures than melt reactions, and therefore the reaction frequently stops if the eutectic temperature

is slightly exceeded. But there are also cases of undercooled liquids that require temperature increases for immediate solid product phase formation.

The inhomogeneity of solid state reactions can frequently be determined by visual inspection of the crystals or under a microscope; nanometer scale homogeneity can only be determined with AFM.<sup>13</sup> Differences of reactivity on different crystal faces or with different crystals can also be determined with the AFM or under the microscope.<sup>13,14</sup>

Differences in reactivity of enantiopure gaseous amines with the crystals of racemic carboxylic acids can be used to decide by microscopic inspection if these occur as racemic crystals or as a conglomerate of enantiomeric crystals.<sup>15</sup> This technique is also useful for the planning of kinetic resolutions by gas–solid reactions of conglomerates.

Solid state circular dichroism (CD) is being used to characterize chiral crystals of achiral molecules giving a (+) or (−) Cotton effect,<sup>6,16</sup> and this elegant technique may replace the tedious X-ray diffraction technique with single crystals using anomalous dispersion. Spectroscopic analyses of solid state reactions must first use solid state techniques (IR, UV/Vis, Raman, luminescence, NMR, ESR, CD, X-ray powder diffraction, DSC, etc.) to secure the solid state conversion before the solution techniques (detection of minor side products, specific rotation, etc.) are applied.

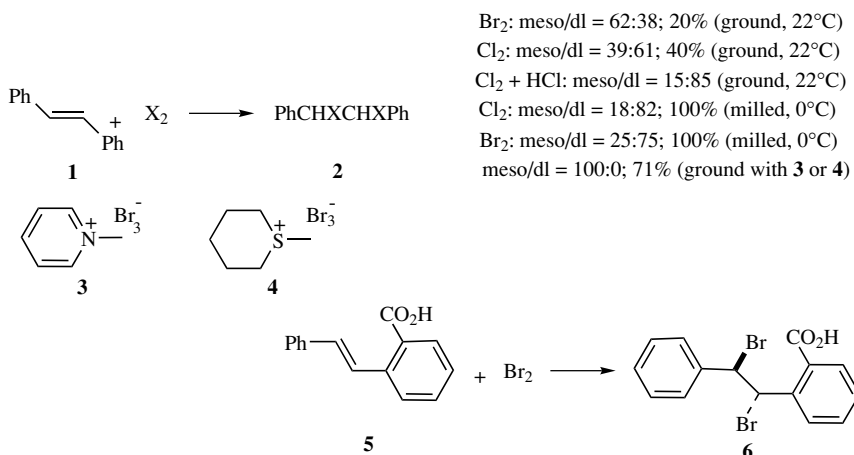
Solid state kinetic data are hard to interpret even if they are of zero or first order. Computational techniques have been summarized<sup>17</sup> and compared to the experimentally secured phase rebuilding mechanism,<sup>2,3</sup> which requires for the first time that the new molecules must find their way out of the crystal lattice immediately after their formation.

Environmentally friendly sustainable gas–solid and solid–solid or intra-solid thermal reactions proceed with 100% yield without side products. Simple by products such as H<sub>2</sub>O, or gases or inorganic salts can be removed without application of solvents (salts may alternatively be washed out with water). In all of these cases, genuine solvent free reactions or syntheses are achieved with highest atom economy as these do not require purification or workup (crystallization, chromatography, etc.). It is therefore most important to run solid state reactions to complete conversion, starting with stoichiometric mixtures of reactants in the solid–solid version. Hard to remove catalysts are rarely required and should be avoided, if possible.

### III. HALOGEN ADDITIONS

The stereochemistry of the addition of chlorine to crystalline *trans*-stilbene (**1**) found some interest as *trans*-additions were judged improbable in the confinement of a crystal. Consequently “exclusive *cis*-addition” to give *dl*-1,2-dichloro-1,2-diphenylethane (**2**, X = Cl) was claimed for single crystals in this

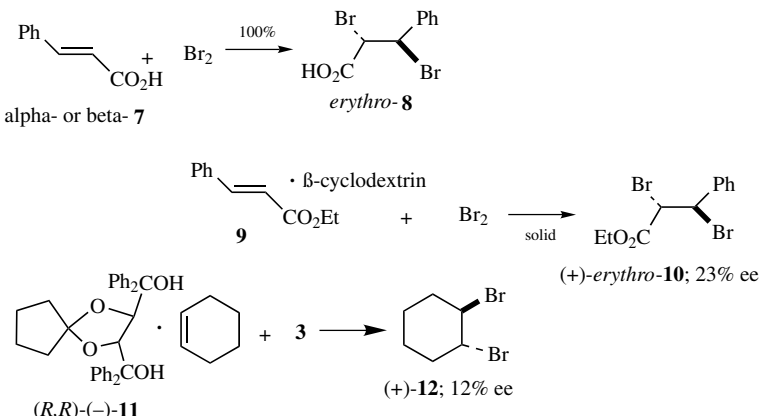
reaction.<sup>18</sup> However, scrutiny with polycrystals of *trans*-stilbene (**1**) gave no more than 61% *cis*-addition of chlorine (providing *d/l*-dichloride **2**) in addition to 39% *trans*-addition (providing *meso*-dichloride, **2**).<sup>19</sup> The *cis*-selectivity could be enhanced to 85% when a 1:1-mixture of Cl<sub>2</sub> and HCl was applied to polycrystals of **1** probably by increasing the rate of the addition.<sup>19,20</sup> However, *trans*-addition was still present in contrast to the previous claims. Clearly, *trans*-addition is facilitated by the molecular-migrations that are necessary for chemical reactivity from the beginning.<sup>2,3</sup> When bromine is added to crystalline *trans*-stilbene, the *trans*-addition prevails (62%) but less strongly than in CS<sub>2</sub> solution (84%).<sup>19,20</sup>



The low yields with ground material are caused by unexpected difficulties with the crystal disintegration. The remedy is to pre-mill **1** to grains of about 1 μm size followed by very cautious addition of the reactive gases. The chemical yields increase to 100%, and the selectivity for *cis*-addition rises considerably.<sup>21</sup> This represents a crystal-size effect as a consequence of the three-step solid state mechanism, with difficulties at the last step that can be engineered. The *meso*-dibromide is the only product if 1-methylpyridinium tribromide<sup>22</sup> (**3**) or tetrahydro-1-methyl(2H-thiopyranium) tribromide<sup>23</sup> (**4**) is used for the solid–solid reaction with *trans*-stilbene. Similarly powdered 2-carboxystilbene **5** provided the (±)-*erythro*-dibromide **6**, selectively.<sup>24</sup>

The addition of bromine gas to solid cinnamic acid (**7**) was first reported in 1863.<sup>25</sup> The then incorrect molecular formula (C<sub>18</sub>H<sub>8</sub>O<sub>4</sub>) derives from incorrect atomic weights, but the reported weight increase supports the correctness of the result. A careful reinvestigation showed that both the α- and β-*trans*-cinnamic

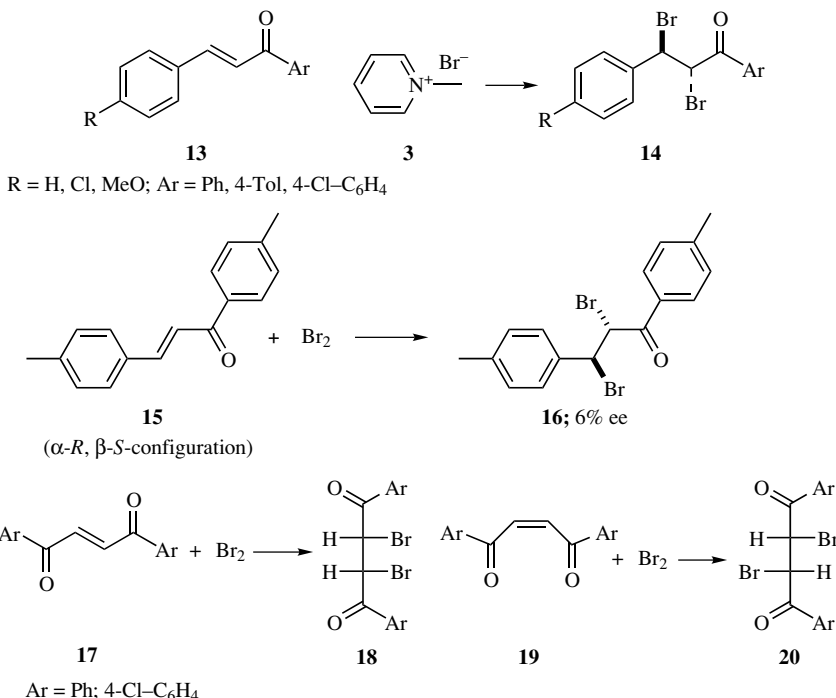
acid polymorphs (**7**) add Br<sub>2</sub> gas rapidly and quantitatively at 20–25 °C to give exclusively the *trans*-addition by forming the ( $\pm$ )-*erythro*-dibromide **8**.<sup>26</sup> The exclusive *trans*-addition in the layered structure points to a long-lived bromonium ion intermediate in the crystal environment where it migrates and therefore opens the possibility for backside attack in the termination of the chemical reaction.



Far-reaching molecular migrations within the crystal are secured by AFM analyses that exhibit different surface features on  $\alpha$ - and  $\beta$ -cinnamic acid (**7**) on different faces that relate closely to the crystal packing.<sup>26</sup> Ethyl *trans*-cinnamate (**9**) can be “solidified” by complexation in chiral  $\beta$ -cyclodextrin, and this gives with bromine the (+)-*erythro*-dibromide **10** with 23% ee.<sup>27</sup> Similarly the host (*R,R*)-(*–*)-**11** includes cyclohexene, which reacts with the solid tribromide **3** to give (+)-**12** with 56% yield and 12% ee.<sup>22</sup>

Chalcones have been subjected to solid state brominations. The solid–solid brominations of various *trans*-chalcones **13** with 1-methylpyridinium tribromide (**3**) and other solid tribromides select exclusive *trans*-addition to give the ( $\pm$ )-*erythro*-dibromides **14**, all with about 90% yield.<sup>22</sup> There was also a report claiming exclusive formation of *erythro*-dibromides from both *trans*- and *cis*-chalcones (**13**, Ar = Ph; R = H, Cl, MeO) upon the action of gaseous bromine.<sup>28</sup> This would, however, mean that unlike the discussion in Hadjoudis<sup>28</sup> the *trans*-chalcones **13** chose the *trans*-addition of bromine and the *cis*-chalcones chose the *cis*-addition of bromine, regardless of mechanistic considerations, which does not appear very reasonable.

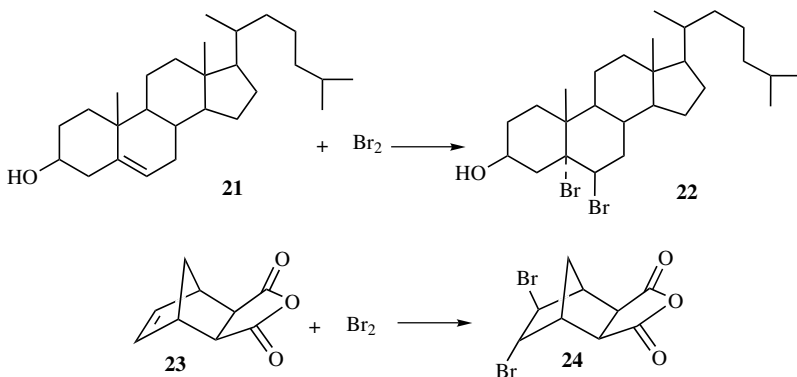
The addition of bromine to 4,4'-dimethylchalcone (**15**) was the subject of a low yield absolute asymmetric synthesis by addition of bromine to a selected



species of chiral crystals with the achiral molecules in ( $\alpha$ -R,  $\beta$ -S)-configuration. The optical yield from the powdered single crystal as measured by polarimetry of the raw brominated material was 6%.<sup>29</sup> Later on, after improvement of the inoculation techniques for the creation of crystals with only one handedness, a so-called quantitative optical yield was claimed.<sup>30</sup> However, the  $[\alpha]_D$ -value of the 6 times recrystallized (+)-( $\alpha$ -R,  $\beta$ -S)-*erythro*-dibromide **16** points rather to a maximum of 16–19% ee and it was *not* secured if there was not also some *threo*-dibromide in the crude reaction mixture.<sup>31</sup> It could be shown that stirred crystallization was superior in obtaining crystals of only one chirality than in unstirred crystallization and the 6% optical yield was confirmed.<sup>32</sup> However, an increase to 13% ee at 73% yield was obtained if chiral crystals of **15**, which showed a (–)-Cotton effect in the solid state CD spectrum, were brominated in an aqueous suspension.<sup>22</sup>

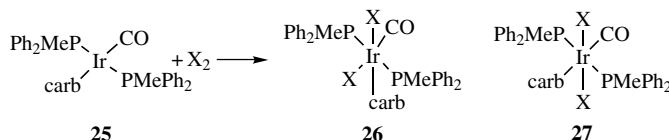
The absolute conformation of the chiral crystal of **15** and the absolute configuration of (+)-**16** were secured by X-ray diffraction techniques. Because of nonplanarity (dihedral angle between the two phenyl groups is 49° in **15**),<sup>31</sup> the approach of bromine to the double bond is asymmetric, leaving the open side apparently more favorable for initial attack by bromine. However, crystal packing effects should also be taken into account.<sup>2,3</sup>

The gas–solid addition of bromine to *trans*- (**17**) and *cis*-dibenzoylethenes (**19**) in analytical experiments gave apparently the *meso*- (**18**) and *d/l*-adducts (**20**), respectively.<sup>33</sup>



Fully stereospecific is the gas–solid *trans*-addition of bromine to cholesterol (**21**). The solid 5α, 6β-dibromide **22** (which is thermodynamically disfavored) is quantitatively obtained.<sup>34</sup> Liquid-state bromine addition did not form an equally pure product after the then necessary recrystallization. Similarly the disubstituted double bond of the crystalline compound **23** adds gaseous bromine in the *trans*-fashion to give the racemic product **24**.<sup>35</sup>

Stereoselective solid state halogen additions to transition metal complexes are also known. For example, the gas–solid addition of chlorine to the carborane-iridium(I) complexes **25** stereospecifically gives rise to the *cis*-addition products having the structure **26** (X = Cl). Conversely, the reactions with gaseous bromine afford 1:1-mixtures of **26** and **27** (X = Br). The chlorine addition in benzene exhibits different selectivities: complex **25a** provides only the *trans*-adduct **27** (X = Cl) and **25b** gives 60% **26** and 40% **27** (X = Cl), respectively.<sup>36</sup>

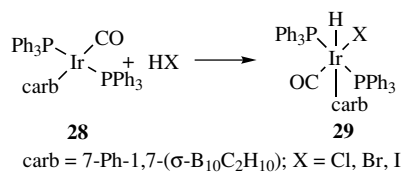


a: carb = 7-Me-1,7-(σ-B<sub>10</sub>C<sub>2</sub>H<sub>10</sub>)

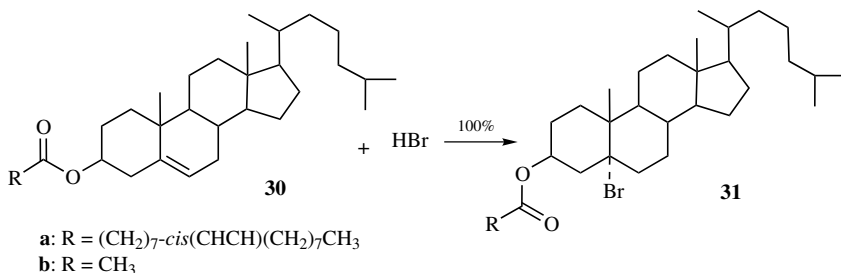
b: carb=7-Ph-1,7-(σ-B<sub>10</sub>C<sub>2</sub>H<sub>10</sub>)

#### IV. HYDROHALOGEN ADDITIONS

The iridium(I) complex **28** undergoes *cis*-additions with gaseous HCl, HBr, and HI. The products **29** are formed stereospecifically in the solid state.<sup>36</sup> Further examples of that type can be found in Coville and Cheng<sup>17</sup> and Ball and Pope.<sup>37</sup>



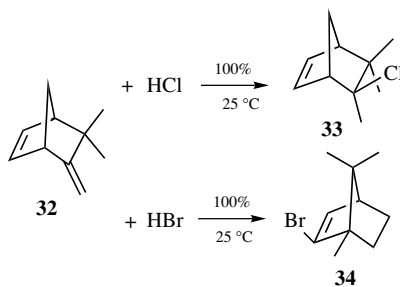
Crystalline cholesteryloleate (**30a**), and less rapidly cholesterylacetate (**30b**), add gaseous HBr quantitatively and stereospecifically to give the 5 $\alpha$ -bromides **31**.<sup>34</sup> These syntheses are performed at -30 °C to -20 °C to avoid melting. Gaseous



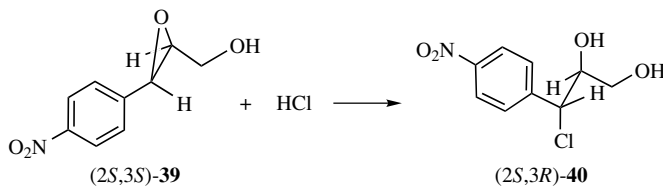
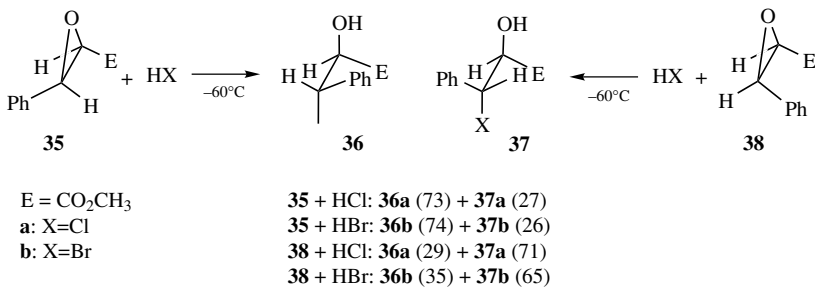
HCl or HI are unreactive, even though they colorize the crystals to light yellow or brown-red. These substrate specificities are not clear, but the 5 $\alpha$ -bromides **31** are most easily prepared by the solid state technique.

Solid (-)-camphene (**32**, m.p. 52 °C) quantitatively adds HCl gas at 25 °C to give camphene hydrochloride (**33**) and this is the easy path to this elusive compound in pure form.<sup>7</sup> Conversely, the addition of HBr immediately provides the rearranged (+)-isobornyl bromide (**34**) stereospecifically and quantitatively.

Ethyl *trans*-cinnamate (**9**) was included in chiral  $\alpha$ - or  $\beta$ -cyclodextrin and the solids were exposed to HBr gas. The result was (*R*)-(+) or (*S*)-(−)-3-bromo-3-phenyl-ethylpropanoate with 46% ee and 31% ee, respectively.<sup>24</sup>

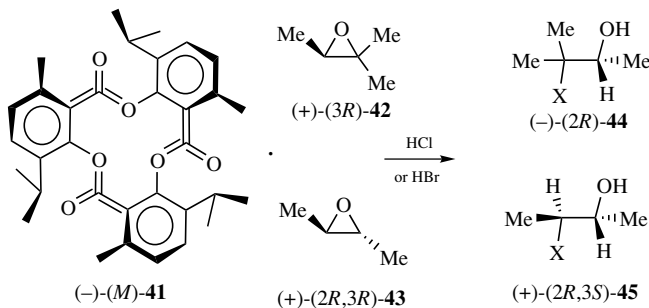


Importantly, numerous solid oxiranes add gaseous HCl or HBr in a stereoselective manner with quantitative chemical yield. The addition to racemic **35** and **38** at  $-60\text{ }^\circ\text{C}$  yield **36** and **37** always with a marked preference for front-side attack of the protonated oxiranes over the backside attack, which is also the case in solution reactions.<sup>38</sup> The reason may derive from “early” formation of the stabilized benzylic cation on the way to the products also in the crystal. The results are included in the reaction scheme and indicate also the full regiospecificity of these reactions. Conversely, the fully stereospecific HCl addition to  $(2S, 3S)$ -**39** yields only the  $(2S, 3R)$ -product **40** by backside attack of the protonated oxirane with lower probability for formation of the benzylic cation than in the cases of **35** or **38**.<sup>38</sup>

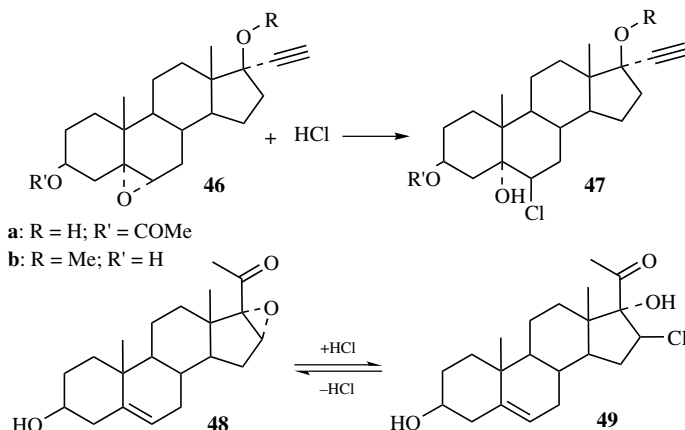


$(-)(M)$ -tri-*o*-thymotide (**41**) (*P3<sub>1</sub>21*) selectively enclathrates the oxiranes **42** or **43** with 13–14% ee for  $(+)-(3R)$ -**42** or 51–55% ee for  $(+)-(2R,3R)$ -**43**. The

isolated molecules in the chiral cages of **41** react stereoselectively with HCl or HBr gas to give the products **44** or **45** in almost stereopure form according to the optical rotations after quantitative reaction under the influence of the chiral environment.<sup>39</sup> The host lattice is preserved during the reactions, but destroyed during liberation of the product molecules.

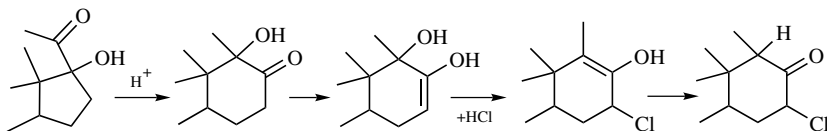


The marked stereoselectivities and clean solid state reactions were used for synthetic purposes in the steroid field. The stereospecifically obtained *trans*-chlorohydrins **47** ensue quantitatively from the crystalline  $5\alpha$ ,  $6\alpha$ -epoxides **46** with gaseous HCl.<sup>38</sup> Similarly the crystalline  $16\alpha$ ,  $17\alpha$ -epoxide **48** reacts with gaseous HCl to yield exclusively the *trans*-chlorohydrin **49**, which easily loses HCl to reform the starting epoxide **48**. Therefore an equilibrium situation is reached in that case.<sup>38</sup>



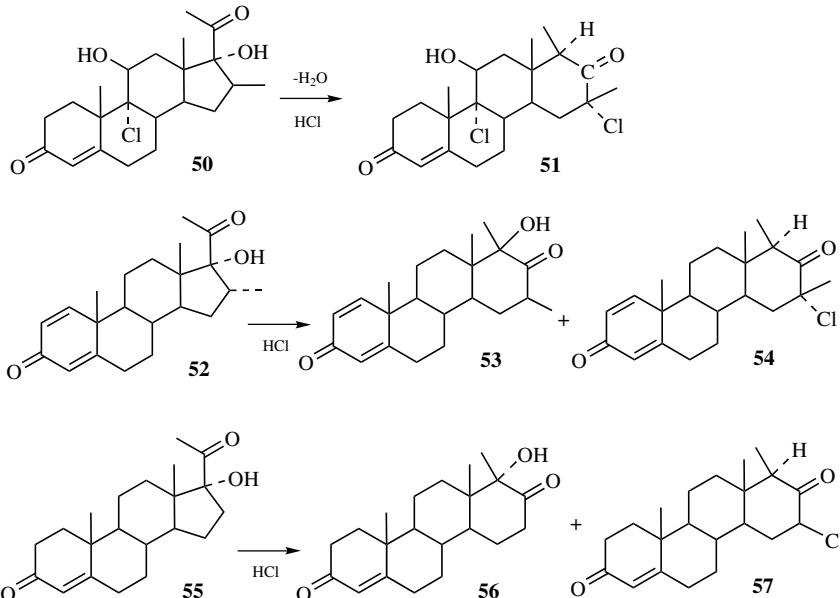
## V. HCl ADDITIONS WITH REARRANGEMENT

The solid state reaction technique opens new possibilities for ring enlargements in the steroid field as schematically sketched in the mechanistic scheme.<sup>38,40</sup> This represents initial acyloin rearrangement followed by HCl-addition with various 1,3-H-shifts.



The steroid acyloin **50** with a  $16\beta$ -methyl substituent undergoes a substitutive rearrangement to give **51** stereospecifically in 100% yield.<sup>40</sup> The most probable mechanism begins with acid catalyzed migration of the 13,17-bond, enolization, vinylogous substitution of OH by Cl and 1,3-H-shift. This unprecedented reaction did not occur in  $\text{CH}_2\text{Cl}_2$ -solution.

The related steroid **52** with a  $16\alpha$ -methyl substituent gives the conventional rearrangement product **53** (two isomers) and the product **54** with a stereospecificity that corresponds to that of **51** at 0 °C without melting. The chlorine is bound to the

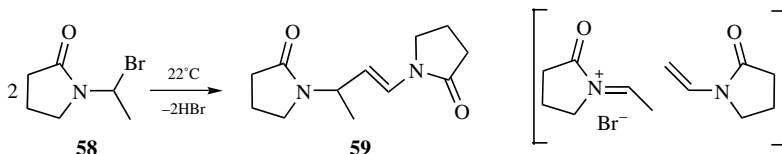


$16\alpha$ -position in both **51** and **54**. If, however, the  $16$ -methyl group is missing as in the starting acyloin **55** a  $16\beta$ -stereospecificity results.<sup>40</sup>

The rearrangement of the acyloin **55** requires the solid state and the HCl gas preferably in the presence of the drying agent  $\text{MgSO}_4 \cdot 2\text{H}_2\text{O}$  to bind the liberated water. Here the intermediate **56** and the final product **57** are formed in 46% yield each (in addition to 8% dehydration product of **55**). Isolated **56** can be transformed to **57** with gaseous HCl. Again, no reaction occurs in  $\text{CH}_2\text{Cl}_2$ .<sup>40</sup>

## VI. ELIMINATIONS

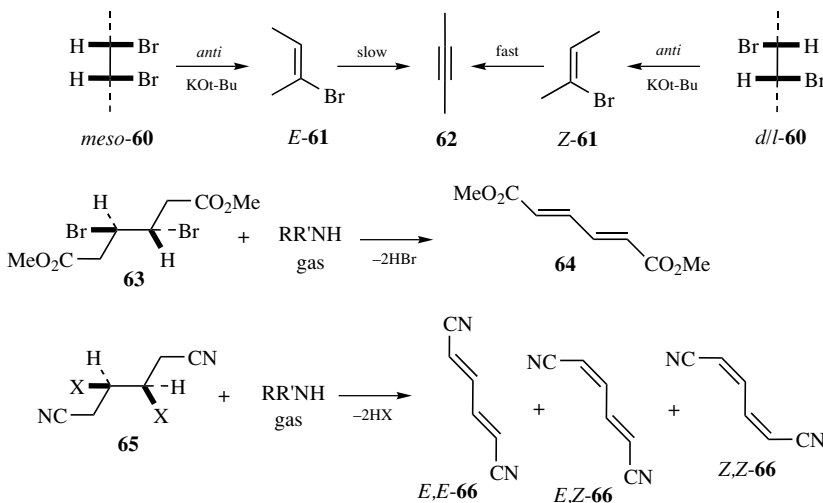
A purely thermal solid state elimination of HBr from the highly reactive solid bromide **58** provides the linear dimer **59** with a *trans*-double bound via the corresponding alkene.<sup>20</sup> Thus, a good yield (65% after recrystallization from acetone) of **59** is obtained after removal of HBr gas from **58** at room temperature without melting. Most likely the intermediates are the cation and the enamide as depicted. This reaction is restricted to the solid state.



Less reactive halogenides require bases for the elimination such as  $\text{KO}t\text{-Bu}$ ,  $\text{NaOH}$ , ammonia or aliphatic amines in gas–solid reactions. Early work has been summarized in Thomas, Morsi, and Desvergne.<sup>41</sup>

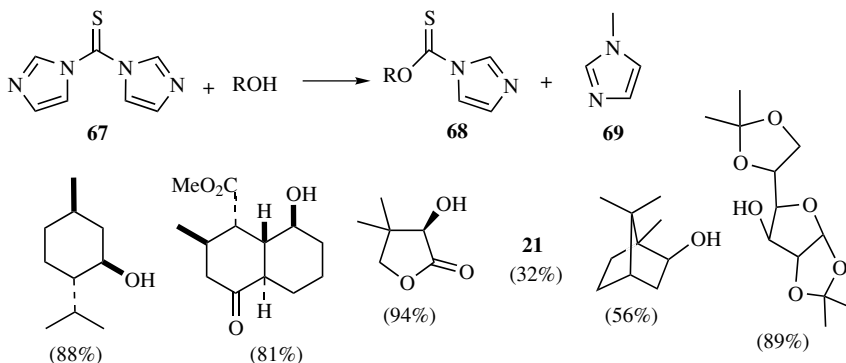
The *anti*-orientation in the gas–solid elimination with the *meso*- and *d/l*-dibromides **60** and  $\text{KO}t\text{-Bu}$  has been secured by the configuration of the olefinic products **61** and the rate differences in their eliminations to give dimethylacetylene **62**.<sup>42</sup>

Solid *meso*- $\beta,\beta'$ -dihalogenoadipates (**63**) give *trans*, *trans*-muconates **64**, whereas solutions provide mixtures of *E/Z*-isomers. While this reaction was termed “topochemical,” the analogous gas–solid elimination of HX from *meso*- $\beta,\beta'$ -dihalogenoadiponitrile (**65**) was termed “reactions at defects” because the three isomers of 1,3-butadiene-1,5-dinitrile (**66**) were formed in the ratio *trans, trans : cis, trans : cis, cis* = 3:5:2 despite different expectations from “topochemistry.”<sup>41</sup> Clearly, the influence of the crystal packing that is so essential for the necessary molecular migrations within the crystal<sup>2,3</sup> was not considered. AFM and SNOM investigations would certainly be able to clarify the differences between **63** and **65**.



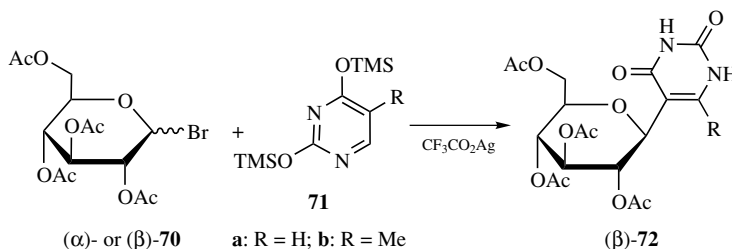
## VII. NUCLEOPHILIC SUBSTITUTIONS

Solid state nucleophilic substitutions of the thiourea derivative **67** with chiral alcohols ROH leads to the chiral thiourethanes **68** and **69**.<sup>43</sup> Some racemic and enantiopure alcohols are listed together with the product yields.

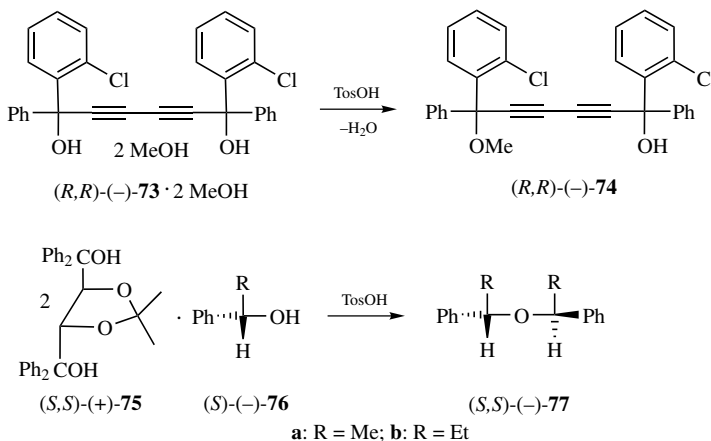


Both 2,3,4,6-tetra-*O*-acetyl- $\beta$ -*D*- and 2,3,4,6-tetra-*O*-acetyl- $\alpha$ -*D*-glucopyranosylbromide **70** provide the  $\beta$ -configured protected glucopyranosyl uracil (**72a**) or -thymine (**72b**) when ball-milled together with **71a,b** and a large excess of silver trifluoroacetate for two days.<sup>44</sup>

Such  $\beta$ -selectivity is not obtainable in the conventional fusion reaction that affords an anomeric mixture. It was not reported if ( $\alpha$ )-**72** would epimerize to

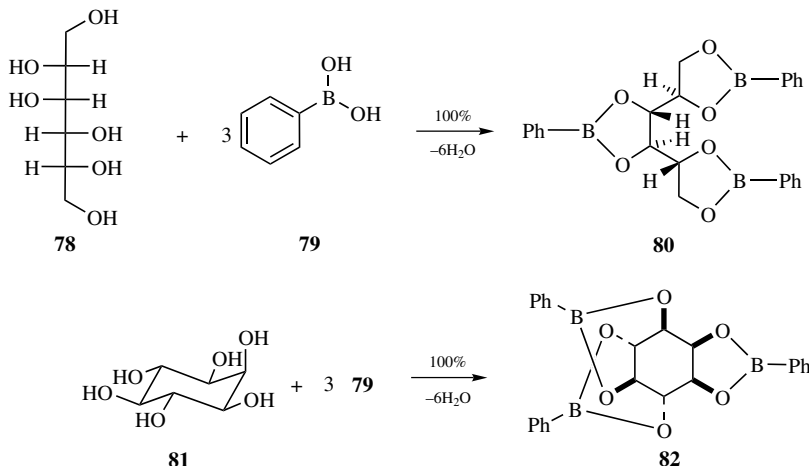


( $\beta$ )-72 upon extended milling. Solid state etherifications of tertiary alcohols as induced by solid *p*-toluenesulfonic acid retain the configuration of the alcohols despite carbonium ion mechanisms. The 1:2 inclusion complex of (*R,R*)-( $-$ )-73 and methanol provides the (*R,R*)-( $-$ )-methoxy derivative 74 with 94% ee.<sup>45</sup> Another enantioselective etherification in the solid state is obtained with the solid inclusion complexes 75 and enantiomerically pure 1-phenylethanol or 1-phenylpropanol (76a, b). Thus, treatment of (75)<sub>2</sub>·76 with TsOH affords the enantiomerically pure ethers (*S,S*)-( $-$ )-77, but not the *meso*-isomers.<sup>45</sup>

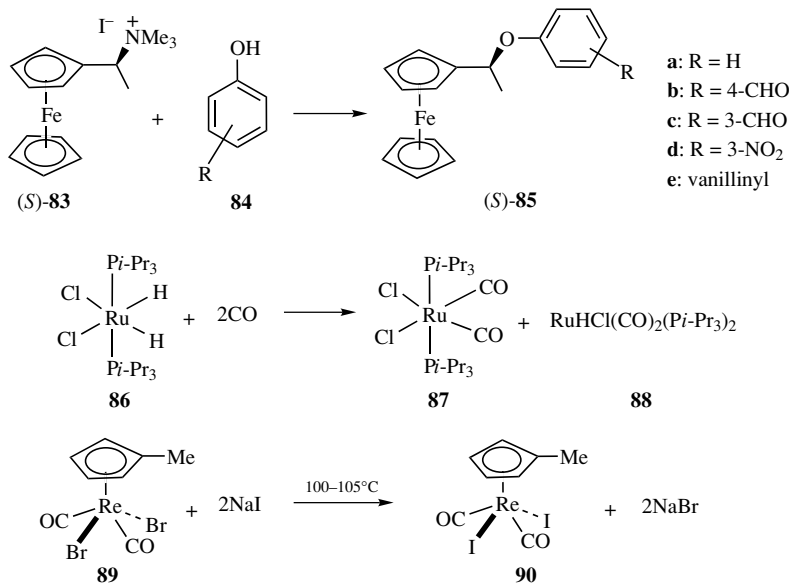


(*D*)-Mannitol (78) reacts quantitatively and stereospecifically at room temperature with three molecules of phenylboronic acid (79) in the ball-mill to give the 1:2,3:4,5:6-product 80 with 2*R*,3*R*,4*R*,5*R*-configuration as a nonsticky powder.<sup>46</sup> This fully protected mannitol is now available with great ease as the water can be removed by drying in a vacuum at 80°C. The same is true for the stoichiometric synthesis of the fully protected *myo*-inositol *rac*-82. It is obtained by milling 81 with three molecules of 79 at 95°C. The *meso*-compound 81 provides specifically the racemate of 82 with one five-membered and two six-membered rings in the given orientation. In both highly remarkable syntheses the

large amounts of the by product water are taken up by the crystal lattice of the tris-boronic esters.<sup>46</sup>



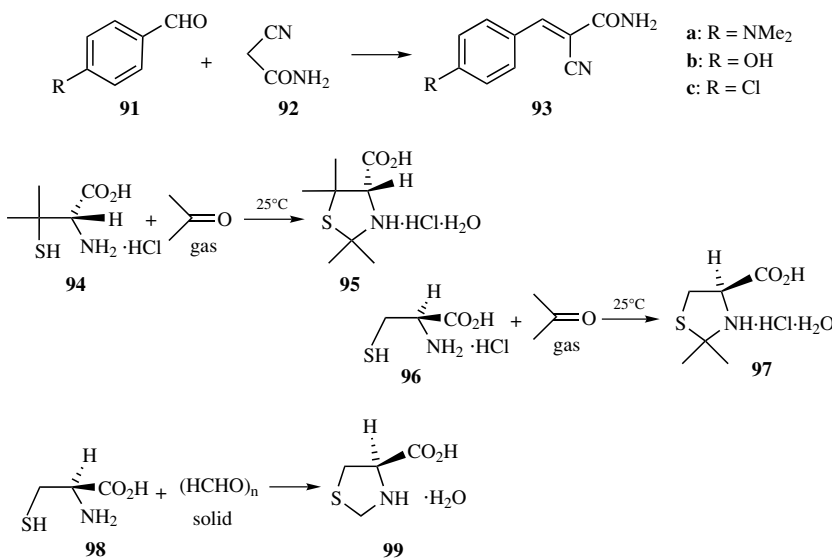
The solid ferrocenyl complex (*S*)-**83** can be substituted at the ligand by solid phenols **84** with retention of the configuration to give (*S*)-**85**. For example, the reaction of **83b** at 70°C in the solid state affords (*S*)-**85b** in 83% yield.<sup>47</sup> It is, however, also possible to substitute ligands in metallorganic complexes and these



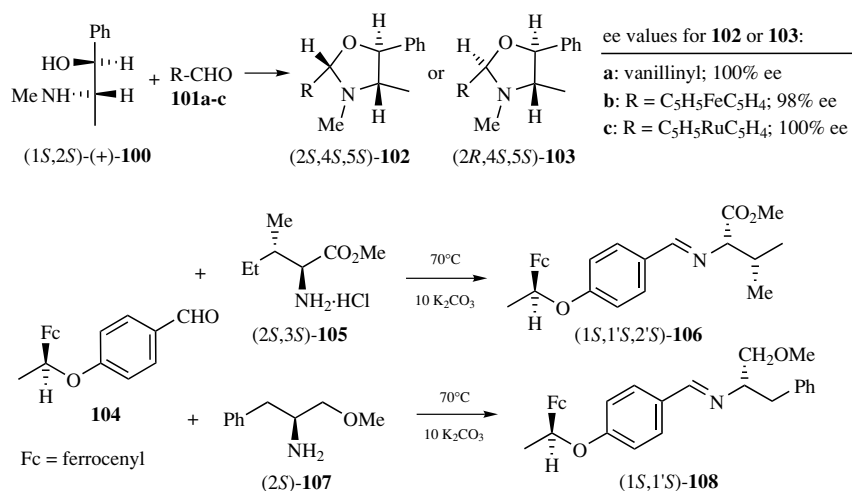
reactions are quite common.<sup>17</sup> The stereochemical course has been elucidated in some cases. For example, the *cis,cis,trans*-complex **86** (distorted variant of a  $D_{4d}$  square antiprism) exchanges its hydrogens by CO to give *cis,cis,trans*-**87**. Additionally the product of H and Cl substitution **88** is obtained by substitution of one H and one Cl.<sup>48</sup> A further example is the double substitution of **89** to give **90** upon solid state reaction with NaI.<sup>49</sup>

### VIII. CARBONYL CONDENSATION REACTIONS

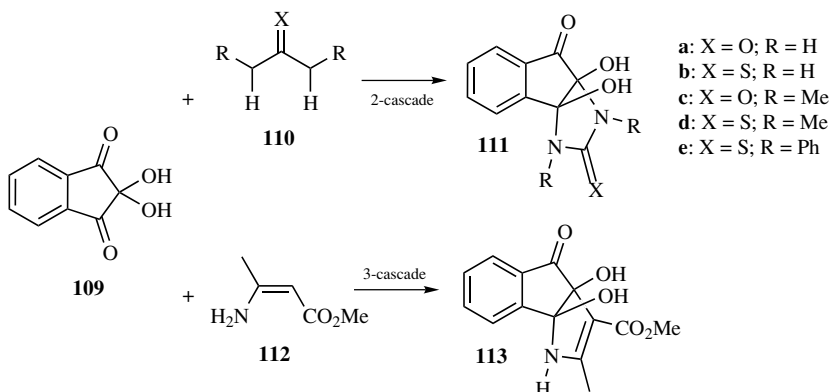
Solid state Knoevenagel condensations with unsymmetrically substituted methylene components give rise to *E/Z*-isomers in the product olefins. For example, aromatic aldehydes **91** and cyanoacetamide (**92**) yield the *E*-isomers **93** in quantitative yield. Similar reactions succeed with methyl cyanoacetate instead of **92**.<sup>50</sup> The same results were obtained in melt reactions. Crystalline D-(–)-penicillamine hydrochloride (**94**·HCl) reacts quantitatively with acetone vapor in the solid state to give D-(**95**) as a solid hydrochloride hydrate. The analogous reaction of L-cysteine hydrochloride (**96**·HCl) gives the thiazolidine L-**97** as a solid hydrochloride hydrate. In none of these cases was it possible to react the more nucleophilic free bases **94** and **96**. AFM measurements indicate surface passivation after an initial start of the reaction, which stopped the further reaction of the free bases.<sup>50</sup> Such passivation is broken by the use of the hydrochlorides. Furthermore, such passivation does not occur in solid–solid reactions with milling, as any passivating layer will be constantly removed. Therefore, both **96**



and neutral L-cysteine (**98**) give **97**·HCl and **99** (both as hydrates), respectively, upon stoichiometric milling with paraformaldehyde in 100% yield.<sup>51,52</sup>



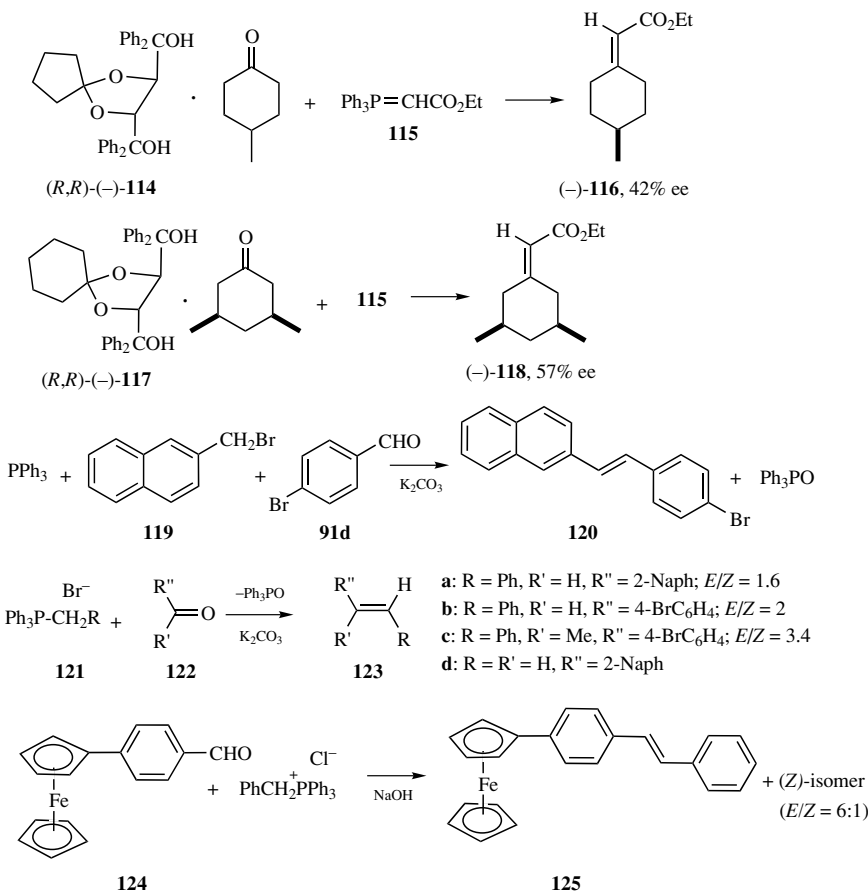
Similarly quantitative yields are obtained when solid (1*S*,2*S*)-(+)-pseudoephedrine (**100**) is reacted with prochiral organic and organometallic solid aldehydes **101a-c** to give one of the epimeric oxazolidines **102** or **103** as a consequence of true solid state reactions upon milling. The configurations of the epimers have not been assigned. If (1*R*,2*S*)-(−)-ephedrine is similarly reacted with **101c**, a one to one mixture of the (2*S*,4*S*,5*R*)- and (2*R*,4*S*,5*R*)-diastereomers ensues with 100% yield in a solid state reaction.<sup>53</sup> Solid state condensation of the chiral metallorganic aldehyde **104** with the chiral amine hydrochlorides **105** and **107** gives the optically pure Schiff's bases **106** and **108** in good yields.<sup>47</sup>



Ninhydrin (**109**) has been quantitatively condensed in stoichiometric solid–solid reactions with (thio)ureas **110** or 3-aminocrotonate (**112**) to give the *cis*-diols **111** and **112** as racemates,<sup>54</sup> The solid compounds **111b** and **113** are remarkably resistant to the elimination of water, despite their N/O-hemiacetal structure.

## IX. WITTIG REACTIONS

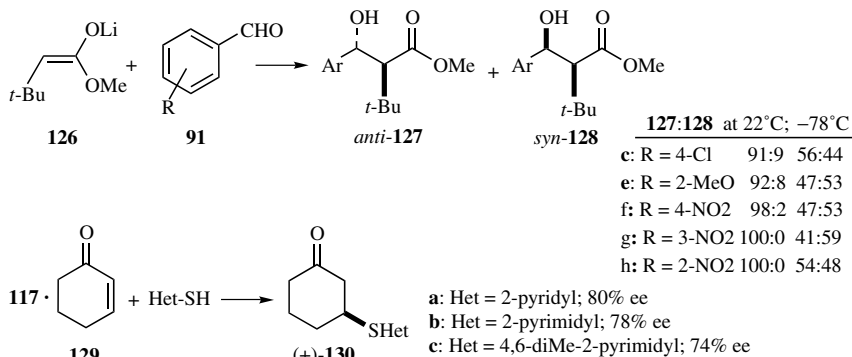
Enantioselective solid–solid Wittig reactions succeed when achiral cyclohexanones are included in suitable chiral hosts, finely powdered together with a phosphorane and heated to 70 °C. For example, the combinations of **114** and **115** or **117** and **115** give 73% (−)-**116** and 42% ee or 58% (−)-**118** and 57% ee, respectively.<sup>55</sup>



Some of the previous experience with ball-milling techniques<sup>3,9</sup> were employed by Balema et al.<sup>56</sup> On the basis of reactive milling for sustainable or “green” chemistry (numerous examples are collected in Tanaka<sup>57</sup> and in Kaupp<sup>135</sup>). Solid state Wittig reactions are reported; however, the term used, “mechanochemical,” is misleading as no tribochemistry (breaking of  $\sigma$ -bonds upon milling of explosives, polymers or infinite covalent crystals<sup>9</sup>) could be executed. It should be reminded here again that the milling just assures repeated contacts of the reacting molecular or ionic crystals in an efficient way.<sup>3</sup> The temperature was judged to stay below 70 °C in the air-cooled device.<sup>56</sup> Moderate *E*-selectivity was reported (which is not available in most Wittig reactions in solution), but triphenylphosphine oxide has to be removed from the products. The products **120** and **123** were obtained in yields of up to 90% with *E/Z*-ratios ranging from 1.6 to 3.5. Clearly, solvent use is required for the workup, and this strongly detracts from the claim that these are “solvent-free” in Balema et al.<sup>56</sup> A preceding study<sup>58</sup> included the total conversion of **124** to give (*E*)-**125** and its (*Z*)-isomer in a 6:1 ratio at total conversion upon 4 minute grinding with the reagents at room temperature. It was, however, not stated if the “solvent-free” or “dry” reaction occurred as a solid state reaction, but the melting points appear to be sufficiently high.

## X. MICHAEL AND ENOLATE ADDITIONS

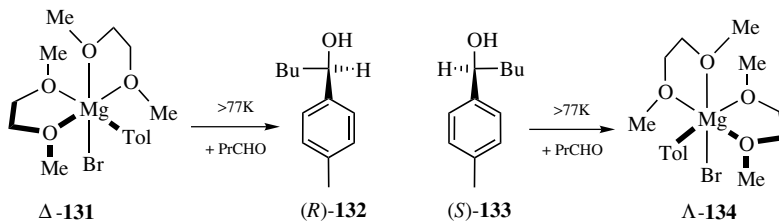
Solid–solid enolate additions to aromatic aldehydes provide the racemic *anti*-**127** and *syn*-**128** products. A marked preference for racemic *erythro*-products was reported at 22 °C, similar to the ratio found in THF solution.<sup>59</sup> However, the melting point of **91e** is not very high. The same reactions at -78 °C provided close to 1:1 mixtures for a series of aromatic aldehydes. It is therefore concluded that the *syn*-products are the thermodynamically controlled diastereomers, while kinetically there is not much differences between the competing transition states.



The enantioselectivity of solid-solid Michael additions can be controlled by inclusion of the enone in chiral hosts. For example, the solid 1:1 inclusion complex of  $(-)(R,R)$ -**117** and 2-cyclohexenone (**129**) yields  $(+)$ -**130** with appreciable ee values upon sonication of powdered mixtures and a catalytic amount of benzyltrimethylammonium hydroxide.<sup>60</sup>

## XI. GRIGNARD REACTIONS

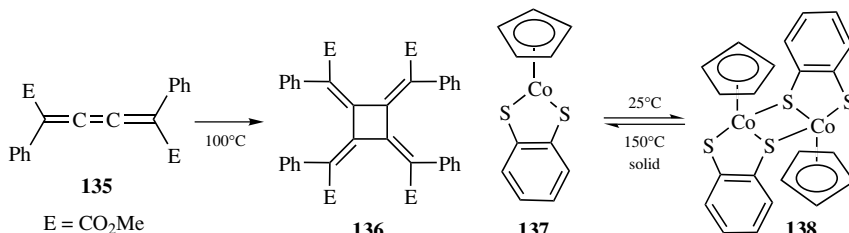
An absolute asymmetric Grignard synthesis uses the spontaneous resolution of hexacoordinated *cis*-magnesium complexes with  $\Delta$ - or  $\Lambda$ -configuration and stereoselective transfer from the  $\Delta/\Lambda$  reagent to *R/S*-product.<sup>61</sup> In the solid state version, the labile Grignard complex is coground with solid aldehyde under liquid nitrogen, and the temperature is allowed to slowly rise to ambient. The enantiomeric excess reaches around 10%. Clearly, advanced low-temperature milling techniques<sup>2,3,9</sup> should be applied in order to increase the yield. The reaction of  $\Delta$ -**131** or  $\Lambda$ -**134**, with butyraldehyde gave  $(R)$ -**132** or  $(S)$ -1-*p*-tolylbutane-1-ol (**133**) in excess, respectively.



Similarly the chiral  $[\text{MgCH}_3(\text{THF})(\text{DME})]^{+}\text{I}^{-}$  complexes react stereoselectively with butyraldehyde and benzaldehyde in their Grignard reactions.<sup>61</sup>

## XII. CYCLOADDITIONS

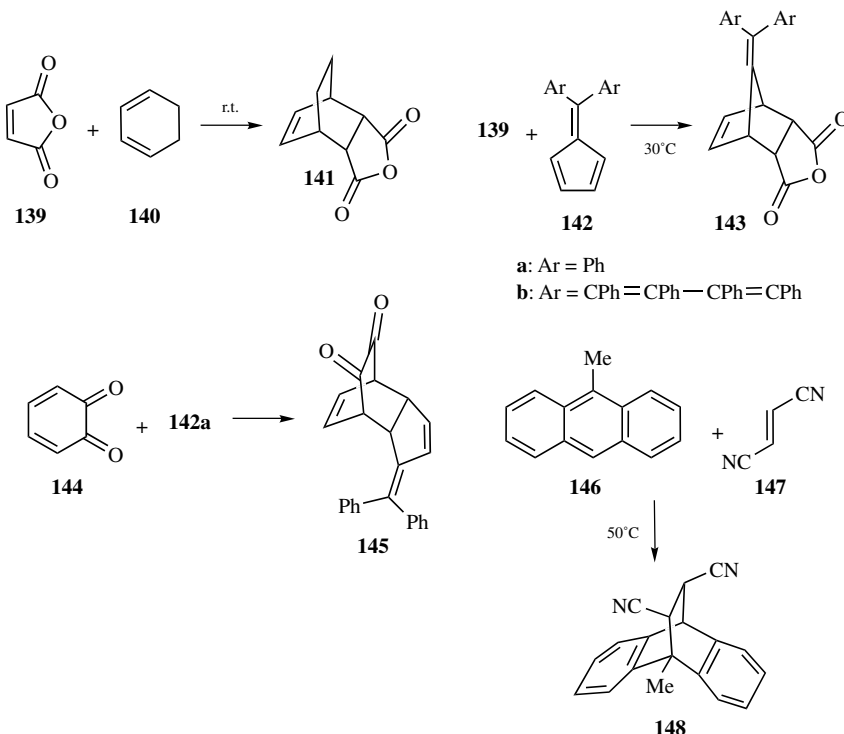
The [2+2]-cycloaddition of the (*E*)-butatriene **135** provides the (1*Z*,2*Z*,3*Z*,4*Z*)-[4]radialene **136** in a stereospecific manner in 75% yield when heated in the



solid state. The unexpected configuration is secured by an X-ray crystal structure determination.<sup>62</sup> Radialene **136**, and a mixture of three stereoisomers is obtained when **135** is heated in toluene.

A reversible thermal solid state [2+2]-cyclodimerization, which is stereospecific and proceeds in single crystals, has been found with ( $\eta^5\text{-C}_5\text{H}_5\text{)}\text{Co}(\text{S}_2\text{C}_6\text{H}_4)$  (**137**). The dimer **138** forms with major conformational changes in the crystal. The reaction is not topotactic, but the crystal shape remains unchanged both upon the dimerization at 25°C and at the cycloreversion at 150 °C. The Co $\cdots$ S interaction distances in the monomer crystal are 4.702 and 4.325 Å, the corresponding bond lengths in the dimer 2.246 and 2.230 Å.<sup>63</sup> The reversible dimerization ( $\Delta H$  for **138** $\rightarrow$ **137** at 150–160 °C is 4.5 kcal mol $^{-1}$ ) profits from favorable differences in the crystal energies of **138** and **137**. The dimer **138** dissociates in organic solvents at 25 °C to give monomer **137**.

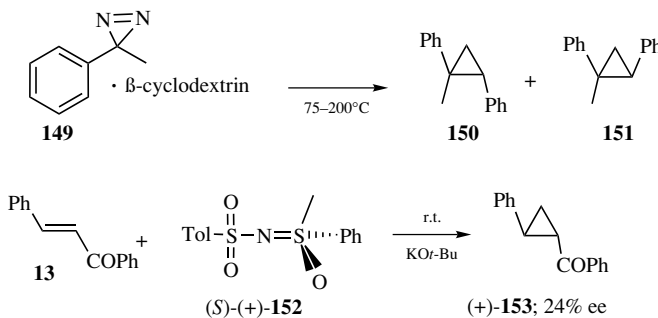
Endoselectivity in some simple gas–solid Diels–Alder reactions has been secured.<sup>64</sup> However, there was not much motivation to repeat more well-known Diels–Alder reactions in the solid state. Solid maleic anhydride (**139**) and cyclohexadiene vapors (**140**) or solid diphenylfulvene (**142**) give the *endo*-adducts



**141** or **143** with 100% yield.<sup>64</sup> Similarly milling of **139** and *o*-benzoquinone (**144**) (prepared by milling pyrocatechol with DDQ) provides adduct **145**.<sup>35</sup> The solid state addition of 9-methylanthracene (**146**) to fumarodinitrile (**147**) at 60°C is complete giving a 100% yield of the *trans*-product (**148**) as a powder.<sup>64</sup> The *trans*-arrangement of the cyano groups is secured by the <sup>1</sup>H NMR coupling constant (4.9 Hz) of the *trans*-H-atoms. The same product is obtained in the melt at 80°C.

Stereoselective solid–solid cycloadditions with carbenes use diazirines, trimethylsulfonium iodide, or trimethylsulfoxonium iodide as precursors. Rather ingenious is the thermal decomposition of the diazirine **149** in β-cyclodextrin (0.9:1 to 1.2:1) which produces high yields (72–87%) of the *trans*-cyclopropane **150** besides minor quantities of the *cis*-compound **151** by cycloaddition of the in situ fragments phenylmethylcarbene and styrene.<sup>65</sup> The β-cyclodextrin- complex of the products does not dissociate when heated to 200°C. Photolytic decompositions of the complex **149** are much inferior and the yield in **150** and **151** drops down to 20% and 8%, respectively, if uncomplexed **149** is heated to 130°C.

An enantioselective solid state cycloaddition of carbene to chalcone (**13**) uses the chiral precursor **152** and KO*t*-Bu. The cyclopropane **153** is obtained with 94% yield and 24% ee.<sup>66</sup> The solid state character of this reaction would be more safe if chalcone **13** or its derivatives are hosts in inclusion complexes. This was tried using the chiral hosts **114** and **117**; however, the *trans*-adducts (derivatives of **153**) were obtained in low yields and low ee values.<sup>66</sup>

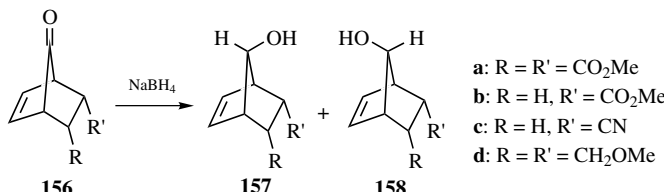
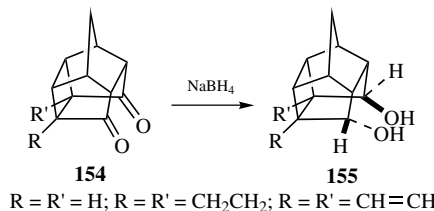


### XIII. REDUCTIONS

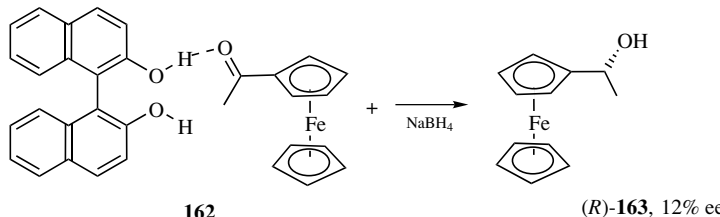
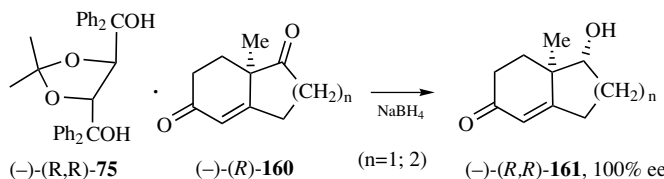
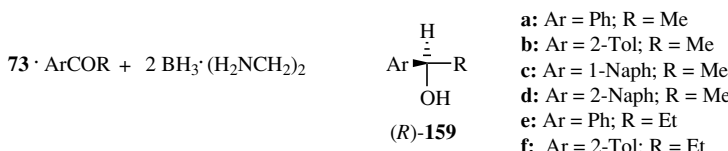
Solid–solid reductions with sodium borohydride tend to be more stereoselective than in solution. The cage diketones **154** afford quantitative yields of the pure *endo,endo*-diols **155** upon grinding followed by agitation, whereas mixtures of **155** with its *endo,exo*-stereomer are obtained in ethanol solution.<sup>67</sup>

A remarkable π-face selectivity was found in the solid state NaBH<sub>4</sub> reduction of a variety of norbornenones **156**. The **157a:158a** ratio is 87:13 at 80% chemical

yield.<sup>68</sup> The solid state reduction of arylepoxydes in  $\beta$ -cyclodextrin with NaBH<sub>4</sub> by ultrasonication gave (*R*)-1-arylethanols in yields of <28% and only very low ee (0.5–9.3).<sup>69</sup> Improvement by milling was not reported.



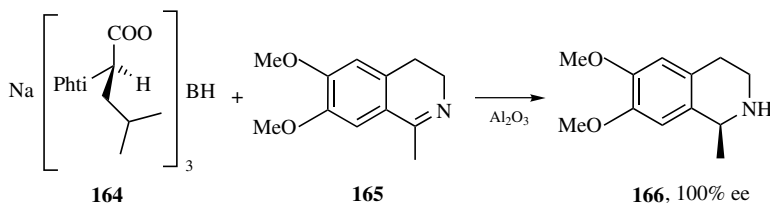
Solid inclusion complexes of ketones in the chiral host (*-(R,R)*-73 can be reduced with the solid borane-ethylenediamine complex by grinding. Chiral secondary alcohols (*R*)-159 with ee values of typically 59% are obtained.<sup>70</sup> The reduction of the inclusion complex 75·160 with NaBH<sub>4</sub> in the solid state



gave  $(-)(R,R)$ -**161** ( $n = 1, 2$ ) with 100% ee in 54% yield.<sup>71</sup> On the other hand, enantioselective reduction of ketones in inclusion complexes with  $\beta$ -cyclodextrin in the solid state proceeded less selectively. The solid complex  $(S)$ -1,1'-bi-2-naphthol · acetylferrocene (**162**) was reduced with NaBH<sub>4</sub> to give the asymmetric induction only in the solid state, when  $(R)$ -**163** was formed with 12% ee.<sup>72</sup>

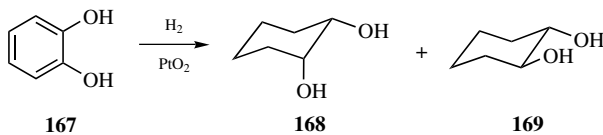
Chiral boron hydrides such as **164** reduced imine **165** in the solid state with 100% ee in 90% yield to give **166**.<sup>73</sup> The reducing agent was suspended on alumina. The chiral reducing agents were obtained from phthaloyl-L-aminoacids.

There is a report of reductive stereoselective (*meso*-diols prevailing) “solid state” pinacol couplings by mixing aromatic aldehydes, ZnCl<sub>2</sub> and Zn at room temperature.<sup>74</sup> However, these reactions could not be transformed into real solid state reductions, since ZnCl<sub>2</sub> or preformed solid ZnCl<sub>2</sub>·ArCHO complexes rapidly become liquid because of their deliquescence in ambient atmosphere. No pinacol coupling occurred in the absence of atmospheric humidity at room temperature in 3 h.<sup>35</sup>



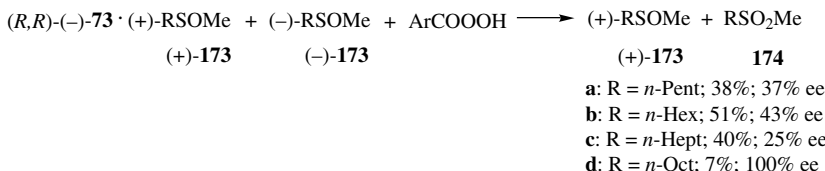
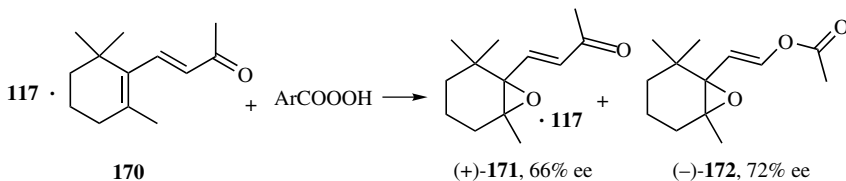
Phti: *N*-phthalimido

Solid state catalytic hydrogenations by “spillover technique” may be stereoselective. Thus pyrocatechol (**167**), when powdered and mixed with PtO<sub>2</sub> under hydrogen (1 bar) at 25 °C, gave a 71:29 mixture of *cis*- (**168**) and *trans*-1,2-dihydroxycyclohexane (**169**).<sup>75a</sup> It is not clear if the products were created as a liquid instead of a solid mixture, because there was also a 12% yield of cyclohexanol reported for this reaction (25 °C; 80% conversion). Interestingly the powder of a left-handed crystal of 3-methyl-4-isopropylphenol (chiral space group P4<sub>3</sub>) upon hydrogenation at 80 °C in the presence of Pt/C and pumping off the volatile liquid products gave a positive optical rotation of the product mixture. Thus, an absolute asymmetric hydrogenation was achieved. However, the structure of the products was not reported.<sup>75b</sup>

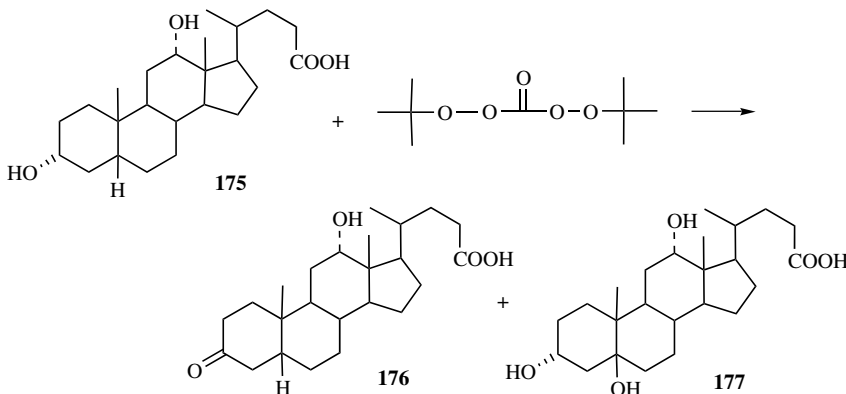


XIV. OXIDATIONS

Enantioselective solid state oxidations of achiral molecules succeed in chiral host inclusion complexes. For example, the solid 1:1 inclusion complex of  $\beta$ -ionone **170** in  $(-)(R,R)$ -**117** reacted with 2 equivalents of coground *m*-chloroperbenzoic acid to give the optical active epoxide **171** still complexed in **117** and the optical active epoxidized product of the Bayer-Villiger oxidation  $(-)$ -**172** not complexed. Clearly, an enantioselective inclusion of the initially formed  $(\pm)$ -**171** protected  $(+)$ -**171** from further oxidation and the uncomplexed  $(-)$ -**171** was further oxidized to give  $(-)$ -**172**.<sup>76</sup>

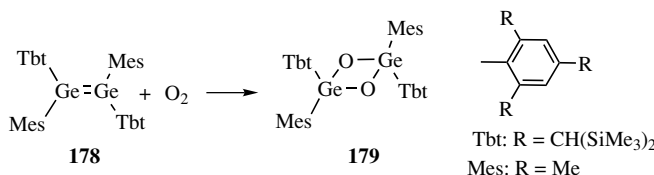


Similar solid state kinetic resolutions use the chiral host  $(-)(R,R)$ -**73** for the protection of the  $(+)$ -sulfoxides **173** while the nonincluded  $(-)$ -sulfoxides of the initial racemate are oxidized by solid *m*-chloroperbenzoic acid to give the sulfones **174**. The nonoxidized  $(+)$ -**173** had ee values between 25 and 100% at varying yields.<sup>76</sup>

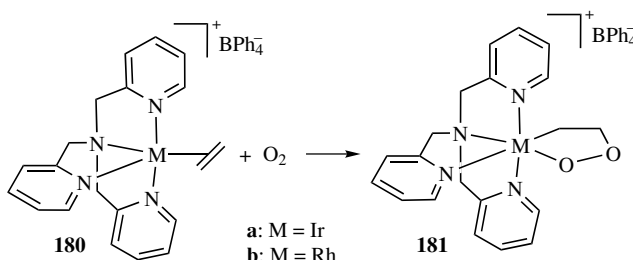


Desoxycholic acid **175** forms a 4:1 crystalline complex with di-*t*-butyldiperoxy carbonate. When heated to 90 °C for 120 h the ketone **176** and the 5-β-hydroxylated product **177** were obtained with 15% yield each.<sup>77</sup> The corresponding solution reaction led to unselective attacks on the various positions of the steroid.

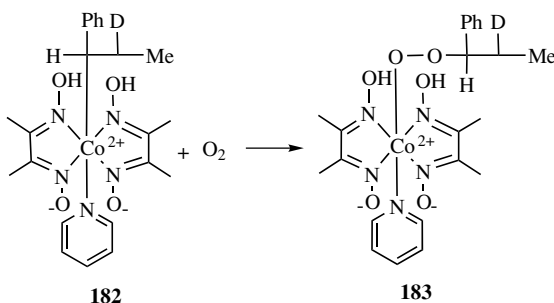
The extremely hindered digermene **178** reacts stereospecifically with oxygen to give the *trans*-substituted 1,3-dioxadigermetane **179**. Two different stable conformational isomers **179** were obtained in 49% and 13% yield but no *cis*-isomer that was additionally formed in the corresponding solution reaction. The structures of the conformational isomers of **179** were determined by X-ray crystallographic analysis.<sup>78</sup>



Gas-solid oxygenation of **180a**, and **b** with oxygen stereospecifically yields only one isomer of the 3-metalla-1,2-dioxolanes **181a**, and **b**. The specificity is lost if the counter anion is PF<sub>6</sub><sup>-</sup> (1:1 mixture with the isomeric 3-metalla-1,2-dioxolane).<sup>79</sup>



The stereoselectively labeled 2-*d*<sub>1</sub>-1-phenylpropylcobaloxime **182** decomposes in the presence of oxygen in hydroxylic solvents with formation of radicals that



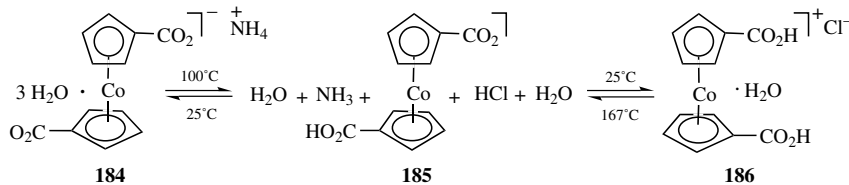
are intercepted by oxygen to give the racemic organoperoxycobaloxime **183**. However, insertion of oxygen in the carbon–cobalt bond of the deuterated 1-phenylpropylcobaloxime takes place stereospecifically in the solid state.<sup>80</sup>

## XV. PROTONATIONS (LIGAND CONFORMATIONS)

The solid amphoteric Co(III) complex **185** that crystallizes in hydrogen-bridged chains with the *transoid* arrangement of the ligands protonates moist ammonia gas and quantitatively forms the hydrated salt **184**, which keeps the *transoid* ligand conformation. If, however, **185** is protonated with gaseous, moist HCl, the crystalline, hydrated salt **186** is quantitatively formed. The conformation of the ligands in crystalline **186** is *cisoid* in a new hydrogen-bridged chain structure. This is shown by X-ray crystal-structure elucidation of the structures **184**, **185**, and **186** and powder diffraction experiments.

The effects of the chain structure for the stereospecific gas-solid reactions have been elucidated with AFM which correlates the surface features formed with the crystal structure. The crystals disintegrate upon reaction, and the neutral structure **185** is reformed upon heating of **184** or **186**.<sup>81</sup> Clearly, the conformational reversal of **185** → **186** or of **186** → **185** is the result of chemical reactions combined with particular crystal properties. This is to be distinguished from crystal phase transitions that are not within the scope of this article.

Similarly protonation of **185** with the vapor of trifluoroacetic acid enforces the *cisoid* conformation in the salt without additional water. On the other hand, the vapor of tetrafluoroboric acid forms a salt with **185** in which an again different chain structure in the *transoid* conformation is obtained.<sup>82</sup>

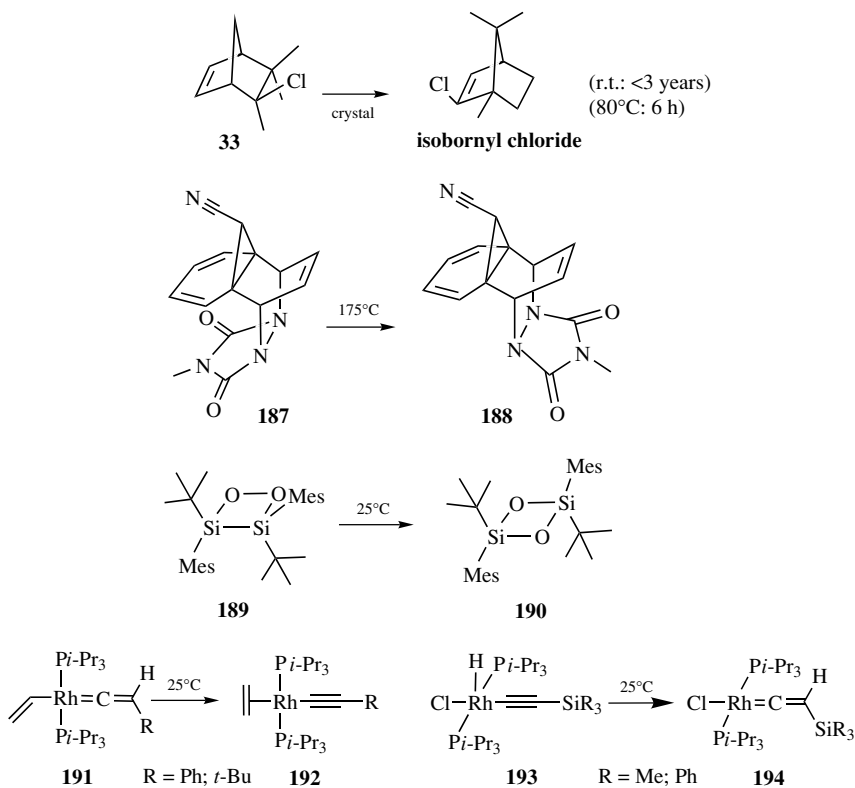


## XVI. THERMAL REARRANGEMENTS

Thermal rearrangements in crystals are comparatively rare. Crystalline camphene hydrochloride (**33**) isomerizes slowly to isobornyl chloride without melting in a solid state stereospecific Wagner-Meerwein rearrangement.<sup>7</sup> A thermal solid state N–N double inversion between kinetically stable invertomers (*exo/endo*-isomerism)

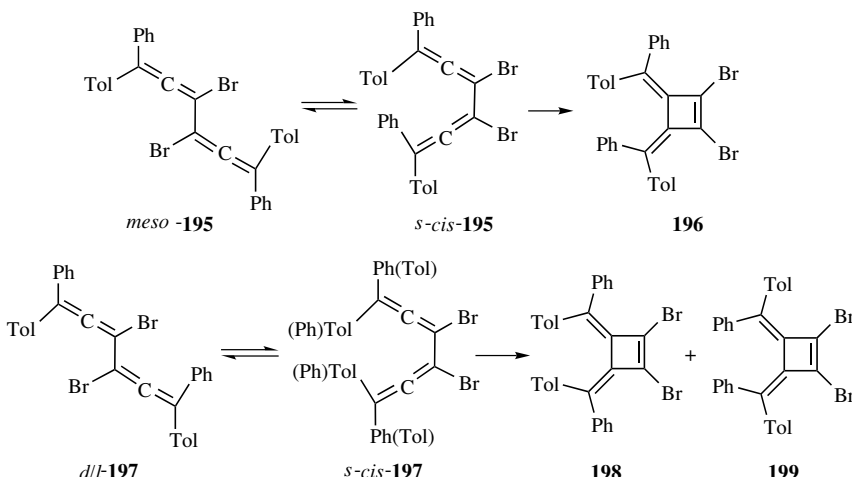
was studied by high temperature X-ray diffraction. The conversion of the less stable isomer of the Diels-Alder product **187** into the more stable isomer **188** occurred at 175 °C from single crystal to polycrystalline material.<sup>83</sup>

The rearrangement of the 1,2-disiladioxetane **189** into the 1,3-disiladioxetane **190** occurs stereospecifically in the crystal (also in solution) at room temperature and below with retention of the configuration at silicon.<sup>84</sup> The crystalline vinyl(vinylidene)rhodium complexes **191a**, and **b** rearrange on standing at room temperature and form the alkinyl(ethene) complexes **192a**, and **b**. Conversely, the corresponding  $\eta^3$ -2,3,4-*trans*-butadienyl complexes are obtained in benzene solution at 50 °C.<sup>85</sup> Furthermore the rearrangement of the rhodium complex **193** to give **194** is stereoselective.<sup>86</sup>

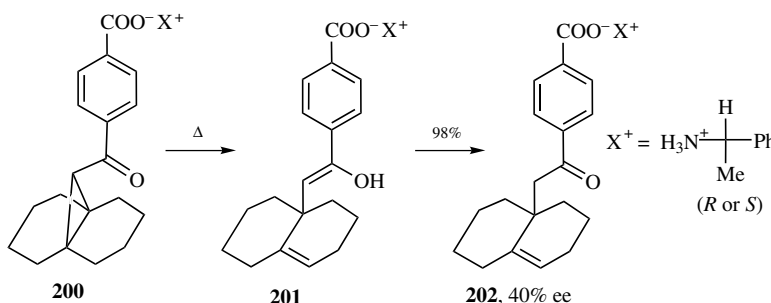


Highly substituted bisallenes cyclize stereospecifically or stereoselectively. Crystalline *meso*-bisallene **195** gives a 100% yield of **196** when heated to 135 °C, undoubtedly via *s-cis*-**195**.<sup>87</sup> Conversely, *racemic* **197** at 125 °C gives a 1:1 mixture of **198 + 199** via *s-cis*-**197**, which is separated by recrystallization.

These reactions were studied by AFM<sup>88</sup> and interpreted on the basis of the crystal structures of the starting materials. Far-reaching anisotropic molecular migrations align features along the most favorable of three cleavage planes of **195**, or in the direction where the molecules find empty space for the required internal rotation and cyclization in the case of **197**.<sup>88</sup>

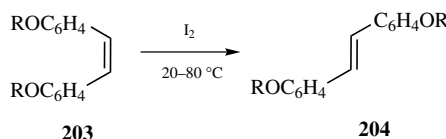


The achiral tricyclo[4.4.1.0] undecane derivative **200** ( $X = H$ ) with its carboxyl group was transformed to various chiral salts **200** by neutralization with enantiomerically pure primary amines to get high-melting salts crystallized in homochiral space groups. When heated (even better when photolyzed), they rearranged to the chiral ketones **202**, presumably via enols **201**. For example, the salt with (*R*)- or (*S*)-1-cyclohexylethylamine gave a 98% yield of the ketone **202** with 40% ee, because the  $\gamma$ -hydrogens  $H_a$  and  $H_b$  are diastereotopic in the chiral crystal.<sup>89</sup> Clearly, conformational enantiomeric preference was transformed into configurational enantiomeric excess.



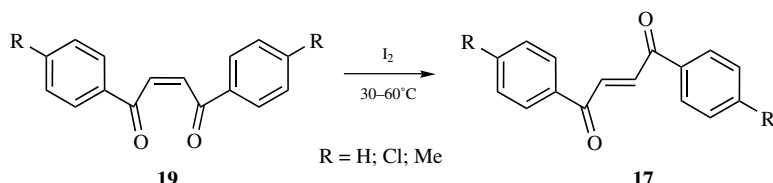
## XVII. SOLID STATE GEOMETRICAL ISOMERIZATIONS

Solid state *E/Z*-isomerizations are more frequently obtained by photolyzing crystals. However, there may be thermal *E/Z*-isomerizations of crystalline olefins catalyzed by iodine. For example, crystalline *cis*-stilbenes **203** can be isomerized to *trans*-stilbenes **204** without intervening liquid phases. The isomerizations follow first order kinetics with various rate constants for 4-MeO, two modifications of 2-MeO, 2-EtO, 2-PrO, and 2-*i*-PrO substitution. The activation energies vary from 20 to 32 kcal mol<sup>-1</sup> but could not be interpreted.<sup>90</sup>



The conclusion that the formation of the *meso*-dibromide upon gas–solid addition of bromine to *cis*-stilbene “is due to *cis-trans* isomerization prior to or during addition”<sup>28,90</sup> cannot be accepted without further proof, as there is also the possibility for *cis*-addition.<sup>19,20</sup> Further solid state isomerizations of crystalline *cis*-1,2-dibenzoyl ethylenes **19** to give **17** are catalyzed by iodine vapors at 30–60°C.<sup>33</sup> After an apparent induction period as evidenced by S-shaped conversion curves (the induction periods were not acknowledged in the publication) first order rate constants and activation energies between 17 and 21 kcal mol<sup>-1</sup> were listed.<sup>33</sup> A mechanistic interpretation was not possible.

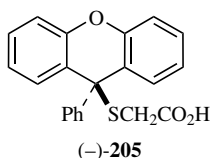
In the case of solid *cis*-chalcone, iodine vapors did not catalyze an *E/Z*-isomerization in the solid state.<sup>91</sup>



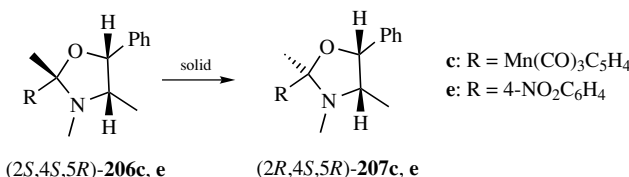
Racemizations in the crystalline state have a long history. It is known, that L- $\alpha$ -amino acids slowly racemize in the solid state.<sup>92</sup> Since this also happens in solid proteins, there are implications not only in pure chemistry but also in biochemistry, nutrition, food technology, and geology. Therefore, techniques have been developed to determine the D/L-ratio of amino acids down to 0.1%, and

inversion rate constants have been determined under acid hydrolysis conditions.<sup>93</sup> One could think of very slow deamination and re-addition of the amine or an enolization mechanism. However, such racemizations can also be induced by photolysis or radiolyses from natural sources.<sup>94</sup>

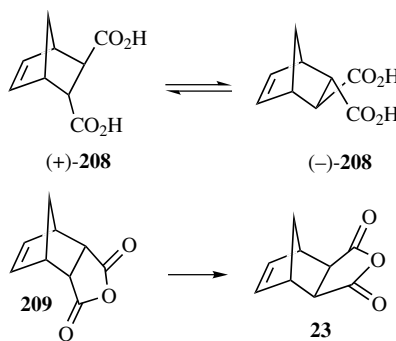
Significantly faster is the solid state racemization of the thioglycolic acid derivative **205**. A solid sample lost its specific rotation upon standing from  $-42.3^\circ$  to  $-36.9^\circ$  in two months and to  $-13.9^\circ$  after 14 months. It is noted that such racemization was more rapid when the acid was exposed to light.<sup>91</sup> A heterolytic dissociation/recombination mechanism within the crystal appears possible.



Chiral N/O-acetals may racemize in the solid state when water of crystallization is present. Examples are the epimerizations of the oxazolidines **206** that contain water from their preparation by stereoselective condensation. Thus the kinetically preferred products **206c**, **206e** (which are admixed to the thermodynamically more stable products **207c**, **207e**) epimerize within some weeks in the solid state to give enantiomerically pure **207c**, **207e**.<sup>53</sup> It appears that the N/O-acetal hydrolyzes and recloses.

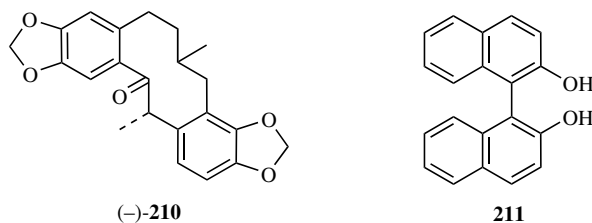


The racemization of Diels-Alder adducts in the solid state appears to proceed via a diradical or complete cycloreversion. For example, (+)-**208** racemizes in the solid state from 130 °C to 155 °C ( $\Delta H^\ddagger = 40.0$  kcal mol<sup>-1</sup>;  $\Delta S^\ddagger = 14$  cal mol<sup>-1</sup> K<sup>-1</sup>) to give (-)-**208**, whereas the melt reaction (eutectic temperature is 165 °C) from 176 °C to 194 °C has much lower activation parameters ( $\Delta H^\ddagger = 29.7$  kcal mol<sup>-1</sup>,  $\Delta S^\ddagger = -6.9$  cal mol<sup>-1</sup> K<sup>-1</sup>).<sup>95</sup> Racemizations in the solid and in the melt follow strictly first-order kinetics.<sup>95</sup> The extrapolated rate in the melt state is about 10 times higher than the rate in the solid state in this unimolecular reaction.



The related endo/exo-isomerization of **209** is easier than the reverse of **23**, and both can also be obtained as solid state isomerizations (eutectic temperature is  $109^\circ\text{C}$ ). These have been termed “solid state isomerizations until the eutectic melting is reached.”<sup>96</sup> However, isomer **209** can be sublimed at  $110\text{--}140^\circ\text{C}$  bath temperature without any signs of isomerization.<sup>35</sup>

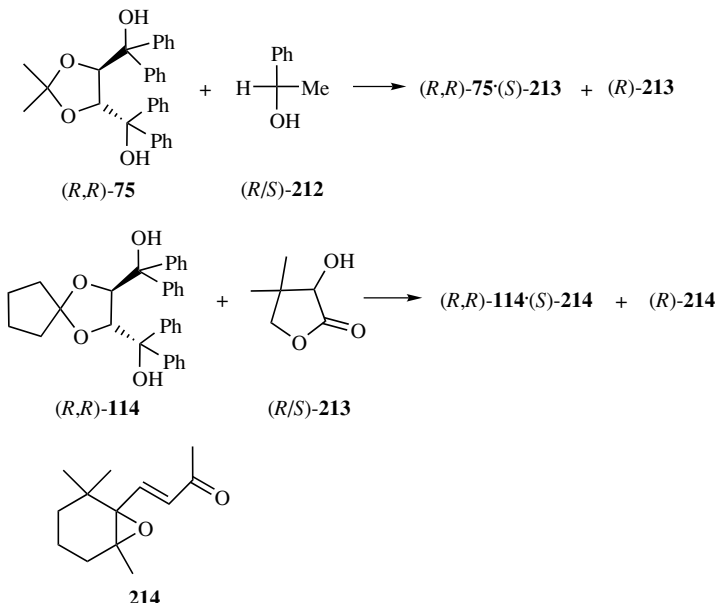
While racemization will probably be faster upon melting of **(-)-corycavine** (**210**), which exhibits a double melting point at  $148\text{--}149^\circ\text{C}$  and  $218^\circ\text{C}$  (racemate),<sup>97</sup> it is not clear if some racemization occurred before the first broad exothermic peak was reached in the DSC experiment. Unfortunately, only one heating rate ( $5^\circ\text{C min}^{-1}$ ) was adopted.



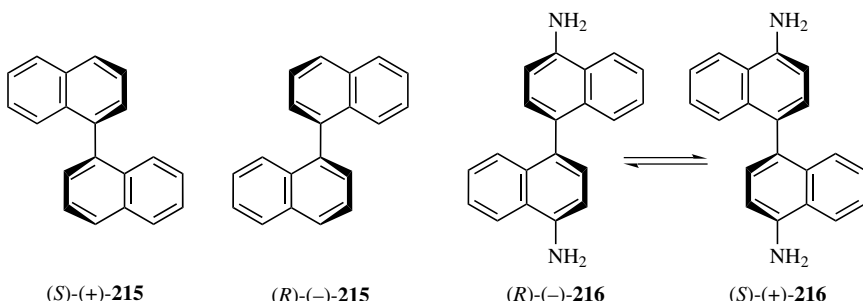
The formation of racemic mixed crystals by mixing and grinding of powdered crystals of **(+)-** and **(-)-2,2'-dihydroxy-1,1'-binaphthyl** **211** in a 1:1 molar ratio was followed by IR spectroscopy.<sup>98</sup>

Resolutions by enantioselective inclusion in host crystals are usually reached by separation of inclusion crystals that were produced from solution or suspension.<sup>99,100</sup> There is also the possibility to obtain enantioselective inhibition from vapors of volatile racemates or of solid-solid enclathration of crystalline racemates into chiral hosts. Such reactions occur under enclathrates

selectively into (*R,R*)-**114** (also into its homologue with cyclohexane ring) both by solid–solid reaction (milling) or short-distance solid-to-solid sublimation (AFM experiment).<sup>102</sup> The success of the enantioselection can be monitored by solid state CD spectroscopy.<sup>100</sup> Similar solid–solid optical resolution of compound **214** was obtained in Toda et al.<sup>76</sup>



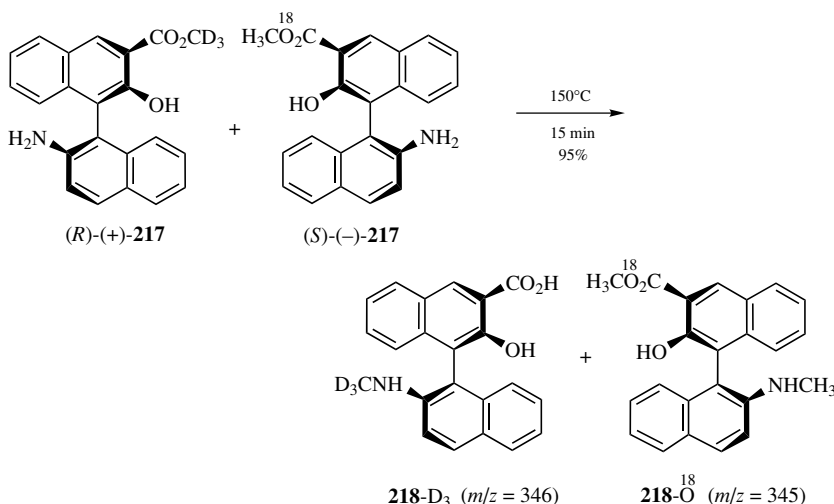
A spontaneous deracemization of near-racemic binaphthyl **215** simply by heating (2 h) its crystals at 76–145°C to form either its (*S*)-(+) or (*R*)(-)enantiomer up to  $[\alpha]_D$ -values of  $\pm 245$  (mp 159°C) represents an absolute



asymmetric syntheses of a stable conformational enantiomer (half live for racemization in solution is 15 min at 50°C).<sup>103</sup> This solid state resolution rests on the partial resolution always obtained from the crystallization of the starting material **215** from its melt, the phase diagram, and, of course, from the possibility for conformational change in the crystal at these temperatures.

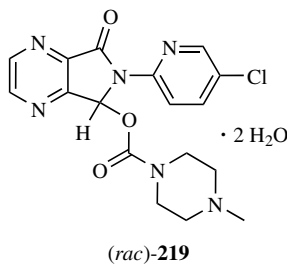
A different phase diagram explains the different behavior of 4,4'-diamino-1,1'-binaphthyl (naphthidine) **216**. Here optical activity of the crystals is lost on storage for several months ( $\tau_{1/2} \approx 2$  months) at room temperature.<sup>104</sup> It is, however, also possible to attain spontaneous resolution at 197–203°C via a solid→melt→solid transformation or at 197°C via a direct solid-solid transformation for up to five hours and the highest rotations obtained are  $[\alpha]_D \pm 49$  while the highest reported<sup>104</sup> specific rotation is  $[\alpha]_D \pm 99$ . If, however, crystalline (S)-(+)-naphthidine (**216**) is heated to 130–195°C (typically 130°C and 150°C where first-order kinetics is obeyed), racemization occurs in the solid state because the racemic crystal is the stable form up to the transition point at 197°C, whereas the resolved crystal is the stable form from 197°C to its m.p. at 204°C.<sup>105</sup> The apparent bias observed for the (S)-(+)-**216** could not be clarified.

A particular case of enantioselection within a racemic crystal has been proved for the S<sub>N</sub>2 transfer of the methyl group in the (unlabeled) 1,1'-binaphthyl **217**.<sup>106</sup> A double-labeling experiment was necessary for rigorous proof. The single crystal X-ray analysis of the racemic crystal **217** suggests

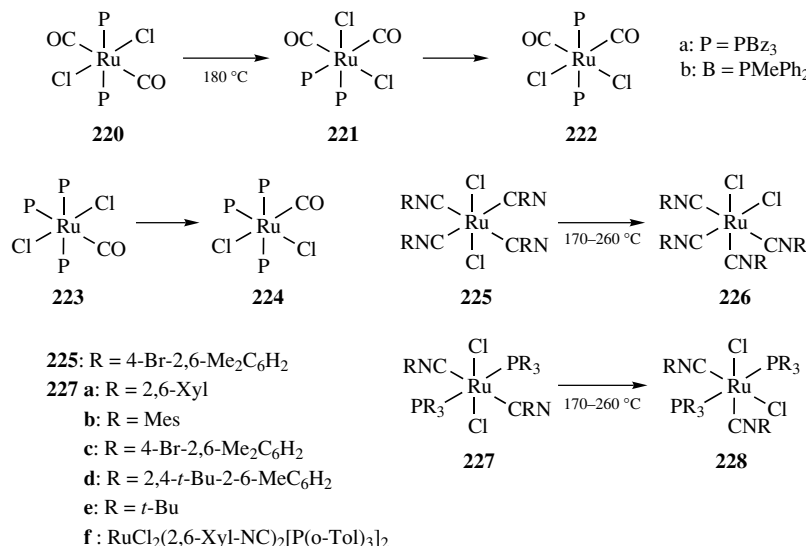


an intermolecular mechanism but not between the centrosymmetric *R* and *S* pairs because the CH<sub>3</sub>O group has a wrong orientation, being too distant (3.79 Å) from NH<sub>2</sub> and having an angle of approach of 94.9°. On the other hand, that distance is only 3.20 Å between the homochiral molecules related by a twofold screw axis and the angle of approach (N—C—O) is 173.2°. Hence the reaction should occur between the (*R*)-(*R*) and (*S*)-(*S*) but not between *R* and *S* molecules. This expectation has been rigorously proved by the depicted double-labeling experiment on the basis of mass spectroscopic analysis. No species containing both labels has been detected. Clearly, the crystal packing is responsible for the unusual stereospecificity, even though the chirality of the labeled products could not be assessed.<sup>106</sup>

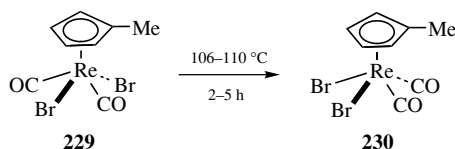
Spontaneous deracemization as in **215** and **216** has to be differentiated from spontaneous separation (more frequently claimed as “resolution”) of racemic crystals into a conglomerate or into racemic twins. The latter processes are pure crystallization effects without configurational change of the molecules. A good example for such processes, which are not the subject of this review, was found with zopiclone dihydrate (**219**). It undergoes a sequential two-step transformation in the solid state upon heating to 75 °C (reversible dehydration) and 112 °C (loss of centrosymmetry) with considerable change of conformation. This step is irreversible and leads to a separation of enantiomers in separate crystals of the enantiomers in the solid state. It could not be determined if there were racemic twins or a conglomerate, though. However, the domain size was larger than 100 nm.<sup>107</sup>



Numerous organometallic Ru(II) complexes exhibit stereoisomerization in the solid state at 140–180 °C or 170–260 °C without intermediate melting. Thus **220a** reacts to **222a** and **221b** to **222b** (the reaction of **220b** to give **221b** involves intermediate melting) or **223** isomerizes to give **224** in preparative useful syntheses.<sup>108</sup> Similarly the *trans* to *cis* isomerizations of **225** to give **226** and the **tcc** to **tcc** conversions of the Ru(II) isonitrile complexes **227** to give **228** have been realized in the solid state.<sup>109</sup>



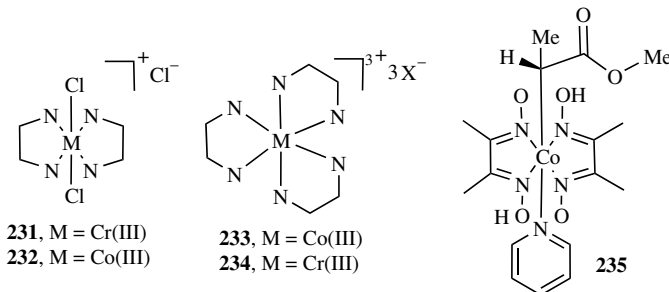
Half-sandwich or four-legged piano stool Re, Mo, W complexes undergo *trans* (diagonal) to *cis* (lateral) isomerizations in the solid state, and numerous examples have been listed by Coville and Levendis.<sup>110</sup> For example, **229** converts unidirectionally to **230** at 110 °C with 98% yield, whereas the reverse reaction is observed in boiling toluene at the same temperature.<sup>111</sup> One of the CO ligands can be exchanged by phosphanes, phosphates, or isocyanides, and Me can be replaced by *t*-Bu or SiMe<sub>3</sub>. Usually the *trans* to *cis* isomerization occurs in the solid state as well as in solution in these cases, but the diiodide [( $\eta^5$ -C<sub>5</sub>H<sub>4</sub>Me)Re(CO)<sub>2</sub>I<sub>2</sub>] proceeds from the *cis* to the *trans* configuration.<sup>110</sup> A multistep turnstile mechanism (three ligands moving) has been proposed for this type of geometric isomerization.<sup>49</sup> However, there may be also movement of only two ligands.<sup>112</sup> No rules could be derived to explain the various facts observed. The complex [( $\eta^5$ -C<sub>5</sub>H<sub>4</sub>Me)Re(CO){P(OPh)<sub>3</sub>}Br<sub>2</sub>] did not change its shape and space group upon reaction.<sup>110</sup> AFM investigations would certainly provide further insights.<sup>12,13</sup>



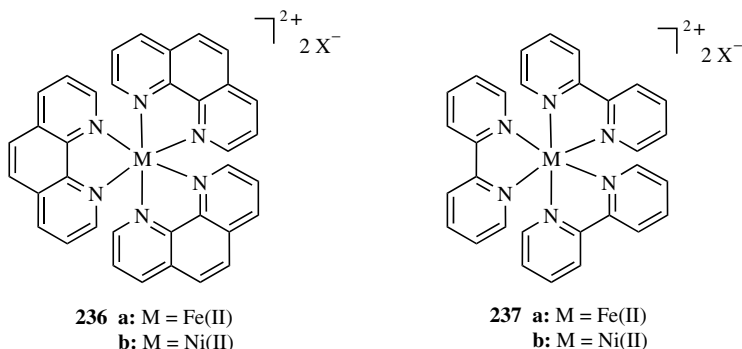
Various types of optical active hexacoordinate heavy metal complexes racemize thermally in the solid state. Both the Cr(III) and Co(III) ethylenediamine complexes

$\Delta$ -*cis*-**231**·H<sub>2</sub>O/ $\Delta$ -*cis*-**232**·H<sub>2</sub>O dehydrate and undergo thermal racemization smoothly at 158 °C in the solid state without any *cis-trans* interconversion. The results are only in accord with a rhombic twist mechanism.<sup>113–115</sup> A different mechanism for the solid state racemization of the Co(III) complex (+)-**233** (X = Cl, Br, SCN, or I) has been described.<sup>113,116</sup> The Cr(III) complex **234** (X = SCN) racemizes at 100–130 °C in the solid state and is accompanied by some “deamination” to *trans*-[Cr(en)<sub>2</sub>(NCS)<sub>2</sub>](NCS).<sup>117</sup>

Only one C–Co bond is involved in the thermal racemization of the cobaloxime complex **235** at 70 °C. The single crystal changes its space group from P2<sub>1</sub> to P2<sub>1</sub>/n within 180 h.<sup>118</sup>

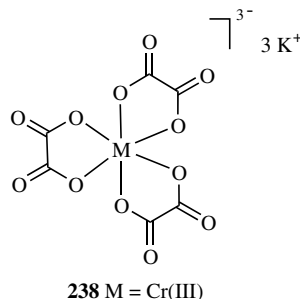


Also the  $\Delta$ -tris-(1,10-phenanthroline) coordination complexes **236** and the tris-(2,2'-bipyridine) complexes **237** of Fe(II) and Ni(II) (X = Cl, Br, I, or ClO<sub>4</sub>) undergo thermal racemization in the solid state. Different racemization mechanisms were proposed for the Ni and Fe complexes.<sup>119–121</sup>



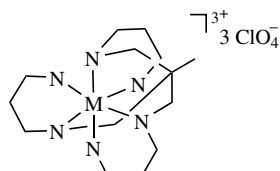
Furthermore the tris-oxalato Cr(III) complex [**238**·(H<sub>2</sub>O)<sub>2</sub>] was resolved, and it racemized in the solid state at temperatures above 200 °C, even when previously

completely dehydrated at a lower temperature. Nevertheless, water vapor catalyzed the process.<sup>122</sup>

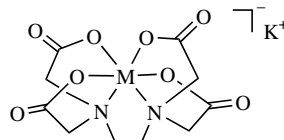


Even coordination complexes with multidentate ligands are known to racemize in the solid state. Thus the chiral form of the [Co(stn)]<sup>3+</sup> complex **239** exhibits facile racemization.<sup>123</sup>

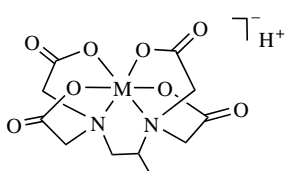
The optically active EDTA-Co(III) complex **240**·(H<sub>2</sub>O)<sub>2</sub> dehydrates at 152 °C and racemizes rapidly at 174 °C.<sup>124</sup> Also the more involved complexes **241** and **242a, 242b** undergo racemization upon heating in the solid state.<sup>125</sup>



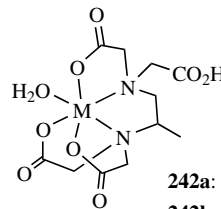
**239**, Me = Co(III)



**240**, M = Co(III)



**241**, M = Cr(III)



**242a**: M = Cr(III)

**242b**: M = Cu(II) and H<sup>+</sup>

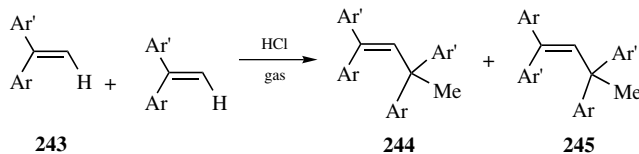
## XVIII. LINEAR DIMERIZATIONS AND POLYMERIZATIONS

Three-dimensional interlocking in molecular crystals will usually inhibit solid state reactivity. Reactivity can be recovered by shrinking the stacks with the

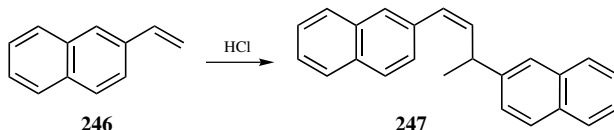
chemical reaction. Shrinking can occur if 1,1-diarylethenes **243** linearly dimerize to give **244**, rather than adding HCl or HBr upon exposure.<sup>21</sup> The catalyzed head-to-tail dimerizations ( $\text{BF}_3$  or  $\text{XeCl}_2$  are also catalyzing) proceed quantitatively and provide interesting *E/Z*-selectivities if two different aryl groups are involved.

The reaction of **243d** gave the same *E/Z*-ratio **244/245** if HBr or BF<sub>3</sub> was the catalyst. Therefore the crystal packing must determine the stereoselectivity, and the shrinking was convincingly shown by AFM investigation to provide craters without walls around them.<sup>21</sup> The known crystal structure of **243d** (**Cc**)<sup>126</sup> indicates that protonation should occur via the methoxy groups to the double bonds from the (100)-face (Figure 9.1). After head-to-tail interaction of the molecules **243dH<sup>+</sup>** and **243d** (before protonation the distance of the centers is 4.380 and 4.417 Å) with the substituents on the same sides, the final liberation of the proton to an adjacent molecule of the next layer appears geometrically easier if the bond rotation turns the larger anisyl group inward while forming the planar double bond in **245d**. The situation in the formation of **245b** should be similar, whereas **243e** exhibits only a very low selectivity.

Interestingly the head-to-tail linear dimerization of 2-vinylnaphthalene in the solid state under the influence of gaseous HCl provides specifically the *cis*-compound **247**.<sup>35</sup>



		T (°C)	244/245
a:	$\text{Ar} = \text{Ar}' = \text{Ph}$	-50	
b:	$\text{Ar} = \text{Ph}, \text{Ar}' = 4\text{-Tol}$	-25	33:67
c:	$\text{Ar} = \text{Ar}' = 4\text{-Tol}$	-25	
d:	$\text{Ar} = \text{Ph}, \text{Ar}' = 4\text{-Anis}$	-25	15:85
e:	$\text{Ar} = 4\text{-Tol}, \text{Ar}' = 4\text{-Anis}$	-25	52:48
f:	$\text{Ar} = \text{Ar}' = 4\text{-Anis}$	r.t.	



Thermal polymerizations of vinylic monomers in the crystal giving isotactic or syndiotactic crystalline polymers are rare (more thoroughly studied are the photochemical or radiolytical versions), because the crystallographic packing

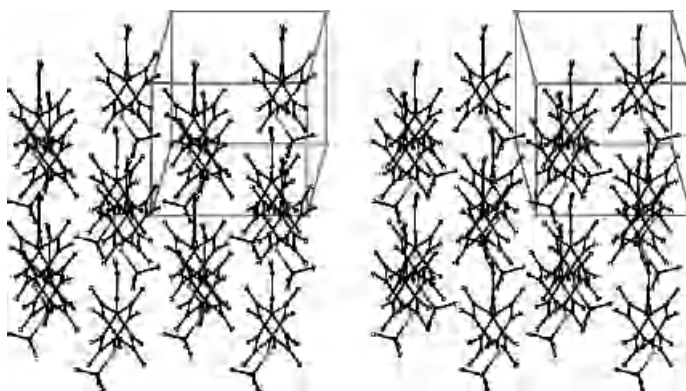
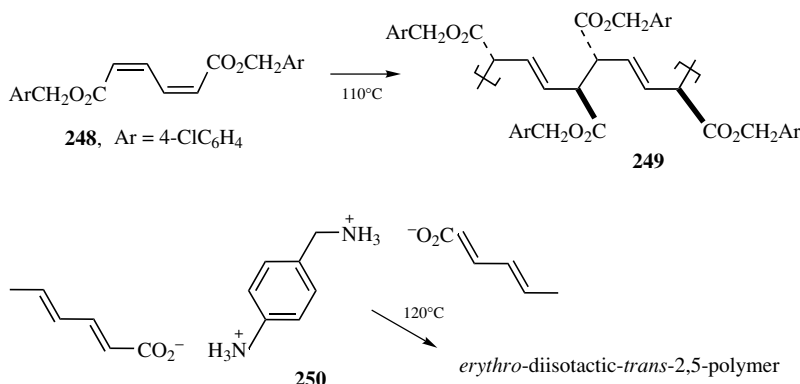


Figure 9.1. Stereoscopic view of the (100) face of 1-(4-anisyl)-1-phenylethene (Cc). See color insert.

requirements are most stringent. The polymer chains can, of course, not exit the crystal, but they must be able to accommodate with the monomer lattice particularly closely. A reconsideration of the possibility for stereoselective thermal (but also photolytical or radiolytical) solid state polymerization met with very limited success.<sup>127</sup> While there are indications that the polymerizability of crystalline vinyl monomers is related to crystal structure, the polymers from 4-acetamidostyrene, 4-benzamidostyrene, and 4-vinylbenzoic acid were atactic, even though the C1…C2 distance was quite short (4.0–4.2 Å) and the double bonds were parallel.<sup>127</sup> The question of the necessary accommodation of the polymer (with largely changed geometry) with the monomer lattice was not addressed, despite the obvious failure of the so-called topochemical principles.

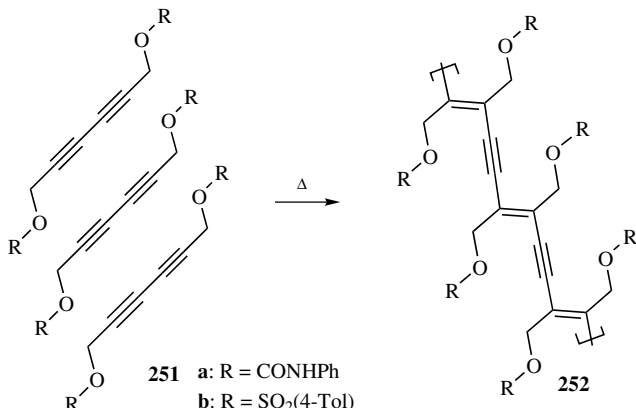
Better results have been achieved with some *E,E*- or *Z,Z*-dienes<sup>128–129</sup> and diynes.<sup>130</sup> Thus, favorable packing has been obtained by crystal engineering in **248** and **250**. Both yielded the stereoregular disisotactic-*trans*-2,5-polymers in up to 96% and 66% yield upon heating.<sup>128</sup> A roughly 5 Å wide, 30–60° inclined stacking of the extended diene-system with respect to the polymerization axis at C–C distances of 3.30–5.69 Å was found geometrically favorable for the polymer to form as it can then accommodate with the monomer lattice. But this was not interpreted in that sense.<sup>128,129</sup> Clearly, the favorable packing could have been easily predicted instead of “trial and error” on the unsuitable basis of topochemistry that could not foresee that unsuitable stacking prohibits reactivity despite C–C distances of <4.2 Å (so known examples in Matsumoto<sup>129</sup>).

The first claim of a homogeneous thermal (also photochemical) polymerization of a polymorph of the bisurethane-substituted 1,3-diacetylene (**251a**, R = CONHPh) at any degree of conversion (“up to 95%”) had to be modified several times. It had to be admitted that the reaction did not run without crystal solvent (e.g., 0.5 dioxane/unit),<sup>131</sup> and a final review from the same research group<sup>132</sup> did not list **251a**



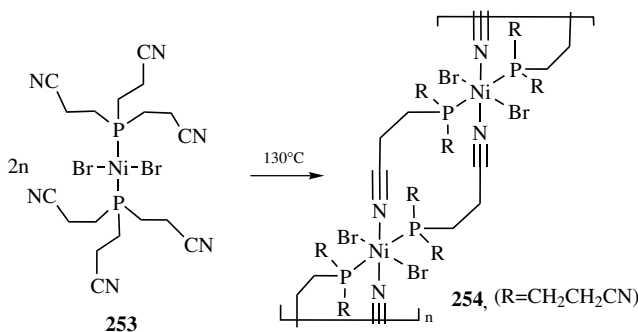
anymore. Furthermore, instead of zero-order kinetics,<sup>129</sup> marked induction periods (followed by a wrongly claimed “first-order” reaction)<sup>132</sup> were found to be general for this type of thermal polymerization and exemplified with the apparently better 4-toluenesulfonate system [**251b**, R =  $\text{SO}_2(4\text{-Tol})$ ].<sup>132</sup> Interestingly, inspection of the curves indicates zero order behavior after the induction period up to 90% conversion instead of “first order”. The stereospecificity of this reaction provided the *trans-tactic* crystalline polymer **252** with few defects.

Most of related diacetylenes proved unreactive in the solid state. As indicated by common bond lengths and angles, there must be columnar stacking at the width of 5 Å with an angle of around 45° enclosed by the diyne moiety and the stacking axis (adjustment to precise bond lengths and angles required). This arrangement achieves a period of the monomer stacking that closely corresponds with the polymer fiber period. Only under these conditions can the polymer accommodate to the monomer structure. This is essential because the polymer cannot migrate and



escape the lattice, of course. However, the mismatch of the periods (**251b/252b**: 3.9%) tells that there must be many migrations of monomer molecules along the stacking axis upon polymerization. Although these considerations appear very helpful and should be taken into account, “topochemical principles” do not give an answer to the question of why certain diacetylenes can be thermally polymerized whereas others with equal packing type but shorter or longer periods (distance of reacting centers always <4.2 Å) are inactive. An AFM investigation on thermolyzed **251b** on (100) revealed ridges along the polymerization axis.<sup>133</sup> The necessary molecular migrations along the b-axis should, however, be studied on the (010)-face, in order to gain more insight into the growth dynamics.<sup>3,4,12</sup> The molecular weights of the polymers are still not disclosed.<sup>132</sup>

The stereospecific quantitative linear polymerization of the square planar Ni(II)-coordination complex **253** to give the octahedral linear coordination polymer **254** in the solid state has been known since 1977.<sup>134</sup> The crystalline polymer exhibits spatial similarities between the packing of monomer and polymer, but the β-angle changes from 90° to 97.5°.



## XIX. CONCLUSIONS

Thermal, stereoselective reactions in the solid state have matured but are far from being extensively used. There is still enormous promise in the application of these powerful techniques that make use of the crystal packing. A large number of sustainable quantitative solid state reactions with 100% yield of one product have been collected in a recent review article<sup>135</sup> and a complete course on these reactions has been widely spread by the OECD since 2001.<sup>136</sup>

Topochemistry, with its dogma of minimal atomic and molecular movements, totally disregards the enormous internal pressure that has to be released if molecular shapes change in the crystal bulk. It was therefore not helpful in the development of these reactions because they require far-reaching molecular

migrations (as AFM evidence tells) to accommodate the original lattice immediately after every single product molecule forms rather than “minimal atomic or molecular movements.” Clearly, “easy paths” will be used in such migrations. If these are not available due to 3D-interlocking, there will be no solid state reactivity.

Although these experimental observations tell that no excessive pressure can be built up within the crystal, they open the opportunity to make use of the crystal packing in order to judge the feasibility of the phase-rebuilding process. The latter is followed by phase transformation (formation of the product phase) and disintegration with formation of new surfaces for further reaction. The interplay of these necessary processes suggests an answer to the question why most such solid state reactions are modestly stereoselective even in the early stages of the reaction at low conversion. Increased yield and stereoselectivity will be obtained if the basic though simple premises of solid state technology are followed. Thus, grinding or better milling is the preferred way to execute solid–solid reactions, and this has nothing to do with tribochemistry (mechanochemistry) in molecular crystals or salts, unlike polymers or infinitely covalent crystals or explosives where ordinary bonds are broken upon crushing. Therefore many of the cited low yield reactions can be easily improved and the reaction times brought down to some minutes, if the proper reaction techniques are applied.

Even scale up capabilities have been demonstrated for gas–solid reactions and solid–solid reactions,<sup>137</sup> and increased selectivity is obtained at lower temperatures. The ingenious three-step mechanism (multistep in the case of cascade reactions) of molecular solid state reactions provides complete reactions rather than the frequently claimed low yields. The latter claims are unfortunate if proper contact between the solid reactants was not assured.

Melting or addition of minor quantities of solvent has to be strictly avoided because the merits of the crystal packing are completely lost under such conditions. These are no longer solid state reactions, and the stereoselectivity will mostly decrease similar to that in solution. Thermal, stereoselective reactions in the solid state will remain an important tool for stereoselective syntheses and numerous yet unexplored applications will certainly emerge because the mechanistic basis have now become very clear.

## REFERENCES

1. For example, the  $\alpha$ - and  $\beta$ -modifications of *o*-acetamidobenzamide are made up of molecules with a different rotational alignment of the amide substituent: Errede, L. A.; Etter, M. C.; Williams, R. C.; Darnauer, S. M.; *J. Chem. Soc., Perkin Trans. 1980*, 2, 233–238.
2. Kaupp, G. In *Comprehensive Supramolecular Chemistry*, Vol. 8. Davies, J. E. D., ed. Elsevier, Oxford, 1996, pp. 381–423 and 21 color plates.

3. Kaupp, G. *Cryst. Eng. Comm.* **2003**, *5*, 117–133, and numerous references therein.
4. Kaupp, G. *Solid-State Reactivity/Gas-Solid and Solid-Solid Reactions*, in *Encyclopedia of Supramolecular Chemistry*, Atwood, J.; Steed, J., eds., Dekker, New York, Internet Edition, July **2005**.
5. Kaupp, G. *Angew. Chem. Int. Ed. Engl.* **1992**, *31*, 592–595, 595–598.
6. Tanaka, K.; Toda, F. *Chem. Rev.* **2000**, *100*, 1025–1074.
7. Kaupp, G.; Schmeyers, J.; Boy, J. *Chemosphere* **2001**, *43*, 55–61.
8. Kaupp, G.; Schmeyers, J.; Naimi-Jamal, M. R.; Zoz, H.; Ren, H. *Chem. Engin. Sci.* **2002**, *57*, 763–765.
9. Kaupp, G.; Naimi-Jamal, M. R.; Ren, H.; Zoz, H. *Process-Worldwide* **2003**, *4*, 24–27; <http://vmg01.dnsalias.net/vmg/process-worldwide.de/download/102327/Long-Version.doc>. *Chemie Technik* **2002**, *31*, 206–208.
10. Kaupp, G.; Herrmann, A.; Schmeyers, J. *Chem. Eur. J.* **2002**, *8*, 1395–1406.
11. Kaupp, G.; Herrmann, A.; Haak, M. *J. Phys. Org. Chem.* **1999**, *12*, 797–807; *EPOC* **1999**, issue *II*; <http://www.wiley.com/epoc>.
12. Kaupp, G. *Curr. Opin. Sol. St. Mater. Sci.* **2002**, *6*, 131–138.
13. Tanaka, K.; Hiratsuka, T.; Ohba, S.; Naimi-Jamal, M. R.; Kaupp, G. *J. Phys. Org. Chem.* **2003**, *16*, 905–912.
14. Kaupp, G.; Schmeyers, J.; Kato, M.; Tanaka, K.; Harada, N.; Toda, F. *J. Phys. Org. Chem.* **2001**, *14*, 444–452.
15. Liu, C.-T.; Curtin, D. Y.; Paul, I. C. *J. Am. Chem. Soc.* **1974**, *96*, 6199–6200.
16. Toda, F.; Tanaka, K. *Supramol. Chem.* **1994**, *3*, 87–88.
17. Coville, N. J.; Cheng, L. *J. Organomet. Chem.* **1998**, *571*, 149–169.
18. Miller, R. S.; Curtin, D. Y.; Paul, I. C. *J. Am. Chem. Soc.* **1972**, *94*, 5117–5119.
19. Kaupp, G.; Matthies, D. *Mol. Cryst. Liq. Cryst.* **1988**, *161*, 119–143.
20. Kaupp, G.; Matthies, D. *Chem. Ber.* **1987**, *120*, 1897–1903.
21. Kaupp, G.; Kuse, A. *Mol. Cryst. Liq. Cryst.* **1998**, *313*, 361–366.
22. Tanaka, K.; Shiraishi, R.; Toda, F. *J. Chem. Soc., Perkin Trans.* **1999**, *1*, 3069–3070.
23. Ohashi, T.; Miyoshi, F.; Sawada, Y. *Nippon Kagaku Kaishi*, **1987**, 1365–1369.
24. Hamazaki, H.; Ohba, S.; Toda, F.; Takumi, H. *Acta Crystallogr.* **1997**, *C53*, 620–624.
25. Schmitt, A. *Liebigs Ann. Chem.* **1863**, *127*, 319–332.
26. Kaupp, G. *Mol. Cryst. Liq. Cryst.* **1994**, *242*, 153–169.
27. Tanaka, Y.; Sakuraba, H.; Oka, Y.; Nakanishi, H. *J. Incl. Phenom.* **1984**, *2*, 841–850.
28. Hadjoudis, E. *Mol. Cryst. Liq. Cryst.* **1986**, *134*, 237–244.
29. Penzien, K.; Schmidt, G. M. *J. Angew. Chem. Int. Ed. Engl.* **1969**, *8*, 608–609.
30. Green, B. S.; Heller, L. *Science* **1974**, *185*, 525–527.
31. Green, B. S.; Rabinovich, D.; Shakked, Z.; Hope, H.; Swanson, K. *Acta Crystallogr.* **1981**, *B37*, 1376–1380.
32. Durand, D.; Kondepudi, D. K.; Moreira, P. F. Jr.; Quina, F. H. *Chirality* **2002**, *14*, 284–287.
33. Hadjoudis, E. *Israel J. Chem.* **1973**, 63–69.
34. Kaupp, G.; Seep, C. *Angew. Chem. Int. Ed. Engl.* **1988**, *27*, 1511–1512.
35. Kaupp, G. Unpublished results.
36. Longato, B.; Morandini, F.; Bresadola, S. *Inorg. Chim. Acta* **1980**, *39*, 27–34.

37. Ball, M. C.; Pope, J. M. *J. Chem. Soc., Dalton Trans.* **1973**, 1802–1804.
38. Kaupp, G.; Ulrich, A.; Sauer, G. *J. Prakt. Chem.* **1992**, *334*, 383–390.
39. Gerdil, R.; Barchietto, G. *Helv. Chim. Acta* **1994**, *77*, 691–708.
40. Kaupp, G.; Jaskulska, E.; Sauer, G.; Michl, G. *J. Prakt. Chem.* **1994**, *336*, 686–689.
41. Thomas, J. M.; Morsi, S. E.; Desvergne, J. P. *Adv. Phys. Org. Chem.* **1977**, *15*, 64–151.
42. Tremelling, M. J.; Hopper, S. P.; Mendelowitz, P. C. *J. Am. Chem. Soc.* **1978**, *43*, 3076–3077.
43. Hagiwara, H.; Ohtsubo, S.; Kato, M. *Mol. Cryst. Liq. Cryst.* **1996**, *279*, 291–293.
44. Im, J.; Kim, J.; Kim, S.; Hahn, B. *Tetrahedron Lett.* **1997**, *38*, 451–452.
45. Toda, F.; Okuda, K. *J. Chem. Soc., Chem. Commun.* **1991**, 1212–1214.
46. Kaupp, G.; Naimi-Jamal, M. R.; Stepanenko, V. *Chem. Eur. J.* **2003**, *9*, 4156–4160.
47. Khrushcheva, N. S.; Belousova, E. E.; Loim, N. M.; Sokolov, V. I. *Russ. Chem. Bull. (Izv. Akad. Nauk., Ser. Khim.) Engl. Transl.* **2000**, *49*, 1106–1108. *Chem. Abs.* **2000**, 700630.
48. Olivian, M.; Marchenko, A. V.; Coalter, J. N.; Caulton, K. G. *J. Am. Chem. Soc.* **1997**, *119*, 8389–8390.
49. Cheng, L.; Coville, N. J. *J. Organometal. Chem.* **1998**, *556*, 111–118.
50. Kaupp, G.; Naimi-Jamal, M. R.; Schmeyers, J. *Tetrahedron* **2003**, *59*, 3753–3760.
51. Kaupp, G.; Schmeyers, J.; Boy, J. *J. Prakt. Chem.* **2000**, *342*, 269–280.
52. Kaupp, G.; Schmeyers, J.; Boy, J. *Tetrahedron* **2000**, *56*, 6899–6911.
53. Khrushcheva, N. S.; Loim, N. M.; Sokolov, V. I.; Makhaev, V. D. *J. Chem. Soc., Perkin Trans. 1997, 1*, 2425–2427.
54. Kaupp, G.; Naimi-Jamal, M. R. *Chem. Eur. J.* **2002**, *8*, 594–600.
55. Toda, F.; Akai, H. *J. Org. Chem.* **1990**, *55*, 3446–3447.
56. Balema, V. P.; Wiench, J. W.; Pruski, M.; Pecharsky, V. K. *J. Am. Chem. Soc.* **2002**, *124*, 6244–6345.
57. Tanaka, K. *Solvent-free Organic Synthesis*. Wiley-VCH, Weinheim, **2003**.
58. Liu, W.; Xu, Q.; Ma, Y.; Liang, Y.; Dong, N.; Guan, D. *J. Organomet. Chem.* **2001**, *625*, 128–131.
59. Wei, Y.; Bakthavatchalam, R. *Tetrahedron* **1993**, *49*, 2373–2390.
60. Toda, F.; Tanaka, K.; Sato, J. *Tetrahedron: Asymmetry* **1993**, *4*, 1771–1774.
61. Vestergren, M.; Eriksson, J.; Hakansson, M. *Chem. Eur. J.* **2003**, *9*, 4678–4686.
62. Nader, F. W.; Wacker, C.-D.; Irngartinger, H.; Huber-Patz, U.; Jahn, R.; Rodewald, H. *Angew. Chem. Int. Ed. Engl.* **1985**, *24*, 852–853.
63. Miller, E. J.; Brill, T. B.; Rheingold, A. L.; Fultz, W. C. *J. Am. Chem. Soc.* **1983**, *105*, 7580–7583.
64. Kaupp, G. Int. Chem. Congress of Pacific Basin Societies, Honolulu, Hawaii, **2000**, Orgn. 1253, Dec. 14–19, **2000**.
65. Abelt, C. J.; Pleier, J. M. *J. Org. Chem.* **1988**, *53*, 2159–2162.
66. Toda, F.; Imai, N. *J. Chem. Soc., Perkin Trans. 1994, 1*, 2673–2674.
67. Marchand, A. P.; Reddy, G. M. *Tetrahedron* **1991**, *47*, 6571–6576.
68. Mehta, G.; Khan, F. A.; Lakshmi, K. A. *Tetrahedron Lett.* **1992**, *33*, 7977–7980.
69. Doussot, J.; Guy, A.; J.-M. Siaugue, C. Ferroud, Guieres, A. F. *Chirality* **1999**, *11*, 541–545.
70. Toda, F.; Mori, K. *J. Chem. Soc. Chem. Commun.* **1989**, 1245–1246.
71. Toda, F.; Kiyoshige, K.; Yagi, M. *Angew. Chem. Int. Ed. Engl.* **1989**, *28*, 320–321.
72. Du, H.-F.; Ding, K.-L.; Meng, J.-B. *Chinese J. Chem.* **2001**, *19*, 716–718.

73. Hajipour, A. R.; Hantehzadeh, M. *J. Org. Chem.* **1999**, *64*, 8475–8478.
74. Tanaka, K.; Kishigami, S.; Toda, F. *J. Org. Chem.* **1990**, *55*, 2981–2983.
75. (a) Sabra, F.; Bassus, J.; Lamartine, R. *Mol. Cryst. Liq. Cryst.* **1990**, *186*, 69–72. (b) Lamartine, R.; Perrin, R.; Thozet, A.; Perrin, M. *Mol. Cryst. Liq. Cryst.* **1983**, *96*, 57–69.
76. Toda, F.; Mori, K.; Matsuura, Y.; Akai, H. *J. Chem. Soc., Chem. Commun.* **1990**, 1591–1593.
77. Friedman, N.; Lahav, M.; Leiserowitz, L.; R. Topovitz-Biro, Tang, C. P.; Zaretskii, Z. *Mol. Cryst. Liq. Cryst.* **1976**, *32*, 127–129.
78. Tokitoh, N.; Kishikawa, K.; Okazaki, R.; Sasamori, T.; Nakata, N.; Takeda, N. *Polyhedron* **2002**, *21*, 563–577.
79. Krom, M.; Peters, T. P. J.; Coumans, R. G. E.; Sciarone, T. J. J.; Hoogboom, J.; ter Beek, S. I.; Schlebos, P. P. J.; Smits, J. M. M.; de Gelder, R.; Gal, A. W. *Eur. J. Inorg. Chem.* **2003**, 1072–1087.
80. Derenne, S.; Gaudemer, A.; Johnson, M. D. *J. Organomet. Chem.* **1987**, *322*, 229–238.
81. Kaupp, G.; Naimi-Jamal, M. R.; Maini, L.; Grepioni, F.; Braga, D. *Cryst. Eng. Comm.* **2003**, *5*, 474–479.
82. Braga, D.; Cojazzi, G.; Emiliani, D.; Maini, L.; Grepioni, F. *Organometallics* **2002**, *21*, 1315–1318.
83. Kaftory, M. *J. Am. Chem. Soc.* **1983**, *105*, 3832–3836.
84. McKillop, K. L.; Gillette, G. R.; Powell, D. R.; West, R. *J. Am. Chem. Soc.* **1992**, *114*, 5203–5208.
85. Wiedemann, R.; Wolf, J.; Werner, H. *Angew. Chem. Int. Ed. Engl.* **1995**, *34*, 1244–1246.
86. Werner, H.; Rappert, T.; Baum, M.; Stark, A. *J. Organomet. Chem.* **1993**, *459*, 319–323.
87. Toda, F.; Tanaka, K.; Tamashima, T.; Kato, M. *Angew. Chem. Int. Ed. Engl.* **1998**, *37*, 2724–2727.
88. Kaupp, G.; Schmeyers, J.; Kato, M.; Tanaka, K.; Toda, F. *J. Phys. Org. Chem.* **2002**, *15*, 148–153.
89. Chong, K. C. W.; Scheffer, J. R. *J. Am. Chem. Soc.* **2003**, *125*, 4040–4041.
90. Hadjoudis, E.; Schmidt, G. M. *J. J. Chem. Soc., Perkin Trans.* **1972**, *2*, 1060–1062.
91. Wallis, E. S.; Adams, F. H. *J. Am. Chem. Soc.* **1933**, *55*, 3838–3851.
92. Dose, K. *Orig. Life* **1981**, *11*, 165–171.
93. Liardon, R.; Ledermann, S.; Ott, U. *J. Chromatogr.* **1981**, *203*, 385–395.
94. Bonner, W. A.; Blair, N. E.; Lemmon, R. M. *Orig. Life* **1979**, *9*, 279–290.
95. Pincock, R. E.; Tong, M.-M.; Wilson, K. R. *J. Am. Chem. Soc.* **1971**, *93*, 1669–1672.
96. Pincock, R. E.; Wilson, K. R.; Kiovsky, T. E. *J. Am. Chem. Soc.* **1967**, *81*, 6890–6897.
97. Kamigauchi, M.; Noda, Y.; Iwasa, K.; Nishijo, Z.; Takao, N. *Arch. Pharm. (Weinheim)* **1993**, *326*, 501–505.
98. Toda, F.; Tanaka, K.; Miyamoto, H.; Koshima, H.; Miyahara, I.; Hirotsu, K. *J. Chem. Soc., Perkin Trans.* **1997**, *2*, 1877–1885.
99. Toda, F.; Tohi, Y. *J. Chem. Soc. Chem. Commun.* **1993**, 1238–1240.
100. Toda, F.; Sato, A.; Tanaka, K.; Mak, T. C. W. *Chem. Lett.* **1989**, 873–876.
101. Kaupp, G.; Schmeyers, J.; Haak, M.; Marquardt, T.; Herrmann, A. *Mol. Cryst. Liq. Cryst.* **1996**, *276*, 315–337.
102. Kaupp, G.; Schmeyers, J.; Toda, F.; Takumi, H.; Koshima, H. *J. Phys. Org. Chem.* **1996**, *9*, 795–800.

103. Pincock, R. E.; Wilson, K. R. *J. Am. Chem. Soc.* **1971**, *93*, 1291–1292.
104. Theilacker, W.; Hopp, R. *Chem. Ber.* **1959**, *92*, 2293–2301.
105. Lu, M. D. M.; Pincock, R. E. *J. Org. Chem.* **1978**, *43*, 601–604.
106. Smrcina, M.; Vyskocil, S.; Hanus, V.; Polasek, M.; Langer, V.; Chew, B. G. M.; Zax, D. B.; Verrier, H.; Harper, K.; Claxton, T. A.; Kocovsky, P. *J. Am. Chem. Soc.* **1996**, *118*, 487–488.
107. Shankland, N.; David, W. I. F.; Shankland, K.; Kennedy, A. R.; Frampton, C. S.; Florence, A. J. *Chem. Commun.* **2001**, 2240–2245.
108. Krassowski, D. W.; Reimer, K.; LeMay H. E. Jr.; Nelson, J. H. *Inorg. Chem.* **1988**, *27*, 4307–4309.
109. Katsuki, K.; Ooyama, Y.; Okamoto, M.; Yamamoto, Y. *Inorg. Chim. Acta* **1994**, *217*, 181–185.
110. Coville, N. J.; Levendis, D. C. *Eur. J. Inorg. Chem.* **2002**, 3067–3078.
111. Cheng, L.; Coville, N. J. *Organometallics* **1996**, *15*, 867–871.
112. Bogadi, R. S.; Levendis, D. C.; Coville, N. J. *J. Am. Chem. Soc.* **2002**, *124*, 1104–1110.
113. LeMay, H. E.; Bailar J. C. Jr. *J. Am. Chem. Soc.* **1968**, *90*, 1729–1733.
114. Banerjea, D.; Bailar J. C. Jr. *Trans. Metal Chem.* **1985**, *10*, 331–333.
115. Banerjee, D. *Trans. Metal Chem.* **1988**, *13*, 160.
116. House, J. E. Jr. *Thermochim. Acta* **1980**, *38*, 59–66.
117. Akabori, K.; Kushi, Y. *J. Inorg. Nucl. Chem.* **1978**, *40*, 1317–1322.
118. Kurihara, T.; Uchida, A.; Ohashi, Y.; Sasada, Y.; Ohgo, Y. *J. Am. Chem. Soc.* **1984**, *106*, 5718–5724.
119. O'Brien, P. *J. Chem. Soc., Dalton Trans: Inorg. Chem.* **1982**, 1173–1174.
120. Fujiwara, T.; Yamamoto, Y. *Inorg. Chem.* **1980**, *19*, 1903–1907.
121. Tatehata, A.; Kumamaru, T.; Yamamoto, Y. *J. Inorg. Nucl. Chem.* **1971**, *33*, 3427–3435.
122. Chowdhury, D. M.; Harris, G. M. *J. Phys. Chem.* **1969**, *73*, 3366–3369.
123. Tomioka, K.; Kashihara, T.; Sakaguchi, U.; Yoneda, H. *Chem. Lett.* **1984**, 1047–1050.
124. Fujiwara, T.; Bailar, J. C. Jr. *Inorg. Chim. Acta* **1988**, *154*, 55–57.
125. De, G.; Suzuki, M.; Uehara, A. *Bull. Chem. Soc. Jpn.* **1987**, *60*, 3444–3446.
126. Wei, Y. Y.; Tinant, B.; Declerc, J. P. *Acta Crystallogr.* **1987**, *C 43*, 86–89.
127. Di, L.; Foxman, B. M. *Supramol. Chem.* **2001**, *13*, 163–174.
128. Nagahama, S.; Matsumoto, A. *Chem. Lett.* **2002**, 1026–1027.
129. Matsumoto, A. *Polymer J.* **2003**, *15*, 93–121.
130. Wegner, G. *Z. Naturforsch.* **1969**, *B24*, 824–932. Kaiser, J.; Wegner, G.; Fischer, E. W. *Israel J. Chem.* **1972**, *10*, 157–171.
131. Wegner, G. *Angew. Chem. Int. Ed. Engl.* **1971**, *10*, 266–267.
132. Enkelmann, V. *Adv. Polym. Sci.* **1984**, *83*, 91–136.
133. Yaji, T.; Izcemi, K.; Isoda, S. *Appl. Surf. Sci.* **2002**, *188*, 519–523.
134. Cheng, K.; Foxman, B. M. *J. Am. Chem. Soc.* **1977**, *99*, 8102–8103.
135. Kaupp, G. *Top. Curr. Chem.*, submitted.
136. Kaupp, G.; Schmeyers, J.; Naimi-Jamal, M. R. *A Practical Students Course: Environmentally Benign Chemical Syntheses*. Case study for distribution by OECD, **2001**. Also available at <http://kaupp.chemie.uni-oldenburg.de>.
137. Kaupp, G. *Int. Chem. Congress of Pacific Basin Societies*, Honolulu, Hawaii, Orgn. 0688, Dec. 15–20, **2005**.

# **Chapter 10**

## **Crystal Structures and Functionalities of Platinum(II) Complexes Controlled by Various Intermolecular Interactions**

MASAKO KATO

*Graduate School of Humanities and Sciences, Nara Women's University,  
Kitauoyahigashi-machi, Nara 630-8506*

- I. Introduction
- II. Thermochromism and Vapochromism of Dicyano(2,2'-bipyridine)platinum(II) Based on the Crystal Structural Change
- III. Ladder Structures for the Platinum(II) Complexes Containing Both Planar and Nonplanar Ligands and the Selective Formation of Integrated Stack with Neutral  $\pi$ -Systems of the Phenanthrene Type
- IV. Deformation of the  $\pi$ -System of Bis(1,10-phenanthroline)platinum(II)
- V. Linkage Isomerism of Bis(thiocyanato)(2,2'-bipyridine)platinum(II) and the Luminescence Properties
- VI. Concluding Remarks

References

### **I. INTRODUCTION**

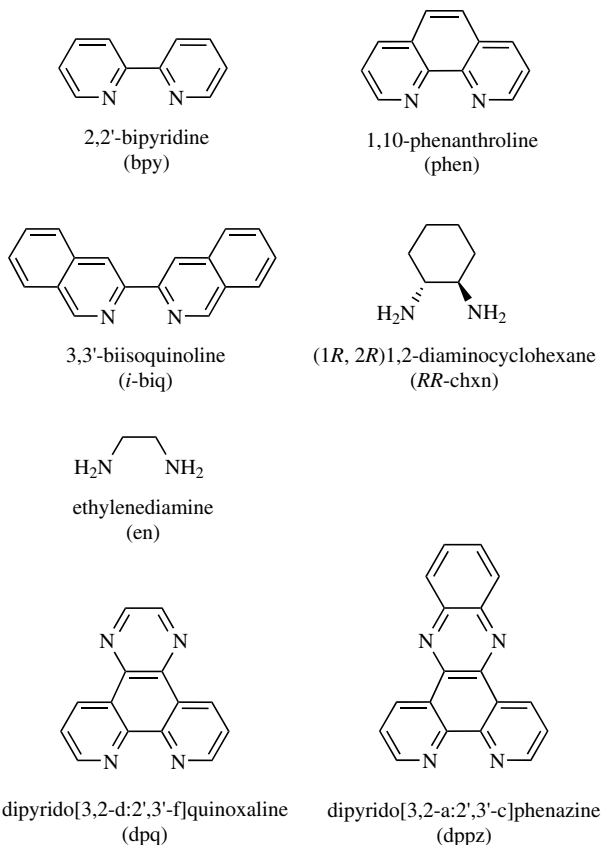
Platinum complexes have been one of the most attractive metal complexes from the viewpoint of stereochemistry in the crystal. Many researchers have been interested in the characteristic solid-state optical properties of several platinum(II) complexes, such as tetracyanoplatinate(II), for a long time.<sup>1,2</sup> Also, in the early days of coordination chemistry, platinum complexes were one of the important tools for the study of stereochemistry. The stereochemistry for discrete

platinum(II) complexes having square-planar geometry is relatively simple, but it is the stacking of these complexes in the solid state that results in the appearance of various interesting properties, such as characteristic color, dichroism, intense luminescence, and electric conductivity. Such interesting properties of platinum complexes depend on the intermolecular interactions that result from the various stacking structures. Thus, the determination of the crystal structures of the complexes is indispensable for understanding their electronic properties, just as in the case of other assembled molecular systems. However, the determination of the crystal structures of platinum complexes by X-ray diffraction has often encountered many difficulties associated with crystallization of the complexes and the structure analysis because the strong anisotropic properties of the complexes tend to produce only very fine needle-like crystals and twined crystals. Fortunately, recent significant advances in techniques and instrumentation, including a CCD camera as a detector, have brought us many new crystal structures.

The author's group has been focusing on the structural design of  $\alpha$ -diimine-platinum(II) complexes using various intermolecular interactions to control the luminescence properties: the metal-metal interaction is the most characteristic intermolecular interaction affecting the luminescence of such complexes and would be controlled primarily by the ligand field strength. The  $\alpha$ -diimine ligands such as 2,2'-bipyridine and 1,10-phenanthroline are expected to control the stacking structures of the platinum complexes on the basis of intermolecular  $\pi\cdots\pi$  interactions. As a result, the polymorphism often occurs for such  $\alpha$ -diimine platinum(II) complexes: for example,  $[\text{PtCl}_2(\text{bpy})]$  provides two crystal forms of yellow and red. The red form has a stacked structure with a Pt $\cdots$ Pt linear chain, while the yellow form has no Pt $\cdots$ Pt stacking but forms  $\pi\cdots\pi$  stacked column comprising the bpy ligands.<sup>3</sup> Also, intermolecular hydrogen bonding should play an important role in the construction of characteristic nanostructures in the crystal. This chapter describes several structural studies on  $\alpha$ -diimine-platinum complexes achieved by the author's group relating to the luminescence properties. The structural formulae and abbreviations for the ligands are summarized in Scheme 10.1.

## II. THERMOCHROMISM AND VAPOCHROMISM OF DICYANO(2,2'-BIPYRIDINE)PLATINUM(II) BASED ON CHANGES IN THE CRYSTAL STRUCTURE

It is well known that square-planar platinum(II) complexes often stack in the solid state to form columnar structures and exhibit characteristic color and luminescence due to Pt $\cdots$ Pt interactions.<sup>4</sup> The red form of  $[\text{Pt}(\text{CN})_2(\text{bpy})]$  is known as a typical example. In the crystal the  $[\text{Pt}(\text{CN})_2(\text{bpy})]$  units are



Scheme 10.1.

stacked with a Pt···Pt distance of ca. 3.35 Å at room temperature, as shown in Figure 10.1.<sup>5</sup> The crystal exhibits intense red luminescence around 600 nm, even at room temperature, which is not observed for the monomeric form in dilute solution.<sup>6</sup> The emission is assigned to that from the metal–metal-to-ligand charge transfer state,  ${}^3\text{MMLCT}$  [ $\text{d}\sigma^*(\text{PtPt}) \rightarrow \pi^*(\text{bpy})$ ], where  $\text{d}\sigma^*(\text{PtPt})$  occurs from the Pt···Pt electronic interactions. Gliemann et al. reported that the emission maximum shifted to longer wavelength with decreasing temperature.<sup>7</sup> Such a striking temperature dependence of the emission spectrum has been noted for several linear-chain platinum complexes, such as  $\text{M}_x[\text{Pt}(\text{CN})_4]\cdot n\text{H}_2\text{O}^2$  and  $[\text{PtCl}_2(\text{bpy})]^4$ , and can be ascribed to changes in the Pt···Pt intermolecular interactions. To obtain direct evidence for a change in the Pt···Pt interactions

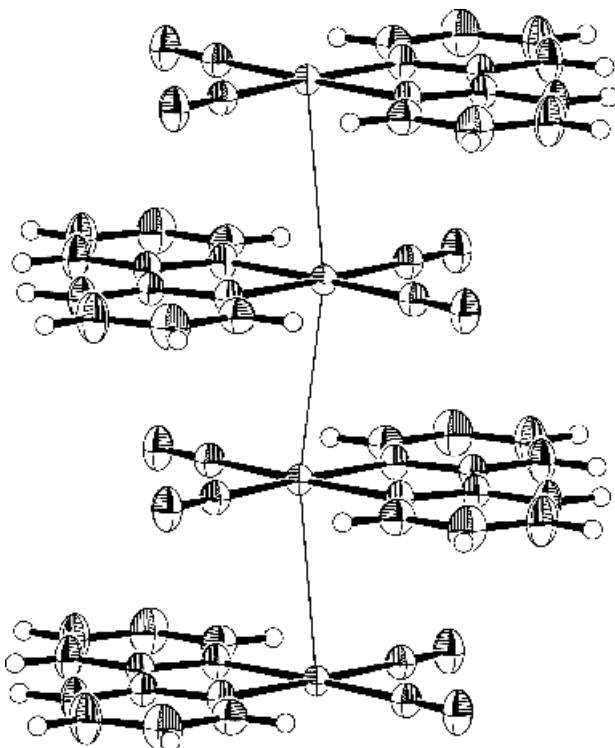


Figure 10.1. The stacking structure for the red form of  $[\text{Pt}(\text{CN})_2(\text{bpy})]$ .

in  $[\text{Pt}(\text{CN})_2(\text{bpy})]$ , we investigated the temperature dependence of the crystal structure, as well as of the emission spectrum and found a good correlation between the emission spectrum and the  $\text{Pt}\cdots\text{Pt}$  distance.<sup>8</sup>

Figure 10.2 shows the emission spectra of the red form of  $[\text{Pt}(\text{CN})_2(\text{bpy})]$  at various temperatures in the range 300 to 15 K. With decreasing temperature the emission band shifts to longer wavelength, increases in intensity, and becomes sharper. At 15 K, the vibrational structure appears and indicates the  ${}^3\text{MMLCT}$   $d\sigma^*(\text{PtPt}) \rightarrow \pi^*(\text{bpy})$  character. Furthermore we observed a temperature-dependent anisotropic change in the lattice constants for the red form of  $[\text{Pt}(\text{CN})_2(\text{bpy})]$  by means of X-ray diffraction. As shown in Figure 10.3, the  $c$  axis, which corresponds with the  $\text{Pt}\cdots\text{Pt}$  stacking direction, contracts significantly with decreasing temperature compared with the other axes ( $a$  and  $b$ ). In proportion to the shrinkage of the  $c$  axis, the  $\text{Pt}\cdots\text{Pt}$  distance contracts from 3.35 Å at room temperature to 3.29 Å at 15 K. The data result in a good correlation with the emission spectrum, which shifts to lower energy as the  $\text{Pt}\cdots\text{Pt}$  distance becomes

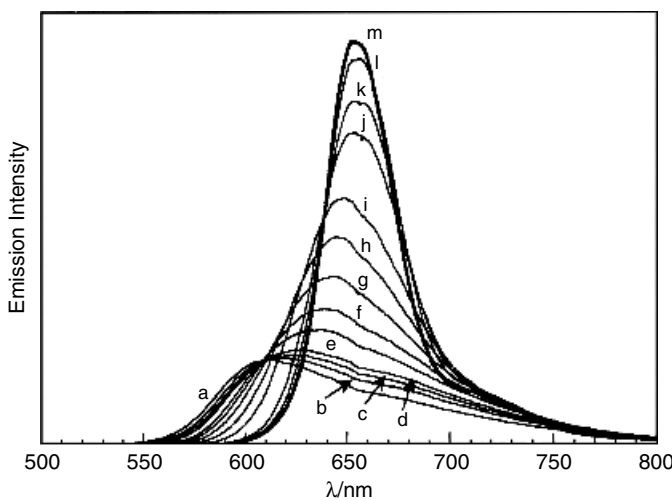


Figure 10.2. The emission spectra of the red form of  $[\text{Pt}(\text{CN})_2(\text{bpy})]$  at different temperatures: (a) 292; (b) 260; (c) 240; (d) 220; (e) 180; (f) 160; (g) 140; (h) 120; (i) 100; (j) 60; (k) 45; (l) 30; (m) 15 K.  $\lambda_{\text{ex}} = 514.5 \text{ nm}$ .<sup>12</sup>

shorter. These observations are interpreted in terms of an increase in the energy of the HOMO, the  $d\sigma^*(\text{Pt})$  orbital derived from the filled  $d_z^2(\text{Pt})$  orbital of the monomer complex, as the  $\text{Pt}\cdots\text{Pt}$  electronic interaction becomes stronger. For the  $[\text{Pt}(\text{CN})_4]^{2-}$  chain, a linear relationship between the emission maxima and  $R^{-3}$

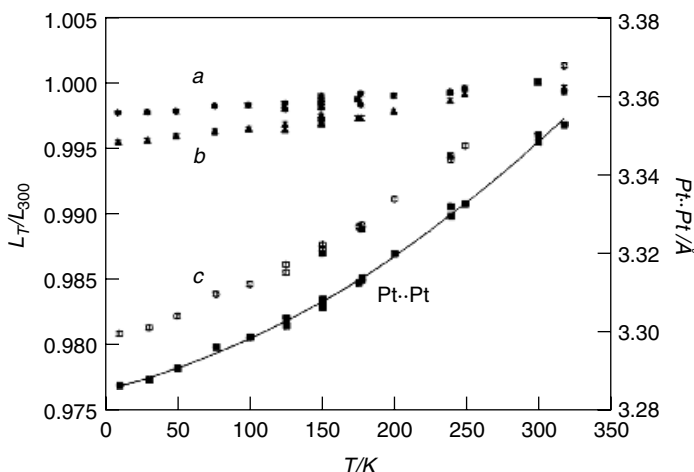


Figure 10.3. Ratio of the unit cell lengths (a, b, and c) relative to that at room temperature (300 K) and the  $\text{Pt}\cdots\text{Pt}$  distance for the red form of  $[\text{Pt}(\text{CN})_2(\text{bpy})]$  plotted as a function of temperature.<sup>12</sup>

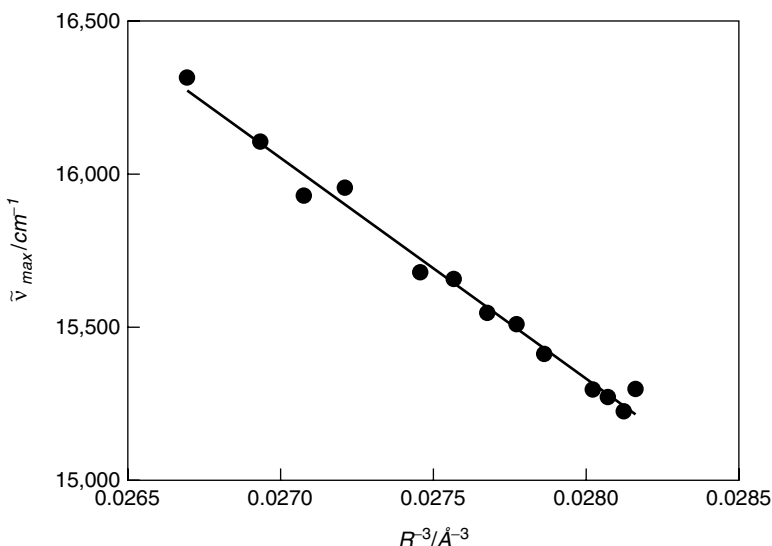


Figure 10.4. Plot of the emission peak energy against  $R^{-3}$  for the red form of  $[\text{Pt}(\text{CN})_2(\text{bpy})]$ , where  $R$  is the Pt...Pt distance.<sup>12</sup>

has been reported, where  $R$  denotes the Pt...Pt distance in the stack.<sup>9</sup> As shown in Figure 10.4, the relationship fits the  $[\text{Pt}(\text{CN})_2(\text{bpy})]$  system well, although the emission state of  ${}^3\text{MMLCT}$  is different from that for the  $[\text{Pt}(\text{CN})_4]^{2-}$  chain ( $d\sigma^* \rightarrow p\sigma$ ).

In addition to the red form  $[\text{Pt}(\text{CN})_2(\text{bpy})]$ , a yellow form is also known.<sup>10</sup> The red form transforms to the yellow form by taking up water molecules reversibly:



The position of the equilibrium is dependent on the vapor pressure of water in the atmosphere. Similar dimorphism is also known for  $[\text{PtCl}_2(\text{bpy})]$ : the red form has a linear Pt...Pt chain, whereas the yellow form consists of  $\pi \cdots \pi$  stacks of the bpy ligands. However, each form is stable and the complex does not exhibit any vapochromic behavior. Thus, much attention has been focused on the difference in the crystal structures of the red and yellow forms of  $[\text{Pt}(\text{CN})_2(\text{bpy})]$ . However, difficulty in getting good single crystals of the yellow form precluded its crystal structure determination until we finally succeeded in 2002.<sup>11</sup> On the basis of the changes in the crystal structure and luminescence spectrum on going from the red to the yellow form, the mechanism of the vapochromic behavior of  $[\text{Pt}(\text{CN})_2(\text{bpy})]$  has been elucidated.

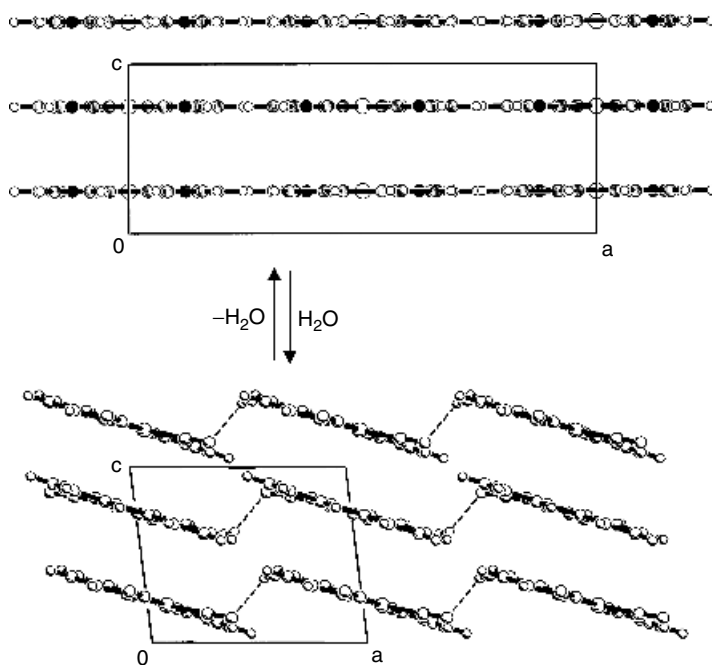


Figure 10.5. Structural conversion between the red (top) and yellow (bottom) forms of  $[\text{Pt}(\text{CN})_2(\text{bpy})]$  induced by water vapor.

For the yellow form  $[\text{Pt}(\text{CN})_2(\text{bpy})]$ , the molecules assemble in inclined stacks, which is a quite different arrangement from that of the yellow form of  $[\text{PtCl}_2(\text{bpy})]$ , where  $\pi \cdots \pi$  stacking of the bipyridine ligands is present. The structure of the yellow form of  $[\text{Pt}(\text{CN})_2(\text{bpy})]$  can be described as a deformation of the infinite chain structure of the red form as shown in Figure 10.5 (bottom). Compared with that for the red form, the stack for the yellow form has more of a zigzag character. There are alternating short and long  $\text{Pt} \cdots \text{Pt}$  distances in the stack (3.3279(3) and 4.6814(3) Å). These distances suggest that the yellow form may be best described as having a dimeric structure when the  $\text{Pt} \cdots \text{Pt}$  interactions are considered. The included water molecules are located near the  $\text{CN}^-$  ligands and interact with the latter through hydrogen bonds.

The transformation between the red and yellow forms of  $[\text{Pt}(\text{CN})_2(\text{bpy})]$  is accompanied by a luminescence change as well as a color change. These changes reflect a change in the  $\text{Pt} \cdots \text{Pt}$  electronic interactions. Figure 10.6 shows the change with time of the emission spectrum of the red form in the presence of water vapor at room temperature. The emission maximum at 602 nm in the initial spectrum gradually shifts to a shorter wavelength and reaches a final value of 566 nm. The

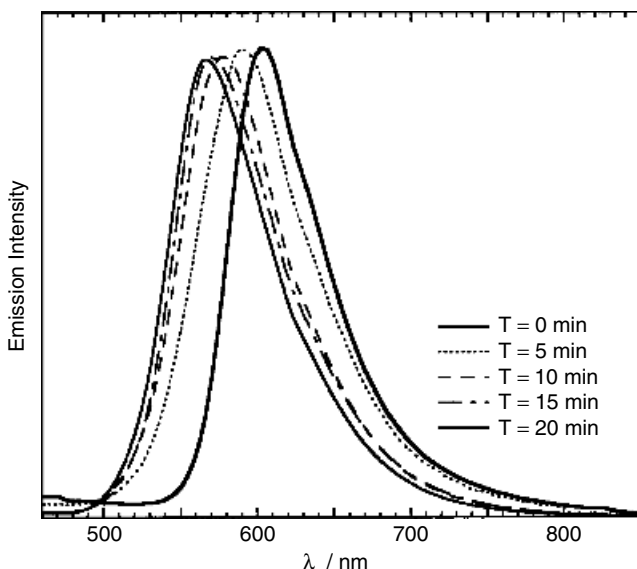


Figure 10.6. Changes in the emission spectrum of the red form of  $[\text{Pt}(\text{CN})_2(\text{bpy})]$  in the presence of water vapor at room temperature.<sup>11</sup>

final spectrum is consistent with that for the yellow form. Thus the transformation from the red form to the yellow form induced by water vapor was confirmed spectroscopically. The origin of the luminescence of the yellow form is assigned to the  ${}^3\text{MMLCT}$  state, which is essentially the same state as that responsible for the luminescence of the red form, on the basis of the similarity of the profiles of the spectra and the emission lifetimes ( $\tau = 56$  and  $109$  ns for the yellow and red forms, respectively). The assignment of the luminescence is also quite reasonable from the viewpoint of the crystal structure: the yellow form of  $[\text{Pt}(\text{CN})_2(\text{bpy})]$  has a short  $\text{Pt}\cdots\text{Pt}$  distance, which is short enough for the metal atoms to interact electronically. However, the interaction is restricted within the dimeric unit and the inclined stack reduces the orbital overlap between the Pt atoms. As a result the  ${}^3\text{MMLCT}$  emission state of the yellow form shifts to a higher energy than that of the red form. A similar behavior has been observed for the crystal of  $[\text{Pt}(\text{CN})_2(i\text{-biq})]$ : the  $\text{Pt}\cdots\text{Pt}$  interaction decreases with increasing inclination of the complex planes in the stack, even if the  $\text{Pt}\cdots\text{Pt}$  distance does not vary.<sup>11</sup> Furthermore the crystal packing of the red form of  $[\text{Pt}(\text{CN})_2(\text{bpy})]$  suggests a reason for the ease of uptake of water molecules. As shown in Figure 10.7, the arrangement of the linear chain stacks in the red form is well-ordered and there are cavities between the stacks that could act as channels for water molecules. However, as each channel is too narrow for water molecules, a change in the stacking arrangement is induced,

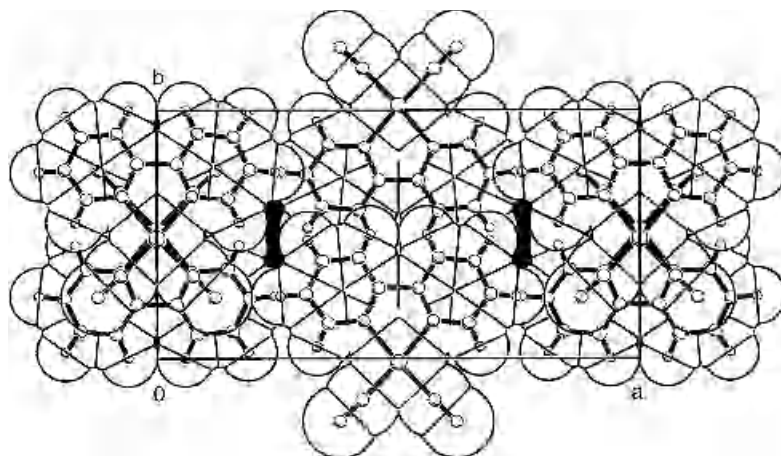


Figure 10.7. Crystal packing of the red form of  $[\text{Pt}(\text{CN})_2(\text{bpy})]$  with van der Waals spheres viewed down the  $c$  axis.<sup>11</sup> There are narrow channels along  $c$  axis indicated in black.

which results in the inclined stacking shown in Figure 10.5. In conclusion, the sensitive vapochromic behavior of  $[\text{Pt}(\text{CN})_2(\text{bpy})]$  crystals can be attributed to the slight deformation of the stacking structure and  $\text{Pt}\cdots\text{Pt}$  chains induced by the insertion of water molecules.

### III. LADDER STRUCTURES FOR PLATINUM(II) COMPLEXES CONTAINING BOTH PLANAR AND NONPLANAR LIGANDS AND SELECTIVE FORMATION OF INTEGRATED STACKS WITH NEUTRAL $\pi$ -SYSTEMS OF THE PHENANTHRENE TYPE

Platinum(II) complexes containing non-planar ligands, such as ethylenediamine (en), do not readily form a columnar structure with a chain of short  $\text{Pt}\cdots\text{Pt}$  interactions because the steric effect between the nonplanar ligands keeps the Pt atoms farther apart. We found that platinum(II) complexes containing both planar and nonplanar ligands,  $[\text{Pt}(\text{diamine})(\alpha\text{-diimine})]^{2+}$  (diamine = en and RR-chxn,  $\alpha$ -diimine = bpy and phen) form a unique ladder-type stacking structure which is constructed by using the  $\pi\cdots\pi$  interactions between the  $\alpha$ -diimine ligands and hydrogen bonding between the en ligand and the counter anion.<sup>13,14</sup> Figure 10.8 shows the ladder-type stacking for  $[\text{Pt}(\text{en})(\text{phen})](\text{PF}_6)_2$ . The  $\pi\cdots\pi$  stack of phen ligands looks like rungs of a ladder and on both sides, the en ligands and  $\text{PF}_6^-$  anions are connected to every other step through hydrogen bonds. It has been found that the interplanar spacings of the phen ligands in the crystal are 3.60(5)

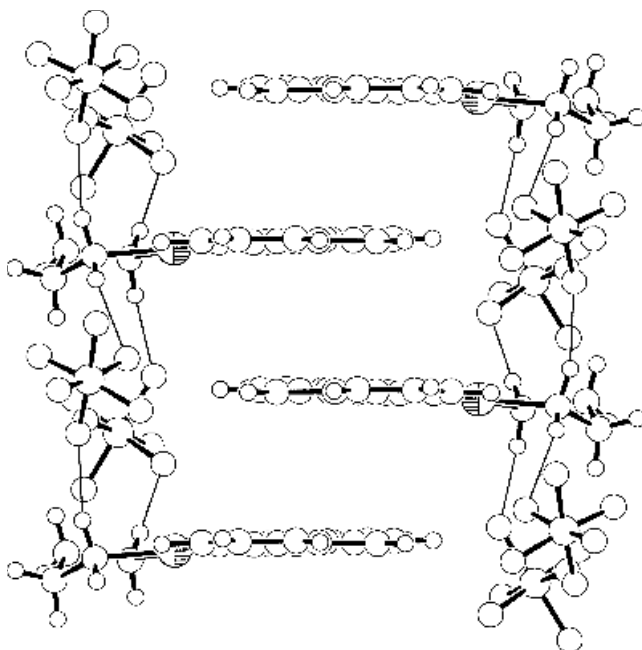


Figure 10.8. Ladder-type stacking of  $[\text{Pt}(\text{en})(\text{phen})](\text{PF}_6)_2$ .<sup>14</sup>

and  $3.56(5)\text{\AA}$ . On the other hand, the interplanar spacings of the  $\pi \cdots \pi$  stack of  $[\text{Pt}(\text{en})(\text{phen})]\text{Cl}_2$ , which contains the smaller  $\text{Cl}^-$  anion, are found to be  $3.38(1)$  and  $3.40(1)\text{\AA}$ . Thus the size of the anion influences the spacings of the pillar-like  $\pi$ -stack of  $\alpha$ -diimine ligands.

Ladder structures of the kind described above may be the sort of loose packed structures that might have inclusion ability. We found that platinum(II) complexes of the type  $[\text{Pt}(\text{en})(\text{L})]^{2+}$  ( $\text{L} = \text{bpy, phen}$ ) co-crystallize selectively with planar neutral  $\pi$ -conjugated compounds of the phenanthrene-type to form 1:1 integrated stacks.<sup>15</sup> The composite crystals,  $[\text{Pt}(\text{en})(\text{L})](\text{PF}_6)_2 \cdot \text{phen} \cdot 2\text{H}_2\text{O}$  ( $\text{L} = \text{bpy, phen}$ ) were readily obtained from an aqueous solution of the components. As shown in Figure 10.9 for the crystal of  $[\text{Pt}(\text{en})(\text{bpy})](\text{PF}_6)_2 \cdot \text{phen} \cdot 2\text{H}_2\text{O}$ , the included phen molecule is arranged parallel to and almost directly over the square-planar complex of  $[\text{Pt}(\text{bpy})(\text{en})]^{2+}$  with interplanar spacings of  $3.43(1)$  and  $3.47(1)\text{\AA}$ . These values suggest that the  $\pi \cdots \pi$  stacks are at their closest separation. The integrated stack is supported by a chain of hydrogen bonds linking water molecules and en ligand in the complex  $\text{NH}_2(\text{en}) \cdots \text{OH}_2 \cdots \text{OH}_2 \cdots \text{N}(\text{en}) \cdots$ , where the free phen's are linked. The  $\text{PF}_6^-$  ions also lie on hydrophilic sites and are linked to en and water molecules by hydrogen bonds. Thus  $\pi \cdots \pi$  interactions and hydrogen

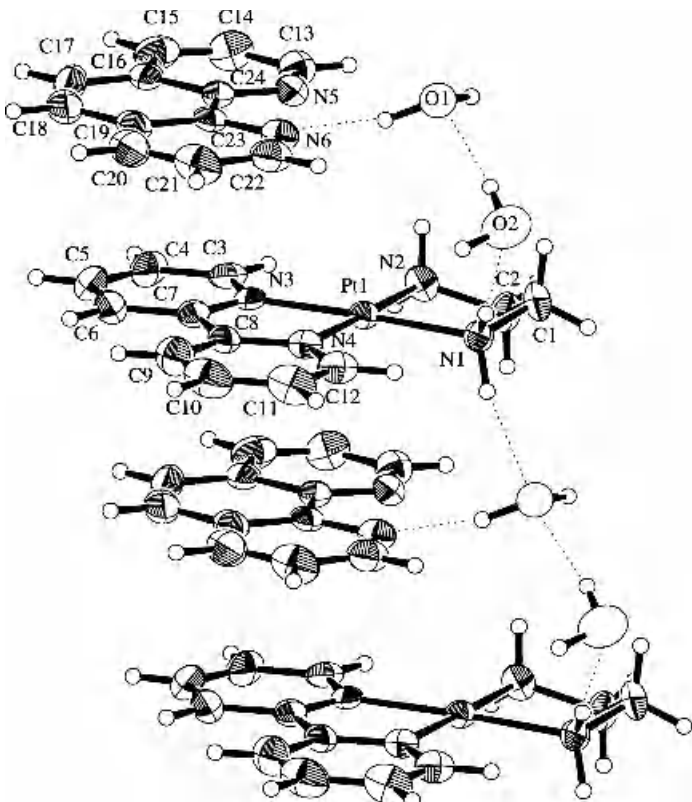


Figure 10.9. Integrated stack in the crystal of  $[\text{Pt}(\text{en})(\text{bpy})](\text{PF}_6)_2 \cdot \text{phen} \cdot 2\text{H}_2\text{O}$ .<sup>15</sup>

bonds cooperatively stabilize the stack. Interestingly, the inclusion of free phen is completely selective. From a mixed solution containing equimolar amounts of  $[\text{Pt}(\text{en})(\text{L})](\text{PF}_6)_2$ , phen, and bpy, only the composite crystal including phen,  $[\text{Pt}(\text{en})(\text{L})](\text{PF}_6)_2 \cdot \text{phen} \cdot 2\text{H}_2\text{O}$ , was obtained. Also all attempts to make composite crystals of  $[\text{Pt}(\text{en})(\text{L})](\text{PF}_6)_2$  with other small aromatic heterocycles such as bpy, quinoline, phenazine, and adenine resulted in failure. In those cases the original complex salts were just recrystallized. For compounds with more extended  $\pi$ -systems like dipyrido[3,2-d:2',3'-f]quinoxaline (dpq) and dipyrido[3,2-a:2',3'-c]phenazine (dppz), composite crystals with independent stacks of the platinum complex and the aromatic heterocycle were obtained, as shown in Figure 10.10, for the dpq co-crystal. Thus, the size and shape of the molecular  $\pi$ -systems could be the main factor influencing the selective formation of the integrated stacks: neither smaller nor bigger  $\pi$ -systems than phen co-crystallised with the  $[\text{Pt}(\text{en})(\text{L})]$

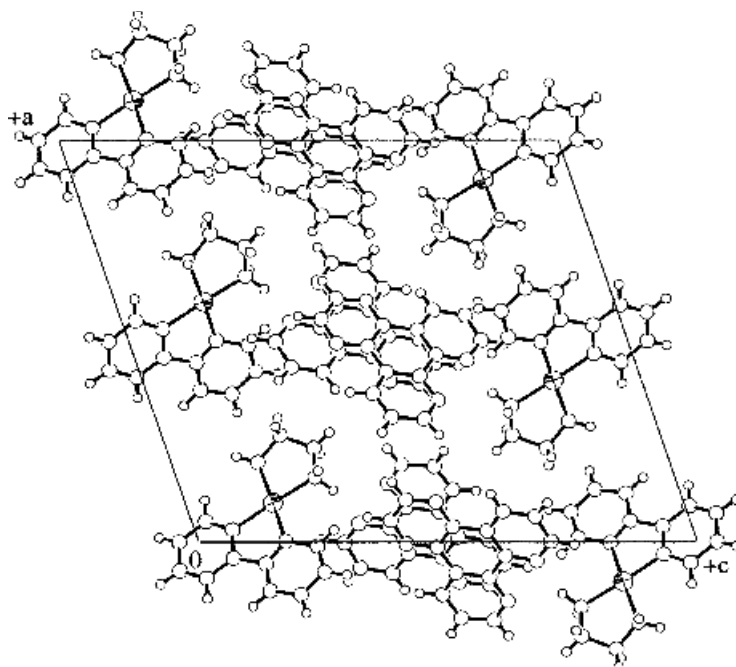


Figure 10.10. Packing structure of  $[\text{Pt}(\text{en})(\text{bpy})](\text{PF}_6)_2 \cdot \text{dpq}$  viewed down the  $b$  axis.

complex and structural isomers of phen with a linear condensed ring, such as phenazine and acridine, were also excluded. As mentioned above, hydrogen bonds might be another major factor for the stabilization of the integrated stacks. Compared with bpy, phen is able to build more effective hydrogen bonds with crystalline water because of the higher basicity of phen ( $\text{pK}_a = 4.93(4)$  for phen,  $4.42(3)$  for bpy at  $25^\circ\text{C}$ ,  $0.1\text{ M}$  ionic strength).

In order to expand the inclusion ability of this type of platinum complexes, we have synthesized platinum(II) complexes in which the en ligand has been replaced by the more bulky *RR*-chxn,  $[\text{Pt}(\text{RR-chxn})(\text{L})](\text{PF}_6)_2$  ( $\text{L} = \text{bpy, phen}$ ).<sup>16</sup> These complexes also adopt ladder stacking in the solid state. As shown in Figure 10.11, the complex cations for  $[\text{Pt}(\text{RR-chxn})(\text{phen})](\text{PF}_6)_2$  are arranged to form stacks of phen ligands and the  $\text{PF}_6^-$  ions are located just between the *RR*-chxn ligands. The  $\pi \cdots \pi$  stack in this ladder structure is obviously weak as in the case of  $[\text{Pt}(\text{en})(\text{phen})](\text{PF}_6)_2$  and the interplanar spacing of the  $\pi \cdots \pi$  stack ( $3.66(2)\text{\AA}$ ) is larger than the normal values ( $3.4\text{--}3.6\text{\AA}$ ). Complexes containing the more bulky *RR*-chxn ligand are expected to be able to include bigger molecules or more guests in the crystal lattice because of the larger space between the complexes in the stack compared with that in the stack of complexes containing the en ligand.

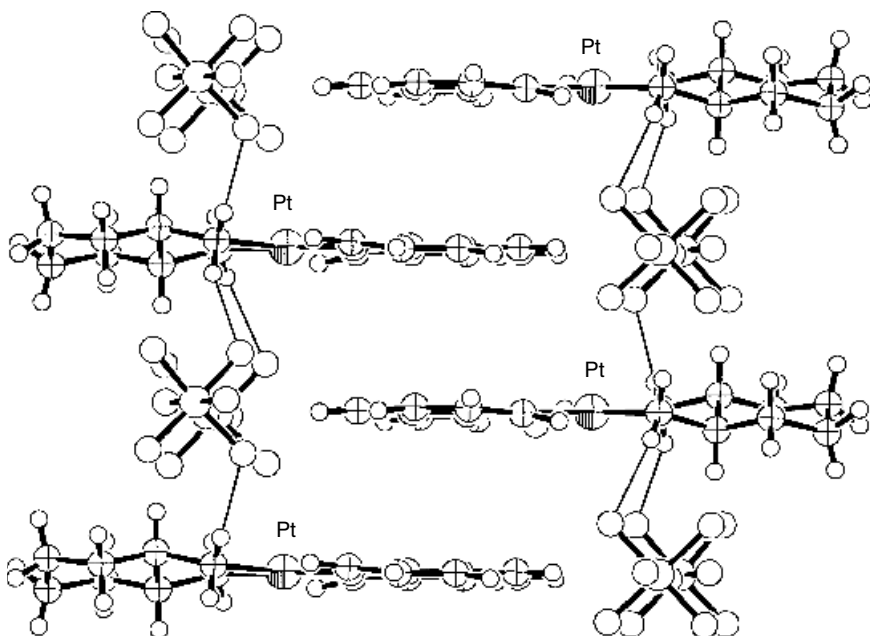


Figure 10.11. The ladder-type stacking of  $[\text{Pt}(\text{RR-chxn})(\text{bpy})](\text{PF}_6)_2$ .<sup>16</sup>

In fact, the 1:3 composite crystal,  $[\text{Pt}(\text{RR-chxn})(\text{bpy})](\text{PF}_6)_2 \cdot 3\text{phen} \cdot 2\text{H}_2\text{O}$ , was obtained on crystallization in the presence of the phen. Interestingly, the crystal contains a 1:2 integrated stack of  $[\text{Pt}(\text{RR-chxn})(\text{bpy})]^{2+}$  and phen, as shown in Figure 10.12. The 1:2  $\pi \cdots \pi$  stack generates large spaces between the RR-chxn ligands and the  $\text{PF}_6^-$  ions successfully fit the spaces. The interplanar spacings in the  $\pi \cdots \pi$  stack (av. 3.35(2) Å) are clearly contracted compared with those for the nonincluded Pt-complex (Figure 10.11). The third phen molecule for  $[\text{Pt}(\text{bpy})(\text{RR-chxn})](\text{PF}_6)_2 \cdot 3\text{phen} \cdot 2\text{H}_2\text{O}$  is located in pairs between the integrated stacks linking them through the hydrogen bonding and the  $\pi - \pi$  interaction. Thus, it has been shown that platinum(II) complexes containing both nonplanar diamine ligands and planar diimine ligands can act as hosts to form interesting composite crystals.

#### IV. DEFORMATION OF THE $\pi$ -SYSTEM OF BIS(1,10-PHENANTHROLINE)PLATINUM(II)

$\pi$ -Conjugated aromatic rings are generally accepted to be planar except for the cases with special molecular structures, such as ball-shaped fullerenes. It has been found, however, that deformation of  $\pi$ -systems also occurs when dictated

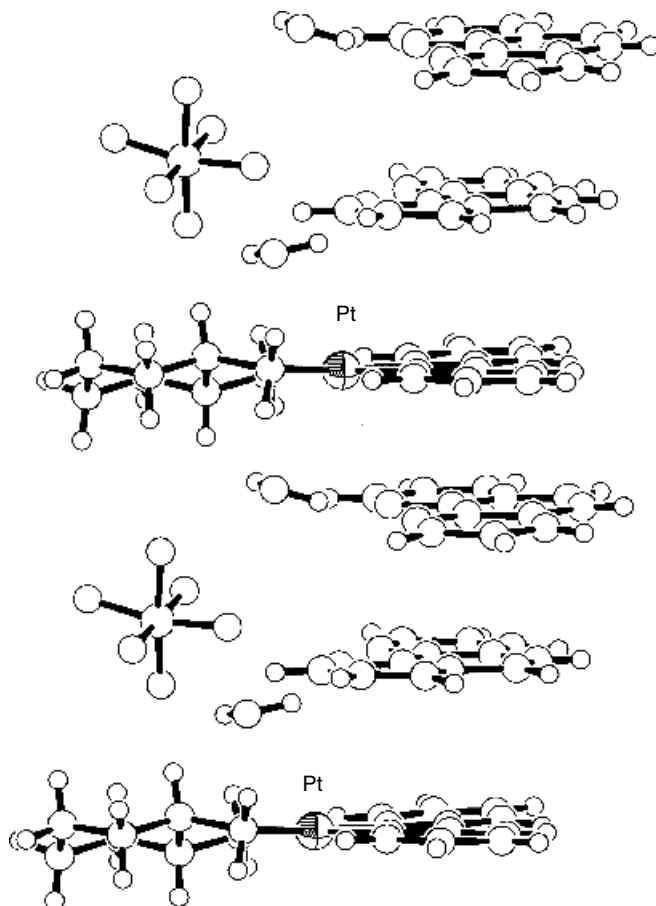


Figure 10.12. The 1:2 integrated stack of  $[\text{Pt}(\text{RR-chxn})(\text{bpy})]^{2+}$  and phen.

by steric constraints. For bis-chelate square-planar complexes or *trans*-bis-chelate octahedral complexes containing aromatic bidentate ligands such as bpy and phen, steric hindrance between the  $\alpha$ -hydrogen atoms of the opposing ligands occurs on coordination, except for complexes involving large metal ions, such as  $\text{Ba}^{2+}$  and  $\text{Sr}^{2+}$ . To avoid the steric hindrance, the complexes are forced to deform.<sup>17</sup> As a result, several types of deformed structures are realized: twist-, bow-, and tilt-conformations, as shown in Figure 10.13. Table 10.1 summarizes the conformations of bis(phen)-type metal complexes determined so far by X-ray crystallography. Complexes containing a rigid fused ring, such as phen, would favor the twist conformation with a deformed coordination plane or

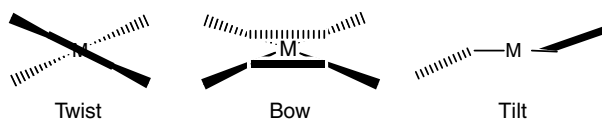


Figure 10.13. Three deformed conformations for bis(phen)-type complexes.

tilt conformations, rather than the bow conformation where two aromatic ligands warp in the opposite directions, especially for the d<sup>8</sup> metal complexes where square-planar coordination is favored. However, it was found that the [Pt(phen)<sub>2</sub>]<sup>2+</sup> complex, which has a ligand with a rigid π-system, can adopt a bow conformation in the solid state if a suitable counter anion is chosen. Figure 10.14 shows the structures of the [Pt(phen)<sub>2</sub>]<sup>2+</sup> cation in the ClO<sub>4</sub><sup>-</sup> and PF<sub>6</sub><sup>-</sup> salts. In the former the cation has the twist conformation, while the bow conformation is found in the latter. To clarify the reason why the bis-phen complex in the PF<sub>6</sub><sup>-</sup> salt takes the bow conformation instead of a twist or tilt conformation, the crystal packing was compared with that of the ClO<sub>4</sub><sup>-</sup> salt. For both salts, the bis-phen complexes are stacked on the phen ligands in the crystals. However, the stacked phen ligands for the PF<sub>6</sub><sup>-</sup> salt are warped in the opposite direction to each other, as shown in Figure 10.15, which seems unfavorable from the viewpoint of the π···π

Table 10.1.

Conformations of Bis(phen)-type Metal Complexes with Coplanar Coordination Geometries

Complex	Conformation	Space Group	M–N / Å	Reference
[Pt(phen) <sub>2</sub> ](PF <sub>6</sub> ) <sub>2</sub>	Bow	C <sub>2</sub> /m	2.038(5)	This work
[Pd(phen) <sub>2</sub> ](PF <sub>6</sub> ) <sub>2</sub>	Bow	C <sub>2</sub> /m	2.050(2)	<sup>24</sup>
[Pt(phen) <sub>2</sub> ](ClO <sub>4</sub> ) <sub>2</sub>	Twist	P <bar{1}< td=""><td>2.042(6)<sub>av</sub></td><td>This work</td></bar{1}<>	2.042(6) <sub>av</sub>	This work
[Pd(phen) <sub>2</sub> ](ClO <sub>4</sub> ) <sub>2</sub>	Twist	I <sub>2</sub> /c	2.059(4), 2.043(4)	<sup>25</sup>
[Hg(phen) <sub>2</sub> ](NO <sub>3</sub> ) <sub>2</sub>	Twist	C <sub>2</sub> /c	2.339(5)	<sup>26</sup>
[Pt(phen) <sub>2</sub> ]Cl <sub>2</sub> ·3H <sub>2</sub> O	Twist	Fddd	2.033(6) <sub>av</sub>	<sup>27</sup>
[Pt(tmphen) <sub>2</sub> ](PF <sub>6</sub> ) <sub>2</sub> ·2bpy	Twist	C <sub>2</sub> /c	2.031(3), 2.039(3)	<sup>24</sup>
<i>trans</i> -[Ru(py) <sub>2</sub> (phen) <sub>2</sub> ](PF <sub>6</sub> ) <sub>2</sub>	Tilt	P <bar{1}< td=""><td>2.096(5), 2.100(5)</td><td><sup>28</sup></td></bar{1}<>	2.096(5), 2.100(5)	<sup>28</sup>
[Sr(OH) <sub>4</sub> (phen) <sub>2</sub> ](ClO <sub>4</sub> ) <sub>2</sub> ·2phen	Planar	P <bar{1}< td=""><td>2.78(1), 2.809(9)</td><td><sup>29</sup></td></bar{1}<>	2.78(1), 2.809(9)	<sup>29</sup>
[Ba(OH) <sub>4</sub> (phen) <sub>2</sub> ](ClO <sub>4</sub> ) <sub>2</sub> ·2phen	Planar	P <bar{1}< td=""><td>2.96(1), 2.96(1)</td><td><sup>29</sup></td></bar{1}<>	2.96(1), 2.96(1)	<sup>29</sup>

Note: tmphen = 3,4,7,8-tetramethyl-1,10-phenanthroline. The suffix av means the averaged value of several data.

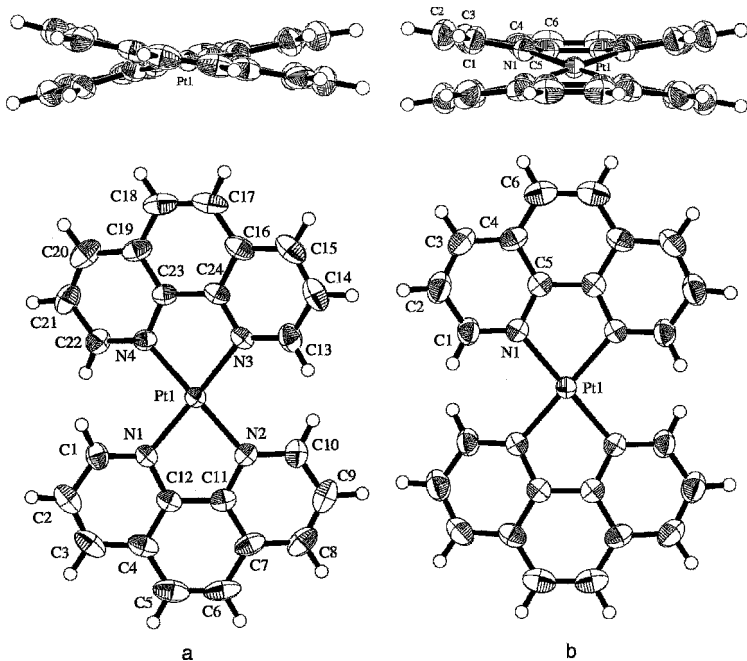


Figure 10.14. Structures of  $[\text{Pt}(\text{phen})_2]^{2+}$  cations for (a) the  $\text{ClO}_4^-$  salt and (b) the  $\text{PF}_6^-$  salts.

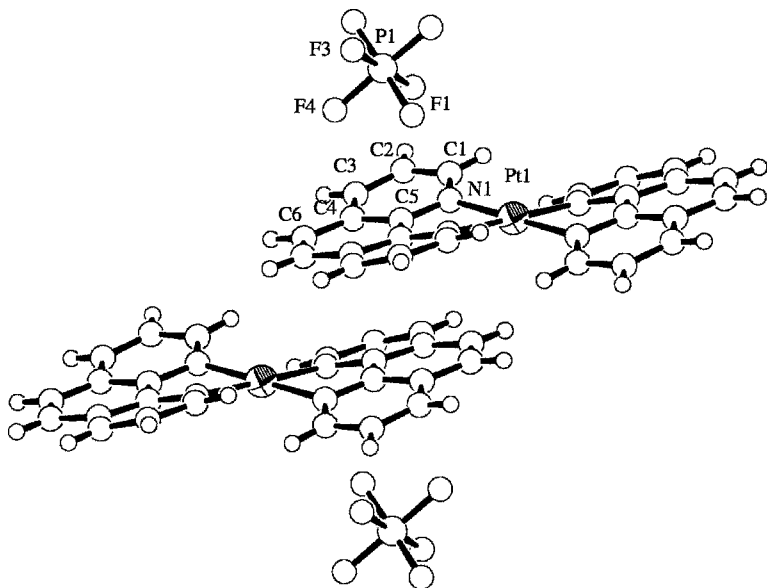


Figure 10.15. The bowed conformation of  $[\text{Pt}(\text{phen})_2]^{2+}$  and the arrangement of the  $\text{PF}_6^-$  anions.

interaction. The bowed deformation of phen may be attributed to the effect of the large spherical  $\text{PF}_6^-$  anions: the phen ligands seem to be bowed so as to fit around the  $\text{PF}_6^-$  anions. On the other hand, the  $\text{ClO}_4^-$  salt does not exhibit such tendency in spite of the similar arrangement of the ions in the crystal. The shape and size of the counter anion might be important factors affecting the conformation of the sterically constrained platinum(II) complexes. Further study including structural and theoretical approaches would be needed to explain the interesting findings of the deformation definitely.

## V. LINKAGE ISOMERISM OF BIS(THIOCYANATO) (2,2'-BIPYRIDINE)PLATINUM(II) AND THE LUMINESCENCE PROPERTIES

Linkage isomerism has been one of the more interesting and significant phenomena observed in coordination chemistry.<sup>18</sup> It often affects not only the molecular structure but also the crystal structure significantly. The thiocyanate ion is a well-known, typical ambidentate ligand. Generally speaking, the softness or hardness of metal ions dictates which form, the *S*-coordinated ( $\text{M-SCN}$ ) or the *N*-coordinated ( $\text{M-NCS}$ ), is favored. For bis(thiocyanato)( $\alpha$ -diimine)platinum(II) complexes,  $[\text{Pt}(\text{SCN})_2(\text{L})]$  ( $\text{L}$  = bpy or substituted bpy), three linkage isomers,  $\text{M-(SCN)}_2$ ,  $\text{M-(SCN)(NCS)}$ , and  $\text{M-(NCS)}_2$ , are possible, excluding cases where SCN ligand acts as binding ligand. The linkage isomerization of these platinum(II) complexes is characterised by their remarkable color change in the solid state. This color change is related to changes in the crystal structure upon isomerization, wherein the intermolecular  $\text{Pt}\cdots\text{Pt}$  interactions are an important factor for coloration and luminescence, as has been demonstrated for several (polypyridine)platinum(II) complexes.<sup>19</sup> Among bis(thiocyanato)( $\alpha$ -diimine)platinum(II) complexes, however, the only crystal structure reported until recently was a low quality one for the red form of  $[\text{Pt}(\text{NCS})_2(\text{bpy})]$ , which was shown to have a columnar stack with a short  $\text{Pt}\cdots\text{Pt}$  distance of  $3.299(2)$  Å.<sup>19</sup> We recently reported the successful isolation and determination of the crystal structures of all three linkage isomers of  $[\text{Pt}(\text{SCN})_2(\text{bpy})]$  as the first reported instance of complete structure determination of all three linkage isomers for bis-thiocyanato type complexes, addition the isomerization behavior of these linkage isomers was investigated.<sup>20</sup>

Figure 10.16 shows the molecular structures of the three linkage isomers,  $[\text{Pt}(\text{SCN})_2(\text{bpy})]$ ,  $[\text{Pt}(\text{SCN})(\text{NCS})(\text{bpy})]$ , and  $[\text{Pt}(\text{NCS})_2(\text{bpy})]$ . Reflecting the differences in the electronic structures of the N and S atoms, the structures of the three isomers are quite different from each other. It is interesting to note that  $[\text{Pt}(\text{SCN})_2(\text{bpy})]$  shows a chiral crystal structure, where the two  $\text{SCN}^-$  ligands are directed to opposite sides of the coordination plane, which results in the molecule having pseudo  $C_2$  symmetry. For  $[\text{Pt}(\text{SCN})(\text{NCS})(\text{bpy})]$ , however, the  $\text{SCN}^-$  ligand is almost in the coordination

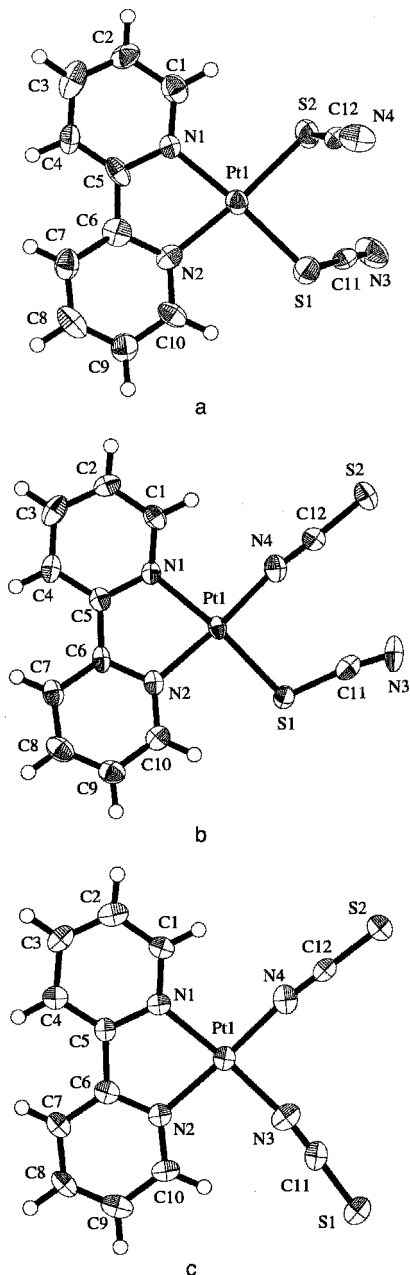


Figure 10.16. Molecular structures of the three linkage isomers: (a)  $[\text{Pt}(\text{SCN})_2(\text{bpy})]$ ; (b)  $[\text{Pt}(\text{SCN})(\text{NCS})(\text{bpy})]$ ; (c)  $[\text{Pt}(\text{NCS})_2(\text{bpy})]$ .<sup>20</sup>

plane and oriented almost parallel to the adjacent  $\text{NCS}^-$  ligand. This geometry probably results from the most compact crystal packing rather than being related to steric effects from the other ligand.  $[\text{Pt}(\text{NCS})_2(\text{bpy})]$  has a completely planar geometry including the two  $\text{NCS}^-$  ligands, because all the atoms lie on a crystallographic mirror plane. The different molecular structures of the isomers affects their packing in the crystals. As shown in Figure 10.17*a*, the non-planar structure of  $[\text{Pt}(\text{SCN})_2(\text{bpy})]$  yields a largely

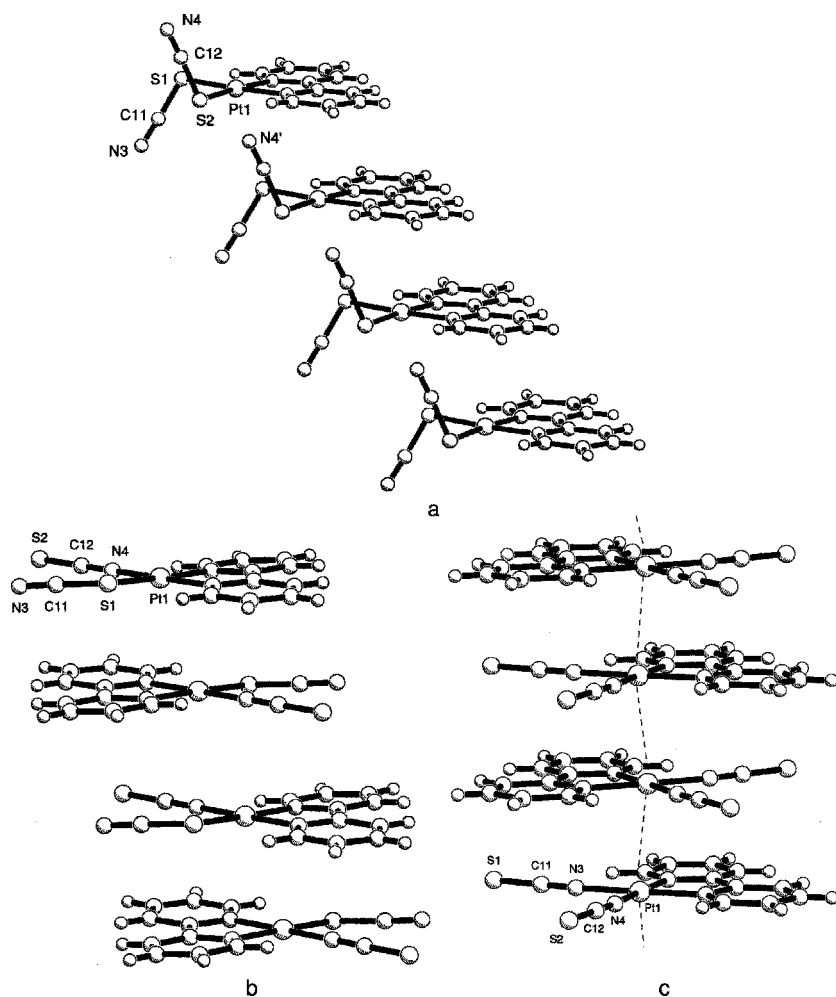


Figure 10.17. Stacking structures of the three isomers: (a)  $[\text{Pt}(\text{SCN})_2(\text{bpy})]$ ; (b)  $[\text{Pt}(\text{SCN})(\text{NCS})(\text{bpy})]$ ; (c)  $[\text{Pt}(\text{NCS})_2(\text{bpy})]$ .<sup>20</sup>

slipped stack with no Pt···Pt interactions. The planar molecules of the other two isomers allow the molecules to stack more vertically. The Pt···Pt distances of the slightly slipped stack for [Pt(SCN)(NCS)(bpy)] also suggest minimal Pt···Pt interactions, as can be seen from Figure 10.17b. On the other hand, in the case of [Pt(NCS)<sub>2</sub>(bpy)], the stacking yields a linear Pt···Pt chain structure with a short Pt···Pt distance (3.237(1) Å), as seen in Figure 10.17c. This structure clearly indicates the presence of Pt···Pt electronic interactions, as in the case of the analogous ( $\alpha$ -diimine) platinum(II) complexes.<sup>11,18</sup>

Of the three isomers, only the red crystals of [Pt(NCS)<sub>2</sub>(bpy)] exhibited intense luminescence with a maximum at 650 nm and a lifetime of 36 ns at room temperature. The spectrum is very similar to those for the red forms of [PtCl<sub>2</sub>(bpy)] and [Pt(CN)<sub>2</sub>(bpy)].<sup>4,12</sup> By analogy, the emission state is reasonably assigned to the <sup>3</sup>MMLCT state, when the linear-chain structure with short Pt···Pt distances is taken into account.

The luminescence features of [Pt(SCN)<sub>2</sub>(bpy)] and [Pt(SCN)(NCS)(bpy)], however, are quite different from that of [Pt(NCS)<sub>2</sub>(bpy)]. These isomers exhibit similar unstructured spectra both in the frozen solution and in the solid state. The spectra for [Pt(SCN)<sub>2</sub>(bpy)] and [Pt(SCN)(NCS)(bpy)] in the solid state can be seen in Figures 10.18 and 10.19, respectively, as spectrum A. The similarity of the spectra for the frozen solution and the crystals indicates that the origin of the emission can be ascribed to the electronic state of the monomeric complex. This is also supported by the crystal structures, since there are no significant Pt···Pt interactions in [Pt(SCN)<sub>2</sub>(bpy)] and [Pt(SCN)(NCS)(bpy)]. Therefore the emission state for [Pt(SCN)<sub>2</sub>(bpy)] and [Pt(SCN)(NCS)(bpy)] can be assigned to the monomeric <sup>3</sup>MLCT state or a charge-transfer state mixed with  $p(S)\rightarrow\pi^*(bpy)$  character, as described for Pt(diimine) complexes containing S-coordinated ligands such as dithiolate.<sup>21</sup>

The linkage isomers can be converted from the kinetically favorable form, [Pt(SCN)<sub>2</sub>(bpy)] to the thermodynamically stable form, [Pt(NCS)<sub>2</sub>(bpy)]. In solution the flip of the thiocyanato ligands occurs stepwise from [Pt(SCN)<sub>2</sub>(bpy)] to [Pt(SCN)(NCS)(bpy)] to [Pt(NCS)<sub>2</sub>(bpy)]. In the solid state, however, direct conversion from [Pt(SCN)<sub>2</sub>(bpy)] to [Pt(NCS)<sub>2</sub>(bpy)] was observed: when neat crystals of [Pt(SCN)(NCS)(bpy)] were kept at 75°C, the solid-state emission spectra measured at 77 K changed as shown in Figure 10.18, indicating the conversion of [Pt(SCN)(NCS)(bpy)] to [Pt(NCS)<sub>2</sub>(bpy)]. On the other hand, the emission spectrum of [Pt(SCN)<sub>2</sub>(bpy)] changed directly to that for [Pt(NCS)<sub>2</sub>(bpy)] without exhibiting the spectrum due to [Pt(SCN)(NCS)(bpy)], as shown in Figure 10.19. Such direct isomerization from [Pt(SCN)<sub>2</sub>(bpy)] to [Pt(NCS)<sub>2</sub>(bpy)] is characteristic of the solid and indicates that [Pt(SCN)(NCS)(bpy)] is not generated or is at least very *transient* in the isomerization process. In the solid state, there are two possibilities for structural transformation: the ligand flips, as is the case in solution, and ligand transfer or exchange. The crystal structures of the three isomers have no close intermolecular contacts between the thiocyanato

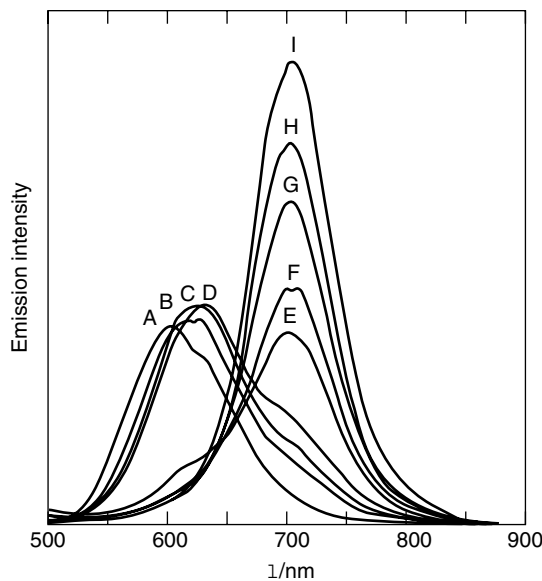


Figure 10.18. Changes in the emission spectrum of  $[\text{Pt}(\text{SCN})(\text{NCS})(\text{bpy})]$  kept at 75°C. The emission spectra ( $\lambda_{\text{ex}} = 340 \text{ nm}$ ) were measured at 77 K after (A) 0 min; (B) 5 min; (C) 10 min; (D) 20 min; (E) 30 min; (F) 40 min; (G) 50 min; (H) 60 min; (I) 70 min.<sup>20</sup>

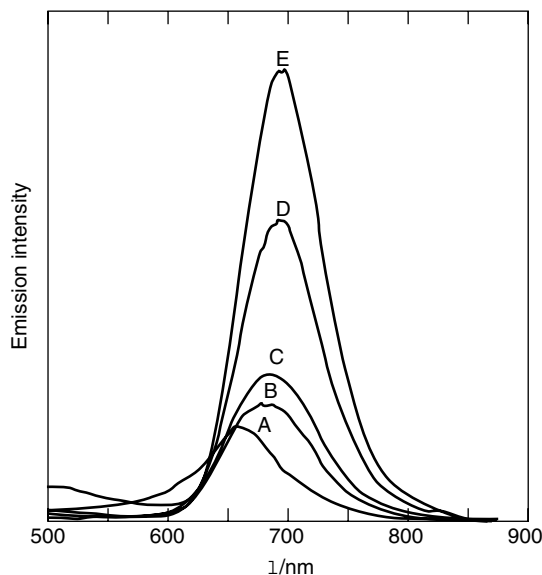


Figure 10.19. Changes in the emission spectrum of  $[\text{Pt}(\text{SCN})_2(\text{bpy})]$  kept at 75°C. The emission spectra ( $\lambda_{\text{ex}} = 40 \text{ nm}$ ) were measured at 77 K: after (A) 0 min; (B) 10 min; (C) 20 min; (D) 30 min; (E) 40 min.<sup>20</sup>

ligands, except for one thiocyanato ligand in the crystal of  $[\text{Pt}(\text{SCN})_2(\text{bpy})]$  which is found to be oriented toward the S atom of a  $\text{SCN}^-$  ligand in an adjacent molecule, as shown in Figure 10.17a ( $\text{S}2\cdots\text{N}4' = 3.83(2)\text{\AA}$ ). The arrangement, however, does not suggest the possibility of concerted ligand transfer of two  $\text{SCN}^-$  ligands in the complex. The flip of the ligands seems much more likely in this arrangement. Thus, isomerization in the solid state presumably occurs by the correlative flip of the ligand, which induces the crystal structure transformation.

## VI. CONCLUDING REMARKS

Platinum(II) complexes are very interesting from the viewpoint of the diversity of the crystal structures and the dramatic variation in color and luminescence in the solid state. Except for above-mentioned examples, we have also synthesized a dinuclear (bipyridine)platinum(II) complex, which exhibits vapor-induced luminescence switching, and amphiphilic platinum(II) complexes with long-alkyl chains.<sup>22,23</sup> In addition, much attention has recently been focused on platinum complexes, as well as other related heavy-metal complexes, as promising light-emitting materials. The development of new luminescent platinum complexes is a continuing important subject.

## REFERENCES

1. Thomas, T. W.; Underhill, A. E. *Chem. Soc. Rev.* **1972**, *1*, 99–120.
2. Gliemann, G.; Yersin, H. *Structure and Bonding* **1985**, *62*, 87–153.
3. Herber R. H.; Croft, M.; Coyer, M. J.; Bilash, B.; Sahiner, A. *Inorg. Chem.* **1994**, *33*, 2422–2426.
4. Houlding, V. H.; Miskowski, V. M. *Coord. Chem. Rev.* **1991**, *111*, 145–152.
5. Connick, W. B.; Henling, L. M.; Marsh, R. E. *Acta Crystallogr.* **1996**, *B52*, 817–822.
6. Che, C.-M.; He, L.-Y.; Poon, C.-K.; Mak, T. C. W. *Inorg. Chem.* **1989**, *28*, 3081–3083.
7. Biedermann, J.; Wallfahrer, M.; Gliemann, G. *J. Lumin.* **1987**, *37*, 323–329.
8. Kato, M.; Sasano, K.; Kosuge, C.; Yamazaki, M.; Yano, S.; Kimura, M. *Inorg. Chem.* **1996**, *35*, 116–123.
9. Day, P. J. *Am. Chem. Soc.* **1974**, *97*, 1588–1589.
10. Bielli, E.; Gidney, P. M.; Gillard, R. D.; Heaton, B. T. *J. Chem. Soc., Dalton* **1974**, 2133–2139.
11. Kishi, S.; Kato, M. *Mol. Cryst. Liq. Cryst.* **2002**, *379*, 303–308.
12. Kato, M.; Kosuge, C.; Morii, K.; Ahn, J. S.; Kitagawa, H.; Mitani, T.; Matsushita, M.; Kato, T.; Yano, S.; Kimura, M. *Inorg. Chem.* **1999**, *38*, 1638–1641.
13. Kato, M.; Kosuge, C.; Yano, S.; Kimura, M. *Acta Crystallogr.* **1997**, *C53*, 838–840.
14. Kato, M.; Takahashi, J. *Acta Crystallogr.* **1999**, *C55*, 1809–1812.
15. Kato, M.; Takahashi, J.; Sugimoto, Y.; Kosuge, C.; Kishi, S.; Yano, S. *J. Chem. Soc., Dalton Trans.* **2001**, 747–752.

16. Koshiyama, T.; Kato, M. *Acta Crystallogr.* **2003**, C59, m446–m449.
17. Hazell, A.; Simonsen, O.; Wernberg, O. *Acta Crystallogr.* **1986**, C42, 1707–1711.
18. Burmeister, J. L. *Coord. Chem. Rev.* **1990**, 105, 77–133.
19. Connick, W. B.; Marsh, R. E.; Schaefer, W. P.; Gray, H. B. *Inorg. Chem.* **1997**, 36, 913–922.
20. Kishi, S.; Kato, M. *Inorg. Chem.* **2003**, 42, 8728–8734.
21. Cummings, S. D.; Eisenberg, R. *J. Am. Chem. Soc.* **1996**, 118, 1949–1960.
22. Kato, M.; Omura, A.; Toshikawa, A.; Kishi, S.; Sugimoto, Y. *Angew. Chem. Int. Ed. Engl.* **2002**, 41, 3183–3185.
23. Kato, M.; Ikemori, M. *Acta Crystallogr.* **2003**, C59, m25–m26.
24. Geremia, S.; Randaccio, L.; Mestroni, G.; Milani, B. *J. Chem. Soc., Dalton Trans.* **1992**, 2117–2118.
25. Rund, J. V.; Hazell, A. C. *Acta Crystallogr.* **1980**, B36, 3103–3105.
26. Grdenić, D.; Kamenar, B.; Hergold-Brundić, A. *Cryst. Struct. Commun.* **1978**, 7, 245–250.
27. Hazell, A.; Mukhopadhyay, A. *Acta Crystallogr.* **1980**, B36, 1647–1649.
28. Bonneson, P.; Walsh, J. L.; Pennington, W. T.; Cordes, A. W.; Durham, B. *Inorg. Chem.* **1983**, 22, 1761–1765.
29. Smith, G.; O'Reilly, E. J.; Kennard, C. H. L.; White, A. H. *J. Chem. Soc., Dalton Trans.* **1977**, 1184–1190.

# SUBJECT INDEX

- Absolute configurations, chiral auxiliaries:  
alcohol resolution, 186–189  
asymmetric syntheses, 182  
carboxylic acid applications, 183–186  
methodology for determination and evaluation,  
178–180  
racemate resolution, 180–182
- Acetone, photodecarbonylation reactions, 217–218
- Acetylcholine esterase (AchE), three-dimensional  
structure, CH/π hydrogen bonds, 286–287
- Achiral molecules:  
chiral conformers, 13–20  
second harmonic generation properties, 171–173
- Acrylic acid, conformational isomer separation,  
6–10
- Acyclic peptides, CH/π hydrogen bonds, 271–274
- Acyloin, HCl-additions with rearrangement,  
314–315
- Acyl radical fragment, photodecarbonylation,  
207–208
- Albicar compounds, homo- and heterochiral crystals,  
engineering methodology, 125–127
- Alcohols:  
resolution:  
camphorsultam dichlorophthalic analysis,  
189–200  
chiral auxiliary molecular design, 186–189  
thermal solid state reactions, nucleophilic  
substitutions, 316–319
- α-Alkyl ketones, photoreactivity, 223–228
- Alkyl groups, cyclopentanone reactivity, 221–223
- α-Networks:  
active unsymmetrical urea, second harmonic  
generation design, 165–173  
pyrimidinone hydrogen bonding, 147
- Amines:  
chiral auxiliaries, alcohol resolution, 188–189  
homo- and heterochiral crystals, racemic  
conglomerate vs. compound, 106–110
- Amino acids, solid state geometrical isomerizations,  
333–341
- Ammonium salts, homo- and heterochiral crystals,  
racemic compounds vs. conglomerates,  
112–114
- Androst-4-ene-3,6,17-trione, pyrimidinone hydrogen  
bonding, 141–143
- 1-(4-Anisyl)-1-phenylethene, linear dimerizations  
and polymerizations, 342–345
- Anomalous racemate, chiral molecules, basic  
properties, 83
- Antimony complexes, CH/π hydrogen bonds,  
277, 279
- Anti-parallel arrangement, N-aryl-pyrimidinone salts,  
C–H···O chain synthon, 147, 149
- Arylepoxydes, reduction reactions, 326
- N-Aryl-2(1H)-pyrimidinone, homo- and heterochiral  
crystals, racemic conglomerate vs. compound,  
104–105
- N-Arylpyrimidinones:  
C–H···O chain synthon, 147–156  
hydrogen bonding mimicry, 143–147  
two-dimensional polar layer arrangement, assembly  
models, 162–165
- Asymmetric syntheses, chiral products, 182
- Atomic-force microscopy (AFM), thermal solid state  
reactions, 305–306
- Atropisomeric compounds, carboxylic acid resolution,  
185–186
- Aziridine compounds, cycloadditions, 325
- Azobenzenes:  
central bond shortening, torsional motion, 36–38  
conformational changes, 38–40
- Ball-milling techniques, Wittig reactions, 322
- 1-Benzazocinone derivative, CH/π hydrogen bonds,  
260–261
- Benzene ring substitution:  
benzylic stabilization, stereoelectronic effects,  
230–231  
chiral crystal conformational isomers, 14–20  
stilbene-type molecules, central bond shortening,  
torsional motion, 34–38
- Benzothiopyran derivative, CH/π hydrogen bonds,  
263, 265
- Benzyl alcohols, resolution, 196–200
- Benzylammonium salt, homo- and heterochiral  
crystals, transformation mechanisms,  
117–119
- N-Benzylideneanilines:  
central bond shortening, torsional motion, 36–38  
conformational change, 40  
“β-phenyl effect,” CH/π hydrogen bonds, 281–283

- Bijvoet method:**  
 absolute configuration of chiral compounds, 178–179  
 alcohol resolution, 199–200
- Bimolecular reactions, crystal photodecarbonylation,** 212
- 1,1'-Binaphthyl, homo- and heterochiral crystals:**  
 racemic compounds vs. conglomerates, 90–99  
 transformation mechanisms, 114–121
- Binaphthyl, solid state geometric isomerizations,** 336–341
- Biopolymers:**  
 $\text{CH}/\pi$  hydrogen bonds, database studies, 291–292  
 three-dimensional structure,  $\text{CH}/\pi$  hydrogen bonds, 283–290  
 nucleic acids, 287–290  
 proteins, 283–287
- Biphenyl-2,2'-dicarboxylic acid, irradiation,** 23–24
- 1,4-Biradical intermediates (BR2),**  
 photodecarbonylation in crystals, 210
- Bisallenes, thermal rearrangements,** 331–332
- 2,2'-(Bisamino)diphenyl ether,  $\text{CH}/\pi$  hydrogen bonds,** 263, 267
- 3,4-Bis(diphenylmethylene)-*N*-methylsuccinamide molecule, chiral arrangement,** 18–20
- 1,3-Bis-(ethylenedithioxy)-2-indanone, electron transfer quenching,** 235–236
- 2,3-Bis-fluoren-9-ylidenesuccinic acid, homo- and heterochiral crystals, racemic conglomerate vs. compound,** 101
- 1,1'-Bis-2-naphthol, homo- and heterochiral crystals, transformation mechanisms,** 121
- Bis(ethylenediamine)glycinatocobalt (III) salts, homo- and heterochiral crystals, racemic compounds vs. conglomerates,** 107
- Bis(1,10-phenanthroline)platinum(II),  $\pi$ -system deformation,** 363–367
- Bis(thiocyanato)(2,2'-bipyridine)platinum(II), linkage isomerism and luminescence,** 367–372
- B3LYP/6-31G methods, alkyl- and carbonyl-ketone reactivity,** 225–228
- Bond dissociation energies (BDE):**  
 alkyl- and carbonyl-ketone reactivity, 226–228  
 stereospecific syntheses, tertiary and quaternary centers, 240–243  
 ketone radicals,  $\alpha$ -substituents, 247
- Bond lengths, stilbene-type molecules:**  
 central bond shortening, torsional motion, 32–38  
 torsional vibration, pedal motion and disorder, 44–45
- Boron hydrides, reduction reactions,** 327
- Boroxine framework, design,** 171–173
- Bowed deformation, bis(1,10-phenanthroline)platinum (II)  $\pi$ -system,** 365–367
- Branched chain organic compounds, homo- and heterochiral crystals, racemic compounds vs. conglomerates,** 98–99
- Bridging auxiliaries, porphyrin/metalloporphyrin metal-ligand coordination, carboxyporphyrin building blocks, polymeric array tailoring,** 70–72
- Bromine compounds:**  
 ethynyl-nitro urea polar crystals, 169–173  
 thermal solid state reactions, halogen-additions, 307–310
- Bromo-nitro urea, second harmonic generation properties,** 170–173
- (4-Bromophenyl)(phenyl-1,2,3,4,5,6-13C6)methanol, alcohol resolution,** 194–200
- Brucine complex, component separation,** 5–6
- Butatriene, cycloadditions,** 323–325
- Cage effects, photodecarbonylation in crystals,** 208–209  
 stereospecificity and scale up, 236–240
- Cambridge Structural Database (CSD),  $\text{CH}/\pi$  hydrogen bonds, small molecular weight compounds,** 290–291
- Camphanic acid, alcohol resolution,** 194–200
- Camphepane compounds:**  
 hydrohalogen additions, 311  
 thermal rearrangements, 330–332
- Camphorsultam dichlorophthalic acid:**  
 alcohol resolution and x-ray crystallographic analysis, 189–200
- chiral auxiliaries:**  
 alcohol resolution, 186–189  
 carboxylic acid applications, 183–186  
 HPLC resolution and x-ray crystallography, alcohol analysis, 189–207
- Carbenes, cycloadditions,** 325
- Carbohydrate-binding protein/carbohydrate complexes, three-dimensional structure,  $\text{CH}/\pi$  hydrogen bonds,** 284–287
- 2-Carbomethoxy-4-cyano-2,4-diphenyl-3-butanon, diastereo- and enantiospecific syntheses,** 240–243
- Carbon-carbon bonds, stilbene-type molecules, central bond shortening,** 32–38
- C–H bond dissociation, phenyl-substituted cyclohexanones, reactivity ranking,** 220–221
- C–H...Br bonds, two-dimensional polar layer arrangement,** 159–162
- C–H...F bonds, two-dimensional polar layer arrangement,** 162
- C–H...O bonds:**  
 active unsymmetrical ureas, second harmonic generation, 170–173  
 N-arylpyrimidinone salts, chain synthon, 147–156  
 pyrimidinone hydrogen bonding, 139–143  
 proof of concept, 143–147  
 two-dimensional polar layer arrangement, 158–162  
 assembly models, 162–165
- CH/ $\pi$  hydrogen bond:**  
 basic conformation, 256–257  
 biopolymer database studies, 291–292  
 chemical characteristics, 257–258  
 database studies, 290–292
- interligand interactions:**  
 coordination compounds, 275  
 enantioselective catalytic reactions, 279–283  
 transition metal compounds, 275–279

- organic compound conformation, 258–259
- peptides, 260–274
  - acyclic peptides, 271–274
  - cyclic peptides, 269–271
- small molecular weight compounds, 290–291
- three-dimensional biopolymer structures, 283–290
  - nucleic acids, 287–290
  - proteins, 283–287
- Carbon-phosphorus bonds, stilbene-type molecules: central bond shortening, 34–38 torsional vibration, pedal motion and disorder, 44–45
- $\alpha$ -Carbonyl ketones, photoreactivity, 223–228
- Carbonyl condensation reactions, thermal solid state reactions, 319–321
- Carboxylic acid:
  - conformal isomer separation, 8–10
  - HPLC resolution and X-ray crystallography, chiral auxiliary, 182–186
- Carboxypeptidase/inhibitor complex, three-dimensional structure, CH/ $\pi$  hydrogen bonds, 284–287
- Carboxyporphyrin building blocks, polymeric array tailoring, 67–72
- Cavity dimensions:
  - crystal stereochemistry, 210–212
  - porphyrins/metalloporphyrin supramolecular networks:
  - open networks, weak interactions, 53–54
  - tessellated extended networks, hydrogen bonds, 57–60
- Central bond shortening, stilbene-type molecules, 32–38
- Central metal atoms, homo- and heterochiral crystals, racemic conglomerate *vs.* compound, 106–110
- Centrosymmetric crystals:
  - homo- and heterochiral crystals, transformation mechanisms, 119–121
  - two-dimensional polar layer arrangement, assembly models, 164–165
- Chain formation:
  - porphyrin polymerization, metal-ligand coordination, 60–64
  - porphyrins/metalloporphyrin supramolecular networks, tessellated extended networks, hydrogen bonds, 56–60
- Chalcones:
  - cycloadditions, 325
  - thermal solid state reactions, halogen additions, 308–310
- Channel-type complex, conformal isomer separation, 6–10
- Chiral auxiliaries:
  - absolute configurations:
    - basic principles, 177–178
    - methodologies, 178–180
  - asymmetric syntheses, 182
  - HPLC resolution and X-ray crystallography: camphorsultam dichlorophthalic analysis, 189–200
- carboxylic acid applications, 182–186
- molecular design for alcohol analysis, 186–189
- racemate resolution, 180–182
- Chiral stationary phase chromatography, homo- and heterochiral crystals, recognition of, 88–89
- Chiral dichlorophthalic acid, alcohol resolution, 189–200
- Chiral molecules. *See also* Heterochiral crystallization; Homochiral crystallization
  - achiral molecules, conformers, 13–20
  - basic properties, 83
  - two-dimensional polar layer arrangement, 156–162
- Chiral N/O-acetals, solid state geometrical isomerizations, 334
- Chiral quasi-racemages, basic properties, 83
- Chiral syntheses, evaluation and methodology, 180–182
- Chirodichroism, homo- and heterochiral crystals, racemic compounds *vs.* conglomerates, 93–99
- Chloride salts, C–H..O chain synthon, 156
- Chlorine compounds, thermal solid state reactions, halogen-additions, 307–310
- Chloro-methyl exchange, pyrimidinone hydrogen bonding, 147–148
- 3-(3-Chlorophenyl)-3-hydroxypropanoic acid, homo- and heterochiral crystals, transformation mechanisms, 117
- Cholesterylacetate, hydrohalogen additions, 311
- Cholesteroleate, hydrohalogen-additions, 311
- Chromium compounds, solid state geometric isomerizations, 339–341
- Cinnamic acid, thermal solid state reactions:
  - halogen additions, 307–310
  - hydrohalogen additions, 311–312
- Circular dichroism (CD):
  - exciton chirality method, absolute configuration of chiral compounds, 178–179
  - thermal solid state reactions, 306
- Cis*-1,2-Dibenzoylethylenes, thermal solid-state reactions, 333
- Cis*-2,6-di(1-cyhexenyl)cyclohexanone,  $\gamma$ -hydrogen abstraction, ultrafast reactions, 231–232
- Cis*-1,4-dihydro-4-tritylpiphenyl, CH/ $\pi$  hydrogen bonds, 262
- Cis*-related structures, porphyrins/metalloporphyrin supramolecular networks, tessellated extended networks, hydrogen bonds, 55–60
- Cis*-stilbenes, thermal solid-state reactions, 333
- $\alpha$ -Cleavage:
  - benzyllic stabilization, stereoelectronic effects, 228–231
  - $\gamma$ -hydrogen abstraction, ultrafast reactions, 231–232
  - photodecarbonylation, 208
  - stereospecificity and scale up, 237–240
- Cobalt compounds:
  - CH/ $\pi$  hydrogen bonds:
    - coordination complexes, 275
    - transition metals, 277–279
  - homo- and heterochiral crystals, racemic compounds *vs.* conglomerates, 106–110
  - porphyrins/metalloporphyrins, metal-ligand coordination, carboxyporphyrin building blocks, polymeric array tailoring, 72

- Cobalt compounds (*continued*)  
 protonations, 330  
 solid state geometric isomerizations, 339–341
- Concerted mechanisms, porphyrins/metalloporphyrin supramolecular assemblies, 74–77
- Condensation reactions, thermal solid state reactions, carbonyl compounds, 319–321
- Conformational isomers:  
 achiral molecules, chiral conformers, 13–20  
 bis(1,10-phenanthroline)platinum(II)  $\pi$ -system deformation, 364–367  
 crystal reaction engineering, 214–215  
 protonations, 330  
 separation, 6–10  
   cyclohexane derivatives, 10–13  
 stereochemistry control, 20–28  
 stilbene-type compounds, torsional motion, 38–40
- Conglomerate crystallization, second harmonic generation properties, 171–173
- Cooperative interaction mechanisms, hydrogen bonds, tessellated extended networks, hydrogen bonds, 55–60
- Coordination compounds:  
 bis(1,10-phenanthroline)platinum(II)  $\pi$ -system deformation, 364–367  
 $\text{CH}/\pi$  hydrogen bonds, interligand interactions, 275  
 solid state geometric isomerizations, 341
- Coordination synthons, porphyrin supramolecular chemistry:  
 concerted mechanisms, 74–77  
 polymeric array tailoring, 69–72
- Copper compounds:  
 $\text{CH}/\pi$  hydrogen bonds, 275  
 enantioselective catalytic reactions, 282–283  
 porphyrins/metalloporphyrins, metal-ligand coordination:  
 carboxyporphyrin building blocks, 69–72  
 pyridylporphyrin building blocks, polymeric array tailoring, 64–67
- Corycavine, solid state geometric isomerizations, 335
- Cotton effect:  
 chiral crystal conformational isomers, 16–20  
 thermal solid state reactions, 306
- Coumarin derivatives, photoirradiation, 26–28
- Counter ions, homo- and heterochiral crystals, racemic conglomerate *vs.* compound, 106–110
- Covalently bound substituents:  
 homo- and heterochiral crystals, racemic compounds *vs.* conglomerates, 110–114  
 stilbene-type molecules, central bond shortening, 32–38
- Crown ethers, porphyrin/metalloporphyrin supramolecular assembly, concerted mechanisms, 75–77
- Crystalline structures:  
 homo- and heterochirality:  
   engineering principles, 121–127  
 racemic conglomerate *vs.* compound:  
   counter ions, central metal atoms and ligands, 106–110  
   covalent substituents, 110–114  
   different compositions, 99–114
- identical composition, 90–99  
 solvates and host-guest inclusion compounds, 100–105
- recognition mechanisms, 87–89
- research background, 81–83
- space groups of symmetry, 83–87
- “switching” between, 89–114
- transformations, 114–121
- light access, 248
- photodecarbonylation reactions:  
 benzylic stabilization, stereoelectronic effects, 228–231  
 diastere- and enantiospecific syntheses, vicinal tertiary and quaternary centers, 240–243  
 electron transfer quenching, 235–236  
 ( $\pm$ )-herbertenolide synthesis, 243–246  
 historical background, 208–210  
 $\gamma$ -hydrogen abstraction, ultrafast competing reactions, 231–232  
 ketone properties, 246–248  
 $\beta$ -phenyl group quenching, 232–235  
 research background, 207–208  
 stereospecificity and scale up, 236–240
- solid state reactions:  
 molecular information, 215–228  
 research background, 206–207  
 thermochemical parameters, 217–218
- stereospecific reactions:  
 cyclopentanones, phenyl and alkyl groups, 221–223  
 energetic considerations, 212–214  
 ketones, 223–228  
 molecularity, 212  
 molecular structure and engineering of, 214–215  
 phenyl-substituted cyclohexanones, 219–221  
 $\alpha$ -substituents, 219–221  
 topochemical postulate and reaction cavity concepts, 210–212  
 supramolecular chemistry, 137–138  
 porphyrin/metalloporphyrin networks, 51–52
- Cyanohydrin:  
 chiral auxiliaries, alcohol resolution, 188–189  
 component separation, 5–6
- Cyano substituents, porphyrins/metalloporphyrin molecular layers, 52–54
- Cyclic peptides,  $\text{CH}/\pi$  hydrogen bonds, 269–271
- Cycloaddition reactions, thermal solid state structures, 323–325
- Cyclodimerization, cycloaddition reactions, 324–325
- Cyclohexane derivatives:  
 conformal isomer separation, 10–13  
 phenyl-substituted cyclohexanones, reactivity ranking, 219–221  
 quenching reactions,  $\beta$ -phenyl groups, 232–235  
 Wittig reactions, 321–322
- Cycloocta-2,4,6-trien-1-one, stereochemistry control, 20–21
- Cyclopentanes:  
 ketone decarbonylation, ( $\pm$ )-herbertenolide synthesis, 246

- photodecarbonylation in crystals, stereospecificity and scale up, 237–240  
quenching reactions,  $\beta$ -phenyl groups, 232–235
- Cyclopentanones, phenyl and alkyl effects, reactivity ranking, 221–223
- Desoxycholic acid, oxidation, 329–330
- Detection and visualization techniques, homo- and heterochiral crystals, 87–89
- Diacetylenes, linear dimerizations and polymerizations, 344–345
- Diamondoid networks:  
homo- and heterochiral crystals, 125–127  
two-dimensional polar layer arrangement, 157–162
- Diastereomorphism:  
chiral molecules, 83  
 $\text{CH}/\pi$  hydrogen bonds, enantioselective catalytic reactions, 281–283  
homo- and heterochiral crystals:  
enantiomorphous space groups, 84–87  
racemic compounds vs. conglomerates, 94–99  
spiral structures, 122
- Diastereospecificity, vicinal tertiary and quaternary centers, 240–243
- Diazine ligands, homo- and heterochiral crystals, racemic compounds vs. conglomerates, 108–109
- 2,3;6,7-Dibenzobicyclo[3.3.1]nona-2,6-diene-4,8-dione, homo- and heterochiral crystals, transformation mechanisms, 115–121
- Dibenzodiazocine esters,  $\text{CH}/\pi$  hydrogen bonds, 262–263
- 1,3-Dibromo-2,4,6-trinitrobenzene, hexagonal network, 171–173
- 1,2-Dichloroethane, conformational isomer separation, 6–10
- Dicyano(2,2'-bipyridine)platinum(II), thermochromism and vapochromism, 352–359
- Diels-Alder adducts:  
endoselectivity, 324–325  
solid state geometric isomerizations, 334–335  
thermal rearrangements, 330–332
- Diene compounds, linear dimerizations and polymerizations, 342
- Digermene compounds, oxidation, 329
- $\alpha$ -Diimine-platinum(II) complexes, structural design, 352
- Diketones, homo- and heterochiral crystals, transformation mechanisms, 116–121
- p*-Dimethylaminophenyl *N*-methyl-*N*-(*p*-nitrophenylsulfonylmethyl)carbamate 1,  $\text{CH}/\pi$  hydrogen bonds, 260
- Dioxolanes, oxidation, 329–330
- 1,2-Diphenylethanates:  
central bond shortening, torsional motion, 36–38  
conformational change, 40
- Diphenylmethanol, alcohol resolution, 191–200
- Dipolar attractions, porphyrins/metalloporphyrin open assemblies, weak interactions, 52–54
- Dipyrido[3,2-*a*:2',3'-*c*f]phenazine (dppz),  $\pi$ -stacking interactions, 361–363
- Dipyrido[3,2-*d*:2',3'-*f*]quinoxaline (dpq),  $\pi$ - $\pi$ -stacking interactions, 361–363
- Direct coordination, porphyrin polymerization, 60–64
- “Discriminator synthon,” active unsymmetrical ureas, second harmonic generation, 170–173
- 1,2-Disaladioxetane, thermal rearrangements, 331–332
- Dissociative reactions:  
crystal stereochemistry, 212–214  
phenyl-substituted cyclohexanones, reactivity ranking, 220–221  
thermochemical parameters, 217–218
- Drug-receptor binding, pyrimidinone hydrogen bonding, 142–143
- Electron spin resonance (ESR) spectroscopy, homo- and heterochiral crystals, racemic compounds vs. conglomerates, 95–99
- Electron transfer, quenching reactions, 235–236
- Eliminations, thermal solid state reactions, 315–316
- Enantiomeric mixtures, homo- and heterochiral crystals, transformation mechanisms, 119–121
- Enantiomer nonsolubility, homo- and heterochiral crystals, 88
- Enantiomeric crystals, racemic compounds vs. conglomerates, 96–99
- Enantiomorphous space groups, homo- and heterochiral crystals, 84–87
- Enantioselective reactions:  
chiral molecules, 83  
 $\text{CH}/\pi$  hydrogen bonds, 279–283  
halogen additions, 310  
Michael-additions, 323  
solid state geometric isomerizations, 335–341  
vicinal tertiary and quaternary centers, 240–243  
Wittig reactions, 321–322
- Endo*-,*endo*-diols, homo- and heterochiral crystals, engineering methodology, 125–127
- Endo*/*exo*-isomerization, solid state geometric isomerizations, 335
- Endoselectivity, cycloaddition reactions, 324–325
- Enkephalins,  $\text{CH}/\pi$  hydrogen bonds, 272–274
- Enolate reactions, solid-solid structures, 322–323
- Enol compounds, component separation, 4–6
- Enthalpy changes, alkyl- and carbonyl-ketone reactivity, 227–228
- Ephedrine, homo- and heterochiral crystals:  
racemic compounds vs. conglomerates, 94–99  
transformation mechanisms, 119–121

- Epoxides, thermal solid state reactions, hydrohalogen additions, 313
- Equatorial conformations, cyclohexane derivatives, 11–12
- Equilibrium mixtures:
- component separation, 2–6
  - stereochemistry control, 20–21
- Erythro-2-amino-1,2-diphenyl ethanol, homo- and heterochiral crystals, racemic compounds *vs.* conglomerates, 106
- Erythro products, Michael- and enolate-additions, 322–323
- Ethane bonds, stilbene-type molecules, central bond shortening, torsional motion, 37–38
- Etherification, thermal solid state reactions, nucleophilic substitutions, 317–319
- Ethylene bonds, stilbene-type molecules, central bond shortening, 33–38
- 4-(4'-Ethynylphenyl)ethynylpyridine, second harmonic generation properties, 171–173
- Ethynyl-nitro urea, tape network design, 169–173
- Excitation wavelengths:
- crystal absorption, 248
  - crystal photodecarbonylation, stereospecificity and scale up, 238–240
- Explosive materials, gas phase reactions, 213–214
- E/Z-isomerizations:
- linear dimerizations and polymerizations, 341–345
  - thermal solid-state reactions, 333–341
- Fecht acid analogue, carboxylic acid resolution, 183–186
- Ferrocenyl complex, thermal solid state reactions, 318–319
- Ferulic acid podand, CH/π hydrogen bonds, 263–264, 268
- “First-order” reaction, linear dimerizations and polymerizations, 344–345
- Flat porphyrin assemblies, open networks, weak interactions, 53–54
- Fluorinated organic compounds, alcohol resolution, 197–200
- Fourier mapping, stilbene-type compounds, conformational changes, 40–41
- Frequency doubling, two-dimensional polar layer arrangement, 164–165
- Gas chromatography, homo- and heterochiral crystals, racemic compounds *vs.* conglomerates, 92–99
- Gas phase reaction, crystal stereochemistry, 212–213
- Gauch-form isomers, conformal separation, 9–10
- Gem*-dialkoxy groups, benzylic stabilization, stereoelectronic effects, 230–231
- Geometrical isomerization, solid state thermal reactions, 333–341
- Gibbs free energy, homo- and heterochiral crystals, transformation mechanisms, 116–121
- Glutamic acid, homo- and heterochiral crystals, racemic compounds *vs.* conglomerates, 99
- Glycoluril, homo- and heterochiral crystals, engineering methodology, 125–127
- Grignard reactions, thermal solid state structures, 323
- Halogen additions, thermal solid state reactions, 306–310
- Halogen compounds:
- homo- and heterochiral crystals, racemic compounds *vs.* conglomerates, 111–114
  - porphyrins/metalloporphyrin molecular layers, weak interactions, 52–54
- Halogenides, thermal solid state reactions, elimination mechanisms, 315–316
- Head-to-tail interactions, linear dimerizations and polymerizations, 342–345
- Heavy metal compounds, solid state geometric isomerizations, 339–341
- Helical structures, two-dimensional polar layer arrangement, 157–162
- “Helical tubulate family,” homo- and heterochiral crystals, racemic conglomerate *vs.* compound, 102–105
- Hemihedry mechanisms, homo- and heterochiral crystals, 88–89
- (±)-Herbertolide synthesis, ketone stereospecific decarbonylation, 243–246
- Herringbone geometry, two-dimensional polar layer arrangement, assembly models, 164–165
- Heterochiral crystallization:
- engineering principles, 121–127
  - racemic conglomerate *vs.* compound:
  - counter ions, central metal atoms and ligands, 106–110
  - covalent substituents, 110–114
  - different compositions, 99–114
  - identical composition, 90–99
  - solvates and host-guest inclusion compounds, 100–105
  - recognition mechanisms, 87–89
  - research background, 81–83
  - space groups of symmetry, 83–87
  - “switching” between hetero- and homochirality, 89–114
  - transformations, 114–121
- Heterogeneous polymers, porphyrins/metalloporphyrins, metal-ligand coordination, 62–64
- Hexameric bracelet, homo- and heterochiral crystals, 122–127
- Hexasubstituted ketones:
- decarbonylation, 206–207
  - stereospecific decarbonylation, 206–207
- Hexa-*tert*-butyl-1,3-dibromotrigermane, homo- and heterochiral crystals, racemic compounds *vs.* conglomerates, 112–114
- Highest occupied molecular orbital (HOMO) calculations, dicyano(2,2'-bipyridine)platinum(II), 355–359
- High-performance liquid chromatography (HPLC): chiral auxiliaries:
- alcohol resolution, 186–189
  - carboxylic acid applications, 182–186

- racemate resolution, chiral syntheses methodology and evaluation, 180–182
- Histidine hydrochloride, homo- and heterochiral crystals, racemic compounds vs. conglomerates, 98–99
- $\text{HNO}_3$ , N-aryl-pyrimidinone salts, C–H···O chain synthon, 149–156
- Hollow porphyrin assemblies, open networks, weak interactions, 53–54
- Homochiral crystallization:
- engineering principles, 121–127
  - racemic conglomerate vs. compound:
    - counter ions, central metal atoms and ligands, 106–110
    - covalent substituents, 110–114
    - different compositions, 99–114
    - identical composition, 90–99
    - solvates and host-guest inclusion compounds, 100–105
  - recognition mechanisms, 87–89
  - research background, 81–83
  - second harmonic generation properties, 171–173
  - space groups of symmetry, 83–87
  - “switching” between hetero- and homochirality, 89–114
  - transformations, 114–121
- Homogeneous polymers:
- linear dimerizations and polymerizations, 343–345
  - porphyrins/metalloporphyrins, metal-ligand coordination, 62–64
- Host-guest inclusion crystallization:
- homo- and heterochiral crystals, racemic compounds vs. conglomerates, 99–114
  - solvates and, 100–105
  - molecule stereochemistry, 20–28
- Human growth hormone-binding protein, three-dimensional structure, CH/π hydrogen bonds, 287–290
- Human plasminogen kringle, three-dimensional structure, CH/π hydrogen bonds, 286–287
- Hydrogen bonds:
- CH/π hydrogen bond:
    - basic conformation, 256–257
    - biopolymer database studies, 291–292
    - chemical characteristics, 257–258
    - database studies, 290–292
    - interligand interactions:
      - coordination compounds, 275
      - enantioselective catalytic reactions, 279–283
      - transition metal compounds, 275–279
    - organic compound conformation, 258–259
    - peptides, 260–274
      - acyclic peptides, 271–274
      - cyclic peptides, 269–271
    - small molecular weight compounds, 290–291
    - three-dimensional biopolymer structures, 283–290
      - nucleic acids, 287–290
      - proteins, 283–287
  - classification, 256
  - conformal isomer separation, 6–10
  - equilibrium mixture compound separation, 2–6
  - homo- and heterochiral crystals, 122–127
- platinum (II)  $\pi$ - $\pi$ -stacking interactions, 360–363
- porphyrin/metalloporphyrin supramolecular assembly, concerted mechanisms, 74–77
- porphyrin polymerization, metal-ligand coordination, 61–64
- porphyrins/metalloporphyrin supramolecular networks:
- open networks, weak interactions, 53–54
  - tessellated extended networks, 54–60
  - supramolecular networks:
    - N-arylpyrimidinone salts, 147–156
    - basic properties, 136–137
    - crystal engineering, 137–138
    - future research issues, 173
    - 2-pyrimidinones, 139–143
      - proof of concept, 143–147
    - two-dimensional polar layer arrangement, 156–162
    - two-dimensional polar layer assembly model, 162–165
    - ureas, 138–139
  - SHG active unsymmetrical design, 165–173
- Hydrogen chloride (HCl):
- N-aryl-pyrimidinone salts, C–H···O chain synthon, 149–156
  - carbonyl condensation reaction, 319–321
  - rearrangement additions, 314–315
- $\gamma$ -Hydrogen abstraction, ultrafast reactions, crystal stereochemistry, 231–232
- Hydrohalogen additions, thermal solid state reactions, 311–313
- Hydrothermal/solvothermal reactions,
- pyridylporphyrin building blocks, polymeric array tailoring, 64–67
- 3-Hydroxy-3-phenylpropionic acids, homo- and heterochiral crystals, racemic compounds vs. conglomerates, 112–113
- Imidazole compounds, component separation, 2–6
- Imidazolium hydrogen mesaconate, two-dimensional polar layer arrangement, 157–162
- Inclusion crystal molecules:
- achiral molecules, chiral conformers, 13–20
  - reduction reactions, 326–327
  - solid state geometric isomerizations, 335–341
  - stereochemistry:
    - basic structures, 1–2
    - selective reactions, 20–28
  - stereoisomer separation, 2–13
  - cyclohexane derivatives, 10–13
  - equilibrium mixture components, 2–6
  - ionone conformational isomers, 6–10
- 2-Indanone derivatives, photodecarbonylation, 208–210
- Interatomic distances, stilbene-type molecules, central bond shortening, 34–38
- Interligand interactions. *See also* Ligand formation
- CH/π hydrogen bond:
    - coordination compounds, 275
    - enantioselective catalytic reactions, 279–283
    - transition metal compounds, 275–279

- Intermolecular interactions:  
 homo- and heterochiral crystals, racemic  
   compounds vs. conglomerates, 112–114  
 platinum(II) crystal structure and functionality:  
   basic principles, 351–352  
   bis(1,10-phenanthroline)  $\pi$ -system, 363–367  
   bis(thiocyanato)(2,2'-bipyridine) linkage  
     isomerism, 367–372  
   dicyano(2,2'-bipyridine) thermochromism/  
     vapochromism, 352–359  
   ladder structures, planar/nonplanar ligands,  
     359–363  
   solid state geometric isomerizations, 337–341
- Internal reference:  
 absolute configuration of chiral compounds, 179  
 carboxylic acid resolution, 183–186
- Interporphyrin organization:  
 porphyrins/metalloporphyrins, metal-ligand  
   coordination:  
     carboxyporphyrin building blocks, polymeric  
       array tailoring, 70  
     organic ligands, 72–74  
     polymerization, 62–64  
     tessellated extended networks, hydrogen bonds,  
       56–60
- Intramolecular interactions:  
 CH/ $\pi$  hydrogen bonds, 267–269  
   coordination compounds, 275  
 stilbene-type molecules, central bond shortening,  
   torsional motion, 37–38
- Iodo nitro urea, second harmonic generation design,  
 168–173
- Ionone isomers:  
 oxidation, 328–330  
 separation, 6–10
- Iridium compounds, hydrohalogen-additions, 311–313
- Iron compounds, porphyrins/metalloporphyrins,  
 metal-ligand coordination, pyridylporphyrin  
   building blocks, polymeric array tailoring,  
     64–67
- Isoleucinamide hydrochloride, *N*-aryl-pyrimidinone  
 salts, C–H...O chain synthon, 153–156
- Isostevio-aniline complex, enantiomorphous space  
 groups, 84–87
- Isotopomeric quasi-racemates (IQR), homo- and  
 heterochiral crystals, 88–89
- Keto diesters, reactivity analysis, 223–228
- Keto-form*, pyridone isolation, 22–27
- Ketones:  
 cyclopentanone reactivity, 222–223  
 photodecarbonylation reactions:  
    $\alpha$ -alkyl-ketones and  $\alpha$ -carbonyl-ketones,  
     223–228  
   benzylidene stabilization, stereoelectronic effects,  
     228–231  
   stereospecific syntheses, vicinal tertiary and  
     quaternary centers, 240–243  
   electron transfer quenching, 235–236  
   ( $\pm$ )-herbartenolide synthesis, 243–246  
   hexasubstituted crystals, 206–207  
   historical background, 208–210
- $\gamma$ -hydrogen abstraction, ultrafast competing  
 reactions, 231–232
- Ketone properties, 246–248
- $\beta$ -phenyl group quenching, 232–235
- research background, 207–208
- stereospecificity and scale up, 236–240
- reduction reactions, 326–327
- triplet energies and yields, 246–247
- Knoevenagel condensations, carbonyl compounds,  
 319–321
- $\beta$ -Lactams:  
 chiral conformers, 16–20  
 intramolecular photoreaction, 23–24  
 2-pyrimidinones, hydrogen bonding, 139–143
- Ladder structures:  
 platinum(II) complexes, 359–363  
 porphyrins/metalloporphyrins, metal-ligand  
   coordination, 62–64
- Lamellar racemic twinning, homo- and heterochiral  
 crystals, enantiomorphous space groups,  
 86–87
- Lattice structures:  
 dicyano(2,2'-bipyridine)platinum(II), 354–359  
 homo- and heterochiral crystals, racemic  
   compounds vs. conglomerates, 99–114  
 reactant/product co-solubility, 248
- Le Chatelier principle, homo- and heterochiral  
 crystals, racemic compounds vs.  
 conglomerates, 99
- Lehn's bracelet structure, homo- and heterochiral  
 crystals, engineering methodology,  
 123–127
- Ligand formation:  
 homo- and heterochiral crystals, racemic  
   conglomerate vs. compound, 106–110  
 platinum(II) complexes, ladder structures,  
 359–363  
 protonations, 330
- Linear-chain platinum complexes, thermochromism  
 and vapochromism, 353–359
- Linear dimerizations, thermal solid state reactions,  
 341–345
- Linkage isomers:  
 bis(thiocyanato)(2,2'-bipyridine)platinum(II),  
 367–372  
 CH/ $\pi$  hydrogen bonds, 277–279
- Luminescence properties:  
 bis(thiocyanato)(2,2'-bipyridine)platinum(II),  
 367–372  
 dicyano(2,2'-bipyridine)platinum(II), 355–359
- Macrocyclic polyethers, CH/ $\pi$  hydrogen bonds, 264,  
 266–267
- Magnesium complexes, Grignard reactions, 323
- Manganese compounds:  
 homo- and heterochiral crystals, racemic  
   compounds vs. conglomerates, 109–110  
 porphyrins/metalloporphyrins, interporphyrin  
   coordination, 72–74
- D-Mannitol, thermal solid state reactions,  
 nucleophilic substitutions, 317–319

- Melting point diagrams, homo- and heterochiral crystals:  
 racemic compounds vs. conglomerates, individual composition, 90–99  
 recognition of, 88–89  
 transformation mechanisms, 114–121
- Metal ion linkers:  
 chiral auxiliaries, alcohol resolution, 186–189  
 polymer array tailoring, porphyrins/  
 metalloporphyrin supramolecular networks, 64–72  
 carboxyporphyrin building blocks, 67–72  
 pyridylporphyrin building blocks, 64–67
- Metal-ligand coordination, porphyrins/  
 metalloporphyrin supramolecular networks, 60–74  
 coordination polymerization, 60–64  
 interporphyrin organic ligands, 72–74  
 metal ion linkers, polymer array tailoring, 64–72  
 carboxyporphyrin building blocks, 67–72  
 pyridylporphyrin building blocks, 64–67
- Metallocarboxylate complexes, porphyrin supramolecular chemistry, polymeric array tailoring, 69–72
- Metal-metal-to-ligand charge transfer (MMLCT), dicyano(2,2'-bipyridine)platinum(II) reactions, 353–359
- (2-Methoxy-2-(1-naphthyl)propionic acid, alcohol resolution, 199–200
- $\alpha$ -Methoxy- $\alpha$ -(trifluoromethyl)phenylacetic acid (MTPA), absolute configuration of chiral compounds, 179
- 4-Methyl-N-(4-methylbenzylidene)aniline, homo- and heterochiral crystals, racemic compounds vs. conglomerates, 93–99
- (4-Methylphenyl)phenylmethanol, alcohol resolution, 191–200
- Michael additions, solid-solid structures, 322–323
- Molecular brick walls, homo- and heterochiral crystals, engineering methodology, 123–127
- Molecularity:  
 crystal photodecarbonylation, 212  
 crystal reaction engineering, 214–215
- Molecular motion. *See also* Torsional motion  
 organic crystals, historical background, 31–32
- Molecular orbital calculations, CH/ $\pi$  hydrogen bonds, 281–283
- Molecular sieve structures:  
 porphyrins/metalloporphyrins, metal-ligand coordination:  
 carboxyporphyrin building blocks, polymeric array tailoring, 69–72  
 polymerization, 62–64  
 tesselated extended networks, hydrogen bonds, 60
- Molecular tweezer conformation, CH/ $\pi$  hydrogen bonds, 262–264
- Molybdenum compounds:  
 CH/ $\pi$  hydrogen bonds, 277  
 solid state geometric isomerizations, 339
- Mosher method, absolute configuration of chiral compounds, 179
- Nanosized structures, pyridylporphyrin building blocks, polymeric array tailoring, 67
- N-[1-(1-Naphthyl)ethylidene]-1-phenyl-2-propylamine, CH/ $\pi$  hydrogen bonds, 260–261
- 2-(1-Naphthyl)propane-1,2-diol, alcohol resolution, 198–200
- Nimodipine, homo- and heterochiral crystals, racemic compounds vs. conglomerates, 90–99
- Ninhydrin:  
 benzilic stabilization, stereoelectronic effects, 230–231  
 condensation reaction, 321
- Nitrate salts, N-aryl-pyrimidinone salts, C–H...O chain synthon, 156
- Nitrogen compounds, HPLC separation, 183
- NCS<sup>−</sup> ligand, bis(thiocyanato)(2,2'-bipyridine)platinum(II) isomers, 369–372
- N–H...O:  
 active unsymmetrical urea, second harmonic generation design, 165–173  
 pyrimidinone hydrogen bonding, 140–143  
 proof of concept, 143–147
- N<sup>+</sup>–H...O<sup>−</sup> bonds, two-dimensional polar layer arrangement, 157–162
- 2-(1-Nitro-2-naphthoxy)propionic acid, homo- and heterochiral crystals, transformation mechanisms, 119–121
- Nitro substituents:  
 active unsymmetrical urea, second harmonic generation design, 165–173  
 porphyrins/metalloporphyrin molecular layers, 52–54
- Noncentrosymmetric cocrystals:  
 active unsymmetrical urea, second harmonic generation design, 165–173  
 N-aryl-pyrimidinone salts, C–H...O chain synthon, 147, 149
- Nonempirical methodology, absolute configuration of chiral compounds, 178–179
- Nonlinear optic (NLO) applications:  
 active unsymmetrical urea, second harmonic generation design 165–173, 165–173  
 two-dimensional polar layer arrangement, 156–162
- Nonplanar ligands, platinum(II) complexes, 359–363
- Norbornenes, reduction reactions, 325–327
- Norrish type-I reaction, photodecarbonylation, 207–208
- Nucleic acids, three-dimensional structure, CH/ $\pi$  hydrogen bonds, 287–290
- Nucleophilic substitutions, thermal solid state reactions, 316–319

- Olefins, *E/Z* isomerization, 333
- One-dimensional networks:
- C–H···O bonds, 160–162
  - hydrogen bonding in ureas, 138–139
  - pyrimidinone hydrogen bonding, 141–143
  - 2-pyrimidinones, 162–165
- Open assemblies, porphyrins/metalloporphyrin molecular layers, weak interactions, 52–54
- Organic compounds:
- CH/π hydrogen bonds, 258–259
  - acyclic peptides, 271–274
  - cyclic peptides, 269–271
  - thermal solid state reactions, 305–310
- Organic crystals:
- N*-aryl-pyrimidinone salts, C–H···O chain synthon, 147–156
  - molecular motion, historical background, 31–32
- Organic ligands, porphyrins/metalloporphyrins, interporphyrin coordination, 72–74
- “Organic zeolites,” porphyrin/metalloporphyrin supramolecular assembly, concerted mechanisms, 75–77
- Orientational disorder, stilbene-type molecules, torsional vibration and pedal motion, 43–45
- ORTEP diagrams, diastereo- and enantiospecific syntheses, vicinal tertiary and quaternary centers, 242–243
- Ortho*-substituted diphenylmethanols, alcohol resolution, 196–200
- Osmium compounds, CH/π hydrogen bonds, 282
- Ostwald’s rule of stages, homo- and heterochiral crystals, racemic compounds vs. conglomerates, 90–99
- 2-Oxasteroids, pyrimidinone hydrogen bonding, 141–143
- 5-Oxatricyclo[5.5.0.0<sup>1,3</sup>]octane-4-one, homo- and heterochiral crystals, racemic compounds vs. conglomerates, 94–95
- Oxidations, solid state molecules, 328–330
- Oxiranes, thermal solid state reactions, hydrohalogen additions, 312
- Oxoamide, chiral crystallization, 14–20
- Oxygen compounds, oxidation, 329–330
- O–H···O<sup>−</sup> bonds, two-dimensional polar layer arrangement, 157–162
- Palladium compounds, porphyrins/metalloporphyrins, metal-ligand coordination, carboxyporphyrin building blocks, 69–72
- Pasteur’s conglomerate, homo- and heterochiral crystals, racemic compounds vs. conglomerates, 100
- Pedal motion:
- azobenzene, 39–40
  - stilbene-type molecules:
    - salicylideneaniline photochromism, 40–42
    - solid state reactivity, 40–43
    - torsional vibration and disorder, 43–45
    - trans*-cinnamamide photodimerization, 42–43
- Peptides, CH/π hydrogen bonds, 260–274
- acyclic peptides, 271–274
  - cyclic peptides, 269–271
- Phase transition, crystal photodecarbonylation, stereospecificity and scale up, 238–240
- Phenanthrene-type platinum complexes, π–π-stacking interactions, 359–363
- bis(1,10-phenanthroline)platinum(II) deformation, 363–367
- Phencyclone Diels–Alder adducts, CH/π hydrogen bonds, 263, 265
- α-Phenyl group, benzylic stabilization, stereoelectronic effects, 228–231
- β-Phenyl groups, quenching by, 232–235
- α-Phenylethylamine (α-PEA), homo- and heterochiral crystals, racemic compounds vs. conglomerates, 106
- 1-Phenylethylammonium hydratropate salt, homo- and heterochiral crystals, racemic compounds vs. conglomerates, 94–99
- Phenyl groups, cyclopentanone reactivity, 221–223
- (Phenyl-2,3,4,5,6-d<sub>5</sub>)phenylmethanol, alcohol resolution, 191–200
- 2-*d*<sub>1</sub>-1-Phenylpropylcobaloxime, oxidation, 329–330
- Phenylpyrimidinone:
- N*-aryl-pyrimidinone salts, C–H···O chain synthon, 150–154
  - hydrogen bonding mimicry, 143–147
  - two-dimensional polar layer arrangement, 158–162
- Phenyl-substituted cyclohexanones, reactivity ranking, 219–221
- Phosphonite salts, homo- and heterochiral crystals, racemic compounds vs. conglomerates, 112–114
- Photochemical reactions:
- crystal stereochemistry, 213–214
  - alkyl- and carbonyl-ketones, 224–228
  - γ-hydrogen abstraction, ultrafast reactions, 231–232
  - β-phenyl groups, quenching reactions, 234–235
  - phenyl-substituted cyclohexanones, reactivity ranking, 219–221
  - stereospecificity and scale up, 237–240
- Photochromism, salicylideneanilines, 40–42
- Photocyclization, achiral molecules, chiral arrangements, 18–20
- Photodecarbonylation reactions:
- crystal stereochemistry:
    - alkyl- and carbonyl-ketone reactivity, 223–228
    - benzylic stabilization, stereoelectronic effects, 228–231
    - stereospecific syntheses, vicinal tertiary and quaternary centers, 240–243
    - electron transfer quenching, 235–236
    - (±)-herbertenolide synthesis, 243–246
    - historical background, 208–210
    - γ-hydrogen abstraction, ultrafast competing reactions, 231–232
    - ketone properties, 246–248
    - β-phenyl group quenching, 232–235
    - research background, 207–208
    - stereospecificity and scale up, 236–240
    - thermochromical parameters, 217–218
- Photodimerization:
- pentane derivatives, 21–22
  - trans*-cinnamamide, 42–43

- Photoirradiation:  
 biphenyl-2,2'-dicarboxylic acid, 23–24  
 inclusion complexes, chiral conformation, 17–20  
 pyridone compounds, 24–27  
 pyridone isolation, 22–27
- Photolysis, benzylic stabilization, stereoelectronic effects, 230–231
- Phthalic acid, *trans*-cinnamamide photodimerization, 43
- Pinacol couplings, reduction reactions, 327
- $\pi$ - $\pi$ -stacking interactions:  
 benzylic stabilization, stereoelectronic effects, 228–231  
 CH/ $\pi$  hydrogen bond, basic characteristics, 257–258  
 platinum(II) complexes, 359–363  
 bis(1,10-phenanthroline) deformation, 363–367  
 porphyrins/metalloporphyrins, 50–52  
 reduction reactions, 325–327
- Planar ligands:  
 bis(thiocyanato)(2,2'-bipyridine)platinum(II)  
 isomers, 369–372  
 platinum(II) complexes, 359–363
- Platinum compounds:  
 platinum(II) crystal structure and functionality, intermolecular interactions:  
 basic principles, 351–352  
 bis(1,10-phenanthroline)  $\pi$ -system, 363–367  
 bis(thiocyanato)(2,2'-bipyridine) linkage  
 isomerism, 367–372  
 dicyano(2,2'-bipyridine) thermochromism/  
 vapochromism, 352–359  
 ladder structures, planar/nonplanar ligands, 359–363  
 porphyrins/metalloporphyrins, metal-ligand coordination, carboxyporphyrin building blocks, 69–72
- Pnma* space group, two-dimensional polar layer arrangement, 160–162
- Polymerization:  
 porphyrin coordination, no external auxiliaries, 60–64  
 porphyrins/metalloporphyrin supramolecular networks, metal ion linker tailoring: 64–72  
 carboxyporphyrin building blocks, 67–72  
 pyridylporphyrin building blocks, 64–67  
 thermal solid state reactions, 341–345
- Polymorphism, homo- and heterochiral crystals, 89  
 racemic compounds vs. conglomerates, 111–114
- Porphyrins/metalloporphyrins:  
 CH/ $\pi$  hydrogen bonds, 275  
 supramolecular networks:  
 basic properties, 49–52  
 concerted mechanisms, 74–77  
 metal-ligand coordination, 60–74  
 coordination polymerization, 60–64  
 interporphyrin organic ligands, 72–74  
 metal ion linkers, polymer array tailoring, 64–72  
 carboxyporphyrin building blocks, 67–72  
 pyridylporphyrin building blocks, 64–67  
 weak interactions, molecular layers, 52–60  
 dipolar attractions, open assemblies, 52–54
- hydrogen bond tressellation, extended networks, 54–60
- Potassium tris(oxalato)cobaltate(III), homo- and heterochiral crystals, racemic conglomerate vs. compound, 105
- Pressure limitations, thermal solid state reactions, 345–346
- Protein Data Bank (PDB):  
 CH/ $\pi$  hydrogen bonds, biopolymer studies, 291–292  
 three-dimensional biopolymers, CH/ $\pi$  hydrogen bonds, 285–287
- Proteins:  
 solid state geometrical isomerizations, 333–341  
 three-dimensional structure, CH/ $\pi$  hydrogen bonds, 283–287
- Protonations, solid ligand conformation, 330
- Proton nuclear magnetic resonance, absolute configuration of chiral compounds, 179
- Pseudoephedrine, carbonyl condensation reaction, 320–321
- Pseudopolymorphism, homo- and heterochiral crystals, 89
- Pseudorotaxane ligands:  
 porphyrin/metalloporphyrin supramolecular assembly, concerted mechanisms, 75–77  
 supramolecular chemistry, 136–137
- Purine ligands, CH/ $\pi$  hydrogen bonds, 279
- 2-Pyridone, stereochemistry control, 22–23
- 4-Pyridone, isolation, 24–25
- Pyridyl moieties, porphyrin polymerization, metal-ligand coordination, 60–64
- Pyridylporphyrin building blocks, polymeric array tailoring, 64–67
- 2-Pyrimidinones:  
 hydrogen bonding mimicry, 139–143  
 proof of concept, 143–147  
 two-dimensional polar layer assembly model, 162–165
- Quasi-racemic compounds:  
 homo- and heterochiral crystals:  
 engineering methodology, 123–127  
 recognition, 88–89  
 pyrimidinone hydrogen bonding, 142–143
- Quaternary centers:  
 benzylic stabilization, stereoelectronic effects, 230–231  
 diastereo- and enantiospecific syntheses, 240–243  
 ketone decarbonylation, ( $\pm$ )-herbertenolide synthesis, 243–246  
 sigma bond in, 206–207
- Quenching reactions:  
 competing reactions in ketones, 247–248  
 electron transfer, 235–236  
 $\beta$ -phenyl groups, 232–235
- Racemates, resolution, chiral syntheses methodology and evaluation, 180–182
- Racemic compounds:  
 alcohol resolution, 196–200  
 chiral molecules, basic properties, 83

- Racemic compounds: (*continued*)  
 homo- and heterochiral crystals:  
   racemic conglomerates:  
 counter ions, central metal atoms and ligands, 106–110  
 covalent substituents, 110–114  
 different compositions, 99–114  
 identical composition, 90–99  
 solvates and host-guest inclusion compounds, 100–105  
 zigzag tape formation, 122–127  
 Michael- and enolate-additions, 322–323  
 solid state geometrical isomerizations, 333–341
- Racemic conglomerates:  
 chiral molecules, basic properties, 83  
 homo- and heterochiral crystals:  
   enantiomorphous space groups, 86–87  
   melting point analysis, 89  
   racemic compound *vs.*:  
 counter ions, central metal atoms and ligands, 106–110  
 covalent substituents, 110–114  
 different compositions, 99–114  
 identical composition, 90–99  
 solvates and host-guest inclusion compounds, 100–105  
   recognition of, 87–89
- Radical reactions:  
 crystall stereochemistry, 206–207  
 photodecarbonylation in crystals, 208–210
- Radical stabilization energies (RSE):  
 alkyl- and carbonyl-ketones, 224–228  
 benzylic stabilization, stereoelectronic effects, 229–231  
 cyclopentanone reactivity, 222–223  
 stereospecific syntheses, vicinal tertiary and quaternary centers, 240–243  
 electron transfer quenching, 235–236  
 $\gamma$ -hydrogen abstraction, ultrafast reactions, 231–232  
 photodecarbonylation reactions, thermochemical parameters, 218
- Reaction cavity:  
 crystal stereochemistry, 210–212  
 thermal solid state reactions, 304
- Rearrangement products, thermal solid state reactions:  
 crystalline structures, 330–332  
 HCl-additions, 314–315
- Red emission spectra:  
 bis(thiocyanato)(2,2'-bipyridine)platinum(II) isomers, 370–372  
 dicyano(2,2'-bipyridine)platinum(II), 352–359
- Reduction reactions, solid state thermal reactions, 325–327
- Resolution:  
 absolute configurations:  
   basic principles, 177–178  
   methodologies, 178–180  
   asymmetric syntheses, 182  
   camphorsultam dichlorophthalic acid, 189–201  
 HPLC and x-ray crystallography:  
   carboxylic acid applications, 182–186  
   molecular design for alcohol analysis, 186–189  
 racemate resolution, 180–182  
 Retinal chromophore, conformal isomer separation, 6–10
- Rhenium compounds, solid state geometric isomerizations, 339
- Rhodium compounds:  
 CH/ $\pi$  hydrogen bonds, 275–279  
 homo- and heterochiral crystals, racemic compounds *vs.* conglomerates, 107–108  
 thermal rearrangements, 331–332
- RR*-chxn ligand, platinum(II)  $\pi$ - $\pi$ -stacking interactions, 362–363
- Ruthenium compounds:  
 CH/ $\pi$  hydrogen bonds, 277–279  
 enantioselective catalytic reactions, 279–283  
 homo- and heterochiral crystals, racemic compounds *vs.* conglomerates, 108  
 solid state geometric isomerizations, 338–339
- Salicylideneanilines, photochromism, 40–42
- Scacchi monohydrated salt, homo- and heterochiral crystals, racemic compounds *vs.* conglomerates, 100
- Scale-up reactions:  
 crystal photodecarbonylation, 236–240  
 thermal solid state reactions, 346
- Schmidt's rule, photodimerization, 21–22
- Schröder-Van Laar-Prigogine-Defay equation, homo- and heterochiral crystals, racemic compounds *vs.* conglomerates, 99
- Second harmonic generation (SHG):  
 two-dimensional polar layer arrangement, 156–162  
 unsymmetrical urea, 165–173
- Self-assemblies, porphyrins/metalloporphyrins, metal-ligand coordination:  
 carboxypporphyrin building blocks, polymeric array tailoring, 69–72  
 polymerization, 61–64  
 pyridylporphyrin building blocks, polymeric array tailoring, 64–67
- Self-association mechanisms, porphyrins/  
 metalloporphyrins, tessellated extended networks, hydrogen bonds, 55–60
- "Shish-kebab" chain polymers, porphyrins/  
 metalloporphyrins, interporphyrin coordination, 72–74
- Sigma bonds:  
 dicyano(2,2'-bipyridine)platinum(II), 354–359  
 stereogenic quaternary centers, 206–207  
 thermal solid state reactions, 305–310  
 Wittig reactions, 322
- Silica gel:  
 chiral auxiliaries, alcohol resolution, 187–189  
 HPLC separation on, nitrogen compounds, 183
- Silver compounds:  
 homo- and heterochiral crystals, racemic compounds *vs.* conglomerates, 109–110  
 pyridylporphyrin building blocks, polymeric array tailoring, 65–67
- Single crystal structures, alcohol resolution, 197–200
- Small molecular weight compounds, CH/ $\pi$  hydrogen bonds, 290–291

- Solid crystals:  
  ketone precursors, 248  
  reactant selection, 248
- Solid solution, chiral molecules, basic properties, 83
- Solid state reactions:  
  crystal stereochemistry:  
    molecular information, 215–217  
    molecular structure and engineering of, 214–215
- cyclopentanones, 221–223
- stereospecific syntheses, vicinal tertiary and  
  quaternary centers, 240–243
- $\gamma$ -hydrogen abstraction, ultrafast reactions, 231–232
- ketone decarbonylation, ( $\pm$ )-herbertenolide  
  synthesis, 243–246
- photochemical initiation, 213–214
- photodecarbonylation in crystals, 209–210  
  benzylic stabilization, 228–231
- quenching reactions,  $\beta$ -Phenyl groups, 232–235
- stilbene-type molecules, pedal motion, 40–43
- thermal stereoselective reactions:  
  basic principles, 303–304  
  carbonyl condensation reactions, 319–321  
  cycloadditions, 323–325  
  eliminations, 315–316  
  Grignard reactions, 323  
  HCl-additions with rearrangement, 314–315  
  hydrohalogen-additions, 311–313  
  linear dimerizations and polymerizations,  
    341–345  
  Michael and enolate additions, 322–323  
  nucleophilic substitutions, 316–319  
  organic solid state chemistry, 305–310  
  oxidations, 328–330  
  protonations (ligands' conformation), 330  
  rearrangements, 330–332  
  reductions, 325–327  
  solid state geometrical isomerizations, 333–341  
  Wittig reactions, 321–322
- thermochemical prediction, 217–218
- topochemical postulate and reaction cavity  
  dimensions, 211–212
- Solvate molecules, homo- and heterochiral crystals,  
  racemic conglomerate vs. compound, host–  
  guest inclusion compounds, 100–104
- Space groups of symmetry, homo- and heterochiral  
  crystals, 83–87
- "Spillover technique," reduction reactions, 327
- Spontaneous deracemization, solid state geometric  
  isomerizations, 338–341
- Spontaneous separation, solid state geometric  
  isomerizations, 338–341
- Square-planar symmetry:  
  bis(1,10-phenanthroline)platinum(II)  $\pi$ -system  
    deformation, 364–367
- carboxyporphyrin building blocks, polymeric array  
  tailoring, 69–72
- linear dimerizations and polymerizations, 345
- porphyrins/metalloporphyrins, supramolecular  
  networks, 50–52
- concerted mechanisms, 74–77
- Stacking geometries. *See also*  $\pi$ - $\pi$ -stacking  
  interactions
- platinum(II) complexes, 359–363
- porphyrins/metalloporphyrin supramolecular  
  networks, open networks, weak  
  interactions, 54
- Stereoelectronic effects, benzylic stabilization,  
  228–231
- Stereogenic quaternary centers, research background,  
  206–207
- Stereoisomers:  
  basic properties, 1–2  
  separation, 2–13  
    cyclohexane derivatives, 10–13  
    equilibrium mixture components, 2–6  
    ionones, 6–10
- Stereospecificity:  
  crystal photodecarbonylation, 236–240  
  ketone decarbonylation, ( $\pm$ )-herbertenolide  
    synthesis, 243–246
- thermal solid state reactions:  
  basic principles, 303–304  
  carbonyl condensation reactions, 319–321  
  cycloadditions, 323–325  
  eliminations, 315–316  
  Grignard reactions, 323  
  halogen-additions, 306–310  
  HCl-additions with rearrangement, 314–315  
  hydrohalogen-additions, 311–313  
  linear dimerizations and polymerizations, 341–345  
  Michael and enolate additions, 322–323  
  nucleophilic substitutions, 316–319  
  organic solid state chemistry, 305–310  
  oxidations, 328–330  
  protonations (ligand conformations), 330  
  rearrangements, 330–332  
  reductions, 325–327  
  solid state geometrical isomerizations, 333–341  
  Wittig reactions, 321–322
- Steric hindrance, bis(1,10-phenanthroline)platinum(II)  
   $\pi$ -system deformation, 364–367
- Stiff stilbenes, central bond shortening, torsional  
  motion, 36–38
- Stilbene-type molecules, torsional motion:  
  central bond shortening, 32–38  
  conformational changes, 38–40  
  disorder and pedal motion, 43–45  
  historical background, 31–32  
  pedal motion and solid state reactivity, 40–43  
    salicylideneaniline photochromism, 40–42  
    trans-cinnamamide photodimerization, 42–43
- $\alpha$ -Substituents:  
  ketone radicals, 247  
  reactivity ranking:  
    cyclopentanones, 221–223  
    phenyl-substituted cyclohexanones, 219–221
- Sulfonate ions, *N*-aryl-pyrimidinone salts, C–H…O  
  chain synthon, 152–154
- Sulfoxides:  
  CH/ $\pi$  hydrogen bond, 256–257  
  oxidation, 328–330
- Sulfur atoms, electron transfer quenching,  
  235–236
- Supramolecular networks:  
  chemical properties, 136–137  
  crystal engineering, 137–138

- Supramolecular networks (*continued*)  
 hydrogen bonds:  
   *N*-arylpurimidinone salts, 147–156  
   basic properties, 136–137  
   crystal engineering, 137–138  
   future research issues, 173  
   2-pyrimidinones, 139–143  
     proof of concept, 143–147  
   two-dimensional polar layer arrangement, 156–162  
   two-dimensional polar layer assembly model, 162–165  
   ureas, 138–139  
     SHG active unsymmetrical design, 165–173  
 porphyrins/metalloporphyrins:  
   basic properties, 49–52  
   concerted mechanisms, 74–77  
   metal-ligand coordination, 60–74  
     coordination polymerization, 60–64  
     interporphyrin organic ligands, 72–74  
     metal ion linkers, polymer array tailoring, 64–72  
       carboxyporphyrin building blocks, 67–72  
       pyridylporphyrin building blocks, 64–67  
     weak interactions, molecular layers, 52–60  
     dipolar attractions, open assemblies, 52–54  
     hydrogen bond tessellation, extended networks, 54–60  
   “Switching” mechanisms, homo- and heterochiral crystals, racemic compounds vs. conglomerates, 93–99  
   counter ions, central metal atoms, or ligands, 106–110  
 Symmetry space groups, homo- and heterochiral crystals, 83–87  
 Synthons:  
   active unsymmetrical urea, second harmonic generation design, 165–173  
   *N*-arylpurimidinone salts, C–H···O chain synthon, 147–156  
   homo- and heterochiral crystal engineering, 121–127  
 porphyrin supramolecular chemistry:  
   concerted mechanisms, 74–77  
   polymeric array tailoring, 69–72  
   supramolecular chemistry, crystal engineering, 137–138  
 “Tailor-made” additives, homo- and heterochiral crystals:  
   enantiomorphous space groups, 86–87  
   racemic compounds vs. conglomerates, 98–99  
 Tautomers, component separation, 2–6  
 Temperature dependence:  
   crystal photodecarbonylation, 248  
   dicyano(2,2'-bipyridine)platinum(II) reactions, 353–359  
   homo- and heterochiral crystals, racemic compounds vs. conglomerates, 100  
 Ternary solubility diagrams, homo- and heterochiral crystals, 88–89  
 Tertiary centers, stereospecific syntheses, 240–243  
 Tessellated extended networks:  
   carboxyporphyrin building blocks, polymeric array tailoring, 69–72  
   hydrogen bonds, porphyrins/metalloporphyrins, 54–60  
   pyridylporphyrin building blocks, polymeric array tailoring, 65–67  
 Tetra(*p*-bromophenyl)ethylene molecules:  
   chiral arrangement, 19–20  
   homo- and heterochiral crystals, racemic conglomerate vs. compound, 102  
 Tetra(4-cyanophenyl)porphyrin, polymerization, metal-ligand coordination, 62–64  
 1,1,3,3 Tetramethyl-2-indanone, benzylic stabilization, stereoelectronic effects, 228–231  
 2,2,5,5 Tetramethylpyrrolidine-3-carboxamide-1-oxy, homo- and heterochiral crystals, racemic compounds vs. conglomerates, 95–99  
 Tetraphenylporphyrin (TPP):  
   polymerization, metal-ligand coordination, 62–64  
   supramolecular networks, 50–52  
 Tetrapyridyl-metallocporphyrin unit, polymerization, metal-ligand coordination, 62–64  
 Thermal ellipsoids, stilbene-type molecules, central bond shortening, torsional motion, 35–38  
 Thermal solid state reactions:  
   basic principles, 303–304  
   carbonyl condensation reactions, 319–321  
   cycloadditions, 323–325  
   eliminations, 315–316  
   Grignard reactions, 323  
   HCl-additions with rearrangement, 314–315  
   hydrohalogen additions, 311–313  
   linear dimerizations and polymerizations, 341–345  
   Michael and enolate additions, 322–323  
   nucleophilic substitutions, 316–319  
   organic solid state chemistry, 305–310  
   oxidations, 328–330  
   protonations (ligand conformations), 330  
   rearrangements, 330–332  
   reductions, 325–327  
   solid state geometrical isomerizations, 333–341  
   Wittig reactions, 321–322  
 Thermochemical parameters:  
   alkyl- and carbonyl-ketone reactivity, 225–228  
   solid state reactivity prediction, 217–218  
 Thermochromism, dicyano(2,2'-bipyridine)platinum(II), 352–359  
 Thiocyanate ions, bis(thiocyanato)(2,2'-bipyridine)platinum(II) isomerism, 367–372  
 Thioglycolic acid derivatives, solid state geometrical isomerizations, 334  
 Thiourea derivatives, thermal solid state reactions, nucleophilic substitutions, 316–319  
 Three-dimensional biopolymer structure:  
   CH/π hydrogen bonds, 283–290  
     nucleic acids, 287–290  
     proteins, 283–287  
   linear dimerizations and polymerizations, 341–345

- Thymotide compounds, thermal solid state reactions, hydrohalogen additions, 312–313
- 4-Toluenesulfonate system, linear dimerizations and polymerizations, 344–345
- Tolyl derivatives:  
  *N*-arylpurimidinone salts, C–H···O chain synthon, 150–154  
  purimidinone hydrogen bonding, 146–147
- Topochemical postulate:  
  crystal stereospecificity, 210–212  
  energetic requirements, 212–214  
  thermal solid state reactions:  
    elimination mechanisms, 315–316  
    internal pressure limitations, 345–346
- Torsional motion, stilbene-type molecules:  
  central bond shortening, 32–38  
  conformational changes, 38–40  
  disorder and pedal motion, 43–45  
  historical background, 31–32  
  pedal motion and solid state reactivity, 40–43  
    salicylideneaniline photochromism, 40–42  
    trans-cinnamamide photodimerization, 42–43
- trans-Cinnamamide, photodimerization, 42–43
- Trans-1,3-diphenyl-2-indanone, reaction cavity dimension, 211–212
- Transformation mechanisms, homo- and heterochiral crystals, 114–121
- Trans-form isomers, conformal separation, 9–10
- Transition metal compounds:  
  CH/π hydrogen bonds, 275–279  
  thermal solid state reactions, halogen-additions, 310
- Transoid conformation, protonations, 330
- Trans-stilbene, thermal solid state reactions, halogen-additions, 306–310
- Triazole compounds, component separation, 2–6
- Triboluminescence, homo- and heterochiral crystals, recognition, 88–89
- Tricyclo[4.4.1.0]undecane derivative, thermal rearrangements, 332
- Triphenyl-2-butanone, photochemical reactions, 234–235
- 1,1,3-Triphenylpropane, photodecarbonylation, 208
- Trost's reagent (MPA), absolute configuration of chiral compounds, 179
- Tunable mix-metatalated compounds, pyridylporphyrin building blocks, polymeric array tailoring, 65–67
- Tungsten compounds, solid state geometric isomerizations, 339
- Twin T-methyl/π interaction, CH/π hydrogen bonds, 289–290
- Twist-boat conformations, β-phenyl groups, quenching reactions, 233–235
- Two-dimensional networks:  
  hydrogen bonding in ureas, 138–139  
  purimidinone hydrogen bonding, 141–143
- Two-dimensional polar layer arrangement:  
  *N*-arylpurimidinone salts, C–H···O chain synthon, 152–154  
  assembly models, 162–165
- hydrogen bonding mimicry, 147
- recurring patterns, 156–162
- Ultrafast reactions, crystal stereochemistry, γ-hydrogen abstraction, 231–232
- Ultraviolet absorption spectra, crystal photodecarbonylation, stereospecificity and scale up, 239–240
- Unimolecular reactions, crystal photodecarbonylation, 212–214
- Unsymmetrical urea compounds, second harmonic generation, active design, 165–173
- Ureas:  
  hydrogen bonding in, 138–139  
  second harmonic generation, active design, 165–173
- Ureylene dicarboxylic acids, hydrogen bonding in, 138–139
- Uronium sulfonate crystal structures, N-aryl-purimidinone salts, C–H···O chain synthon, 152–154
- Valine hydrochloride, homo- and heterochiral crystals, racemic compounds vs. conglomerates, 99
- Van der Waals dimensions:  
  dicyano(2,2'-bipyridine)platinum(II), 358–359  
  ketone triplet energies and yields, 246–247  
  porphyrins/metalloporphyrin supramolecular networks:  
    metal-ligand coordination, polymerization, 63–64  
    open networks, weak interactions, 54  
    tessellated extended networks, hydrogen bonds, 55–60  
  quenching reactions, β-phenyl groups, 234–235  
  topochemical postulate and reaction cavity dimensions, 211–212
- Van't Hoff's rule, homo- and heterochiral crystals, racemic compounds vs. conglomerates, 100
- Vapochromism, dicyano(2,2'-bipyridine)platinum(II), 352–359
- Vicinal tertiary centers, stereospecific syntheses, 240–243
- Vinylic monomers, linear dimerizations and polymerizations, 342–345
- Viscosity effects, crystal photodecarbonylation, stereospecificity and scale up, 238–240
- Wagner-Meerwein rearrangement, solid state compounds, 330–332
- Wallach rule, chiral molecules, 83
- Water uptake:  
  dicyano(2,2'-bipyridine)platinum(II), 358–359  
  platinum (II) π–π-stacking interactions, 360–363
- Weak interactions, molecular layers:  
  hydrogen bonds, 256  
  porphyrins/metalloporphyrin supramolecular networks, 52–60  
  dipolar attractions, open assemblies, 52–54  
  hydrogen bond tressellation, extended networks, 54–60

- Weizmann Institute hypothesis, homo- and heterochiral crystals, racemic compounds *vs.* conglomerates, 98–99
- Wittig reactions, thermal solid state chemistry, 321–322
- X-ray diffraction:  
absolute configuration of chiral compounds, 178–179  
absolute configurations:  
basic principles, 177–178  
methodologies, 178–180  
asymmetric syntheses, 182  
camphorsultam dichlorophthalic acid, 189–207  
dicyano(2,2'-bipyridine)platinum(II), 354–359
- HPLC resolution and:  
carboxylic acid applications, 182–186  
molecular design for alcohol analysis, 186–189  
racemate resolution, 180–182
- stilbene-type molecules:  
central bond shortening, 32–38  
conformational change, 38–40  
thermal solid state reactions, halogen additions, 309–310
- Yellow emission spectra, dicyano(2,2'-bipyridine)platinum(II), 356–359
- Zinc compounds:  
 $\text{CH}/\pi$  hydrogen bonds, 275  
homo- and heterochiral crystals, racemic compounds *vs.* conglomerates, 108  
porphyrins/metalloporphyrins, metal-ligand coordination:  
carboxyporphyrin building blocks, polymeric array tailoring, 70–72  
interporphyrin organic ligands, 72–74
- Zopiclone, homo- and heterochiral crystals, transformation mechanisms, 119–121

## CUMULATIVE AUTHOR INDEX

Index comprises the names of contributors to Volumes 1–25 of **Topics in Stereochemistry**.

- Aaron, H. S., *Conformational Analysis of Intramolecular-Hydrogen-Bonded Compounds in Dilute Solution by Infrared Spectroscopy*, **11**, 1.
- Addadi, L., *A Link Between Macroscopic Phenomena and Molecular Chirality, Crystals as Probes for the Direct Assignment of Absolute Configuration of Chiral Molecules*, **16**, 1.
- Allen, L. C., *see* Buss, V., **7**, 253.
- Altona, C., *see* Romers, C., **4**, 39.
- Arad-Yellin, R., *see* Green, B. S., **16**, 131.
- Arigoni, D., *Chirality Due to the Presence of Hydrogen Isotopes at Noncyclic Positions*, **4**, 127.
- Arnett, E. M., *see* Stewart, M. V., **13**, 195.
- Ashby, E. C., *see* Boone, J. R., **11**, 53.
- Barton, D. H. R., *Conformational Analysis—The Fundamental Contributions of D. H. R. Barton and O. Hassel*, **6**, 1.
- Bauman, L. E., *see* Malloy, T. B. Jr., **11**, 97.
- Bell, R. A., *Some Chemical Applications of the Nuclear Overhauser Effect*, **7**, 1.
- Benfield, R. E., *see* Johnson, B. F. G., **12**, 253.
- Benner, S. A., *Stereospecificity in Enzymology: Its Place in Evolution*, **19**, 127.
- Berkovitch-Yellin, Z., *see* Addadi, L., **16**, 1.
- Berti, G., *Stereochemical Aspects of the Synthesis of 1,2-Epoxides*, **7**, 93.
- Binsch, G., *The Study of Intramolecular Rate Processes by Dynamic Nuclear Magnetic Resonance*, **3**, 97.
- Blanco, M.-J., *Transition-Metal-Templated Synthesis of Rotaxanes*, **23**, 125.
- Blaney, J. M., *see* Ripka, W. C., **20**, 1.
- Bonne, J. R., *Reduction of Cyclic and Bicyclic Ketones by Complex Metal Hydrides*, **11**, 53.
- Bonner, W. A., *Origins of Chiral Homogeneity in Nature*, **18**, 1.
- Bosnich, B., *Asymmetric Synthesis Mediated by Transition Metal Complexes*, **12**, 119.
- Brewster, J. H., *Helix Models of Optical Activity*, **2**, 1.
- Brunner, H., *Enantioselective Synthesis of Organic Compounds with Optically Active Transition Metal Catalysts in Substoichiometric Quantities*, **18**, 129.
- Brunsveld, L., *Chiral Discotic Molecules: Expression and Amplification of Chirality*, **24**, 373.
- Buckingham, D. A., *Conformational Analysis and Configurational Effects for Chelate Complexes*, **6**, 219.
- Bucourt, R., *The Torsion Angle Concept in Conformational Analysis*, **8**, 159.
- Bures, M. G., *Searching Techniques for Databases of Three-Dimensional Chemical Structures*, **21**, 467.
- Buss, V., *The Electronic Structure and Stereochemistry of Simple Carbonium Ions*, **7**, 253.
- Buyss, H. R., *see* Romers, C., **4**, 39.

- Carreira, L. A., *see* Malloy, T. B. Jr., **11**, 97.  
Cavallo, L., *see* Guerra, G., **24**, 1.  
Chambron, J.-C., *see* Blanco, M.-J., **23**, 125.  
Choi, N. S., *see* Goodman, M., **5**, 69.  
Clark, C. I., *see* White, J. M. **22**, 137.  
Closs, G. L., *Structures of Carbenes and the Stereochemistry of Carbene Additions to Olefins*, **3**, 193.  
Cohen, M. D., *see* Green, B. S. **16**, 131.  
Corradini, Paolo., *see* Guerra, G., **24**, 1.  
Corriu, R. J. P., *Stereochemistry at Silicon*, **15**, 43.  
Crabbé, P., *Applications of Optical Rotatory Dispersion and Optical Circular Dichroism in Organic Chemistry*, **1**, 93.
- Dale, J., *Multistep Conformational Interconversion Mechanism*, **9**, 199.  
De Rosa, Claudio, *Chain Conformation, Crystal Structures, and Structural Disorder in Stereo regular Polymers*, **24**, 71.  
DeSantis, G., *see* Silvestri, M. G., **23**, 267.  
Diederich, F., *see* Thilgen, C., **23**, 1.  
Dodziuk, H., *Unusual Saturated Hydrocarbons: Interaction Between Theoretical and Synthetic Chemistry*, **21**, 351.  
Drabowicz, J., *see* Mikolajczyk, M., **13**, 333.  
Duax, W. L., *Crystal Structures of Steroids*, **9**, 271.  
Duddeck, H., *Substituent Effects on <sup>13</sup>C Chemical Shifts in Aliphatic Molecular Systems. Dependence on Constitution and Stereochemistry*, **16**, 219.
- Eliel, E. L., *see* Arigoni, D., **4**, 127.  
Enemark, J. H., *see* Feltham, R. D., **12**, 155.  
Evans, D. A., *Stereoselective Aldol Condensation*, **13**, 1.
- Facelli, J. C., *Molecular Structure and Carbon-13 Chemical Shielding Tensors Obtained from Nuclear Magnetic Resonance*, **19**, 1.  
Fahey, R. C., *The Stereochemistry of Electrophilic Additions to Olefins and Acetylenes*, **3**, 237.  
Farina, M., *The Stereochemistry of Linear Macromolecules*, **17**, 1.  
Feltham, R. C., *Structures of Metal Nitrosyls*, **12**, 155.  
Fenoglio, D. J., *see* Karabatos, G. J., **5**, 167.  
Fenwick, D. R., *Asymmetric Amplification*, **22**, 257.  
Fiaud, J. C., *see* Kagan, H. B., **10**, 175; **18**, 249.  
Flood, T. C., *Stereochemistry of Reactions of Transition Metal-Carbon Sigma Bonds*, **12**, 37.  
Floss, H. G., *Stereochemistry of Biological Reactions at Protoprochiral Centers*, **15**, 253.  
Freedman, T. B., *Stereochemical Aspects of Vibrational Optical Activity*, **17**, 113.  
Fryzuk, M. D., *see* Bosnich, B., **12**, 119.  
Fuchs, B., *Conformations of Five-Membered Rings*, **10**, 1.  
Fuji, K., *see* Kawabata, T., **23**, 175.  
Fujiki, M., *Chirality in Polysilanes*, **24**, 209.
- Gallagher, M. J., *Stereochemical Aspects of Phosphorus Chemistry*, **3**, 1.  
Gielen, M., *The Stereochemistry of Germanium and Tin Compounds*, **12**, 217.  
Garcia-Garibay, M. A., *see* Mortko, C. J., **25**, 205.  
Glasfield, A., *see* Benner, S. A., **19**, 127.  
Goldberg, I., *Supramolecular Networks of Porphyrins*, **25**, 71.  
Goodman, M., *Concepts of Polymer Stereochemistry*, **2**, 73; *Polypeptide Stereochemistry*, **5**, 69.

- Gosse, I., *see* Thilgen, C., **23**, 1.
- Gottarelli, G., *Some Correlations Between Molecular and Cholesteric Handedness*, **24**, 425.
- Graczyk, P. R., *Anomeric Effect: Origin and Consequences*, **21**, 159.
- Grant, D. M., *see* Facelli, J. C., **19**, 1.
- Green, B. S., *Stereochemistry and Organic Solid-State Reactions*, **16**, 131.
- Green, M. M., *Mass Spectrometry and the Stereochemistry of Organic Molecules*, **9**, 35.
- Guérin, C., *see* Corriu, R. J. P., **15**, 43.
- Guerra, G., *Chirality of Catalysts for Stereospecific Polymerizations*, **24**, 1.
- Hanson, K. R., *see* Hirschmann, H., **14**, 183.
- Harada, J., *Torsional Motion of Stilbene-type Molecules in Crystals*, **25**, 31.
- Harada, N., *Chiral Auxiliaries Powerful for Both Enantiomer Resolution and Determination of Absolute Stereochemistry by X-ray Crystallography*, **25**, 177.
- Hassel, O., *see* Barton, D. H. R., **6**, 1.
- Haubenstock, H., *Asymmetric Reductions with Chiral Complex Aluminum Hydrides and Tricoordinate Aluminum Reagents*, **14**, 231.
- Havinga, E., *see* Romers, C., **4**, 39.
- Heathcock, C. H., *see* Oare, D. A., **19**, 227; **20**, 87.
- Hilvert, D., *Stereoselective Reactions with Catalytic Antibodies*, **22**, 83.
- Hirsch, J. A., *Table of Conformational Energies—1967*, **1**, 199.
- Hirschmann, H., *On Factoring Chirality and Stereoisomerism*, **14**, 183.
- Hofer, O., *The Lanthanide Induced Shift Technique: Applications in Conformational Analysis*, **9**, 111.
- Hoover, D. J., *see* Pirkle, W. H., **13**, 263.
- Hutchins, R. O., *see* Maryanoff, B. E., **11**, 187.
- Janzen, E. G., *Stereochemistry of Nitroxides*, **6**, 177.
- Jenkins, I. D., *see* Gallagher, M. J., **3**, 1.
- Jimenez, M. C., *see* Blanco, M.-J., **23**, 125.
- Johnson, B. F. G., *Stereochemistry of Transition Metal Carbonyl Clusters*, **12**, 253.
- Kagan, H. B., *see* Fenwick, D. R., **22**, 257.
- Kagan, H. B., *New Approaches in Asymmetric Synthesis*, **10**, 175; *Kinetic Resolution*, **18**, 249.
- Kalinowski, H.-O., *Fast Isomerizations about Double Bonds*, **7**, 295.
- Karabatsos, G. J., *Rotational Isomerism about  $sp^2-sp^3$ Carbon–Carbon Single Bonds*, **5**, 167.
- Kato, M., *Crystal Structures and Functionalities of Platinum(II) Complexes Controlled by Various Intermolecular Interactions*, **25**, 351.
- Kaupp, G., *Stereoselective Thermal Solid State Reactions*, **25**, 303.
- Kawabata, T., *Memory of Chirality: Asymmetric Induction Based on the Dynamic Chirality of Enolates*, **23**, 175.
- Keese, R., *see* Luef, W., **20**, 231.
- Kellie, G. M., *Nonchair Conformations of Six-Membered Rings*, **8**, 225.
- Kessler, H., *see* Kalinowski, H.-O., **7**, 295.
- Kinbara, K., *Chiral Discrimination During Crystallization*, **23**, 207.
- Klärner, F.-G., *Walk Rearrangements in [n.1.0] Bicyclic Compounds*, **15**, 1.
- Koe, J. R., *see* Fujiki, M., **24**, 209.
- Krebs, P. J., *see* Porter, N. A., **18**, 97.
- Kostyanovsky, R. G., *see* Levkin, P. A., **25**, 81.
- Krow, G., *The Determination of Absolute Configuration of Planar and Axially Dissymmetric Molecules*, **5**, 31.

- Lahav, M., *see Addadi, L.*, **16**, 1.  
Lambert, J. B., *Pyramidal Atomic Inversion*, **6**, 19.  
Leiserowitz, L., *see Addadi, L.*, **16**, 1.  
Lenev, D. A., *see Levkin, P. A.*, **25**, 81.  
Levkin, P. A., *Homo- and Heterochirality in Crystals*, **25**, 81.  
Luef, W., *Strained Olefins: Structure and Reactivity of Nonplanar Carbon–Carbon Double Bonds*, **20**, 231.
- Malloy, T. B., Jr., *Conformational Barriers and Interconversion Pathways in some Small-Ring Molecules*, **11**, 97.  
Martin, Y. C., *see Bures, M. G.*, **21**, 467.  
Maryanoff, B. E., *Stereochemical Aspects of Phosphorus-Containing Cyclohexanes*, **11**, 187.  
Maryanoff, C. A., *see Maryanoff, B. E.*, **11**, 187.  
Mason, S. F., *The Foundations of Classical Stereochemistry*, **9**, 1.  
Masuda, Y., *see Goodman, M.*, **5**, 69.  
McKenna, J., *The Stereochemistry of the Quaternization of Piperidines*, **5**, 275.  
Meijer, E. W., *see Brunsved, L.*, **24**, 373.  
Mikolajczyk, M., *Chiral Organosulfur Compounds*, **13**, 333.  
Mikolajczyk, M., *see Graczyk, P. R.*, **21**, 159.  
Mislow, K., *Molecular Chirality*, **22**, 1.  
Mislow, K., *Stereoisomeric Relationships of Groups in Molecules*, **1**, 1. *See also Raban, M.*, **2**, 199.  
Mitchell, M., *see Silvestri, M. G.*, **23**, 267.  
Moreau, J. J. E., *see Corriu, R. J. P.*, **15**, 43.  
Moriarity, R. M., *Stereochemistry of Cyclobutane and Heterocyclic Analogs*, **8**, 271.  
Mortko, C. J., *Engineering Stereospecific Reactions in Crystals: Synthesis of Compounds with Adjacent Stereogenic Quaternary Centers by Photodecarbonylation of Crystalline Ketones*, **25**, 205.  
Musso, H., *see Osawa, E.*, **13**, 117.
- Nafie, L. A., *see Freedman, T. B.*, **17**, 113.  
Nakashima, H., *see Fujiki, M.*, **24**, 209.  
Nakazaki, M., *The Synthesis and Stereochemistry of Chiral Organic Molecules with High Symmetry*, **15**, 199.  
Nangia, A., *Supramolecular Synthesis of 1D Chains and 2D Layers in Hydrogen Bond Networks of Ureas and 2-Pyrimidinones*, **25**, 135.  
Nelson, J. V., *see Evans, D. A.*, **13**, 1.  
Nishio, N., *The CH/π Hydrogen Bond: An Important Molecular Force in Controlling the Crystal Conformation of Organic Compounds and Three-Dimensional Structure of Biopolymers*, **25**, 255.  
Nolte, R. J. M., *see Brunsved, L.*, **24**, 373.
- Oare, D. A., *Stereochemistry of the Base-Promoted Michael Addition Reaction*, **19**, 227; *Acylic Stereocontrol in Michael Addition Reactions of Enamines and Enol Ethers*, **20**, 87.  
Ogawa, K., *see Harada, J.*, **25**, 31.  
Okamoto, Y., *Optically Active Polymers with Chiral Recognition Ability*, **24**, 157.  
Oki, M., *Recent Advances in Atropoisomerism*, **14**, 1.  
Osawa, E., *Applications of Molecular Mechanics Calculations to Organic Chemistry*, **13**, 117.
- Palyulin, V. A., *see Zefirov, N. S.*, **20**, 171.  
Persoons, A., *see Verbiest, T.*, **24**, 519.

- Peterson, M. J., *see* Vedejs, E., **21**, 1.
- Pethrick, R. A., *see* Wyn-Jones, E., **5**, 205.
- Piccirilli, J. A., *see* Benner, S. A., **19**, 127.
- Pirkle, W. H., *NMR Chiral Solvating Agents*, **13**, 263.
- Porter, N. A., *Stereochemical Aspects of Radical Pair Reactions*, **18**, 97.
- Raban, M., *Modern Methods for the Determination of Optical Purity*, **2**, 199; *See also* Mislow, K., **1**, 1.
- Riddell, F. G., *see* Kellie, G. M., **8**, 225.
- Ripka, W. G., *Computer Graphics and Molecular Modeling in the Analysis of Synthetic Targets*, **20**, 1.
- Rohrer, D. C., *see* Duax, W. L., **9**, 271.
- Romers, C., *Geometry and Conformational Properties of Some Five-and Six-Membered Heterocyclic Compounds Containing Oxygen and Sulfur*, **4**, 39.
- Rowan, A. E., *see* Brunsved, L., **24**, 373.
- Ruch, E., *The Stereochemical Analogy Model—A Mathematical Theory of Dynamic Stereochemistry*, **4**, 99.
- Saigo, K., *see* Kinbara, K., **23**, 207.
- Saito, Y., *Absolute Stereochemistry of Chelate Complexes*, **10**, 95.
- Sandström, J., *Static and Dynamic Stereochemistry of Push-Pull and Strained Ethylenes*, **14**, 83.
- Sargeson, A. M., *see* Buckingham, D. A., **6**, 219.
- Sasai, H., *see* Shibasaki, M., **22**, 201.
- Saunders, J. K., *see* Bell, R. A., **7**, 1.
- Sauvage, J.-P., *see* Blanco, M.-J., **23**, 125.
- Schleyer, P. V. Ragué., *see* Buss, V., **7**, 253.
- Schlögl, K., *Stereochemistry of Metallocenes*, **1**, 39.
- Schlosser, M., *The Stereochemistry of the Wittig Reaction*, **5**, 1.
- Schnur, J. M., *see* Spector, M. S., **24**, 281.
- Scott, J. W., *Enantioselective Synthesis of Non-Racemic Chiral Molecules on an Industrial Scale*, **19**, 209.
- Selinger, J. V., *see* Spector, M. S., **24**, 281.
- Shibasaki, M., *Asymmetric Catalysis with Chiral Lanthanoid Complexes*, **22**, 201.
- Sih, C. J., *Resolution of Enantiomers via Biocatalysis*, **19**, 63.
- Silvestri, M. G., *Asymmetric Aldol Reactions Using Aldolases*, **23**, 267.
- Simamura, O., *The Stereochemistry of Cyclohexyl and Vinylidyl Radicals*, **4**, 1.
- Sloan, T. E., *Stereochemical Nomenclature and Notation in Inorganic Chemistry*, **12**, 1.
- Spada, G. P., *see* Gottarelli, G., **24**, 425.
- Spector, M. S., *Chiral Molecular Self-Assembly*, **24**, 281.
- Stewart, M. V., *Chiral Monolayers at the Air-Water Interface*, **13**, 195.
- Stoddart, J. F., *Chiral Crown Ethers*, **17**, 207.
- Stothers, J. B., *see* Wilson, N. K., **8**, 1.
- Sullivan, G. R., *Chiral Lanthanide Shift Reagents*, **10**, 287.
- Taber, T. R., *see* Evans, D. A., **13**, 1.
- Thilgen, C., *Chirality in Fullerene Chemistry*, **23**, 1.
- Toda, F., *Stereochemistry of Molecules in Inclusion Crystals*, **25**, 1.
- Torbeev, V. Y., *see* Levkin, P. A., **25**, 81.
- Toromanoff, E., *Steric Course of the Kinetic 1,2 Addition of Anions to Conjugated Cyclohexenones*, **2**, 157.

- Toyoda, S., *see* Fujiki, M., **24**, 209.  
Tsai, M.-D., *see* Floss, H. G., **15**, 253.
- Ugi, L., *see* Ruch, E., **4**, 99.  
Umezawa, Y., *see* Nishio, M., **25**, 255.
- Vedejs, E., *Stereochemistry and Mechanism of the Wittig Reaction*, **21**, 1.  
Verbiest, T., *Nonlinear Optics and Chirality*, **24**, 519.  
Verdini, A. S., *see* Goodman, M., **5**, 69.
- Walba, D. M., *Ferroelectric Liquid Crystal Conglomerates*, **24**, 457.  
Weeks, C. M., *see* Duax, W. L., **9**, 271.  
Weissbuch, I., *see* Addadi, L., **16**, 1.  
White, J. M., *Stereoelectronic Effects of the Group 4 Metal Substituents in Organic Chemistry*, **22**, 137.  
Wilen, S. H., *Resolving Agents and Resolutions in Organic Chemistry*, **6**, 107.  
Willett, P., *see* Bures, M. G., **21**, 467.  
Wilson, N. K., *Stereochemical Aspects of <sup>13</sup>C NMR Spectroscopy*, **8**, 1.  
Wong, C.-H., *see* Silvestri, M. G., **23**, 267.  
Woodard, R. W., *see* Floss, H. G., **15**, 253.  
Wu, S.-H., *see* Sih, C. J., **19**, 63.  
Wynberg, H., *Asymmetric Catalysis by Alkaloids*, **16**, 87.  
Wyn-Jones, E., *The Use of Ultrasonic Absorption and Vibrational Spectroscopy to Determine the Energies Associated with Conformational Changes*, **5**, 205.
- Yamamoto, C., *see* Okamoto, Y., **24**, 157.  
Yashima, E., *see* Okamoto, Y., **24**, 157.  
Young, D. W., *Stereochemistry of Metabolic Reactions of Amino Acids*, **21**, 381.
- Zefirov, N. S., *Conformational Analysis of Bicyclo[3.3.1]nonanes and their Hetero Analogs*, **20**, 171.

# CUMULATIVE TITLE INDEX

	VOL.	PAGE
Absolute Configuration of Chiral Molecules, Crystals as Probes for the Direct Assignment of ( <i>Addadi, Berkovitch-Yellin, Weissbuch, Lahav, and Leiserowitz</i> ) .....	16	1
Absolute Configuration of Planar and Axially Dissymmetric Molecules ( <i>Krow</i> ) .....	5	31
Absolute Stereochemistry of Chelate Complexes ( <i>Saito</i> ) .....	10	95
Acetylenes, Stereochemistry of Electrophilic Additions ( <i>Fahey</i> ) .....	3	237
Acyclic Stereocontrol in Michael Addition Reaction of Enamines and Enol Ethers ( <i>Oare and Heathcock</i> ) .....	20	87
Aldolases, Asymmetric Aldol Reactions Using ( <i>Silvestri, DeSantis, Mitchell and Wong</i> ) .....	23	267
Aldol Condensations, Stereoselective ( <i>Evans, Nelson, and Taber</i> ) .....	13	1
Alkaloids, Asymmetric Catalysis by ( <i>Wynberg</i> ) .....	16	87
Aluminum Hydrides and Tricoordinate Aluminum Reagents, Asymmetric Reductions with Chiral Complex ( <i>Haubenstock</i> ) .....	14	231
Amino Acids, Stereochemistry of Metabolic Reactions of ( <i>Young</i> ) .....	21	381
Analogy Model, Stereochemical ( <i>Ugi and Ruch</i> ) .....	4	99
Anomeric Effect: Origin and Consequences ( <i>Graczyk and Mikołajczyk</i> ) .....	21	159
Antibodies, Catalytic, Stereoselective Reactions with ( <i>Hilvert</i> ) .....	22	83
Asymmetric Aldol Reactions Using Aldolases ( <i>Silvestri, DeSantis, Mitchell and Wong</i> ) .....	23	267
Asymmetric Amplification ( <i>Fenwick and Kagan</i> ) .....	22	257
Asymmetric Catalysis by Alkaloids ( <i>Wynberg</i> ) .....	16	87
Asymmetric Catalysis with Chiral Lanthanoid Complexes ( <i>Shibasaki and Sasai</i> ) .....	22	201
Asymmetric Reductions with Chiral Complex Aluminum Hydrides and Tricoordinate Aluminum Reagents ( <i>Haubenstock</i> ) .....	14	231
Asymmetric Synthesis, New Approaches in ( <i>Kagan and Fiaud</i> ) .....	10	175
Asymmetric Synthesis Mediated by Transition Metal Complexes ( <i>Bosnich and Fryzuk</i> ) .....	12	119
Atomic Inversion, Pyramidal ( <i>Lambert</i> ) .....	6	19
Atropisomerism, Recent Advances in ( <i>Oki</i> ) .....	14	1
Axially and Planar Dissymmetric Molecules, Absolute Configuration of ( <i>Krow</i> ) .....	5	31
Barriers, Conformational, and Interconversion Pathways in Some Small Ring Molecules ( <i>Malloy, Bauman, and Carreira</i> ) .....	11	97

	VOL.	PAGE
Barton, D. H. R., and Hassel, O., Fundamental Contributions to Conformational Analysis ( <i>Barton and Hassel</i> ) .....	6	19
Bicyclic Compounds, Walk Rearrangements in [n.1.0] ( <i>Kärner</i> ).....	15	1
Carbene Additions to Olefins, Stereochemistry of ( <i>Closs</i> ).....	3	193
Carbenes, Structure of ( <i>Closs</i> ).....	3	193
sp <sup>2</sup> -sp <sup>3</sup> Carbon-Carbon Single Bonds, Rotational Isomerism about ( <i>Karabatsos and Fenoglio</i> ) .....	5	167
Carbonium Ions, Simple, the Electronic St Hydrogen Isotopes at Noncyclic Positions Chelate Complexes, Absolute Stereochemistry of ( <i>Saito</i> ) .....	10	95
Catalysis, Asymmetric, with Chiral Lanthanoid Complexes ( <i>Shibasaki and Sasai</i> ) .....	22	201
Catalytic Antibodies, Stereoselective Reactions with ( <i>Hilvert</i> ) .....	22	83
<sup>13</sup> C Chemical Shielding Tensors Obtained from NMR, Molecular Structure and ( <i>Facelli and Grant</i> ) .....	19	1
<sup>13</sup> C Chemical Shifts in Aliphatic Molecular Systems, Substituent Effects on Dependence on Constitution and Stereochemistry ( <i>Duddeck</i> ).....	16	219
CH/π Hydrogen Bond: An Important Molecular force in Controlling the Crystal Conformation of Organic Compounds and Three-Dimensional Structure of Biopolymers, The ( <i>Nishio, Umezawa</i> ) .....	25	255
Chiral Auxiliaries Powerful for Both Resolution and Determination of Absolute Configuration by X-ray Crystallography ( <i>Harada</i> ) .....	25	177
Crystal Structures and Functionalities of Platinum(II) Complexes Controlled by Various Intermolecular Interactions ( <i>Kato</i> ) .....	25	351
Chiral Crown Ethers ( <i>Stoddart</i> ) .....	17	207
Chiral Discotic Molecules: Expression and Amplification of Chirality ( <i>Brunsveld, Rowan, Nolte, and Meijer</i> ) .....	24	373
Chiral Discrimination during Crystallization ( <i>Kinbara and Saigo</i> ). ....	23	207
Chiral Homogeneity in Nature, Origins of ( <i>Bonner</i> ) .....	18	1
Chirality Due to the Presence of Hydrogen Isotopes at Noncyclic Positions ( <i>Arigoni and Eliel</i> ) .....	4	127
Chirality in Fullerene Chemistry ( <i>Thilgen, Gosse and Diederich</i> ) .....	23	1
Chirality, Molecular ( <i>Mislow</i> ) .....	22	1
Chiral Lanthanide Shift Reagents ( <i>Sullivan</i> ) .....	10	287
Chiral Lanthanoid Complexes, Asymmetric Catalysis with ( <i>Shibasaki and Sasai</i> ) .....	22	201
Chiral Monolayers at the Air-Water Interface ( <i>Stewart and Arnett</i> ) .....	13	195
Chiral Organic Molecules with High Symmetry, The Synthesis and Stereochemistry of ( <i>Nakazaki</i> ) .....	15	199
Chiral Organosulfur Compounds ( <i>Mikołajczyk and Drabowicz</i> ).....	13	333
Chiral Recognition Ability, Optically Active Polymers with ( <i>Okamoto, Yashima, and Yamamoto</i> ). ....	24	157
Chiral Solvating Agents, in NMR ( <i>Pirkle and Hoover</i> ) .....	13	263
Cholesteric Handedness, Some Correlations Between Molecular and ( <i>Gottarelli and Spada</i> ) .....	24	425
Classical Stereochemistry, The Foundations of ( <i>Mason</i> ) .....	9	1
Conformational Analysis, Applications of the Lanthanide-induced Shift Technique in ( <i>Hofer</i> ) .....	9	111

	VOL.	PAGE
Conformational Analysis of Bicyclo[3.3.1]nonanes and Their Hetero Analogs ( <i>Zefirov and Palyulin</i> ).....	20	171
Conformational Analysis, The Fundamental Contributions of D. H. R. Barton and O. Hassell ( <i>Barton and Hassel</i> ) .....	6	1
Conformational Analysis of Intramolecular Hydrogen-Bonded Compounds in Dilute Solution by Infrared Spectroscopy ( <i>Aäron</i> ) .....	11	1
Conformational Analysis of Six-membered Rings ( <i>Kellie and Riddell</i> ) .....	8	225
Conformational Analysis of Steric Effects in Metal Chelates ( <i>Buckingham and Sargeson</i> ) .....	6	219
Conformational Analysis and Torsion Angles ( <i>Bucourt</i> ) .....	8	159
Conformational Barriers and Interconversion Pathways in Some Small Ring Molecules ( <i>Malloy, Bauman and Carreira</i> ) .....	11	97
Conformational Changes, Determination of Associated Energy by Ultrasonic Absorption and Vibrational Spectroscopy ( <i>Wyn-Jones and Pethrick</i> ) .....	5	205
Conformational Changes by Rotation about $sp^2-sp^3$ Carbon-Carbon Single Bonds ( <i>Karabatsos and Fenoglio</i> ) .....	5	167
Conformational Energies, Table of ( <i>Hirsch</i> ) .....	1	199
Conformational Interconversion Mechanisms, Multi-step ( <i>Dale</i> ) .....	9	199
Conformations of 5-Membered Rings ( <i>Fuchs</i> ) .....	10	1
Conjugated Cyclohexenones, Kinetic 1,2 Addition of Anions to, Steric Course of ( <i>Toromanoff</i> ) .....	2	157
Crystals as Probes for the Direct Assignment of Absolute Configuration of Chiral Molecules, A Link Between Macroscopic Phenomena and Molecular Chirality ( <i>Addadi, Berkovitch-Yellin, Weissbuch, Lahav, and Leiserowitz</i> ) .....	16	1
Crystal Structures of Steroids ( <i>Duax, Weeks, and Rohrer</i> ) .....	9	271
Cyclobutane and Heterocyclic Analogs, Stereochemistry of ( <i>Moriarty</i> ).....	8	271
Cyclohexyl Radicals, and Vinylic, The Stereochemistry of ( <i>Simamura</i> ).....	4	1
Databases of Three-Dimensional Chemical Structures, Searching Techniques for ( <i>Bures, Martin and Willett</i> ).....	21	467
Double Bonds, Fast Isomerization about ( <i>Kalinowski and Kessler</i> ) .....	7	295
Electronic Structure and Stereochemistry of Simple Carbonium Ion, ( <i>Buss, Schleyer, and Allen</i> ) .....	7	253
Electrophilic Additions to Olefins and Acetylenes, Stereochemistry of ( <i>Fahey</i> )	3	237
Enantioselective Synthesis of Non-Racemic Chiral Molecules on an Industrial Scale ( <i>Scott</i> ) .....	19	209
Enantioselective Synthesis of Organic Compounds with Optically Active Transition Metal Catalysts in Substoichiometric Quantities ( <i>Brunner</i> ) .....	18	129
Engineering Stereospecific Reactions in Crystals: Synthesis of Compounds with Adjacent Stereogenic Quaternary Centers by Photodecarbonylation of Crystalline Ketones ( <i>Mortko and Garcia-Garibay</i> ) .....	25	205
Enzymatic Reactions, Stereochemistry of, by Use of Hydrogen Isotopes ( <i>Arigoni and Eiel</i> ) .....	4	127
Enzymology, Stereospecificity in: Its Place in Evolution ( <i>Benner, Glasfeld and Piccirilli</i> ) .....	19	127

	VOL.	PAGE
1,2-Epoxides, Stereochemistry Aspects of the Synthesis of ( <i>Berti</i> ) . . . . .	7	93
EPR, in Stereochemistry of Nitroxides ( <i>Janzen</i> ) . . . . .	6	177
Ethylenes, Static and Dynamic Stereochemistry of Push-Pull and Strained ( <i>Sandstrom</i> ) . . . . .	14	83
Five-Membered Rings, Conformations of ( <i>Fuchs</i> ) . . . . .	10	1
Foundations of Classical Stereochemistry ( <i>Mason</i> ) . . . . .	9	1
Fullerene Chemistry, Chirality in ( <i>Thilgen, Gosse and Diederich</i> ) . . . . .	23	1
Geometry and Conformational Properties of Some Five- and Six-Membered Heterocyclic Compounds Containing Oxygen or Sulfur ( <i>Romers, Altona, Buys, and Havinga</i> ) . . . . .	4	39
Group 4 Metal Substituents, Stereoelectronic Effects of the ( <i>White and Clark</i> ) . . . . .	22	137
Hassel, O. and Barton, D. H. R., Fundamental Contributions to Conformational Analysis ( <i>Hassel and Barton</i> ) . . . . .	6	1
Helix Models, of Optical Activity ( <i>Brewster</i> ) . . . . .	2	1
Heterocyclic Compounds, Five- and Six-Membered, Containing Oxygen or Sulfur, Geometry and Conformational Properties of ( <i>Romers, Altona, Buys and Havinga</i> ) . . . . .	4	39
Heterocyclic Four-Membered Rings, Stereochemistry of ( <i>Moriarty</i> ) . . . . .	8	271
Heterotopism ( <i>Mislow and Raban</i> ) . . . . .	1	1
Homo- and Heterochirality in Crystals ( <i>Levkin, Torbeev, Lenev, and Kostyanovsky</i> ) . . . . .	25	81
Hydrocarbons, Unusual Saturated: Interaction between Theoretical and Synthetic Chemistry ( <i>Dodziak</i> ) . . . . .	21	351
Hydrogen-Bonded Compounds, Intramolecular, in Dilute Solution, Conformational Analysis of, by Infrared Spectroscopy ( <i>Aaron</i> ) . . . . .	11	1
Hydrogen Isotopes at Noncyclic Positions, Chirality Due to the Presence of ( <i>Arigoni and Eliel</i> ) . . . . .	4	127
Infrared Spectroscopy, Conformational Analysis of Intramolecular Hydrogen-Bonded Compounds in Dilute Solution by ( <i>Aaron</i> ) . . . . .	11	1
Intramolecular Hydrogen-Bonded Compounds, in Dilute Solution, Conformational Analysis of, by Infrared Spectroscopy ( <i>Aaron</i> ) . . . . .	11	1
Intramolecular Rate Processes ( <i>Binsch</i> ) . . . . .	3	97
Inversion, Atomic, Pyramidal ( <i>Lambert</i> ) . . . . .	6	19
Isomerization, Fast, About Double Bonds ( <i>Kalinowski and Kessler</i> ) . . . . .	7	295
Ketones, Cyclic and Bicyclic, Reduction of, by Complex Metal Hydrides ( <i>Boone and Ashby</i> ) . . . . .	11	53
Lanthanide-induced Shift Technique—Applications in Conformational Analysis ( <i>Hofer</i> ) . . . . .	9	111
Lanthanide Shift Reagents, Chiral ( <i>Sullivan</i> ) . . . . .	10	287
Lanthanoid Complexes, Chiral, Asymmetric Catalysis with ( <i>Shibasaki and Sasai</i> ) . . . . .	22	201
Liquid Crystal Conglomerates, Ferroelectric ( <i>Walba</i> ) . . . . .	24	457

	VOL.	PAGE
Mass Spectrometry and the Stereochemistry of Organic Molecules ( <i>Green</i> ) . . . . .	9	35
Memory of Chirality: Asymmetric Induction Based on the Dynamic Chirality of Enolates ( <i>Kawabata and Fuji</i> ) . . . . .	23	175
Metal Chelates, Conformational Analysis and Steric Effects in ( <i>Buckingham</i> and <i>Sargeson</i> ) . . . . .	6	219
Metal Hydrides, Complex, Reduction of Cyclic and Bicyclic Ketones by ( <i>Boone and Ashby</i> ) . . . . .	11	53
Metallocenes, Stereochemistry of ( <i>Schlogl</i> ) . . . . .	1	39
Metal Nitrosyls, Structures of ( <i>Feltham and Enemark</i> ) . . . . .	12	155
Michael Addition Reaction, Stereochemistry of the Base-Promoted ( <i>Oare</i> and <i>Heathcock</i> ) . . . . .	19	227
Michael Addition Reactions of Enamines and Enol Ethers, Acyclic Stereocontrol in ( <i>Oare and Heathcock</i> ) . . . . .	20	87
Molecular Chirality ( <i>Mislow</i> ) . . . . .	22	1
Molecular Mechanics Calculations—Applications to Organic Chemistry ( <i>Osawa and Musso</i> ) . . . . .	13	117
Molecular Modeling, Computer Graphics and, in the Analysis of Synthetic Targets ( <i>Ripka and Blaney</i> ) . . . . .	20	1
Monolayers, Chiral, at the Air-Water Interface ( <i>Stewart and Arnett</i> ) . . . . .	13	195
Multi-step Conformational Interconversion Mechanisms ( <i>Dale</i> ) . . . . .	9	199
Nitroxides, Stereochemistry of ( <i>Janzen</i> ) . . . . .	6	177
Non-Chair Conformations of Six-Membered Rings ( <i>Kellie and Riddell</i> ) . . . . .	8	225
Nuclear Magnetic Resonance, $^{13}\text{C}$ Chemical Shifts in Aliphatic Molecular Systems, Substituent Effects on, Dependence on Constitution and Stereochemistry ( <i>Duddeck</i> ) . . . . .	16	219
Nuclear Magnetic Resonance Chiral Lanthanide Shift Reagents ( <i>Sullivan</i> ) . . . . .	10	287
Nuclear Magnetic Resonance, $^{13}\text{C}$ Stereochemical Aspects of ( <i>Wilson and</i> <i>Stothers</i> ) . . . . .	8	1
Nuclear Magnetic Resonance, Chiral Solvating Agents in ( <i>Pirkle and</i> <i>Hoover</i> ) . . . . .	13	263
Nuclear Magnetic Resonance, for Study of Intra-Molecular Rate Processes ( <i>Binsch</i> ) . . . . .	3	97
Nuclear Magnetic Resonance, Molecular Structure and Carbon-13 Chemical Shielding Tensors Obtained from ( <i>Facelli and Grant</i> ) . . . . .	19	1
Nuclear Overhauser Effect, Some Chemical Applications of ( <i>Bell and</i> <i>Saunders</i> ) . . . . .	7	1
Olefins, Stereochemistry of Carbene Additions to ( <i>Class</i> ) . . . . .	3	193
Olefins, Stereochemistry of Electrophilic Additions to ( <i>Fahey</i> ) . . . . .	3	237
Olefins, Strained: Structure and Reactivity of Nonplanar Carbon-Carbon Double Bonds ( <i>Luef and Keese</i> ) . . . . .	20	231
Optical Activity, Helix Models of ( <i>Brewster</i> ) . . . . .	2	1
Optical Circular Dichroism, Recent Applications in Organic Chemistry ( <i>Crabbé</i> ) . . . . .	1	93
Optical Purity, Modern Methods for the Determination of ( <i>Raban and Mislow</i> ) . .	2	199
Optical Rotatory Dispersion, Recent Applications in Organic Chemistry ( <i>Crabbé</i> ) . . . . .	1	93

	VOL.	PAGE
Optics, Nonlinear, and Chirality ( <i>Verbiest and Persoons</i> ) . . . . .	24	519
Organic Solid-State, Stereochemistry and Reactions ( <i>Green, Arad-Yellin, and Cohen</i> ) . . . . .	16	131
Organosulfur Compounds, Chiral ( <i>Mikołajczyk and Drabowicz</i> ) . . . . .	13	333
Origins of Chiral Homogeneity in Nature ( <i>Bonner</i> ) . . . . .	18	1
Overhauser Effect, Nuclear, Some Chemical Applications of ( <i>Bell and Saunders</i> ) . . . . .	7	1
Phosphorus Chemistry, Stereochemical Aspects of ( <i>Gallagher and Jenkins</i> ) . . . . .	3	1
Phosphorus-containing Cyclohexanes, Stereochemical Aspects of ( <i>Maryanoff, Hutchins, and Maryanoff</i> ) . . . . .	11	186
Piperidines, Quaternization Stereochemistry of ( <i>McKenna</i> ) . . . . .	5	275
Planar and Axially Dissymmetric Molecules, Absolute Configuration of ( <i>Krow</i> ) . . . . .	5	31
Polymerizations, Chirality of Catalysts for Stereospecific ( <i>Guerra, Cavallo, and Corradini</i> ) . . . . .	24	1
Polymers, Chain Conformation, Crystal Structures, and Structural Disorder in Stereoregular ( <i>De Rosa</i> ) . . . . .	24	71
Polymer Stereochemistry, Concepts of ( <i>Goodman</i> ) . . . . .	2	73
Polypeptide Stereochemistry ( <i>Goodman, Verdini, Choi, and Masuda</i> ) . . . . .	5	69
Polysilanes, Chirality in the ( <i>Fujiki, Koe, Nakashima, and Toyoda</i> ) . . . . .	24	209
Pyramidal Atomic Inversion ( <i>Lambert</i> ) . . . . .	6	19
Quaternization of Piperidines, Stereochemistry of ( <i>McKenna</i> ) . . . . .	5	75
Radical Pair Reactions, Stereochemical Aspects of ( <i>Porter and Krebs</i> ) . . . . .	18	97
Radicals, Cyclohexyl and Vinylidic, The Stereochemistry of ( <i>Simamura</i> ) . . . . .	4	1
Reduction, of Cyclic and Bicyclic Ketones by ( <i>Sih and Wu</i> ) . . . . .	19	63
Resolution, Kinetic ( <i>Kagan and Fiaud</i> ) . . . . .	18	249
Resolving Agents and Resolutions in Organic Chemistry ( <i>Wilen</i> ) . . . . .	6	107
Rotational Isomerism about $sp^2-sp^3$ Carbon-Carbon Single Bonds ( <i>Karabatos and Fenoglio</i> ) . . . . .	5	167
Rotaxanes, Transition-Metal-Templated Synthesis of ( <i>Blanco, Chambron, Jiménez and Sauvage</i> ) . . . . .	23	125
Self-Assembly, Chiral Molecular ( <i>Spector, Selinger, and Schnur</i> ) . . . . .	24	281
Silicon, Stereochemistry at ( <i>Corriu, Guerin, Mauman, and Carreira</i> ) . . . . .	11	97
Stereochemical Aspects of $^{13}\text{C}$ NMR Spectroscopy ( <i>Wilson and Stothers</i> ) . . . . .	8	1
Stereochemical Aspects of Phosphorus-containing Cyclohexanes ( <i>Maryanoff, Hutchins, and Maryanoff</i> ) . . . . .	11	186
Stereochemical Aspects of Radical Pair Reactions ( <i>Porter and Krebs</i> ) . . . . .	18	97
Stereochemical Aspects of Vibrational Optical Activity ( <i>Freedman and Nafie</i> ) . . . . .	17	113
Stereochemical Nomenclature and Notation in Inorganic Chemistry ( <i>Sloan</i> ) . . . . .	12	1
Stereochemistry, Classical, The Foundations of ( <i>Mason</i> ) . . . . .	9	1
Stereochemistry, Dynamic, A Mathematical Theory of ( <i>Ugi and Ruch</i> ) . . . . .	4	99
Stereochemistry of Biological Reactions at Propropochiral Centers ( <i>Floss, Tsai, and Woodard</i> ) . . . . .	15	253
Stereochemistry of Chelate Complexes ( <i>Saito</i> ) . . . . .	10	95

	VOL.	PAGE
Stereochemistry of Cyclobutane and Heterocyclic Analogs ( <i>Moriarty</i> ) .....	8	271
Stereochemistry of Germanium and Tin Compounds ( <i>Gielen</i> ) .....	12	217
Stereochemistry of Linear Macromolecules ( <i>Farina</i> ) .....	17	1
Stereochemistry of Nitroxides ( <i>Janzen</i> ) .....	6	177
Stereochemistry of Organic Molecules, and Mass Spectrometry ( <i>Green</i> ).....	9	35
Stereochemistry of Push-Pull and Strained Ethylenes, Static and Dynamic ( <i>Sandström</i> ) .....	14	83
Stereochemistry of Reactions of Transition Metal-Carbon Sigma Bonds ( <i>Flood</i> ) ...	12	37
Stereochemistry at Silicon ( <i>Corriu, Guérin, and Moreau</i> ).....	15	43
Stereochemistry of Transition Metal Carbonyl Clusters ( <i>Johnson and Benfield</i> ) .....	12	253
Stereochemistry of Molecules in Inclusion Crystals ( <i>Toda</i> ).....	25	1
Stereoselective Thermal Solid State Reactions ( <i>Kaupp</i> ) .....	25	303
Stereoselective Reactions with Catalytic Antibodies ( <i>Hilvert</i> ) .....	22	83
Stereoisomeric Relationships, of Groups in Molecules ( <i>Mislow and Raban</i> ) ...	1	1
Stereoisomerism, On Factoring Chirality and ( <i>Hirschmann and Hanson</i> ) .....	14	183
Stereoselective Aldol Condensations ( <i>Evans, Nelson, and Taber</i> ).....	13	1
Stereoelectronic Effects of the Group 4 Metal Substituents in Organic Chemistry ( <i>White and Clark</i> ).....	22	137
Stereospecificity in Enzymology: Its Place in Evolution ( <i>Benner, Glasfeld, and Piccirilli</i> ) .....	19	127
Steroids, Crystal Structures of ( <i>Duax, Weeks, and Rohrer</i> ) .....	9	271
Strained Olefins: Structure and Reactivity of Nonplanar Carbon-Carbon Double Bonds ( <i>Luef and Keese</i> ).....	20	231
Supramolecular Networks of Porphyrins ( <i>Goldberg</i> ).....	25	71
Supramolecular Synthesis of 1D Chains and 2D Layers in Hydrogen Bond Networks of Ureas and 2-Pyrimidinones ( <i>Nangia</i> ).....	25	135
Transition-Metal-Templated Synthesis of Rotaxanes ( <i>Blanco, Chambron, Jiménez and Sauvage</i> ) .....	23	125
Torsion Angle Concept in Conformational Analysis ( <i>Bucourt</i> ) .....	8	159
Torsional Motion of Stilbene-type Molecules in Crystals ( <i>Harada, Ogawa</i> ) ...	25	31
Ultrasonic Absorption and Vibrational Spectroscopy Use of, to Determine the Energies Associated with Conformational Changes ( <i>Wyn-Jones and Pethrick</i> ).....	5	205
Unusual Saturated Hydrocarbons: Interaction Between Theoretical and Synthetic Chemistry ( <i>Dodziuk</i> ) .....	21	351
Vibrational Optical Activity, Stereochemical Aspects of ( <i>Freedman and Nafe</i> )...	17	113
Vibrational Spectroscopy and Ultrasonic Absorption, Use of, to Determine the Energies Associated with Conformational Changes ( <i>Wyn-Jones and Pethrick</i> ).....	5	205
Vinylic Radicals, and Cyclohexyl. The Stereochemistry of ( <i>Simamura</i> ).....	4	1
Wittig Reaction, Stereochemistry of ( <i>Schlosser</i> ) .....	5	1
Wittig Reaction, Stereochemistry and Mechanism of the ( <i>Vedejs and Peterson</i> ).....	21	1